ACTA TECHNICA

ACADEMIAE SCIENTIARUM HUNGARICAE

REDIGIT: M. MAJOR

TOMUS 76
FASCICULI 1—2

AKADÉMIAI KIADÓ, BUDAPEST 1974

ACTA TECHNICA

SZERKESZTŐ BIZOTTSÁG

BARTA ISTVÁN, BÖLCSKEI ELEMÉR, GESZTI P. OTTÓ,
HELLER LÁSZLÓ

Az *Acta Technica* angol, francia, német és orosz nyelven közöl értekezéseket a műszaki tudományok köréből.

Az *Acta Technica* változó terjedelmű füzetekben jelenik meg, több füzet alkot egy kötetet.

A közlésre szánt kéziratok a következő címre küldendők:

Acta Technica
1051 Budapest, Münnich Ferenc u. 7.

Ugyanerre a címre küldendő minden szerkesztőségi és kiadóhivatali levelezés.

Megrendelhető a belföld számára az „Akadémiai Kiadó"-nál (1363 Budapest Pf. 24. Bankszámla 215 11448) a külföld számára pedig a „Kultúra" Könyv- és Hírlap Külkereskedelmi Vállalatnál (1389 Budapest 62, P.O.B. 149 Bankszámla: 218 10990) vagy annak külföldi képviseleteinél és bizományosainál.

Die *Acta Technica* veröffentlichen Abhandlungen aus dem Bereiche der technischen Wissenschaften in deutscher, englischer, französischer und russischer Sprache.

Die *Acta Technica* erscheinen in Heften wechselnden Umfanges. Vier Hefte bilden einen Band.

Die zur Veröffentlichung bestimmten Manuskripte sind an folgende Adresse zu senden:

Acta Technica
1051 Budapest,
Münnich Ferenc u. 7.
Ungarn

An die gleiche Anschrift ist auch jede für die Schriftleitung und den Verlag bestimmte Korrespondenz zu richten. Abonnementspreis pro Band: $ 24.00

Bestellbar bei dem Buch- und Zeitungs-Außenhandels-Unternehmen »Kultúra« (1389 Budapest 62, P.O.B. 149 Bankkonto Nr. 218 10990) oder bei seinen Auslandsvertretungen und Kommissionären.

ACTA TECHNICA

ACADEMIAE SCIENTIARUM HUNGARICAE

REDIGIT: M. MAJOR

TOMUS 76

AKADÉMIAI KIADÓ, BUDAPEST 1974

INDEX

Verő J. A. 70 Jahre. — For *Verő J. A.*, 70th Anniversary. 243

Mándi A. 1891—1972 249

Bitó, J. F.—Antal, K. G.: A Capacitive Discharge Method for Determining Gas Impurities Quantitively — Eine kapazitive Entladungsmethode für die quantitative Bestimmung von Gasverunreinigungen — *Вито, Я., Антал, К.:* Метод емкостных газовых разрядов для количественного определения газовых примесей 65

Bitó, J. F.—Antal, K. G.: Examination of the Structure of Functional Relations among Physical Quantities and some Application there of in Discharge Physics — Die Struktur von funktionellen Zusammenhängen zwischen physikalischen Größen und die Anwendung derselben in der Entladungsphysik — Исследование структуры функциональных зависимостей между физическими величинами и ее применение для газых разрядов 257

Bhargava, R. D.—Miss Bhargava R. R.: An Infinite Elastic Plate under Tension with a Crack and a Circular Inclusion — Zug einer unendlichen Scheibe, die einen geraden Einschnitt und eine kreisförmige Einbettung besitzt — *Баргава, Р. Д., Баргава, Р. Р.:* Вытяжка бесконечной по размерам плоской пластины ....

Buócz, Z.—Janositz, J.: Ein neues Verfahren zur Lösung der Doppelpunkteinschaltung durch Streckenmessung — A New Method of the Double-Point Insertion on the Basis of Distance Measurement — *Буоц, З., Яношитуц, Я.:* Новый метод решения проблемы двойной привязки точки, основывающейся на данных измерения расстояния 87

Ecsedi, I.: An Approximate Method for the Analysis of Flexible Torsion of Round Bars of Variable Diameters — Eine Näherungsmethode zur Analyse der elastischen Verdrehung von Rundstäben mit veränderlichen Durchmessern — *Эчеди, И.:* Приближенный метод исследования упругого кручения круглых стержней переменного сечения 93

Hajdú, L.— Zahorán, J.: Hermetically Sealed Silver-Zinc Batteries Operating in the Silver (I) Oxide (Ag_2O) Phase — In der (Ag_2O)-Phase von Silber (I)-Oxyd funktionierender gasdicht verschlossener Silber-Zink-Akkumulator — *Хайду, л., Захоран, Я.:* Герметизированный серебряно-цинковый аккумулятор, работающий в фазе одновалентного серебра (Ag_2O) 153

Holnapy, D.: Numerical Algorithm to Determine the Difference Operators of Boundary-Value Problems — Numerischer Algorithmus zur Ermittlung der Differenzoperatoren von Randwertaufgaben — Численный алгоритм для определения разностных операторов задач краевых значений 413

Kalló, P.: Critical Summary of the Design Methods of Form-independent Thin Triplet Systems — Kritische Zusammenfassung der Entwurfsmethode der gestaltungsabhängigen dünnen Schichten des Triplex — Критическое об-обшение метода проэктирования форманезависимой тоской системы триплета 255

Kis, S.: Rational Assumption of Interpolation Reference Points in the Case of Bivariate Lagrange Interpolation — Zweckmässige Festlegung der Grundpunkte für die Lagrangesche Interpolation bei zwei Variablen — Целесообразное принятие интерполяционных опорных точек в случае интерполяции Лагранжа с двумя переменными 425

Kereszty, P.: Role of the Centre Plate and Side Bearing in the Safe Riding of Rail Vehicles — Rolle des Drehtellers und der Gleitstütze in der Fahrsicherheit der Schienenfahrzeuge — *Яерести, П.:* Роль вагонного подпятника и боковой опоры в надержности движения железнодорожного подвижного средства 129

Kollár, L.: Continuum Method of Analysis for Double-Layer Space Trusses with Upper and Lower Chord Planes of Different Rigidities — Berechnung zweischichtiger Raumfachwerke mit unteren und oberen Gurtebenen von verschiedenen Steifigkeiten mit dem Kontinuumverfahren — *Коллар, Л.:* Расчет двухслойных пространственных ферм различной жесткости, имеющих верхнюю и нижнююплоскости пояса 53

Kollár, L.: Analysis of Double-Layer Space Trusses with Diagonally Square Mesh by the Continuum Method — Berechnung zweischichtiger, im Grundriß diagonalviereckiger Raumfachwerke mit dem Kontinuumverfahren — Расчем бвухслойныхпространственных решеток с диагонального-квадратным планом методом wконтинуума 273

Kozarov, M.—Ivanov, Ts. P.: Wave Propagation in an Infinite Transversely Isotropic Cylinder of Elliptical Cross-Section — Wellenfortpfanzung in einem in der Querrichtung isotropen Zylinder elliptischen Querschnitts — *Козаров, М., Иванов, Ч. И.:* Распространение волн в поперечном направлении изотропном бесконечном цилиндре эллиптического сечения 21

Márkus, Gy.: Circular Plate Foundations of Spherical Gas Tanks on Point Supports — Kreisplatten-Fundamente von Kugelgasbehältern mit punktförmigen Abstützungen — Круглая плита фундамента шарового газольдера, покоящегося на точечных опорах 435

Mistéth, E.: Dimensioning of Structures for Flood Discharge According to the Theory of Probability — Bemessung von Bauwerken für Hochwasser-Ableitung aufgrund der Wahrscheinlichkeitstheorie — *Миштет, Э.:* Расчет технических сооружений на основе теории вероятности на отвод паводковых вод 107

Megahid Ahmed, A.—Lenkei, P.: The Effect of the Cross-Section Dimensions on the Ductility of Concrete — Einfluß der Querschnittsdimensionen auf die Verformungsfähigkeit des Betons — Влияние поперечных размеров на предельные деформации бетона 391

Murty, J. .S: Comparative Study of Some Creep-rupture Extrapolating Formulae — Vergleichende Untersuchung einiger Extrapolationsformeln für die Auswertung von Zeitdauern — Сравнительное исследование некоторых экстраполяционных формул для оценки продолжительностей 293

Patkó, J.—Jr. Vajta, M.: Determination of the Thermal Breakdown Voltage for D. C. and A. C. Voltages — Bestimmung der Labilitätsspannung für Gleich- und Wechselspannung — *Патко, Я., МЛ. Вайта, М.:* Определение напряжения лабильности при постоянном и переменном токах 183

Schatt, W.: Grundlegende Vorgänge bei der Gefügeentwicklung — Basic Phenomena in Structure Development — *Шатт, В.:* Основные процессы формирования материальной структуры 39

Somogyi, K. — *Pődör, B.:* A Simple Sample Holder and Cryostat for Measuring Thermoelectric Power of Semiconductors in the Temperature Range of 80—400 K — Ein einfacher Probenhalter und Kryostat für die Messung der thermoelektrischen Spannung von Halbleitern im Temperaturbereich 80—400 K — *Шомоди, К., Педер, Б.:* Простой держатель образца и криостат для измерения термоэлектрических полупроводников в интервале температур от 80 до 400 К 177

Пацельт, И.: Интеграционный метод для решения контрактной задачи упругих систем с односторонними — *Páczelt, I.:* Iteration Method Applied to the Solution of Contact Problems of Elastic Systems Having Elements in Unilateral Relation — Iterationsverfahren zur Lösung der Kontakt-Fragen von elastischen Systemen mit einseitigen Anschluß .....

Tarnai, T.: Spherical Grids of Triangular Network — Sphärische Dreiecksfachwerke — *Тарнаи, Т.:* Сферические решетчатые конструкции с треугольной сеткой..... 307

Timár, A.: Testing the Plastic Properties of Cohesive-and Intermediate-Type Soils by Extrusion — Untersuchung der plastischen Eigenschaften von bindingen Übergangsböden mit Hilfe von Stangenpressung — Исследование пластических свойств связанних и переходних грунтов прессованием прутков 355

Wedig, W.: Stabilitätsbedingungen für ein Schwingungssystem mit zufälliger Parametererregung — Conditions of Stability for a System under Random Parametric Excitation — *Ведиг, В.:* Условия стабильности колебательной системы, возбуждаемой случайным параметром 1

Zolnay, L.: L'approvisionnement en eau des villes et châteaux-forts hongrois au moyen-âge — Water Supply of Mediaeval Hungarian Towns and Fortresses — Wasserversorgung mittelalterlicher ungarischer Städte und Burgen 337

Varga, L.: Displacement Functions of Orthogonally Anisotropic Cylindrical Shells — Verschiebungsfunktionen von ortogonal-anisotropischen zylindrischen Schalen — Функции смещение ортогональных анизотропных цилиндрических оболочек 371

Acta Technica Academiae Scientiarum Hungaricae, Tomus 76 (1—2), pp. 1—19 (1974)

STABILITÄTSBEDINGUNGEN FÜR EIN SCHWINGUNGSSYSTEM MIT ZUFÄLLIGER PARAMETERREGUNG*

W. WEDIG**

Das Stabilitätsverhalten eines parametererregten Schwingungssystems, dessen Bewegungsverhalten durch eine Einzeldifferentialgleichung mit stochastischen Koeffizienten beschrieben werden kann, wird über die FOKKER—PLANCK-Gleichung untersucht. Die Bedingungen für die Stabilität der Ruhelage im quadratischen Mittel werden näherungsweise mit Hilfe einer Störungsrechnung hergeleitet. Für stochastische Koeffizienten, deren Spektraldichten über ein breites Frequenzband verteilt sind, ergeben die kritischen Erregerspektren Instabilitätsbereiche, deren tiefster Punkt in der Nähe der doppelten Eigenfrequenz des Schwingungssystems liegt. Bei Schmalfanderregungen gibt man als erste Näherung die Wurzel der kritischen Erregervarianz in Abhängigkeit der mittleren Erregerfrequenz an und erhält dadurch einen Instabilitätsbereich, der seinen Schwellwert ebenfalls in der Nähe der Parameterresonanz erreicht.

Einleitung

Das Stabilitätsverhalten elastischer Körper unter schwingenden äußeren Lasten ist in den letzten Jahren eingehend untersucht worden. Für den praktisch wichtigsten Fall harmonisch pulsierender Erregungen beantwortet eine allgemeine Theorie von E. METTLER [1] alle wesentlichen Fragen. Diese Theorie kann das Stabilitätsproblem in einfachen Fällen mit Hilfe einer homogenen, linearen Einzeldifferentialgleichung vom Schwingungstyp lösen, in der die äußere Erregung als ein zeitlich veränderlicher Koeffizient enthalten ist. Derartige Erregungen heißen Parametererregungen und haben auch in anderen Bereichen der Schwingungstechnik eine selbständige Bedeutung.

Neuerdings gewinnen über harmonische Erregungen hinaus auch Zufallserregungen an Bedeutung. Dann enthält die Bewegungsgleichung des parametererregten Schwingungssystems Zufallsfunktionen als zeitlich veränderliche Koeffizienten, die ähnlich wie periodische Koeffizienten die Ruhelage des Schwingungssystems destabilisieren können. Diese Problemstellung wurde zunächst von J. C. SAMUELS [2] sowie von T. K. CAUGHEY und J. K. DIENES [3] bearbeitet. Für den einfachen Fall einer Erregung durch gaussisches weißes

* Dieser Beitrag wurde anläßlich eines Partnerschaftsbesuchs am 19. 10. 1971 im Institut für Technische Mechanik der Technischen Universität Budapest vorgetragen.

** W. WEDIG, Institut für Technische Mechanik, Karlsruhe, BRD

Rauschen haben sie die quadratischen Momente des Systems berechnet und eine Bedingung hergeleitet, die die Stabilität der Ruhelage im quadratischen Mittel sichert.

In dem vorliegenden Beitrag wird die destabilisierende Wirkung von wirklichkeitsnäheren Erregerprozessen untersucht, die man durch Tiefpaß- und Bandpaßfilter aus gaussischem weißen Rauschen erzeugen kann. Es wird sich zeigen, daß die obenerwähnte Momentenstabilitätsuntersuchung bei zufälligen Parametererregungen mit stark veränderlichen Spektren auf frequenzabhängige Instabilitätsbereiche führt, deren tiefster Punkt ähnlich wie bei der Struttschen Karte der Mathieu-Gleichung in der Nähe der doppelten Eigenfrequenz des Schwingungssystems liegt.

2. Schwingungsgleichungen

Ein einfacher Sonderfall der kinetischen Stabilitätstheorie liegt z. B. vor, wenn man nach der Stabilität der gestreckten Ruhelage eines geraden Stabes fragt, der an seinen Enden momentenfrei gelagert ist und durch pulsierende Kräfte axial belastet wird (Fig. 1). Bei einer Anfangsstörung in Querrichtung wird der Stab Transversalschwingungen $w(x, t)$ um seine Gleichgewichtslage ausführen, die durch die Bewegungsgleichung

$$EJw_{xxxx}+P(t)w_{xx}+\beta w_t+\mu w_{tt}=0 \tag{1}$$

beschrieben werden. Hierin ist EJ die Biegesteifigkeit des Stabes, μ ist seine Masse je Längeneinheit und β ist die Konstante einer geschwindigkeitsproportionalen, ebenfalls auf die Längeneinheit bezogenen Dämpfungskraft. Die Axialkraft $P(t)$ besteht aus einem konstanten Anteil P_0 und aus einem um diesen Mittelwert schwingenden Anteil $P_1x(t)$, so daß die zeitliche Veränderlichkeit der Kraft allein durch die dimensionslose Zufallsfunktion $x(t)$ bestimmt wird.

Die Bewegungsgleichung (1) gilt nur bei Vernachlässigung der Rotationsträgheit der Stabelemente und der Längsschwingungen im Stabe, so daß die äußere Belastung $P(t)$ für jeden Stabquerschnitt konstant bleibt. Außerdem muß die Untersuchung der Stabbiegeschwingungen auf kleine Schwingungsausschläge beschränkt bleiben, weil bei großen Durchbiegungen die elastische Rückstellung des Stabes durch nichtlineare Terme zu ergänzen ist. Die Bewegungsgleichung (1) kann daher nur zur Untersuchung der Stabilität der Ruhelage des Stabes herangezogen werden.

Der aus den Eigenfunktionen gebildete Produktansatz

$$w(x, t) = y(t) \cdot \sin(\pi n x/l)$$

erfüllt die Randbedingungen, die an den Enden des Stabes durch die frei drehbaren Lager vorgeben sind und führt die Bewegungsgleichung (1) für die erste Eigenfunktion ($n = 1$) auf eine homogene lineare Einzeldifferentialgleichung zweiter Ordnung zurück.

$$\ddot{y}+2D\omega_1\dot{y}+\omega_1^2[1-\varepsilon x(t)\,y=0\,. \tag{2}$$

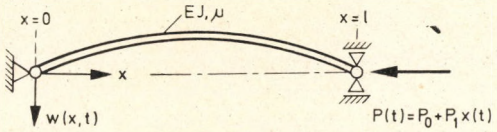

Fig. 1

Hierin ist ω_1 die tiefste Eigenkreisfrequenz der ungedämpften Eigenschwingungen, die der Stab für $\beta = 0$ und $P_1 = 0$ ausführen würde, D ist das dimensionslose Lehrsche Dämpfungsmaß, und ε ist ein ebenfalls dimensionsloser Parameter, der klein gegen Eins ist.

$$\omega_n^2 = (n^2 P_E + P_0)(\pi n)^2/\mu l^2, \qquad \beta/\mu = 2D\omega_n\,,$$
$$\varepsilon = P_1/(n^2 P_E - P_0),\ n = 1, 2, \ldots \qquad P_E = EJ\,(\pi/l)^2.$$

Die Gleichung (2) nennt man die Stabilitätsgleichung des Stabes, weil sich an ihr entscheiden läßt, ob die Querschwingungen $w(x, t)$ des Stabes nach einer kleinen Anfangsstörung auf- oder abklingen, und damit auch die Frage nach der Stabilität der gestreckten Gleichgewichtslage des Stabes beantwortet werden kann. Bei einer zufälligen Parametererregung wird dieses Zeitverhalten des Schwingungssystems über die statistischen Kenndaten der Zufallsschwingungen $y(t)$ beschrieben. Entsprechend diesen Kenndaten gibt es daher auch verschiedene Stabilitätsdefinitionen, von denen hier nur die Stabilität im quadratischen Mittel betrachtet werden soll. Danach nennt man die Ruhelage des Systems, das durch die stochastische Differentialgleichung (2) beschrieben wird, im quadratischen Mittel stabil, wenn die zweiten Momente der Lage und Geschwindigkeit des Systems

$$\lim_{t\to\infty} E[y^2 t)] \leq c_1\,, \quad \lim_{t\to\infty} E[y(t)\,\dot{y}(t)] \leq c_2\,, \quad \lim_{t\to\infty} E[\dot{y}^2(t)] \leq c_3 \tag{3}$$

für unbegrenzt wachsende Zeit endlich bleiben [4].

Für eine etwas einfachere Auswertung dieser Momentenstabilitätsdefinitionen ist es zweckmäßig, zuvor noch über den Exponentialansatz

$$y(t) = T(t)\exp(-D\omega_1 t)$$

die Zeitfunktion $T(t)$ für die Lagekoordinate $y(t)$ einzuführen. Damit nimmt die Einzeldifferentialgleichung (2) des parametererregten Schwingungssystems die Form

$$\ddot{T} + \nu_1^2 T = \varepsilon_1 \nu_1^2 x(t) T \tag{4}$$

an. Sie enthält mit

$$\nu_1 = \sqrt{1 - D^2}$$

die gedämpfte Eigenkreisfrequenz des Systems und mit $\varepsilon_1 = \varepsilon/(1 - D^2)$ einen dimensionslosen Parameter, der bei kleinen Dämpfungen ebenfalls klein ist. Für die Lagekoordinate $z_1 = T$ und für die Geschwindigkeitskoordinate $z_2 = \dot{T}$ erhält man aus (4) schließlich ein System von zwei Differentialgleichungen erster Ordnung

$$\dot{z}_1 = z_2\,, \quad \dot{z}_2 = -\nu_1^2 z_1 + \varepsilon_1 \nu_1^2 x(t)\, z_1\,, \tag{5}$$

die zur Aufstellung der Differentialgleichungen der quadratischen Momente benötigt werden.

3. Erregung durch gaussisches weißes Rauschen

Zur Einführung in die folgenden Stabilitätsuntersuchungen wird zunächst der bereits bekannte Sonderfall [5] betrachtet, daß die Parametererregung $x(t)$ des Schwingungssystems ein stationärer gaussischer Zufallsprozeß $\xi(t)$ mit dem Mittelwert $E[\xi(t)] = 0$ ist, dessen Autokorrelationsfunktion mit

$$E[\xi(t_1)\xi(t_2)] = S_0 \sigma(t_1 - t_2)$$

(Fig. 2) durch die Diracsche Deltafunktion und durch das konstante Spektrum

$$S\xi(\omega) = S_0 = \text{konst.}$$

(Fig. 3) vorgegeben ist. Dieser Zufallsprozeß $\xi(t)$ — kurz gaussisches weißes Rauschen genannt — hat den Vorteil, daß er als Erregermechanismus dynamischer Systeme auf Markov-Prozesse führt, deren bedingte Wahrscheinlichkeitsdichte $p(z, t; z_0, t_0)$ für $t \geqslant t_0$ relativ einfach über die zugehörige Fokker—Planck-Gleichung

$$\frac{\partial p}{\partial t} = -\sum_{i=1}^{2} \frac{\partial}{\partial z_i}(a_i\, p) + \frac{1}{2} \sum_{i,j=1}^{2} \frac{\partial^2}{\partial z_i\, \partial z_j}(b_{ij}\, p)$$

zu ermitteln ist. Hierin ist $z = (z_1, z_2)^T$ der Zustandsvektor des Schwingungssystems und die Koeffizienten a_i, b_{ij} $(i, j = 1, 2)$ sind die infinitesimalen Mo-

mente, die man aus den Zustandsänderungen Δz_i $(i = 1, 2)$ des Systems nach einer Erwartungswertbildung und einem Grenzübergang mit $\Delta t \to 0$ erhält [6].

$$a_i = \lim_{\Delta t \to 0} \frac{1}{\Delta t} E[\Delta z_i], \quad b_{ij} = \lim_{\Delta t \to 0} \frac{1}{\Delta t} E[\Delta z_i \, \Delta z_j], \qquad i, j = 1, 2.$$

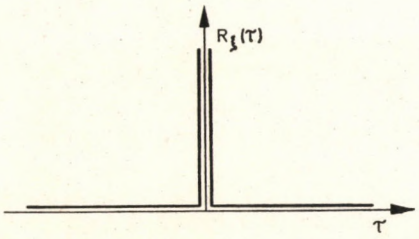

Fig. 2

Diese Rechnung liefert für das vorgegebene System (5)

$$a_1 = z_2, \qquad a_2 = -\nu_1^2 z_1,$$
$$b_{11} = b_{12} = b_{21} = 0, \quad b_{22} = \varepsilon_1^2 \nu^4 S_0 z_1^2,$$

so daß die Fokker – Planck-Gleichung folgende Form annimmt:

$$\frac{\partial p}{\partial t} = -z_2 \frac{\partial p}{\partial z_1} + \nu_1^2 z_1 \frac{\partial p}{\partial z_2} + \frac{1}{2} \varepsilon_1^2 \nu_1^4 S_0 z_1^2 \frac{\partial^2 p}{\partial z_2^2}.$$

Um daraus die Erwartungswerte der Lage z_1 und der Geschwindigkeit z_2 des parametererregten Schwingungssystems zu ermitteln, werden entsprechend der Definition

$$M_{k_1 k_2}(t) = E[z_1^{k_1} z_2^{k_2}] = \int_{-}^{+} \int_{\infty}^{\infty} z_1^{k_1} z_2^{k_2} p dz_1 \, dz_2$$

beide Seiten der Fokker–Planck-Gleichung mit Potenzen der Zustandskoordinaten z_i $(i = 1, 2)$ multipliziert und über den gesamten Phasenraum integriert. Dann stehen auf der linken Seite der Gleichung bereits die zeitlichen Ableitungen der Erwartungswerte, während ihre rechte Seite noch durch eine partielle Integration umzuformen ist. Danach erhält man eine gewöhnliche Differentialgleichung für die Erwartungswerte $(k_1 + k_2)$-ter Ordnung:

$$\dot{M}_{k_1 k_2} = k_1 M_{k_1 - 1, k_2 + 1} - k_2 \nu_1^2 M_{k_1 + 1, k_2 - 1} + k_2 (k_2 - 1) \frac{1}{2} \varepsilon_1^2 \nu_1^4 S_0 M_{k_1 + 2, k_2 - 2}.$$

Diese Gleichung ergibt speziell für die quadratischen Momente $(k_1 +$

$+ k_2 = 2$) ein System aus drei linearen homogenen Differentialgleichungen erster Ordnung, das in der Matrizenschreibweise

$$\dot{\mathbf{M}} = (\mathbf{A} + \varepsilon_1^2 \mathbf{R})\,\mathbf{M} \tag{6}$$

angegeben wird. Hierin ist $\mathbf{M}$ der Momentenvektor, $\mathbf{A}$ ist die Matrix das für $\varepsilon = 0$ ungestörten Systems und $\mathbf{R}$ ist die Matrix der Erregung.

$$\mathbf{M} = \begin{pmatrix} M_{2,0} \\ M_{1,1} \\ M_{0,2} \end{pmatrix}, \quad \mathbf{A} = \begin{pmatrix} 0 & 0 & 0 \\ -\nu_1^2 & 0 & 1 \\ 0 & -2\nu_1^2 & 0 \end{pmatrix}, \quad \mathbf{R} = \begin{pmatrix} 0 & 0 & 0 \\ 0 & 0 & 0 \\ \nu_1^4 S_0 & 0 & 0 \end{pmatrix}.$$

Die Matrizen $\mathbf{A}$ und $\mathbf{R}$ enthalten nur konstante Koeffizienten. Der Exponentialansatz $\mathbf{M}(t) = \mathbf{C}e^{\lambda t}$ liefert daher eine hinreichend allgemeine Lösung des Systems und führt nach Einsetzen in (6) auf ein homogenes Gleichungssystem

$$(\lambda \mathbf{E} - \mathbf{A} - \varepsilon_1^2 \mathbf{R})\,\mathbf{C} = 0\,, \tag{7}$$

in dem $\mathbf{E}$ die Einheitsmatrix ist. Der noch unbestimmte Amplitudenvektor $\mathbf{C}$ hat nur dann nichtverschwindende Komponenten, wenn die zu (7) gehörende Koeffizientendeterminante gleich Null und also λ eine Wurzel der charakteristischen Gleichung ist.

Das Gleichungssystem (7) wird näherungsweise mit Hilfe der Störungsrechnung gelöst. Dazu macht man für den Exponenten λ und für den Amplitudenvektor $\mathbf{C}$ einen Reihenansatz

$$\lambda = \lambda^{(0)} + \varepsilon_1^2 \lambda^{(1)} + \varepsilon_1^4 \lambda^{(2)} + \ldots,$$
$$C = C^{(0)} + \varepsilon_1^2 C^{(1)} + \varepsilon_1^4 C^{(2)} + \ldots$$

und führt diese Potenzreihen in (7) ein. Der Koeffizientenvergleich gleich hoher Potenzen des kleinen Parameters ε_1^2 liefert dann eine Folge von algebraischen Gleichungen

$$(\varepsilon_1^2)^i\colon \quad (\lambda^{(0)}\,\mathbf{E} - \mathbf{A})\,\mathbf{C}^{(i)} = \mathbf{R}\,\mathbf{C}^{(i-1)} - \sum_{j=0}^{i-1} \lambda^{(i-j)}\,\mathbf{C}^{(j)},$$

welche rekursibel lösbar sind. Die Gleichung

$$(\lambda^{(0)}\,\mathbf{E} - \mathbf{A})\,\mathbf{C}^{(0)} = 0$$

der nullten Näherung besitzt mit der imaginären Einheit i und mit den Integrationskonstanten a_m für $m = 0, \pm 1$ drei Wurzeln und drei zugehörige Amplitudenvektoren.

$$\lambda_m^{(0)} = i2\nu_1 m\,. \quad C_m^{(0)} = \alpha_m [1, im\nu_1, (1 - 2m^2)\,\nu_1^2]^T, \quad m = 0, \pm 1\,.$$

Diese Grundlösung hat man anschließend in die Gleichung der ersten Näherung einzusetzen und erhält daraus

$$\lambda_m^{(1)} = \frac{1}{2} \nu_1^2 S_0 \frac{1}{1-3m^2}, \quad m = 0, \pm 1$$

als eine erste Korrektur der Grundlösung. Setzt man beide Ergebnisse in die oben angeführte Potenzreihe ein, so hat man die Wurzeln mit

$$\lambda_m = i2\nu_1 m + \varepsilon_1^2 \frac{1}{1-3m^2} \frac{1}{2} \nu_1^2 S_0 + 0(\varepsilon_1^4), \quad m = 0, \pm 1$$

bis auf Reihenglieder der Größenordnung, ε_1^4 bestimmt.

Man erkennt, daß die erste Wurzel λ_0 den größten Realteil besitzt. Sie bestimmt daher das Wachstumsverhalten der quadratischen Momente von $z_1 = T$ und $z_2 = \dot{T}$ und zusammen mit der eingangs eingeführten Exponentialfunktion

$$y(t) = T(t) \exp(-D\omega_1 t)$$

auch das Wachstumsverhalten der quadratischen Momente von Lage $y(t)$ und Geschwindigkeit $\dot{y}(t)$ des parametererregten Schwingungssystems. Das Moment

$$E[y^2] = M_{2,0} \exp(-2D\omega_1 t)$$

und auch die übrigen quadratischen Momente des Systems haben somit stets ein abklingendes Zeitverhalten, wenn der Realteil $\varepsilon_1^2 \nu_1^2 S_0/2$ der ersten Wurzel kleiner als die Dämpfungskonstante $2D\omega_1$ des Schwingungssystems ist. Setzt man in diese Stabilitätsbedingung noch die gedämpfte Eigenkreisfrequenz ν_1 und den in (4) eingeführten kleinen Parameter ε_1 ein, so erhält man schließlich die bereits bekannte Stabilitätsgrenze [5]

$$\varepsilon^2 \omega_1 S_0 = 4D(1 - D^2). \tag{8}$$

Diese Stabilitätsbedingung wurde in der untenstehenden Abbildung (Fig. 4) für kleine Dämpfungsbeiwerte $D \ll 1$ ausgewertet. Dabei wurde die kritische Spektraldichte $\varepsilon^2 S_0$ der zufälligen Erregung $\varepsilon\xi(t)$ mit dem Faktor ω_1 geeignet dimensionslos gemacht und über der Erregerfrequenz ω aufgetragen. Überschreitet das Erregerspektrum den Schwellwert $4D$, dann ist die Ruhelage des parametererregten Schwingungssystems im quadratischen Mittel instabil. Nur wenn das Erregerspektrum unterhalb des schraffiert angegebenen Instabilitätsbereiches liegt, haben die quadratischen Momente des Systems ein exponentiell abklingendes Zeitverhalten. Auffällig an diesem Ergebnis ist, daß bei einer Erregung durch gaussisches weißes Rauschen die

Erregerfrequenzen keinen Einfluß auf das Stabilitätsverhalten des Systems haben. Ganz anders als bei harmonischen Erregungen ist die Grenzkurve des in Fig. 4 gezeichneten Instabilitätsbereiches über der Frequenzachse konstant. Dies erscheint aber plausibel, da auch bei zufälligen Parametererregungen nur dann eine Frequenzabhängigkeit in den Stabilitätsbedingungen auftreten kann, wenn die Spektraldichte der Erregung nicht gleichmäßig verteilt ist.

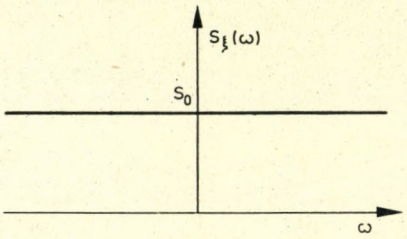

Fig. 3

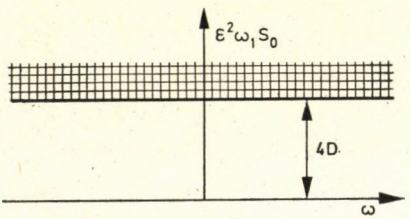

Fig. 4

4. Erregung durch gefiltertes weißes Rauschen

Zufallsprozesse mit frequenzabhängigen Spektraldichteverteilungen können über Formfilter aus gaussischem weißen Rauschen $\xi(t)$ erzeugt werden. Betrachtet wird zunächst der einfache Fall eines Tiefpaßfilters erster Ordnung, dessen Differentialgleichung in der Form

$$\dot{x}+\omega_g x = \omega_g \xi(t) \tag{9}$$

vorgegeben wird. Seine Grenzkreisfrequenz ist ω_g. Sie bestimmt sowohl die Bandbreite als auch die Einschwingzeit des Filters. Nach der Einschwingzeit ist der gefilterte Prozeß $x(t)$ stationär. Er besitzt dann den Mittelwert $E[x(t)]=$ $= 0$ und die Varianz $\sigma_x^2 = \omega_g S_0/2$. Die zugehörige Autokorrelationsfunktion

$$R_x(\tau) = E[x(t_1)\, x(t_2)]$$

und die Spektraldichteverteilung $S_x(\omega)$ lauten

$$R_x(\tau) = \frac{1}{2}\omega_g S_0 \exp\left(-\omega_g|\tau|\right), \quad S_x(\omega) = S_0 \frac{\omega_g^2}{\omega_g^2+\omega^2}$$

und sind in Fig. 5 und 6 aufgezeichnet. Wie in Abschnitt 3 wird das Spektrum $\varepsilon^2 S_x(\omega)$ der zufälligen Parametererregung $\varepsilon x(t)$ mit der Eigenkreisfrequenz ω_1 des Systems geeignet dimensionslos gemacht und in Abhängigkeit der Erregervarianz $(\varepsilon\sigma_x)^2$ angegeben.

$$\varepsilon^2 \omega_1 S_x(\omega) = (\varepsilon\sigma_x)^2 \frac{2\omega_1 \omega_g}{\omega_g^2 + \omega^2} . \tag{10}$$

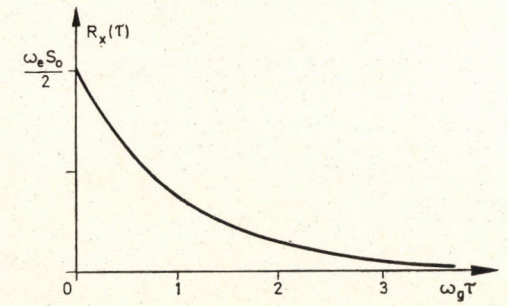

Fig. 5

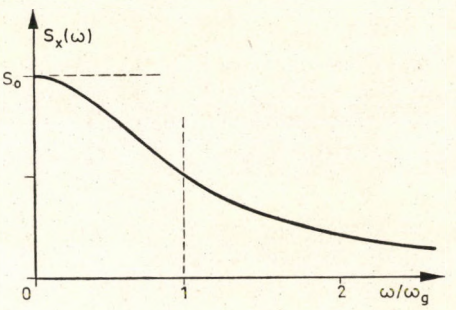

Fig. 6

Für die weitere Rechnung hat man jedoch wieder von der ungefilterten Erregung $\xi(t)$, dem gaussischen weißen Rauschen, auszugehen und demzufolge neben den Zustandskoordinaten $z_1 = T$ und $z_2 = \dot{T}$ des Schwingungssystems noch eine dritte Zustandskoordinate $z_3 = x$ für das Erregersystem einzuführen. In dieser Betrachtungsweise liegt dann ein System aus drei Differentialgleichungen vor

$$\begin{aligned} \dot{z}_1 &= z_2 , \\ \dot{z}_2 &= -\nu_1^2 z_1 + \varepsilon_1 \nu_1^2 z_1 z_3 , \\ \dot{z}_3 &= -\omega_g z_3 + \omega_g \xi(t) , \end{aligned}$$

das inhomogen und nichtlinear ist. Der Zustandsvektor $\mathbf{z} = (z_1, z_2 z_3)^T$ dieses Systems ist ebenso wie die Erregung $\xi(t)$ ein Markov-Prozeß. Seine bedingte

Wahrscheinlichkeitsdichte $p(z, t; z_0, t_0)$ kann man daher über die zugehörige Fokker-Planck-Gleichung

$$\frac{\partial p}{\partial t} = -\sum_{i=1}^{3} \frac{\partial}{\partial z_i}(a_i\, p) + \frac{1}{2}\sum_{i,j=1}^{3} \frac{\partial^2}{\partial z_i\, \partial z_j}(b_{i,j}\, p)$$

ermitteln und berechnet durch eine Integration über den gesamten Phasenraum die Erwartungswerte $(k_1 + k_2 + k_3)$-ter Ordnung

$$M_{k_1 k_2 k_3}(t) = E\left[T^{k_1}(t)\, \dot{T}^{k_2}(t)\, x^{k_3}(t)\right],$$

$$M_{k_1 k_2 k_3}(j) = \iiint_{-\infty}^{+\infty} z_1^{k_1}\, z_2^{k_2}\, z_3^{k_3}\, p\, dz_1\, dz_2\, dz_3$$

des Schwingungs- und Erregersystems. Aus dieser Rechnung erhält man schließlich die gewöhnliche Differentialgleichung

$$\dot{M}_{k_1 k_2 k_3} = -k_3\, \omega_g\, M_{k_1 k_2 k_3} + k_1\, M_{k_1-1, k_2+1, k_3} - k_2\, \nu_1^2\, M_{k_1+1, k_2-1, k_3} + \\ + \omega_g\, k_3\, (k_3 - 1)\, \sigma_x^2\, M_{k_1, k_2, k_3-2} + k_2\, \varepsilon_1\, \nu_1^2\, M_{k_1+1, k_2-1, k_3+1}$$

und speziell für alle Indizes $k_1 + k_2 = 2$ ein System aus drei Differentialgleichungen, das in der Matrizenschreibweise

$$\dot{\mathbf{M}}_k = A_k\, \mathbf{M}_k + \omega_g\, k\, (k-1)\, \sigma_x^2\, \mathbf{M}_{k-2} + \varepsilon_1\, R\mathbf{M}_{k+1},$$

$$\mathbf{M}_k = \begin{pmatrix} M_{2,0,k} \\ M_{1,1,k} \\ M_{0,2,k} \end{pmatrix}, \quad A_k = \begin{pmatrix} -k\,\omega_g & 2 & 0 \\ -\nu_1^2 & -k\,\omega_g & 1 \\ 0 & -2\nu_0^2 & -k\,\omega_g \end{pmatrix}, \quad R = \begin{pmatrix} 0 & 0 & 0 \\ \nu_1^2 & 0 & 0 \\ 0 & 2\nu_1^2 & 0 \end{pmatrix} \tag{11}$$

angegeben wird. Setzt man für den dritten Index $k_3 = k$ zunächst die Zahl Null, so stehen in dem Momentenvektor $\mathbf{M}_0$ die bereits erwähnten quadratischen Erwartungswerte des Schwingungssystems, deren Zeitverhalten zu überprüfen ist. Man erkennt, daß $\mathbf{M}_0$ über den kleinen Parameter ε_1 und über die Erregermatrix $\mathbf{R}$ mit $\mathbf{M}_1$ schwach gekoppelt ist und damit auch mit den Momentenvektoren $\mathbf{M}_k$ der k-ten Ordnung gekoppelt ist, dessen Erwartungswerte neben den Zustandskoordinaten z_1 und z_2 des Systems auch k-te Potenzen der Parametererregung $x(t)$ enthalten. Für eine Erregung durch gefiltertes weißes Rauschen liefert die Fokker – Planck-Gleichung demnach eine Folge linearer Differentialgleichungen mit konstanten Koeffizienten.

Dieses Differentialgleichungssystem kann man näherungsweise mit Hilfe einer Störungsrechnung lösen. Dazu macht man für den Momentenvektor $\mathbf{M}_k(t)$ einen Exponentialansatz, dessen Exponent λ und dessen Amplitudenvektor $\mathbf{C}_k$ in Potenzreihen des kleinen Parameter ε_1 zu entwickeln sind.

$$\mathbf{M}_k(t) = \mathbf{C}_k\, \exp\,(\lambda t), \qquad \lambda = \lambda^{(0)} + \varepsilon_1\, \lambda^{(1)} + \varepsilon_1^2\, \lambda^{(2)} + \ldots,$$

$$\mathbf{C}_k = \mathbf{C}_k^{(0)} + \varepsilon_1 \mathbf{C}_k^{(1)} + \varepsilon_1^2\, \mathbf{C}_k^{(2)} + \ldots.$$

Diese Potenzreihen werden in die Matrizengleichung (11) eingeführt und liefern nach dem Koeffizientenvergleich gleich hoher Potenzen von ε_1 eine Folge linearer algebraischer Gleichungen.

$$\varepsilon_1^i\colon\ (\lambda^{(0)} E - A_k)\,\mathbf{C}_{k_1}^{(i)} = \omega_g k(k-1)\,\sigma_x^2\,\mathbf{C}_{k-2}^{(i)} + \\ + R\mathbf{C}_{k+1}^{(i-1)} - \sum_{j=0}^{j-1} \lambda^{(i-j)}\,\mathbf{C}_k^{(j)}, \qquad i,k = 0,1,2\ldots \tag{12}$$

In (12) ist **E** die Einheitsmatrix und der hochgestellte Index i gibt den Grad der Näherungen an. Für eine rekursible Lösung dieser Gleichungen hat man zunächst die homogene Grundgleichung

$$(\lambda^{(0)}\,\mathbf{E} - \mathbf{A}_0)\,\mathbf{C}_0^{(0)} = 0$$

heranzuziehen und berechnet aus ihr die drei Wurzeln $\lambda_m^{(0)}$ sowie die drei zugehörigen Amplitudenvektoren $\mathbf{C}_{0,m}^{(0)}$ der nullten Näherung.

$$\lambda_m^{(0)} = i2\nu_1\, m, \quad \mathbf{C}_{0,m}^{(0)} = \alpha_m\,[1, i\nu_1\, m, (1-2m^2)\,\nu_1^2]^T \quad m = 0, \pm 1. \tag{13}$$

Hierin ist i die imaginäre Einheit und die Koeffizienten $\alpha_m\,(m = 0, \pm 1)$ sind Integrationskonstanten, die an beliebig vorgebbare Anfangsbedingungen anzupassen sind. Für eine weitere Auflösung von (11) muß man noch den zur Grundlösung (13) gehörenden Amplitudenvektor $\mathbf{C}_{1,m}^{(0)}$ aus der nullten Näherungsgleichung berechnen. Mit diesem Vektor ist dann die rechte Seite der ersten Näherungsgleichung

$$(\lambda^{(0)}\,\mathbf{E} - \mathbf{A}_0)\,\mathbf{C}_0^{(1)} = -\lambda^{(1)}\,\mathbf{C}_0^{(0)} + \mathbf{R}\mathbf{C}_1^{(0)}$$

bis auf $\lambda^{(1)}$ bekannt. Ihre drei Komponentengleichungen liefern eine Bestimmungsgleichung für $\lambda^{(1)}$ sowie zwei weitere Gleichungen zur Berechnung zweier Komponenten des Amplitudenvektors $C_0^{(1)}$. Eine Komponente, z. B. die erste, dieses Vektors bleibt wegen der Homogenität der Gleichungen unbestimmt. Konventionell darf sie gleich Null gesetzt werden. Ähnlich kann man anschließend auch die Gleichungen der höheren Näherungen lösen. Um diesen Auflösungsprozeß zu systematisieren, werden die Gleichungen (12) für die ersten Indizes k und für die ersten Potenzen von ε_1 angeschrieben und zweckmäßig in ein dreieckförmiges Tableau eingeordnet.
Das darin eingezeichnete Schema zeigt, auf welche Weise die Grundlösungen in die Gleichungen der nächst höheren Näherung eingehen und welche Amplitudenvektoren $C_k^{(i)}$ zu berechnen sind, wenn die Wurzeln z. B. bis zur Größenordnung von ε_1^2 ermittelt werden sollen.

Im Einzelnen erhält man dann für die erste Korrektur der drei Wurzeln mit $\lambda_m^{(1)} = 0$ $(m = 0, \pm 1)$ keinen Beitrag, und erst die Gleichung der zweiten Näherung liefert eine Verbesserung der in (13) aufgestellten Grundlösung. Dabei weist die erste Wurzel λ_0 den größten Realteil auf. Für eine Stabilitätsuntersuchung braucht daher auch nur diese Wurzel angegeben zu werden. Ihr Wert wurde bis auf Potenzen ε_1^6 formelmäßig berechnet [7].

$$\frac{\lambda_1}{\omega_g} = \frac{(\varepsilon_1 \sigma_x \nu_1)^2}{\omega_g^2 + 4\nu_1^2} + \frac{(\varepsilon_1 \sigma_x \nu_1)^4}{\omega_g^2 + 4\nu_1^2)^2} \alpha + 0(\varepsilon_1^6);$$

$$\alpha = \frac{4\nu_1^2 - \omega_g^2}{4\nu_1^2 + \omega_g^2} + \frac{11\nu_1^2 + 2\omega_g^2}{\nu_1^2 + \omega_g^2}.$$

Die zu dieser Wurzel gehörende Partikulärlösung bestimmt das Wachstumsverhalten der quadratischen Momente des parametererregten Schwingungssystems und entscheidet zusammen mit dem Dämpfungsbeiwert des Systems die Stabilität seiner Ruhelage im quadratischen Mittel. Die Stabilitätsgrenze wird erreicht, wenn λ_0 gerade gleich $2D\omega_1$ ist. Diese Stabilitätsbedingung ist eine quadratische Gleichung für die Varianz $(\varepsilon\sigma_x)^2$ der zufälligen Erregung $\varepsilon x(t)$ und liefert nach Auflösung die kritische Erregervarianz

$$(\varepsilon\sigma_x)^2_{\text{krit}} = (1 - D^2)^2 \frac{\omega_g^2 + 4\nu_1^2}{2\alpha\nu_1^2} \left[\sqrt{1 + \frac{\sqrt{8D\alpha}}{1D^2} \frac{\nu_1}{\omega_g}} - 1 \right].$$

Setzt man die kritische Erregervarianz in die Beziehung (10) ein, so kann man schließlich auch die kritische Spektraldichte der zufälligen Parametererregung angeben.

$$[\varepsilon^2 \omega_1 S_x(\omega)]_{\text{krit}} = \frac{(\varepsilon\sigma_x)^2_{\text{krit}}}{\sqrt{1 - D^2}} \frac{2\omega_g \nu_1}{\omega_g^2 + \omega^2}.$$

Diese Erregerspektren sind in Fig. 7 für das Lehrsche Dämpfungsmaß $D = 0{,}025$ und für verschiedene Grenzfrequenzen ω_g aufgezeichnet.

Für große Bandbreiten $\omega_g \gg \omega_1$ liegen zufällige Parametererregungen mit flachen, schwach veränderlichen Spektraldichteverteilungen vor. Um das Stabilitätsverhalten des Schwingungssystems bei derartigen Erregerprozessen zu kennzeichnen, genügt es, den bereits erwähnten Schwellwert (8) anzugeben, den die Erregerspektraldichte

$$\varepsilon^2 \omega_1 S_x(\omega = 2\omega_1)$$

an der Stelle der doppelten Eigenkreisfrequenz des Systems nicht überschreiten darf, wenn die Stabilität der Ruhelage im quadratischen Mittel gesichert

sein soll. Diese spezielle Stabilitätsbedingung wurde bereits 1958 von R. L. STRATONOVICH und Y. M. ROMANOVSKII [8] aufgestellt und davon unabhängig später auf anderem Wege von F. WEIDENHAMMER [9] und P. W. U. GRAEFE [10] bestätigt. Sind die Grenzfrequenzen dagegen von der Größenordnung

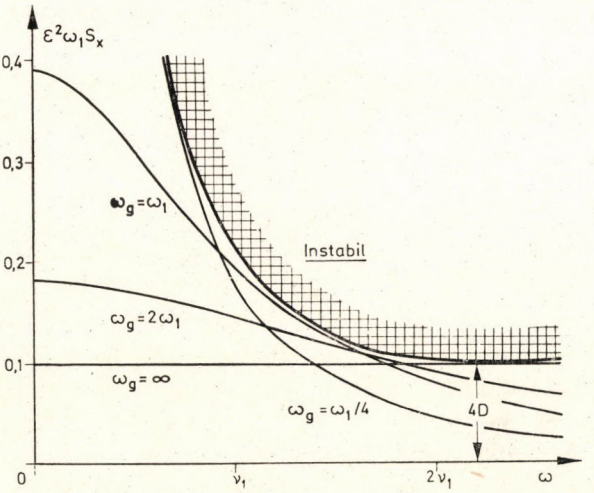

Fig. 7

der Eigenfrequenz oder sogar kleiner, so liegen die in der Fig. 7 gezeichneten kritischen Werte

$$\varepsilon^2\,\omega_1\,S_x\,(\omega = 2\omega_1)$$

an der Parameterresonanzfrequenz bereits erheblich unterhalb des Schwellwertes $4D$. Die spezielle Momentenstabilitätsbedingung wird dann zu ungenau. Vielmehr werden bei derartigen stark veränderlichen Erregerspektraldichten die unterhalb der Parameterresonanz liegenden Erregerfrequenzen kritisch, so daß man mit der Einhüllenden der kritischen Erregerspektraldichten auch eine frequenzabhängige Stabilitätsgrenze erhält. Bei einer Spektraldichte

$$\varepsilon^2\,\omega_1\,S_x\,(\omega)$$

der zufälligen Parametererregung, die mit ihrem gesamten Funktionsverlauf unterhalb dieser Stabilitätsgrenze liegt, haben die quadratischen Momente $E[y^2]$, $E[\dot{y}^2]$ und $E[y\dot{y}]$ des Schwingungssystems stets ein abklingendes Zeitverhalten (3), und die Ruhelage des Systems ist im quadratischen Mittel stabil. Reicht dagegen auch nur ein kleiner Abschnitt der Erregerspektraldichte in den schraffiert angegebenen Instabilitätsbereich, so wachsen die quadratischen Momente exponentiell an.

Im Bereich tieferer Erregerkreisfrequenzen zeigt der in Fig. 7 angegebene Instabilitätsbereich bereits den typischen frequenzabhängigen Verlauf, wie er ähnlich auch bei harmonischen Parametererregungen vorkommt. Insbesondere erreicht er seinen tiefsten Punkt in der Nähe der Parameterresonanz bei der doppelten Eigenfrequenz des Schwingungssystems, und eine Erhöhung der Dämpfung führt auch hier zu einer Verengung des kritischen Frequenzbereiches. Um auch für höhere Erregerfrequenzen einen frequenzabhängigen Instabilitätsbereich zu erhalten, werden im folgenden zufällige Parametererregungen untersucht, die man durch Bandpaßfilter aus gaussischen weißen Rauschen erzeugen kann.

5. Bandpaßerregungen

Ein derartiger Bandpaß kann z. B. aus einem Tiefpaßfilter und einem nachgeschalteten Hochpaßfilter gebildet werden. Die Differentialgleichungen beider Filter werden in der Form

$$\dot{x} + \omega_e x = \dot{\eta}(t), \qquad \dot{\eta} + \omega_e \eta = \omega_e \xi(t)$$

vorgegeben. Nach der Einschwingzeit ist der Ausgangsprozeß $x(t)$ stationär und besitzt eine Autokorrelationsfunktion (Fig. 8), die nur noch von der Zeitdifferenz $\tau = t_1 - t_2$ abhängt. Die zugehörige Spektraldichte hat den in Fig. 9 gezeichneten Verlauf.

$$R_x(\tau) = \frac{1}{4}\omega_e S_0 (1 - \omega_e|\tau|)\, e^{-\omega_e|\tau|}, \qquad S_x(\omega) = S_0 \left[\frac{\omega_e \omega}{\omega_e^2 + \omega^2}\right]^2.$$

Hierbei ist die mittlere Frequenz des Prozesses durch die obere bzw. untere Grenzkreisfrequenz ω_e vorgegeben, die für beide Filter gleich ist. Nach der Wahl dieser mittleren Frequenz läßt sich die Bandbreite des Spektrums nicht mehr variieren.

Um das Stabilitätsverhalten des Schwingungssystems bei dieser speziellen Bandpaßerregung zu untersuchen, werden auch hier die Differentialgleichungen der quadratischen Momente über die zugehörige Fokker – Planck-Gleichung aufgestellt und ähnlich wie vorhin gezeigt mit Hilfe der Störungsrechnung näherungsweise bis auf Potenzen ε_1^6 gelöst. Nach längerer Rechnung erhält man dann mit $x = \omega_e/\nu_1$ die kritische Varianz [11]

$$(\varepsilon_1 \sigma_x)^2_{\text{krit}} = [1 - \sqrt{1 - \mu D \omega_1/16\omega_e}]\,(x^2+4)^2\, 8/\mu;$$

$$\mu = \frac{492 - 5x^2}{x^2+4}\, x^2 - 3\,\frac{22x^6 + 75x^4 + 201x^2 + 256}{(x^2+1)^3}$$

und kann damit auch die zugehörige Spektraldichte

$$\varepsilon^2 \omega_1 S_x(\omega) = \left[2\varepsilon\sigma_x \frac{\omega\omega_e}{\omega^2 + \omega_e^2}\right]^2 \frac{\omega_1}{\omega_e}$$

der zufälligen Erregung angeben.

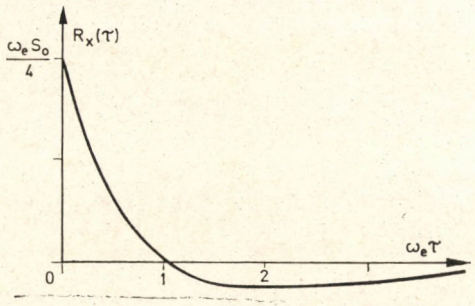

Fig. 8

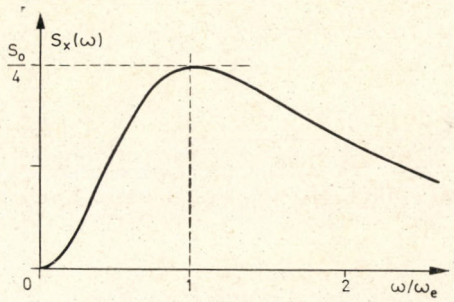

Fig. 9

Diese kritischen Spektraldichteverteilungen sind in der Fig. 10 für einige Werte des mittleren Frequenzverhältnisses $\varkappa = \omega_e h_1$ und für $D = 0{,}025$ aufgezeichnet. Ihre Einhüllende führt auf einen Instabilitätsbereich, dessen Grenzkurve anders als bei Tiefpaßerregungen auch bei höheren Erregerfrequenzen wieder ansteigt. Man erkennt, daß eine Bandpaßerregung ihre stärkste destabilisierende Wirkung besitzt, wenn die mittlere Erregerfrequenz in der Nähe der Parameterresonanz bei der doppelten Eigenfrequenz des Schwingungssystems liegt. Bei dieser Resonanzerregung genügt bereits eine geringe Erregerspektraldichte, um die Ruhelage des Systems zu destabilisieren. Eine Erhöhung der Dämpfung vermindert die Resonanzgefahr und führt auch hier auf eine Verengung des gefährlichen Frequenzbereiches.

Vergleicht man die destabilisierende Wirkung dieses Zufallsprozesses mit der einer harmonischen Parametererregung, so kann folgendes festgestellt werden. Bei der Bandpaßerregung muß das Lehrsche Dämpfungsmaß des

Schwingungssystems von der Größenordnung ε^2 sein, um die Stabilität der Ruhelage im quadratischen Mittel zu sichern. Diese zufällige Parametererregung ist demnach weniger stabilitätsgefährdend als harmonische Erregungen, bei denen bereits ein Lehrsches Dämpfungsmaß von der Größenordnung ε^1 erforderlich ist. Dies liegt offenbar daran, daß die Energiebeiträge sowohl der Bandpaßerregung als auch der vorhin untersuchten Tiefpaßerregung über ein zu breites Frequenzband verteilt sind.

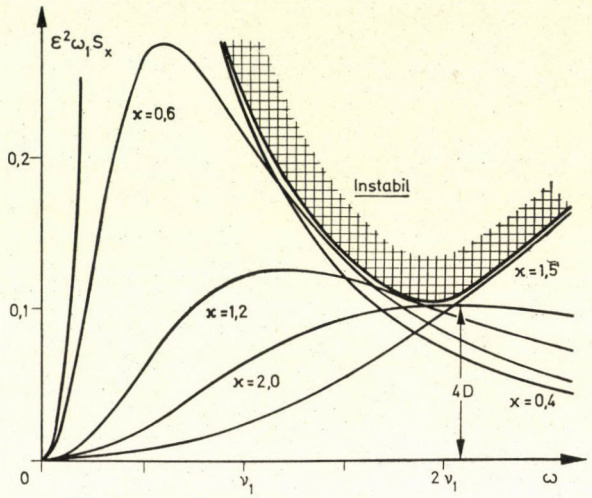

Fig. 10

6. Schmalbanderregungen

Die oben geäußerte Vermutung wird bestätigt, wenn man die destabilisierende Wirkung einer schmalbandigen Parametererregung untersucht, die entsprechend den Filtergleichungen

$$\ddot{x} + 2\delta_e \dot{x} + \omega_e^2 x = 2\delta_e \dot{\eta}(t); \qquad \dot{\eta} + \omega_\infty \eta = \omega_\infty \xi(t)$$

realisiert werden kann. Hierin bestimmen die Frequenzkonstante ω_e und die Dämpfungskonstante σ_e des Hochpaßfilters die mittlere Erregerfrequenz und die Bandbreite der Erregerspektraldichte. Die Eingangsgröße $\dot{n}(t)$ des Hochpasses wird von einem vorgeschalteten Tiefpaßfilter geliefert. Seine Grenzkreisfrequenz ω_∞ liegt weit oberhalb der Erregerfrequenzen und geht insbesondere nach einem Grenzübergang gegen unendlich weder in die Autokorrelationsfunktion noch in die Spektraldichte der Schmalbanderregung ein.

$$R_x(\tau) = \delta_e S_0 e^{-\delta_e|\tau|}\left(\cos \nu_e \tau - \frac{\delta_e}{\nu_e} \sin \nu_e |\tau|\right),$$

$$S_x(\omega) = \frac{4\omega^2 \delta_e^2 S_0}{(\omega_e^2 - \omega^2)^2 + (2\delta_e \omega)^2}, \quad \nu_e^2 = \omega_e^2 - \delta_e^2.$$

Beide Funktionen gelten also für $\omega_\infty \to \infty$ und sind in Fig. 11 und 12 für zwei verschiedene Bandbreiten δ_e aufgezeichnet.

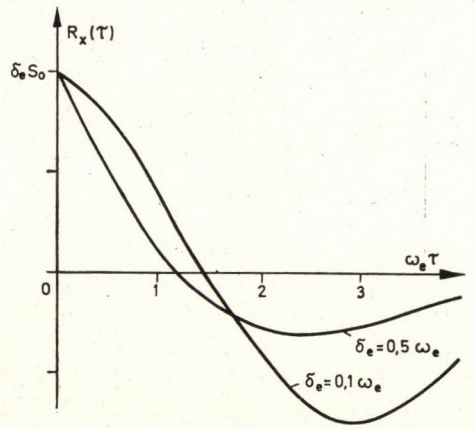

Fig. 11

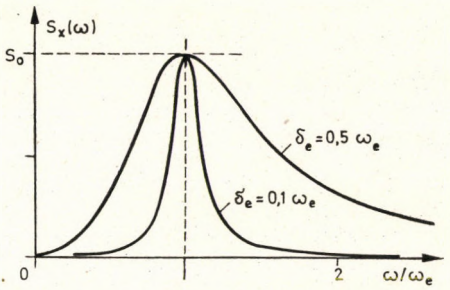

Fig. 12

Ähnlich wie vorhin gezeigt wurde, kann man auch hier die quadratischen Momente des Schwingungssystems über die Fokker — Planck-Gleichung und mit Hilfe der Störungsrechnung näherungsweise berechnen. Allerdings wird diese Rechnung für den gewählten Schmalbandprozeß so aufwendig, daß man die Potenzreihen der Lösungen bereits nach der ersten Korrektur abbrechen muß und die Wurzeln nur bis zu dem Reihenglied ε_1^2 berechnen kann. Die Bedingung $\lambda_0 = 2D\omega_1$, daß die quadratischen Momente des Schwingungssystems kein aufklingendes Zeitverhalten haben, führt dann auf die Erregervarianz [12].

$$(\varepsilon_1 \sigma_x)^2_{\text{krit}} = \frac{2D\omega_1}{2\delta_e 4\nu_1^4} [(4\delta_e \nu_1)^2 + (\omega_e^2 - 4\nu_1^2)^2].$$

Mit der kritischen Erregervarianz ist dann auch die Spektraldichte $\varepsilon^2 \omega_1 S_x(\omega)$

der zufälligen Parametererregung bekannt, bei der die Ruhelage des Systems gerade noch stabil ist. Allerdings erhält man mit dieser Näherungsberechnung nur den tiefsten Punkt des zugehörigen Instabilitätsbereiches, weil die in

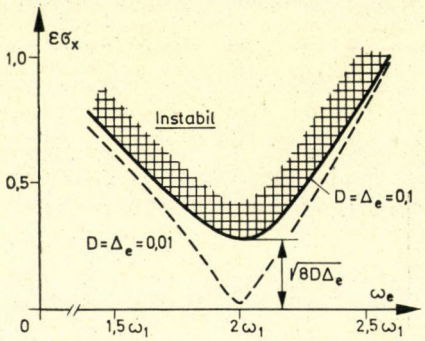

Fig. 13

zweiter Näherung berechneten kritischen Erregerspektraldichten für alle Bandbreiten σ_e und für alle Erregerfrequenzen ω_e den Wert

$$\varepsilon^2 \omega_1 S_x(\omega = 2\omega_1) = 4D$$

an der Stelle der Parameterresonanz annehmen. Die sich daran anschließenden übrigen Werte des Instabilitätsbereiches lassen sich erst dann ermitteln, wenn man ebenso wie bei den oben untersuchten Tiefpaß- und Bandpaßerregungen noch die Gleichungen der nächst höheren Näherung berücksichtigt.

Unabhängig davon kann man aber gerade eine Zufallserregung mit schmaler Bandbreite physikalisch anschaulich durch ihre mittlere Erregerkreisfrequenz ω_e und durch ihre Varianz $(\varepsilon\sigma_x)^2$ charakterisieren. Überdies liefert die Wurzel $\varepsilon\sigma_x$ aus der Erregervarianz ein Maß für die mittlere Amplitude der Zufallserregung $\varepsilon x(t)$. Insofern ist es für schmalbandige Zufallserregungen durchaus sinnvoll, nicht mehr ihre kritischen Spektraldichteverteilungen aufzuzeichnen, sondern die kritischen Werte $\varepsilon\sigma_x$ in Abhängigkeit der mittleren Erregerkreisfrequenzen ω_e aufzutragen.

$$(\varepsilon\sigma_x)_{\text{krit}} = \sqrt{\frac{2D}{\Delta_e}\left[4\Delta_e^2 + \left(\frac{\omega_e^2}{4\omega_1^2} - 1\right)^2\right]}.$$

Man erhält dann ebenfalls einen Instabilitätsbereich, der in Fig. 13 für zwei Parameterwerte der kleinen Dämpfung $D \ll 1$ und der relativen Bandbreite $\Delta_e = \sigma_e/2\omega_1$ aufgezeichnet wurde. Man erkennt, daß schmalbandige Zufallserregungen das Stabilitätsverhalten eines parametererregten Schwingungssystems durchaus ähnlich wie harmonische Erregungen beeinflussen. Insbesondere genügt auch hier bereits eine mittlere Amplitude von der Größenordnung $\varepsilon\sigma_x$, um die Ruhelage des Systems zu destabilisieren.

SCHRIFTTUM

1. METTLER, E.: Eine Theorie der Stabilität der elastischen Bewegung, *Ing.-Archiv.* **16** (1947) 135; Allgemeine Theorie der Stabilität erzwungener Schwingungen elastischer Körper, *Ing.-Arch.* **17** (1949), 418
2. SAMUELS, J. C.: On the Stability of Random Systems and the Stabilization of Deterministic Systems with Random Noise, *J. Acoust. Soc. Am.* **32** (1960), 594
3. CAUGHEY, T. K.—DIENES, J. K.: The Behaviour of Linear Systems with Random Parametric Excitation, *J. Math. Phys.* **40** (1962), 300
4. BERTRAM, J. E.—SARACHIK, P. E.: Stability of Circuits with Random Time-Varying Parameters, *Trans. Inst. Radio Engr. P.G.F.* (1959) 2—5, 260
5. ARIARATNAM, S. T.: Dynamic Stability of Structures, Hrsgg. von G. Herrmann, New York 1967, Insbes. S. 255
6. ARIARATNAM, S. T.—GRAEFE, P. W. U.: Linear System with Stochastic Coefficients, *Int. Journ. of Control*, **1** (1955), 239; **2** (1965), 161; **3** (1965), 205
7. WEDIG, W.: Stabilitätsbedingungen für parametererregte Schwingungssysteme mit breitbandigen Zufallserregungen (Vortrag auf der GAMM-Tagung 1971 in Mannheim), im Druck
8. KUZNETZOV, P. I.—STRATONOVICH, R. L.—TIKHONOV, V. I.: Non-Linear Transformations of Stochastic Processes, New York 1965, Insbes. S. 327
9. WEIDENHAMMER, F.: Stabilitätsbedingungen für Schwinger mit zufälligen Parametererregungen, *Ing.-Arch.* **33** (1964), 404
10. GRAEFE, P. W. U.: Stability of a Linear Second Order System under Random Parametric Excitation, *Ing.-Arch.* **35** (1966), 276
11. WEDIG, W.: Instabilitätsbereich spezieller Spektraldichteverteilungen bei einem parametererregten Schwingungssystem, im Druck *(ZAMP)*
12. WEDIG, W.: Stabilitätsbedingungen für parametererregte Schwingungssysteme mit schmalbandigen Zufallserregungen, im Druck *(ZAMM* 1972, 52—3, S. 161—166)

Conditions of Stability for a System under Random Parametric Excitation. The stability of a parametric excited system, the motions of which can be described by a differential equation with stochastic coefficients, is investigated by using the FOKKER—PLANCK equation. The conditions of the mean square stability for the equilibrium position are approximately derived by applying a perturbation method. In case of stochastic coefficients, the spectral densities of which are distributed upon a broad frequency band, the critical spectral densities are giving instability regions, the lowest point of which is situated near twice the natural frequency of the system. In case of narrow band excitations one has to specify as first approximation the root of the critical excitation variance as a function of the mean excitation frequency.

Условия стабильности колебательной системы, возбуждаемой случайным параметром. Производится исследование колебательной системы параметрического возбуждения в отношении ее поведения с точки зрения стабильности с использованием уравнения Фоккера—Планка, условия движения которой можно описать дифференциальным уравнением со стохастическим коэффициентом. Определение условий стабильности, действительных для положения равновесия, квадратичным средним значением производится приближенным способом применением метода вычисления возмущения. В случае таких стохастических коэффициентов, плотности спектра которых распределяются в широкой полосе частот, в результате получают такие области нестабильности критических возбуждающих спектров, наиболее глубоко лежащая точка которых находится вблизи двухкратной частоты собственных колебаний колебательной системы. В случае узкополосных возбуждений в качестве первого приближения необходимо указать корень квадратичного разброса критического возбуждения в функции от средней возбуждающей частоты, и вследствие этого получается такая область нестабильности, которая достигает своего предельного значения также вблизи параметрического резонанса.

Acta Technica Academiae Scientiarum Hungaricae, Tomus 76 (1—2), pp. 21—38 (1974)

WAVE PROPAGATION IN AN INFINITE TRANSVERSELY ISOTROPIC CYLINDER OF ELLIPTICAL CROSS-SECTION

M. KOZAROV* and Ts. P. IVANOV**

[Manuscript received 4 February 1972]

The propagation of harmonic waves in a transversely isotropic cylinder of elliptical cross-section on the basis of the linear theory of elasticity is investigated. The result is obtained by Mathieu's function. The condition that the cylindrical surface is stressfree is given in the form of an infinite determinant which is equal to zero. From the general result it is possible to obtain two special cases: wave propagation in an isotropic cylinder of elliptical cross-section and wave propagation in a transversely isotropic cylinder of circular cross-section.

Symbols

x_i $(i = 1, 2, 3)$	— elliptical co-ordinates,
ε_{ii}, $1/2\,\gamma_{ij} (i \neq j)$	— components of the tensor of strain,
u_i	— components of displacement,
h^2	$= 1/2\, l^2(\cosh x\, 2_1 - \cos 2\, x_2)$,
$2l$	— focal length of the ellipse,
σ_{ij}	— components of the tensor of stresses,
c_{ij}	— elastic constants, satisfying the inequalities (5),
t	— time,
ϱ	— density,
$2\pi/\alpha$	— wave length,
$\omega/2\pi$	— wave frequency,
$c = \omega/\alpha$	— velocity of wave propagation in the axis direction x_3,
∇	— Laplacian operator, defined in (9),
λ_i, k_i $(i = 1, 2)$	— roots of the equations (11),
k_3	— constant, defined in (18),
q_i	$= \alpha^2 l^2 k_i$,
$ce_m(x_2, q_i)$, $se_m(x_2, q_i)$	— solutions of equations (21), which are represented in the form (23),
$Ce_m(x_1, q_i)$, $Se_m(x_1, q_1)$	— solutions of the equations (22),
$Fe_m(x_1, q_i)$ or $Fey_m(x_1 q_i)$,	
$Ge_m(x_1, q_i)$ or $Gey_m(x_1\, q_i)$,	— second linearly independent solutions of equations (22),
$a_m^{(i)}$ $b_m^{(i)}$	— characteristic numbers, defined in (25),
${}^iU_{2r+1}^{2n+1}, V_{2r+1}^{2n+1}, \ldots, Z_{2r+1}^{2n+1}$	— functions of x_1, defined in (34),
T	— determinant, defined in (37),
T_{2N-1}	— subdeterminant of T with $3N$ rows and columns counted from the left upper corner of T,
H_{2N-1}	— determinant, defined in (38),
λ, μ	— Lame constants,
$J_m(\alpha\sqrt{k_i}r)$	— Bessel functions of the first kind.

* Prof. C. T. Sc. Eng. MARIN MARINOV KOZAROV High Civil Engineering Institute bul. Smirnenski, 1, Sofia, Bulgaria

** Sc. A. TSOLO PETROV IVANOV Institute of Mathematics and Mechanics, Bulgarian Academy of Sciences, ul. 36, block VIII, Sofia 13, Bulgaria

1. Introduction

The propagation of harmonic waves in an infinite cylinder with a stress-free cylindrical surface is investigated on the basis of the linear theory of elasticity by POCHHAMMER [1] and CHREE [2] for the case of an isotropic, circular cylinder. The following investigations developed in two directions: investigation of the wave propagation in aeolotropic circular cylinders [3] — [7] and in isotropic non-circular cylinders — investigated is the case of a cylinder with an elliptical cross-section [8]. In these works exact solutions of the problems are given. At the same time isotropic and aeolotropic cylinders with different cross-sections have obtained approximate solutions, references of which can be found in the above quoted works and also in [9] — [11].

In this paper the propagation of harmonic waves in an infinite transversely isotropic cylinder of elliptical cross-section is investigated. By the introduction of potential functions and the separation of variables, the solution of the set problem is reduced to the solution of Mathieu's equations. The condition that the cylindrical surface is stressfree is obtained in the form of an infinite determinant which is equal to zero. The elements of the determinant contain Mathieu's functions and their derivatives. Two special cases can be obtained from the derived results: the wave propagation in an isotropic cylinder of elliptical cross-section [8] and wave propagation in a transversely isotropic cylinder of circular cross-section [4].

2. Formulation of the problem and the drawing of the basic equations

The relations between the components of the displacement u_i $(i = 1, 2, 3)$, the strain ε_{ii}, $\gamma_{ij}(i, j = 1, 2, 3, i \neq j)$ and the stress $\sigma_{ij}(i, j = 1, 2, 3)$ for the three dimensional transversely isotropic body in an elliptical co-ordinate system $x_i(i = 1, 2, 3)$ take the form

$$\varepsilon_{11} = \frac{1}{h}\frac{\partial u_1}{\partial x_1} + \frac{1}{h^2}\frac{\partial h}{\partial x_2}u_2, \quad \gamma_{23} = \frac{1}{h}\frac{\partial u_3}{\partial x_2} + \frac{\partial u_2}{\partial x_3},$$

$$\varepsilon_{22} = \frac{1}{h}\frac{\partial u_2}{\partial x_2} + \frac{1}{h^2}\frac{\partial h}{\partial x_1}u_1, \quad \gamma_{13} = \frac{1}{h}\frac{\partial u_3}{\partial x_1} + \frac{\partial u_1}{\partial x_3}, \tag{1}$$

$$\varepsilon_{33} = \frac{\partial u_3}{\partial x_3} \qquad \gamma_{12} = \frac{\partial}{\partial x_1}\left(\frac{u_2}{h}\right) + \frac{\partial}{\partial x_2}\left(\frac{u_1}{h}\right),$$

$$\sigma_{11} = c_{11}\varepsilon_{11} + c_{12}\varepsilon_{22} + c_{13}\varepsilon_{33}, \qquad \sigma_{23} = c_{44}\gamma_{23},$$

$$\sigma_{22} = c_{12}\varepsilon_{11} + c_{11}\varepsilon_{22} + c_{13}\varepsilon_{33}, \qquad \sigma_{13} = c_{44}\gamma_{13}, \tag{2}$$

$$\sigma_{33} = c_{13}\varepsilon_{11} + c_{13}\varepsilon_{22} + c_{33}\varepsilon_{33}, \qquad \sigma_{12} = c_{66}\gamma_{12},$$

where

$$2c_{66} = c_{11} - c_{12}$$

and

$$2h^2 = l^2(ch\ 2x_1 - \cos 2x_2) \tag{3}$$

$2l$ indicate the focal length of the family of ellipses $x_1 = \text{const}$, $0 \leqq x_2 < 2\pi$, $x_3 = 0$ and

$$a = l\cosh x_1, \qquad b = l\sinh x_1, \qquad e = (\cosh x_1)^{-1} \tag{4}$$

are the semimajor axis, the semiminor axis and the eccentricity, respectively. The elastic constants $c_{ij} = c_{ji}$ satisfy the following inequalities

$$c_{11} > |c_{12}|, \qquad (c_{11} + c_{12})\, c_{33} > 2c_{13}^2, \qquad c_{44} > 0, \tag{5}$$

since the strain energy density is positive definite.

The equations of motion in elliptic co-ordinates take the form:

$$\begin{aligned}
\varrho h^2 \frac{\partial^2 u_1}{\partial t^2} &= \frac{\partial}{\partial x_1}(h\sigma_{11}) + \frac{1}{h}\frac{\partial}{\partial x_2}(h^2\sigma_{12}) + h^2\frac{\partial \sigma_{13}}{\partial x_3} - \frac{\partial h}{\partial x_1}\sigma_{22}, \\
\varrho h^2 \frac{\partial^2 u_2}{\partial t^2} &= \frac{\partial}{\partial x_2}(h\sigma_{22}) + \frac{1}{h}\frac{\partial}{\partial x_1}(h^2\sigma_{12}) + h^2\frac{\partial \sigma_{23}}{\partial x_3} - \frac{\partial h}{\partial x^2}\sigma_{11}, \\
\sigma h^2 \frac{\partial^2 u_3}{\partial t^2} &= h^2\frac{\partial \sigma_{33}}{\partial x_3} + \frac{\partial}{\partial x_1}(h\sigma_{13}) + \frac{\partial}{\partial x_2}(h\sigma_{23}),
\end{aligned} \tag{6}$$

where ϱ is density. Equations (1) and (6) can be obtained, as a special case, from the corresponding equations for arbitrary orthogonal co-ordinates, given in [12].

The solution of the problem will be sought in the form

$$\begin{aligned}
hu_1 &= \left(\frac{\partial \varphi}{\partial x_1} + \frac{\partial \psi}{\partial x_2}\right)\cos(\alpha x_3 + \omega t) \\
hu_2 &= \left(\frac{\partial \varphi}{\partial x_2} - \frac{\partial \psi}{\partial x_1}\right)\cos(\alpha x_3 + \omega t), \\
u_3 &= \lambda\varphi \sin(\alpha x_3 + \omega t),
\end{aligned} \tag{7}$$

where $2\pi/\alpha$ is the wave length, $\omega/2\pi$ — its frequency, $c = \omega/\alpha$ is the phase velocity of the propagation in the direction of the x_3 axis. $\varphi(x_1, x_2)$ and $\psi(x_1, x_2)$ are unknown functions, λ is a constant which will be defined later.

Substituting (7) into (1) and the result obtained in (2) we have

$$\sigma_{11} = \left[c_{12}\nabla\varphi + 2\frac{c_{66}}{h^2}\frac{\partial^2\varphi}{\partial x_1^2} + 2\frac{c_{66}}{h^2}\frac{\partial^2\psi}{\partial x_1\partial x_2} + 2\frac{c_{66}}{h^3}\frac{\partial h}{\partial x_2}\left(\frac{\partial\varphi}{\partial x_2} - \frac{\partial\psi}{\partial x_1}\right) - \right.$$
$$\left. - 2\frac{c_{66}}{h^3}\frac{\partial h}{\partial x_1}\left(\frac{\partial\varphi}{\partial x_1} + \frac{\partial\psi}{\partial x_2}\right) + c_{13}\alpha\lambda\varphi\right]\cos(\alpha x_3 + \omega t),$$

$$\sigma_{22} = \left[c_{12}\nabla\varphi + 2\frac{c_{66}}{h^2}\frac{\partial^2\varphi}{\partial x_2^2} - 2\frac{c_{66}}{h^2}\frac{\partial^2\psi}{\partial x_1\partial x_2} - 2\frac{c_{66}}{h^3}\frac{\partial h}{\partial x_2}\left(\frac{\partial\varphi}{\partial x_2} - \frac{\partial\psi}{\partial x_1}\right) + \right.$$
$$\left. + 2\frac{c_{66}}{h^2}\frac{\partial h}{\partial x_1}\left(\frac{\partial\varphi}{\partial x_1} + \frac{\partial\psi}{\partial x_2}\right) + c_{13}\alpha\lambda\varphi\right]\cos(\alpha x_3 + \omega t), \tag{8}$$

$$\sigma_{33} = [c_{13}\nabla\varphi + c_{33}\alpha\lambda\varphi]\cos(\alpha x_3 + \omega t),$$

$$\sigma_{23} = \frac{c_{44}}{h}\left[\lambda\frac{\partial\varphi}{\partial x_2} - \alpha\left(\frac{\partial\varphi}{\partial x_2} - \frac{\partial\psi}{\partial x_1}\right)\right]\sin(\alpha x_3 + \omega t),$$

$$\sigma_{13} = \frac{c_{44}}{h}\left[\lambda\frac{\partial\varphi}{\partial x_1} - \alpha\left(\frac{\partial\varphi}{\partial x_1} + \frac{\partial\psi}{\partial x_2}\right)\right]\sin(\alpha x_3 + \omega t),$$

$$\sigma_{12} = \left[\frac{c_{66}}{h^2}\left(\frac{\partial^2\varphi}{\partial x_1\partial x_2} - \frac{\partial^2\psi}{\partial x_1^2}\right) - 2\frac{c_{66}}{h^3}\frac{\partial h}{\partial x_1}\left(\frac{\partial\varphi}{\partial x_2} - \frac{\partial\psi}{\partial x_1}\right) + \frac{C_{66}}{h^2}\right.$$
$$\left.\left(\frac{\partial^2\varphi}{\partial x_1\partial x_2} + \frac{\partial^2\psi}{dx_2^2}\right) - 2\frac{c_{66}}{h^3}\frac{\partial h}{\partial x_2}\left(\frac{\partial\varphi}{\partial x_1} + \frac{\partial\psi}{\partial x_2}\right)\right]\cos(\alpha X_3 + \omega t)$$

where ∇ indicates the Laplacian operator

$$\nabla = \frac{1}{h^2}\left(\frac{\partial^2}{\partial x_1^2} + \frac{\partial^2}{\partial x_2^2}\right). \tag{9}$$

By substituting (8) into (6) it is to be seen that the equations (6) will be satisfied, if the equations

$$\begin{aligned} c_{11}\nabla\varphi + [\varrho\omega^2 - \alpha^2 c_{44} + \lambda\alpha(c_{44} + c_{13})]\varphi &= 0, \\ [\lambda c_{44} - \alpha(c_{44} + c_{13})]\nabla\varphi + \lambda(\varrho\omega^2 - \alpha^2 c_{33})\varphi &= 0, \\ c_{66}\nabla\psi + (\varrho\omega^2 - \alpha^2 c_{44})\psi &= 0 \end{aligned} \tag{10}$$

are also satisfied. In order to satisfy the first two equations in (10) simultaneously, the constant λ must be so chosen as to satisfy the equations

$$\frac{\lambda(\varrho\omega^2 - \alpha^2 c_{33})}{\lambda c_{44} - \alpha(K c_{44} - c_{13})} = \frac{\varrho\omega^2 - \alpha^2 c_{44} + \lambda\alpha(c_{44} + c_{13})}{c_{11}} = \alpha^2 k. \tag{11}$$

This is only possible in the case when

$$\alpha(c_{44} + c_{13}) \neq 0.$$

When

$$\alpha(c_{44} + c_{13}) = 0$$

a solution is sought for u_3 in the form

$$u_3 = f(x_1, x_2) \sin(\alpha x_3 + \omega t). \tag{12}$$

Then the second equation of (10) is replaced by the equation

$$c_{44} \nabla f + (\varrho\omega^2 - \alpha^2 c_{33}) f = 0. \tag{13}$$

After that the case

$$\alpha(c_{44} + c_{13}) \neq 0$$

is investigated. The case

$$\alpha(c_{24} + c_{13}) = 0$$

can be investigated in an analogous way.

When λ is eliminated from equation (11) and divided by α^4 we obtain

$$Ak^2 + Bk + C = 0 \tag{14}$$

where

$$\begin{gathered} A = c_{11}c_{44} > 0, \quad B = c_{11}c_{33} - c_{13}^2 - 2c_{13}^2 c_{44} - \\ p(c_{11} + + c_{44}), \quad C = (p - c_{33})(p - c_{44}) \end{gathered} \tag{15}$$

and

$$p = \varrho c^2.$$

Now the case $c_{33} > c_{44}$, $c_{11} \neq c_{44}$ will be investigated. The other cases may be investigated in an analogous way.

If we denote by k_i $(i = 1, 2)$ the roots of equation (14) and $D = B^2 - 4AC$, when we use the relations of VIÈTE, the following is obtained:

a) if $c_{44} < p < c_{33}$, that means $C < 0$, then $k_1 > 0, k_2 < 0$;

b) if $p = c_{33}, c_{44}$, that means $C = 0$, then $k_1 = 0, k_2 = -B/A$;

c) if $0 < p < c_{44}$ or $p > c_{33}$, that means $C > 0$ and

c_1. $p < M$, that means $B > 0$, then $k_1, k_2 < 0$, if $D \geqq 0$ or k_1 and k_2 are complex numbers, if $D < 0$.

c_2. $p = M$, that means $B = 0$, then k_1 and k_2 are purely imaginary numbers.

c_3. $p > M$, that means $B < 0$, then k_1, $k_2 > 0$, if $D > 0$ or k_1 and k_2 are complex numbers, if $D < 0$. In these formulae the notation

$$M = \frac{c_{11} c_{33} - c_{13}^2 - 2 c_{13} c_{44}}{c_{11} + c_{44}} \tag{16}$$

has been used. It is not difficult to show that $M < c_{33}$.

When is written

$$B^2 = (c_{11} + c_{44})^2 (p - M)^2, \tag{17}$$

$$4AC = 4c_{11}c_{44}(p - c_{33})(p - c_{44})$$

and indicated with D_0 the quantity of D for $p = 0$, the following is obtained:

a) If $c_{44} < M < c_{33}$ and

a_1) $D_0 > 0$ then it is possible that $D < 0$ for $p < 0$, only when the equation $D = 0$ has two real roots $p_i > 0$ $(i = 1, 2)$. (It is not difficult to see, that the equation $D = 0$ can in this case have two real roots both of which are positive or negative or two complex roots.) For these roots we have $0 < p_1 < p_2 < c_{44}$ or $c_{33} < p_1 < p_2$. Then $D < 0$ for $p_1 < p < p_2$.

a_2) $D_0 = 0$, then it is possible that $D < 0$ only when for the roots of equation $D = 0$, which are real in this case, obey the condition $0 = p_1 < p_2$. Then $p_2 < c_{44}$ and $D < 0$ for $0 < p < p_2$.

a_3) $D_0 < 0$, then $D < 0$ for $0 < p < p_2$, where $p_2 < c_{44}$ is the positive root of the equation $D = 0$. (The root p_1 is negative.)

b) If $0 < M \leqq c_{44}$, then $D < 0$ for $\max(p_1, 0) < p < p_2$ where $0 < p_2 \leqq c_{44}$.

c) If $M \leqq 0$, then it is not difficult to show that $D_0 < 0$. The equation $D = 0$ has two real roots p_1 and p_2 where

$$p_1 < 0 < p_2 < c_{44} \quad \text{and} \quad D < 0 \quad \text{for} \quad 0 < p < p_2.$$

From these results it is possible to determine the type of roots k_i $(i = 1, 2)$ of equation (14) as a function of the velocity c. It is evident that for high enough values of c the roots of (14) are always positive.

The quantity

$$k_3 = \frac{pc^2 - c_{44}}{c_{66}} \tag{18}$$

is negative for $0 < p < c_{44}$ and positive for $p < c_{44}$.

3. Solution of the basic equations

The equations (10) will be satisfied if the equations

$$\begin{aligned} \nabla \varphi_i + \alpha^2 k_i \varphi_i &= 0, \\ \nabla \psi + \alpha^2 k_3 \psi &= 0 \end{aligned} \tag{19}$$

are satisfied, where $i = 1$ or 2. $\varphi_i(x_1, x_2)(i = 1, 2)$ are the potential functions, corresponding to the roots k_i $(i = 1, 2)$. The solutions of the equations (19) are sought for in the form

$$\begin{aligned} \varphi_i(x_1, x_2) &= g_{i1}(x_1)\, g_{i2}(x_2), \qquad (i = 1, 2), \\ \psi(x_1, x_2) &= g_{31}(x_1)\, g_{32}(x_2). \end{aligned} \tag{20}$$

When (20) is substituted in (19) we obtain

$$\frac{d^2 g_{i2}}{dx_2^2} + (\eta_i - 2 q_i \cos 2 x_2)\, g_{i2} = 0\,, \qquad (i = 1, 2, 3) \tag{21}$$

$$\frac{d^2 g_{i1}}{dx_1^2} - (\eta_i - 2 q_i \operatorname{ch} 2 x_1)\, g_{i2} = 0\,, \qquad (i = 1, 2, 3)$$

where

$$4 q_i = \alpha^2 l^2 k_i \ (i = 1, 2, 3). \tag{22}$$

η_i $(i = 1, 2, 3)$ are the separation constants. The equations (21) are Mathieu's equations and the equations (22) are the modified equations of Mathieu. Because the solution has to be periodic in x_2 with period 2π, the separation constants must be chosen equal to the characteristic numbers of the corresponding equations. All information on Mathieu's equations and also for the notation used can be found in the book of McLachlan [13].

Only the case when $q_i > 0$ $(i = 1, 2, 3)$ will be considered, that means when the velocity c is sufficiently large. The other cases corresponding to small velocities can be considered in an analogous way.

The periodic solutions of the equations (21) and the two linearly independent solutions of every one of the equations (22) are respectively

$$g_{i2}(x_2) = \begin{cases} ce_{2n}(x_2, q_i) = \sum_{r=0}^{\infty} A_{2r}^{2n}(q_i) \cos 2 r x_2\,, \\ ce_{2n+1}(x_2, q_i) = \sum_{r=0}^{\infty} A_{2r+1}^{2n+1}(q_i) \cos (2r+1) x_2\,, \\ se_{2n+1}(x_2, q_i) = \sum_{r=0}^{\infty} B_{2r+1}^{2n+1}(q_i) \sin (2r+1) x_2\,, \\ se_{2n+1}(x_2, q_i) = \sum_{r=0}^{\infty} B_{2r+2}^{2n+2}(q_i) \sin (2r+2) x_2\,, \end{cases} \tag{23}$$

$$g_{i1}(x_1) = \begin{cases} Ce_{2n}(x_1, q_i)\,; \;\; Fe_{2n}(x_1, q_i) & \text{or } Fey_{2n}(x_1, q_i) \\ Ce_{2n+1}(x_1, q_i); \;\; Fe_{2n+1}(x_1, q_i) & \text{or } Fey_{2n+1}(x_1, q_i), \\ Se_{2n+1}(x_1, q_i); \;\; Ge_{2n+1}(x_1, q_i) & \text{or } Gey_{2n+1}(x_1, q_i)\,. \\ Se_{2n+2}(x_1, q_i); \;\; Ge_{2n+2}(x_1, q_i) & \text{or } Gey_{2n+2}(x_1, q_i) \end{cases} \tag{24}$$

where the corresponding characteristic numbers are

$$\eta_i = a_{2n}^{(i)}, \;\; \eta_i = a_{2n+1}^{(i)}, \;\; \eta_i = b_{2n+1}^{(i)}, \;\; \eta_i = b_{2n+1}^{(i)}, \;\; (i = 1, 2, 3). \tag{25}$$

It is possible to satisfy the boundary conditions for four types of harmonic waves, for which the following conditional designations are used, analogous to those introduced for a circular cylinder:

A. Flexural waves of the 1st type

$$\begin{aligned} \varphi_i(x_1, x_2) &= \sum_{n=0}^{\infty} [C_{2n+1}^{(i)} Ce_{2n+1}(x_1, q_i) + F_{2n+1}^{(i)} Fe_{2n+1}(x_1, q_i)]\, ce_{2n+1}(x_2, q_i), \\ \psi(x_1, x_2) &= \sum_{n=0}^{\infty} [S_{2n+1}^{(3)} Se_{2n+1}(x_1, q_3) + G_{2n+1}^{(3)} Ge_{2n+1}(x_1, q_3)] se_{2n+1}(x_2, q_3)\,. \end{aligned} \tag{26}$$

For this solution when $x_1 = \text{const}$ the displacements u_1 and u_3 are symmetric with respect to the major axis and antisymmetric with respect to the minor axis and the displacement u_2 is antisymmetric with respect to the major axis and symmetric with respect to the minor axis. (The displacements are defined by equations (7), where φ is substituted by $\varphi_1 + \varphi_2$, and $\lambda\varphi$ is substituted by $\lambda_1\varphi_1 + \lambda_2\varphi_2$.)

B. Flexural waves of the 2nd type

$$\begin{aligned} \varphi_i(x_1, x_2) &= \sum_{n=0}^{\infty} [S_{2n+1}^{(i)} Se_{2n+1}(x_1, q_i) + G_{2n+1}^{(i)} Ge_{2n+1}(x_1, q_i)]\, se_{2n+1}(x_2, q_i), \\ \psi(x_1, x_2) &= \sum_{n=0}^{\infty} [C_{2n+1}^{(3)} Ce_{2n+1}(x_1, q_3) + F_{2n+1}^{(3)} Fe_{2n+1}(x_1, q_3)]\, ce_{2n+1}(x_2, q_3). \end{aligned} \tag{27}$$

For this solution when $x_1 = \text{const}$ the displacements u_1 and u_3 are antisymmetric with respect to the major axis and symmetric with respect to the minor axis and the reverse for the displacement u_2.

C. Longitudinal waves

$$\begin{aligned} \varphi_1(x_1, x_2) &= \sum_{n=0}^{\infty} [C_{2n}^{(i)} Ce_{2n}(x_1, q_i) + F_{2n}^{(i)}(x_1, q_i)] ce_{2n},(x_2, q_i) \\ \psi(x_1, x_2) &= \sum_{n=0}^{\infty} [S_{2n+2}^{(3)} Se_{2n+2}(x_1, q_3) + G_{2n+2}^{(3)} Ge_{2n+2}(x_1, q_3)]\, se_{2n+2}(x_2, q_3). \end{aligned} \tag{28}$$

For this solution when $x_1 = \text{const}$, the displacements u_1 and u_3 are symmetric with respect to the major and minor axis, while u_2 is antisymmetric.

D. Torsional waves

$$\varphi_i(x_1, x_2) = \sum_{n=0}^{\infty} \left[S_{2n+2}^{(i)} Se_{2n+2}(x_1, q_i) + G_{2n+2}^{(i)} Ge_{2n+2}(x_1, q_i)\right] Se_{2n+2}(x_2, q_i),$$
$$\psi(x_1, x_2) = \sum_{n=0}^{\infty} \left[C_{2n}^{(3)} Ce_{2n}(x_1, q_3) + F_{2n}^{(3)} Fe_{2n}(x_1, q_2)\right] ce_{2n}(x_2, q_3). \tag{29}$$

For this solution when $x_1 = \text{const}$ the displacements u_1 and u_3 are antisymmetric with respect to the major and minor axis, while u_2 is symmetric.

In the equations (26)—(29) $C_m^{(i)}$, $F_m^{(i)}$, $S_m^{(i)}$ and $G_m^{(i)}$ are constants, which will be determined by the boundary conditions. In some cases it is more expedient to use instead of functions $Fe_m(x_1, q_i)$ and $Ge_m(x_1, q_i)$ the functions $Fey_m(x_1, q_i)$ and $Gey_m(x_1, q_i)$ because for them we can apply the relations derived in [13].

4. Equation for determining the phase velocity of waves

The boundary conditions, that the cylindrical surface is stressfree, takes the form

$$\sigma_{11} = \sigma_{12} = \sigma_{13} = 0 \tag{30}$$

for $x_1 = \xi_0$ and $\xi(\xi_0, \xi$ are const) in the case of a hollow elliptical cylinder ($\xi_0 \leq x_1 \leq \xi$). The solutions (26)—(29) can be applied to this case.

In the case of a solid elliptical cylinder the boundary condition (30) must be satisfied for $x_1 = \xi(0 \leq x_1 \leq \xi, \xi_0 = 0)$. For this case we set $F_m^{(i)} = G_m^{(i)} = 0$ $(i = 1, 2, 3)$ in the solutions (26)—(29) because the functions $Fe_m(x_1, q_i)$ and $Ge_m(x_1, q_i)$ lead to unbounded displacements at the points of the straight lines parallel to axis x_3 and going through the focus of the ellipse.

In the case of an infinite space with elliptic opening the boundary conditions (30) must be satisfied for $x_1 = \xi_0(\xi_0 \leq x_1 < \infty, \xi = \infty)$. It is also necessary that the displacements and strains should be restrained at infinity. In this case the same solution can be used as that for the solid cylinder. It gives bounded displacements and strains at infinity. This can be proved by using the asymptotic representation of the functions $Ce_m(x_1 q_i)$ and $Se_m(x_1 q_i)$ for large values of x_1, which are from the type

$$\beta \left(\frac{2}{\pi z_i}\right)^{1/2} \begin{matrix} \sin \\ \cos \end{matrix} \left(z_i + \frac{\pi}{4}\right),$$

where β is a constant dependent on m and q_i, but not on x_1; $z_i = \sqrt{q_i}\, e^{x_1}$, it is to be mindered that we are considering the case $q_i > 0$).

Because the following calculations are very lengthy we will take into consideration only one of the possible cases: propagation of flexural waves of the 1st type in a solid elastic cylinder. For the purpose of simplification of the notation we will write ${}^{i}A_{2r+1}^{2n+1}$ instead of $A_{2r+1}^{2n+1}(q_i)$ for $i = 1.\ 2$ and S_{2n+1}, B_{2r+1}^{2n+1}, q, b_{2n+1} instead of $S_{2n+1}^{(3)}$ $B_{2r+1}^{2n+1}(q_3), q_3$, $b_{2n+1}^{(3)}$.

When we use the equations (23) we obtain

$$\varphi_i(x_1, x_2) = \sum_{n=0}^{\infty} \sum_{r=0}^{\infty} C_{2n+1}^{(i)}\, Ce_{2n+1}(x_1, q_i)\, {}^{i}A_{2r+1}^{2n+1} \cos(2r+1)\, x_2\,,$$

$$\psi(x_1, x_2) = \sum_{n=0}^{\infty} \sum_{r=0}^{\infty} S_{2n+1}\, Se_{2n+1}(x_1, q)\, B_{2r+1}^{2n+1} \sin(2r+1)\, x_2\,. \tag{31}$$

By substituting (31) in (8) and using the identities

$$\sum_{r=0}^{\infty} A_r \cos 2x_2 \cos(2r+1)\, x_2 = \sum_{r=0}^{\infty} \tilde{A}_r \cos(2r+1)\, x_2\,,$$

where

$$2\tilde{A}_0 = A_0 + A_1 \text{ and } 2\tilde{A}_r = A_{r-1} + A_{r+1} \text{ for } r \geqq 1\,,$$

$$\sum_{r=0}^{\infty} A_r \cos 2x_2 \sin(2r+1)\, x_2 = \sum_{r=0}^{\infty} \tilde{A}_r \sin(2r+1)\, x_2\,,$$

where

$$2\tilde{A}_0 = A_1 - A_0 \text{ and } 2\tilde{A}_r = A_{r-1} + A_{r+1} \text{ for } r \geqq 1\,, \tag{32}$$

$$\sum_{r=0}^{\infty} A_r \sin 2x_2 \sin(2r+1)\, x_2 = \sum_{r=0}^{\infty} \tilde{A}_r \cos(2r+1)\, x_2\,,$$

where

$$2\tilde{A}_0 = A_0 + A_1 \text{ and } 2\tilde{A}_r = A_{r+1} - A_{r-1} \text{ for } r \geqq 1\,,$$

$$\sum_{r=0}^{\infty} A_r \sin 2x_2 \cos(2r+1)\, x_2 = \sum_{r=0}^{\infty} \tilde{A}_r \sin(2r+1)\, x_2\,,$$

where

$$2\tilde{A}_0 = A_0 - A_1 \text{ and } 2\tilde{A}_r = A_{r-1} - A_{r+1} \text{ for } r \geqq 1$$

and the equations (22) and (3), for the stresses of interest we obtain

$$h^4 \sigma_{11} = l^2 \sum_{n=0}^{\infty} \sum_{r=0}^{\infty} \left[\sum_{i=1}^{2} C_{2n+1}^{(i)}\, {}^{i}U_{2r+1}^{2n+1}(x_1) + S_{2n+1}\, X_{2r+1}^{2n+1}(x_1) \right] \cdot$$

$$\cdot \cos(2r+1)\, x_2 \cos(\alpha x_3 + \omega t),$$

$$h^4\sigma_{12} = c_{66}\, l^2 \sum_{n=0}^{\infty}\sum_{r=0}^{\infty}\left[\sum_{i=1}^{2} C_{2n+1}^{(i)}\, V_{2r+1}^{2n+1}(x_1) + S_{2n+1}\, Y_{2r+1}^{2n+1}(x_1)\right]\cdot$$
$$\cdot \sin(2r+1)x_2 \cos(\alpha x_3 = \omega t), \tag{33}$$

$$h\sigma_{13} = c_{44} \sum_{n=0}^{\infty}\sum_{r=0}^{\infty}\left[\sum_{i=1}^{2} C_{2n+1}^{(i)}\, {}^{i}W_{2r+1}^{2n+1}(x_1) + S_{2n+1}\, Z_{2r+1}^{2n+1}(x_1)\right]\cdot$$
$$\cdot \cos(2r+1)\, x_2 \sin(\alpha x_3 + \omega t),$$

where

$${}^{i}U_{2r+1}^{2n+1}(x_1) = \left\{\frac{l^2}{8}\left[(2\cosh^2 2x_1 + 1)\, {}^{i}A_{2r+1}^{2n+1} - 4\, {}^{i}k_{2r+1}^{2n+1}\cosh 2x_1 + \right.\right.$$
$$+ {}^{i}L_{2r+1}^{2n+1}\Big] C c_{13}\,\alpha\lambda_i - c_{12}\,\alpha^2 k_i) + c_{66}\,(a_{2n+1}^{(i)} - 2q_i\cosh 2x_1)({}^{i}A_{2r+1}^{2n+1}\cosh 2x_1 -$$
$$\left. - {}^{i}k_{2r+1}^{2n+1}) - c_{66}\, {}^{i}M_{2r+1}^{2n+1}\right\} Ce_{2n+1}(x_1, q_i) - c_{66}\sinh 2x_1\, {}^{i}A_{2r+1}^{2n+1}\, C\acute{e}_{2n+1}(x_1, q_i),$$

$$X_{2r+1}^{2n+1}(x_1) = c_{66}\left\{\left[(2r+1)\cosh 2x_1\, B_{2r+1}^{2n+1} - N_{2r+1}^{2n+1}\right] S'\acute{e}_{2n+1}(x_1, q) - \right.$$
$$\left. - (2r+1)\, B_{2r+1}^{2n+1}\sinh 2x_1\, Se_{2n+1}(x_1, q)\right\},$$

$${}^{i}V_{2r+2}^{2n+1}(x_1) = \left[{}^{i}P_{2r+1}^{2n+1} - (2r+1)\, {}^{i}A_{2r+1}^{2n+1}\cosh 2x_1\right] C\acute{e}_{2n+1}(x_1, q_i) + \tag{34}$$
$$+ (2r+1)\, {}^{i}A_{2r+1}^{2n+1}\sinh 2x_1\, Ce_{2n+1}(x_1, q_1).$$

$$Y_{2r+1}^{2n+1}(x_1) = \frac{1}{2}\left[(b_{2n+1} - 2q\cosh 2x_1)(Q_{2r+1}^{2n+1} - B_{2r+1}^{2n+1}\cosh 2x_1) - \right.$$
$$- (2r+1)^2\, B_{2r+1}^{2n+1}\, ch\, 2x_1 + \left. R_{2r+1}^{2n+1}\right] Se_{2n+1}(x_1, q) +$$
$$+ B_{2r+1}^{2n+1}\sinh 2x_1\, S\acute{e}_{2n+1}(x_1, q),$$

$${}^{i}W_{2r+1}^{2n+1}(x_1) = (\lambda_i - \alpha)\, {}^{i}A_{2r+1}^{2n+1}\, C\acute{e}_{2n+1}(\alpha_1, q_i),$$
$$Z_{2r+1}^{2n+1}(x_1) = -\alpha(2r+1)\, B_{2r+1}^{2n+1}\, Se_{2n+1}(x_1, q),$$

$$2\, {}^{i}K_1^{2n+1} = {}^{i}A_3^{2n+1} + {}^{i}A_1^{2n+1}, \qquad 2\, {}^{i}K_{2r+1}^{2n+1} = {}^{i}A_{2r+3}^{2n+1} + {}^{i}A_{2r+1}^{2n+1},\ r \geq 1$$

$$2\, {}^{i}L_1^{2n+1} = {}^{i}A_5^{2n+1} + {}^{i}A_3^{2n+1}, \qquad 2\, {}^{i}L_3^{2n+1} = {}^{i}A_7^{2n+1} + {}^{i}A_1^{2n+1},$$
$$2\, {}^{i}L_{2r+1}^{2n+1} = {}^{i}A_{2r+5}^{2n+1} + {}^{i}A_{2r-3}^{2n+1},\ r \geq 2$$

$$2\, {}^{i}M_1^{2n+1} = 3\, {}^{i}A_3^{2n+1} + {}^{i}A_1^{2n+1}, \qquad 2\, {}^{i}M_{2r+1}^{2n+1} = (2r+3)\, {}^{i}A_{2r+3}^{2n+1} -$$
$$- (2r-1)\, {}^{i}A_{2r-1}^{2n+1}\ \ r \geq 1$$

$$
{}^{i}P_1^{2n+1} = 2\,{}^{i}A_3^{2n+1} - {}^{i}A_1^{2n+1}, \qquad {}^{i}P_{2r+1}^{2n+1} = (r+2)\,{}^{i}A_{2r+3}^{2n+1} + (r-)\,{}^{i}A_{2r-1}^{2n+1}, \quad r \geqq 1
$$

$$
N_1^{2+n1} = 2B_3^{n+1} + B_1^{2n+1}, \qquad N_{2r+1}^{2n+1} = (r+2)\,B_{2r+3}^{2n+1} + (r-1)\,B_{2r-1}^{2n+1}, \quad r \geqq 1
$$

$$
2Q_1^{2n+1} = B_3^{2n+1} - B_1^{2n+1} \qquad 2Q_{2r+1}^{2n+1} = B_{2r+3}^{2n+1} + B_{2r-1}^{2n+1}, \quad r \geqq 1
$$

$$
2R_1^{2n+1} = 15B_3^{2n+1} - 3B_1^{2n+1} \qquad 2R_{2r+1}^{2n+1} = (2r+3)(2r+5)\,B_{2r+3}^{2n+1} + (2r-1)(2r-3)\,B_{2r-1}^{2n+1}, \quad r \geqq 1
$$

$$
- i = 1, 2, \ (n = 0, 1, 2, \ldots)
$$

where the prime denotes the derivative of x_1 and $\lambda_i\,(i = 1, 2)$ are the roots of the equation (11).

When the equations (33) are used and the linear independency of the trigonometric functions, it is seen in order to satisfy the boundary conditions (30), that we have

$$
\begin{aligned}
&\sum_{n=0}^{\infty}\left[\sum_{i=1}^{2} C_{2n+1}^{(i)}\,{}^{i}U_{2r+1}^{2n+1}(\xi) + S_{2n+1}\,X_{2r+1}^{2n+1}(\xi)\right] = 0\\
&\sum_{n=0}^{\infty}\left[\sum_{i=1}^{2} C_{2n+1}^{(i)}\,{}^{i}V_{2r+1}^{2n+1}(\xi) + S_{2n+1}\,Y_{2r+1}^{2n+1}(\xi)\right] = 0\,, \qquad (36)\\
&\sum_{n=0}^{\infty}\left[\sum_{i=1}^{2} C_{2n+1}^{(i)}\,{}^{i}W_{2r+1}^{2n+1}(\xi) + S_{2n+1}\,Z_{2r+1}^{2n+1}(\xi)\right] = 0\,,\\
&\qquad (r = 0, 1, 2\ldots).
\end{aligned}
$$

In order to obtain a solution, the infinite system of homogeneous equations (36) with an infinite number of unknowns $C_{2n+1}^{(1)}$, $C_{2n+1}^{(2)}$, S_{2n+1} $(n = 0, 1, 2, \ldots)$ the determinant of the coefficients must be equal to zero:

$$
T \equiv \begin{vmatrix}
{}^{1}U_1^1(\xi) & {}^{2}U_1^1(\xi) & X_1^1(\xi) & {}^{1}U_1^3(\xi) & {}^{2}U_1^3(\xi) & X_1^3(\xi)\ldots\\
{}^{1}V_1^1(\xi) & {}^{2}V_1^1(\xi) & Y_1^1(\xi) & {}^{1}V_1^3(\xi) & {}^{2}V_1^3(\xi) & Y_1^3(\xi)\ldots\\
{}^{1}W_1^1(\xi) & {}^{2}W_1^1(\xi) & Z_1^1(\xi) & {}^{1}W_1^3(\xi) & {}^{2}W_1^3(\xi) & Z_1^3(\xi)\ldots\\
{}^{1}U_2^1(\xi) & {}^{2}U_3^1(\xi) & X_3^1(\xi) & {}^{1}U_3^3(\xi) & {}^{2}U_3^3(\xi) & X_3^3(\xi)\ldots\\
{}^{1}V_3^1(\xi) & {}^{2}V_3^1(\xi) & Y_3^1(\xi) & {}^{1}V_3^3(\xi) & {}^{2}V_3^3(\xi) & Y_3^3(\xi)\ldots\\
{}^{1}W_3^1(\xi) & {}^{2}W_3^1(\xi) & Z_3^1(\xi) & {}^{1}W_3^3(\xi) & {}^{2}W_3^3(\xi) & Z_3^3(\xi)\ldots\\
\cdot & \cdot & \cdot & \cdot & \cdot & \cdot\\
\cdot & \cdot & \cdot & \cdot & \cdot & \cdot\\
\cdot & \cdot & \cdot & \cdot & \cdot & \cdot
\end{vmatrix} = 0 \qquad (33)
$$

The equation (37) is the secular equation, from which the possible velocities of wave propagation are determined. Seeking solution of (37) on a mathematical basis is rather difficult.

That is the reason why only a mechanical interpretation of the method used will be given. Let $x_1 = \xi_1$, $x_2 = \Theta_1, \Theta_3, \Theta_5, \ldots \Theta_{2N-1}$, $-\infty < x_3 < \infty$ be N arbitrary straight lines over the cylindrical surface, parallel to the axis x_3. In order to satisfy the boundary conditions (30) for the points of every one of these straight lines, the solution is searched for in the form (31), where the summing up to n is made from 0 to $N-1$, instead of from 0 to ∞. For the stresses σ_{1l} $(l = 1, 2, 3)$ we have (33), where the summing up to n is made only from 0 to $N-1$. When boundary conditions (30) are used we have a system of linear homogeneous equations with $3N$ unknowns $C^{(1)}_{2n+1}$, $C^{(2)}_{2n+1}$, S_{2n+1} $(n = 0, 1, 2, \ldots, N-1)$. In order to obtain a solution for this system the determinant of coefficients of the unknowns must be equal to zero:

$$H_{2N-1} \equiv \begin{vmatrix} \sum_{r=0}^{\infty} {}^1U^1_{2r+1}(\xi)\cos(2r+1)\Theta_1 \ldots \sum_{r=0}^{\infty} X^1_{2r+1}(\xi)\cos(2r+1)\Theta_1 \ldots \sum_{r=0}^{\infty} X^{2N-1}_{2r+1}(\xi)\cos(2r+1)\Theta_1 \\ \sum_{r=0}^{\infty} {}^1V^1_{2r+1}(\xi)\sin(2r+1)\Theta_1 \ldots \sum_{r=0}^{\infty} Y^1_{2r+1}(\xi)\sin(2r+1)\Theta_1 \ldots \sum_{r=0}^{\infty} Y^{2N-1}_{2r+1}(\xi)\sin(2r+1)\Theta_1 \\ \sum_{r=0}^{\infty} {}^1W^1_{2r+1}(\xi)\cos(2r+1)\Theta_1 \ldots \sum_{r=0}^{\infty} Z^1_{2r+1}(\xi)\cos(2r+1)\Theta_1 \ldots \sum_{r=0}^{\infty} Z^{2N-1}_{2r+1}(\xi)\cos(2r+1)\Theta_1 \\ \sum_{r=0}^{\infty} {}^1U^1_{2r+1}(\xi)\cos(2r+1)\Theta_3 \ldots \sum_{r=0}^{\infty} X'_{2r+1}(\xi)\cos(2r+1)\Theta_3 \ldots \sum_{r=0}^{\infty} X^{2N-1}_{2r+1}(\xi)\cos(2r+1)\Theta_3 \\ \cdots\cdots\cdots\

the determinant H_{2N-1} by the substitution of all infinite series with finite sums to r from 0 to $N-1$. It is to be proved, in order that $H^*_{2N-1}=0$ for arbitrarily chosen $0 \leqq \Theta_{2m+1} < 2\pi$ $(m=0,1,2\ldots N-1)$ we must have $T_{2N-1}=0$, where T_{2N-1} is the subdeterminant which is obtained from the determinant T when we take $3N$ rows and columns, counted from the left upper corner of T.

The first, fourth ... $(3N-2)^{\text{th}}$ row are multiplied by the constants $D_1, D_3, \ldots, D_{2N-1}$, respectively, and are added to the first row. The second, fifth, ..., $(3N-1)^{\text{th}}$ row are multiplied by the constants $E_1, E_3, \ldots, E_{2N-1}$, respectively, and are added to the second row. The third, sixth, ..., $(3N)^{\text{th}}$ row are multiplied with $D_1, D_3, \ldots, D_{2N-1}$, respectively, and are added to the third row. Thus we obtain

$$H^*_{2N-1} \equiv \begin{vmatrix} \sum_{r=0}^{N-1} {}^1U^1_{2r+1}(\xi) \sum_{m=0}^{N-1} D_{2m+1} \cos(2r+1)\Theta_{2m+1} \ldots \\ \qquad \ldots \sum_{r=0}^{N-1} X^{2N-1}_{2r+1}(\xi) \sum_{m=0}^{N-1} D_{2m+1} \cos(2r+1)\Theta_{2m+1} \\ \sum_{r=0}^{N-1} {}^1V^1_{2r+1}(\xi) \sum_{m=0}^{N-1} E_{2m+1} \sin(2r+1)\Theta_{2m+1} \ldots \\ \qquad \ldots \sum_{r=0}^{N-1} Y^{2N-1}_{2r+1}(\xi) \sum_{m=0}^{N-1} E_{2m+1} \sin(2r+1)\Theta_{2m+1} \\ \sum_{r=0}^{N-1} {}^1W^1_{2r+1}(\xi) \sum_{m=0}^{N-1} D_{2m+1} \cos(2r+1)\Theta_{m+1} \ldots \\ \qquad \ldots \sum_{r=0}^{N-1} Z^{2N-1}_{2r+1}(\xi) \sum_{m=0}^{N-1} D_{2m+1} \cos(2r+1)\Theta_{2m+1} \\ \sum_{r=0}^{N-1} {}^1U^1_{2r+1}(\xi) \cos(2r+1)\Theta_3 \ldots \\ \qquad \ldots \sum_{r=0}^{N-1} X^{2N-1}_{2r+1}(\xi) \cos(2r+1)\Theta_3 \\ \hline \sum_{r=0}^{N-1} {}^1W^1_{2r+1}(\xi) \cos(2r+1)\Theta_{2N-1} \ldots \\ \qquad \ldots \sum_{r=0}^{N-1} Z^{2N-1}_{2r+1}(\xi) \cos(2r+1)\Theta_{2N-1} \end{vmatrix} = 0 \qquad (39)$$

If the determinant of the coefficients of the unknown D_{2m+1} in the system

$$\sum_{m=0}^{N-1} D_{2m+1} \cos(2r+1)\Theta_{2m+1} = 0 \quad (r=0,1,2,\ldots,N-1) \qquad (40)$$

denoted by Δ, is equal to zero or the determinant of the coefficients of the unknowns E_{2m+1} in the system

$$\sum_{m=0}^{N-1} E_{2m+1} \sin(2r+1)\Theta_{2m+1} = 0 \quad (r = 0, 1, 2, \ldots, N-1) \tag{41}$$

denoted by σ, is equal to zero, then H^*_{2N-1} is identically zero. If $\Delta \neq 0$ and $\sigma \neq 0$, then at least one of the subdeterminant of the elements of the first row of Δ and σ will be different from zero. Let for example the subdeterminant of the elements $\cos\Theta$, and $\sin\Theta$, marked with Δ_1, and σ_1, respectively, be different from zero. Then the systems

$$\begin{aligned} &\sum_{m=1}^{N-1} D_{2m+1} \cos(2r+1)\Theta_{2m+1} = \cos(2r+1)\Theta_1, (r = 1, 2, \ldots, N-1), \\ &\sum_{m=1}^{N-1} E_{2m+1} \sin(2r+1)\Theta_{2m+1} = \sin(2r+1)\Theta_1, \ (r = 1, 2, \ldots, N-1) \end{aligned} \tag{42}$$

have a non-zero solution. (It is assumed $D_1 = E_1 = -1$)

$$D_{2m+1} = \frac{\Delta_{1,2m+1}}{\Delta}, \quad E_{2m+1} = \frac{\sigma_{1,2m+1}}{\sigma_1} \ (m = 1, 2, \ldots, N-1). \tag{43}$$

The determinant $\Delta_{1,2m+1}$ and $\sigma_{1,2m+1}$ are obtained from Δ_1, and σ_1, respectively, by the substitution of the column with elements

$$\begin{matrix}\cos \\ \sin\end{matrix}(2r+1)\Theta_{2m+1} \ (r = 1, 2, \ldots, N-1)$$

with the column

$$\begin{matrix}\cos \\ \sin\end{matrix}(2r+1)\Theta_1 (r = 1, 2, \ldots, N-1).$$

When we use (43) we obtain

$$\begin{aligned} \sum_{m=0}^{N-1} D_{2m+1} \cos\Theta_{2m+1} &= -\frac{1}{\Delta_1}\left(\Delta_1 \cos\Theta_1 - \right. \\ &\left. - \sum_{m=1}^{N-1} \Delta_{1,2m+1} \cos\Theta_{2m+1}\right) = -\frac{\Delta}{\Delta_1} \neq 0, \end{aligned} \tag{44}$$

$$\begin{aligned} \sum_{m=0}^{N-1} E_{2m+1} \sin\Theta_{2m+1} &= -\frac{1}{\delta_1}\left(\sigma_1 \sin\Theta_1 - \right. \\ &\left. - \sum_{m=1}^{N-1} \sigma_{1,2m+1} \sin\Theta_{2m+1}\right) = -\frac{\sigma}{\sigma_1} \neq 0. \end{aligned}$$

Therefore the equation $H_{2N-1} = 0$ can be written in the form

$$\begin{vmatrix} {}^1U_1^1(\xi) & \dots X_1^1(\xi) & \dots X_1^{2N-1}(\xi) \\ {}^1V_1^1(\xi) & \dots Y_1^1(\xi) & \dots Y_1^{2N-1}(\xi) \\ {}^1W_1^1(\xi) & \dots Z_1^1(\xi) & \dots Z_1^{2N-1}(\xi) \\ \sum_{r=0}^{N-1} {}^1U_{2r+1}^1(\xi)\cos(2r+1)\Theta_3 \dots & \sum_{r=0}^{N-1} X_{2r+1}^1(\xi)\cos(2r+1)\Theta_3 \dots & \sum_{r=0}^{N-1} \cdot X_{2r+1}^{2N-1}(\xi)\cos(2r+1)\Theta_3 \\ \cdot & \cdot\cdot\cdot\cdot & \cdot\cdot\cdot\cdot \\ \cdot & \cdot\cdot\cdot\cdot & \cdot\cdot\cdot\cdot \\ \cdot & \cdot\cdot\cdot\cdot & \cdot\cdot\cdot\cdot \\ \sum_{r=0}^{N-1} {}^1W_{2r+1}^1(\xi)\cos(2r+1)\Theta_{2N-1} \dots & \sum_{r=0}^{N-1} Z_{2r+1}'(\xi)\cos(2r+1)\Theta_{2N-1} \dots & \sum_{r=0}^{N-1} \cdot Z_{2r-1}^{2N-1}(\xi)\cos(2r+1)\Theta_{2N-1} \end{vmatrix} =$$

The first row of the determinant from (45) is multiplied with $\cos\Theta_3, \cos\Theta_5, \dots, \cos\Theta_{2N-1}$, respectively, and is substracted from the 4th, 7th, $\dots$, $(3N-2)^{\text{th}}$ row and analogously with the second and third rows. Then for all elements of the determinant from the third row down we obtain sum r from 1 to $N-1$. Repeating these transformations several times we can transform the equation

$$H_{2N-1}^* = 0 \quad \text{to} \quad T_{2N-1} = 0.$$

Therefore the determinant H_{2N-1}^* is either identically equal to zero, or if it is not identically equal to zero, so that, in order to get $H_{2N-1}^* = 0$ we must have $T_{2N-1} = 0$. But the equation $T_{2N-1} = 0$ does not depend on the selection of the points Θ_{2m+1} $(m = 0, 1, 2, \dots, N-1)$. Therefore, no matter how we chose the points Θ_{2m+1}, if the determinant H_{2N-1} is a good enough approximation of the determinant H_{2N-1}, it can be considered, that the equation $T_{2N-1} = 0$ approximately represents the condition the cylinder surface to be free from loading and this condition will be more accurate, as N is chosen to be bigger.

5. Special cases

From these results we may obtain two special cases. If we set

$$c_{11} = c_{33} = \lambda + 2\mu, \quad c_{44} = c_{66} = \mu, \quad c_{13} = c_{12},$$

where λ and μ are Lame constants, we obtain the case of wave propagation in an isotropic cylinder with an elliptical cross-section. When we take into consideration

$$\alpha^2 k_1 = \frac{\varrho\,\omega^2}{\lambda+2\mu} - \alpha^2, \quad \alpha^2 k_2 = \frac{\varrho\,\omega^2}{\mu} - \alpha^2, \quad \lambda_1 = -\alpha, \quad \lambda_2 = \frac{\varrho\omega^2}{\mu\alpha} - \alpha,$$

it is obvious that the formulae (34) differ by only multiplying factors from the formulae (37)—(44), given in [8]. (Possibly because of a printing mistake, before the coefficients $\overline{\Theta}_{2r+1}^{2m+1}$ and $\overline{I}_{2r+1}^{2m+1}$ in the formula (39) of [8] and $\overline{\epsilon}_{2r+1}^{2m+1}$ in formula (43) of [8] the plus sign is taken instead of minus.)

The case of wave propagation in transversely isotropic cylinders with a circular cross-section, investigated in [4], is obtained from the present formulae as l tends to zero and x_1 tends to infinity in such a way, that $lchx_1$ should tend to r, this means that the ellipse with the semimajor axis r tends to a circle with the same radius. When we take into consideration, that ${}^{i}A_{2r+1}^{2n+1}$ and B_{2r+1}^{2n+1} tend to zero for $r \neq n$ and to one for $r = n$, $a_{2n+1}^{(i)}$ $(l = 1, 2)$ and b_{2n+1} tend to $(2n + 1)^2$ and

$$Ce_m(x_1, q_i) \to p'_m J_m(\alpha\sqrt{k_i}\,r), \qquad (m \geqq 0),$$

$$Se_m(x_1, q_i) \to S'_m J_m(\alpha\sqrt{k_i}\,r), \qquad (m \geqq 1),$$

$$\frac{d}{dx_1} Ce_m(x_1 q_i) \to p'_m r \frac{d}{dr} J_m(\alpha\sqrt{k_i}\,r), \qquad (m \geqq 0),$$

$$\frac{d}{dx_1} Se_m(x_1, q_i) \to S'_m r \frac{d}{dr} J_m(\alpha\sqrt{k_i}\,r), \qquad (m \geqq 1)$$

where p'_m, S'_m, are constants, and $J_m(\alpha\sqrt{k_i}r)$ are Bessel functions of the first kind the formulae (34) are transformed in the corresponding formulae to a circular cylinder. Because

$${}^{1}U_{2r+1}^{2n+1}(\xi) = {}^{i}V_{2r+1}^{2n+1}(\xi) = {}^{i}W_{2r+1}^{2n+1}(\xi) = X_{2r+1}^{2n+1}(\xi) = Y_{2r+1}^{2n+1}(\xi) = Z_{2r+1}^{2n+1}(\xi) = 0$$

when $r \neq n$ is fulfilled, then the determinant T reduces to the product of infinite number of finite determinants, every one of which can be put equal to zero, in order that the boundary condition (30) should be satisfied.

6. Conclusion

Propagation of harmonic waves in a cylinder with an elliptical cross-section has a considerably more complicated character when compared with the propagation of such waves in a circular cylinder. That necessitates the

use of more complicated mathematical apparatus, as a result of which it is not always possible to give exact proofs of the considered problems. Concerning the determination of the possible phase velocities of wave propagation, this can be achieved only if we use the most contemporary computation techniques.

REFERENCES

1. POCHHAMMER, L.: Über Fortpflanzungsgeschwindigkeiten kleiner Schwingungen, *Journ. Rein. Angew. Math.*, **81** (1876), 324—336
2. CHREE, C.: The Equations of an Isotropic Solid in Polar and Cylindrical Coordinates, *Trans. Camb. Phil. Soc.* **14** (1889), 250
3. CHREE, C.: On Longitudinal Vibrations of Aelotropic Bars with One Axis of Material Simmetry, *Quart. J. of Math.*, **24** (1890), 340—358
4. MIRSKY, I.: Wave Propagation in Transversely Isotropic Circular Cylinders, *J. Acoust. Soc. of America* **37** (1965), 1016—1026
5. NOWINSKY, J. L.: Propagation of Longitudinal Waves in Circular Cylindrically Orthotropic Bares, *Trans. of ASME*, Ser. B, **89** (1967), 408—412
6. BERNSTEIN, P. J.: Wolni krutzenia w anisotropnom neenorodnom cylindritscheskom sterschne. *Ing. Journal* **5** (1965), 572—574
7. KOZAROV, M.—IVANOV, Ts. P.: Wave Propagation in Elastic Orthotropic Circular Cylinders National Conference on Applied Mechanics, Bucharest—June 1969, *Rumania or Rozprawy Inzynierskie* **17** (1969) (in Polish)
8. WONG, P. K.—MIKLOWITZ, J.—SCOTT, R. A.: Propagation of Harmonic Flexural Waves in an Infinite Elastic Rod of Elliptical Cross Section, *J. Acoust. Soc. of America* 393—398
9. MEDICK, M. A.: Extensional Waves in Elastic Bars of Rectangular Cross Section, *J. Acoust. Soc. of America* **43** (1968)
10. NIGRO, N. J.: Wave Propagation in Anisotropic Bars of Rectangular Cross Section, *J. Acoust. Soc. of America* **43** (1968), 958—965
11. FRASER, W. B.: Stress Wave Propagation in Rectangular Bars, *Internat. J. Solids and Struct.* **5** (1969), 379—397
12. MCCONNELL, A. J.: Application of Tensor Analysis, Dover publ., Inc., New York 1957
13. MCLACHLAN, N. W.: Theory and Application of Mathieu Functions, Dover Publ., Inc., New York 1964

Wellenfortpflanzung in einem in der Querrichtung isotropen Zylinder elliptischen Querschnitts. Die Fortpflanzung harmonischer Schwingungswellen in einem in der Querrichtung isotropen Zylinder von elliptischem Querschnitt mit Hilfe der linearen Elastizitätstheorie wird behandelt. Das Ergebnis wurde durch die Mathieusche Funktion erhalten. Als Bedingung der Spannungslosigkeit der Zylinderoberfläche ist eine unendliche Determinante gleich Null angegeben. Aus dem allgemeinen Ergebnis können zwei Spezialfälle erhalten werden: Wellenfortpflanzung in einem isotropen Zylinder von elliptischem Querschnitt und Wellenfortpflanzung in einem in der Querrichtung isotropen Zylinder mit Kreisquerschnitt.

Распространение волны в поперечном направлении изотропном бесконечном цилиндре эллиптического сечения. Изучение распространения гармонических колебательных волн в цилиндре эллиптического сечения из материала, являющегося изотропным в поперечном направлении, на основе теории линеарной упругости. Результат получается на основе функции Mathieusche. Условие, касающееся ненапряженности поверхности цилиндра, дано в форме бесконечного детерминанта, равного нулю. На основе общего результата можно вывести два специальных случая, а именно: распространение колебаний в изотропном цилиндре эллиптического сечения и распространение колебаний в цилиндре круглого сечения, являющегося изотропным в поперечном направлении.

Acta Technica Academiae Scientiarum Hungaricae, Tomus 76 (1—2), pp. 39—52 (1974)

GRUNDLEGENDE VORGÄNGE BEI DER GEFÜGEENTWICKLUNG*

W. SCHATT**

Es wird eine Darstellung der wichtigsten, bei der Gefügeentwicklung von metallischen Werkstoffen in Lösungen ablaufenden elektrochemischen Vorgänge gegeben: Ätzen unter Wasserstoffbildung, durch Reduktion eines Oxydationsmittels und mit Komplexbildung. Sodann werden die Ursachen für die physikalische und chemische Inhomogenität der realen Werkstoffoberfläche erörtert, derzufolge die Gefügebestandteile selektiv vom Ätzmittel angegriffen und im Mikroskop beobachtbar werden.

1. Einleitung

In der metallographischen Ätztechnik herrschen heute noch die empirischen Methoden vor. Weniger bekannt sind jedoch ihre ursächlichen Zusammenhänge, die zur Entwicklung des Gefüges führen, und deren Kenntnis es ermöglicht, die Gefügeentwicklung systematischer vornehmen zu können. Von diesen Zusammenhängen soll versucht werden, ein in etwa abgerundetes Bild zu geben, wobei sich die Darlegungen auf den praktisch häufigsten Fall, die Gefügeentwicklung in Lösungen, beschränken sollen.

Der Ätzvorgang in Lösungen ist ein elektrochemischer Korrosionsvorgang, bei dem Metallionen in Lösung gehen. Für die nähere Betrachtung dieses Vorganges stehen zwei Fragen im Vordergrund: Welcher Art sind die elektrochemischen Vorgänge, die beim Ätzen ablaufen, und durch was ist im System Metalloberfläche/Ätzmittel die für eine selektive Lösung der einzelnen Gefügebestandteile notwendige Potentialdifferenz gegeben.

2. Elektrochemische Vorgänge beim Ätzen

Gehen die Metallatome als Kationen in Lösung, bildet sich an der Metalloberfläche eine elektrische Doppelschicht aus. Erst wenn sich für die freigewordenen Elektronen ein Abnehmer findet, läuft der Vorgang weiter.

* Vorgetragen im Sept. 1972 an der Technischen Universität Budapest.

** Prof. Dr. Ing. habil. W. SCHATT, Techn. Universität Dresden, DDR

Für ein unedles Metall in einer nichtoxydierenden Säure, z. B. Eisen in Salzsäurelösung, treten dabei folgende Reaktionen auf:

$$\text{Als anodische Teilreaktion} \quad Me \rightarrow Me^{z+} + 2e^- \tag{1a}$$

$$\text{u. als katodische Teilreaktion} \quad 2H^+ + 2e^- \rightarrow H_2 \tag{1b}$$

Das Metall löst sich unter Wasserstoffentwicklung. Der Wasserstoff dient als Elektronennehmer. Dieser Vorgang läßt sich mit Hilfe eines Stromdichte-Potential-Schaubildes beschreiben (Bild 1). $\varepsilon_{0,1}$ und $\varepsilon_{0,2}$ sind die Gleichgewichtspotentiale beider Teilvorgänge, die in Abhängigkeit von der jeweiligen Ionenkonzentration durch die Nernstsche Gleichung

$$\varepsilon_0 = E_n + \frac{RT}{n \cdot F} \ln C \tag{2}$$

gegeben sind. Mit zunehmender Stromdichte polarisieren die Potentiale der Metallauflösung zu edleren, die der Wasserstoffbildung zu unedleren Werten. Es bildet sich ein Mischpotential ε_M aus, bei dem anodischer und katodischer Teilvorgang mit einer dem Betrag nach gleichen Stromdichte ablaufen. Das System ist nach außen stromlos. Die Teilstromdichte i_k ist als Maß für die Intensität des Ätzprozesses anzusehen.

Während die Gleichgewichtspotentiale $\varepsilon_{0,1}$ und $\varepsilon_{0,2}$ thermodynamisch durch Gleichung (2) gegeben sind, hängt der Wert des Mischpotentials ε_M von der Lage der Teil-Stromdichte-Potential-Kurven ab. Ist der Vorgang der Metallauflösung wenig gehemmt (anodische Teilkurve verläuft steiler, kleinere Polarisation), dann ist das Mischpotential negativer (unedler), ist er stärker gehemmt (anodische Teilkurve verläuft flacher, größere Polarisation), dann ist ε_M positiver (edler). Das heißt aber auch, daß im Gegensatz zu den Gleichgewichtspotentialen die Größe des Mischpotentials und damit die Intensität des Ätzangriffes stark von den Eigenschaften der Metalloberfläche abhängt. Eine verformte Oberfläche z. B. löst sich leichter als eine nicht verformte. Da der Zustand der Metalloberfläche schwer definierbar ist, sind die Mischpotentiale auch oftmals nicht reproduzierbar.

Andererseits ist die Lage des Mischpotentials und die Ätzstromdichte vom p_H-Wert der Ätzlösung über $\varepsilon_{0_{H_2}} = -0{,}058\ p_H$ abhängig (Bild 2). Je größer der p_H-Wert, d. h. je geringer die Wasserstoffionenkonzentration ist, umso unedler sind das Gleichgewichtspotential der katodischen Reaktion und das Mischpotential und umso kleiner wird die Ätzstromdichte i_k. Auf diesem Wege läßt sich durch geeignete Veränderung der Ätzmittelkonzentration ein in vielen Fällen günstigerer milderer Angriff der Ätzlösung auf die Metalloberfläche einstellen.

Aus dem Vorangegangenen muß man folgern, daß ein Metall, dessen Gleichgewichtspotential edler als das der Wasserstoffentwicklung ist, unter den genannten Bedingungen kein Mischpotential bilden kann. Es kann selbst in starken Säuren nicht unter H_2-Bildung angeätzt werden.

Um auch solche Metalle ätzen zu können, muß das System so geartet sein, daß die freiwerdenden Elektronen durch Reduktion des Sauerstoffs

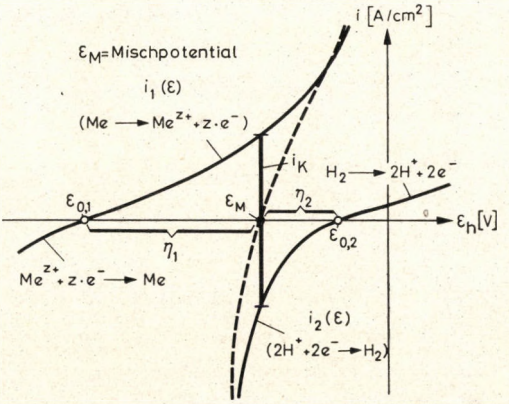

Bild 1. Stromdichte-Potential-Kurven für die Auflösung eines unedlen Metalls unter Wasserstoffbildung [1]

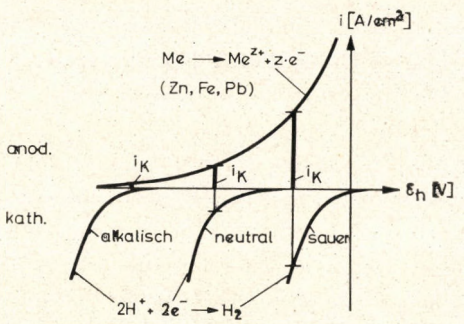

Bild 2. pH-Abhängigkeit der Korrosionsstromdichte i_k [1]

oder eines anderen geeigneten Oxydationsmittels verbraucht werden. Im Falle der Sauerstoffreduktion verläuft dann der Vorgang in sauren Lösungen gemäß

$$Me \rightarrow Me^{z+} + ze^- \tag{4a}$$

$$O_2 + 4H^+ + 4e^- \rightarrow 2H_2O \tag{4b}$$

und in neutralen bis alkalischen Lösungen nach

$$Me \rightarrow Me^{z+} + ze^- \tag{4a}$$

$$O_2 + 2H_2O + 4e^- \rightarrow 4OH^- \tag{4c}$$

Bild 3 zeigt diesen Vorgang wieder in der i-ε-Darstellung. Auch hier beeinflußt die Anionenkonzentration c_{O_2} die Größe der Ätzstromdichte.

Die Ätzlösungen für die Gefügeentwicklung edlerer Metalle enthalten deshalb Zusätze von Säuren mit oxydierender Wirkung bzw. von Oxydationsmitteln, wie Salpeter-, Chrom- und Pikrinsäure, Wasserstoffperoxid, Persulfate u. a. So ätzt z. B. die Salpetersäure das Cu nicht auf Grund ihrer sauren Eigenschaften, sondern allein als Redoxsystem mit hohem positiven Redoxpotential. Um die Ätzlösungen universeller verwenden zu können und damit die Lagerhaltung zu vereinfachen, enthalten die meisten von ihnen von vornherein derartige Oxydationsmittel, so daß sie sowohl für die Ätzung unedlerer wie auch edlerer metallischer Werkstoffe geeignet sind. Diese Gruppe von Ätzmitteln ist heute in der Ätztechnik am häufigsten und vielfältigsten in Anwendung.

Wie dargelegt wurde, ist die anodische Auflösung des Metalls an das Auftreten eines Mischpotentials im System Metalloberfläche/ Ätzlösung gebunden. Je edler das Potential für den anodischen Teilvorgang ist, bei umso positiveren Potentialen muß auch die katodische Teilreaktion verlaufen, da sich sonst kein Mischpotential ausbilden kann. Das war im vorangegangenen Fall dadurch erreicht worden, daß ein Ätzmittel gewählt wurde, bei dem an Stelle der bei negativeren Potentialen ablaufenden Wasserstoffentwicklung der katodische Vorgang durch eine Sauerstoffreduktion gegeben ist. Es ist jedoch auch möglich, daß bei einem gegebenen Potential der katodischen Reaktion die Bildung eines Mischpotentials dadurch erreicht wird, daß das zunächst edlere Potential der Metallauflösung zu unedleren Potentialen verschoben wird.

Enthält nämlich das Ätzmittel einen Komplexbildner für das Metallion und weist die dann entstehende Komplexverbindung eine feste Bindung auf (kleine Komplexdissoziationskonstante), dann wird die *i*-ε-Kurve der Metallauflösung stark nach negativeren Potentialen verschoben. Durch die Komplexbildung werden Metallionen verbraucht. Die Metallionenkonzentration der Lösung nimmt ab und gemäß Gleichung (2) wird das Potential des Metalls gegen die Ätzlösung negativer. Im Falle des Cu beispielsweise bildet sich der Komplex

$$[Cu(CN)_4]^{--} \rightleftharpoons Cu^{++} + 4CN^{-}, \tag{5}$$

der z. T. dissoziiert. Die Dissoziation ist jedoch so gering, daß der Vorgang im wesentlichen nach links verläuft.

Bild 4 veranschaulicht schematisch diesen Vorgang für einige edle Metalle in gesättigter KCN-Lösung ($p_H \approx 11$). Die Verschiebung des Au-Gleichgewichtspotentials geht so weit, daß das Au in Gegenwart von Sauerstoff gelöst wird. Die Verschiebung des Cu-Gleichgewichtspotentials ermöglicht sogar bei Abwesenheit von Sauerstoff eine langsame Lösung des Cu unter Wasserstoff-

entwicklung. Für das Ag ergibt sich unter diesen Bedingungen nur eine schwache Auflösung. Durch die Zugabe von Komplexbildnern zum Ätzmittel kann in bestimmten Fällen der Ätzangriff verstärkt und damit die Gefügeentwicklung, insbesondere bei edleren Werkstoffen, verbessert werden.

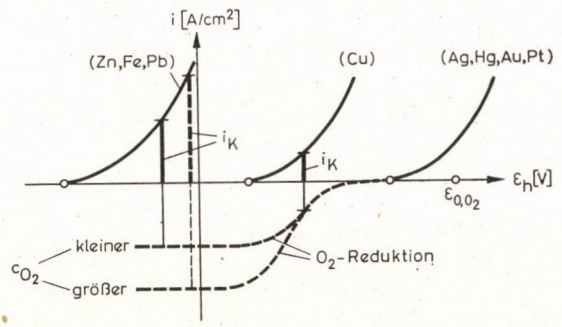

Bild 3. Korrosion durch Sauerstoffreduktion [1]

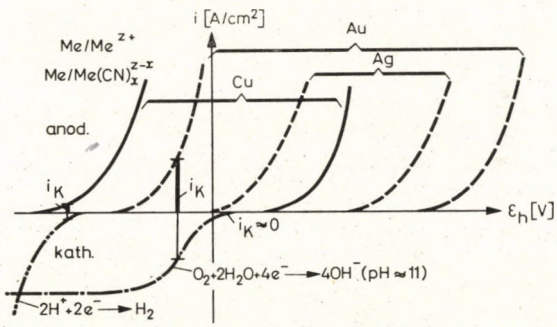

Bild 4. Korrosion von edlen Metallen unter Komplexbildung [1]

Bei all diesen Ätzvorgängen war vorausgesetzt worden, daß das Metall mit dem Ätzmittel direkt in Berührung steht, d. h. eine aktive Auflösung des Metalls vorliegt. Freilich kann die Ätzreaktion in Lösungen auch zur Bildung schwer löslicher Verbindungen führen, die sich als Schicht auf der Metalloberfläche ablagern. Diese weniger häufige Möglichkeit soll jedoch in diesem Zusammenhang nicht betrachtet werden.

3. Selektive Löslichkeit der Gefügebestandteile

Mit Hilfe der dargelegten allgemeinen Grundzüge des elektrochemischen Metallabtrages beim Ätzen allein ist es jedoch nicht möglich, die Gefügeentwicklung am metallischen Werkstoff erklären zu können. Für die Gefügeentwicklung ist es notwendig, daß der Abtrag der Oberfläche nicht schlechthin,

sondern in einer für das Gefüge charakteristischen Weise erfolgt, d.h. daß bestimmte Gefügebestandteile stärker und andere nicht oder weniger stark abgetragen werden, so daß im Zuge des Ätzvorganges anstelle der ursprünglich ebenen Schliff-Fläche ein Oberflächenrelief entsteht, an dem das im Mikroskop einfallende Licht so reflektiert bzw. gestreut wird, daß ein das Gefüge richtig wiedergebendes Bild entsteht.

Die Forderung einer selektiv unterschiedlichen Löslichkeit bzw. Abtragungsrate der einzelnen Gefügebestandteile erfüllen die metallischen Werkstoffe von Natur aus. Jede Metalloberfläche ist physikalisch und/oder chemisch inhomogen. Sie weist Bereiche auf, die einen unterschiedlichen elektrochemischen Charakter und somit über die Bildung von Lokal -bzw. Korrosionselementen eine differenzierte Löslichkeit haben.

Die Oberfläche nimmt insofern eine Sonderstellung ein, als sich an ihr alle Eigenschaften des Körpers unstetig ändern. Die Atome der Oberfläche sind in Abweichung von den im Innern untergebrachten Atomen nicht allseitig durch Bindungen zu benachbarten Atomen abgesättigt. Demzufolge ist die Oberfläche der Sitz einer freien Energie, der Oberflächenenergie. Die spezifische Oberflächenenergie eines kristallinen Körpers ist anisotrop, d. h. sie ist von der kristallographischen Orientierung der Fläche abhängig. Sie ist umso kleiner, je größer die Oberflächenkoordinationszahl, d. h. je größer die Belegungsdichte der Oberfläche mit Atomen ist. Beispielsweise beträgt sie beim krz Wolfram

für die (111)-Fläche 6690 erg cm^{-2}
für die (100)-Fläche 6430 erg cm^{-2} und
für die (110)-Fläche 5510 erg cm^{-2}.

Da die Triebkraft für den Ätzvorgang in der Erniedrigung der totalen Oberflächenenergie zu suchen ist, hängt auch die Tendenz, Ätzreaktionen einzugehen, von der kristallographischen Orientierung der Oberfläche ab. Das kommt z. B. auch in den an Al-Einkristallen verschiedener Oberflächenorientierung in einem Na_2SO_4-Elektrolyten ($p_H = 4$) ermittelten Ruhepotentialen zum Ausdruck:

Fläche	Spez. Oberflächenenergie erg cm^{-2}	Ruhepotential mV
(100)	1916	−936
(111)	1664	−852

d. h. die (100)-Fläche mit der niedrigeren atomaren Belegungsdichte hat eine größere spez. Oberflächenenergie, sie verhält sich unedler als die dichtest gepackte (111)-Fläche. Bei ihr läuft der Auflösungsvorgang mit einer geringeren Hemmung ab, so daß die Kristallpolarisation $\eta_{K(100)} < \eta_{K(111)}$ ist.

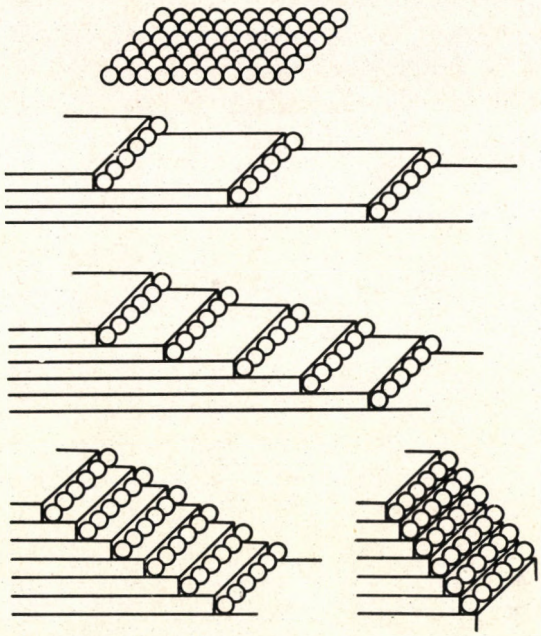

Bild 5. Schematische Darstellung des Aufbaues höherindizierter Kristallflächen

Des weiteren ist zu berücksichtigen, daß bei Kristallen nur "einfache", dichtgepackte Flächen, wie die (110) bei krz oder die (111) bei kfz Kristallen, atomar glatt sind. Höher indizierte Flächen, sog. Vizinalen, weisen atomare Stufen, die von einfachen Flächen gebildet werden, und Ecken auf (Bild 5). Bei Temperaturen oberhalb des absoluten Nullpunktes wird durch Fluktuation von Oberflächenatomen das atomare Relief weiter "aufgerauht" (Bild 6),

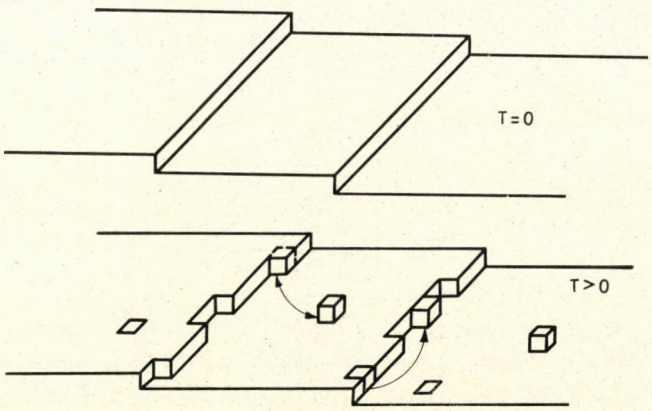

Bild 6. Schematische Darstellung einer realen Kristalloberfläche [2]

bis sich im Gleichgewicht eine quasistationäre Oberflächenstruktur ausbildet, wobei Ecken und Stufen weiter entstehen und verschwinden, die mittlere Charakteristik der Oberfläche aber erhalten bleibt.

Die in den Stufen und Ecken untergebrachten Atome sind mit einer geringeren Energie als die in einer Fläche oder im Kristallinneren gelegenen Atome an das Kristallgebäude gebunden. Während beispielsweise ein in

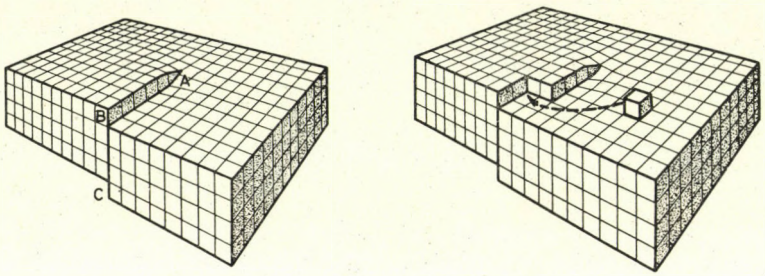

Bild 7. Schematische Darstellung der Stufenbildung durch eine Schraubenversetzung

einer (111)-Oberfläche eines kfz-Kristalls gelegenes Atom von 9 nächsten Nachbarn umgeben ist, hat das in einer von dieser Fläche gebildeten Stufe untergebrachte Atom 7 und das am Stufenbeginn, an der Ecke, 6 nächste Nachbarn und ist gegenüber einem Atom im Kristallinneren, das 12 nächste Nachbarn aufweist, nur noch mit der halben Gitterenergie an das Kristallgitter gebunden. Man bezeichnet deshalb die Lage an der Ecke auch als Halbkristall-Lage.

Beim realen metallischen Werkstoff wird die Zahl der Halbkristallagen außer durch die Temperatur noch dadurch erhöht, daß die Metalloberfläche von ihrer Bearbeitung her mehr oder weniger rauh ist und zahlreiche Versetzungen enthält. Jede die Oberfläche durchstoßende Schraubenversetzung erzeugt eine Stufe, die die Halbkristallage enthält (Bild 7).

Die energetisch begünstigten Halbkristallagen haben für den Lösungsvorgang beim Ätzen eine besondere Bedeutung. Ähnlich wie beim Kristallabbau in die Gasphase kommen für den Abbau in Lösungen ($Me_{Gitter} \rightarrow Me_{ad} \rightarrow Me^{z+}$) vorzugsweise jene Gitterplätze in Frage, auf denen die Oberflächenatome weniger stark gebunden sind (Bild 8). Daraus folgt, daß bei einer Kornschnittfläche, die höher indiziert, stärker aufgerauht ist und eine größere Anzahl von Halbkristallagen enthält, die Neigung, eine Abbaureaktion einzugehen, größer ist als bei einer Kornschnittfläche, die weniger aufgerauht ist, und die sich deshalb edler verhält und weniger abgetragen wird. Sind beide im polykristallinen Werkstoff leitend miteinander verbunden, so bildet sie beim Ätzen ein Lokalelement. Haben sie eine gemeinsame Korngrenze, so erscheint

diese nach dem Ätzvorgang infolge des zwischen den Kornschnittflächen entstandenen Niveauunterschiedes als Kante, die das senkrecht einfallende Licht streut (Korngrenzenätzung, Bild 9).

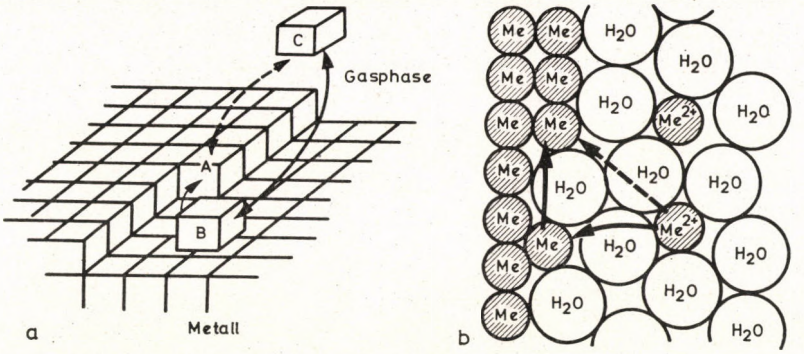

Bild 8. Schematische Darstellung (a) des Auf- und Abbaus eines Kristalls in der Gasphase und (b) des Übertritts eines Metallions in den Elektrolyten [3]

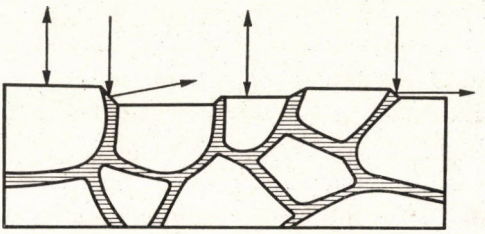

Bild 9. Schematische Darstellung der Entwicklung des Korngrenzenbildes im Mikroskop

Der Zustand minimaler geometrischer Größe einer willkürlichen Kristalloberfläche ist nicht gleichbedeutend mit einem Minimum an Oberflächenenergie. Da die Bausteine des festen Körpers nicht in dem Sinne wie in einer Flüssigkeit beweglich sind, wird deshalb beim Ätzen die kristallographisch zufällige Oberfläche verändert: Auf den Kornschnittflächen entsteht eine Terassenstruktur (Bild 10), die von Flächenelementen niedriger Oberflächenenergie gebildet wird. Da diese beim Vielkristall in Bezug auf das im Mikroskop einfallende Licht von Kornschnittfläche zu Kornschnittfläche unterschiedlich angeordnet sind (Bild 11), wird auch das Licht an den jeweiligen Kornschnittflächen verschieden reflektiert (dislozierte Reflexion), so daß die Kornschnittflächen in unterschiedlichen Hell-Dunkel-Tönen erscheinen (Kornflächenätzung).

Die Bildung einer solchen Terassenstruktur muß man sich wie folgt vorstellen: Der Lösungsvorgang darf als ein dem Kristallwachstum kinematisch reziproker Vorgang aufgefaßt werden. In Bild 12 ist das Wachstum einer konvexen Kristalloberfläche schematisch dargestellt. Es zeigt sich, daß die

schnell wachsenden Flächen verschwinden, so daß der Kristall in seiner Endgestalt von Flächen mit der geringsten Wachstumsgeschwindigkeit begrenzt ist, und das sind niedrig indizierte Flächen. Das Auftreten schnell wachsender Flächen in konkaven Oberflächenbereichen hat, wie das untere Teilbild zeigt, nur vorübergehenden Charakter. Denkt man sich diesen Vorgang kinematisch umgekehrt, so ergibt sich, daß bei der Auflösung in einer Kristallhohlhalbkugel dieselben einfach indizierten Flächen wie beim Wachstum eines Konvexkörpers erzeugt werden. Diese Vorstellung läßt sich auf die Metalloberfläche übertragen, wenn man berücksichtigt, daß in ihr zahlreiche submikroskopische halbkugelige Hohlräume bestehen. In jedem Fall sind dies die Raumecken der atomar aufgerauhten Oberfläche, von denen der Ätzangriff ausgeht und so fortschreitet, daß an die Stelle der ehemals zufällig orientierten Kornschnittfläche eine aus niedrig indizierten mikroskopischen Flächenanteilen aufgebaute Terassenstruktur tritt.

Aus dem vorliegenden Untersuchungsmaterial geht jedoch hervor, daß nicht in jedem Falle — wie zunächst zu erwarten wäre — die Kornschnittfläche so abgetragen wird, daß Flächenelemente dichtester Packung entstehen. Eingehendere Untersuchungen hierzu sind vor allem am Al vorgenommen worden, von dem bekannt ist, daß bei der Ätzung in HCl- bzw. HCl-HF-Lösung Würfelflächen (Bild 10) und nicht die dichtest belegten Oktaederflächen freigelegt werden. MAHL und STRANSKI [5] erklären das damit, daß sich während des Ätzens auf der Al-Oberfläche eine monomolekulare Oxidschicht bildet, die dem Al-Gitter genau angepaßt ist, und deren Bildungsgeschwindgkeit größer als die Auflösungsgeschwindigkeit ist. Dadurch gelangt nicht das kfz Al-Gitter, sondern das Ionengitter des Oxids primär zur Auflösung. Für diese Bedingungen ist dann, wie die Autoren zeigen konnten, die Würfelfläche die Gleichgewichtsformfläche.

Eine andere Erklärung gibt POLITYCKI [6], der den Ätzabbau des Al in HF-, HCl,- HBr- und HJ-Lösungen untersucht hat. Er führt den beobachteten kristallographisch unterschiedlichen Abtrag allein auf die in der Phasengrenze Oberfläche/Ätzlösung bestehenden sterischen Verhältnisse zurück (Bild 13): Die Fluorionen sind kleiner als die Al-Atome, sie können sich deshalb bei Adsorption jeder dargebotenen Fläche anpassen; der Abtrag erfolgt so, daß glatte Flächen entstehen. Die Cl- und Br-Ionen können sich nur an der weiter gepackten Würfelfläche dicht anpassen, es entstehen also beim Ätzen Würfelflächen. Die Jod-Ionen sind zu groß, um sich an einer Fläche bevorzugt anpassen zu können; deshalb entsteht beim Angriff die Gleichgewichtsfläche (111).

Es ist noch nicht möglich, in jedem Falle eine endgültige Erklärung zu geben. Man darf aber annehmen, daß dort, wo beim Ätzen nicht die dichtest besetzten Ebenen entstehen, Passivierungs- oder Inhibitionsvorgänge eine Rolle spielen, die die kristallographische Form der Gleichgewichtsfläche ver-

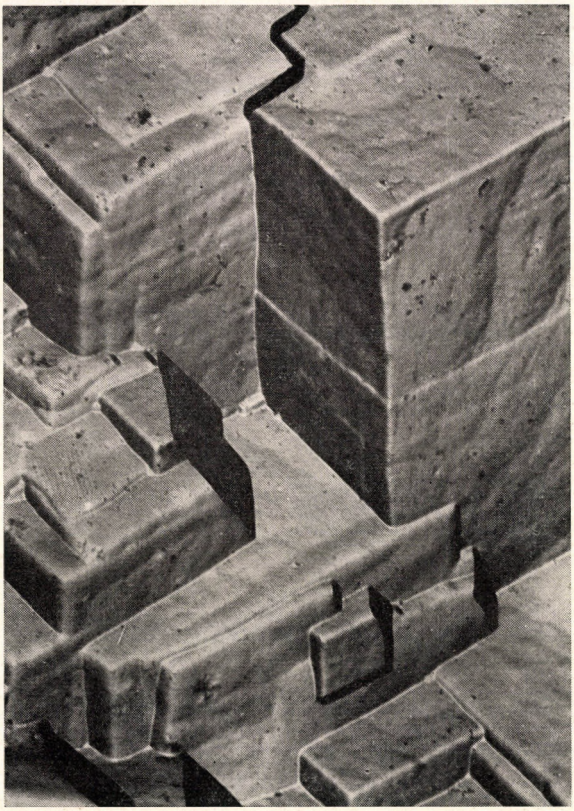

Bild 10. Elektronenmikroskopische Aufnahme einer geätzten Al-Oberfläche

ändern. — Es sei noch erwähnt, daß an derartig geätzten Kornschnittflächen mit Hilfe eines optischen Goniometers auch Kornorientierungsbestimmungen vorgenommen werden können [7], wenn die Ätzflächenform bekannt ist.

Das Streben nach Erniedrigung der totalen Oberflächenenergie kommt auch in der bei der Korngrenzenätzung vielfach anzutreffenden Furchenbildung

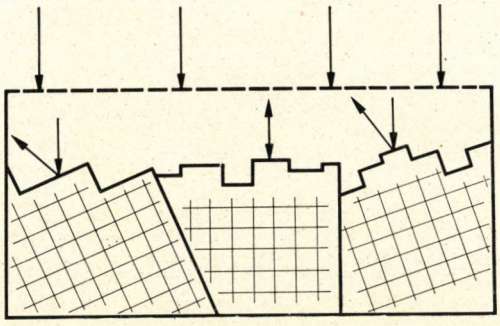

Bild 11. Schematische Darstellung der dislozierten Reflexion

zum Ausdruck. Die Korngrenze stellt eine Zone dar, in der das Atomgitter stark gestört ist, und die deshalb bevorzugt angegriffen werden kann. Die Bildung der Korngrenzenfurche geschieht so, daß beiderseits der Korngrenze

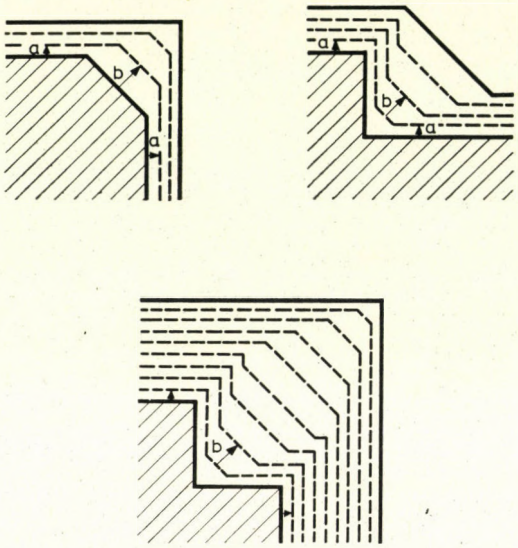

Bild 12. Verschiebungsstadien einer langsam wachsenden (a) und einer schnell wachsenden (b) Fläche [4]

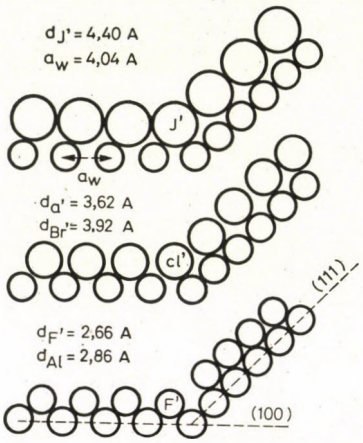

Bild 13. Anpassung der Halogenionen an die Würfel- und Oktaederfläche des Al [6]

Flächen niedrigerer Oberflächenenergie entstehen (Bild 14). Sie strebt einer Gleichgewichtskonfiguration zu, die durch die Beziehung

$$\frac{\sigma_{AB}}{\sin\gamma} = \frac{\sigma_A}{\sin\alpha} = \frac{\sigma_B}{\sin\beta} \tag{6}$$

gekennzeichnet ist [8] (σ_A, σ_B Oberflächenspannung des Kornes A, B; σ_{AB} Korngrenzenspannung). In technischen Werkstoffen allerdings dürfte beim Ätzen in Lösungen der Einfluß der Oberflächenenergie in den Hintergrund treten und der Einfluß der chemischen Inhomogenität der Korngrenzenzone bei der Furchenbildung dominieren. Die von der Entstehung des Werkstoffes

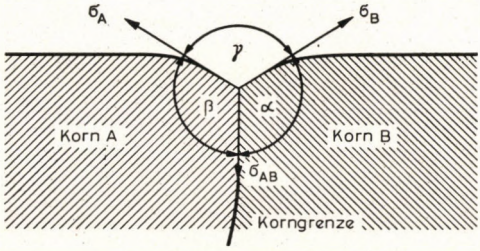

Bild 14. Gleichgewichtskonfiguration an einer Korngrenze [8]

her im Korngrenzenbereich angereicherten Verunreinigungen, die edler oder unedler als ihre Umgebung sein können, bilden mit dieser Lokalelemente, denen zufolge die Korngrenzensubstanz selektiv gelöst wird.

In noch stärkerem Maße von Einfluß auf die Gefügeausbildung beim Ätzen ist die chemische Inhomogenität bei mehrphasigen metallischen Werkstoffen. Die oft auch vom Kristallgitter her, in jedem Falle aber hinsichtlich ihrer chemischen Zusammensetzung verschiedenen Phasen weisen meist ausgeprägte Unterschiede in ihrem elektrochemischen Verhalten auf, die den Einfluß physikalischer Inhomogenitäten, wie sie im Vorangegangenen dargelegt wurden, überdecken. Die Tatsache, daß in der Schliefffläche eines solchen Werkstoffes elektrochemisch edlere und unedlere Gefügebestandteile nebeneinander liegen und im Kornverband leitend miteinander verbunden sind, hat die Bildung von Korrosionselementen zur Folge. Als Beispiel hierfür sei nur die Ätzung des zweiphasigen α-β-Messungs erwähnt, bei dem die zinkreichere β-Phase einen bevorzugten Angriff erleidet. Der mit der Betätigung derartiger Korrosionselemente verbundene unterschiedliche Abtrag der Gefügebestandteile ist oft so stark, daß die jeweilige Kornschnittfläche in etwa gleichmäßig abgebaut bzw. in beliebiger Weise strukturiert wird und keine aus kristallographisch definierten Flächenelementen bestehende Terassenstruktur entsteht.

SCHRIFTTUM

1. Vetter, K. J.: Elektrochemische Kinetik. Springer-Verlag, Berlin/Göttingen/Heidelberg 1961, S. 588 ff.
2. Geguzin, Ja. E. in: »Diffusion in metallischen Werkstoffen«. VEB Deutscher Verlag für Grundstoffindustrie, Leipzig 1970, S. 295 ff.

3. KAESCHE, H.: Die Korrosion der Metalle. Springer-Verlag, Berlin/Heidelberg/New York 1966, S. 102 ff.
4. MUTAFTSCHIEW, B.: *Phys. Stat. Sol.* **8** (1965), 233—238
5. MAHL, H.—STRANSKI, J. N.: *Z. Physik. Chemie* **51** (1942), 319—346
6. POLITYCKI, A.: *Metall* **8** (1954), 173—176
7. SCHATT, W.: *Radex-Rundschau* (1967), H. 3/4, 567—575
8. JEGLITSCH, F.: *Radex-Rundschau* (1967), H. 3/4, 679—685

Basic Phenomena in Structure Development. The author describes the most important phenomena of the structure development of metallic materials in solutions: edging with hydrogen development, by reduction of an oxydizing agent and with formation of a complex. Subsequently the causes for the physical and chemical inhomogeneity of the real surface are discussed, which causes the structural components to be attacked selectively by the edging agent, so that they can be observed under the microscope.

Основные процессы формирования материальной структуры. Автор описывает важнейшие процессы формирования структуры металлических материалов в растворе: травление при выделении водорода, травление путем восстановления окисляющим веществом и травление образованием комплекса. После чего рассматриваются причины физической и химической негомогенности действительной материальной поверхности, вследствие чего травильное средство селективно разлагает структурные компоненты, так что они становятся пригодными для наблюдений под микроскопом.

Acta Technica Academiae Scientiarum Hungaricae, Tomus 76 (1–2), pp. 53–63 (1974)

CONTINUUM METHOD OF ANALYSIS FOR DOUBLE-LAYER SPACE TRUSSES WITH UPPER AND LOWER CHORD PLANES OF DIFFERENT RIGIDITIES

L. KOLLÁR*
DOCTOR OF TECHN. SC.

[Manuscript received 23 July, 1971]

A general method has been presented for determining equivalent continua of double-layer space trusses with two different, arbitrary chord plane meshes. Differential equation system and boundary conditions of the equivalent continuum are derived. In addition to the deflection function describing the plate deformation, a stress function is still needed to describe the internal force system of the substituting continuum, similarly as for ribbed plates.

1. Introduction

The problem of the continuum method of analysis of double-layer space trusses has been solved for the case where both chord planes have rigidity characteristics that are identical or differ only by a multiplying factor [7], [3]. The problem, however, becomes more complicated if rigidity characteristics of chord planes deviate by different degrees or qualitatively (e.g. the one has, and the other lacks shear rigidity etc.), approaching the internal force system to that of a plate with two-way ribs on one side [1].

A previous publication [4] presented a solution for a special kind of space trusses with different chord planes: where there was no shear rigidity in the lower chord plane, only in the upper one, this latter could, however, only support normal forces equal in x and y directions. In the following, a generalized method will be described, according to which the continuum equation for space trusses with lower and upper chord planes of any rigidity characteristics may be written down.

2. Setting the problem. Assumptions

Let us assume a double-layer space truss of parallel chord planes at spacing h. Chord planes are only required to be homogeneous i.e. with identical rigidity characteristics throughout, besides, components of deformation and of internal forces should be in a mutually inambiguous, linear relationship.

* Dr. KOLLÁR Lajos Karap u. 9 1122 Budapest, Hungary

Otherwise, chord plane rigidities may be perfectly arbitrary, i.e. each chord plane may be generally anisotropic (aeolotropic). The connecting diagonals are required not to inhibit chord plane deformations. A space truss meeting these conditions is illustrated in Fig. 1.

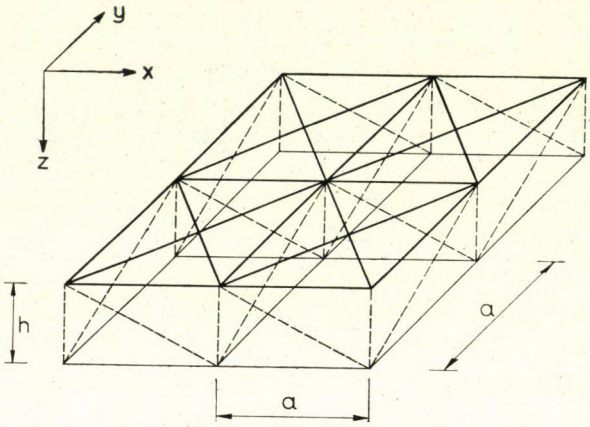

Fig. 1

Let us mention that this method is also valid for inhomogeneous chord planes (of variable rigidity), only coefficients of the differential equation will vary from place to place.

From the aspects of statics, the chord planes are characterized by strain and shear rigidities against deformations in their plane, as defined in the reference system xy by the matrix relationship

$$\begin{bmatrix} n_x \\ n_y \\ n_{xy} \end{bmatrix} = \begin{bmatrix} A_{11} & A_{12} & A_{13} \\ A_{21} & A_{22} & A_{23} \\ A_{31} & A_{32} & A_{33} \end{bmatrix} \begin{bmatrix} \varepsilon_x \\ \varepsilon_y \\ \gamma_{xy} \end{bmatrix} \tag{1a}$$

or briefly

$$\mathbf{n} = \mathbf{A}\boldsymbol{\epsilon} \tag{1b}$$

where $\mathbf{n}$ is the vector of the internal (membrane) forces of the chord plane, $\boldsymbol{\epsilon}$ is the deformation vector, and $\mathbf{A}$ is the rigidity matrix, this latter always being symmetric in virtue of the theorem of virtual work.

In what follows, subscripts l and u will refer to lower and upper chord planes, respectively.

3. Description of the method

Let us divide the rigidity matrix of e.g. the upper chord plane:

$$\mathbf{A}^u = \mathbf{A}^u_{\mathrm{I}} + \mathbf{A}^u_{\mathrm{II}} . \tag{2}$$

The part $\mathbf{A}_{\mathrm{I}}^{u}$ is so chosen that its elements are k times the rigidities of the lower chord plane:

$$\mathbf{A}_{\mathrm{I}}^{u} = k \cdot \mathbf{A}^{l} . \tag{3}$$

Thereby the "differential" rigidity matrix $\mathbf{A}_{\mathrm{II}}^{u}$ represents, in fact, the qualitative differences between the upper and the lower chord plane rigidities.

The entire force system and deformation of the structure will also be divided into two parts. Part 1 will consist of the pure flexural deformation

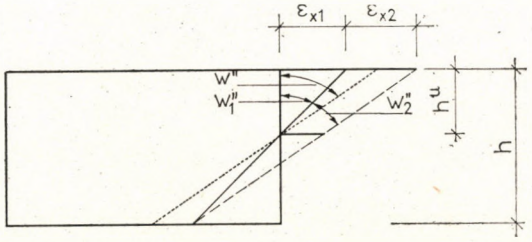

Fig. 2

w_1 and related internal forces of the lower chord plane of rigidity $\mathbf{A}^{l}$ and of the upper one of proportional rigidity $\mathbf{A}_{\mathrm{I}}^{u}$. Among these, the internal forces of the lower chord plane assume their final value. In the upper chord plane, however, deformations $\epsilon_{\mathrm{I}}^{u}$ due to flexural deformation w_1 produce internal forces corresponding to rigidity $\mathbf{A}_{\mathrm{II}}^{u}$ too, rather than only those corresponding to $\mathbf{A}_{\mathrm{I}}^{u}$. In general, however, these do not constitute an equilibrium force system in themselves. Hence, the upper chord plane is compelled into an accessory plane deformation (subscript 2) resulting in internal forces to offset the unbalanced forces in the bending part 1 of deformation (subscript 1). Of course, this accessory deformation must be a compatible one.

Naturally, these two parts of the force system cannot be determined separately, but only together, since none of them is an equilibrium force system in itself.

The plane deformation of the upper chord plane 2 produces no plane deformation of the lower chord plane (namely earlier it was assumed that the connecting diagonals do not counteract deformations of either chord plane), but the entire structure undergoes further bending deformation (w_2 in Fig. 2). The corresponding bending moments (together with the moments of the unbalanced forces of deformation part 1) are the corresponding membrane forces of the upper chord plane multiplied by their distance h^u from the neutral line (4). These moments, however, carry no vertical load, since they are due to a force system in equilibrium, hence, also the righthand side of the plate equation containing these moments will be zero.

4. Basic equations

In conformity with the decomposition of deformation and force systems into two parts: 1 and 2, these will be characterized by the bending deflection function w_1, and by the stress function Φ defining the accessory plane force system, respectively.

Since the deflection function w_1 ensures compatibility of related deformations, w_1 has only to meet the plate equation expressing equilibrium. Stress function Φ ensures the equilibrium of plane forces defined by the same, thus, it has to meet the compatibility equation. Thereby two simultaneous differential equations will be established.

For part 1 of the force system (bending) it is expedient to define the bending rigidity matrix $\mathbf{B}$ of the space truss. This is equal to the moment of inertia of chord rigidity matrices $\mathbf{A}^l$ and $\mathbf{A}_1^u$, having a ratio k to each other, referred to their common gravity line at a depth:

$$h^u = h \frac{1}{1+k} . \tag{4}$$

Thus, the matrix of bending rigidity:

$$\mathbf{B} = h^2 \frac{k}{1+k} \mathbf{A}^l \tag{5}$$

relating the second derivatives of the bending deformation w_1 i.e. curvatures and (double) twist, to the specific moments affecting the entire space truss:

$$\begin{bmatrix} m_x \\ m_y \\ m_{xy} \end{bmatrix} = - \begin{bmatrix} B_{11} & B_{12} & B_{13} \\ B_{21} & B_{22} & B_{23} \\ B_{31} & B_{32} & B_{33} \end{bmatrix} \begin{bmatrix} w_1'' \\ w_1^{\cdot\cdot} \\ 2w_1'^{\cdot} \end{bmatrix}, \tag{6a}$$

(superscripts $'$ and $\cdot$ indicating differentiations with respect to x and y, respectively), hence:

$$\mathbf{m} = - \mathbf{B} \cdot L_1 \, w_1 , \tag{6b}$$

L_1 denoting the following differential operator:

$$L_1 = \begin{bmatrix} \dfrac{\partial^2}{\partial x^2} \\ \dfrac{\partial^2}{\partial y^2} \\ 2 \dfrac{\partial^2}{\partial x \, \partial y} \end{bmatrix} . \tag{7}$$

Now, the known differential equation of plate equilibrium [6]:

$$m_x'' + m_y'' + 2\, m_{xy}'' = -p \tag{8a}$$

can be simplified into:

$$L_1^* \mathbf{m} = -p\,. \tag{8b}$$

Substituting here (6b) we obtain the differential equation of bending deformation w_1 in case of a plate of general anisotropy:

$$L_1^*\ \mathbf{B}\ L_1 w_1 = p. \tag{9}$$

For the analysis of the complementary plane deformation, i.e. part 2 of the force system, it has to be considered that the force system

$$\mathbf{n}_2 = \begin{bmatrix} n_{x2} \\ n_{y2} \\ n_{yx2} \end{bmatrix} = \mathbf{A}^u \cdot \boldsymbol{\epsilon}_2 \tag{10}$$

resulting from the accessory plane deformation of the upper chord plane

$$\boldsymbol{\epsilon}_2 = \begin{bmatrix} \varepsilon_{x2} \\ \varepsilon_{y2} \\ \gamma_{xy2} \end{bmatrix} \tag{11}$$

will not be in equilibrium in itself, but only together with the unbalanced part $\mathbf{n}_{1\,II}$ of forces due to (bending) deformation 1. According to what has been stated before, these unbalanced forces $\mathbf{n}_{1\,II}$ may be obtained by multiplying tensile deformations of the upper chord plane due to bending deformation w_1 ([3], Fig. 2)

$$\boldsymbol{\epsilon}_1 = \begin{bmatrix} \varepsilon_{x1} \\ \varepsilon_{y1} \\ \gamma_{xy1} \end{bmatrix} = h^u L_1 w_1 \tag{12}$$

by the corresponding elements of differential rigidity matrix $\mathbf{A}_{II}^u$:

$$\mathbf{n}_{1\,II} = \begin{bmatrix} n_{x1\ II} \\ n_{y1\ II} \\ n_{xy1\ II} \end{bmatrix} = \mathbf{A}_{II}^u \cdot \boldsymbol{\epsilon}_1\,. \tag{13}$$

Thus, stress function Φ has to be so chosen as to provide equilibrium of the sum of forces $n_{1\,II}$ and n_2, i.e.:

$$\begin{aligned} \Phi'' &= n_{x1\,II} + n_{x2}\,, \\ \Phi'' &= n_{y1\,II} + n_{y2}\,, \\ -\Phi'' &= n_{xy1\,II} + n_{xy2}\,, \end{aligned} \tag{14a—c}$$

or introducing differential operator

$$L_2 = \begin{bmatrix} \dfrac{\partial^2}{\partial y^2} \\ \dfrac{\partial^2}{\partial x^2} \\ -\dfrac{\partial^2}{\partial x\,\partial y} \end{bmatrix}^{:} \tag{15}$$

$$L_2 \Phi = \mathbf{n}_{1\,II} + \mathbf{n}_2\,, \tag{16}$$

Let us now see the compatibility equation of plane deformation, of the known form [5]:

$$L_2^* \boldsymbol{\epsilon} = \varepsilon_x'' + \varepsilon_y'' - \gamma_{xy}'' = 0\,. \tag{17}$$

In principle, only complementary deformation $\boldsymbol{\epsilon}_2$ is required to meet compatibility equation (17), deformation $\boldsymbol{\epsilon}_1$ due to w_1 (12) being compatible anyhow. Nevertheless, from Eqs (14) and (16) it appears that ε_2 cannot be expressed by Φ alone, namely Φ includes part of forces due to deformation $\boldsymbol{\epsilon}_1$. Hence, Eq. (16) will be completed by forces $\mathbf{n}_{1I}$ from part 1 of the force system, and the compatibility will be written for the entire deformation (1 + 2).

In fact, these missing forces $\mathbf{n}_{1I}$ equal chord forces resulting from bending:

$$\mathbf{n}_{1I} = -\,\mathbf{m}/h, \tag{18a}$$

i.e. from (6b):

$$\mathbf{n}_{1\,I} = \frac{1}{h}\,\mathbf{B} \cdot L_1\, w_1\,. \tag{18b}$$

Thus, the complete force system in the upper chord plane, also taking (16) into consideration, is:

$$\mathbf{n}_{1\,I} + \mathbf{n}_{1\,II} + \mathbf{n}_2 = \frac{1}{h}\,\mathbf{B}\, L_1\, w_1 + \mathbf{L}_2\, \Phi. \tag{19}$$

The corresponding total strain $\boldsymbol{\epsilon}_1 + \boldsymbol{\epsilon}_2$ is obtained by inverting Eqs (1):

$$\boldsymbol{\epsilon}_1 + \boldsymbol{\epsilon}_2 = (\mathbf{A}^u)^{-1} \cdot (\mathbf{n}_{1\,I} + \mathbf{n}_{1\,II} + \mathbf{n}_2) = (\mathbf{A}^u)^{-1} \left(\frac{1}{h}\,\mathbf{B}\, L_1\, w_1 + L_2\, \Phi \right), \tag{20}$$

which substituted into (17) delivers the other differential equation describing the force system in the space truss:

$$L_2^*\, (\mathbf{A}^u)^{-1} \left(\frac{1}{h}\,\mathbf{B}\, L_1\, w_1 + L_2\, \Phi \right) = 0. \tag{21}$$

The system of Eqs (9) and (21) — together with the boundary conditions — defines functions w_1 and Φ, hence, the entire force system. Boundary condi-

tions, are, however, given for the entire deflection w rather than for w_1 alone. Hence, equations are to be rewritten so as to contain w rather than w_1. This total deflection w is the sum of deflection w_1 due to part 1 of the (bending) force system and w_2 due to accessory plane deformation 2:

$$w = w_1 + w_2. \tag{22}$$

Since the lower chord plane remains unaffected by deformation 2, deflection w_2 may be expressed by strain ϵ_2 according to Fig. 2:

$$\begin{aligned} w_2'' &= \frac{\varepsilon_{x2}}{h}, \\ w_2'' &= \frac{\varepsilon_{y2}}{h}, \\ 2w_2' &= \frac{\gamma_{xy2}}{h}, \end{aligned} \tag{23a}$$

that is,

$$L_1 w_2 = \frac{1}{h}\epsilon_2. \tag{23b}$$

(22) is used to express $L_1 w_1$ in Eqs (9) and (21) by w and ϵ_2:

$$L_1 w_1 = L_1 w - \frac{1}{h}\epsilon_2. \tag{24}$$

Now, ϵ_2 has to be expressed by Φ and w. Both sides of Eq. (20) are multiplied by $\mathbf{A}^u$, then ϵ_1 will be expressed by w_1 making use of (12), w_1 by w and ϵ_2 on the basis of (24). Thus, the equation will include, beside ϵ_2, only functions w and Φ, lending themselves to express ϵ_2:

$$\mathbf{A}^u\left[h^u\left(L_1 w - \frac{1}{h}\epsilon_2\right) + \epsilon_2\right] = \frac{1}{h}\mathbf{B}\left(L_1 w - \frac{1}{h}\epsilon_2\right) + L_2\Phi. \tag{25}$$

Rearranging and taking into consideration the identity based on (5):

$$\frac{h - h^u}{h}\mathbf{A}^u + \frac{1}{h^2}\mathbf{B} = \frac{k}{1+k}(\mathbf{A}^u + \mathbf{A}^l)$$

ϵ_2 will be expressed as:

$$\epsilon_2 = h L_1 w + \frac{1+k}{k}(\mathbf{A}^u + \mathbf{A}^l)^{-1}(L_2\Phi - h\mathbf{A}^u L_1 w), \tag{26}$$

which, when substituted into (24), yields $L_1 w_1$ expressed by w and Φ:

$$L_1 w_1 = \frac{1}{h}\,\frac{1+k}{k}(\mathbf{A}^u + \mathbf{A}^l)^{-1}(h\mathbf{A}^u L_1 w - L_2\Phi). \tag{27}$$

Substituting (27) into (9) and (21) [and, for the sake of uniformity, expressing $\mathbf{B}$ by $\mathbf{A}^l$ according to (5)] yields the system of differential equations containing the total deflection w and the stress function Φ:

$$hL_1^* \mathbf{A}^l (\mathbf{A}^u + \mathbf{A}^l)^{-1} (h \mathbf{A}^u L_1 w - L_2 \Phi) = p, \tag{28a}$$

$$L_2^* (\mathbf{A}^u)^{-1} [\mathbf{A}^l (\mathbf{A}^u + \mathbf{A}^l)^{-1} (h \mathbf{A}^u L_1 w - L_2 \Phi) + L_2 \Phi] = 0. \tag{28b}$$

Thus, (28a, b) may be considered as the system of continuum differential equations describing the behaviour of the general double-layer space truss.

Proportionality factor k vanishes from the system of differential equations, hence, k can be assumed arbitrarily.

Of course, Eqs (28a, b) assume invertibility of matrices $\mathbf{A}^u$ and $(\mathbf{A}^u + \mathbf{A}^l)$. In a subsequent paper, cases not meeting this condition will be considered.

In the special case where rigidities of the two chord planes are proportional ($\mathbf{A}^u = k\mathbf{A}^l$) then, because of

$$\mathbf{A}^l (\mathbf{A}^u + \mathbf{A}^l)^{-1} = \frac{1}{1+k} \mathbf{E} \quad \text{and} \quad (\mathbf{A}^u)^{-1} \mathbf{A}^u = \mathbf{E}, \tag{28a}$$

(28a) and (28b) contain the products of operators $L_1 L_2$ multiplied by Φ and w, respectively, zero in outcome. Hence, equation system (28a, b) is composed of two independent equations: the first one determines deflection w of the plate with the bending rigidity matrix

$$\mathbf{B} = h^2 \frac{k}{1+k} \mathbf{A}^l$$

and the other provides for the deformational compatibility of the complementary stress function Φ, but in case of boundaries not affected by loads in the upper chord plane, $\Phi \equiv 0$.

Internal forces of the substituting continuum obtained by solving Eqs (28a, b), also taking boundary conditions into consideration, can be converted into bar forces according to [7], [2] or [3].

5. Boundary conditions

In what follows, equations of freely supported (hinged) boundary conditions will be written down, and for the sake of simplicity, only for the boundary parallel to the x axis:

zero deflection: $w = 0,$ (29a)

zero bending moment normal to the boundary: $m_y = 0,$ (29b)

zero horizontal (membrane) force normal to the boundary in the upper chord plane: $$n_y = n_{y1} + n_{y2} = 0, \tag{29c}$$

zero (membrane) shear force in the upper chord plane: $$n_{xy} = n_{xy1} + n_{xy2} = 0. \tag{29d}$$

Making use of (18a), (29b) yields $n_{y1\,I} = 0$, hence (29c) becomes, taking (14b) into consideration:

$$\Phi'' = 0. \tag{29c*}$$

The moment needed for (29b) can be expressed by w and Φ by substituting (27) into (6b). Taking also (5) into consideration, we obtain

$$\mathbf{m} = -h\ \mathbf{A}^l(\mathbf{A}^u + \mathbf{A}^l)^{-1}(h\mathbf{A}^u\ L_1\ w - L_2\Phi). \tag{29b*}$$

The component of this moment vector normal to the boundary (in this case m_y) has to be zeroed.

Finally, the internal force vector $\mathbf{n}_{1I}$ needed for (29d) can be written in the form

$$\mathbf{n}_{1\,I} = \frac{hk}{1+k}\,\mathbf{A}^l L_1\, w_1$$

making use of (18b) and (5). Substituting (27), $\mathbf{n}_{1I}$ can be expressed by w and Φ as:

$$\mathbf{n}_{1I} = \mathbf{A}^l(\mathbf{A}^u + \mathbf{A}^l)^{-1}(h\mathbf{A}^u\, L_1\, w - L_2\,\Phi). \tag{29d*}$$

Boundary condition (29d) can be written by taking the component n_{xy1I}, and adding $-\Phi''$ in conformity with (14c).

6. Application

Let us write down continuum differential equations of the space truss with identical rigidity characteristics in directions x and y, Fig. 1, by means of general equations (29a, b).

This space truss is characterized by the rigidity matrix of the lower chord plane taking the form:

$$\mathbf{A}^l = \begin{bmatrix} A_l & 0 & 0 \\ 0 & A_l & 0 \\ 0 & 0 & 0 \end{bmatrix}$$

and of the upper chord plane (see in [2]):

$$\mathbf{A}^u = \begin{bmatrix} A & \nu A & 0 \\ \nu A & A & 0 \\ 0 & 0 & A_{xy} \end{bmatrix}$$

According to (3):

$$k = \frac{A}{A_l} .$$

Establish now matrices $(\mathbf{A}^u)^{-1}$ and $(\mathbf{A}^u + \mathbf{A}^l)^{-1}$:

$$(\mathbf{A}^u)^{-1} = \begin{bmatrix} \frac{1}{A(1-\nu^2)} & \frac{-\nu}{A(1-\nu^2)} & 0 \\ \frac{-\nu}{A(1-\nu^2)} & \frac{1}{A(1-\nu^2)} & 0 \\ 0 & 0 & \frac{1}{A_{xy}} \end{bmatrix} .$$

$$\mathbf{A}^u+\mathbf{A}^l)^{-1} = \begin{bmatrix} \frac{(A_l+A)}{(A_l+A)^2-\nu^2 A^2} & \frac{-\nu A}{(A_l+A)^2-\nu^2 A^2} & 0 \\ \frac{-\nu A}{(A_l+A)^2-\nu^2 A^2} & \frac{(A_l+A)}{(A_l+A)^2-\nu^2 A^2} & 0 \\ 0 & 0 & \frac{1}{A_{xy}} \end{bmatrix} .$$

After the indicated operations, Eqs (28a, b) become:

$$\frac{h}{(1+k)^2-k^2\nu^2}\{h\,k\,A_l[(1+k-k\nu^2)\,w^{IV}+2\nu\,w'''+(1+k-k\nu)\,w''] + \\ + [k\nu\,(\Phi^{IV}+\Phi'') - 2(1+k)\,\Phi''']\} = p,$$

$$\frac{h}{(1+k)^2-k^2\nu^2}[-k(w^{IV}+w'')+2(1+k)\,w'''] - \\ - \frac{1}{[(1+k)^2-k^2\nu^2]\,k(1-\nu^2)A_l}\{[1+k(1+\nu^2)]\,(\Phi^{IV}+\Phi'') - \\ - 2\nu\,(1+2k)\,\Phi'''\} + \frac{1}{k(1-\nu^2)\,A_l}(\Phi^{IV}+\Phi''-2\nu\Phi''') + \frac{\Phi'''}{A_{xy}} = 0.$$

Neglecting the transverse contraction of the upper chord plane ($\nu = 0$), these equations simplify into:

$$h^2\frac{k}{1+k}A_l\left(w^{IV}+w''-\frac{2\Phi'''}{hkA_l}\right) = p$$

and

$$\frac{2h}{1+k}w''' + \frac{1}{(1+k)A_l}(\Phi^{IV}+\Phi'') + \frac{\Phi'''}{A_{xy}} = 0 .$$

For $\nu = 0$ and freely supported edges, boundary conditions are simply:

$$w = 0, \tag{29a}$$

$$\Phi'' = 0, \tag{29c*}$$

Boundary condition (29b*) would be

$$h\ A\ w'' - \Phi'' = 0$$

but because of (29c*) it can be further simplified to

$$w'' = 0, \tag{29b*}$$

and finally (since element 33 of $\mathbf{A}_{\mathrm{I}}^{u} = k\mathbf{A}^{l}$ is zero) $n_{xy11} = 0$, thus (29d) becomes:

$$\Phi'' = 0. \tag{29d}$$

Notice, however, that neglect of the transverse contraction anyhow involves an approximation, since according to [2], no chord plane mesh with two-way tensile and shear rigidities, of exactly zero transverse contraction coefficient, exists.

REFERENCES

1. Giencke, E.: Die Grundgleichungen für die orthotrope Platte mit exzentrischen Steifen. *Der Stahlbau* **24** (1955), 128—129
2. Hegedüs, I.: Analysis of Meshes with Bars in Four or More Directions by Means of the Continuous Computational Model. (In press)
3. Kollár, L.—Hegedüs, I.: Solution of Double-Layer Space Trusses of General Triangular Grid by the Equivalent Continuum Model. *Acta. Techn. Hung.* **74** (1972), 363—381
4. Kollár, L.: Analysis of Double-Layer Space Trusses with Diagonally Square Mesh by the Continuum Method. *Acta. Techn. Hung.* **74** (1972), 521—540
5. Timoshenko, S.—Goodier, J. N.: Theory of Elasticity, Second Edition. McGraw-Hill, New York—Toronto—London 1951
6. Timoshenko, S.—Woinowski-Krieger, S.: Theory of Plates and Shells. McGraw-Hill, New York—Toronto—London 1959
7. Wright, D. T.: A Continuum Analysis for Double-Layer Space Frame Shells. *Publ. Int. Assoc. Bridge Struct. Eng.* Zurich, **26** (1966)

Berechnung zweischichtiger Raumfachwerke mit unteren und oberen Gurtebenen von verschiedenen Steifigkeiten mit dem Kontinuumverfahren. Ein allgemeines Verfahren wird angegeben für die Bestimmung des gleichwertigen Kontinuums von zweischichtigen Raumfachwerken, deren beiden Gurtebenen aus unterschiedlichen, beliebigen Netzwerken bestehen. Differentialgleichungssystem und Randbedingungen des gleichwertigen Kontinuums werden abgeleitet. Außer der Durchbiegungsfunktion, die die Plattenverformung beschreibt, ist noch eine Spannungsfunktion nötig für die Kennzeichnung des Kräftespiels des Ersatzkontinuums, ähnlich dem Fall der Rippenplatten.

Расчет двухслоный пространственных ферм различной жесткости, имеющих верхнюю и нижнюю плоскости пояса. В работе излагается общий метод определения эквивалентного континуума двухслойных пространственных ферм, у которых две плоскости пояса состоят из любых, различающихся друг от друга сетей. Выводится система дифференциальных уравнений и краевые условия эквивалентного континуума. Определяется, что кроме функции изгиба, характеризующей деформацию плит, необходима и функция напряжений — для характеристики работы замещающего континуума подобно случаю ребристых плит.

Acta Technica Academiae Scientiarum Hungaricae, Tomus 76 (1—2), pp. 65—85 (1974)

A CAPACITIVE DISCHARGE METHOD FOR DETERMINING GAS IMPURITIES QUANTITATIVELY

J. F. BITÓ*
DOCTOR OF TECHN. SC.

and

K. G. ANTAL**

[Manuscript received: 20th Dec. 1971]

An original statistical model allowing theoretical determination of the critical breakdown field strength is presented. The applicability of the method is shown for argon. A good agreement has been found between the values of the critical breakdown field strength calculated by means of the proposed model and obtained experimentally. The revealed microphysical relationships lead to a quick quantitative method of gas analysis. By showing the possibilities of improving the model underlying theoretical considerations the importance of further information available is emphasized in this way.

Introduction

In manufacturing fluorescent lamps, a number of different gases impairing discharge parameters and regarded as impurities are released or retained during certain operations of vacuum technology. Thus, for example, liberation of air can be expected as a result of an inefficient pumping and that of CO_2 and CO with a decomposition of the oxide cathodes. A very important degrading may be caused by these residual gases and vapours in argon as filling gas at a pressure of 2,5 mm of mercury even with a partial pressure of the order of 10^{-4} mm Hg, so that a quick indication and location of impurity sources in the mass production of fluorescent lamps are justified. A satisfactory solution by available gas analysis methods such as mass spectrography, for example, is impossible because of the lengthiness of measurements and the fact that an accurate fault location would require the breaking up of a large number of lamps, increasing the costs of an analysis extremely. Thus, a discharge method of determining impurities by non-destructing measurements on the lamps was urgently required. However, an analysis of the main discharge between the two oxide cathodes failed to furnish the desired results because of the large number of factors involved. Thus arose the idea of using a capacitive discharge between two clamps placed externally on the glass tube of the lamp to detect low-concentration impurities. This, in turn, required an

* Dr. J. F. Bitó, Korompai u. 22/a, 1124 Budapest, Hungary
** K. G. Antal, Vécsey ltp. 4, 1204 Budapest, Hungary

elaborate theoretical and experimental study of alternating-current capacitive discharges.

A survey and systematization of the literature on available discharge criteria and the processes introducing a discharge [1, 2] have shown that no breakdown criterion based on experimental results in the pressure range and at the frequencies of interest is available.

It was decided to develop a statistical model for argon gas at pressures in the order of a few millimetres of mercury at a frequency of 50 Hz which could readily be generalized to include other inert gases and allowing a study of breakdown phenomena as well as to interpret the relationship between measurable parameters of a capacitive discharge and microparameters of the operating gas and, after having cleared up these phenomena to such an extent to develop a gas analysing method that could be used for industrial purposes. In the following, an account of the theoretical and experimental results obtained and of the method developed on this basis as well as its applicability will be given. To allow a good grasp of the situation, the summary of these results which follows here is restricted to the case of a fluorescent lamp.

1. Low-frequency breakdown criterion for argon gas

By using the microcharacteristics of the gas, the external dimensions of the discharge tube and the characteristics of the applied field, the domain to be analysed here can be characterized by the inequalities

$$\lambda < d, r; \omega < \nu; \omega u_d/d \tag{1}$$

where

λ — free mean path of an electron; r and d characteristic dimensions of the discharge tube (length and radius);
ω — frequency of the applied field;
ν — frequency of the collisions between electrons and neutral gas atoms;
u_d — electron drift velocity.

(For a more detailed classification of discharge conditions see [1—2]). In this case, breakdown criteria in [3—7] are generally based on a corpuscle balance by analogy with Townsend's model, primary and secondary ionisation coefficients being characterized by α and γ as calculated for direct current or determined experimentally.

In the case of a capacitive discharge in a discharge vessel having insulating walls as investigated by the authors, very small values of γ can be assumed but this secondary emission coefficient γ varies considerably from one point to another according to the state of the particular elementary surfaces, so that it would be difficult to substitute a proper value—computed or measured —for γ_{eff} in the breakdown criterion based on a corpuscule balance.

Instead, a spatial electron multiplication is intended to be taken into account by using the energetic conception [1, 2] although it the importance of the part played by wall processes in establishing a discharge is realized. As a matter of fact, the breakdown criterion has been stated with the restriction that the mean energy characterizing a particular electron or electron cloud should attain the ionization energy of a neutral atom in the operating gas, which, apparently, would involve a neglection of the secondary phenomena although they have been taken into account indirectly as a necessary condition for the secondary processes to take place.

The breakdown criterion based upon the energetic conception has the nature of a lower limit alone, in the way in which it has been defined. However, this is only an apparent disadvantage over the breakdown criteria based upon the particle balance which in principle includes a necessary and sufficient condition for a breakdown to take place.

In this connection, an equal or even larger error may be made in both directions in determining the critical breakdown voltage (or field intensity) when the coefficients α and γ characterizing a spatial ionization and secondary emission, respectively, are taken into account with an non-adequate accuracy.

With these remarks in mind, a breakdown criterion for the investigated case has been formulated as follows.

A discharge begins when the kinetic energy of the charged particles initially present in the discharge space as averaged over a half cycle of the applied field attains the energy which is necessary to ionize the operating gas.

In developing the breakdown criterion presented here, a statistical description has been chosen.

In order to determine mean thermal (random) and oriented (drift) velocity components of electrons for the one-dimensional case, a Maxwell—Boltzmann equation including a perturbation caused only by the applied electric field (H = 0) will be used,

$$\begin{aligned} &\frac{\partial f_0}{\partial t} + \frac{v}{3} \cdot \frac{\partial f_1}{\partial x} + \frac{e\,E}{3mv^2} \cdot \frac{\partial}{\partial v}(v^2 f_1) + S_0 = 0 \\ &\frac{\partial f_1}{\partial t} + v\frac{\partial f_0}{\partial x} + \frac{e\,E}{m} \cdot \frac{\partial f_0}{\partial v} + S_1 = 0 \end{aligned} \tag{2}$$

where

f_0 — symmetric component without perturbation of the distribution function;
f_1 — asymmetric component with a perturbation of the distribution function, taken as a first approximation;
x — co-ordinate in the direction of the field;
v — electron velocity;
m — electron mass;
e — electron charge;
E — applied electric field;
S_0 — zeroth moment of the collision integral;
S_1 — first moment of the collision integral.

(For a detailed derivation of Eqs (2) see [1] and [2]).

The moments of the breakdown integral will be taken into account in the form

$$S_0 = -\frac{1}{v^2} \cdot \frac{\partial}{\partial v}\left[\frac{v^3}{m} \cdot \frac{k\,T_g}{\lambda(v)} \cdot \frac{\partial f_0}{\partial v} + \frac{v^4 f_0}{\lambda(v)}\right] \tag{3}$$

and

$$S_1 = \frac{v}{\lambda(v)} f_0 \tag{4}$$

developed by DAVIDOV [20],

where k — Boltzmann constant;
T_g — temperature of the gas;
$\lambda(v)$ — free mean path of an electron.

Thus, a system of simultaneous equations serving to determine the distribution function

$$f(v) = f_0 + \frac{u_d}{v} f_1 \tag{5}$$

can be written down in a final form as:

$$\frac{\partial f_0}{\partial t} + \frac{v}{3} \cdot \frac{\partial}{\partial x} f_1 + \frac{1}{3} \cdot \frac{e}{m} E \frac{1}{v^2} \cdot \frac{\partial}{\partial v}(v^2 f_1) - \\ - \frac{1}{v^2} \cdot \frac{\partial}{\partial v}\left[\frac{v^3\,k\,T_g}{m\,\lambda} \cdot \frac{\partial f_0}{\partial v} + \frac{v^4 f_0}{\lambda}\right] = 0 \tag{6}$$

and

$$\frac{\partial f_1}{\partial t} + v \frac{\partial}{\partial x} f_0 + \frac{e}{m} E \frac{\partial f_0}{\partial v} + \frac{v}{\lambda} f_1 = 0. \tag{7}$$

In Equations (3) and (4) expressing the moments of collision integral inelastic interactions have been disregarded. Taking these interactions into account in determining the distribution function makes an analysis extremely difficult, and a solution to the equation is to be found only by some numerical methods.

To determine the mean electron energy (temperature) an approximate method taking inelastic collisions into account is widely used [8, 9], this being based upon an analysis of the energy balance for electron cloud. The main point of the method lies in the fact that instead of determining a mean energy directly through a complicated distribution function the factors augmenting or reducing the energy of the electrons are expressed in the form of an energy balance based upon some physical considerations, and the mean random and drift velocities involved are given by means of a simpler distribution function allowing for inelastic interactions only. A simpler differential equation that includes the energy dependence of these mean values and collision cross-sec-

tions characterizing elastic collisions can be analysed more easily, and a good approximation is then attained in determining mean electron energy.

By using this method the elementary processes resulting in an energy gain (P) and energy loss (N) in the given case will now be investigated.

Processes leading to an energy gain:

An electron traversing a distance $dx = u_d\,dt$ in time dt in the applied field, E receives an average energy

$$P_1 = e\,E\,u_d\,dt \tag{8}$$

from this field, where u_d is the mean drift velocity of the electrons.

On the other hand, the energy that can be obtained during inelastic interactions with the excited atoms present in the field can be written as

$$P_2 = v_r\,n_a\,\sigma_a\,eU_a\,dt \tag{9}$$

where

n_a — concentration of the excited electrons;
v_r — mean random velocity of electrons;
σ_a — cross-section of an inelastic collision between an electron and an excited atom, resulting in an energy transfer;
U_a — potential corresponding to the mean energy of an excited atom.

Processes leading to an energy loss:

Energy loss occurs in the case of an elastic collision between an electron and a neutral gas atom. The energy loss in a collision is

$$\Delta K_e = -\frac{2m}{M}(K_e - K_g) = \Delta[e\,U_e] = -\frac{2m}{M}\,e(U_e - U_g) \tag{10a}$$

where

$K_{e,g}$ — kinetic energy of an electron and a gas atom, respectively;
$U_{e,g}$ — potential corresponding to kinetic energy.

The energy loss during dt is

$$N_1 = \Delta[e\,U_e]\frac{v_r}{\lambda}\,dt = -\frac{2m}{M}\,e\,(Ue - U_g)\,n_g\,\sigma\,v_r \tag{10b}$$

where

λ — free mean path of an electron with an energy eU_e;
n_g — concentration of gas atoms;
σ — elastic collision cross-section in the case of an electron energy of eU_e.

Finally, the energy loss caused by an inelastic collision can be written in the form of a sum yielding

$$N_2 = -\,v_r\,n_g\,e\sum_k \sigma_k\,U_k\,dt \tag{11}$$

where

σ_k — inelastic collision cross-section;
U_k — excitation and ionization potentials of the atoms.

Based on elementary processes leading to the above energy gain and loss, a balance equation to determine the electron mean energy can be written in the form

$$\frac{dU_e}{dt} = \frac{2}{3} E u_d - \frac{2}{3} v_r n_g \sigma \left[\frac{2m}{M} (U_e - U_g) + \sum_k \frac{\sigma_k}{\sigma} U_k - \frac{n_a}{n_g} \cdot \frac{\sigma_a}{\sigma} U_a \right] \tag{12}$$

where d/dt is the total differential, i.e.

$$\frac{d}{dt} = \frac{\partial}{\partial t} + u_d \frac{\partial}{\partial x} .$$

An energy balance written in such a general form is not only applicable to processes preceding a breakdown but can also be regarded as a useful basic equation in discharge physics [8, 9].

In the case to be analysed here Equations (6) and (7) will be used to determine u_d and v_r.

It should be noted in passing that, in the pressure range investigated, the ratio λ/d has a value [10]

$$\frac{\lambda}{d} \sim 10^{-2} < 1 .$$

In other words, when dimension d of the discharge vessel is regarded as a characteristic dimension, a good approximation is obtained by neglecting coordinate dependence both in Eq. (6) and (7) serving to determine the distribution function and in Eq. (12) characterizing the energy balance. Furthermore, time dependence can be expressed in the form exp $(-i\,\omega t)$ when the analysis is restricted to the period before discharge (immediately before breakdown, static fields due to a changing process of the walls need not to be taken into account).

Consequently, the simultaneous differential equations (2) to be used in determining the distribution function may be analysed in a stationary homogeneous case. A necessary condition for the given approximation to be applicable is given by the inequality [1, 2]

$$\frac{e^2 E^2}{m k T(\omega^2 + \nu^2)} \ll 1 \tag{13}$$

where T is the electron temperature.

In a low frequency case where $\omega < \nu$, a.c. field intensity E can be replaced by a d.c. effective value E_{eff} and by using the relationship

$$E_{\text{eff}}^{=2} = E_{\text{eff}}^{\sim 2} \frac{1}{1 + \dfrac{\omega^2}{\nu^2}}$$

with

$$k\,T \sim m\,v_r^2\,;$$

$$u_d = \frac{e\,E}{m\,\nu}$$

the criterion (13) limits the value of the "small" parameter u_d/v_r in the series expansion of the distribution function:

$$\frac{u_d}{v_r} < 1.$$

Previous experiments and an estimate of the corresponding parameter have shown that this condition is fulfilled in the case investigated here [10] so that

$$\frac{u_d}{v_r} \sim 10^{-2} < 1.$$

To solve the system of simultaneous equations in (6) and (7) a further, well-known approximation will be made [1, 2]. The symmetric component of the distribution function is assumed to be characterized by a Maxwell—Boltzmann distribution, so that the two associated equations become independent of each other and u_d can be computed directly from (7) and (8). After integration,

$$u_d = \frac{e}{m}\,\frac{E}{\bar{\nu} - i\omega} \tag{14}$$

where

$$\bar{\nu} = v_{\max}/\lambda(v_{\max})\,. \tag{15}$$

This value of $\bar{\nu}$ is obtained by considering $\lambda(v)$ to have a slow variation as compared to that of $\partial f_0/\partial v$ so that its value can be determined at a velocity $v_{\max}$ corresponding to the maximum value of this function. In Eq. (12), $v_{\max}$ is substituted for v_r as well and by averaging over a half cycle energy balance it can be written in a final form as follows [10]:

$$\begin{aligned} U_e = {} & \frac{4}{3\pi}\,E^2\,\frac{e}{m}\left[\frac{1}{\bar{\nu}\,\omega} + i\,\frac{1}{\bar{\nu}^2}\right] - \\ & - \frac{8}{3\pi}\sqrt{\frac{8}{\pi}}\sqrt{\frac{e}{m}}\cdot\frac{m}{M}\cdot\frac{U_e^{3/2}}{\lambda}\,[1+i] - \\ & - \frac{4}{3\pi}\sqrt{\frac{8}{\pi}}\sqrt{\frac{e}{m}}\cdot\frac{1}{\lambda}\cdot\frac{\sigma_k}{\sigma}\,U_k\,U_e^{1/2}\,[1+i] + \\ & + \frac{4}{3\pi}\sqrt{\frac{8}{\pi}}\sqrt{\frac{e}{m}}\cdot\frac{U_a}{\lambda}\cdot\frac{n_a}{n_g}\cdot\frac{\sigma_a}{\sigma}\,U_e^{1/2}\,[1+i]. \end{aligned} \tag{16}$$

In averaging along half a cycle a linear energy dependence of the cross-sections has been taken into account.

In Equation (16) potential U_e corresponding to a mean electron energy according to the breakdown criterion will be replaced by the ionization potential U_i of the neutral gas atoms and then real and imaginary parts separated to yield the following two equations [10]:

$$U_i = \frac{4}{3\pi} \cdot \frac{e}{m} \cdot \frac{1}{\bar{\nu}\,\omega} E^2 - \frac{8}{3\pi} \sqrt{\frac{8}{\pi}} \sqrt{\frac{e}{m}} \cdot \frac{1}{\lambda} \times \\ \times \left[\frac{m}{M} U_i^{3/2} + \frac{\sigma_k U_k U_i^{1/2}}{\sigma} - \frac{n_a}{n_g} \cdot \frac{\sigma_a}{\sigma} U_a U_i^{1/2} \right] \tag{17}$$

and

$$0 = \frac{4}{3\pi} \cdot \frac{e}{m} \cdot \frac{1}{\bar{\nu}^2} E^2 - \frac{8}{3\pi} \sqrt{\frac{8}{\pi}} \sqrt{\frac{e}{m}} \cdot \frac{1}{\lambda} \times \\ \times \left[\frac{m}{M} U_i^{3/2} + \frac{\sigma_k U_k U_i^{1/2}}{\sigma} - \frac{n_a}{n_g} \cdot \frac{\sigma_a}{\sigma} U_a U_i^{1/2} \right]. \tag{18}$$

An inspection of the equations obtained from the real part (17) and imaginary part (18) shows that Eq. (18) does not include the frequency of the applied field causing a perturbation so that Eq. (17) alone has a physical reality. With the specific argon gas parameters substituted, it can be seen that the highest energy losses are caused by inelastic collisions, which is obvious since ionization cross-section in the vicinity of the ionization threshold is very small. On the other hand, of the processes resulting in energy gains, the energy gained from the excited atoms is very small as compared to the energy obtained from the field. With the corresponding parameters substituted, Eq. (17) yields a critical breakdown field intensity of 66 V/cm for 2,5 mm Hg as a final result.

The theoretical value of the critical breakdown field strength obtained above for a lower limit shows a good agreement within 5 per cent with that obtained experimentally for the given gas pressure (Fig. 2). However, this occurred near the minimum of $E = f(p\,d)$. Since the proposed model has been developed with considerable simplifications in order to make an analysis possible, it is thought that a breakdown criterion the valability of which could be extended to a wider pressure range will be obtained by further improving this model (for example, by using larger time resolution instead of averaging over half a cycle).

2. Experimental conditions, methods, results

2.1 *Experimental conditions*

Experimental investigations relative to low frequency capacitive discharges with external electrodes were carried out by means of two different types of discharge vessels.

In support of the theoretical analysis, experiments have been carried out on a cylindrical quartz discharge tube having a simple geometry. Two copper clamps 25 mm wide and of 0,2 mm width spaced at a distance of 18 mm were used as external electrodes. The dimensions of the discharge vessel used in the latter experiments were the same as those of a standard 40-watt fluorescent lamp to allow a direct adaptability of the obtained results of measurements.

The internal walls of the quartz discharge vessel were degassed for 20 minutes at a final vacuum of 10^{-7} mm Hg before filling the vessel with the gas. On the other hand, heat treatment of the discharge tube having the same geometry as a fluorescent lamp, was made according to the prescription of fluorescent lamps.

Gas filling of the discharge tubes by freezing out with liquified air was accomplished with a special filling system [11] eliminating recontamination mechanisms and allowing at the same time the introduction of impurity gases at a pressure of about 10^{-4} mm Hg.

In experimental work, noble gases (A, Ne, He) of spectral purity and their mixtures with mercury at a pressure of 2×10^{-3} mm Hg were used as filling gases (at a wall temperature of 25°C).

2.2 *Experimental methods*

In these investigations, pressure was measured by means of a MÜ-81-type ionization vacuum meter, McLeod-type mercury vacuum meter and a MÜ-71-type vacuum meter, according to the pressure range and a mercury manometer was used for a more accurate determination of higher pressure values.

Typical current jumps in capacitive discharges were investigated in an arrangement shown schematically in Fig. 1 for both types of discharge vessels.

The voltage of a stabilized a. c. power supply STF type EKM-1834II with a high stabilization factor, connected to the 220 V mains through an insulating transformer Tr was applied through a toroidal coil to the primary of a high-voltage transformer. Because of the impedance of this high-voltage transformer, a Metrohm-type 10-kiloohm variable resistor P was inserted into the secondary circuit to allow, at the same time, an accurate control of the voltage on the electrodes, that is, on the clamps. This voltage applied to the electrodes *via* loading resistor R was indicated by a 0,2-class voltmeter V, which was replaced by the Y input of a TR-4602 type double-beam oscilloscope O when studying phase conditions of the current impulses within a half cycle. To measure the discharge current, input X of this oscilloscope was used to indicate the voltage drop across R. In order to obtain a proper signal level,

load resistor R was chosen of 0,5 megohms with regard to the system time constant.

A Brüel and Kjaer 2304 level recorder with integrating input I was used to registrate the electric charges accumulated on the walls during current jumps.

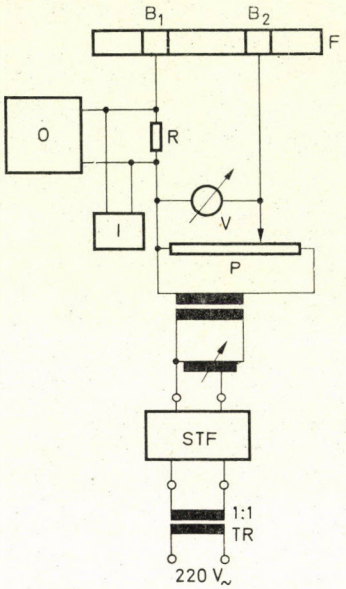

Fig. 1. Schematic diagram of the equipment to investigate capacitive discharges

2.3 *Results and their theoretical interpretation*

These experimental investigations were carried out with the double aim of producing experimental support for the theoretical results by means of a discharge tube having idealized geometry and of obtaining some results which could readily be used in practice by means of a discharge vessel having the geometry of a fluorescent lamp, characterizing the connection between microparameters of gas space and measurable voltage—ampere characteristics of a capacitive discharge system.

Since the special literature on capacitive discharges [13, 14] gives but a very incomplete survey of the pressure dependence of capacitive breakdown voltages (field intensities) in various noble gases it seemed to be a necessary step, as a beginning to investigate pressure dependence of critical field intensities (voltages) for argon, neon, and helium regarded as important rare gases, in our case in the pressure range from 10^{-1} to 50 mm Hg.

In addition to their importance in industry, these gases are of interest from a theoretical point of view since on the basis of the velocity dependence

of electron free mean paths they can be grouped in three basic classes being typical for other gases as well, by arranging them according to their increasing ionization potentials $\lambda_e \approx v^{-n}$ for argon, $\lambda_e \approx$ constant for neon and $\lambda_e \approx v$ for helium.

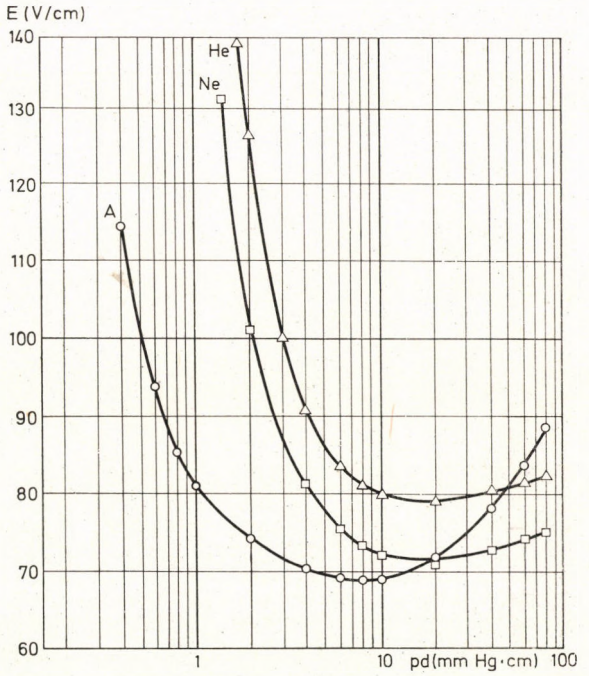

Fig. 2. pd dependence of critical breakdown field intensities for A, Ne and He

The functions $E = f(p\ d)$ obtained experimentally for these noble gases and their mixtures with mercury vapours at a pressure of 2×10^{-3} mm Hg are shown in Figs 2 and 3. The product of pressure times, distance was plotted on the horizontal axis on a logarithmic scale, while the vertical axis shows the critical field strength at which the first typical current jump of an a.c. capacitive discharge appears (Fig. 4). An inspection of these curves shows that for each of the three noble gases a minimum critical breakdown field intensity can be attained by varying pressure (or distance), and the same situation is found in a mixture with mercury vapours. Consequently, pressure dependence of breakdown field intensity in a capacitive discharge bears some resemblance in this sense to the Paschen curves for a direct current discharge. An inspection of the minimum value of these functions shows that in the order of increasing ionization potentials they are shifted toward a higher and higher field intensity both for pure noble gases and their mixtures with mercury vapour. Above a pressure of 10 mm Hg a very interesting steep increase in the

critical breakdown field intensity is experienced for argon without any explanation, by using the proposed theoretical model with the simplifications presented. As it was pointed out in the analysis of the theoretical model, it is thought that the validity of the proposed breakdown criterion that is based upon an analysis of the energy balance can be improved and extended to other

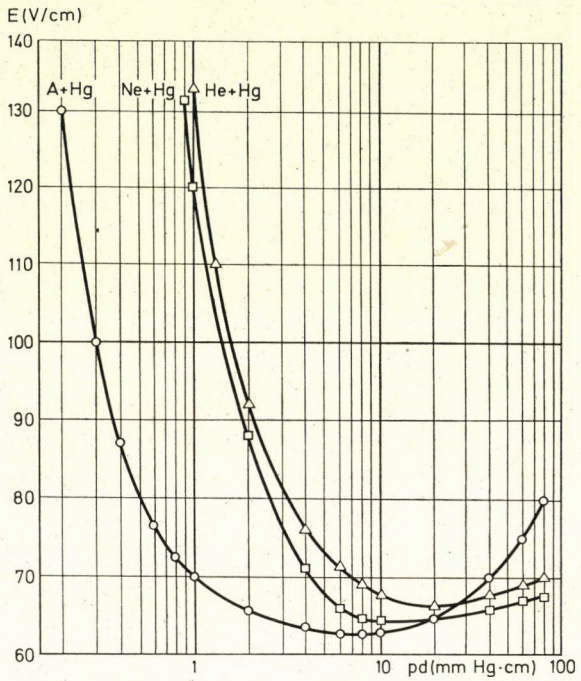

Fig. 3. pd dependence of critical breakdown field intensity for A, Ne, He in a mixture with mercury vapour at 2×10^{-3} mm Hg

noble gases by an appropriate consideration of experimental observations. As a first step in this direction, effort was made to adopt a theoretical method based upon the analysis of the structure of functional relationships between the physical quantities in the domain of discharge physics. The main point of this method lies in the fact that—by using the dimension theory—a functional relationship, accurate within a constant factor, can be obtained between the basic parameters determining the given physical phenomenon. A choice of these basic parameters can be made by reason of physical considerations or by the use of some parameters in the system of simultaneous equations describing the phenomenon. By using this method in [15], random and drift velocities well-known in the literature have been obtained for the three basic groups of velocity dependence of the free path lengths in a d.c. case without a series expansion of the Maxwell—Boltzmann equations as presented in the

discussion by using some approximate methods. Even in the case, however, when no system of equations is available, this is a very useful method for stating the extent to which the model or physical picture to be used to describe the phenomenon can be supported by functional relations experimentally determined. It is intended, among others, to try to evaluate the functions shown in Figs 2 and 3 by the method mentioned above.

Experimental observations made when introducing mercury vapours into noble gases revealed the possibility of an additional improvement of the model based upon an energy balance. In this case, an important decrease of the critical breakdown field intensity can be observed even at a mercury vapour pressure, very low as compared to the pressure of the operating gas (Fig. 2). Only a very slight variation in the calculated value of critical breakdown field strength occurs when free path lengths and ionization potentials characterizing the mixture of argon and mercury vapours are substituted in the balance equation, and energies which can be received from excited atoms are disregarded. As a matter of fact, mercury can be considered as an energy storing element in the field because of its metastable levels and, at the same time, an important part is played by photoionization. This latter assumption has been supported by spectral investigations of capacitive current pulses as well as the phenomena observed in the case when the discharge space has been exposed to a light source emitting an intensive spectrum line at 2537 Å.

To sum up, the functions $E_{cr} = f(p\ d)$ measured in a mixture of the investigated noble gases and mercury vapours in a wide pressure range and shown in Figs 2 and 3 can be interpreted by the use of the model based on a statistical analysis of the energy balance. On the other hand, additional methods are needed to obtain a proper pressure dependence along some sections, for example, at pressures higher than 10 mm of mercury.

Experiences gained in the course of the experimental investigations cleared up not only the information needed in industrial applications but also some ways leading to an improvement of the model outlined above.

Figures 4—12 show typical current jumps in a capacitive discharge and time variation of individual impulses. The model described here gives a correct picture only in the moment when the first current impulse appears (Figs 4 and 5) since charges are generated in the field and carried to the walls where they give rise to a retardant static field and thus the movement of a charged particle will now be determined both by the applied field intensity and this static field. A study of the initial phase of current jumps and impulse wave forms [16] led to the establishment of a direct relationship between microparameters of the operating gas and the measured volt-ampere characteristics of the capacitive discharge with the given geometry taken into account.

Time variation of a current impulse may be characterized by a simple "picture" allowing for the discharge geometry and gas microparameters.

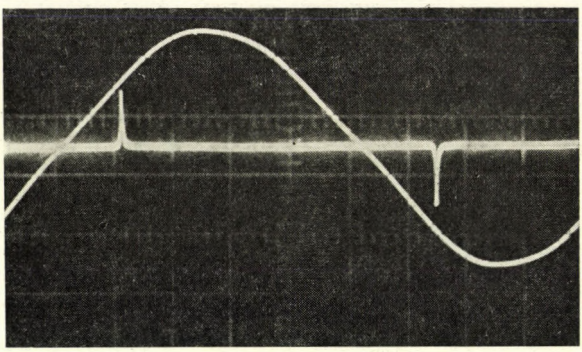

Fig. 4. A typical capacitive discharge oscillogram

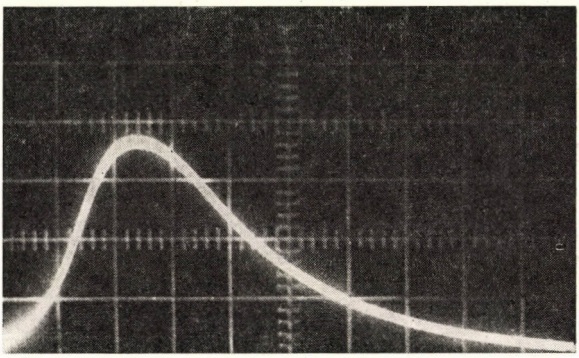

Fig. 5. Waveform of a capacitive current impulse

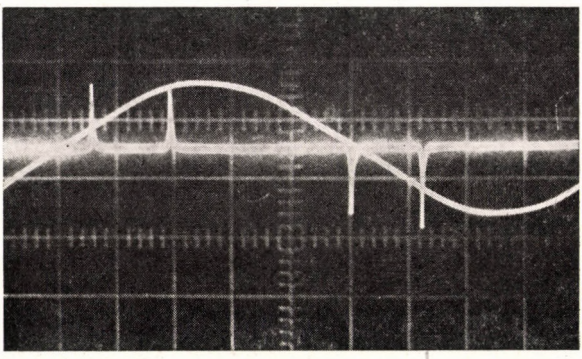

Fig. 6. A typical capacitive discharge oscillogram

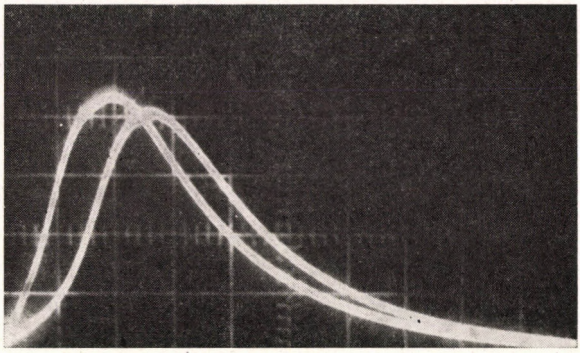

Fig. 7. Waveform of the capacitive current impulse

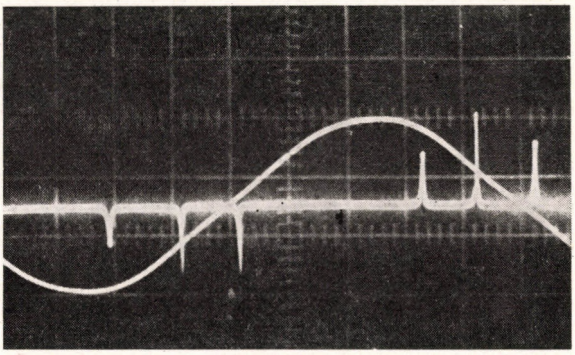

Fig. 8. Typical capacitive discharge oscillogram

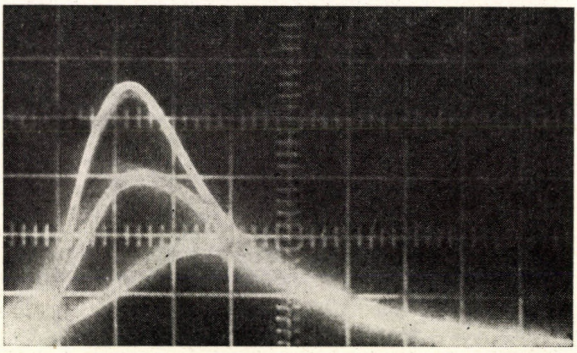

Fig. 9. Waveform of the capacitive current impulse

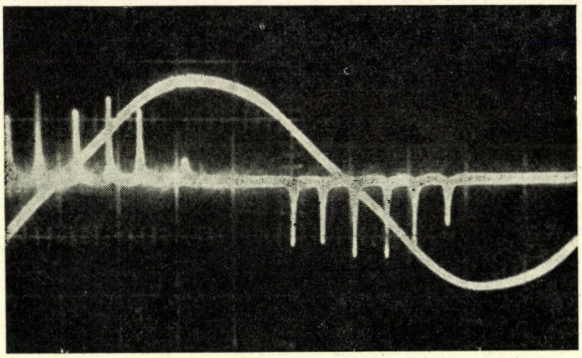

Fig. 10. Typical capacitive discharge oscillogram

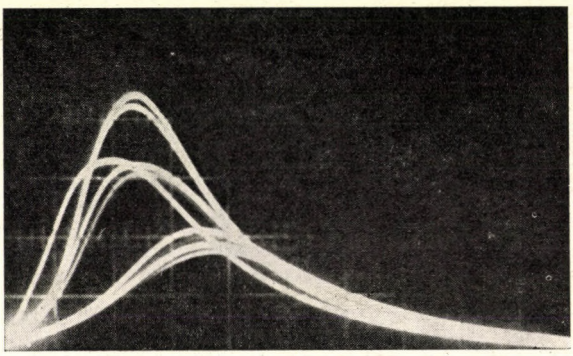

Fig. 11. Waveform of the capacitive current impulse

Figure No.	Beam X		Beam Y	
	Horizontal axis μs/cm	Vertical axis V/cm	Horizontal axis ms/cm	Vertical axis V/cm
4	2000	2	2	75
5	20	0,5	—	—
6	2000	5	2	150
7	20	0,5	—	—
8	2000	5	2	150
9	20	0,5	—	—
10	2000	5	2	150
11	20	0,5	—	—

Calibration table of the quadratic net for the oscillograms in Figs 4—11.

A discharge vessel can be regarded as three condensers connected in series giving a resultant capacity of

$$C_{er} = \frac{2C_F C_G}{2C_F + C_G} \tag{19}$$

where

C_F — capacity between the external electrode and the internal wall of the discharge vessel ($C_F \sim 100\,\mu\mu$F in the given case);
C_G — capacity of the gas space ($\sim 10\,\mu\mu$F).

Before the beginning of a discharge there is a capacitive current which flows in the load resistor circuit $R_M C_{er}$ and is determined by the applied voltage and impedance. When a discharge is started gas space capacity may be considered to be shorted by the discharge as a first approximation. A current jump appears then in the circuit with the amplitude

$$i_{imp} = E_d \left(\frac{1}{R_M + \frac{1}{i\,\omega\,C_{er}}} - \frac{1}{R_M + \frac{1}{i\,\omega\,2C_r}} \right). \tag{20}$$

This picture fails to present time variation for a current impulse. To do this, let us consider the first impulse (Fig. 5) with the assumption that no charges have been accumulated on the walls as yet. In this approximate "picture" impulse rising time is disregarded and it is assumed that the current at $t = t_0 + \delta t$ (immediately following the discharge) may be characterized by i_{imp} determined by the external circuit and geometry (20). Current density j corresponding to this current intensity i_{imp} can be written in terms of micro-parameters as

$$j = e\ n\ b\ E_\Sigma \tag{21}$$

where

E_Σ — resultant field intensity between the internal walls of the discharge vessel;
b — mobility characterized by the gas parameters.

With the charges accumulated on the walls taken into account, the resultant field intensity E_Σ can be written as

$$E_\Sigma = E_0 \sin(\omega t + \chi) - \frac{1}{C_G\,d} \int_0^t i\,dt \tag{22}$$

where χ is the initial phase angle of the applied field at $t = t_0 = 0$, i.e., at the moment of discharge ($E_{\text{crit.}} = E_0 \sin \chi$).

By using Eqs (21) and (22), time variation of the current density is given by the integral equation

$$j = e\,n\,b \left[E_0 \sin(\omega t + \chi) - \frac{F}{C_G\,d} \int_0^t j\,dt \right] \tag{23}$$

where F designates the wall area under the electrodes.

Obviously, rising time is excluded from this formula, that is,

$$j\big|_{t\leq 0} = 0; \qquad j\big|_{t=0+\delta t} = j_{imp} \tag{24}$$

is assumed, where j_{imp} depends on the external circuit.

Subsequent impulses are characterized in the same way except that static fields caused by the charges which have been carried to the walls by preceding impulses should also be taken into account and the initial phase angle of the applied field will be altered accordingly. Shifts of the initial phase angle can be followed in Figs 4, 6, 8 and 10. The first impulse appears near the maximum of the applied field (not reaching it because the first impulse following a breakdown gives rise to a static field altering the phase angle of the first current impulse appearing in the following half cycle of the same polarity) as is to be seen in Fig. 4, while in Fig. 10 it occurs in a negative half cycle of the applied field.

These simple "pictures" will suffice to clearly show that, in addition to the critical breakdown field intensity of the capacitive discharge (the apppearance of the first current impulse), the voltage (field strength) giving rise to subsequent impulses also provide some information on the gas space microparameters.

To sum up, it can be seen that, with a given external electric circuit and discharge geometry, besides the critical breakdown field strength, initial phases of subsequent current impulses, the corresponding field intensities as well as time dependence of current impulses provide independent information on the gas space parameters.

3. Practical aspects

On the basis of detailed theoretical and experimental investigations of capacitive discharges a gas-purity testing method has been developed by using measured critical breakdown field intensities [17]. By determining the firing voltage U_1 of the first current impulse as well as that of the second impulse (U_2) and the extinction voltage U_{10} of the first impulse three connected parameters have been found to construct calibration curves by the use of which a quantitative gas analysis can be then performed [18].

A detailed description of the equipment used in these investigations is given in Section 2 of the present paper. By using a special filling system calibration curves shown in Figs 13—16 have been constructed for some types of impurities most frequently encountered in the gas space of a fluorescent lamp such as air, carbon dioxide, water vapour, oil vapour. These curves show the dependence of the three selected parameters upon the partial pressure of the impurities introduced into argon at 2,5 mm Hg and mercury vapour at 2×10^{-3}

mm Hg in the pressure range of interest for the industry. In these figures, "o" designates parameters relative to a fluorescent lamp with "pure" gas space.

In Section 2.3, attention has drawn to a relationship between the measurable volt-ampere characteristics of a capacitive discharge and the micro-

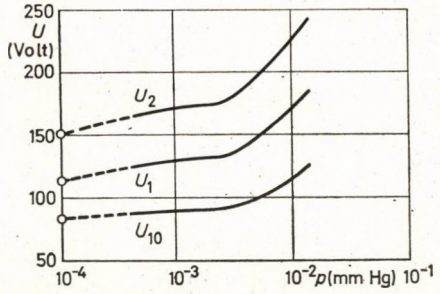

Fig. 13. First firing voltage U_1, second firing voltage U_2 and first extinction voltage U_{10} as functions of the partial pressure of air in a mixture of 2.5 mm Hg A + 2×10^{-3} mm Hg mercury vapour.

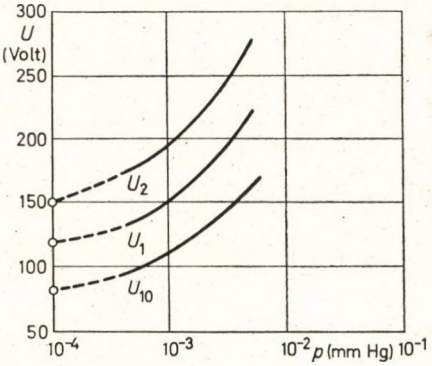

Fig. 14. First firing voltage U_1, second firing voltage U_2, and first extinction voltage U_{10} as functions of the partial pressure of carbon dioxide in a mixture of A (2.5 mm Hg) and mercury vapour (2×10^{-3} mm Hg)

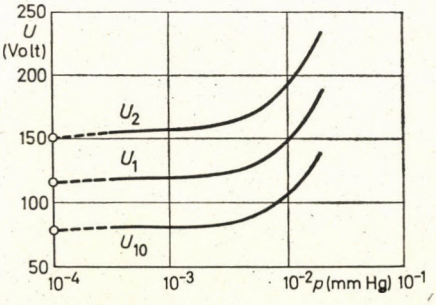

Fig. 15. First firing voltage U_1, second firing voltage U_2, and first extinction voltage U_{10} as functions of the partial pressure of water vapours introduced into a mixture of A (2.5 mm Hg) and mercury vapour (2×10^{-3} mm Hg)

parameters of a gas space. The revealed relationship suggests a number of parameters allowing the construction of calibration curves useful in practice. The choice of the three parameters proposed for industrial purposes (U_1, U_2 and U_{10}) was justified by the fact that they could be registered simply and rapidly.

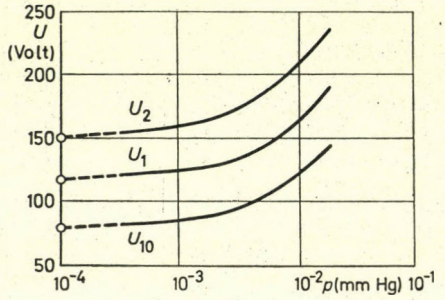

Fig. 16. First firing voltage U_1, second firing voltage U_2, and first extinction voltage U_{10} as functions of the partial pressure of oil vapour introduced into a mixture of A (2.5 mm Hg) and mercury vapour (2×10^{-3} mm Hg)

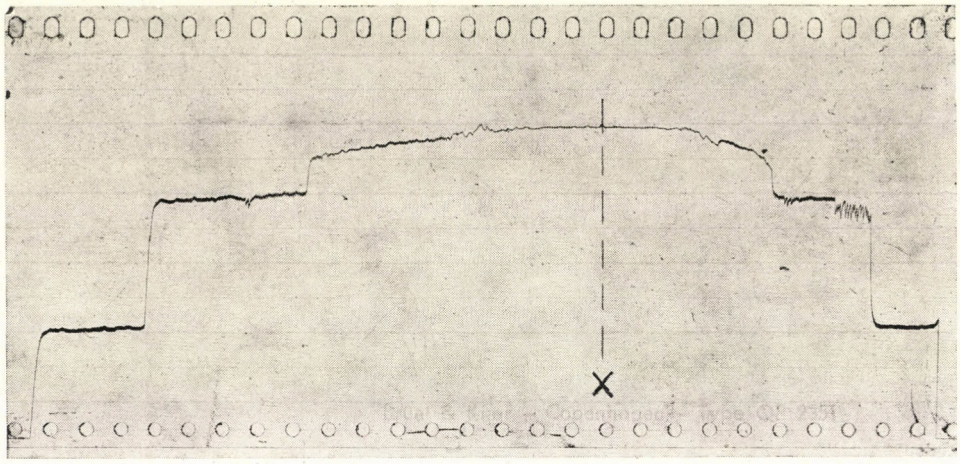

Fig. 17. Integrated record of current impulses within half a cycle as a means for determining the amount of charges accumulated on the walls

The oscillogram used in laboratory investigations is that shown in Fig. 17, which shows an integrated form of the current impulses as a function of voltage. In this figure, the formation and decay of a capacitive discharge obtained with a recorder are shown. Up to point X of the horizontal axis, an increase of voltage (field intensity) gives rise to a sequence of current jumps, the area of which integrated over a half cycle is obtained in this case in a loga-

rithmic scale. From point X, the voltage (field intensity) decreases and the recorder reveals an extinction characteristic. By knowing the current jumps corresponding to discrete voltages and their areas the amounts of charges on the wall can be determined. From this point of view, the record corresponds to an improvement on the old method; it gives more detailed information on the gas space composition.

REFERENCES

1. ANTAL, K.: Dissertation, 1971
2. BITÓ, J.—ANTAL, K.: *Műszaki Tudomány*, at press
3. FUCHS, W.: *Z. Physik* **10** (1936), 709
4. FUCHS, W.: *Appl. Sci. Res.*, Hague, *B*6 (1955)
5. FUCHS, W.—GRAF, L.—MUES, G.—MÜLLER, H. G.: *Z. Phys.* **145** (1956), 1
6. FUCHS, W.: *Proceedings of the Third International Conference on Ionization Phenomena in Gases*, Venice 1957
7. VLAARDINGERBROEK, M. T.: *Appl. Sci. Res.*, Hague, **85** (1955), 139
8. HERTZ, G.: *Verh. d..D. Phys. Ges.* **19** (1917), 268
9. GRANOWSKI, V. L.—DAN SU: **26** (1940), 873
10. BITÓ, J. F.—ANTAL, K. G.: *Acta Phys. Hung.* **30** (1970), 23
11. BITÓ, J. F.—ANTAL, K. G.: *Tungsram Symposium*, Moscow, Paper **10** (1969)
12. BHATAWDEKAR, M. G.: *Doctoral Dissertation*, University of Rajputana Jaipur, Rajasthan (India) 1957
13. LOEB, L. B.—EL-BAKKAL, J. M.: *Fifth International Conference on Ionization Phenomena in Gases*, Munich, **I** (1961), 734
14. EL-BAKKAL, J. M.—LOEB, L. B.: *J. of Applied Phys.* **133** (1962), 1564
15. BITÓ, J. F.—ANTAL, K. G.: *Acta Phys. Hung.*, at press
16. BITÓ, J. F.—ANTAL, K. G.: *Acta Techn. Hung.*, at press
17. GÁCS, I.—SZIGETI, GY.—ROTTER, A.—SZABÓ, J.: Hungarian Patent No. 134 181.
18. BITÓ, J. F.—ANTAL, K. G.: *Acta Techn. Hung.*, at press

Eine kapazitive Entladungsmethode für die quantitative Bestimmung von Gasverunreinigungen. Die Verfasser stellen das von ihnen ausgearbeitete statistische Modell vor, mit dessen Hilfe die kritische Durchschlagsfeldstärke theoretisch bestimmt werden kann. Die Anwendbarkeit der Methode wird für Argon vorgeführt. Die auf Grund des Modells berechneten und die versuchsweise erhaltenen kritischen Durchschlagsspannungen stimmen gut überein. Im Besitz der aufgedeckten mikrophysikalischen Zusammenhänge wird eine gut verwendbare, schnelle, quantitative Methode zur Gasanalyse angegeben. Die Verfasser verweisen auf die Möglichkeiten für die Verfeinerung des Modells, welches die Grundlage der theoretischen Betrachtungen bildet, und zeigen so die Bedeutung der auf diesem Wege erhältlichen weiteren Informationen.

Метод емкостных газовых разрядов для количественного определения газовых примесей. Описывается разработанная нами статистическая модель, при использовании которой теоретическим путем можно определить критическую напряженность поля при пробое. Применимость метода демонстрируется в случае аргона. Между значениями критической напряженности поля при пробое, вычисленными на основе модели и полученными экспериментальным путем, установлено удовлетворительное совпадение. Располагая вскрытыми микрофизическими зависимостями, авторами приводится отлично применимая на практике скоростная методика количественного газового анализа. Вскрывая возможности усовершенствования модели, служащей в качестве теоретических соображений, дастся ссылка на значение дальнейших информаций, которые можно получить таким путем.

Acta Technica Academiae Scientiarum Hungaricae, Tomus 76 (1—2), pp. 87—91 (1974)

EIN NEUES VERFAHREN ZUR LÖSUNG DER DOPPELPUNKTEINSCHALTUNG DURCH STRECKENMESSUNG

Z. BUOCZ und J. JANOSITZ

[Eingegangen am 10. September 1971]

Die Arbeit bringt eine neuartige, von der herkömmlichen abweichende Behandlung des Problems der Doppelpunkteinschaltung durch Streckenmessung. Der wahrscheinlichste Wert einer Strecke wird von zwei gemessenen und berechneten Abständen bestimmt. Ein in der Fachliteratur bereits mitgeteiltes numerisches Beispiel dient zur Darstellung der Vorteile des Verfahrens.

Zeichenerklärung

s_i $(i = 1, 2, \ldots, 5)$	genaue Werte der Strecken [m]
$\overline{S}_i$ $(i = 1, 2, \ldots, 5)$	wahrscheinlichste Werte der Strecken [m]
S_i' $(i = 1, 2, \ldots, 5)$	gemessene Werte der Strecken [m]
S_i'' $(i = 1, 2, \ldots, 5)$	berechnete Werte der Strecken [m]
S_i^* $(i = 1, 2, \ldots, 5)$	die in der Fachliteratur [2] ermittelten Werte der Strecken [m]
S_i^{**} $(i = 1, 2, \ldots, 5)$	die in der Fachliteratur [3] ermittelten Werte der Strecken [m]
μ_0	Mittelfehler der Längeneinheit $[\sqrt{\text{m}^2/\text{m}}]$
$\mu_{\overline{s}_i}$ $(i = 1, 2, \ldots, 5)$	Mittelfehler der Streckenwerte $\overline{S}_i$ $[\mu_0]$
$\mu_{s_i'}$ $(i = 1, 2, \ldots, 5)$	Mittelfehler der Streckenwerte S_i' $[\mu_0]$
$\mu_{s_i''}$ $(i = 1, 2, \ldots, 5)$	Mittelfehler der Streckenwerte S_i'' $[\mu_0]$
x_A, x_B, x_C, x_D y_A, y_B, y_C, y_D	bekannte Koordinatenwerte der Punkte A, B, C, D [m]
x_{N_1}, y_{N_1}	Koordinatenwerte, berechnet aus den Streckenwerten S_3, S_4 und den bekannten Koordinaten der Punkte C und D [m]
x_{M_1}, y_{M_1}	Koordinatenwerte, berechnet aus den Streckenwerten S_2, S_5 und den bekannten Koordinaten der Punkte B und N_1 [m]
M_0, N_0	(bezw. x_M, x_N, y_M, y_N) Werte dieser Koordinaten als Endergebnis [m]
M_0^*, N_0^*	die in der Fachliteratur [2] ermittelten Endergebnisse für die Punkte M und N [m]
M_0^{**}, N_0^{**}	die in der Fachliteratur [3] ermittelten Endergebnisse für die Punkte M und N [m]

Der Aufsatz befaßt sich mit dem Problem der Doppelpunkteinschaltung, worüber in der Fachliteratur [2, 3] bereits berichtet wurde. Aufgrund der Bezeichnung des Bildes 1 läßt sich das Problem folgendermaßen aufstellen:

Es seien die Koordinaten der Punkte A, B, C und D gegeben. Wir wollen die Abstände

$$S_1, S_2, S_3, S_4 \text{ und } S_5$$

in gleicher Weise und mit denselben Meßgeräten ermitteln. Mit den erhaltenen Werten sollen die wahrscheinlichsten Werte der Koordinaten der Punkte

$$M \text{ und } N$$

bestimmt werden.

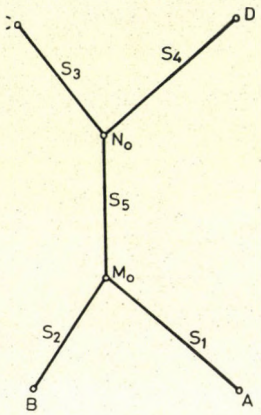

Fig. 1

Das Prinzip der hier entwickelten Lösungsmethode weicht von jenem der Empfehlungen der zitierten Facharbeiten [2, 3] nicht ab, wie dies auch aus den Endergebnissen ersichtlich ist. Doch glauben wir, daß unsere Methode den Vorteil einer einfacheren Programmierung für die Rechenmaschine bietet.

Zur Berechnung der Koordinaten der Punkte M und N sollen die höchstwahrscheinlichen Werte der Abstände $\bar{S}_i$ $(i = 1, 2, \ldots, 5)$, bestimmt werden. Auf Grund der in der Facharbeit [1] dargelegten Ableitung stehen uns für den Wert S_i zwei voneinander unabhängige Informationen, S_i' und S_i'', zur Verfügung. Hieraus ergibt sich der wahrscheinlichste Wert von S_i, nämlich $\bar{S}_i$:

$$\bar{S}_i = \frac{S_i'/\mu_{s'}^2 + S_i''/\mu_{s_i'}^2}{1/\mu_{s_i'}^2 + 1/\mu_{s_i''}^2}, \tag{1}$$

wo μ die betreffende mittlere Abweichung (Streuung) bedeutet. Es wurde bewiesen, daß in Kenntnis der Werte S_i' und S_i'' der «beste», also der mit dem kleinsten mittleren Fehler behaftete Wert für S_i durch $\bar{S}_i$ (1) erhalten wird, wobei der kleinste mittlere Fehler $\mu_{\bar{s}_i}$ sich folgenderweise berechnen läßt:

$$\mu_{\bar{s}}^2 = \frac{1}{1/\mu_{s'}^2 + 1/\mu_{s_i''}^2}. \tag{2}$$

Für den auf Bild 1 dargestellten Fall ergeben sich folgende Werte:

S_i' die sich aus der Messung des i Abstandes ergebende Information,

S_i'' der i Abstand, berechnet aus den Abstandswerten S_j

wobei $j = 1, 2, \ldots, 5$, jedoch mit $j \neq i$.

Mit Rücksicht darauf, daß S_i' als Meßergebnis erhalten wurde und durch Einbeziehung der Formeln

$$\begin{aligned}(x_C - x_{N_1})^2 + (y_C - y_{N_1})^2 &= S_3'^2, \\ (x_D - x_{N_1})^2 + (y_D - y_{N_1})^2 &= S_4'^2\end{aligned} \tag{3}$$

x_{N_1} und y_{N_1} bestimmt werden können, ergeben sich die Formeln:

$$\begin{aligned}(x_{N_1} - x_{M_1})^2 + (y_{N_1} - y_{M_1})^2 &= S_5'^2, \\ (x_B - x_{M_1})^2 + (y_B - y_{M_1})^2 &= S_2'^2,\end{aligned} \tag{4}$$

und aus diesen lassen sich die Koordinaten des Punktes M_1 bestimmen.

Mit diesem Wert erhalten wir den Abstand

$$S_1'' = \overline{AM_1}, \tag{5}$$

und in ähnlicher Weise erhält man die berechneten Werte für

$$S_2'', S_3'', S_4'' \quad \text{und} \quad S_5''.$$

Voraussetzungsgemäß wurden die Messungen nach ein- und demselben Prinzip und mit genau denselben Meßgeräten durchgeführt, und so ergibt sich folgende Beziehung:

$$\mu_{S_i'}^2 = S_i \, \mu_0^2, \tag{6}$$

wo μ_0 den mittleren Fehler der Längeneinheit bedeutet.

Nach dem Fehlerfortpflanzungsgesetz gilt:

$$\mu_{S_i''}^2 = \sum_{\substack{j=1 \\ j \neq}}^{5} \left(\frac{\partial S_i''}{\partial S_j'} \right)^2 \cdot \mu_{S_j'}^2. \tag{7}$$

In der Fachliteratur [1] finden wir den Beweis dafür, daß man im Falle der Vernachlässigbarkeit der Glieder zweiter Ordnung — übrigens einer Voraussetzung des Fehlerfortpflanzungsgesetzes — in der Reihenentwicklung

$$S_i = S_i \, (S_j) \qquad (j = 1, 2, \ldots, 5; \; j \neq i), \tag{8}$$

die Formel aufschreiben kann:

$$\frac{\partial S_i'}{\partial S_j} \cong - \frac{S_i'' - S_i'}{S_j'' - S_j'} \tag{9}$$

Aus dem Besagten geht hervor, daß zur Berechnung des Abstandswertes S_i die Kenntnis des mittleren Fehlers μ_0 der Längeneinheit nicht erforderlich ist. Die Beweisführung gemäß der Fachliteratur [1] enthält noch folgende Feststellung:

Falls die Koordinaten der Punkte M_0 und N_0 aus den Werten S_i berechnet werden, so kann zwischen den, aus den Koordinaten von zwei benachbarten Punkten berechenbaren Abstandswerten und den diesen zugeordneten $\bar{S}_i$ Werten kein Widerspruch bestehen.

Zum besseren Verständnis sei hier das numerische Beispiel gemäß der Fachliteratur [2, 3] dargestellt.

Es seien die gegebenen Koordinaten der genannten Punkte A, B, C und D (Werte in [m]):

	A	B	C	D
x	+ 766,66	+ 639,55	+1816,38	+2134,12
y	+2036,85	+1319,56	+ 752,53	+1672,81

Nun folgt die Tafel mit den gemessenen und den berechneten Werten, wozu bemerkt sei, daß die Werte S_i^* der Quelle [2] und die Werte S_i^{**} der Quelle [3] entnommen wurden.

Es soll darauf hingewiesen werden, daß die Einheit $[\mu_0^2]$ für die Größen $\mu_{S_i'}^2$ und $\mu_{S_i''}^2$ der 2. und 4. Reihe sich aus den Zusammenhängen (6) und (7) ergibt.

Größe und Einheit	1	2	3	4	5
S_i' [m]	585,97	461,41	561,07	713,60	576,21
$\mu_{S_2'}^2$ $[\mu_0]$	585,97	461,41	561,07	713,60	576,21
S_i'' [m]	585,37088	460,49289	560,53257	712,73659	575,71797
$\mu_{S_i''}^2$ $[\mu_0]$	2092,1240	5813,9437	1593,8928	4848,4214	1230,0273
S_i [m]	585,83891	461,34257	560,93007	713,48922	576,0534
S_i^* [m]	585,835	461,353	560,928	713,487	676,046
S_i^{**} [m]	585,83856	461,34366	560,93139	713,48928	576,04950

Es folgt die Tafel die die aus den Werten S_i berechneten Koordinatenwerte und zum Vergleich die korrespondierenden Werte für M_0^* und N_0^* aus Quelle [2] und für M_0^{**} und N_0^{**} aus Quelle [3] (Werte in [m]) enthält

	M_0	M_0^*	M_0^{**}
x	1052,41252	1052,421	1052,4140
y	1525,42773	1524,438	1524,4885

	N_0	N_0^*	N^{**}
x	7558,79999	1558,803	1558,7985
y	1250,62216	1250,824	1250,8234

Zur numerischen Kontrolle wollen wir die Differenzen bzw. Abweichungen miteinander vergleichen, indem wir die drei Differenzwerte anführen, die sich ergeben, wenn man von der Streckenlänge M_0N_0, die aus den Punktkoordinaten der Punkte M_0 und N_0 erfolgt, den korrespondierenden Wert S_5 abzieht:

$$\overline{M_0 N_0} - S_5 = 0{,}00053 \text{ [m]},$$

$$\overline{M_0^* N_0^*} - S_5 = 0{,}006 \text{ [m]},$$

$$\overline{M_0^{**} N_0^{**}} - S_5 = 0{,}00017 \text{ [m]}.$$

Diese Ziffern beweisen, daß die Genauigkeit der drei Verfahren nur unwesentlich variiert.

LITERATUR

1. Janositz, J.: Mérésekből nyert információk értékelése a bányászati paraméterek becslésénél (Wertung von Meßinformationen bei der Schätzung von Bergbau-Parametern), *Műszaki Tudomány* (Unter Druck)
2. Panther, A.: Doppelpunkteinschaltung durch Streckenmessung [Ausgleichung nach bedingten Beobachtungen], *Allg. Verm. Nachr.* **77** (1970), 22—28
3. Tárczy-Hornoch, A.: Zur Doppelpunkteinschaltung durch Streckenmessung aus je zwei gegebenen Punkten *(Neue Bautechnik.* — Wiss. Zeitschrift für Bergbau-Geowiss. und Aufbereitung. **1.** Jahgr. H. 6, S. 407—410

A New Method of the Double-point Insertion on the Basis of Distance Measurement
In this paper a new estimation method is described in order to find, in a certain way that deviates from the accustomed, the solution of the problem of how to carry out a double-point insertion on the basis of distance is defined by two independent informations, the latter being obtained from measured and calculated values. The numeric example, already published in the literary sources serves to demonstrate the advantages of the new method.

Новый метод решения проблемы двойной привязки точки, основывающейся на данных измерения расстояния. В работе проблема двойной привязки точки, основывающейся на данных измерения расстояния, рассматривается отличным от обычного решения образом. Наиболее вероятное значение определяется на основе двух независимых друг от друга информаций, а именно с помощью значений измеренных и рассчитанных расстояний. Преимущества данного метода иллюстрируются с помощью числового примера, сообщенного также в специальной статье по теме.

Acta Technica Academiae Scientiarum Hungaricae, Tomus 76 (1—2), pp. 93—105 (1974)

AN APPROXIMATE METHOD FOR THE ANALYSIS OF ELASTIC TORSION OF ROUND BARS OF VARIABLE DIAMETERS

I. ECSEDI*

[Manuscript received 21 October, 1971]

An approximate method for the analysis of round bars with variable diameter is being reported. The differential equation

$$\frac{\partial^2 \Phi}{\partial r^2} - \frac{3}{r}\frac{\partial \Phi}{\partial r} + \frac{\partial^2 \Phi}{\partial z^2} = 0 \qquad \text{(a)}$$

defining the stress function of torsion by taking into account the appropriate boundary conditions, is solved according to the method of the partial discretization with respect to z.

Notation

The following symbols are used in this paper:

$\begin{bmatrix} r \\ \varphi \\ z \end{bmatrix}$ polar coordinates of point P (Fig. 1),

$\begin{bmatrix} \vec{e}_r \\ \vec{e}_\varphi \\ \vec{e}_z \end{bmatrix}$ unit vectors of the system of polar coordinates r, φ, z,

$\begin{bmatrix} x \\ y \\ z \end{bmatrix}$ Cartesian coordinates of point P,

$\begin{bmatrix} \vec{i} \\ \vec{j} \\ \vec{k} \end{bmatrix}$ unit vectors of the system of coordinates x, y, z,

$\vec{r} = x\vec{i} + y\vec{j} + z\vec{k}$,

$\vec{\varrho}_z$ stress vector acting in point P, in the plane perpendicular to z,

$\vec{R} = x\vec{i} + y\vec{j}$, $\vec{r} = \vec{R} + z\vec{k}$,

$\begin{bmatrix} \tau_{r\varphi} \\ \tau_{\varphi z} \end{bmatrix}$ stress of direction $\begin{bmatrix} \vec{e}_\varphi \\ \vec{e}_z \end{bmatrix}$ acting in point P in plane normal to $\begin{bmatrix} \vec{e}_r \\ \vec{e}_\varphi \end{bmatrix}$.

M_c torsional moment acting on the cross-section K of the bar,

$\begin{bmatrix} \vec{F}_S \\ \vec{M}_S \end{bmatrix}$ resulting dual vector of the system of internal forces acting on the cross-section K, reduced to the centre of gravity S of the cross-section K,

$\vec{q}$ intensity vector of the system of external forces distributed through the volume,

*I. Ecsedi, Franklin u. 17, 3528 Miskolc, Hungary.

$\Phi = \Phi(r, z)$ stress function of the torsion,

$\Phi_\infty^+ = \Phi_\infty^+(r) = \lim_{z \to \infty} \Phi(r, z)$,

$\Phi_\infty^- = \Phi_\infty^-(r) = \lim_{z \to -\infty} \Phi(r, z)$,

$\begin{bmatrix} z_1^- \\ z_2^+ \\ z_1^\times \\ z_2^\times \end{bmatrix}$ characteristic-co-ordinates z

h step distance at the difference quotients with respect to z,
G shear modulus of elasticity of the bar material,
$\mathbf{A}, \mathbf{V}, \mathbf{\Lambda}$ quadratic matrices,
$\Phi, u, f, v, \ldots$ column vectors,
ψ coefficient of deformation,
V tangential displacement,
$C_{i,1}, C_{i.2}$ integration constants,
φ, ψ auxiliary variables,
other variables are explained in the text.

1. Introduction

By way of preliminary let us summarize the major findings relating to the elastic torsion of prismatic bars of circular cross-section with variable diameter.

The cross-section K of the prismatic bar is subjected to torsion in the case where the resulting dual vector of the system of the internal forces acting on the cross-section, reduced to the centre of gravity S of the cross-section (Fig. 1):

$$\vec{F}_s = \int_{(A)} \vec{\varrho}_z \, xA = \vec{0}, \tag{1}$$

$$\vec{M}_s = \int_{(A)} \vec{R} \times \vec{\varrho}_z \, dA = M_c \vec{k}. \tag{2}$$

In the case of pure torsion, in any P point of the bar, in the system of polar coordinates (r, φ, z) the form of the matrix of the stress tensor is as follows

$$\mathbf{F} = \begin{bmatrix} 0 & \tau_{r\varphi} & 0 \\ \tau_{\varphi r} & 0 & \tau_{\varphi z} \\ 0 & \tau_{z\varphi} & 0 \end{bmatrix}. \tag{3}$$

It is well known that in the case in question, the governing equations of the theory of elasticity are satisfied under the condition $-\vec{q} = \vec{0}$, if the scalar co-ordinates of the stress tensor differing from zero, will be derived from a so-called stress function $\Phi = \Phi(r, z)$, according to Eqs (5) and (6), which, above the region depicted in Fig. 2 satisfies the partial differential equation

$$\frac{\partial^2 \Phi}{\partial r^2} - \frac{3}{r} \frac{\partial \Phi}{\partial r} + \frac{\partial^2 \Phi}{\partial z^2} = 0, \tag{4}$$

$$\tau_{r\varphi} = -\frac{1}{r^2}\frac{\partial \Phi}{\partial z}, \tag{5}$$

$$\tau_{z\varphi} = \frac{1}{r^2}\frac{\partial \Phi}{\partial r}. \tag{6}$$

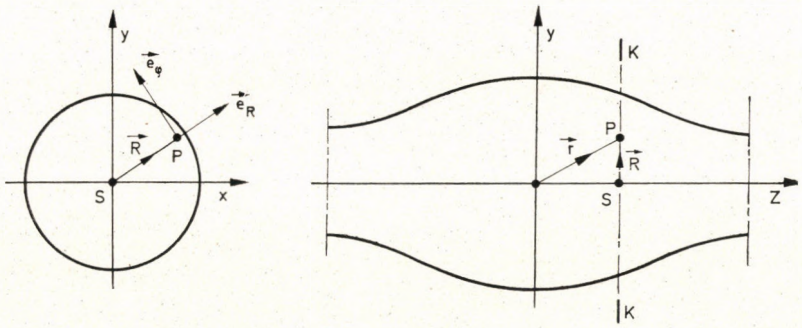

Fig. 1

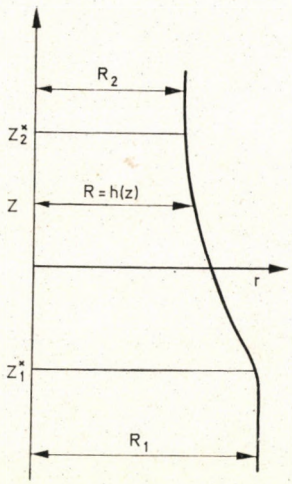

Fig. 2

Since in the case of the problem in question, the mantle of the investigated bar is not subjected to any load, therefore, [3] the value of Φ along the meridian line — which is the delineation of the bar — is constant. A torsional moment acting on any cross-section if the function $\Phi = \Phi(r, z)$ is known, may be expressed as follows [3]:

$$M_c = 2\pi\,[\Phi[R(z), z] - \Phi(0, z)]\,. \tag{7}$$

From the validity of the equation

$$\tau_{r\varphi}(r, z)|_{r=0} = 0$$

follows that $\Phi = \Phi(r, z)$ at the point $r = 0$ — on the z-axis — is constant. Since this constant does not affect the magnitude of the stresses, its value will consequently be chosen to be equal to zero.

2. Solution of the problem

The meridian lines of round bars with variable diameter discussed in this paper (Fig. 2) may be given in the following form:

$$R = R(z) = \begin{cases} R_1 & z \leq z_1^x, \\ h(z), & \text{if } z_2^x \leq z \leq z_1^x, \\ R_2 & z \geq z_2^x. \end{cases} \tag{8}$$

Here it will be assumed that the meridian line does not contain sharp entails, and no abrupt and significant variation of the radius of curvature of the envelope along the z-direction occurs.

For determining the stress function, Saint-Venant's principle[1] will be utilized. According to this principle, in the case of a sufficient high value of $|z|$ ($z \leq z_1^-$, i.e., $z \geq z_2^+$) it can be assumed that Φ is independent of z. Thus, in the case of appropriately selected z_1^- or z_2^+, the function $\Phi(r, z)$ will take the forms $\Phi_\infty^-(r)$ or $\Phi_\infty^+(r)$. $\Phi_\infty^-(r)$ and $\Phi_\infty^+(r)$ may be written in the forms

$$\Phi_\infty^- = \Phi_\infty^-(r) = \frac{M_c}{2\pi R_1^4} r^4, \qquad (0 \leq r \leq R_1) \tag{9}$$

$$\Phi_\infty^+ = \Phi_\infty^+(r) = \frac{M_c}{2\pi R_2^4} r^4, \qquad (0 \leq r \leq R_2) \tag{10}$$

respectively.

Accordingly, the following extreme value problem should be solved above the delimited region T depicted in Fig. 3.

[1] Thereby it will be avoided that the partial differential equation (4) should be solved above the region (shown in Fig. 2) extending to the infinity both in $+z$ and in $-z$ direction. with the boundary conditions

$$\begin{gathered} \lim_{z \to \infty} \Phi(r, z) = \Phi_\infty^+(r), \\ \lim_{z \to -\infty} \Phi(r, z) = \Phi_\infty^-(r), \\ \Phi(0, z) = 0 \quad \text{and} \quad \Phi[R(z), z] = M_c/2\pi = \text{const}. \end{gathered} \tag{8a}$$

The function $\Phi = \Phi(r, z)$ should be determined which is continuous within and at the boundary of region T and within this region satisfies the homogenic second order, elliptic-type partial differential equation

$$\frac{\partial^2 \Phi}{\partial r^2} - \frac{3}{r}\frac{\partial \Phi}{\partial r} + \frac{\partial^2 \Phi}{\partial z^2} = 0, \tag{11}$$

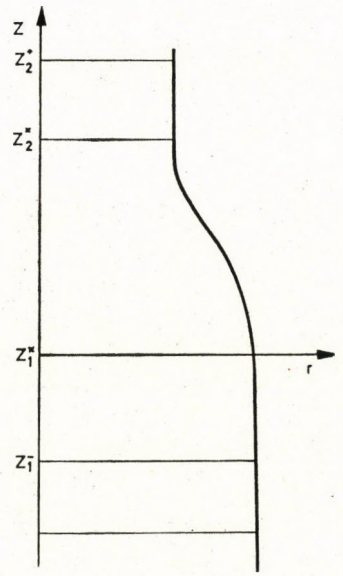

Fig. 3

and, at the boundary of region T, the boundary condition

$$\Phi = \begin{cases} 0, & r = 0, \quad z_1^- \leq z \leq z_2^+, \\ \dfrac{M_c}{2\pi}, & r = R(z) \quad z_1^x \leq z \leq z_2^x, \\ \dfrac{M_c}{2\pi}, & r = R_1, \quad z_1^- \leq z \leq z_1, \\ \text{if} & \\ \dfrac{M_c}{2\pi}, & r = R_2, \quad z_2^x \leq z \leq z_2^+, \\ \dfrac{M_c}{2\pi R_1^4} r^4, & z = z_1, \quad 0 \leq r \leq R_1, \\ \dfrac{M_c}{2\pi R_2^4} r^4, & z = z_2, \quad 0 \leq r \leq R^2. \end{cases} \tag{12}$$

The problem of extreme value set up by (11) and (12) may be solved by the

method of the partial discretization with respect to z. The partially discretized variety of the boundary value problem is the set of equation

$$\left.\frac{\partial^2 \Phi}{\partial r^2} - \frac{3}{r}\frac{\partial \Phi}{\partial r} + \frac{\partial^2 \Phi}{\partial z^2}\right|_{z=z_i} = 0, \qquad (13)$$

$$(i = 1, 2, \ldots, n-1)$$

and the set of boundary conditions

$$\Phi = \begin{cases} 0, & r = 0, & z^- \leq z_i \leq z^+, \\ \dfrac{M_c}{2\pi}, & r_i = R(z_i), & z_1^x \leq z_i \leq z_2^x, \\ \dfrac{M_c}{2\pi}, & r = R_1, & z_1^- \leq z_i \leq z_1^x, \\ & \text{if} & \\ \dfrac{M_c}{2\pi}, & r = R_2, & z_2^x \leq z_i \leq z_2^+, \\ \dfrac{M_c}{2\pi R_1^4} r^4, & z = z_1^-, & 0 \leq r \leq R_1, \\ \dfrac{M_c}{2\pi R_2^4} r^4, & z = z_2^+, & 0 \leq r \leq R_2. \end{cases} \qquad (14)$$

Let us approximate the derivative $\partial^2\Phi/\partial z^2$ in Eq. (13) by a change ratio.

This approximation — by making use in z of the discretization of step rate h — leads, by the application of the central differences, to the following result (see e.g. [1]):

$$\frac{\partial^2 \Phi}{\partial z^2} = \frac{\Phi(r_1 z_{i+1}) - 2\Phi(r_1 z_i) - \Phi(r_1 z_{i-1})}{h^2} + O(h^2). \qquad (15)$$

By applying the approximation (15) containing an error of $O(h^2)$ order of magnitude, the Eq. (13) will be

$$\frac{d^2 \Phi_i}{dr^2} - \frac{3}{r}\frac{d\Phi_i}{dr} + \frac{\Phi_{i+1} - 2\Phi_i + \Phi_{i-1}}{h^2} = 0 \qquad (16)$$

wherein

$$\Phi_i = \Phi(r, z_i) = \Phi_i(r),$$

$$\left.\frac{d\Phi_i}{dr} = \frac{\partial \Phi(r_1 z)}{\partial r}\right|_{z=z_i} = \Phi_i'(r), \qquad (16a)$$

$$\frac{d^2\Phi_i}{dr^2} = \frac{\partial^2 \Phi(r_1 z)}{\partial r^2}\bigg|_{z=z_i} = \Phi_i''(r),$$

$$(i = 1, 2, \ldots, n-1)\,.$$

By using these symbols the set of boundary conditions (12) may be written in the form

$$\begin{aligned} &\text{a)} \quad \Phi_i(0) = 0, \\ &\text{b)} \quad \Phi(R_i) = \frac{M_c}{2\pi}, \\ &\text{c)} \quad \Phi_0 = \Phi_{\infty}^{-}(r) = \frac{M_c}{2\pi R_1^4} r^4, \\ &\text{d)} \quad \Phi_n = \Phi_{\infty}^{+}(r) = \frac{M_c}{2\pi R_2^4} r^4, \end{aligned} \tag{17}$$

herein

$$\kappa_i = R(z_i)\,, \qquad (i = 1, 2, \ldots, n-1)\,.$$

The problem of boundary value set by (16) and (17), by introducing the column vectors

$$\Phi = \begin{bmatrix} \Phi_1 \\ \Phi_2 \\ \cdot \\ \cdot \\ \cdot \\ \Phi_{n-1} \end{bmatrix} \qquad f = \begin{bmatrix} -\dfrac{\Phi_0}{h^2} \\ 0 \\ \cdot \\ \cdot \\ 0 \\ -\dfrac{\Phi_n}{h^2}\,. \end{bmatrix} \tag{17a}$$

and the matrix of continuance-type

$$\mathbf{A} = \frac{1}{h^2}\begin{bmatrix} -2 & 1 & 0 & & & & & 0 \\ 1 & -2 & 1 & & & & & \cdot \\ \cdot & \cdot & \cdot & & & & & \cdot \\ \cdot & \cdot & \cdot & & & & & \cdot \\ & & & & & 1 & -2 & 1 \\ 0 & 0 & 0 \ldots & & \ldots & 0 & 1 & -2 \end{bmatrix} \tag{17b}$$

may be condensed into the vector-scalar differential equation

$$\frac{d^2\Phi}{dr^2} - \frac{3}{r}\frac{d\Phi}{dr} + \mathbf{A}\Phi = f. \tag{18}$$

Now let the matrix transforming the matrices be $\mathbf{V}$ and $\mathbf{A}$ by similarity transformation into the diagonal matrix $\mathbf{\Lambda}$

$$\mathbf{\Lambda} = \mathbf{V}\mathbf{A}\mathbf{V}^{-1}, \tag{19}$$

$$\frac{d^2\mathbf{V}\Phi}{dr^2} - \frac{3}{r}\frac{d\mathbf{V}\Phi}{dr} + \mathbf{V}\Phi = \mathbf{V}f. \tag{20}$$

Let us introduce the vector variable

$$v = \mathbf{V}\Phi \tag{21}$$

and the known vector

$$d = \mathbf{V}f. \tag{22}$$

With these notation (16) will be

$$\frac{d^2v}{dr^2} - \frac{3}{r}\frac{dv}{dr} + \mathbf{\Lambda}v = d. \tag{23}$$

As is known, the $\mathbf{\Lambda}$ is the following diagonal matrix (see e.g. [4]):

$$\mathbf{\Lambda} = \langle \lambda_1, \lambda_2, \ldots, \lambda_k, \ldots \lambda_{n-1} \rangle \tag{24}$$

wherein

$$\lambda_k = -\frac{4}{h^2}\sin^2\frac{k\pi}{2n}, \tag{25}$$

$$(k = 1, 2, \ldots n-1)$$

and V may be built up in the following form from the eigenvectors of $\mathbf{A}$:

$$\mathbf{V} = [a_1, a_2, \ldots a_k, \ldots, a_{n-1}] \tag{26}$$

wherein

$$a_k = \sqrt{\frac{2}{n}} \begin{bmatrix} \sin\dfrac{k\pi}{n} \\ \sin\dfrac{2k\pi}{n} \\ \vdots \\ \sin\dfrac{(n-1)k\pi}{n} \end{bmatrix} \tag{27}$$

$$(k = 1, 2, \ldots, n-1).$$

$\mathbf{V}^{-1}$ -- the inverse of $\mathbf{V}$ — being aware of $\mathbf{V}$ may be obtained by transposition

$$\mathbf{V}^{-1} = \mathbf{V}^T. \tag{28}$$

By making use of (24) to (27) the following scalar equations are obtained being equivalent to (23)

$$\frac{d^2 v_k}{dr^2} - \frac{3}{r}\frac{dv_k}{dr} + \lambda_k v_k = d_k, \tag{29}$$

$$(k = 1, 2, \ldots, n-1).$$

The general solution to this common, second order, linear inhomogenic differential equation will be found by summing up the general solution of the homogenic differential equation

$$\frac{d^2 v_k}{dr^2} - \frac{3}{r}\frac{dv_k}{dr} + \lambda_k^2 v_k = 0, \tag{30}$$

$$(k = 1, 2, \ldots, n-1)$$

and one of the particular solutions of the inhomogenic differential equation (29).

The disturbing term of the inhomogenic differential equation evolved in detail:

$$d_k = \sqrt{\frac{2}{n}} \sum_{s=1}^{n-1} f_s \sin\frac{sk\pi}{n} =$$

$$= -\sqrt{\frac{2}{n}}\frac{1}{h^2}\left[\Phi_0 \sin\frac{k\pi}{n} + \Phi_n \sin\frac{(n-1)k\pi}{n}\right] =$$

$$= -\frac{M_c}{2h^2}\sqrt{\frac{2}{n}}\left[\frac{1}{R^4}\sin\frac{k\pi}{n} + \frac{1}{R_2^4}\sin\frac{(n-1)k\pi}{n}\right] r^4 = \tag{31}$$

$$= -D_k r^4,$$

$$(k = 1, 2, \ldots, n-1).$$

Here the notation

$$D_k = -\frac{M_c}{2h^2}\sqrt{\frac{2}{n}}\left[\frac{1}{R_1^4}\sin\frac{k\pi}{n} + \frac{1}{R_2^4}\sin\frac{(n-1)k\pi}{n}\right],$$

$$(k = 1, 2, \ldots, n-1)$$

has been introduced. The particular solution of (29) is sought for in the form

$$V_{kp} = r^4, \tag{32}$$

$$(k = 1, 2, \ldots, n-1)$$

wherein C_k, for the moment is an unknown constant. By replacing (32) into (29) it will be found that such a function can be the solution of the differential equation only in the case, if

$$\lambda_k C_k = -D_k \tag{32a}$$

that is,

$$C_k = -\frac{D_k}{\lambda_k}, \tag{33}$$

$$(k = 1, 2, \ldots, n-1).$$

Thus, a particular solution to the inhomogenic differential equation (29) is e.g. the function

$$v_{kp} = -\frac{D_k}{\lambda_k} r^4, \tag{34}$$

$$(k = 1, 2, \ldots, n-1).$$

The homogenic differential equation (30) with the variable

$$\varrho_k = \sqrt{\lambda_k}\, r, \tag{35}$$

$$(k = 1, 2 \ldots, n-1)$$

will be the differential equation of the following form

$$\frac{d^2 v_k}{d\varrho_k^2} - \frac{3}{\varrho_k}\frac{dv_k}{d\varrho_k} + v_k = 0, \tag{36}$$

$$(k = 1, 2, \ldots, n-1).$$

Seeking for the general solution to Eq. (36) in the form

$$v_k = \varphi_k \psi_k, \tag{37}$$

$$(k = 1, 2, \ldots, n-1)$$

the following differential equation may be written down for the functions φ_k and ψ_k:

$$\varphi_k'' \psi_k + \varphi_k' \left(2\psi_k' - \frac{3}{\varrho_k}\psi_k\right) + \varphi_k \left(\psi_k'' - \frac{3}{\varrho_k}\psi_k' + \psi_k\right) = 0, \tag{38}$$

$$(k = 1, 2, \ldots, n-1).$$

Let us select the function ψ_k in such a way, that the coefficient of the function φ_k be equal to zero. In this case, for example,

$$\psi_k = \varrho_k^{3/2} \tag{39}$$

$$(k = 1, 2, \ldots, n-1).$$

By replacing (39) into Eq. (38), the differential equation defining φ_k will be obtained:

$$\varphi_k'' + \left(1 - \frac{15}{4}\,\frac{1}{\varrho_k^2}\right)\varphi_k = 0, \tag{40}$$

$$(k = 1, 2, \ldots, n-1)\,.$$

From the form

$$\varphi_k'' + \left[1 - \frac{\frac{3}{2}\left(\frac{3}{2}+1\right)}{\varrho_k^2}\right]\varphi_k = 0, \tag{41}$$

$$(k = 1, 2, \ldots, n-1)$$

of Eq. (40), by making use of [2] the solution to (40) may be easily obtained:

$$\varphi_k = \sqrt{\varrho_k}\,[C_{1,k} J_2(\varrho_k) + C_{2,k} N_2(\varrho_k)], \tag{42}$$

$$(k = 1, 2, \ldots, n-1)$$

wherein $\begin{bmatrix} J_2(\varrho) \\ N_2(\varrho) \end{bmatrix}$ represent a Bessel-function of second order and of the $\begin{bmatrix} \text{first} \\ \text{second} \end{bmatrix}$ kind.

On the basis of Eqs (35), (36), ..., (42), the general solution to the homogenic differential equation (30) may be given in the form:

$$v_{kh} = \lambda_k r^2\,[C_{1,k} J_2(\sqrt{\lambda_k}\,r) + C_{2,k} N_2(\sqrt{\lambda_k}\,r)]\,, \tag{43}$$

$$(k = 1, 2, \ldots, n-1)\,.$$

Therefore, the general solution to the inhomogenic differential equation (29) will be:

$$v_k = -\frac{D_k}{\lambda_k} r^4 + \lambda_k r^2\,[C_{1,k} J_2(\sqrt{\lambda_k}\,r) + C_{2,k} N_2(\sqrt{\lambda_k}\,r)], \tag{44}$$

$$(k = 1, 2, \ldots, n-1)\,.$$

From the boundary condition (17a) it follows that

$$C_{2,k} = 0\,, \tag{45}$$

$$(k = 1, 2, \ldots, n-1)$$

for $\Phi_s(0)$ is of finite — zero — value, thus

$$v_k = \sqrt{\frac{2}{n}} \sum_{s=1}^{n-1} \Phi_s \sin \frac{ks \cdot \pi}{n}$$

also is finite in the place $r = 0$, which can only be fulfilled, if

$$C_{2,k} = 0\,,$$

$$(k = 1, 2, \ldots, n-1)\,.$$

The constants $C_{1,k}$ may only be determined with the aid of the boundary condition (17b), from the set of equations

$$\sum_{s=1}^{n-1} J_2\left(\sqrt{\lambda_s}\, R_k\right) \lambda_s R_k^2 \sin \frac{ks\pi}{n} C_{1,s} = \\ = \frac{h}{2\pi} \sqrt{\frac{n}{2}}\, M_c + \sum_{s=1}^{n-1} \frac{D_s}{\lambda_s} R_k^4 \sin \frac{ks\pi}{n}, \\ (k = 1, 2, \ldots, n-1) \tag{46}$$

found by the fulfilment of the boundary condition.

Finally by inverting Eq. (21), one may obtain from v_k the value of Φ_s:

$$\Phi_s = \sqrt{\frac{2}{n}} \sum_{k=1}^{n-1} v_k \sin \frac{ks\pi}{n}, \\ (s = 1, 2, \ldots, n-1). \tag{47}$$

Replacing the partially discretized stress function into Eqs (5) and (6), one finds the following relations for the stresses $\tau_{r\varphi}$ and $\tau_{\varphi z}$:

$$\tau_{r\varphi} = \tau_{r\varphi}(r, z_1^- + ih) = -\frac{1}{r^2} \frac{\Phi_{i+1}(r) - \Phi_{i-1}(r)}{2h}, \tag{48}$$

$$\tau_{\varphi z} = \tau_{\varphi z}(r, z_1^- + ih) = \frac{1}{r^2} \frac{d\Phi_i(r)}{dr}, \\ (i = 0, 1, 2, \ldots, n-1, n). \tag{49}$$

Here

$$\Phi_{-1} = \Phi(r, z_1^- - h) = \Phi_\infty^-(r) \tag{50}$$

and

$$\Phi_{n+1} = \Phi(r, z_2^+ + h) = \Phi_\infty^+(r). \tag{51}$$

Being aware of the stress function we can determine the value

$$\psi = \frac{V}{r} \tag{52}$$

used in analysing the displacements; i.e., the relative angle of torsion of an elementary ring of unit length and of a radius r (see, for example, [3]), on the basis of the differential equation

$$\Psi_{i+1} = \Psi_{i-1} + \frac{1}{r^3} \cdot \frac{2h}{G} \cdot \frac{d\Phi_i}{dr} \\ (i = 0, 1, 2, \ldots, n-1) \tag{53}$$

established on the basis of the relation

$$Gr^3 \frac{\partial \Psi}{\partial z} = \frac{\partial \Phi}{\partial r}. \tag{54}$$

Herein

$$\Psi_0 = 0\,, \tag{55}$$

$$\psi_{-1} = \psi(r, z_1^- - h) = -\frac{2}{\pi}\frac{M_c}{GR_1^3}h, \tag{56}$$

if the torsion is considered with respect to the cross-section designated by "0", having the coordinate $z = z_1^{-2}$.

3. Note

If the body of revolution of the considered meridian curve is symmetric with respect to the plane $z = 0$, then the relation

$$\Phi_i = \Phi_{n-i}\,, \tag{57}$$
$$(i = 0, 1, \ldots, n)$$

will be used. And from this,

$$C_{1,i} = C_{1,n-i}\,, \tag{58}$$
$$(i = 1, 2, \ldots, n-1)$$

will be obtained for the integration constants.

REFERENCES

1. Demidowitsch, B. P.—Maron, J. A.—Shuvalova, E. S.: Numerische Methoden der Analysis, Akademie Verlag, Berlin 1968
2. Pattantyús Á,G.: Manual for Mechanical and Electrical Engineers, V. I, Műszaki Kiadó, Budapest 1961 (In Hungarian)
3. Timoshenko, S.—Goodier, J. N.: The Theory of Elasticity, McGraw-Hill Book Company, Inc. New York—Toronto—London 1951
4. Zurmühl, R.: Matrizen, Springer Verlag, Berlin—Göttingen—Heidelberg 1964

Eine Annäherungsmethode zur Analyse der elastischen Verdrehung von Rundstäben mit veränderlichen Durchmessern. Eine Näherungsmethode zur Analyse der elastischen Verdrehung von Rundstäben mit veränderlichen Durchmessern wird behandelt. Die Differentialgleichung

$$\frac{\partial^2 \Phi}{\partial r^2} - \frac{3}{r}\frac{\partial \Phi}{\partial r} + \frac{\partial^2 \Phi}{\partial z^2} = 0,$$

die die Spannungsfunktion der Verdrehung definiert, wird bei den entsprechenden Randbedingungen durch partielle Diskretisation nach z gelöst.

Приближенный метод исследования упругого кручения круглых стержней переменного сечения. В работе описывается приближенный метод анализа упругого кручения круглых стержней переменного сечения. Дифференциальное уравнение

$$\frac{\partial^2 \Phi}{\partial r^2} - \frac{3}{r}\frac{\partial \Phi}{\partial r} + \frac{\partial^2 \Phi}{\partial z^2} = 0,$$

определяющее функцию напряжения кручения, при соответствующих краевых условиях решается методом дискретирования по частному производному z.

[2] In a strict sense, not a cross-section is dealt with but with a surface of a constant angle of torsion. Such surfaces, being at a sufficiently great distance to the segment of axis of variable diameter, may be assumed, with a reasonable approximation, to be planes, perpendicular to the axis of revolution.

Acta Technica Academiae Scientiarum Hungaricae, Tomus 76 (1—2), pp. 107—127 (1974)

DIMENSIONING OF STRUCTURES FOR FLOOD DISCHARGE ACCORDING TO THE THEORY OF PROBABILITY

E. MISTÉTH*
CAND. OF TECHN. SC.

[Manuscript received 22 November, 1971]

The flood discharge capacity of structures is treated depending on the geometric proportions, discharge factor and random variables. Also an arbitrary probable value of the flood discharge in connection with the service life of the structure might be determined with the aid of one of the extremal distributions. The purpose of the new method of dimensioning is to ensure that the flood discharge capacity should, by a given probability, be higher than the design discharge. The risk incurred may, depending on the amount of damages caused by accidental failure, be established by only economical considerations.

Notation

The following symbols are used in this paper:

R	— flood discharge capacity of structure,
Q	— discharge to be led through structure,
$Y = R - Q$	— discharge reserve to led through structure,
$G(\xi_1, \xi_2, \ldots, \xi_n)$	— function established from geometric proportions of structure and characterizing flood discharge,
v	— discharge factor,
ξ, η	— random variables,
$\xi(t), \eta(t), \zeta(t)$	— stochastic processes,
$a = M(\xi)$	— mean value,
$s = D(\xi)$	— dispersion,
$v = s/a$	— variation factor, relative dispersion,
$\mu_j = M\{[\xi - M(\xi)]^j\}$	— jth order central moment,
$f = \mu_3/s^3$	— asymmetry,
$c = \mu_4/s^4 - 3$	— kurtosis,
$1/r$	— risk incurred,
$F(x)$	— probability distribution function,
$f(x)$	— probability density function,
$m = (\xi - a)/s$	— independent variable of standardized distribution function,
t	— time,
T	— durability of structure,
$C(r)$	— rebuilding cost of structure,
D	— total amount of damages caused by failure of structure, profit loss included,
$L(r)$	— maintenance cost of structure,
q	— rate of interest.

* Dr. E. MISTÉTH, 1085 Budapest Csepreghy u. 2, Hungary.

1. Introduction

A great number of bridges built over small rivers, water courses, are being destroyed by the demolishing effect of floods. The question arises: Why does this happen? Why are they not damaged upon the effect of loads? Why only structures over minor water courses overbalance and bridges of large rivers remain firmly standing? To answer these questions, the safety of passing down flood discharges should be investigated.

The method deducted hereafter does not want to present either new hydraulic [1, 2] or new hydrologic [3, 4] theorems, only in consequence of the scatter of the parameters comprised by the existing functional relations — defines the economically optimal cross-sectional area with the aid of stochastic relations based on the theory of probability. Finally a definition of flood safety is given, based on probability theory.

2. Discharge capacity of the structure

The discharge capacity of the structure shown in Fig. 1 may be characterized by the following deterministic function:

$$R = \nu G(\xi_1, \xi_2, \ldots, \xi_n) \tag{1}$$

Herein, for example,

$\xi_1, \xi_2, \ldots$ — geometric dimensions,
ξ_{n-1} — tailwater elevation,
ξ_n — critical headwater surface,
ν — discharge factor.

The critical headwater surface is the water level at which the structure, upon the effect of the arriving discharge, will hydraulically fail. Description of the different ways of hydraulic failure (backwash of the foundations, adjoining dykes, washing away of superstructure, etc.) will not be discussed here.

The question is, whether the distribution probability function $F_R(R)$ or the probability density function $f_R(R)$ of the discharge capacity (R) might be determined, if the distribution of the independent geometrical dimensions is normal: with a mean value a_i, a dispersion s_i, a density function

$$f_i(x_i) = \frac{1}{\sqrt{2\pi}\, s_i} \exp\left[-\frac{(x_i - a_i)^2}{2s_i^2}\right]$$

and with a discharge factor ν being independent of the geometric dimensions the probability density function of which, for example, according to Pearson III

$$f_\nu(\nu) = \frac{\lambda^\alpha}{\Gamma(\alpha)} (\nu - \nu_0)^{\alpha-1} \exp\left[-\lambda(\nu - \nu_0)\right]$$

then, the density function of the discharge capacity will be

$$f_R(R) = \frac{\lambda^\alpha}{\sqrt{(2\pi)^n}\,\Gamma(\alpha)\,s_1, s_2, \ldots, s_n} \int_{-\infty}^{\infty} \cdots \int_{-\infty}^{\infty} \left[\frac{R}{G(x_1, x_2, \ldots, x_n)} - v_0\right]^{\alpha-1} \times$$

$$\times \exp\left\{-\left[\lambda\left(\frac{R}{G(x_1, x_2, \ldots, x_n)} - v_0\right) + \frac{(x_1 - a_1)^2}{2s_1^2} + \frac{(x_2 - a_2)^2}{2s_2^2} + \ldots + \right.\right.$$

$$\left.\left. + \frac{(x_n - a_n)^2}{2s_n^2}\right]\right\} \times \frac{dx_1\, dx_2 \ldots dx_n}{|G(x_1, x_2, \ldots, x_n)|}. \qquad (2)$$

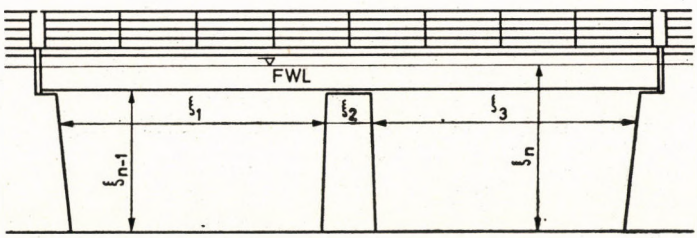

Fig. 1. A structure and its discharge gates

Although the above assumptions are the simplest possible, expression (2), i.e., the density function of the discharge capacity leads, however, to an intricate definite integral only to be solved numerically.

If the probability characteristics of the discharge factor v: the mean value a_v, dispersion s_v, the asymmetry f_v, the kurtosis c_v and the probability characteristics of the geometric dimensions of normal distribution a_i, s_i are given and their relative dispersion $v_i \leq 0.07$, then the probability characteristics a_R, s_R, f_R and c_R are as follows:

$$a_R = M(R) = \bar{R} = a_v G(a_1, a_2, \ldots, a_n) + \ldots,$$

$$s_R^2 = D^2(R) = s_v^2[G(a_1, a_2, \ldots, a_n)]^2 + a_v^2 \sum_{i=1}^{n} G_i^2 s_i^2 + \ldots,$$

$$f_R = f_v \left(\frac{s_v}{s_R}\right)^3 [G(a_1, a_2, \ldots, a_n)]^3 + \ldots, \qquad (3)$$

$$c_R = \frac{1}{s_R^4}\left\{(c_v + 3)\, s_v^4[G(a_1, a_2, \ldots, a_n)]^4 + 3a_v^4 \sum_{i=1}^{n} G_i^4 s_i^4 + \right.$$

$$\left. + 6a_v^2 s_v^2[G(a_1, a_2, \ldots, a_n)]^2 \sum_{i=1}^{n} G_i^2 s_i^2 + 6a_v^4 \sum_{\substack{i=1 \\ j=1}}^{n} G_i^2 G_j^2 s_i^2 s_j^2 + \ldots\right\} - 3.$$

The expression (3) may be obtained from expression (1) by expending the second term of this latter, the function $G(\xi_1, \xi_2, \ldots, \xi_n)$ into Taylor's

series at the place $(a_1, a_2, \ldots, a_n)$. Since $v_i \leqq 0.07$, it is sufficient only to take the terms of the first degree into account. Hereafter, the first four moments of the polynomial algebraic expression consisting of terms of the first degree should be determined, wherefrom expression (3) may be computed. Should $v_i > 0.07$, then also the terms of higher order might be required. If $|f_R| < 0.1$

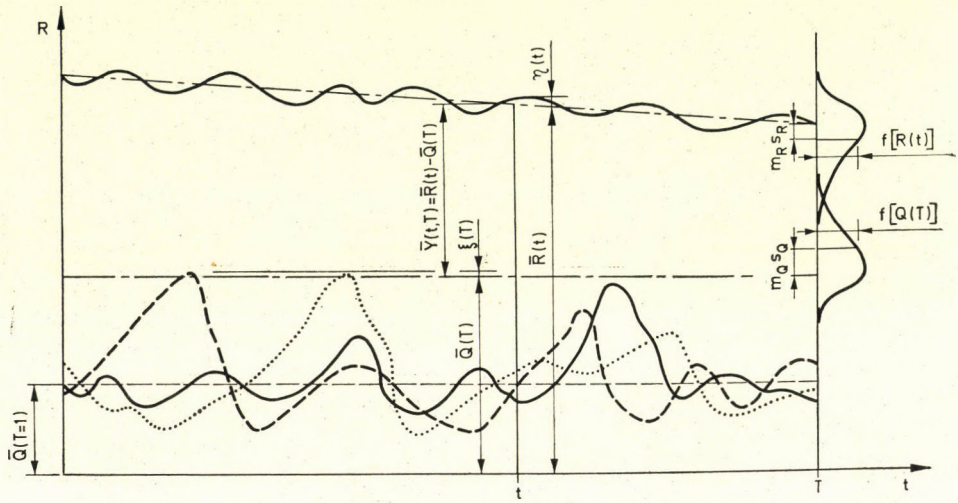

Fig. 2. Time sequences of discharge capacity and maximum discharges $R = R(t)$ and $Q = Q(T)$

and $|c_R| < 0.2$, so the distribution of the flood discharge capacity may be regarded as normal.

In the expression (3)

$$G_i = \left(\frac{\partial G}{\partial \xi_i}\right)_{\substack{\xi_1 = a_1 \\ \xi_n = a_n}} \qquad (i = 1, 2, \ldots, n) .$$

The inaccuracy of the calculation must be involved in the dispersion s_v of the discharge factor v.

As a matter of fact, the flood discharge capacity forms a time sequence $R = \bar{R}(t) + \eta(t)$ because the river varies its geometric dimensions (the dimensions of the bed) in dependence on time. In Fig. 2a realization is represented (the time-dependent discharge capacity of a certain structure of the river). If there exists a periodically repeated maintenance, so $\bar{R}(t) =$ constans; and $\eta(t)$ is a stationary and ergodic stochastic process, so that $M[\eta(t)] = 0$.

Should the maintenance of the structure be dispensed with, so the flood discharge capacity would also be monotonously decreasing (Fig. 2) during the service life of the structure. In this case, $\bar{R}(t)$ might be described, for example, by a trend-like decreasing rational function.

If the discharge capacity cannot be described with the expression (1), i.e., the discharge factor does not depend on the geometric dimensions, the expression $R = R(\xi_1, \xi_2, \ldots, \xi_{n,v})$ should be expanded into Taylor's series at the place $a_1, a_2, \ldots, a_\eta, a_\nu$ and the first four moments of the polynomial power series should be determined for each term.

According to the foregoing, any probabilistic lower limit of the flood discharge capacity of any structure might be determined

$$R_H = \bar{R} - ms_R,$$
$$m = m(f_R, c_R, r). \tag{4}$$

The value of m in expression (4) depends on the distribution described in (2) and on the prescribed $1/r$ probability.

3. Design durability

The structures may, from the viewpoint of their durability conveniently be classified into two groups: permanent structures and temporary constructions. The permanent structures may be designed for a service life of $\tau = 50$ years and the temporary ones for $\tau = 5$ years; extraordinarily large structures should be designed for a durability of $\tau = 100$ to 160 years. Whilst a flood return period of 50 years might be considered in the case of a permanent structure, for example, as a mean value, in the case of a provisional flood discharge clearance, this is to be considered as an event of 10 per cent encounter probability. If

$$\text{Prob}\,[Q(T_1) \leq X_1] = \text{Prob}\,[Q(T_2) \leq X_2]$$

and

$$T_1 > T_2$$

then

$$X_1 > X_2 \tag{5}$$

Expression (5) states that the flood discharge of the same probability of a structure of longer service life is larger that that of a structure of shorter durability.

4. The design flood discharge

For the water stages of rivers and thus for the discharges to be calculated from them, records forming a time sequence of several decades are available. It may be assumed that the yearly maxima of these records con-

stitute a representative homogeneous and independent set. From this set an arbitrary probabilistic flood discharge should be determined by taking into account the service life of the structure.

If the observation period was long enough and furnished a set consisting of a great number of elements, then the distribution fitted to the yearly maxima T_1 should be of the same construction as that fitted to the yearly maxima T_2. Obviously, both distributions should be derivable to the yearly maxima, or, from the distribution drawn on one of their monotonic functions and it might be posited that all the three distributions are upper extrema of the same character. Be the distribution fitted to the yearly maxima

$$\text{Prob}\,[Q(T_0 = 1) \leq x] = F_0(x) \tag{6}$$

the distribution fitted to the maxima of years T_1

$$\text{Prob}\,[Q(T_1) \leq x] = F_1(x) \tag{7}$$

the distribution fitted to the maxima of years T_2

$$\text{Prob}\,[Q(T_2) \leq x] = F_2(x)\,. \tag{8}$$

Thus, the following relation should be true between the distributions

$$\begin{aligned} F_1(x) &= [F_0(x)]^{T_1} = F_0[a(T_1)x + b(T_1)]\,, \\ F_2(x) &= [F_0(x)]^{T_2} = F_0[a(T_2)x + b(T_2)]\,. \end{aligned} \tag{9}$$

Expression (9) states that any one of the upper extrema is derived from the basic distribution by linear transformation. The constraint expressed in relations (9) is, for the distributions sought for, a functional equation. This functional equation was solved by Fréchet [5] in 1927 and by Fisher and Tipett [6] in 1928. In the case at hand, from the three extremal solutions given by them, only two can be taken into account, i.e., the solutions type I and type III.

Type I holding true for all values of x is

$$\begin{gathered} F_\infty(x) = \exp\{-\exp[-\varrho(x - x_0)]\} \\ -\infty < x < \infty \\ \varrho > 0 \end{gathered} \tag{10}$$

and type III holding true only for the values $x > x_0$ is

$$\begin{aligned} F_{-k}(x) &= \exp\{-[\varrho(x - x_0)^{-k}\}\,, \quad \text{if} \quad x > x_0 \\ F_{-k}(x) &= 0 \quad \text{if} \quad x \leq x_0\,, \quad k > 0\,, \quad \varrho > 0 \end{aligned} \tag{11}$$

To which attraction region of extremal distribution a river stretch belongs can only be decided by determining the asymmetry and the kurtosis. For the determination of the attraction region Ruy Aguiar da Silva Leme [8] set up theoretic mathematical conditions.

The upper extremum, type I contains two parameters: the form parameter ϱ and the position parameter x_0. If the service life of the construction is T, so the distribution function of the extremal stochastic process is

$$F_{\infty}(x, T) = \exp\left(-\exp\left\{-\varrho(T)[x - x_0(T)]\right\}\right). \tag{12}$$

The central moments of the distribution type I figuring in expression (12), are as follows:

$$\begin{aligned}
\mu_1(T) &= \bar{Q}(T) = x_0(T) + \frac{0{,}57722}{\varrho(T)}, \\
\mu_2(T) &= [s_Q(T)]^2 = \frac{1{,}64493}{[\varrho(T)]^2}, \\
\mu_3(T) &= \frac{2{,}40411}{[\varrho(T)]^3}, \\
\mu_4(T) &= \frac{14{,}6136}{[\varrho(T)]^4}, \\
x_0(T) &= x_0 + \frac{\ln T}{\varrho(T)}, \\
\varrho(T) &= \varrho .
\end{aligned} \tag{13}$$

The value of ϱ and x_0 may be determined from the basic distribution fitted to the yearly maxima, from the first, second and fifth line of the set of expressions (13).

The asymmetry and the kurtosis of the distribution will be

$$\begin{aligned}
f_Q(T) &= \frac{\mu_3(T)}{[\mu_2(T)]^{3/2}} = 1{,}13955, \\
c_Q(T) &= \frac{\mu_4(T)}{[\mu_2(T)]^2} - 3 = 2{,}4000 .
\end{aligned} \tag{14}$$

From expression (14) it is evident, that the asymmetry and kurtosis of the distribution is a constant figure independent of durability. These two constant figures form a constraint in defining the rivers whose distribution of flood discharge belongs to the upper extremal distribution type I. Commonly, for the case of quiet water flows (as for example, the Danube), $f < 1{,}14$, while in the with disquiet flows of a wide stage-fluctuation range (as, for

example, the river Tisza) $f > 1{,}14$. The determination of a flood discharge $Q_M(T)$ of arbitrary probability $100/r$ per cent, consists in calculating the value of x of the equation

$$F_\infty(x) = 1 - \frac{1}{r}.$$

The solution of the above equation is

$$Q_M(T) = [x,T]_{(100/r)\%} = \frac{\ln (r - \Delta)\, T}{\varrho} + x_0,$$

$$\Delta = \frac{r \ln \left(1 - \frac{1}{r}\right) + 1}{\ln \left(1 - \frac{1}{r}\right)}, \qquad (15)$$

$$\lim_{r \to \infty} \Delta = 0{,}5.$$

In expression (15) the boundary transition may be carried out by a twice repeated application of L'Hopital's rule.

The question arises: if $f_a \neq 1.13955$ and $c_a \neq 2{,}4$, how should one proceed? If $0{,}1 < f_a < 1{,}14$, then the distribution may be expressed with the aid of the first extremal distribution as follows:

$$F_\infty(x, T) = \exp\left\{- \exp\left[- \varrho \left(x^n - x_0 - \frac{\ln T}{\varrho}\right)\right]\right\}. \qquad (16)$$

From expression (16), a flood discharge of arbitrary $100/r$ probability per cent, the design discharge will, for example, be

$$Q_M(T) = [x, T]_{(100/r)\%} = \left[\frac{\ln (r - \Delta)\, T}{\varrho} - 0{,}57722\right]^{1/n}. \qquad (17)$$

In expression (17) the value of Δ is the same as that determined in expression (15). The value of n should be determined from the expression (17) as follows.

The new random variable $\eta = \xi^n - M(\xi^n)$ should be established.

$$[M(\xi) = 0,\ M(\xi^2) = \mu_2, \ldots, M(\xi^i) = \mu_i, \ldots (i = 1, 2, \ldots n).$$

From equation

$$\frac{\mu_3^{(n)}}{[\mu_2^{(n)}]^{3/2}} = 1{,}13955$$

the value of n may be calculated by applying the trial-and-error method. On the basis of the thus obtained value of n the new random variable should be

determined in respect of which the central moments should directly be defined; after repeatedly checking the values of f and c, the expression (16) gives the distribution, while the expression yields the flood discharge of an arbitrary probability.

The characteristics $a_\eta - t$, $s_\eta - t$, $f_\eta - t$ and $c_\eta - t$ of the random variable η are given by expression (13). The probability characteristics a_Q, s_Q, f_Q, c_Q of the random variable ξ to be calculated from it might be similarly determined to the expression (3). If $f_a > 1{,}14$ and $c_a > 2{,}4$, further $x > x_0$, then the distribution function of the extremal stochastic process of type III is

$$F_{-k}(x,T) = \exp(-\{\varrho(T)\,[x - x_0(T)]\}^{-k}. \tag{18}$$

The central moments of the distribution in expression (18) are

$$\begin{aligned}
\mu_1(T) &= \bar{Q}(T) = x_0(T) + \frac{\alpha_1}{\varrho(T)}, \\
\mu_2(T) &= [s_Q(T)]^2 = \frac{\alpha_2}{[\varrho(T)]^2}, \\
\mu_3(T) &= \frac{\alpha_3}{[\varrho(T)]^3}, \\
\mu_4(T) &= \frac{\alpha_4}{[\varrho(T)]^4}, \\
x_0(T) &= x_0, \\
\varrho(T) &= \frac{\varrho}{\sqrt[k]{T}},
\end{aligned} \tag{19}$$

The values of k,ϱ and x_0 figuring in expression (19) should be calculated from the basic distribution to be fitted to the yearly maxima

$$\begin{aligned}
f_Q(k) &= \frac{\mu_3(T)}{[\mu_2(T)]^{3/2}} = \frac{\alpha_3}{[\alpha_2]^{3/2}}, \\
c_Q(k) &= \frac{\mu_4(T)}{[\mu_2(T)]^2} - 3 = \frac{\alpha_4}{[\alpha_2]^2} - 3.
\end{aligned} \tag{20}$$

From expression (20) it is evident, that the asymmetry and kurtosis of the distribution may be calculated from the basic distribution and they are independent of the durability of the construction. The asymmetry and kurtosis is plotted against k in Fig. 3. The values of α in expression (20) are as follows

$$\alpha_1 = \pi\left(-\frac{1}{k}\right),$$

$$\alpha_2 = \pi\left(-\frac{2}{k}\right) - \pi^2\left(-\frac{1}{k}\right),$$

$$\alpha_3 = 2\pi^3\left(-\frac{1}{k}\right) - 3\pi\left(-\frac{1}{k}\right)\pi\left(-\frac{2}{k}\right) + \pi\left(-\frac{3}{k}\right), \tag{21}$$

$$\alpha_4 = \pi\left(-\frac{4}{k}\right) - 4\pi\left(-\frac{3}{k}\right)\pi\left(-\frac{1}{k}\right) + 6\pi\left(-\frac{2}{k}\right)\pi^2\left(-\frac{1}{k}\right) - 3\pi^4\left(-\frac{1}{k}\right).$$

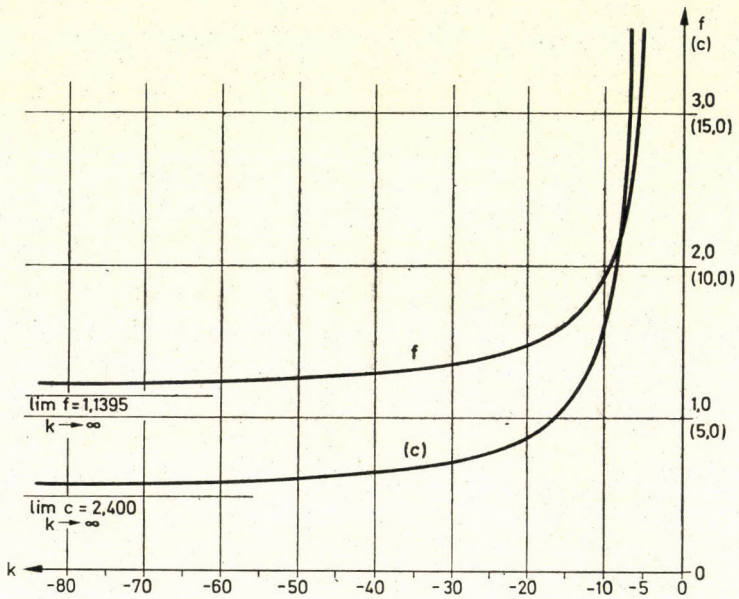

Fig. 3. The asymmetry and kurtosis of extremal distribution III depending on the exponent parameter k. $f = f(k)$ and $c = c(k)$

The values of α of the expression (21) are presented in Table I.

$\pi(z) = z!$ is the Gaussian function.

The parameters of the distribution should be determined from the basic distribution fitted to the yearly maxima, with the aid of Figure 3 and Table I. First, the value of k and in the second step that of ϱ should be calculated. In the calculation, the condition that the dispersions of the values $\alpha_i (i = 2, 3, 4)$ are not equal should be taken into account. Finally, the value of x_0 should be determined from the first line of the expression (19).

The distribution according to the expression (18) is a flood discharge value of an arbitrary probability of $100/r$ per cent, for example, the determi-

Table I

Characteristics of the extremal distribution III (Formulas 20 and 21)

k	α_1	$\frac{\alpha_2}{10^{-2}}$	$\frac{\alpha_3}{10^{-3}}$	$\frac{\alpha_4}{10^{-4}}$	$f=\frac{\alpha_3}{(\alpha_2)^{3/2}}$	$c=\frac{\alpha_4}{(\alpha_2)^2}-3$
−100	1,0059	0,0169	0,0026	0,0016	1,201	2,672
− 90	1,0065	0,0209	0,0036	0,0025	1,207	2,779
− 80	1,0074	0,0266	0,0053	0,0041	1,216	2,799
− 70	1,0084	0,0349	0,0080	0,0071	1,227	2,851
− 60	1,0099	0,0478	0,0130	0,0135	1,243	2,929
− 50	1,0119	0,0694	0,0231	0,0292	1,264	3,045
− 45	1,0133	0,0863	0,0324	0,0457	1,279	2,124
− 40	1,0151	0,1100	0,0473	0,0754	1,297	3,229
− 35	1,0173	0,1452	0,0731	0,1342	1,321	3,368
− 30	1,0204	0,2003	0,1213	0,2632	1,354	3,562
− 28	1,0219	0,2314	0,1526	0,3571	1,370	3,664
− 26	1,0237	0,2706	0,1956	0,4968	1,390	3,783
− 24	1,0258	0,3206	0,2564	0,7122	1,412	3,929
− 22	1,0284	0,3858	0,3452	1,0582	1,440	4,108
− 20	1,0315	0,4733	0,4799	1,6426	1,474	4,333
− 19	1,0333	0,5286	0,5741	2,0873	1,494	4,470
− 18	1,0353	0,5942	0,6946	2,6935	1,516	4,628
− 17	1,0376	0,6729	0,8512	3,5370	1,542	4,811
− 16	1,0402	0,7684	1,0584	4,7389	1,571	5,026
− 15	1,0432	0,8858	1,3383	6,4989	1,605	5,282
− 14	1,0466	1,0324	1,7257	9,1600	1,645	5,594
− 13	1,0507	1,2188	2,2773	13,3386	1,692	5,980
− 12	1,0555	1,4608	3,0896	20,2063	1,750	6,468
− 11	1,0614	1,7833	4,3355	32,1440	1,821	7,108
− 10,0	1,0686	2,2262	6,3455	54,4114	1,910	7,979
− 9,5	1,0729	2,5127	7,8264	72,8779	1,965	8,543
− 9,0	1,0778	2,8587	9,8020	99,9372	2,028	9,229
− 8,5	1,0833	3,2819	12,4961	140,8991	2,102	10,081
− 8,0	1,0897	3,8074	16,2648	205,3577	2,189	11,166
− 7,5	1,0971	4,4713	21,6979	311,6771	2,295	12,590
− 7,0	1,1058	5,3272	29,8178	497,5963	2,425	14,534
− 6,5	1,1162	6,4577	42,5003	847,9752	2,590	17,334
− 6,0	1,1288	7,9958	63,4325	1577,733	2,806	21,678
− 5,5	1,1444	10,1663	100,5340	3330,190	3,101	29,221
− 5,0	1,1642	13,3761	172,9396	8604,590	3,535	45,092
− 4,5	1,1902	18,4256	335,2587	33543,46	4,239	95,801

nation of design discharge is, as a matter of fact, the calculation of the values of x of the equation

$$F_{-k}(x) = 1 - 1/r\,.$$

$$Q_M(T) = [x, T]_{(100/r)\%} = x_0 + \frac{\sqrt[k]{(r-\Delta)T}}{\varrho}\,. \tag{22}$$

The value Δ of the expression (22) is equal to that of expression (15). From expression (21) it may be concluded that $k > 4$, or else, $1/k$, $2/k$, $3/k$ or $4/k$ might be negative integrals and the function has a pole, thus, some of the values of the moments $\mu_i (i = 2, 3, 4)$ to be calculated from them are infinitely high.

For the extremal distribution type III it can be proved that

$$\begin{aligned} &\lim_{k\to\infty} f = 1{,}13955, \\ &\lim_{k\to\infty} c = 2{,}4000\,. \end{aligned} \tag{23}$$

Expression (23) states that the third extremal distribution tends to the extremal distribution type I with the increase of k.

5. A new method of dimensioning

The new dimensioning method treats in Chapter 2 the probability characteristics of the discharge capacity of the structure and, in Chapter 4, those of the flood discharge capacity of the cross-section in question. The structure is designed adequately if

$$\operatorname{Prob}\{[R(t)-Q(T)] \geqq 0\} \geqq 1 - \frac{1}{r}, \qquad 0 < t \leqq T \tag{24}$$

In expression (24) the time sequence is combined of two parts, one of them being the trend character, and the other, a stochastic process

$$\operatorname{Prob}\left(\{[\bar{R}(t) - \bar{Q}(T)] + [\eta(t) - \xi(T)]\} \geq 0\right) \geq 1 - \frac{1}{r}\,. \tag{25}$$

In expression (25) the second part between the square brackets is also a steady state and in the second order an ergodic stochastic process

$$\zeta(t, T) = \eta(t) - \xi(T)$$

the mean value of which is

$$M[\zeta(t,T)] = 0\,.$$

The structure should be so dimensioned that the flood discharge capacity, during its service life, should, by a pre-determined probability, be higher than the flood discharge flowing through the stretch of river dimensioned and related to the durability of the structure. The above relation may be seen in Fig. 2. It might also be stated, that the reserve of discharge which can be led through the structure during the designed working life could be equal to zero only at a value lower than a pre-determined probability.

The probability characteristics of expression (24), in case it is independent of $R(t)$ and $Q(T)$ are

$$a_Y(t,T) = \bar{Y}(t,T) = \bar{R}(t) - \bar{Q}(T),$$

$$[s_Y(t,T)]^2 = [s_R(t)]^2 + [s_Q(T)]^2,$$

$$f_Y(t,T) = -\left\{ f_R(t)\left[\frac{s_R(t)}{s_Y(t,T)}\right]^3 - f_Q(T)\left[\frac{s_Q(T)}{s_Y(t,T)}\right]^3, \right. \tag{26}$$

$$c_Y(t,T) = [c_R(t)+3]\left[\frac{s_R(t)}{s_Y(t,T)}\right]^4 + [c_Q(T)+3]\left[\frac{s_Q(T)}{s_Y(t,T)}\right]^4 + 6\left\{\frac{[s_R(t)]\,[s_Q(T)]}{[s_Y(t,T)]^2}\right\}^2 - 3.$$

If $|f_Y(t,T)| < 0{,}1$ and $|c_Y(t,T)| < 0{,}2$, so, one could calculate with a normal distribution. In this case

$$\bar{R}(t) = \bar{Q}(T) + m\sqrt{[s_Q(T)]^2 + [s_R(t)]^2},$$

$$0 < t \leq T, \tag{27}$$

$$m = m(r).$$

The expression (27) holds true also in the case, where the distribution of $Y(t,T)$ is not normal, however, then $m = m(f_Y, c_Y, r)$, i.e., the value of m does not depend only on the risk incurred, but also on the type of the distribution, as well as on the asymmetry and on the kurtosis. The question arises: how is $Y(t,T)$ distributed? In fact, $Y(t,T)$ is the convolution of the distributions ($R(t)$ and $Q(t)$. Its density function is

$$f_Y(Y) = \int_{-\infty}^{\infty} f_R(R) \cdot f_Q(R - Y)\, dR. \tag{28}$$

The density function of $f_R(R)$ might be obtained from expression (2), whilst the density function $f_Q(Q)$ is the first derivative of the expression (12) or (18), with respect to x taking also the expressions (13) and (19) into consideration. As long as the density function $f_v(v)$ is not clarified by a sufficient number of tests, for density function $f_Y(Y)$ the Pearson's III or IV might be proposed instead of the expression (28).

In this case one of the Pearson's distributions should, with the aid of the method of moments, be fitted to the probability characteristics (a_Y, s_Y, f_Y, c_Y) calculated from expression (26).

In the case where the failure of the structure is characterized by the critical amount of water, the yearly maxima of the water quantity should be established and not the maxima of the yearly discharge. The former being important in the case of earthworks, dikes, may be determined in such a way that in the proximity of the yearly maxima of discharges, discharges associated with the water level above the foot of the dam should be established and summarized according to the continuous period.

6. The optimal risk

In connection with expression (27) only one problem remained unsolved, i.e., the selection of the value of m. On the basis of what was said in the preceding chapter, the value of m depends only on the risk taken. The risk taken may be prescribed by a code rule, the value of which, depending on the significance of the structure may vary between $5 \cdot 10^{-2}$ and $2 \cdot 10^{-3}$.

Be the rebuilding cost of the structure $C(r)$, the risk incurred in respect to the design durability of the structure $1/r$, and the interest rate of the allowance for depreciation q, then, the annual depreciation rate is

$$j = \frac{q^T(q-1)}{q^T - 1} C(r).$$

If the structure fails after a period $t < T$, so the allowance for depreciation of the sum $j(T-t)$ will fall off. This sum — capitalized at the moment of failure — will be

$$j = \frac{q^{(T-t)} - 1}{q^{(T-t)}(q-1)}.$$

If from the preceding expression the depreciation rate will be replaced into this latter one, the remaining allowance for depreciation for the structure, capitalized at the moment of failure, will be

$$\frac{q^T - q^t}{q^T - 1} C(r).$$

D designates the amount of damages arising at the moment of failure of the structure the profit loss included. The total cost (first cost plus the allowance for depreciation fallen off plus the rth part of the amount of damages):

$$K(r) = C(r) + \frac{1}{r}\left[C(r)\left(1 + \frac{q^T - q^t}{q - 1}\right) + D\right]. \tag{29}$$

The minimum cost might occur at the point where the first derivative of the cost function with respect to r is equal to zero.

According to expression (27), the discharge capacity varies linearly if the independent variable is m, and thus $R = Q + ms$. The discharge capacity grows proportionally with the increase of the cross-sectional area of the water flow $R \cong \varphi\tau$. Between the cost of the structure and the cross-sectional area — in a narrow region — there is a linear interdependence: $C(r) \cong A + B\mathfrak{F}$. In the case of fixed f and c, $m = \psi_0 + \psi_1 \log r$ if $r > 0$. With the help of regression calculation it may be established that, for example, in the case of Pearson's III distribution, if $f = 1{,}0$, $m = 0{,}04 + 1{,}48 \log r$ in the region of $20 < r < 10\,000$. The divergence from the preceding linear relation is at most 4 per cent.

Replacing the above expressions into each other,

$$C(r) = \left(A + \frac{BQ}{\varphi} + \frac{Bs\psi_0}{\varphi}\right) + \frac{B\psi_1}{\varphi} \log r \tag{30}$$

and with new symbols the relation

$$C(r) = C_0(b_0 + b_1 \log r) \tag{31}$$

may be written down. Regression calculation has also been carried out in a numerical example, justifying the usefulness of relation (31) with about 3 per cent divergence. The most convenient value of C_0 is the rebuilding cost associated with the $1/e = 0.3679$ times the optimal risk r_0. After deriving the function (29) and making the findings equal to zero, one obtains

$$r(t) = \frac{b_0 + b_1 \log r/e}{b_1 \log e}\left[\frac{D}{C_0(b_0 + b_1 \log r/e)} + \left(1 + \frac{q^T - q^t}{q^T - 1}\right)\right]. \tag{32}$$

In this expression, between the square brackets, the maximum of the second term — in the case of $t = 0$ — is equal to 2. If the maintenance of the structure and its environment is continuous, the distribution of t is, for example, uniform and $M(t) = T/2$ then:

$$M\left(\frac{q^T - q^t}{q^T - 1}\right) \sim \frac{q^T - q^{T/2}}{q^T - 1}$$

and in the case if $q = 1.06$ and $T = 50$,

$$M\left(\frac{q^T - q^t}{q^T - 1}\right) \sim 0{,}8.$$

In consequence of the conveniently selected value of C_0 the value of the numerator is equal to 1. Hence

$$r_{\max} = \frac{1}{0{,}4343\, b_1} \left(\frac{D}{C_0} + 2 \right) . \tag{33}$$

The value of r is variable depending on the amount of damages resulting from the incidental failure and on the significance of the traversing structure, between 20 and 500. It is to be seen that the risk incurred varies between $5 \cdot 10^{-2}$ and $2 \cdot 10^{-3}$. The upper limit is valid for the smaller bridges of secondary roads, in general, for structures of minor importance, while the lower limit holds for bridges of important roads, structures of major significance.

The second constraint is that the yearly rate of the allowance for depreciation

$$\frac{q^T(q-1)}{q^T - 1} C(r)$$

and the total of the maintenance costs per year should be the so-called total minimum cost. It is assumed that the variation of the maintenance cost is given by the relation

$$L(r) = L_0 \left(b_3 + \frac{b_2}{\log r} \right) . \tag{34}$$

The expression (34) is not verified, it is only analogous to expression (31). The convenient value of L_0 is the maintenance cost associated with the optimal risk; in this case, the value of the term between the brackets is equal to 1. The relation (34) reflects a stochastic connection and in the practice of mechanical engineers, where one should reckon with significant maintenance costs, it has been adopted [9]. On the basis of the minimum of the yearly costs, the condition

$$r = 10^{\sqrt{\frac{L_0 b_2 (q^T - 1)}{C_0 b_1 q^T (q-1)}}} \tag{35}$$

should be satisfied. If $T \sim 50$ years and $q - 1 = p$, so

$$r \cong 10^{0{,}95\sqrt{\frac{L_0 b_2}{C_0 b_1 p}}} \tag{36}$$

From between the conditions (33) and (36) this is the critical one which gives the larger value of r. From the combination of the two expressions one has

$$\frac{D}{C_0} \geq 0{,}4343\, b_1\ 10^{0{,}95\sqrt{\frac{L_0 b_2}{C_0 b_1 p}}} - 2 \tag{37}$$

By satisfying the expression (37) the value of r should be determined with the

aid of the expression (33). If the amount of damages caused by the failure of the structure is lower than that given by expression (37), then the value of r is given by the expression (36). Since near the optimum, the cost function to be described by expression (29) hardly varies, in determining the values of r one may proceed, on a certain large scale, by rounding the value upwards.

7. Numerical example

The dimensioning of the river barrage at Kisköre for flood has been carried out with the help of the new method as follows.

The arrangement of the discharge openings of the barrage are shown in Fig. 4. The first task was to determine the discharge capacity of the barrage. The height of the dams of the storage reservoir above the main construction was 93.20 m. The highest water level at

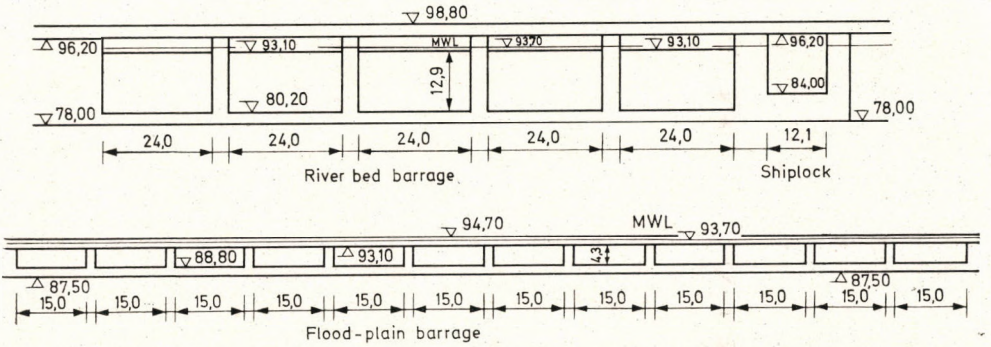

Fig. 4. Outlines of the river barrage at Kisköre

which the structure could pass the flood without being damaged, was 93,70 m (critical head-water level) which means that the water level dammed up over the lower edge of the structure by 0.60 m just does not endanger the stability of the structure. This is the mean value of the critical water level at which the structure hydraulically comes into limit state. In this case, the storage dams should be elevated by an emergency-dam of 1.0 m height.

According to the data of the discharge curve verified by the model-test, at the level 93.20 m, the discharge capacity was $\overline{R} = 6840$ m³/sec; the probability characteristics of the above discharge were

$$s_R = 500 \text{ m}^3/\text{sec} ,$$
$$f_R = 0.8 ,$$
$$c_R = 1.0 .$$

The statistical characteristics of the yearly maxima between 1901 and 1960 of the gauge near Taksony were

$\overline{Q}(1) = 1778$ m³/sec

$$a_Q = 1.0 ,$$
$$s_{\overline{Q}} = 0.1558 ,$$
$$\mu_3 = 0.0814 ,$$
$$\mu_4 = 0.1041 ,$$
$$v_Q = 0.3947 ,$$

$$f_Q = \frac{0.0814}{0.1558 \cdot 0.3947} = 1.324\,,$$

$$c_Q = \frac{0.1041}{0.1558^2} - 3 = 1.288$$

The risk taken in respect of the hydraulic failure of river and flood-plain barrages of different dimensions was investigated for design durability of $T = 100$ years and $T = 50$ years. The results of these investigations are summarized in Table II. In Fig. 5, the conjugate points are shown. With the aid of regression calculation the cost functions have been determined for a durability of $T = 100$ years

$$C(r) = 14.7(0.2401 + 0.5253 \log r) \cdot 10^6\ \$\,,$$

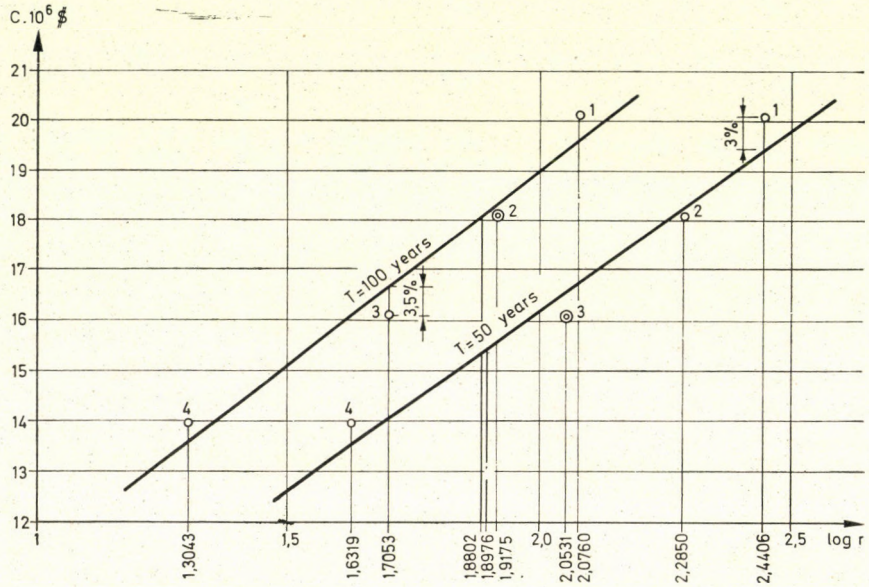

Fig. 5. First costs in dependence on the risk incurred
$C = C_0 (b_0 + b_1 \log r)$ Table II

Table II

Cost and risk data of different designs of the river barrage at Kisköre

No.	Denomination: River bed barrage m	Denomination: flood-plain m	head-water rising, cm	cross-section area, m²	r: T = 50 years	r: T = 100 years	Cost 10⁶$
1	6×24 = 144	14×15 = 210	36,0	2 870	275,8	119,1	20,07
2	5×24 = 120	12×15 = 180	50,6	2 433	193,0	82,7	18,07
3	4×24 = 96	10×15 = 150	72,7	1 992	113,0	50,7	16,07
4	3×24 = 72	7×15 = 105	112,7	1 488	42,8	20,6	13,95

i.e., for a durability of $T = 50$ years

$$C(r) = 12.4(0.1339 + 0.5869 \log r) \cdot 10^6 \text{ \$} .$$

In connection with the amount of damages caused by the failure of the structure, the following list gives information.

Other parts of the main construction failed	40.10^6 \$
Demolition prior to rebuilding	8.10^6 \$
Loss of electric energy for six years	20.10^6 \$
Standstill in irrigation for six years	137.10^6 \$
Bridge over the river Tisza and damages caused by traffic loss	8.10^6 \$
50 human lives $50.0,14.10^6$	7.10^6 \$
Flood protection, other damages	5.10^6 \$
Total	$D = 225.10^6$ \$

Handling human life as money value might be objectionable: herein, the evaluation of the insurance companies has been used.

$$T = 100 \text{ years} ,$$

$$b_1 = 0.5253 ,$$

$$\frac{D}{C_0} = \frac{225}{14.7} = 15.3 ,$$

$$r_{\max} = \frac{2.303}{0.5253}(15.3 + 2) = 75.9; \text{ in the case of five spans; } r = 82.7 ,$$

$$T = 50 \text{ years} ,$$

$$b_1 = 0.5869 ,$$

$$\frac{D}{C_0} = \frac{225}{12.4} = 18.1 ,$$

$$r_{\max} = \frac{2.303}{0.5869}(18.1 + 2) = 79; \text{ for five spans; } r = 113 .$$

From the data of the Table it is evident that the flood gates of the spillway in the barrage at Kisköre should be built for 5×24 m river barrage spans and 12×15 m flood-plain spans for a durability of $T = 100$ years. Would the durability be $T = 50$ years, so would 4×24 m river barrage spans and 10×15 m flood-plain barrage spans be sufficient.

8. Conclusions

On the basis of the above discussion and the numerical example presented, the questions put in the introduction may be answered. The flood discharge safety of bridges taking also into account the design durability, is not satisfactory because the lowest edge of the structure should be designed in the flood level of 5 to 10 years, and not above the 100 year flood by 0.5 to 1.0 m. The lowest edge of the structure, shown in the numerical example would be designed — if one disregards navigation — above the 100 year flood by 1.0 on the level 92.26 m. The bridge positioned at this level would

— in all probability — hydraulically fail. The elevation of the lowest edges of structures erected over navigable rivers furnishes convenient hydraulic safety for floods to pass. This is why the hydraulic failure endangers only bridges built over unnavigable rivers.

In the case of bridges with spans narrower than 15 m, where flat foundations have been constructed by one or two meters under the bottom of the river bed, the danger of hydraulic failure is increased. The foundations of such bridges — independent of the quality of the bedrock — should always be designed on pile foundation, to ensure a stable support for the infrastructure of the bridge against accidental wash-outs. Further, it is advisable to connect the superstructure of the bridges of unnavigable rivers to the supports in accordance with their deadweight. In order to obtain a more favourable discharge factor, not only the piers, but also the abutments should be designed with an arched profile.

The flood safety of these structures — as was also verified by the numerical example — is about 1 to 10 per cent. The mechanical safety on the effect of the loads is 0.2 to 0.05 per cent 10, by two or three orders of magnitude higher than the flood safety. Finally the definition: By flood safety a capacity is meant which, during the design period may be measured with the encounter probability of all of the most unfavourable simultaneous hydraulic and meteorologic effects causing the failure of the structure.

The following statements may be concluded:

1. The flood safety of the structures is only definitely defined by the preestablishment of the design durability. It is advisable to give different periods of durability for structures according to their design character, i.e., temporary, permanent or large structures of great significance.

2. For the determination of flood discharge the extremal distribution I or III might be posited. These distributions also permit the conclusion from time sequences of insufficient length to the discharge distributions by also taking into account the design durability.

3. For the determination of the discharge capacity a sufficient number of small model-tests are to be performed, for being able to define the probability characteristics of the discharge factor and flood discharge (i.e., the mean value, dispersion, asymmetry, kurtosis).

4. It is practicable to use the above procedure for dimensioning of hydrologically analysed water flows, for the distribution of the discharge reserves Pearson's III distribution might temporarily be used.

Permanent structures of hydrologically unexplored water courses should be dimensioned for a flood discharge of 500 to 1000 years; the clearance safety should be 0.3 to 0.5 m. In such conditions it is enough to design temporary structures for a 100-year flood discharge and it is convenient to design the lowest edge of the structure by 0.3 m above the 100-year flood line.

REFERENCES

1. AGROSKIN, I. I.—DIMITRIEV, G. T.—PIKALOV, F. I.: Hydraulics. Tankönyvkiadó, Budapest 1952*
2. KOZÁK, M.: Hydraulics. Lecture notes. Manuscript 1964*
3. VAN TE CHOW: Handbook of Applied Hydrology. McGraw-Hill Book Company, New York—London 1964
4. NÉMETH, E.: Hydrologics and Hydrometry. Tankönyvkiadó, Budapest 1954*
5. FRÉCHET, M.: Sur le loi de probabilité de l'écart maximum. *Ann. Soc. Polonaise Math.* (Cracow) **6** (1927)
6. FISHER, R. A.—TIPETT, L. H. C.: Limiting Force of the Frequency Distribution of the Smallest and Largest Member of a Sample. *Proc. Cambridge Phil. Soc.* **24** (1928)
7. STAROSOLSZKY, Ö.—MUSZKALAY, L.: Manual for Hydraulic Structures II. Műszaki Könyvkiadó, Budapest 1961*
8. Ruy Aguiar da Silva LEME: Os Extremos de Amostras Ocasionais e Suas Aplicações à Engenharia, São Paulo 1954
9. SZÁSZ GY.: Safety in Technics. *Szabványügyi Közlemények* (1965), 10, 12*
10. MISTÉTH E.: Some Safety Problems. 8th Congress of the I.A.B.S.E, New York 1968. Final Report

* In Hungarian

Bemessung von Bauwerken für Hochwasserableitung aufgrund der Wahrscheinlichkeitstheorie. Die Hochwasserschluckfähigkeit der Bauwerke wird in Abhängigkeit der geometrischen Abmessungen und des Durchflussfaktors als Zufallsgrössen dargelegt. Ein beliebiges Maß der Wahrscheinlichkeit kann auch unter Berücksichtigung der vorgesehenen Lebensdauer, mit Hilfe irgendeiner extremalen Verteilung ermittelt werden. Das Wesentliche der neuen Bemessung besteht in der Sicherung einer Schluckfähigkeit, die um eine bestimmte Wahrscheinlichkeit höher als der maßgebende Durchfluss ist. Dieses Risiko kann, in Abhängigkeit von dem Schaden, verursacht durch die zufällige Zerstörung des Bauwerkes, auch nur aufgrund von wirtschaftlichen Erwägungen ermittelt werden.

Расчет технических сооружений на основе теории вероятности на отвод паводковых вод. В работе описывается способность технических сооружений отводить паводковые воды в функции от переменных вероятности, а именно геометрических размеров и фактора расхода. Некоторый произвольный вероятный масштаб расхода паводковых вод может быть определен также с учетом запроектированного срока службы данного технического сооружения, с помощью какого-нибудь экстремального распределения. Новым методом расчета является то условие, что необходимо обеспечить, чтобы водопоглощающая способность была бы с некоторой определенной вероятностью больше размерного расхода паводковых вод. Этот взятый риск, в зависимости от ущерба, вызванного возможным разрушением, может быть определен также на основе только экономических соображений.

Acta Technica Academiae Scientiarum Hungaricae, Tomus 76 (1—2), pp. 129—152 (1974)

ROLE OF THE CENTRE PLATE AND SIDE BEARING IN THE SAFE RIDING OF RAIL VEHICLES

P. KERESZTY*

[Manuscript received: 1 February, 1972]

In the construction technique of rail vehicles, the design of the support of the vehicle underframe on the bogie by a centre plate has been applied for nearly a century. This solution has the advantage of allowing the rocking of the vehicle body on its two bogies. However, if this motion becomes too intense, and causes oscillation of the body. this will already be unfavourable. Astonishingly the RIV and RIC-statutes regulating the change of railway cars on international level do not contain any prescriptions in this connection; in turn, in the PPV-regulation there are to be found some indications in respect to this question which, however, can only be considered as a first step in proposing a regulation.

Introduction

Up to the early forties, for realizing a suitable connection between the rail vehicle and its bogie a simple centre plate or pivot was applied. Since then, a number of designs have been suggested to replace these traditional devices, however, with comparative success. The deficiencies of such new schemes which did not work in the practice, usually revealing themselves only after a few years in the railway working which may be considered as a matter of course, because new designs should only be tested in service after thorough preliminary theoretical investigation.

In the railway operation a vehicle is submitted to a great many effects, which may also act in a number of different combinations. Carrying out supervisory investigations for every possible combination, would require preterhuman effort, not to mention that this work should be done during the period of designing the vehicle, though, it is commonly known that in order to reasonably satisfy the command on vehicles, this period should be limited to a relatively short terme, at most to one or one and a half years. In such cases, the designer is only dependent on his intuition which may be called constructor's inspiration.

After a certain working time when deficiencies on the new construction are beginning to occur, the practice itself shows the effects proving them-

* P. KERESZTY, Zirzen J. u. 8, 1125 Budapest, Hungary.

selves decisive. Unfortunately, these experiences are still rather indistinct, and therefore, thorough investigation work should be carried out in order to throw light on the causes of the occurred deficiencies beginning with the collection of experiences obtained during the service, continued by their evaluation and concluded by establishment of different theoretical processes, i.e., by the selection of the most probable one of them. This would be a rather lengthy work, taking also into account that for this time — as has already been mentioned — the practice itself sorted out the factors which, in the course of the supervisory investigation need not be considered. As good examples for those said above, the supporting device of the bogies of the cars series *Cak* might be mentioned as well as the facility replacing the centre plate of the five axle motor coaches series *Bbmot*.

The fact that, in reality, how far from simple the relationships are, is verified by the present paper. Such a particular phenomenon will be investigated in the fullest detail as that occurring on the centre plate equipment, that is, on the simplest support imaginable and which so-far was unknown by the designers and operators of the rail vehicles.

1. Selection of the type of centre plate

Two kinds of centre plate designs are in use in general [1]; the spherical bogie centre and the flat centre plate, the conceptual schemes of which are depicted in Fig. 1. Certain railways as, for example, are also the Hungarian State Railways, mainly apply the spherical centre plate on their vehicles, while on the freight cars of other companies (U.S.S.R., U.S.A., BR), almost exclusively flat centre plates are to be found [2], [3], [4].

In the spherical centre plate the position of the vehicle body is not accurately defined, therefore the body can freely tilt towards both sides, whilst in the case of flat centre plate, no tilting can occur. Accordingly, the common belief is that if spherical centre plates are applied as supports, the body takes an unstable position because it can tilt both to the left-hand side and to the right-hand side, as much as is allowed by the side pads. On the other hand, owing to the plane supporting surface, it seems that the vehicle body remains stable, that is, in a definitely determined position.

However, in the case of a few tank wagons, having flat centre plate supports, the position of the tank became more unstable than in the case of the spherical centre plate support. Such tank wagons frequently derailed on poorly maintained tracks, and it was remarkable that much more derailments occurred with loaded than with unloaded vehicles, although, as is commonly known, empty wagons are more liable to the danger of derailment. This phenomenon made a detailed investigation necessary in connection with the support of the vehicle underframe on the bogie centre.

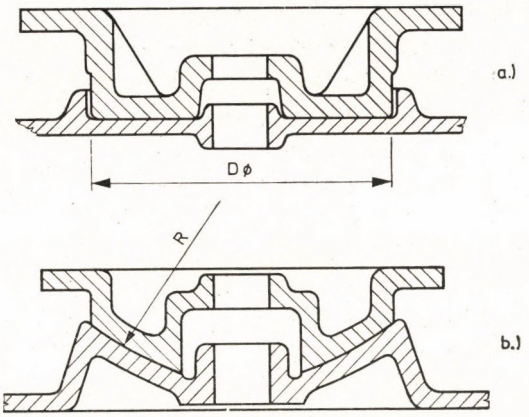

Fig. 1

1.1. *Role of the centre plates*

The centre plate of the bogie vehicles has a number of functions:

— transfers the weight of the body to the bogie;

— permits the rotation of the bogie in the horizontal plane under the vehicle underframe (at the cost of friction causing a resisting force as little as possible):

— realizes the design position of the vehicle body in the design vehicle gauge;

— by the friction between the top and bottom spherical plates hinders the tilting of the vehicle body about its longitudinal axis or, in the case of a flat centre plate, by the fact that the vehicle body can tilt about the edge of the centre plate only under the effect of a turning moment higher than a given one;

— by the mechanical connection between the masses of the bogie frame and vehicle body damps the harmful motions of the bogie, and

— at the same time, also the damaging oscillation of the vehicle body.

Both kinds of the centre plates may more or less fulfil the above functions.

1.2. *Conditions of fitting of the centre plates*

Both during manufacturing and periodical maintanence of the rail vehicles the bogies and the vehicle body are made and repaired separately, respectively. Hereafter, the bogies are situated one after the other, and the vehicle body or tank is lowered onto them. The two bolsters of the two bogies will never lie in the same plane, because neither are their support springs of the same height, nor their specific deflection is exactly identical, further-

more, the structural heights of the parts of the supported construction are not equal, in short, there are tolerances of manufacture everywhere to be found which, on the whole, cause the two bolsters to incline at an angle α_0 (Fig. 2). In Fig. 2, the bolsters of two bogies are to be seen in front elevation, the nearer one being drawn with a full line, and the rear one with a dashed line.

The springs drawn at both ends of the bolster at a basic spacing b, represent the resulting spring suspension on both sides of the bogie, with a spring rate f. The half of the body weight (P) should act on each of the bolsters; let us assume that this load is symmetrically distributed, therefore it acts exactly at the bogie centres. In the figure, the two side pads, lying at a distance e from each other are also to be seen.

To change the obliquity of the two bolsters, a turning moment M should be imposed on each of them, both of the same value but of opposite signs. Under the effect of the moments $+M$ and $-M$, the angle α_0 changes by $\Delta\alpha$, the value of which can be determined. The additional force attacking the springs is equal to $\pm M/b$; the deflections of the springs being equal to $\pm f\ M/b$, therefore, the bolster rotates by a value

$$\sin \Delta \frac{\alpha}{2} = \frac{2fM}{b^2} \approx \frac{\Delta\alpha}{2}.$$

As will be shown later, in the numerical examples, actually, very small angular displacements occur, therefore, the sines and tangents of the angles may be assumed to be equal to the lengths of the arcs. Accordingly, the angle α_0 changes under the effect of the moment M by a value

$$\Delta\alpha \approx \frac{4f}{b^2} M$$

and it will be found that

$$\alpha = \alpha_0 - \Delta\alpha.$$

Let us now see the vehicle body at which tolerances of manufacture also exist, in consequence of which the top parts of the centre plates do not lie in a common plane, but their planes are inclined at an angle β_0. In Fig. 3, only the two cross-sections of the vehicle body are depicted in which it is supported on the two bolsters.

The angle of torsion β_0 of the vehicle body or, in the case in question, of the tank, is negative according to the direction of α_0 represented in Fig. 2.

If, similarly to the case of the bolsters, also on the tank, a pair of moments $\pm M$ are acting, also the angle β_0 will vary by a value $\Delta\beta$.

$$\beta = (-\beta_0) - (-\Delta\beta).$$

Let us denote the specific torsional capacity of the tank by ψ mm/kp which is usually measured at the basic spacing e of the side pads. This factor shows that under the effect of 1 kp lifting force, acting on one of the bearing pads, the corner hoisted by how many mms will be lifted above the plane defined by the other three supports [5]. As a matter of course, the 1 kp lifting

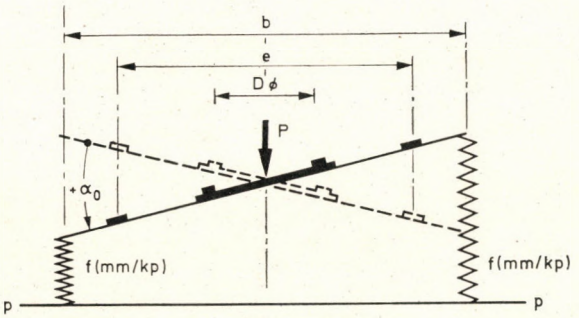

Fig. 2

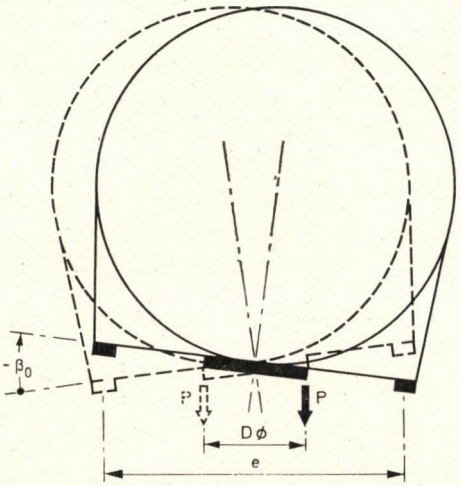

Fig. 3

force is an additional force above the reaction force induced at the point of support of the tank. Accordingly, under the effect of the moment M acting with an arm e, the tank will be twisted by an angle $\Delta\beta$, the value of which is

$$\sin \Delta\beta = \frac{\psi M}{e^2} \approx \Delta\beta .$$

Let us put the tank shown in Fig. 3 upon the two bolsters sketched in Fig. 2. Then, the support will be realized at the two edges of the top centre

plates denoted by P; that is, the eccentric forces P are acting at these points, and induce the moments denoted with M. Also the reacting moments of the twisting moments attacking the bolsters and tank body are equal, only of opposed signs; they constitute the internal moment of the vehicle construction and twist the tank or the vehicle body.

By putting the body into position the angle formed by the bolsters are changing to

$$\alpha = [\alpha_0 - (+\Delta\alpha)],$$

while the angle formed by the two main cross-beams (bolster beams) under the tank will be

$$\beta = [(-\beta_c) - (-\Delta\beta)].$$

The top and bottom centre plates exactly fit together in the case when $\alpha = \beta$.

Accordingly

$$\alpha_0 - \frac{4f}{b^2} M_1 = (-\beta_0) + \frac{\psi}{e^2} M_1,$$

$$\alpha_0 + \beta_0 = \left(\frac{4f}{b^2} + \frac{\psi}{e^2}\right) M_1.$$

By M_1 the moment has been denoted which, in the case of the flat seating of the centre plates partly twists the tank body, partly raises unequal load distribution on the two supports of the bolsters on the bogies.

1.3. *Measurement results obtained on two vehicles*

On the left-hand-side of Figure 4, the variation of the angles of α and β are illustrated with the numerical characteristics of a very stiff tank wagon, versus the moment M. At the right-hand-side of the same figure, the variations of the angles calculated with the data of a four-axle passenger car of a less stiff structure are presented. In both cases, it has been assumed that between the two ends of the bolsters 10 mm of local height difference exists (measured at the basic spacing 2000 mm of the springs) and also 10 mm height difference occurs in the vehicle body or tank, however, this latter, at the basic spacing of 1500 mm of the side bearing pads. The angles α_0 and β_0 are assumed to cause opposite torsions as is also represented in Figs 2 and 3. Thus at the left-hand-side and right-hand-side of the figure, both of the vehicle constructions are illustrated with the identical initial twist

$$\frac{10}{2000} = 0{,}005 \quad = \tan\alpha_0\,; \quad \alpha_0 \simeq 0^\circ 17',$$

$$\frac{10}{1500} = 0{,}0067 = \tan\beta_0\,; \quad \beta_0 \simeq -\,0^\circ 23'.$$

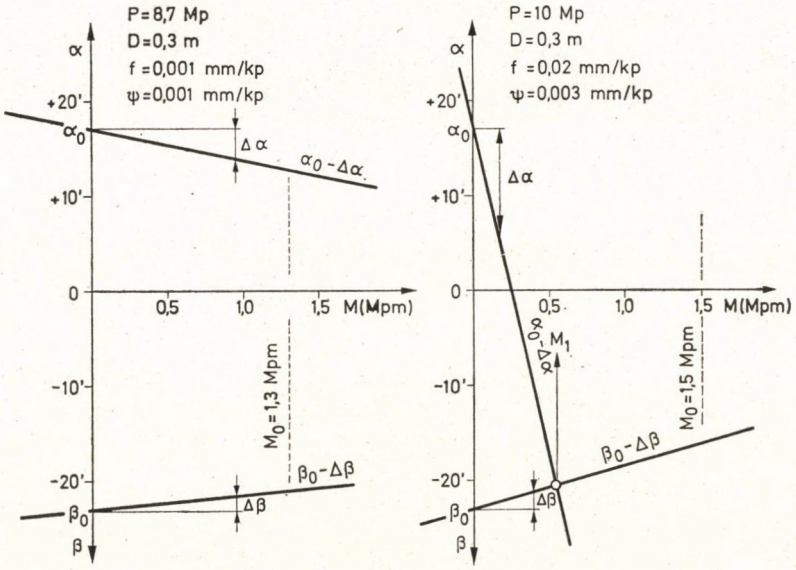

Fig. 4

The equality $\alpha = \beta$ evidently occurs where the two inclined straight lines intersect. The abscissa associated with this point of intersection defines the moment M_1

$$M_1 = \frac{\alpha_0 + \beta_0}{\frac{4f}{b^2} + \frac{\psi}{e^2}} . \tag{1}$$

This point of intersection is found, in the case of the passenger cars at $M_1 = 0{,}55$ Mpm, while in the case of the tank wagons this point lies far outside the area of Fig. 4 which may also be seen from its calculated value

$$M_1 = \frac{0{,}005 + 0{,}0067}{0{,}001 + 0{,}000445} = 8{,}1 \ Mp\,m .$$

However, the dead load of the vehicle body can induce a moment at most of a magnitude

$$M_0 = P\frac{D}{2} \tag{2}$$

and if the bolsters would impose a larger angular displacement since the arm of the force cannot increase, the vehicle body cannot follow the angular displacements of the bolsters, it will only be supported by the edges of the top centre plates. Accordingly, the value of M_0 represents the limiting case where the plates can exactly fit together.

In Fig. 4, also the max. M_0 moments are represented, and here is to be seen that in the case of the passenger car $M_1 < M_0$. Therefore, here, the flat centre plates fit together. However, in the case of the tank wagon the two inclined straight lines do not intersect within the moment-coordinates $\pm M_0$, consequently, the tank will only be supported at two points on the bogies. Therefore, the tank may easily become tilted.

Thus, an empty tank will be supported only at one point on each bogie and got into an unstable, tilting position around the line connecting these points. This circumstance is unfavourable because of the uncertain position of the tank in the design gauge of the vehicle, and mainly, because the vehicle body may come into an undesirable oscillation in running, and this oscillation cannot be damped by any effect. Lastly, neither the load may be transferred symmetrically to the four wheels if the load is *always* transferred to the edge of the centre plate, and thus, also the safety of riding will become worse.

In turn, in the case of a loaded vehicle, the force P^r acting on the centre plate is greater which, in the case of the vehicle investigated, was about $P^r = 34$ Mp. This can already exert a moment $M_0^r = 34{,}0 \cdot 0{,}15 = 5{,}1$ Mpm if the weight of the body rests on the edge of the flat centre plate. However, also in this case there is $M_0^r = 5{,}1$ Mpm $\ll M_1 = 8{,}1$ Mpm. That is why one man alone can sway the tank of a vehicle of such a high gross weight with only the weight of his own body which is altogether about 80 kp. The example of the tank wagon also clearly shows that an unloaded vehicle body gets sooner into this tilting position, than the loaded one, because $M_0^{\text{empty}} < M_0^{\text{loaded}}$.

Such unfavourable conditions cannot occur in the case of the application of a spherical centre plate because here, the upper and lower surfaces fit together in every position at any values of the angles α and β.

1.4. *The vehicle body under which it is desirable to apply spherical centre plate*

According to that said above, in the working condition of the flat centre plate support a change will be caused if the twisting moment M_1 will be augmented above the value of M_0, because in the case of $M_1 > M_0$ tilting of the vehicle body may occur. From the equality $M_1 = M_0$

$$\frac{\alpha_0 + \beta_0}{\frac{4f}{b^2} + \frac{\psi}{e^2}} = P\frac{D}{2}$$

and from this, the following desideratum may be derived:

$$\alpha_0 + \beta_0 \leq P\frac{D}{2}\left(\frac{4f}{b^2} + \frac{\psi}{e^2}\right). \tag{3}$$

Provided that, due to the inaccuracies of the manufacture and assembling, the value of $(\alpha_0 + \beta_0)$ might be higher than the right-hand-side of the equation, then, to avoid tilting, in lieu of the flat centre plate spherical one should conveniently be applied. However, the application of this rule is also desirable below the value of the right-hand-side of the equation in order to make allowance for the dynamic effects which may contribute in bringing the vehicle body into sway. Namely, the investigations carried out so far, were only of a static character.

The spherical centre plate, the construction cost of which is higher than that of the flat centre plate, is in such cases more advantageous than the latter because, as was already mentioned, in applying it, the difference between the angles α_0 and β_0 is indifferent.

1.5. *Running on track twist*

When a railway vehicle comes to a twisted track section, for example, over dipped sleepers or run-off of superelevation, then the track under the bogies is not level, as is exhibited in Fig. 5. In this figure, for simplification's

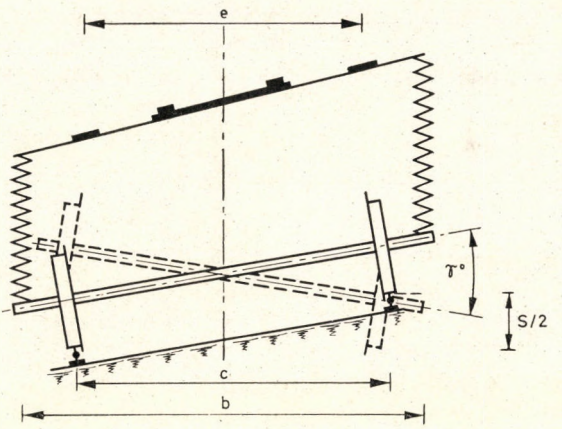

Fig. 5

sake, two wheel sets are represented in the front elevation in the plane of the centre plates, the angle γ formed by the axles of which characterizes the twist of the track measured at a spacing of bogie centres $2(S/2) = S$. By the angle γ, the angle α formed by the bolsters has been changed; only the question arises: to what extent? When the vehicle is running through such a track twist, its structure will be torsioned more and more.

The spring loads are augmented by a couple

$$\frac{b}{c}\,\frac{S}{4f+\psi}$$

[5], and the twisting moment of this couple

$$M_t = \frac{b^2}{c}\,\frac{S}{4f+\psi} \tag{4}$$

will be added to the internal moment M_1 twisting the tank. With the increase of S, according to the equation, proportionally increases also the value of M_t. Therefore, it is to be feared that the body of the passenger car considered to be of very favourable behaviour may also get into a tilting position when the car runs on such a twisted track.

The moment M_1 twisting the structure of the vehicle may increase from its initial value — as has already been stated — only up to reaching the value $+M_0$ or $-M_0$. Accordingly, the value of the twisting moment $\pm M_t$ induced by the track twist must not be allowed to surpass the value

$$|\pm M_t| \leq |\pm M_0 - M_1| \quad |M_0| - |M_1| \geq \frac{b^2}{c}\,\frac{S}{4f+\psi}$$

that is,

$$\left|P\frac{D}{2}\right| - \left|\frac{\alpha_0+\beta_0}{\frac{4f}{b^2}+\frac{\psi}{e^2}}\right| \geq \frac{b^2}{c}\,\frac{S}{4f+\psi}\,.$$

This relation is represented in Fig. 6 which, calculated with the data of the passenger car treated above, shows the region at the shaded areas in which the vehicle body is supported only on two points and thus, comes into a tilting position. In the figure, only the values of the moments may be read off but, with the help of Eq. (4) the amount of the twist S of the track may easily be determined which, in the case of a passenger car of bogie centres $t = 17{,}2$ m corresponds to track twists (at $+M_t$) 1 : 590 and (at $-M_t$) through the runoff of the superelevation 1 : 273.

Thus, as is seen, also the body of a passenger car may come into a tilting position, since track twists to this extent frequently occur. However, such track twists are fortunately short, the vehicles quickly run over them and, hereafter, the vehicle body will rest again on stable supports.

However, these numerical data draw the attention to the practicability of remaining with the value of the moment M_1 as much as possible below the value of M_0.

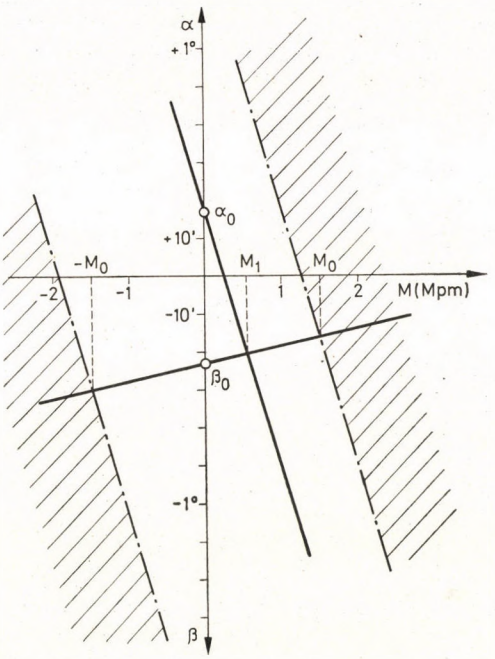

Fig. 6

2. Side bearing pads

According to the traditional design of the railway bogie vehicles the vehicle body is supported at the centre plates on the bogies and on each bogie side pads prevent it in tilting sideways too far. This tilting is permitted by the larger or smaller v-clearances between the vehicle under-frame and side pads. The main purpose of such a vehicle construction design is to interpose between the vehicle body and track a separate structure — the bogie — whose task is to accept the impacts and other undesirable effects from the track and transfer them already in a damped condition to the vehicle body as much as possible. This requires a connection between the vehicle underframe and bogie as loose as possible involving the requirement that they should have a single contact point. This, however, would allow the tilting of the car body which should be prevented first in order to assure the body of remaining within the design gauge of the vehicle, furthermore, to prevent it from taking up a lateral motion with too large amplitudes during running.

It might be said, if this lateral motion is damaging, no clearances should be left between the vehicle underframe and side pads ($v = O$). That kind of support also exist — namely the centre pivot design — where the pivot applied instead of the centre plate, serves only for *axis of rotation* of the bogie

in comparison with the vehicle body, while the load transfer is realized by the side bearings.

However, this design cannot be applied on any kind of vehicle, as it will be seen below. In fact, the movements of the vehicle underframe and bogie are too manifold, their construction should satisfy a number of requirements, and not only permitting the few motions treated in the foregoing.

2.1. *Twisting of the vehicle*

The rail track consists, in general, of two rails which define a plane. Also the *underframe* of the vehicle is constructed, in general, as a plane structure, the points of support of the wheels on the rails also lie in a common plane.

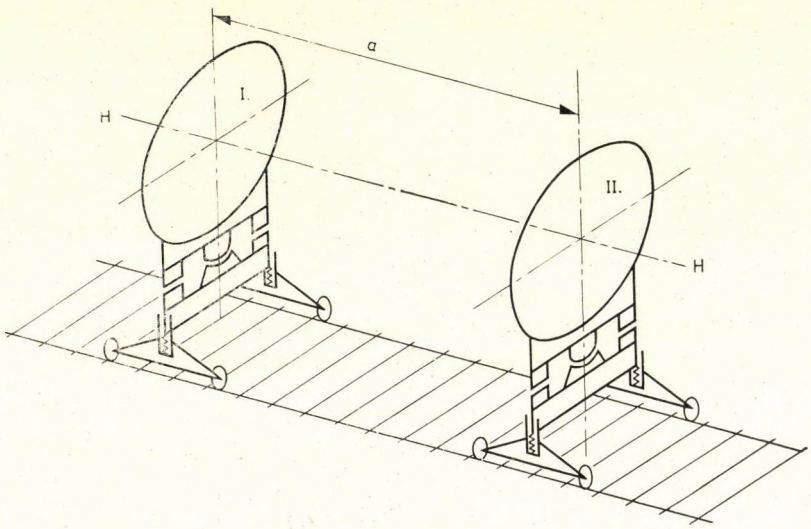

Fig. 7

On such a track with such vehicles, the most favourable condition takes place, where the gross weight of the vehicle is symmetrically distributed, the wheels bearing the approximately identic magnitude of load.

This ideal state in plane is illustrated in Fig. 7 where above the *plane of the track* two *bogies* spaced at bogie centres "a" and above them the principal cross-sections I and II of the vehicle body — tank — are depicted in outlines.

As soon as this, idealistic in plane design, is changed — that is, the vehicle goes over a track twist, for example, over a run-off of super-elevation — the ideal load of the wheels will change, some of them will decrease, others increase. Namely, also the vehicle structure must be distorted in order to have the wheels fitted together with the rails of the twisted track.

The stronger the track twist, the larger is the change in the wheel load. Is the track twist extraordinarily strong, so it may occur that no weight falls on one of the wheels at all, moreover, a wheel may be raised from the *rail head* or, as sometimes one says, the rail is running out from under the wheel.

In this way, the twists in the track reduce the *safe running* of the wheels; the twists and asymmetry in the vehicle construction have the very same consequence [6].

Let us consider in place of the cross-sections I and II in Fig. 7 a continuous stiff tank of a length "a" which does not allow the two cross-sections (the two bogies) to rotate in comparison to each other, that is, does not allow the wheels to fit together with the rails. However, if the cross-sections I and II are connected, by and large, by a *flat underframe* then the two *bogies* can fit, so to say, without difficulty together with the track for, to twist a long flat plate only a little effort is needed.

This explains the phenomenon that the same *bogies* show a *more pronounced tendency to derailment* under a *tank* than under a *flat underframe.*

2.2. *Liquidation of the disadvantage*

The disadvantage of the stiff vehicles is usually eliminated by prescribing a *clearance* between the *side pads* the wider the more stiff the vehicle is. Namely, this clearance, v at the side pads permits the two *bogies* to rotate freely, as compared to each other, in opposed directions (denoted by $+M$ and $-M$ in Fig. 8) under the vehicle body, leaving the *vehicle body* without torsion. Although, the whole vehicle *structure* will be twisted in such cases, the body remains untwisted.

This favourable process lasts until the *side bearing pads* come into contact. Subsequently, the whole vehicle construction is again as stiff, as it was initially when the clearance between the *side bearing pads* did not yet existed [7]. As a matter of course, the stiffer such a vehicle body is against torsion, the larger clearance should be prescribed as a minimum for the type of vehicle in question. Besides, the top limit of the clearance should also be established, because the *amplitude* of the oscillation of the vehicles should be limited and neither should one go beyond the *design gauge of the vehicle.*

Considering the above viewpoints, the purpose is to maintain a *clearance* between the *side pads* which will fall between a prescribed maximum and minimum. As a matter of course the maintenance of the clearance should be checked by operation and should be carried out on a plane track stretch where the structure of the vehicle is not in a twisted state and thus, the magnitude of the *clearance* between the *side pads* will not change. In the case of such a condition of support, the state of the vehicle body is only stable in two extreme positions when the body, besides the centre plates is also supported at one or

the other side by its side pads. Thus, the magnitude of the clearance may change at one of the side pads from zero up to its whole value according to which way the vehicle body rests, for the moment, on its bogies. However, the sum of the two *side-pad clearances* remains always the same within one bogie.

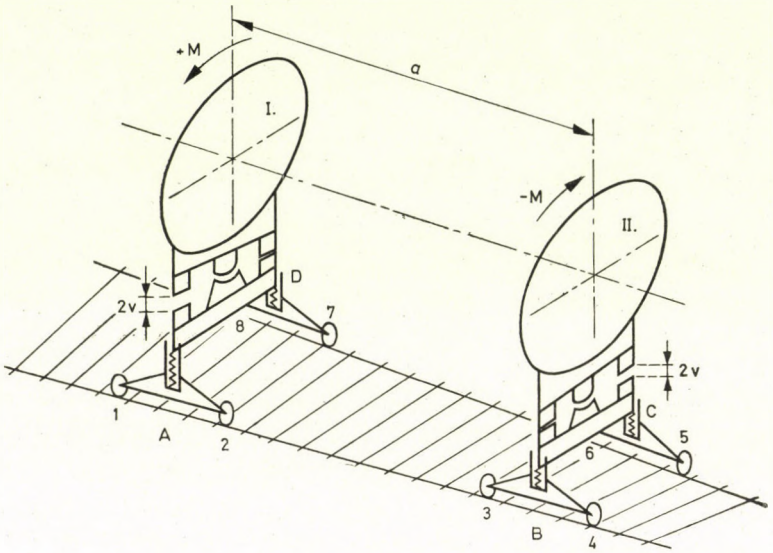

Fig. 8

Accordingly, it is convenient to supervise the *sum* of the clearances because, in this way, the check measurement is made independently on the unstable position of the vehicle body [8].

In Fig. 8, a frame of a vehicle standing on a track twist is to be seen where this twist distorted the vehicle construction towards the directions shown by the arrows $+M$ and $-M$. The torsion took place easily, even so to say without a hitch, as long as a clearance existed between the side pads. At the moment when this clearance disappeared, that is, one of the extreme positions had been reached, as it is depicted in Fig. 8, then, from that moment on, the side pads on the diagonal $B-D$ of the vehicle will limit the torsion which took place up to this moment softly. In turn, on a track twist *opposite* to that represented in the figure, the directions $+M$ and $-M$ will interchange, and in this latter case, the sum of the clearances to be found on the other diagonal of the vehicle marked with $A-C$ will define the possible extent of the soft torsion. Accordingly, to make sure that the vehicles will run over track twists or any direction with the same safety, the sum of the clearances between the side pads on the diagonals of the vehicles standing on a level track should

be larger than a given minimum, however, this should be related to *both diagonals.*

Thereby, the significance of the clearance between the side pads in the safe riding of the stiff vehicles has been verified. Two important rules in connection with this clearance have also been established:

1) the *sum* of two clearances *within a bogie* should be higher than a required minimum V, and lower than a given W maximum;

2) the *sum* of two clearances to be found on the *diagonals of the vehicle* should also be higher than a given V minimum.

2.3. *Manufacturing and supervision*

The statements made in connection with a practical instance of a tank wagon, are well represented in Fig. 9. The magnitudes of V and W theoretically established are considered as the limiting values to the region of tolerances. For the tank wagon selected as an example, the values $V = 15$ mm and $W = 20$ mm will be adopted. The same values are also applied by the railways. This proved to be necessary due to the extraordinary stiffness of the tank body, as well as to the characteristics of the track to be covered [9]. These limiting values of the sum of the clearances will symmetrically be distributed between the side pads, thus, the value $v = 8{,}75 \pm 1{,}25$ mm will be obtained. Herewith, it should be noted that for vehicle structures of torsional stiffness the symmetric construction always has a decisive significance.

In Fig. 9, at the centre, the top view of a four-axle tank wagon is to be seen with the four side pads, denoted with the capitals $A-B-C-D$. To the left, the possible values of the side-pad clearances of the bogie $A-D$ are to be seen and to the right, those of the bogie $B-C$. The abscissas represent the different positions of the body between the two possible extreme cases where the body is supported either on the side pads D and C or on those of A and B. The tank, as was mentioned, is so stiff that its twist caused by the friction on the centre plate can be neglected. These two figures represent the rule 1) in Chapter 2.2. That one under 2) is illustrated by the rectangle below in Fig. 9, which has been obtained by the simple superposition of the two figures.

In this superposed diagram any possible position of the vehicle body is represented by a common ordinate because the simultaneous values of the four clearances between the side pads may always be read off from a single ordinate. Be, for example, the vehicle body, for the moment, in the position marked in the figure with $z-z$. Then, the values of the clearances might be

at A and B $\quad 6 \sim 11$ mm,

at C and D $\quad 14 \sim 9$ mm.

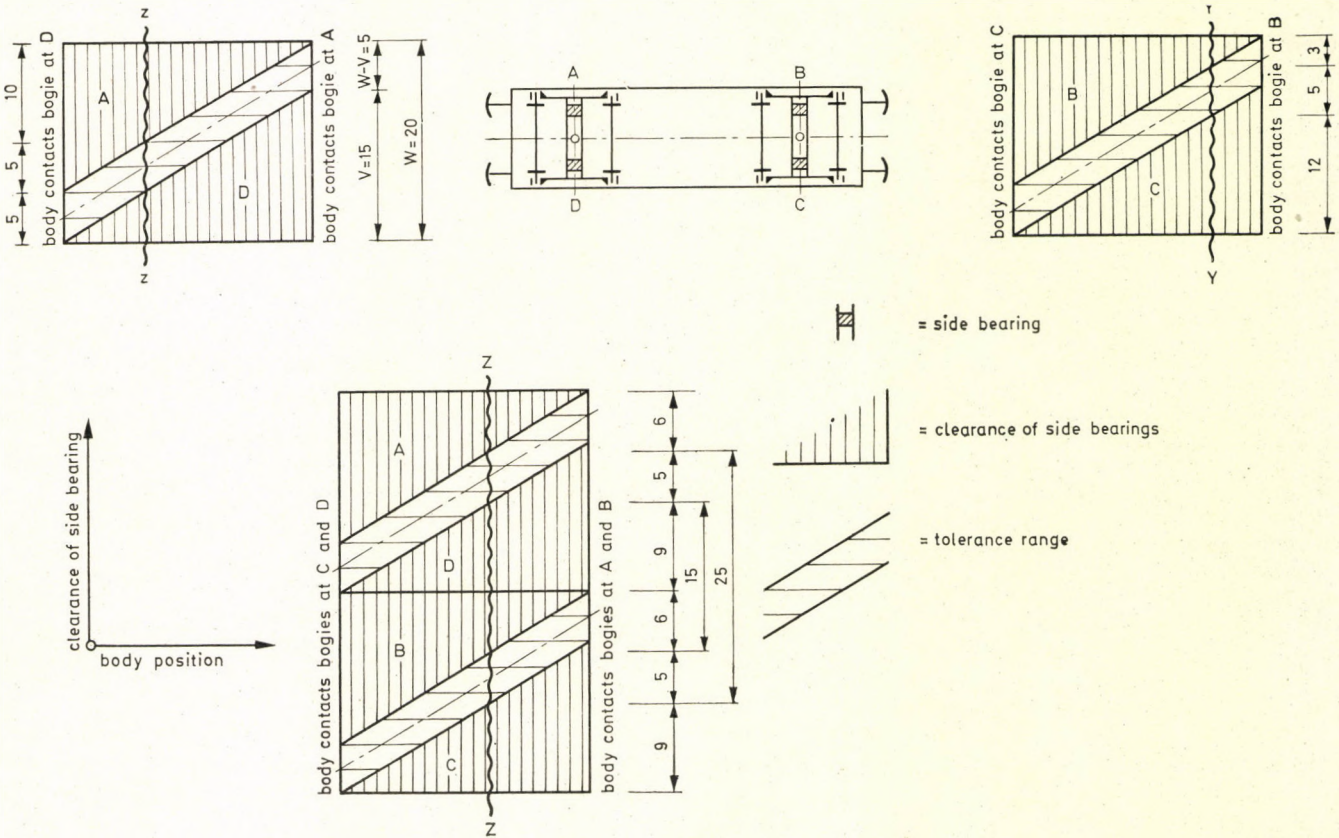
body contacts bogie at D
body contacts bogie at A
body contacts bogie at C
body contacts bogie at B
body contacts bogies at C and D
body contacts bogies at A and B
clearance of side bearing
body position
= side bearing
= clearance of side bearings
= tolerance range
A
B
C
D
Z
Y
W-V=5
V=15
W=20
10
5
5
3
5
12
6
5
9
6
5
9
15
25

Fig. 9

These clearances differ from a mean value $\bar{v}$ at most, only by a tolerance value $\pm\tau$, which can be determined as follows,

$$\bar{v} = \frac{W + V}{4} \qquad \text{and} \qquad \tau = \frac{W - V}{4}.$$

The question may be raised if — due to the reasons already mentioned — the values $\bar{v} = 8{,}75$ mm $\pm|\tau| = 1{,}25$ mm cannot be measured in the symmetric position of the tank and therefore the *sum* of the two side-pad clearances should be measured then this condition does represent difficulties from the viewpoint of the manufacturing technique or supervision of the manufacture.

By some railways, internal rules, valid within the company itself prescribe the condition that $A = B = C = D = \bar{v} \pm \tau$. Let us assume such a manufacturing technique where after putting into position the tanks upon their bogies for the first time the above given clearance values might have been complied with a 86 per cent probability. This means a scatter $\sigma = \tau$ in the case of a Gaussian distribution.

According to the suggestion of the author, only the value of the *sums* should be checked in the following way:

$$\begin{aligned} A + B &= 2\bar{v} \pm 2\tau = 2(\bar{v} \pm \tau), \\ B + C &= 2\bar{v} \pm 2\tau = 2(\bar{v} \pm \tau), \\ A + C &> 2\bar{v} - 2\tau = 2(\bar{v} - \tau), \\ D + B &> 2\bar{v} - 2\tau = 2(\bar{v} - \tau). \end{aligned}$$

According to one familiar theorem of the theory of probability [10] the scatter of the *sum* of the random variables (here A, B, C, D) comes to

$$\sigma_t = \sigma\sqrt{2} < 2\tau.$$

This means that in the case of a manufacturing technique fully identical with the above one, this new prescription relating to the sum of the clearances may be observed with a probability of 95 per cent. Thereby, besides the practicability of the method of determination of the clearances by measuring their sums, the manufacture of the vehicles becomes far more economical because from among a hundred vehicles only in the case of five should the body be removed again after the first assembly, in order to correct the side pad clearance.

(In this connection it should be noticed that the described consideration of the theory of probability is only valid in connection with the independent random variables. However, it may be assumed that the criterion of the independence is fulfilled with reasonable approximation.)

3. Co-operation of the centre plate and side pads

In investigating the centre plate, the condition of the fitting together of the top and bottom centre plates, it was our endeavour to clarify, whilst in the chapter dealing with the side pads the clearance and its distribution between them were revealed. However, the two equipments are mounted on the main cross-beam of the vehicle underframe and on the bolster of the bogie, thus, they are compelled to co-operate to a certain degree.

As the condition of fitting together the top and bottom centre plates it was found in Chapter 1 that the unequality $M_1 < M_0$ should be fulfilled. This is a fact, otherwise the vehicle body comes into a tilting position. In turn, tilting occurs only in the case when this is permitted by the clearance v between the side pads. Fig. 10 shows the level of the side pads during manufacturing before the bogies might be connected under the vehicle body. Should such supervision not be carried out or should it be made carelessly, so it might occur that the height values denoted with A_r and B_r would equal zero. In this case, the vehicle body cannot tilt towards that side about the edge of the centre plate but, at most, only about the edge of the side pad; to which, however, the moment

$$M_{cs} > P\frac{e}{2}$$

is required.

Even more disadvantageous would be the situation when one of the values A_r and B_r would be negative and, in addition, $A_r + B_r$ would be less than zero. In such cases, the centre plates never fit together, and the body will always be in a tilting position with respect to the edge.

The investigations pronouncedly showed three threshold values of the twisting moment, whose numerical magnitude — in the case of the two vehicles investigated in Section 1.3 — are as follows

Table I

Symbol of the moment	Passenger car	Empty tank	Loaded tank
M_0	1,5 Mpm	1,305 Mpm	5,134 Mpm
M_1	0,55 Mpm	8,1 Mpm	8,1 Mpm
M_{cs}	7,5 Mpm	6,52 Mpm	25,7 Mpm

These values show how the three vehicles characterized by them will behave in service. In addition, let us imagine that the vehicle body is always placed upon the bogies with the aid of cranes. On this occasion, the bogie

tends to form the position of the two bolsters gradually to its own shape (β) while, in turn, these perform a twisting effect on the body.

This process

— discontinues in the case of passenger cars already at a twisting moment $M_1 = 0{,}55$ Mpm because at this time, the centre plates lie in a common plane $\alpha = \beta$;

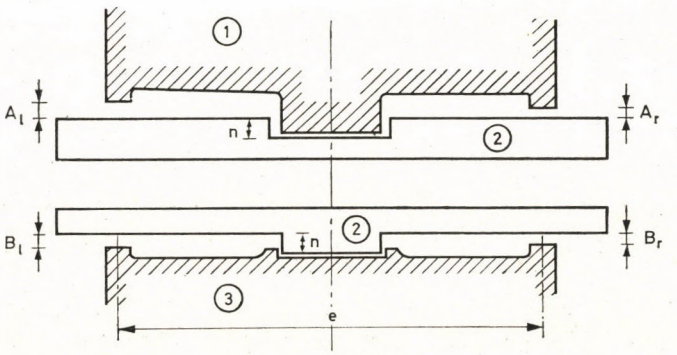

Fig. 10

— the empty tank wagon will, in turn, only be supported on the edge of the centre plates, that is, it will tilt if this would be allowed by the size of the clearance left between the side pads, because $M_1 > M_0$;

— or if there is no sufficient clearance between the side pads when it is supported on the edges of these latter and is tilting. In fact, $M_1 > M_{cs}$ and thus tilting may occur;

— the loaded tank wagon will be supported on the edges and tilt about them because $M_1 > M_0$;

— but if no sufficient clearance has been left at side the pads, the body will be supported on the side bearings, however, without tilting because $M_1 < < M_{cs}$.

By the right determination of the clearance between the side pads — according to Chapter 2 — a very significant other advantage offers. Heretofore, it has been assumed that the track stretch under the vehicle was formed by two *parallel* rails. Now considering the wheel-loads of the vehicle acting on the rails of the twisted track, it should be taken into account that the distorted track tends to twist the structure of the vehicle, as was mentioned in Sections 1,5 and 2,1. Accordingly, a new twisting moment is acting which either augments or reduces the twisting moment to which the vehicle structure was subjected up to that moment. If one investigates the safe riding then only that case is interesting, where the moment twisting the vehicle structure increases. As a consequence of the twist, the weight of one or the other wheel decreases, thereby

also the safety of running will be reduced, thus, the practical value of the investigation performed so far, might be demonstrated.

It would go beyond the scope of this paper to discuss the method of calculation of the wheel-load; the question is treated in detail in [5], [6], [7] and [9]. For carrying out the calculations the following further data are required relating to the passenger and freight cars treated in this paper.

Denomination	Passenger car	Tank wagon	
		empty	loaded
Gross weight of the vehicles . . .	32 000 kp	25 552 kg	76 648 kp
Ideal wheel-load	4 000 kp	3 194 kp	9 581 kp
Bogie centres	15 200 mm	7 800 mm	7 800 mm
Bogie wheel-base	2 950 mm	1 800 mm	1 800 mm

The main cross-dimensions (basic spacing of side pads, basic spacing of spring supports, etc.) of the different cars hardly differ, therefore, they have been taken to be identical. The numerical data of Table II which summarizes the results of the investigations were obtained in this way.

The second line of this table gives information about the magnitude of the twisting moment M_1 which depends on the care of manufacture in relation to the moments M_0 and M_{cs}. In the third line, two pairs of extreme cases are considered. In the case of every vehicle it was assumed for the most unfavourable case that on of the diagonals, no clearances are at disposal between the side pads. The contrary of this is that the clearances between the side pads are symmetrically distributed.

In lines IV, V, VI favourable phenomena are denoted by the "no"-squares, whilst those containing "yes" designate unfavourable cases. The most favourable is the passenger car with symmetrically distributed side-pad clearances. However, the stiff tank — if its car has been made insensible to track imperfections — is always in tilting position and therefore, the vehicle may behave unfavourably from the viewpoint of the dynamics of riding. For the elimination of this unfavourable phenomenon, in lieu of the flat centre plate the application of the spherical one might be suggested.

Reduction of the wheel-load is markedly shown in lines IX and X. Track and body twists cause quite insignificant changes in the wheel-loads of the passenger car, accordingly, they are the safest in riding. However, the problem of the tank wagons is already not so simple.

3.1.1. Let us roll the tank wagon step by step upon a track twist and assume that on a level track clearances are at disposal at each side pad. In such cases — as already mentioned — the two bogies may without any difficulty fit together with the deformed track, thus, only the initial deformation

twists the vehicle body. As a matter of course, the wheel-load will accordingly be reduced. Let us call this state "primary tilting position," that is, where the tank is tilting about the edge of the centre plate. Rolling the wagon upon a more and more twisted track it will come to such a portion of the track where the clearance between the side pads lying on one of the diagonals of the vehicle

Table II

I.	Characteristics of the vehicle			Passenger car		Freight wagon			
						loaded		tare	
II.	Order of magnitude of the twisting moments			$M_1<M_0<M_{cs}$		$M_0<M_1<M_{cs}$		$M_0<M_{cs}<M_1$	
III.	Sum of the clearances between the side bearing pads lying on a diagonal of the vehicle		v_A+v_C	0	4	0	13	0	13
			v_B+v_D	8	4	26	13	26	13
IV.	Is the vehicle body supported on the edge of the centre plate (or side pads)?			yes	no	yes	yes	yes	yes
V.	Is the vehicle body resting in a tilting position?			no	no	no	yes	yes	yes
VI.	Is the vehicle sensitive to track imperfections?			yes	no	yes	no	yes	no
VII.	Reduction of wheel-load	due to initial deformations (kp)		183	183	2700	1712	2175	435
VIII.		due to 1 : 300 track twist (kp)		713	631	4060	420	2170	420
IX.		Total:	(kp)	896	814	6760	2132	2170	855
X.			(%)	22,4	20,4	70,5	22,2	68,1	26,8
XI.	Sum of the clearances between the side pads on a diagonal of the vehicle (mm)		v_A+v_C	—	—	—	8	—	8
			v_B+v_D	—	—	—	8	—	8
XII.	Reduction of wheel-load	due to 1 : 300 track twist		—	—	—	1820	—	1820
XIII.		Total	(kp)	—	—	—	3532	—	2170
XIV.			(%)	—	—	—	36,8	—	68,1

disappear. Thereby, the "primary tilting" discontinues and subsequently, the track twist causes the tank to distort as far as the value of M_{cs} will be reached. In the case of an empty vehicle this equals 2170 kp (that is, 68 per cent) wheel-load reduction. Hereafter, the "secondary tilting position" will

already take place about the edges of the side pads. However, the wheel-loads cannot be reduced any more on a track of any strong twist because the tank again became independent on the two bogies dancing under it. This is why in the column last but one of the line IX only the wheel-load reduction corresponding to the moment M_{cs} instead of the sum stands.

3.1.2. If no clearance would exist, neither initially, between the side pads then, in the process described in Section 3.1.1. only that change will take place that the "primary tilting position" will not occur and the "secondary tilting position" will take already place on a moderate track twist. The maximum wheel-load reduction also remains in this case as 2170 kp. However, it should be noted that, nevertheless, the safety of riding will still be reduced because the same reduction in the wheel-load occurs on a *less accentuated* track twist.

3.2. Let us load the same tank wagon to its full capacity and roll it also in this state to the track twist treated above, joining to a level section. Also now two cases may occur.

3.2.1. If initially no clearance existed between the side pads then the tank will not tilt as far as a twisting moment, higher than M_{cs} increased by the effect of the load carried by the vehicle, does not act. Therefore, the wheel-loads will be more and more reduced as they are running on a more and more twisted track as far as the reduction by 89,5 per cent will be reached. This is the "second tilting position."

3.2.2. In turn, if some clearance existed between the side pads, then — as was to be seen in Section 3.1.1. — a primary tilting position takes place which will be followed by the free torsion of the bogies and only hereafter, by the "second tilting position." Thus, in this latter case, the second tilting position occurs on a stronger track twist whereby the running safety of the vehicle is increased.

3.3. In the lines IX and X of the table, the deviations expressed in percentage are not so accentuated (only 68,1 per cent in comparison with 89,5 per cent) because in the table a track twist 1 : 300 is indicated as a specified maximum value. However, it is well known from the practice [9] that actually much sharper track twists occur.

Otherwise, from the lines IX and X of the table it is obvious that by the twists of the vehicle body and track quite insignificant changes in the wheel-loads of the passenger car are caused. Thus, this vehicle is the safest in riding.

In turn, the riding safety of a rigid tank wagon is satisfactory if the side-pad clearances on a diagonal are symmetrically distributed. Besides, also the magnitude of the clearance is of importance because, if instead of 6,5 + 6,5 mm (lines IX and X) only 4 + 4 mm would be provided for, then, according to the values in lines XIII and XIV the empty tank wagon would become dangerous to derailment.

4. Conclusions

The particular behaviour of the stiff tank wagons in being more inclined to derailment in loaded state than in tare, has been explained. (Sections 3.1. and 3.2.). For securing the safe running of the vehicle, the following measures should be fulfilled;

— Select conveniently the magnitude of the clearance between the side pads and

— distribute it as symmetrically as possible,

— make perceptible the effect of the angles of α_0 and β_0 depending on the accuracy of manufacture.

The investigations have justified that from the viewpoint of the safety of riding, the fact that if the tank could freely tilt on the bogies or the bogies could move as freely as possible under the stiff vehicle body, was favourable. However, it should not be left out of consideration that the investigations were only of quasistatic character. Taking also the dynamics of riding of the vehicles into account, a vehicle body freely tilting may easily get into oscillation which, from the viewpoint of safe riding should at all means be avoided. For this reason vibration dampers should be inserted between the vehicle body and bogies which, besides the costliness, is rather undesirable in the freight car service. A much simpler solution would be the application of spherical centre plate instead of the flat one. The friction in the spherical centre plate realizes on the one hand the required damping effect and on the other — as was seen earlier — eliminates the unfavourable effects of the difference between the angles α_0 and β_0.

REFERENCES

1. WALMSLEY: Non Metallic Liners for Rolling Stock Bearing Surfaces, *Railway Gazette* (1970), May 15
2. VINOKUROV: Vagony, Moscou 1959. Transeldorisdat
3. Car Builders Cyclopedia. 21st edition. Simmons—Bordman Publ. Corp. New York 1961
4. KOFFMAN: Limitations of the Three-Piece Bogie, *Railway Gazette* **15** (1970), 5
5. KERESZTY: La capacité de gauchissage des véhicules. Acta Techn. Hung. **26.** (1959)
— — Moyens propres à assurer la circulation normale des wagons sur des voies présentant des gauches. Question B 55/RPI. UIC—ORE. Utrecht octobre 1964.
KOFFMAN: Torsional Stiffness of Wagons, *Railway Gazette* **15** (1963), 2
6. KERESZTY: Role of Twist of Rail Vehicles in the Process of Derailment. *Közlekedéstudományi Szemle* (1967), No. 1. (In Hungarian)
7. KERESZTY: Some Problems in Analysing the Derailment of Railway Vehicles. *Járművek, Mezőgazdasági Gépek* (1960), April (In Hungarian)
8. PPV-Regulation. 5. Annex III.
9. Moyens propres à assurer la circulation normale des wagons sur des voies présentant des gauches. *Question ORE*, B. 55. *Bulletin de l'ORE.* Utrecht, No. 24. Janvier, 1967

Rolle des Drehtellers und der Gleitstütze in der Fahrsicherheit der Schienenfahrzeuge. Beinahe seit einem Jahrhundert ist im Schienenfahrzeugbau die Bauweise bekannt, wo das Untergestell des Wagens durch Drehteller auf den Drehgestellen unterstützt wird. Diese Lösung bietet dem Wagenkasten eine günstige Möglichkeit über den beiden Drehgestellen eine

schwankende Bewegung vollführen zu können. Wird aber diese Bewegung übertrieben, so wird der Wagenkasten in eine schädliche Schwingung gebracht. Die die Wagenaustauschung im internationalen Verkehr regulierenden Vorschriften RIV und RIC enthalten in dieser Hinsicht interessanterweise keine Verordnungen. Jedoch kann man in den PPV Vorschriften eine Hinweisung finden, die aber nicht mehr als ein Anfangsschritt betrachtet werden kann.

Роль вагонного подпятника и боковой опоры в надежности движения железнодорожного подвижного средства. В области техники железнодорожного движения уже приблизительно в течение одного века известно то решение, при котором рама подвижного средства опирается на поворотную тележку через вагонный подпятник. Такое решение является выгодным для кузова, чтобы кузов мог качаться между двумя своими поворотными тележками. Однако, если такое движение возрастает слишком сильно и достигнет колебательного состояния, то такое явление будет уже вредным. Правила RIV и RIC, систематизирующие в международном отношении обмен вагонами, интересным образом по данному вопросу не содержат никаких указаний. В правилах PPV же можно найти определенную ссылку по данному вопросу, что, конечно, можно считать только начальным шагом. В работе дается числовой анализ данного вопроса; этот анализ может служить основой в сборнике условий для более точного урегулирования данного вопроса.

Acta Technica Academiae Scientiarum Hungaricae, Tomus 76 (1—2), pp. 153—175 (1974)

HERMETICALLY SEALED SILVER–ZINC BATTERIES OPERATING IN THE SILVER (I) OXIDE (Ag_2O) PHASE

L. HAJDU and J. ZAHORÁN

[Manuscript received 24 March, 1972]

The paper briefly reviews the characteristics of the hermetically sealed miniature silver—zinc storage cells enhancing the problems resulting primarily from their hermetic sealing. It deals in detail with the problem of gas formation in sealed silver—zinc cells, and particularly with the factors which permit to influence the amount of gas formation. The influence of the silver structure on the size of the Ag_2O (silver monoxide) phase developing during the charging is analysed, then the design and experimental work is reviewed which enabled the development of hermetically sealed miniature silver—zinc cells working exclusively in the Ag_2O phase. Information is given on the electrical and storing characteristics and the life of such cells, finally they are compared to other cells, pointing out in what direction further research and development should proceed on the base of the very positive results obtained so far.

1. Introduction

The fundamental problem of miniaturized portable instruments and telecommunication engineering devices is the relatively large weight and volume of their supply sources. The high specific energy storage capacity sealed miniature silver–zinc batteries, produced in series by the Hungarian Medicor Works several years ago, and the production of which has been started recently by the joint Hungarian–British company Medicharge, feature the advantages offered by the silver–zinc system die, exactly, to its high specific energy storage.

Earlier publications by authors [1], [2] report in detail on the essential features and development of the silver–zinc battery system. Thus here only the specific energy storage capacity will be compared in Table 1, which clearly illustrates the advantages of the silver–zinc system. Another important advantage of the silver–zinc system is the high loadability, however, with a rather short period of time (starter character).

These two advantages have made the silver–zinc batteries as power sources nonpareil in many fields of application. The hermetically sealed silver–zinc miniature batteries produced by Medicor Works in metal casing may be optionally located in the consumer devices, due exactly to the hermetic seal, either as individual cells, or as batteries consisting of such cell units.

In addition to their advantageous characteristics, the silver–zinc batteries have, however, certain disadvantages as well.

One such drawback is the relatively high world market price of the silver, representing the basic material of the positive electrode and, thereby, that of the batteries proper. True, in theory only 2,02 g silver is required for the production of 1 Ah, but in practice the multiple of this quantity is used. The

Table I

Comparison of the energy densities of conventional and up-to-date silver–zinc accumulators

No.	System	Ah/kg	Wh/kg	Ah/dm³	Wh/dm³
1	Acidic lead accu.	10÷15	20÷30	20÷30	40÷60
2	Alkaline nickel–cadmium accu.	15÷20	18÷24	30÷50	36÷60
3	Silver–zinc accu.	40÷60	60÷75	80÷100	120÷150

silver will not be annihilated by the destruction of the battery, and can be recovered in the form of pure silver with minor losses, still the user is only interested in the purchase price of the new battery.

In addition to the relatively high price the cycle life of even the best quality silver–zinc batteries is only about 60 to 100 cycles [3], assuming full discharge and subsequent recharge in every cycle. Thus, even if the total amount of Ah or, more precisely, Wh values that can be recovered during the life of a silver–zinc battery is considered, the cost per Wh is still high.

As for their treatment, if the specifications of use are adhered to, there is no essential difference between silver–zinc and other (lead, nickel–cadmium, etc.) batteries. Attention must be drawn, however, to the increased sensitivity of the silver–zinc batteries to overcharge, as well as repolarization if they represent batteries consisting of series connected cells.

On the basis of the facts described above, the research team under the direction of authors has focussed its activity, as a first step, on the work to eliminate reverse polarity, the results where of have already been reported on in detail elsewhere [1], [2]. In Chapter 6 of the same publication, authors outline the promising efforts in producing a hermetically sealed miniature silver–zinc battery where, by using the same silver weight, the charge corresponding to the rated capacity can be provided for at a potential level conforming to silver(I)oxide (Ag_2O). Silver–zinc accumulators of a charge of this type have, undoubtedly, great advantages as against a normal accumulator [1], [2]. Practical realization of the possibilities thus explored obviously demanded systematic research and development for the pourpose of clarifying all the relevant problems. In this paper authors report in detail on the research

and development activities directed to produce a sealed miniature silver–zinc accumulator operating in the pure silver(I)oxide phase, on the basis of which the production of such accumulators is carried out in a serial scale today.

2. Gas formation in the sealed silver–zinc accumulator

Processes characteristic of the operation of accumulators, taking place in the course of energy consumption (storage) and power supply, which have been described in detail by the publications referred to [1], [2], are actually chemical reactions where, theoretically, no gas is produced. Reference was made in these papers to the several secondary processes similarly characteristic of the system under operational conditions. These processes, some of which being associated with gas production, are detrimental to the hermetically sealed system. So here only the secondary reactions associated with gas formation will be discussed which are due, essentially, to one of two reasons:

(1) raw material properties, and

(2) the operational conditions of the accumulator.

The most detrimental are the gas forming processes due to raw material characteristics, since they are "spontaneous" which means that they occur during storage after assembly, that is, when the accumulator is at standstill, and because in extreme cases may lead to the complete destruction of the hermetic seal.

In silver–zinc accumulators (but, we believe, this applies to every electrochemical source), examination of the active agents of the charged state is of critical importance, not only because they are to be stable in this condition to meet the preconditions of use, but also because in an essentially identical electrolyte — through a more or less complete separation — two energetically entirely different substances are present: mixture of the silver oxides, and metal zinc.

The stability of silver oxides in basic electrolytes was studied by a number of research workers in recent years [4], [5].

In general, solubility is not associated with gas formation and the silver oxides form, usually, colloid solutions. If the electrolyte contains a sufficient quantity of reducing agent (such as the polybasic alcohol plasticizers of cellophane separators), then the oxides are reduced, and the silver will be resolved in the form of a metal colloid. There is no gas production in there cases since the reducing agent will bind the oxygen.

The situation is entirely different when, in order to utilize the silver to a maximum extent, the positive electrodes of the accumulators are dimensioned in such a manner as to make the use of the so-called peroxide phase (AgO) indispensable for operation at the rated capacity. In such cases the silver oxide

mixture may contain in a considerable quantity certain higher order oxides which discharge oxygen in the course of spontaneous decomposition, e.g.:

$$Ag_2O_3 = 2AgO + 1/2\ O_2\ . \tag{1}$$

This phenomenon is in correlation with the purity of the basic silver material. If the silver contains contaminations decreasing the overvoltage of oxygen separation from the active material, then the silver cannot reach the adequate

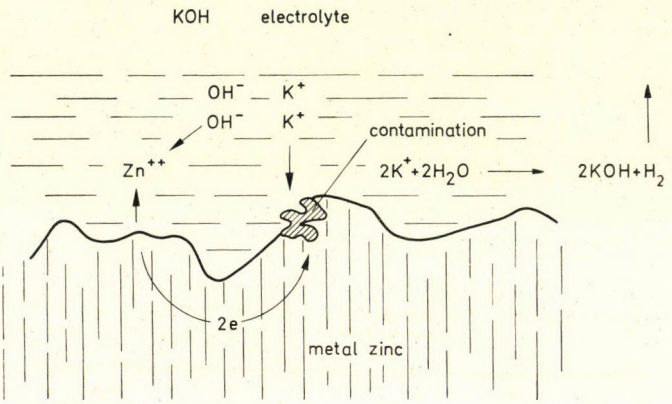

Fig. 1. Detrimental effect of contamination on the zinc electrode

specific charge (no AgO/Ag_2O mixture of adequate ratio can be produced) since the oxide mixture is usually produced by anodic oxidation in these cases, and in the course of this process oxygen production can already be observed.

According to TVARUSHKO, these metal impurities are mainly Co, Ni, Zr, Ce, Pd, and W, where the sequence of the enumeration reflects that of the oxygen overvoltage reduction. At a certain concentration of impurities and anodic current density, AgO cannot even be produced but only the lower order Ag_2O oxide.

As for the behaviour of the active agent, this is related to the operational (charge or discharge) conditions which will be discussed later on.

The behaviour of zinc electrodes in KOH electrolyte is less favourable than that of silver, as in the former case serious gas formation must be reckoned with. According to the well-known reaction

$$Zn + 2KOH + 2H_2O = K_2Zn(OH)_4 + H_2 \tag{2}$$

the zinc will be dissolved by the electrolyte, and this process is in connection with the zinc impurities. Absolutely pure zinc could never be dissolved. Impurities which are, in general, more electropositive than the zinc, form with

the latter a shorted galvanic cell within the electrode, where they act as the cathode and the zinc will be anodically dissolved.

Essentially, this is an electrochemical corrosion of the zinc. The rate of the process depends on the quality of the contaminations. The more electropositive the contamination is as compared to the zinc in the solution, the higher is the speed of the process. The dependence of the differential rate of dissolution on the impurities was studied by means of a simple experiment:

Four zinc plate samples of identical geometry and weight used as basic anode materials of different iron contents, although with approximately identical other impurities were placed into the electrolyte and, after an identical period of time, the volume of the gas trapped by the hydrogen gas collector burette located above the vessel, used for the dissolution process, was measured. During the experiment the temperature was maintained at constant, whereas the pressure was corrected according to the barometric pressure value.

Iron contamination, %	H_2 (in mm³) produced within an identical period of time
0,0004	80
0,001	155
0,0018	195
0,0025	280

With respect to the easier separation of the H_2 gas there is another factor playing a detrimental role which cannot be neglected, either. The majority of impurities will reduce the overvoltage of H_2 separation in zinc, and there is hardly any exception among the most common impurities from this aspect. This process demands, therefore, the possibly maximum purity of basic anode materials as a compulsory specification. Generally, all the contaminations more electropositive than zinc are detrimental, including Fe, Cr, Na, Cu, Pt and C. The very few exceptions increase the potential of H_2 separation in the zinc.

A special action is exerted by mercury which, in addition to the above effect, forms an amalgam with the electropositive impurities and will disperse them in the active anode as against the characteristic nature of Fig. 1 where the contaminant is concentrated, whereby the production of a surface of the same potential is promoted. Thus, an increased potential homogeneity may reduce the process. This is why mercury is deliberately employed in most power sources using zinc anodes to compensate for the effect of impurities. This possibility, however, should never alleviate the requirements set to high-purity anode materials. As an example, the critical contaminant concentrations

of the zinc anodes in sealed silver–zinc accumulators do not exceed 10^{-3} per cent and, in addition, amalgamation of the residual impurities is by 2 to 4 per cent mercury.

By-processes associated with the operational conditions of accumulators may also lead to gas formation. Operational conditions mean here, above all, how charge and discherge are performed.

If the fundamental current producing or accumulating process is assumed to take place as described earlier by authors [1], [2], this may hold true only with the stipulation that the efficiency of the transformation between electric and chemical energies is increasing with a reduced current density in the case of both charge and discharge. Since, on the other hand, current density cannot be reduced infinitely, as this would eliminate the power source character, a compromise is necessary with respect to efficiency. Although the efficiency cf the silver–zinc system is one of the very best part of the energy difference determined by this efficiency is still wasted for secondary processes leading to gas production.

As mentioned earlier, in the case of both charge and discharge the oxidation and reduction of the active substances should be spoken about. In addition, as shown by the fundamental processes, the oxygen uptake of the reduced active agent (Ag) is performed indirectly, by the intermediary of the electrolyte, from the oxidized active substance (ZnO). In charge, for example, the zinc oxide transfers its oxygen through a transmission process to the silver (which gives silver oxide and zinc), while in discharge a vice versa process is completed. When charging with an extremely small current density, the oxygen quantity in the silver oxides thus produced will be exactly equal to the Coulomb number used for charging. If, on the other hand, charging is still acceptable in practice with a finite current density then, in addition to the useful

$$ZnO + 2Ag = Ag_2O + Zn \tag{3}$$

process another process producing oxygen gas, that is,

$$2OH^- = H_2O + 1/2\ O_2 + 2e^- \tag{4}$$

will also take place.

Because of the diffusive and boundary layer inhibitions this process can be observed mainly on the positive electrode while, due to similar reasons, hydrogen may be produced on the negative electrode.

Since oxygen transport is by electrolyte ions, at a high current density the K^+ ions may be neutralized and hydrogen produced instead of the useful reaction (separation of the oxygen atom from the ZnO molecule) at the zinc oxide electrode:

$$2K^+ + 2H_2O + 2e^- = 2KOH + H_2,$$

$$2H_2O + 2e^- = 2OH + H_2. \tag{5}$$

Naturally, it would be a mistake to believe that a charge quantity corresponding to the total amount of energy difference, determined by the efficiency of the energy or even by the current efficiency, might be used for gas producing secondary reactions. This would result in the production of such great gas quantities, even in the extremely high current efficiency silver–zinc accumulators, whereby sealing would be precluded.

Gas producing process connected to the operational conditions will accompany every use where the overcharge or overdischarge of the active substances is involved. Here the two terms, referred to above, mean that the active agents have been transformed quantitatively in the direction of the desired reaction, there is no more active material to be transformed (oxidized or reduced) and, therefore, a by-process associated with gas production (water decomposition) will take place.

In order to avoid such consequences, the quantity of active substances in each accumulator system will be dimensioned to more than the nominal capacity of the accumulator, and the charge as well as discharge conditions will have to satisfy certain requirements (ultimate voltage) which, depending on the current density, enable in both the "charged" and "discharged" state of the accumulator the maintenance of a sufficient quantity of active material reserve conforming to the opposite state. This technical know-how is particularly important in sealed systems.

Gas formation must be avoided in hermetically sealed systems not only because the pressure increase may lead to mechanical damages, deformations, and the destruction of the hermetic seal, but also because the gases thus produced would create inclusions in the active material usually of high porosity, even if the construction could resist all the above effects. Inclusions would then "shield" part of the active surfaces by displacing the electrolyte therefrom. This, in turn, leads to the reduction of the actually active surface, whereafter the current intensity specified as a precondition of use creates an increased current density over this reduced surface. Finally, this will enhance all the consequences brought about by the gas producing processes taking place under operational conditions as described above. This is why gas formation would increasingly accelerate the destruction of any accumulator.

All the possibilities (material purity, precise specification of the operational conditions, dimensioning) available to minimize gas production (it cannot be completely eliminated) are made good use of the hermetically sealed silver–zinc miniature accumulators manufactured by Medicor Works.

In the application of the dual depolarizer preventing reverse polarization, as described in [1] and [2], one of the preconditions was to find a material which, if not as its main requirement, could reduce gas formation at the positive electrode. This is actually accomplished, indeed, by cadmium oxide finally employed for the purpose.

According to the measurement results of TVARUSHKO [4], the gas production of a silver oxide electrode made of absolutely pure (99,99 per cent) silver is 23 μl/g/day, whereas that of a cadmium alloyed silver electrode is only 16 μl/g/day.

The most interesting is that the reduced spontaneous gas formation as described above was associated with a similarly reduced gas production in the accumulator used. Further reduction in the gas formation was achieved by

Table II

Comparison of the gas quantities produced in conventional double depolarizer and lead additive type accumulators

Construction	Condition	Gas quantity (mm²)	
		+ electrode	− electrode
I. Conventional	After charge	150	50
	After 60 cycles	200	500
II. Double depolar.	After charge	50	50
	After 100 cycles	200	200
III. Lead additive	After charge	35	35
	After 150 cycles	35	50

Note: Data represent the average of at least 6 cells, each. The initial deformation of the cells (a few tenth of a mm) begins at a gas quantity of about 500 or 600 mm³.

using another material again, not primarily for this purpose, but to promote better silver utilization, namely a lead additive. Reduction of the gas quantity produced in hermetically sealed accumulators is illustrated by Table II where data of conventional, dual depolarizer, and lead additive accumulators are compared (average data of 6 cells).

The value of these results is further increased by the fact that an increased cycle number could be achieved in the sequence of enumeration.

Electrochemical refinement, amalgamation, and the high purity of the basic materials are the factors in the negative electrode which reduce gas formation to an acceptable level. Still, further research cannot be considered as superfluous although spectacular results of several orders of magnitude influence are not to be expected.

3. Effect of the silver structure on the Ag_2O phase size

Literary data and our own experiences confirm that, if the grain size of the silver active agent can be decreased while the necessary value (50 to 60 per cent) of the electrode porosity is maintained, the quantity readily charged

within the Ag_2O phase will increase at an identical current density. This is a natural consequence of the fact that the actual current density will decrease with the reduction of the active grain size (surface increase).

It was experienced, however, that the quantity which could be charged in the Ag_2O phase did not proportionally increase with the reduction of the silver dust grain size, but that the reduction of the average grain size to 40 or 50 per cent would permit only a 10 to 15 per cent higher charge in that phase.

Accordingly, in our activity studies about 140 mAh/g quantities of silver dust, slightly dependent on grain size have been observed, that could be charged in the Ag_2O phase. The pressing parameters of the test electrodes were kept constant.

The situation is entirely different in the case of active silver developed over an intact silver wire core [6], [7], where the active substance is not self-pressed but has a density corresponding to its development (chlorination). The specific charge in the Ag_2O phase with this active silver type is 157 mAh/g, that is, essentially greater than the same figure for powder.

As is well known, in silver–zinc systems the reduction of the silver(I)oxide capacity during the silver electrode cycles is due mainly to the agglomeration (specific surface reduction) of the active grains.

This process depends on the current density [8] as well as on the additives. Test results obtained with silver of lead content revealed that, after repeated cycle studies, the quantity which could be charged initially in the Ag_2O phase could not be maintained if electrodes pressed from active powder have been used (this quantity decreased, of course), whereas in the case of active silver formed on wire electrodes it did not change as compared to the initial value, even if a number of cycles had been completed. Literature explains this phenomenon [9] by the formation of silver plumbates over the surface of the silver grains as early as during the formation process proper which, then, as a "protective film" prevents the agglomeration of the grains, and ensures a permanent specific surface for a long period of time.

A rather interesting feature of the phenomenon is that, initially, the lead additive will not necessarily improve the specific values. On the contrary, it will slightly impair these figures during the formation cycle (Fig. 2, curves a and b). Fig 2 presents the life test results of accumulators in a comparative illustration. Curve "a" represents the data of accumulators with lead additives, while curve "b" indicates the same without such an additive, in the function of cycle number. In other words, this is the charge in the Ag_2O phase.

The next target was to determine the lead concentration ensuring the most favourable effect. Application of the suggested [10] 1 per cent Pb as related to active silver was found to cause increased damage in the cellophane separator as compared to cells without an additive, whereas an additive of 0,5 per cent could not exert the desired effect. Subsequent experiments, there-

fore, have been performed with a Pb additive of 0,8 per cent active silver weight. This, finally, has led to a construction which, at a reduced silver quantity, makes the production of accumulator cells operating in the Ag_2O phase possible.

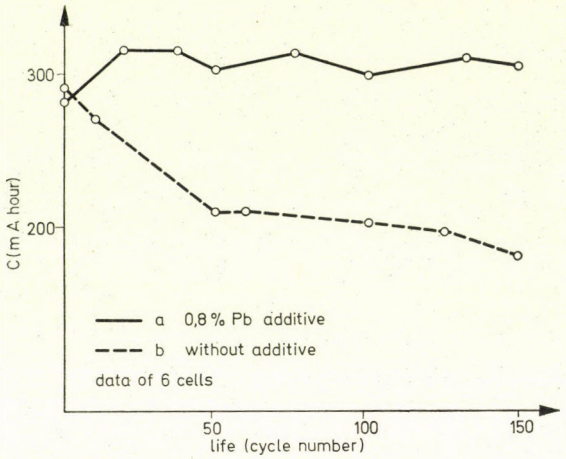

Fig. 2. Comparison of the charge of accumulators with and without a lead additive, via the positive electrode

4. Experimental

Prior to the beginning of the experimental work the constructional principles had to be elaborated according to the theory described above, whereby the miniature silver–zinc accumulators operating in the silver (I)oxide phase could then be produced in series with sufficient safety. These fundamental principles were as follows:

(a) No basic contructional modification was needed which would have meant a significant change as compared to the accumulators series produced for several years. This applied to both the main components of the individual cell types (housing, cover, sealing ring, separator, etc), and the main technological processes.

(b) An eventual modification of the construction was not to cause surplus cost in the manufacture of the products. This applied, above all, to the silver quantity used which, up to a certain limit, would have increased the ratio of the silver(I)oxide phase but this should have resulted in a considerable extra cost.

(c) A constructional modification was to result not only the possibility of charging into the accumulators the quantity corresponding to their rated capacity actually within the silver(I) phase, and make the accumulators

maintain this advantageous characteristic practically along their entire life, but also to improve their other parameters as well, up to the feasible degree. This applied to both cycle life figures.

(d) No constructional modification should affect the very good results of earlier development (the unique construction and technology of the silver

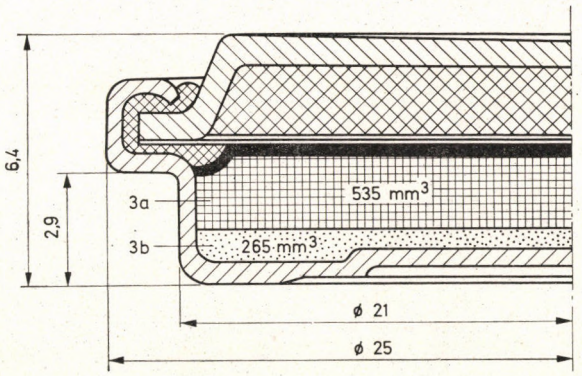

Fig. 3. Sectional view of the B—300 DP lead additive type miniature accumulator

electrode, favourable properties of the zinc electrode, the effect of the secondary depolarizer eliminating reverse polarization, etc.) which have made the premodification accumulators nonpareil in their field.

By taking these fundamental principles into consideration, the new construction design has made use of the constructional principles of the accumulators equipped with a secondary depolarizer including, however, the supplementations aiming at the accomplishment of the final objectives as well. In order to verify the practical adaptability of the systematic research efforts, let us deal in detail with the practical features of the construction design.

Every silver–zinc accumulator is characterized by the fact that the quantity of active agents theoretically required for its operation, is considerably overdimensioned. Practically the same principle was followed in the production of the silver–zinc accumulators manufactured by Medicor. Overdimensioning the quantity of active agents is all the more justified here, as operation under hermetically sealed conditions demands the prevention of appreciable gas formation at the electrodes regardless of the circumstances (see Section 2).

Details of the construction will be illustrated by the example of a 300 mAh rated capacity miniature accumulator cell (Fig. 3). The schematic illustration in this Figure where, nevertheless, all the main dimensions and the two electrode space volumes can be clearly seen, represents the con-

struction of a cell operating in the pure silver(I)oxide phase. In a cell of normal construction the positive electrode areas 3/a and 3/b contain a total of 2,95 g pure silver weight activated [6], [7] silver electrodes made of 0,14 mm silver wire. In reduced state the average porosity of the silver electrodes is

$$P_{red} = \frac{1 - \gamma_{apparent}}{\gamma_{actual}} = \frac{1 - 3.7}{10.4} = 0.645 = 64.5\ \%$$

where

$$\gamma_{apparent} = \frac{2.95}{0.8} = 3.7\ g/cm^3$$

$$\gamma_{actual} = 10{,}4\ g/cm^3$$

It will have to be noted here that the average porosity after the electrode has been installed, that is, when about 56% of the 2,95 g total silver weight is already oxidized in AgO state, will decrease to about 57 per cent. In this state the charge quantity that can be recovered from the silver electrode is about 780 mAh. Addition of the secondary depolarizer made the elimination of the overcapacity of the silver electrode, as compared to that of the zinc electrode possible. This, in turn, has led to the reduction of the wire electrode weight which, together with the experiments [6], [7] aimed at an increased specific silver utilization, and continued simultaneously with the original research project, enabled us to employ a 2,05 g weight silver wire electrode of an average capacity of 650 mAh (appr. 65% utilization). Reduction in the weight of the wire electrode permitted its compression to a smaller volume at practically the same porosity whereby room was made available for the secondary depolarizer.

In the determination of the required secondary depolarizer quantities the aspects studied in detail during previous research [1], [2] had to be taken into consideration. The CdO active agent had to be employed in such a quantity as to be capable of ensuring a voltage of about 0,4 V for 3 or 4 hours, and to have a silver dust quantity acting as conductor additive enough to supplement, as a silver easy to charge in the Ag_2O phase, the Ag_2O phase of the wire electrode up to the rated capacity of the cell, in addition to providing for the conductivity needed.

The CdO quantity still providing for one-third (100 mAh) of the nominal cell capacity, with the about 75% electrochemical efficiency known in the reduction of CdO taken into account, is

$$\frac{0{,}100}{0{,}75 \cdot 0{,}418} = 0{,}32\ g$$

where 0,418 Ah/g is the theoretical equivalent of CdO. A CdO quantity of 0,35 g was selected for safety reasons, corresponding practically to 110 mAh.

Earlier research confirmed that if, as a conductor additive, active silver dust is mixed to the CdO in a ratio of 30 : 70 or 40 : 60 per cent, this will already provide for the desired conductivity. Thus, in our case the problem was to find the active silver dust quantity within the above ratio range which could complete, in the course of charging, the Ag_2O phase of the wire electrode to the rated capacity. Previous investigations conducted with silver wire electrodes revealed in good agreement with literary data that, in the course of the first cycles, about 1/3 of the total electrode capacity or, more precisely, on the average its 31,4 per cent could be charged into the electrode within the Ag_2O phase. Again on the average, the 31,4 per cent as related to the total capacity of the silver wire electrode means a capacity of

$$0{,}314 \cdot 650 = 205 \text{ mAh}$$

that can be recharged in the Ag_2O phase, with a 650 mAh total wire electrode capacity in mind.

Although the capacity that can be charged into the active silver dust in the silver(I)oxide phase is slightly depedent on the Ag : CdO ratio, it is about 140 mAh/g in the range of the ratios reckoned with.

Again for safety reasons a silver dust quantity of 0,75 g was selected which would provide, theoretically, for an Ag_2O phase of

$$0{,}75 \cdot 140 = 105 \text{ mAh.}$$

Thus, theoretically, the capacity that can be charged in the silver(I) phase is

$$Ag_2O = 205 + 105 = 310 \text{ mAh.}$$

The powder mix thus obtained contains 68 per cent silver and 32 per cent CdO. Its calculated specific weight is 9,5 g/cm^3, whereby the porosity of the second depolarizer compressed to the given volume (2b) will be:

$$P_{\text{second}} = \frac{1 - \gamma_{\text{app}}}{\gamma_{\text{act}}} = 1 - \frac{5{,}15}{9{,}5} = 0{,}565 = 56{,}5\ \%$$

where

$$\gamma_{\text{app}} = \frac{G_{\text{second}}}{V_{\text{second}}} = \frac{1{,}1}{0{,}265} = 5{,}15 \text{ g/cm}^3$$

Thus, the porosity of the secondary depolarizer is seen to be practically identical to that of the oxidized wire electrode, which means that the average porosity of the positive electrode area remained unchanged as compared to the original construction.

In the modified construction the active agent content of the zinc electrode too, had to be changed. More precisely, it had to be increased to such a degree

whereby the metal zinc content of the electrode could make the total reduction of both the silver wire electrode included in an oxidized form and the CdO active substance possible. In the reduction of the zinc electrode employed [12] its electrochemical efficiency was, according to our earlier investigations, at least 95 per cent, thus a zinc electrode of

$$\frac{650 + 115}{0{,}95} 1{,}22 = 975\,\text{mg}$$

average zinc content could be realized. During the so-called "zero discharge" of the total zinc quantity of the new cells, that is, when only the capacity of the silver wire electrode installed in oxidized state would be discharged, not more than 85 per cent would be transformed to $Zn(OH)_2$, whereas 15 per cent would remain in metal zinc form. During the next charge this residual metal zinc will act as a retransformation core and, according to experience, improve the operation of the zinc electrode.

Experimental cells produced according to the construction described above could take up a charge of 280 or 290 mAh in the Ag_2O phase as early as during the very first charge following the "zero discharge" and, therefore, still representing part of the production process. This increased during the next few cycles to 300 or 310 mAh but, in the subsequent cycles, each cell exhibited a considerable decrease as far as the quantity that could be charged in the Ag_2O phase was concerned (line "b" in Fig. 2). Thus, the experiment unequivocally verified that, in the case of a rational construction, the rated capacity might be charged into the double depolarizer type cells practically within the silver(I)oxide phase, although the same cells proved that during subsequent cycles, because of the silver structure changes described in detail in Section 3, the quantity that might be charged in the Ag_2O phase would necessarily decrease.

The effect exerted by the lead additive on the silver structure as descirbed similarly in Section 3 made, on the other hand, it evident to attempt the compensation of the unfavourable structure variation taking place along the successive cycles by the action of a correctly selected lead additive in such a manner as to keep the initial advantageous Ag_2O phase maintained practically during the entire life of the cell.

Determination of the necessary lead additive quantity, and the method of its addition to the positive electrode was described in Section 3.

Since in the lead additive quantities reckoned with here, the lead can be safely dissolved in the electrolyte, and its structure affecting influence is caused by the lead separated from the solution over the silver surface, the lead had to be added to the secondary depolarizer powder mix in the form of lead oxide (PbO), and to mix the two materials in a homogeneous manner.

The quantity was determined in our case with respect to the ratio of the activated silver of the secondary depolarizer and the activated part of the wire electrode; it was found to be, in practice, 0,8 per cent of the total active silver. As an intersting feature of the cells with additive, in the cycle following the "zero discharge" the charging quantity was reduced as compared to the cells with no additive supplementation in the Ag_2O phase (Fig. 2). In the sub-

Table III

Quantity of charging in the Ag_2O phase with conventional, double depoliarizer and lead additive B—300 type accumulators, in the function of the cycle number

Cycle	Conventional	Double depolar.	Lead additive
1	130	290	280
10	125	247	273
20	125	229	293
30	115	234	281
40	105	235	304
50	100	192	290
60	80	205	293
70		204	290
80		195	305
90		193	304
100		194	290
130			291
150			300

sequent cycles the Ag_2O phase corresponding to the rated capacity could still be reached at a rather slow rate, although it was stabilized later on, at around the value of the nominal capacity, and no significant reduction took place like those after 20 or 30 cycles with the earlier cells without additive, which permitted an Ag_2O phase charge of only 200 to 220 mAh after such an operational period.

All this is made evident by Table III where the conventional, double depolarizer and lead additive cells are compared with respect to their Ag_2O phase charges in the function of the cycle number. The Table clearly shows that the Ag_2O utilization was very low in the traditional accumulators because, in order to provide an efficient hermetic seal, the capacity of the cell had to be over-dimensioned in silver.

Utilization is much better in the case of double depolarizer cells, since here the capacity of the negative (zinc) electrode exceeds that of the silver, whereby the latter will always be completely discharged and, when charging,

the entire Ag_2O phase will function. This in itself would lead to a considerable surplus capacity in the Ag_2O phase, although the capacity decrease due to agglomeration might again be similarly considerable.

The situation is entirely different in the case of accumulators containing lead additive, as the excessive Ag_2O phase developed during the first few

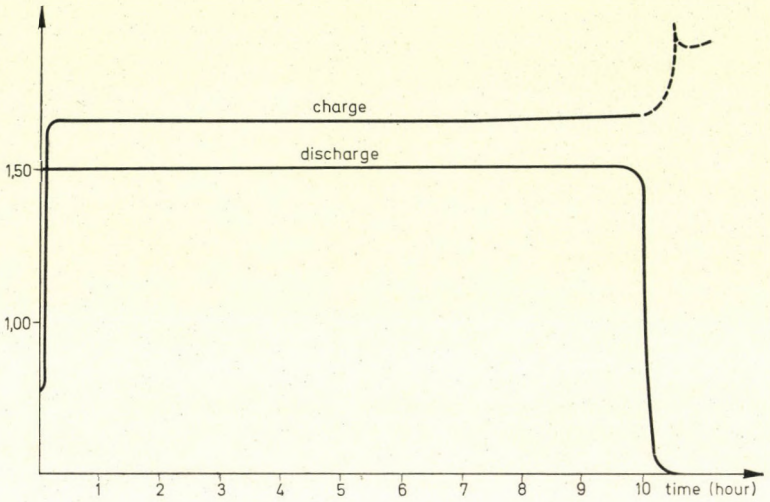

Fig. 4. Characteristics of lead additive type accumulators

cycles will remain constant along the whole life of the cell. The charge and discharge characteristics of such an accumulator operating in the silver(I) oxide phase are presented in Fig. 4.

5. Electric, life, and storage properties of silver-zinc accumulators operating in the silver(I)oxide phase

As a result of the research-development project described in detail in the first Section, today the Medicor Works and the joint Hungarian–British undertaking Medicharge (with headquarters in the U.K.) manufacture a whole family of hermetically sealed miniature accumulators.

Table IV illustrates this accumulator family with their most important electric and mechanical data.

Both manufacturers assemble higher voltage and capacity aggregates by using these miniature accumulator cells. Because of their wide assortment they cannot be described in detail here.

Ever since the introduction of the research and development results referred to here and earlier [1], [2] into the field of production, the hermetically sealed miniature silver–zinc accumulators have acquired, in addition to the

Table IV

Hermetically sealed silver–zinc miniature accumulator family produced by Medicor Works

Type	Rated voltage V	Rated capacity mAh	Diameter mm	Height mm
B—300	1,5	300	25,0	6,4
B—200	1,5	200	20,0	7,0
B—150	1,5	150	20,0	6,3
B—80	1,5	80	15,5	7,0
B—50	1,5	50	11,5	6,4

maintenance of their excellent original properties (high specific storage capacity, starter character, etc.), a number of new outstanding characteristics.

The hazards of reverse polarization, characteristic of any accumulator system, and produced in the course of discharging higher voltage accumulators developed by using series connected cells, have been practically eliminated by the secondary depolarizer

This does not mean of course that if, either deliberately or by negligence, an accumulator is forgotten in the discharge circuit for a long time after full discharge (up to the ultimate discharge voltage specified), there should not be any eventual damages to be reckoned with. Just as in the case of any hermetically sealed power source, the primary hazard of reverse polarization is represented here by the gas formation to an impermissible extent in the cell. Operation of the accumulator exclusively in the Ag_2O phase is of utmost importance, because of the reasons described in detail in Section 2, with respect to the gas production within the cells. Since the accumulators constructed on the basis of the above research results can be charged with the quantity corresponding to the rated capacity in the silver (I) oxide phase, no gas formation whatsoever is possible in the silver electrode area during charge, and only to a limited extent in the zinc electrode space, owing to the high hydrogen overvoltage brought about by the mercury content of the zinc.

The possibility of charging the rated capacity in the Ag_2O phase leads to a number of electrotechnical advantages. If, when charging, no silver(II) oxide (AgO) is produced at all then, when discharging after charge, this discharge will be at a practically constant voltage (Fig. 4). This characteristic feature is displayed only by this type of silver–zinc accumulators. The constant value of terminal voltage is one of the most important quality characteristics of the electric energy supplied by the power source. On the other hand, when discharging an accumulator that can also be charged in the silver(II)oxide phase, particularly if discharge is within a short period of time after charge, a higher voltage characteristic of the AgO compound must also be reckoned with in the first part of the discharge period. This voltage exceeding the rated

voltage of the cell by about 20 per cent is hardly tolerated by the most up-to-date devices of the integrated circuit type, if at all. After the quantity charged in the silver(I) phase could be successfully adjusted to around that corresponding to the rated capacity, and since the cells maintain this feature practically along their whole life, it has become feasible to construct chargers whose simple built-in automatic sensor will detect the about 0,3 V jump in the terminal voltage of the cell at the boundary of the silver(I)oxide and silver(II)-oxide phases, whereafter no charging current will be supplied. As the boundary of the two phases is represented, in practice, by the rated capacity of the cell, the most advantageous operational method for the accumulator can be adjusted if this type of a charger is employed, in such a manner as to have it used for discharge (as the power source in a consumer apparatus) only according to the conditions of use and, independently of the quantity discharged, switch it over to charge again. In this case the charger will again charge up the accumulator to the rated capacity, thus it will be available for the next discharge period as such. If the accumulator was correctly selected for the consumer appliance, this operation would represent the optimum method of use.

Results achieved in the field of cycle life deserve detailed discussion. So far, the cycle life of the highest quality silver–zinc accumulators [3] was estimated to be maximum 60 to 100 cycles, with full charge and discharge assumed. According to all the known literary data and authors' experience, the most typical cause of silver–zinc accumulator breakdown is the failure of the separator employed. Prior, therefore, to presenting the life results achieved, the separation problems of silver–zinc accumulators should be dealt with in general.

As mentioned earlier [1], [2], experiences show a difference in the behaviour of the separators depending on the silver oxidation phase, the unit had been charged up to. A number of studies in literature and several Hungarian pilot experiments revealed that, of all the foils known at present, the plasticizer-free cellpohanes and acetate cellulose foils of the longest cellulose chain, that is, of the highest polymerization degree, would be both the most suitable and most commonly used materials for this purpose.

Medicor Works use plasticizer-free cellophane because a number of experiments verified that the use of any other foil, particularly of the plastic base types, would result in an inadmissible increase of the compactness or low porosity of these materials, without any considerable improvement in life, compensating for the above drawback.

So it was self-evident to assume that if a constant lower oxidation grade silver can be provided for in the operation of the accumulator, this should exert a favourable influence on separator stability and, thereby, the new accumulators might be expected to exhibit a significantly longer life. This assumption has been confirmed as follows.

For quite some time, as the breakdown index of separators the silver mg reduced in the separator layers after a certain cycle number has been used, as determined by per layer analysis. The realistic character of this index is supported by two findings:

(1) The silver of reduced state in the separator will oxidize the materials of the latter, thus open up the saccharose rings of the cellulose molecule, and lead to chain ruptures (depolymerization).

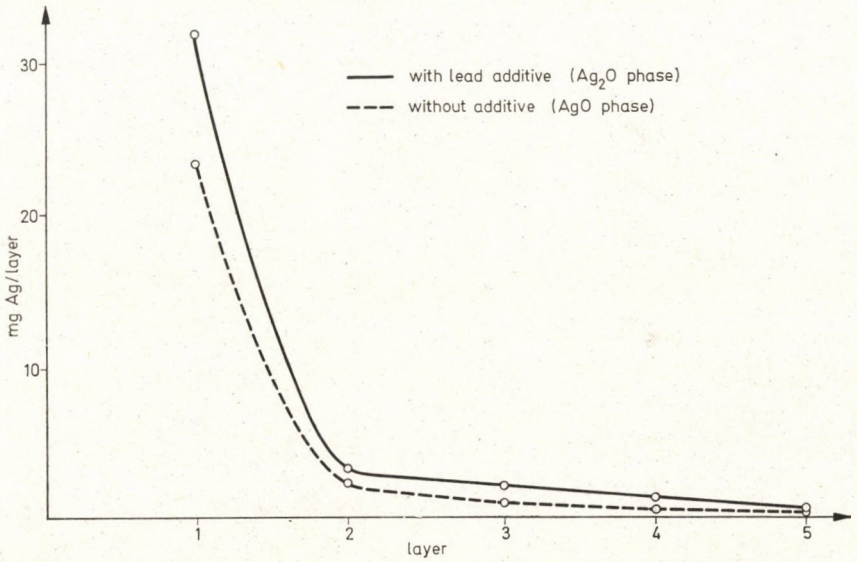

Fig. 5. Silver penetration into the separator layers after 140 cycles

(2) In the other layers farther away from the silver electrode, it will increase the possibility of slow shorts as the separator saturated with silver acts like a metallic conductor, and will lose its separating possibility.

Examinations involved the dismantling of accumulators of different age and previous storage figures, and the analysis of their separator layers (Fig. 5).

The diagram shows that, in the accumulators operated only in the Ag_2O phase, each separator layer contains a greater quantity of silver than in those charged up in the AgO phase as well. However, opening up the cells confirmed that these separators were much more stable mechanically, did not exhibit any damages and, what was still more important, reached a much longer life. In general, they have become "conductive" or "leaking," which favours failure, but without gas production and cell deformation, usually after 120 to 150 cycles.

In the storage test the accumulators were opened after 2, 4, 6, and 9 months of storage, respectively, and the silver content of their separators is

presented in Table V. These data show that silver penetration during storage is much less than in operation, and that the "saturation" of the individual layers with silver is a time process, where damages to the second layer will

Table V

Silver content of the separator layers in the function of the storage period, mg Ag/layer

Storage period	Layers					
	1	2	3	4	5	Total
New cells	0,06	0,01	0	0	0	0,07
After 2 months	2,50	0,20	0,20	0,01	0	2,71
After 4 months	9,00	0,50	0,15	0,05	0,01	9,71
After 6 months	9,40	0,37	0,09	0,05	0,01	9,92
After 9 months	8,10	1,90	0,14	0,03	0,01	10,18
Cells tested after 150 cycles	15,70		2,15	0,14	0,05	18,04

start only after the saturation of the first one. Significant silver enrichment of the first layer will take place between the 2nd and 4th month, while that of the second layer during the storage period of the 6th to 9th months.

To sum up the experiences collected in separator testing, it may be said that the elimination of the higher oxidation degree silver oxide (AgO) has somewhat increased the hazards of silver migration (due to the several orders of magnitude better colloid solubility of Ag_2O) but, at the same time, the oxidative damages to the separators would be considerably reduced which has led to an unequivocally significant life extension. This was obvious because the destructive effect exerted by Ag_2O on the separator had been of a considerably lesser degree than the similar AgO effect.

The storage parameters of the Ag_2O phase charged accumulators are rather favourable. As for the number of cycles completed, the life indices of new accumulators did not differ appreciably from the figures shown by units stored already for 9 months (Table VI).

Table VI

	Cycles up to breakdown
New cells	156
After 2 months of storage	159
4	147
6	162
9	151

Note: The cycle number represents in each storage phase the average of 6 B—300 DP type cells

6. Summary

As a result of the research-development project described in detail, a family of hermetically sealed miniature silver–zinc accumulators could be produced which, as compared to the silver–zinc accumulators representing the world standard (3), would reveal a number of further advanced features.

The extent of specific storage capacity may be illustrated by the following comparison: the nominal dimensions of the LR-2 type, 1,5 V, 2 Ah capacity non-sealed cell produced by the Yardney (USA) company in a plastic housing, including the shoes, are $15 \times 43{,}5 \times 64$ mm, which means a volume of 41,66 cm^3. Thus, the specific rated charge capacity per cm^3 is

$$\frac{2000}{41{,}66} = 48 \text{ mAh/cm}^3$$

(Without the clamps the dimensions are $15 \times 43 \times 55$ mm, meaning a volume of 35,89 cm^3 and a specific storage capacity of 56 mAh/cm^3.)

The nominal dimensions of the B-300 DP type 1,5 V, 0,3 Ah capacity miniature accumulator manufactured by Medicor are $\varnothing$ $25 \times 6{,}4$ mm, with a corresponding volume of 3,14 cm^3. So the specific rated storage capacity per cm^3 is

$$\frac{300}{3{,}14} = 95{,}5 \text{ mAhc/m}^3 .$$

This practically doubled specific storage capacity is particularly remarkable, if we take into consideration that the ratio of housing to the internal active volume of this 0,3 Ah capacity accumulator is certainly greater than that of a 2Ah capacity accumulator. The criterion of hermetic seals, according to which no gas must be produced in the course of either charge or discharge, justify the lower utilization of the active agents as against the open system accumulators. In this context the high specific storage capacity achieved with the miniaturized accumulators seems to be of a still greater significance.

Hermetic sealing offers particularly important advantages in a number of fields of application. However, it requires at the same time the incorporation of the active ingredients in a "ready-to-use" form, and the addition of the electrolyte quantity necessary for operation in the course of manufacture. This, in turn, has the advantage that if such an accumulator type is to be used, there is no need to perform the unpleasant and inconvenient operations of electrolyte fill-up and "formation" cycles, as the unit can be used normally as soon as it has been unpacked. Since the manufacturer supplies the accumulators in a charged-up condition, their use will start with immediate installation and discharge (power producing process).

In practice, the secondary depolarizer has solved the problem of reverse polarization in the case of series connected accumulators. Extension of the silver(I)oxide phase practically to the rated capacity has led to the following particular advantages:

(a) it will prevent any gas formation at the silver electrode if charged to the rated capacity;

(b) since silver(II)oxide will not develop at all, the stress on the separator is greatly reduced which, beyond an increased number of cycles, will increase the storage period as well;

(c) it makes the employment of simple automatic chargers feasible whereby the accumulators can safely be charged up to almost the rated capacity, independently of their charge prior to re-charge.

On the basis of the various investigations conducted with a great number of accumulators ever since their series production has been started, authors are convinced that further efficient research might lead, beyond the advantages already achieved, to the accomplishment of the old objective, that is, extension of the life of silver–zinc accumulators to several hundred cycles.

This, however, requires much persistent work in order to improve separation and the reversibility of the zinc electrodes. Research projects have already been started, but their efficiency can only be assessed in the future through the expected significant increase of the cycle life.

REFERENCES

1. HAJDU, L.—dr. ZAHORÁN J.: Latest Research Results in the Field of Hermetically Sealed Miniature Silver—Zinc Accumulators, *Műszaki Tudomány* **45** (1972) (in Hungarian)
2. HAJDU, L.—dr. ZAHORÁN J.: Recent Research Results in the Field of Hermetically Sealed Miniature Zinc—Silver Storage Batteries, *Acta Techn. Hung.* **73** (1972)
3. Service and Operating Instructions for the Yardney Silvercell—Yardney Electric Corp. (N.Y. 1970)
4. TVARUSHKO, A.: The Decomposition of AgO in Alkaline Solution, *Journal of the El. Chem. Soc.* **116** (1969) 61, 62
5. GAINES, L.: Secondary Silver—Zinc Battery Technology, *Journal of the El. Chem. Soc.* **116** (1969), 61,02
6. HEGYESSY, L.: Activation of the Silver Electrodes of Batteries I, *Magyar Kémikusok Lapja* **3** (1970) (in Hungarian)
7. HEGYESSY, L.: Activation of the Silver Electrodes of Batteries II, *Magyar Kémikusok Lapja* **3** (1970) (in Hungarian)
8. DIRKSE, T. P.: The Cathodic Behaviour of AgO in Alkaline Solution, *Journal of the El. Chem. Soc.* **9** (1969)
9. RUETSCHI, P.: USA Patent No. 3.085.186
10. British Patent No. 905.603
11. Hungarian Patents No. HA—1386 and HA—1459
12. Hungarian Patent No. HA—662

In der (Ag_2O-Phase von Silber (I)-Oxyd funktionierender gasdicht verschlossener Silber-Zink-Akkumulator. Die Arbeit faßt kurz die Eigenschaften des gasdicht verschlossenen Miniatur Silber—Zink-Akkumulators zusammen mit nachdrücklicher Betonung der Probleme, die sich in erster Reihe aus dem gasdichten Verschluß ergeben. Eingehend behandelt die

Arbeit die Frage der Gasbildung bei Luftdicht verschlossenen Silber—Zink-Akkumulatoren, wobei die Faktoren besonders hervorgehoben werden durch welche das Ausmaß der Gasbildung beeinflußt werden kann. Der Einfluß der Silberstruktur auf die Größe der sich beim Laden entwickelnden Ag_2O-Phase (Silbermonoxyd) wird untersucht, und dann wird die experimentelle und konstruktive Arbeit besprochen, durch die es gelungen ist, einen ausschließlich in der Ag_2O-Phase funktionierenden hermetisch verschlossenen Miniatur Silber—Zink-Akkumulator zu entwickeln. Über die elektrischen und Lagereigenschaften sowie die Lebensdauer solcher Akkumulatoren wird informiert, und schließlich werden diese mit anderen Akkumulatoren verglichen, unter Hervorhebung der Richtung, in welcher auf Grund der bisherigen sehr positiven Ergebnisse weitere Forschung und Entwicklung benötigt sind.

Герметизированный серебряно-цинковый аккумулятор, работающий в фазе одновалентного серебра (Ag_2O). Данное сообщение является как бы продолжением прежних публикаций [1], [2] авторов и в нем сначала обобщаются свойства герметизированных миниатюрных аккумуляторов серебряно-цинковой системы, особо рассматривая те проблемы, которые вытекают в первую очередь из герметизации. В связи со сказанным детально разбирается вопрос газообразования в герментизированных серебряно-цинковых аккумуляторах, особо подчеркивая те факторы, которые могут быть использованы для влияния на масштабы газообразования. Примыкая к 6-ой главе уже упомянутой выше работы [1], [2], детально анализируется воздействие структуры серебра на величину фазы Ag_2O (окись серебра), формирующейся во время процесса заряда. После выяснения теоретических основ авторы в связи с конкретным примером описывают ту конструкторскую и экспериментальную работу, с помощью которой удалось оформить герметизированные миниатюрные серебряно-цинковые аккумуляторы, работающие чисто в фазе Ag_2O. В сообщении дается подробная информация относительно электрических свойств, свойств хранения и срока службы таких аккумуляторов, которые с точки зрения потребителей являются наиболее интересными. В заключение на основе имеющихся достижений сообщается сравнение с прочими аккумуляторами, подчеркивая то, что на основе достигнутых до сих пор очень положительных результатов — в каком направлении считают авторы необходимым продолжать дальнейшие исследовательские работы по развитию этих типов аккумуляторов.

Acta Technica Academiae Scientiarum Hungaricae Tomus 76 (1—2), pp. 177—181 (1974)

A SIMPLE SAMPLE HOLDER AND CRYOSTAT FOR MEASURING THERMOELECTRIC POWER OF SEMICONDUCTORS IN THE TEMPERATURE RANGE OF 80—400 K

K. SOMOGYI* and B. PŐDÖR**

[Manuscript received 4 August, 1972]

A simple sample holder and cryostat system is described, suitable for measuring the temperature dependence of the thermoelectric power of semiconductors in the temperature range of 80—400 K.

The measurement of thermoelectric power (TEP) of semiconductors involves many well-known experimental difficulties, though in principle the measurement is quite simple. Several designs of the sample holders and cryostats were already described in the literature [1—6] emphasizing different aspects of the measurement. In the present paper a measuring system is described which was constructed on the below-mentioned general principles. Its main difference from other designs is that the ends of the sample are fixed inside the copper blocks, which in turn are heated from inside and the sample is in the vapour of boiling nitrogen. This system is easy to handle and very useful for serial measurements affording high accuracy.

In Figs 1 and 2 the schematic outlines and the photos of the relevant parts of the sample holder are shown, respectively. The most important parts are the copper blocks 1 and 2, each one fitted with a T-shaped movable piece 3, fixed by brass screws 4 and springs 5. The ends of the sample 6 are to be attached between the copper blocks and the T-shaped parts. The termocouples 7 go through the copper block, then through a hole into the T-shaped moving part, touching the sample. In this way the heat conduction through the thermocouples is minimized. The material of the thermocouples is chromel-alumel, having a diameter of 0.4 mm, therefore the effects of possible inhomogeneities in the thermocouple wires are ruled out [4]. The ends of the thermocouples are soldered to the moving T-shaped parts of the sample holder.

The copper blocks are heated by heaters 8 placed inside the blocks. In this way the heat transfer to the surrounding medium takes place through the sample blocks, minimizing both the heat transfer to the nitrogen gas and

* K. Somogyi, Research Institute for Technical Physics of the Hungarian Academy of Sciences 1325 Budapest, P. O. Box 76.

** B. Pődör, Research Institute for Technical Physics of the Hungarian Academy of Sciences 1325 Budapest, P. O. Box 76.

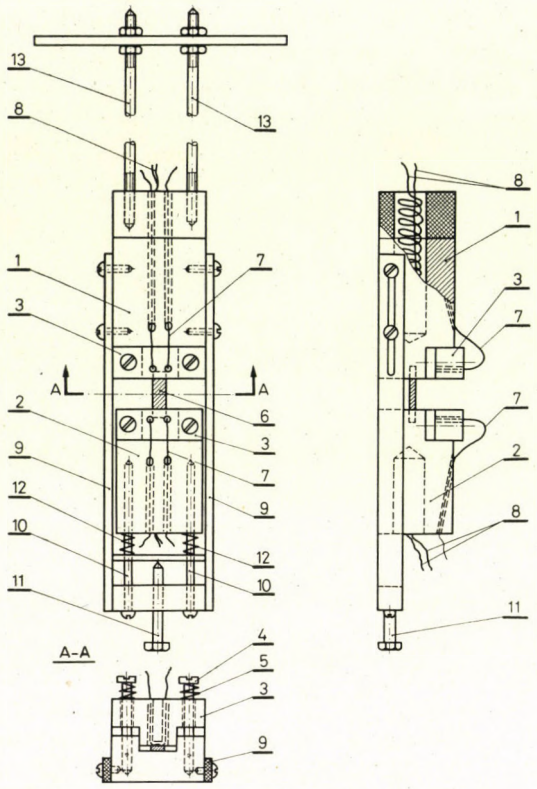

Fig. 1. Schematic outline of the sample holder (See text)

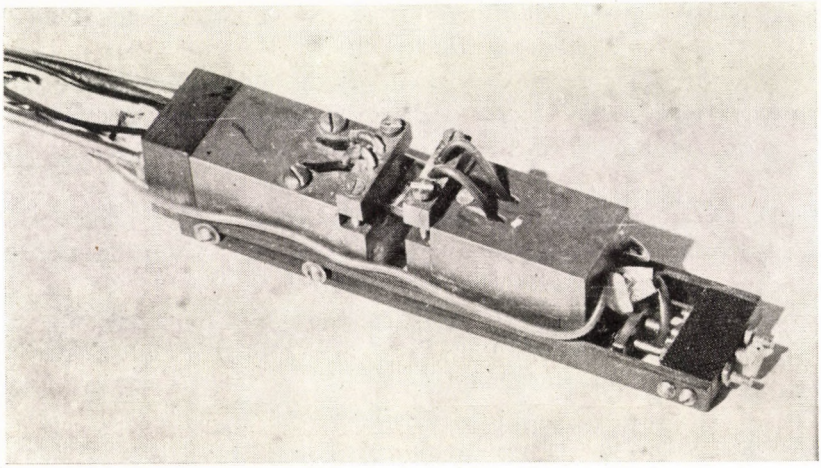

Fig. 2. Photo of the sample holder

the convection of the latter. Moreover, the maximum temperature of the surrounding medium does not exceed the temperature of the copper blocks.

The two copper blocks are connected by textile-bakelite rods 9 and brass rods 10 in such a way that with the aid of screw 11 the distance between them can be varied, while spring 12 assures the elastic connection between

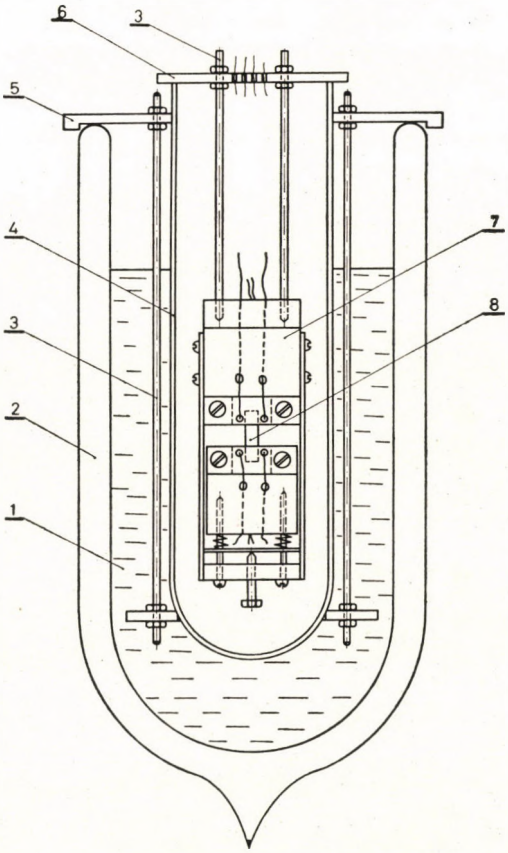

Fig. 3. The Dewar system. *1* — liquid nitrogen, *2* — Dewar, *3* — rods of low conductivity material, *4* — glass tube, *5* — top of the Dewar, *6* — top of the sample holder, *7* — sample holder, *8* — sample

the copper blocks. The sample ends can be clamped between the moving and fixed parts of the copper blocks, or if necessary, they can be simply pressed between them. Those parts of the copper blocks which make direct contact with the sample are covered by a 20—30 μm thick gold foil to ensure good electrical and thermal contacts as well. The sample holder system is mounted on two rods of low heat conductivity 13. The sample holder is in a thick walled (1.5—2 mm) glass tube, whose lower end and the whole assembly is lowered into a Dewar containing liquid nitrogen (Fig. 3). Liquid nitrogen is poured

into the glass tube, too, up to the middle of the lower copper block. In this way the sample holder and the sample are in the vapour of boiling nitrogen. Without switching on the heater of the lower block, its temperature reaches 77 K, and nearly the same temperature can be measured on the lower end of the sample. With the other heater a convenient temperature gradient can be established and maintained during the measurements simultaneously regulat-

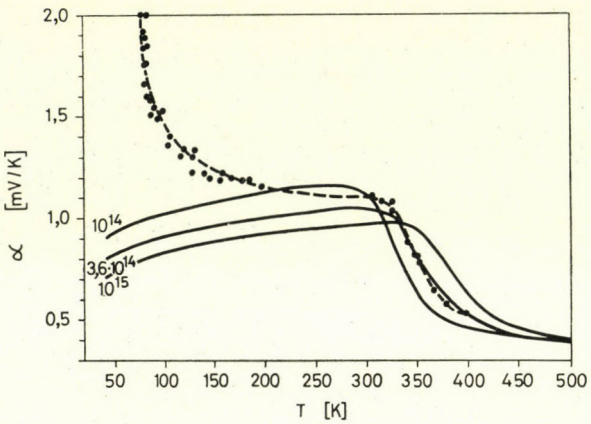

Fig. 4. Typical results of measurements on a Ge sample with a donor concentration $N_d = 3.6 \times 10^{14}$ cm^{-3}. Theoretical curves without phonon drag contribution for donor concentrations 1×10^{14}, 3.6×10^{14} and 1×10^{15}, respectively

ing the input power of the two heaters. During the heating the nitrogen content of the glass tube boils off. At measurements above room temperature the outer Dewar can be filled with water.

The convection of the nitrogen gas does not influence the measurement procedure because the thermocouples go partly through the copper blocks [2], [5], and on the other hand, the big copper blocks ensure an effective thermal screening of the sample.

The temperature gradient on the sample can be varied between wide limits. According to our experience the most suitable temperature gradient was 5—10 K.In this case the lowest limit of measurements was about 80—85 K (the average temperature of the sample). The upper temperature limit is influenced by the contacting material used for making electrical contacts to the sample, etc., and in our case it was about 400 K.

The accuracy of the measurements is better than 10%. Near and above room temperature it might even be better. In order to control the set up we made measurements of TEP on pure Ge samples. In Fig. 4 a typical result of such a measurement is shown and compared with theoretical curves, not taking into account the phonon drag effect which predominates at low tem-

peratures. Our experimental results favourably compare with those found in the literature [7] and near and above room temperature with the theoretical ones, too, where the neglect of the phonon drag effects is justified.

REFERENCES

1. Geballe, T. H.—Hull, G. W.: *Phys. Rev.* **94** (1954), 1134
2. Middleton, A. E.—Scanlon, W. W.: *Phys. Rev.* **92** (1953), 219
3. Фистуль, В. И., Черкас, К. В.: *ФТТ* **4** (1962), 3288
4. Goland, A. N.—Ewald, A. W.: *Phys. Rev.* **104** (1956), 948
5. Somogyi, K.—Szidjakin, V. G.: *Híradástechnika*, Budapest, **20** (1969), 262
6. Давиденко, Н. И., Факидов, И. Г.: *ПТЭ* No. **5** (1967), 254
7. Smith, R. A.: Semiconductors, University Press Cambridge 1959

Ein einfacher Probenhalter und Kryostat für die Messung der thermoelektrischen Spannung von Halbleitern im Temperaturbereich 80÷400K. Ein einfacher Probenhalter und Kryostat für die Messung der Temperaturabhängigkeit der thermoelektrischen Spannung von Halbleitern im Bereich 80—400 K werden beschrieben.

Простой держатель образца и криостат для измерения термо э. д. с. полупроводников в интервале температур от 80 до 400 К. Описывается простая система измерения для термо э. д. с. полупроводников в зависимости от температуры в интервале температур от 80 до 400К.

Acta Technica Academiae Scientiarum Hungaricae, Tomus 76 (1—2), pp. 183—206 (1974)

DETERMINATION OF THE THERMAL BREAKDOWN VOLTAGE FOR D.C. AND A.C. VOLTAGES

J. PATKÓ

and

M. VAJTA Jr.*

After the definition of the conceptions "thermal breakdown" and "thermal instability" a short survey of the history of the thermal breakdown theories is given. After writing up the general instability equations for D.C. voltages the expression of the thermal breakdown voltage for a specified temperature dependence of the resistivity is derived, then the same derivation for A.C. voltages is performed in a similar way. The individual temperature distributions are calculated for both cases, the obtained results tabulated by a computer are presented and the effects of some parameters on the value of the thermal breakdown voltage are investigated.

1. Introduction

The problem of thermal breakdown attains ever greater importance due to the permanent increase of the nominal voltages and operational temperatures. The higher nominal voltages and operational temperatures of the insulation materials are economically justified.

The suitability of the insulation material is mostly determined — from among the great number of the electrical and non-electrical parameters — by the breakdown voltage. The breakdown voltage, — unlike the other electrical characteristics, — is no integrated value, but always the breakdown voltage of the weakest point in the insulation, or the insulating material.

The breakdown processes can generally only be described in a qualitative manner. The relationships between the macroscopic and the microscopic characteristics may in many cases be described with a good approximation, especially for crystalline and homogeneous structured materials [1—6]. But in the case of the practically most frequent amorphous materials of no homogeneous structure only empirical relationships, established by measurements are available [7—15].

Three types of breakdown in solid dielectrics are generally distinguished:

a) pure electrical breakdown,

b) breakdown by internal or surface ionization,

c) thermal breakdown.

* Ifj. dr. VAJTA MIKLÓS, 1041 Budapest, Dessewffy u. 41, Hungary.

The individual types of breakdown are not sharply separated: during the complete breakdown process two, or even all three types may appear. The first two types are not dealt with here, only references are made in this connection to the literature [16—20].

In the thermal breakdown an important role is played by the losses occurring always in the insulation materials, causing the warming up of the material. The temperature has a decided effect on the breakdown due to the non-linear temperature dependence of the electrical characteristics of the materials. This is why the thermal breakdown is also called "high temperature breakdown." In thermal breakdown a breakdown voltage, the so-called thermal breakdown voltage may be defined, whose characteristics are:

1) — its very low dependence on the electrical field homogenity,
2) — its high dependence on the duration of the voltage application,
3) — its very high dependence on the ambient temperature, i.e.,

the temperature rise and the heat transfer conditions, respectively. Although the thermal breakdown can be distinguished from the electrical breakdown by the properties listed above, yet it seems to be important to point out the very essential difference between the thickness dependence of the breakdown voltages in both cases. In electrical breakdown the breakdown field strength is specified as a characteristic value of the materials permitting the calculation of the breakdown voltage for the given arrangement always in the same manner. In the case of homogeneous fields a linear relationship prevails between the breakdown voltage and the thickness of the dielectric medium. This relationship is fundamentally modified in the case of the thermal breakdown; namely with increasing thicknesses the breakdown voltage increasingly falls short of the linear rise with the thickness and tends towards a limit value. It is important to emphasize this deviation, regarding that one of the fundamental aims of the thermal breakdown theories was to clear up the thickness dependence of the thermal breakdown voltage.

2. The conception of the thermal instability, the thermal breakdown voltage

From the above it is to be seen that non-linear temperature dependence of the electrical parameters has a fundamental part in the development and appearance of the thermal breakdown. The losses occurring permanently in the dielectric, generally depend on the temperature and the local field strength in the following form [21—22]:

$$q_b(\vartheta,\ U) = K \cdot e^{b(\vartheta-\vartheta_0)} \cdot E^2 \tag{1}$$

where q_b — loss pro unit volume [W/m³]
E — electrical field strength [V/m]
ϑ_0 — reference temperature [°C]
b — temperature coefficient characterizing the temperature dependence [1/°C]
K — constant, depending on the layout and the material characteristics [A/m · V]

Accordingly the occuring losses depend, in general, exponentially on the temperature, but the heat quantity available for transfer to the environment (not regarding radiation) varies only in a linear way [23]:

$$Q_{tr} = \alpha \cdot F(\vartheta_s - \vartheta_a) \tag{2}$$

where Q_{tr} — heat quantity available for transfer [W]
α — heat transfer coefficient [W/m² °C]
F — heat transfer surface [m²]
ϑ_s — surface temperature [°C]
ϑ_a — ambient temperature [°C]

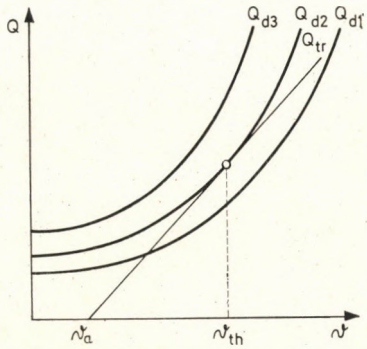

Fig. 1. The heat quantities developing in the dielectric ($Q_{d3} > Q_{d2} > Q_{d1}$) and those available for transfer to the environment (Q_{tr}) versus temperature

From the above it directly follows that a limit state must exist, beyond which a greater heat quantity is formed that can be transferred and so a heat instability appears. Fig. 1 shows the forming and the transferable heat quantities versus the temperature. This relationship permits to write up the conditions of the thermal instability in the following form:

$$Q_d = Q_{tr} \qquad \text{and} \qquad \frac{\partial Q_d}{\partial \vartheta} = \frac{\partial Q_{tr}}{\partial \vartheta} \tag{3}$$

where

$$Q_d = \int_V q_d \cdot dV \ [W]$$

is the heat quantity formed in the total volume of the dielectric.

Although the above conditions seem to be trivial, their calculation is rather complicated, especially if the thickness dependence of the temperature is also to be allowed for in equation (1). Between the electric potential and the field strength there exists an unequivocal relationship [24], which may be — in many cases, — mathematically complicated. With the aid of this relationship a $Q_d(\vartheta)$ — curve can be plotted for each voltage value. The voltage

producing exactly the heat quantity Q_d which corresponds to the instability is called, according to the definition, the thermal breakdown voltage. In thermal breakdown the breakdown voltage is always understood to be the thermal breakdown voltage, in spite of the fact that in principle the thermal breakdown should occur only in an infinite time period at the instability (thermal breakdown-) voltage, but at higher voltages than this value it occurs within a finite time period in any case.

3. Differential equation, the applied model

By the instability condition (3) it is clear that for its accurate calculation the temperature distribution developing in the dielectric under the given boundary conditions must be known. The general thermal state of the mate-

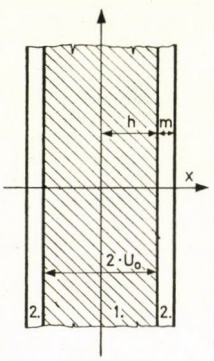

Fig. 2. Plane model 1. — dielectric, 2. — electrode

rials having an internal heat source is given for the stationary case by the so-called Kirchhoff–Fourier equation [25]:

$$\operatorname{div}(\lambda_1 \operatorname{grad} \vartheta) + q_b(\vartheta) = 0 \tag{4}$$

where λ_1 — thermal conductivity (of the dielectric in this case) [W/m°C]. The general solution of this equation in a closed formula is unknown. The application of a model with only one-dimensional heat flow seems to be advisable (concerning the three-dimensional solution BELLMANN [26] made a valuable statement). Our plane model is shown in Fig. 2. The arrangement corresponds e.g. to a coil insulation where the coil length exceeds the thickness by several orders of magnitude. The form of our differential equation is considerably reduced in this way:

$$\frac{d^2\vartheta}{dx^2} + \frac{q_b(\vartheta)}{\lambda_1} = 0\,. \tag{5}$$

The boundary conditions required for the solution of this differential equation may be written up on the basis of the following considerations. The point $x=0$ is a symmetry axis, therefore the maximum temperature is developing here and the heat flow in this plane is zero. At the boundary surface between the electrode and the dielectric ($x = h$) the temperature is identical, but the tem-

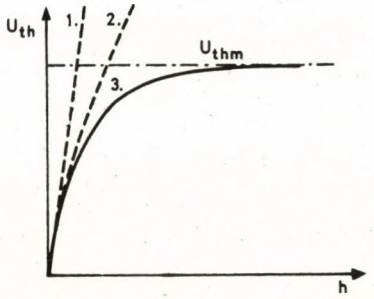

Fig. 3. Thermal breakdown voltage versus the thickness. 1. According to Wagner's theory; 2. according to intermediate theories; 3. according to the exact theory

perature distribution shows an inflection point due to the continuity of the heat flow. We assume that heat is transferred from the surface of the outer electrode to the constant temperature environment. Based on the above we have [25]:

$$\left(\frac{d\vartheta}{dx}\right)_{x=0} = 0\,,$$

$$\lambda_1 \cdot F \left(\frac{d\vartheta}{dx}\right)_{x=h-0} = \lambda_2 \cdot F \left(\frac{d\vartheta}{dx}\right)_{x=h+0}, \tag{7}$$

$$-\lambda_2 \cdot F \left(\frac{d\vartheta}{dx}\right)_{x=h+m} = \alpha \cdot F(\vartheta_s - \vartheta_a), \tag{8}$$

where λ_2 — the thermal conductivity of the electrode [W/m °C],
m — thickness of the electrode [m].

The development of the individual thermal breakdown theories is unequivocally connected with the increasingly more accurate solution of the differential equation (5). The primary aim of the research is the expression of the thermal breakdown voltage as a function of the parameters of the dielectric. According to the experiments the thickness-dependence of the thermal breakdown voltage is as shown in Fig. 3. The increasingly more accurate theories reflect the development from the linear approximation to the accurate function.

4. The approximation theories

Attention was focussed on the phenomenon of the thermal breakdown at the turn of the century and the first comments and observation on the breakdown also originate from this period. M. WALKER [27], K. W. WAGNER [28] and E. H. RAYNER [15] were among the first to investigate this phenomenon more thoroughly. K. W. WAGNER elaborated an especially interesting theory starting from the empirical fact that the breakdown does not appear in the whole material, but only along a narrow channel. He applied several approximations in his theory, therefore his results, showing that the thermal breakdown voltage is directly proportional with the thickness of the dielectric, were only of an approximative nature, but nevertheless had a great significance in creating the foundation of the thermal breakdown theories. His results were criticized by several authors, among others by W. ROGOWSKY, DREYFUS, T. KARMAN, A. GEMANT, S. WHITEHEAD, etc. [29—34]. Unlike WAGNER they set out from a model of a uniformly homogeneous dielectric. Although they were unable to derive the general expression of the thermal breakdown voltage, yet they succeeded in extending their results to two extreme cases. They have shown that for very little thickness the thermal breakdown voltage varies by the square root as a function of the thickness, i.e.

$$U_{th}(h \approx 0) = \text{const.} \sqrt{h} \tag{9}$$

where U_{th} is the thermal breakdown voltage [V].

Their results agreed well with the experimental data. The other extreme case they studied was that of very thick dielectrics and they established that the thermal breakdown voltage tends to a maximum with the increase of the thickness, i.e.,

$$U_{th}(h \to \infty) = U_{thm} = \text{const.} \tag{10}$$

Unfortunately they were unable to establish the thickness dependence of the thermal breakdown voltage between both the extreme cases. These initial theories may also be illustrated by the initial tangent (Wagner's theory), or the initial section of the accurate $U_{th} = f(h)$ curve to be described further on as shown in Fig. 3.

5. General instability equations for D. C. voltages

An abrupt change in the thermal breakdown theories came about when the Russian physicist V. A. FOK succeeded in solving the differential equation (5) with specified boundary conditions and in adapting this to the instability condition [35]. Simultaneously with FOK similar results were obtained by

others, but nobody managed to derive the instability equations for the general temperature dependence of the resistance. As we are dealing now with a D.C. voltage case (4), our differential equation is;

$$\operatorname{div}(\lambda_1 \operatorname{grad} \vartheta) + \gamma(\operatorname{grad} \varphi)^2 = 0 \tag{11}$$

where φ — electrical potential and γ — the electric conductivity. For the electric potential we can write down the following equation:

$$\operatorname{div}(\gamma \operatorname{grad} \varphi) = 0. \tag{12}$$

It can be shown that the isothermal points of the temperature distribution curves representing the solution of the equations (11) and (12) coincide with the potential levels. Let us introduce the following variable:

$$u = -2 \int \lambda_1(\vartheta) \cdot \varrho(\vartheta) \cdot d\vartheta \tag{13}$$

where $\lambda_1(\vartheta)$ and $\varrho(\vartheta)$ may be perfect general temperature functions and ϱ the electric resistivity in [Ω m]. For our one-dimensional model the equations are considerably reduced:

$$\frac{d}{dx}\left(\lambda_1 \frac{d\vartheta}{dx} + \gamma \cdot \varphi \frac{d\varphi}{dx}\right) = 0, \tag{14}$$

$$\frac{d}{dx}\left(\gamma \frac{d\varphi}{dx}\right) = 0. \tag{15}$$

For the electric potential the following conditions may be given in addition to the thermal boundary conditions (6)—(8):

$$\varphi = +U_0 \text{ if } x = h \quad \text{and} \quad \varphi = -U_0 \text{ if } x = -h. \tag{16}$$

From equation (15) the current density J flowing in the dielectric may be directly obtained by integration. With the aid of (13) the following integral may be defined:

$$\varphi^2 = -2 \int_{\vartheta}^{\vartheta_m} \lambda_1(\vartheta) \cdot \varrho(\vartheta) \cdot d\vartheta = u(\vartheta) - u(\vartheta_m). \tag{17}$$

By integrating equation (14), expressing the potential with the aid of (17) and integrating again with the substitution $x = h$ we obtain:

$$J \cdot h = \int_{\vartheta_1}^{\vartheta_m} \frac{\lambda_1(\vartheta) \cdot d\vartheta}{\sqrt{u(\vartheta) - u(\vartheta_m)}}. \tag{18}$$

The temperature distribution in the electrode will be linear (as it has no internal heat source) and by taking the boundary conditions into account it can be written in the following form:

$$\vartheta = \vartheta_1 - g \cdot \frac{x - h}{h} (\vartheta_1 - \vartheta_a) \quad \text{and} \; g = \frac{\alpha \cdot h}{\alpha \cdot m + \lambda_2} \tag{19}$$

where ϑ_1 is the temperature at point $x = h$.
By taking the boundary conditions into consideration and by eliminating the unknown current density from (18) the following two equations are obtained:

$$F_1(\vartheta_1, \vartheta_m) \equiv \int_{\vartheta_1}^{\vartheta_m} \frac{\lambda_1(\vartheta) \cdot d\vartheta}{\sqrt{u(\vartheta) - u(\vartheta_m)}} - g \cdot \frac{\lambda_2}{U_0} (\vartheta_1 - \vartheta_a) = 0, \tag{20}$$

$$F_2(\vartheta_1, \vartheta_m) \equiv u(\vartheta_1) - (\vartheta_m) - U_0^2 = 0\,. \tag{21}$$

By both these equations the temperature and potential distribution relations in the dielectric could be expressed by the parameters ϑ_1 and ϑ_m. It can be seen by these equations that with increasing voltage (with the other parameter values unchanged) ϑ_1 and ϑ_m must increase. In the case when no real solutions for the equations (20) and (21) can be given any longer, we speak of the critical voltage, that we have defined as the thermal breakdown voltage. The mathematical condition for the disappearance of the real solutions of these equations is the disappearance of the corresponding Jacobi determinant, i.e.,:

$$\det \text{ Jacobi} = \begin{vmatrix} \dfrac{\partial F_1}{\partial \vartheta_1} & \dfrac{\partial F_1}{\partial \vartheta_m} \\ \dfrac{\partial F_2}{\partial \vartheta_1} & \dfrac{\partial F_2}{\partial \vartheta_m} \end{vmatrix} = 0\,. \tag{22}$$

This equation is indeed the mathematical formulation of the instability condition (3) in a different form. The equation of the instability condition is obtained by developing the determinant and by eliminating the differential quotients, [35—36] as:

$$F_3(\vartheta_1, \vartheta_m) \equiv g \cdot \frac{\lambda_2}{U_{th}} - \lambda_1(\vartheta_1) \cdot \varrho(\vartheta_1) \int_{\vartheta_1}^{\vartheta_m} \frac{\dot{\gamma}(\vartheta)\, d\vartheta}{\sqrt{u(\vartheta) - (\vartheta_m)}} = 0 \tag{23}$$

where

$$\dot{\gamma} = \frac{d\gamma(\vartheta)}{d\vartheta}\,.$$

The thermal breakdown voltage can be calculated with the knowledge of the geometrical and cooling conditions, by the elimination of the parameters ϑ_1 and ϑ_m, by the equations (20), (21) and (23). The great virtue of the result

is that it is valid for the temperature dependence and the thermal conductivity dependence of the general resistivity for the given model. In practice the expressions are reduced to simpler forms, as the thermal conductivity of the dielectrics may be assumed to be temperature-independent in certain temperature ranges [23].

6. Determination of the thermal breakdown voltage for D. C. voltages

The expression of the thermal breakdown voltage is easily derived from the general instability equations in characterizing the temperature dependence of the resistivity by the following function relationship [16—18]:

$$\gamma(\vartheta) = \gamma_0 \cdot e^{\frac{\vartheta}{T}} . \tag{25}$$

By performing the integration of (13) we obtain:

$$u(\vartheta) = 2 \cdot \lambda_1 \cdot \varrho_0 \cdot T \cdot e^{-\frac{\vartheta}{T}} \tag{25}$$

where T — is the temperature coefficient characterizing the temperature dependence of the electrical conductivity. Let us introduce the following dimensionless quantities:

$$\Theta = \frac{\vartheta}{T}, \qquad v = \frac{U_{th}}{\sqrt{2 \cdot \lambda_1 \cdot \varrho_0 \cdot T}}, \qquad c = g \cdot \frac{\lambda_2}{\lambda_1} . \tag{26}$$

With these notations the equations (20), (21) and (23) may be brought to the following forms:

$$\int_{\Theta_1}^{\Theta_m} \frac{d\Theta}{\sqrt{e^{-\Theta} - e^{-\Theta_m}}} - \frac{c}{v}(\Theta_1 - \Theta_a) = 0 , \tag{27}$$

$$e^{-\Theta_1} - e^{-\Theta_m} - v^2 = 0 , \tag{28}$$

$$\int_{\Theta_1}^{\Theta_m} \frac{e^{\Theta}\, d\Theta}{\sqrt{e^{-\Theta} - e^{\Theta_m}}} - \frac{c}{v} e^{\Theta_1} = 0 . \tag{29}$$

Although the above integrations can be performed in principle [36—37], it seems to be more advisable to introduce a new parameter:

$$\cos^2 \xi = e^{\Theta_1 - \Theta_m}, \qquad 0 \leqq \xi \leqq \frac{\pi}{2} . \tag{30}$$

By performing the integrations with this new parameter and after reducing the equations, the thermal breakdown voltage may be expressed as:

$$U_{\text{th}}^{=} = \sqrt{2 \cdot \lambda_1 \cdot \varrho_0 \cdot T} \cdot e^{-\frac{\vartheta a}{2T}} \cdot \Psi(c), \tag{31}$$

where

$$\Psi(c) = \sin \xi \cdot e^{-\frac{\xi \cdot \tan \xi}{c}}, \tag{32}$$

and

$$c = \frac{\sin \xi}{\cos^3 \xi} (\xi + \sin \xi \cdot \cos \xi). \tag{33}$$

The function (32) is called Fok-function after Fok, who derived it for the first time. The ranges of interpretation of the functions can easily be determined as:

$$0 \leqq c \leqq \infty, \qquad 0 \leqq \xi \leqq \frac{\pi}{2}, \qquad 0 \leqq \Psi(c) \leqq 1.$$

With our results (31), (32) and (33) we managed to express the thermal breakdown voltage through the auxiliary parameter exclusively as a function of the geometrical and heat transfer relations of the dielectric. The expression (31) is in harmony with the previous expositions, i.e., with increasing thickness (c increases) the thermal breakdown voltage tends to a maximum value:

$$U_{\text{thm}}^{=} = 1{,}414 \sqrt{\frac{\lambda_1 \cdot T}{\gamma(\vartheta_a)}}. \tag{34}$$

We have tabulated the functions $\Psi(c)$ and $c(\xi)$ with the aid of a digital computer. The results are presented in Figs 4 and 5 on the basis of the table found in the Appendix. The stepping interval of the table is so dense that the intermediate values may be interpolated with an accuracy satisfying all practical demands. Fig. 4 shows the function $\Psi(\xi)$ versus the auxiliary parameter ξ, while Fig. 5 gives the function $\Psi(c)$ versus the parameter c. This latter Figure illustrates well the saturating, i.e., limited nature of $\Psi(c)$.

The temperature distributions developing in the dielectric can also be tabulated. The results, without deriving them (see [36] for the derivations) are:

$$\Theta_m - \Theta_1 = \frac{1}{T} (\vartheta_m - \vartheta_1) = -2 \cdot \ln [\cos \xi], \tag{35}$$

$$\Theta_1 - \Theta_a = \frac{1}{T} (\vartheta_1 - \vartheta_a) = 2 \frac{\xi \cdot \tan \xi}{c}. \tag{36}$$

$$\Theta_m - \Theta_a = \frac{1}{T} (\vartheta_m - \vartheta_a) = 2 \frac{\xi \cdot \tan \xi}{c} - 2 \cdot \ln [\cos \xi]. \tag{37}$$

The individual temperature distributions were also calculated by a computer and the results are shown in Figs 6, 7 and 8. As it is seen in Fig. 6, the instability temperature rise is not limited, in principle it may increase indeed ad infinitum, contrary to the temperature rise at A.C. voltages. This agrees

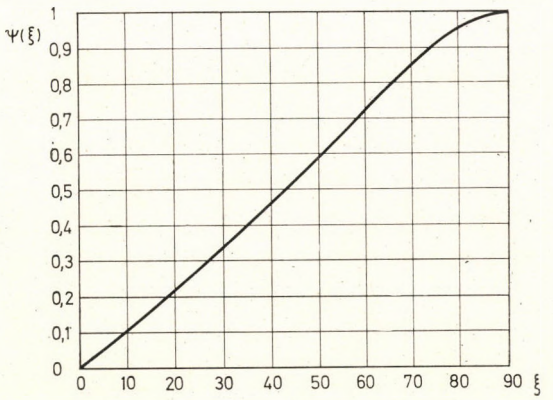

Fig. 4. The function $\psi(\xi)$ for D.C. voltage

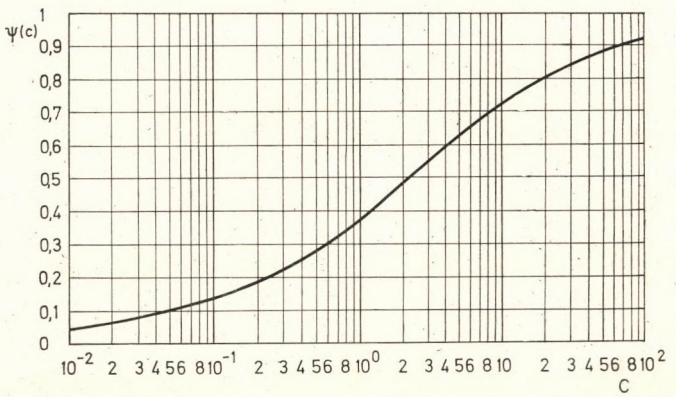

Fig. 5. The function $\psi(c)$ for D.C. voltage

with the evidence of several authors [6], [18], [22], and its cause is, on the one hand, that the electrical field distribution at D.C. voltages is primarily determined by the conductivity, whereas at A.C. voltages it is determined by the permittivity; and on the other hand at D.C. voltages the current density was assumed to be continuous, while at A.C. voltages the field strength is assumed to be continuous.

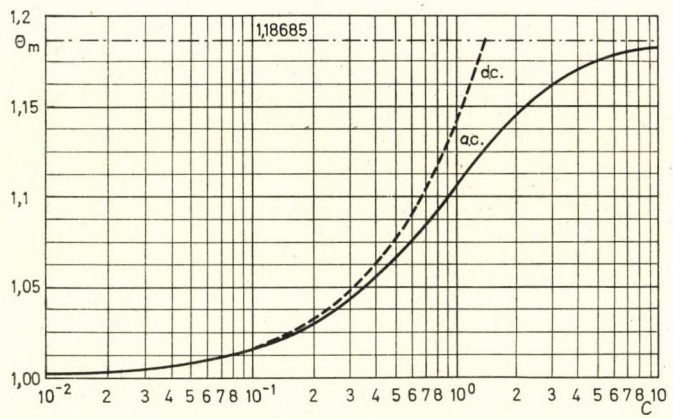

Fig. 6. Relative instability temperature-rise of the dielectric. - - - - - at D.C. voltage; ——— at A.C. voltage

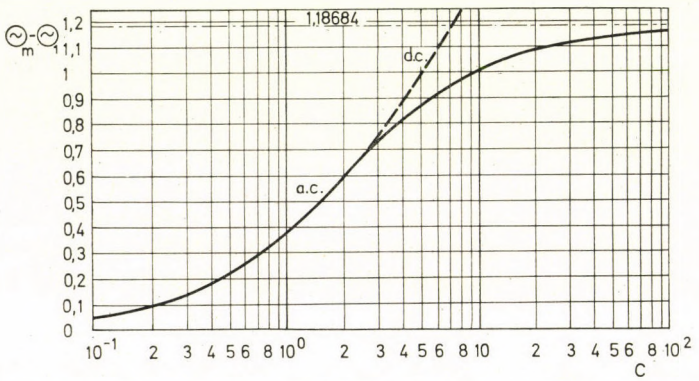

Fig. 7. Relative instability temperature difference between the dielectric and environment. - - - - - at D.C. voltage; ——— at A.C. voltage

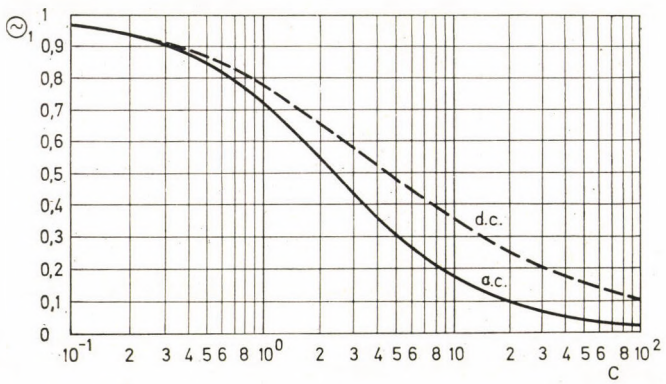

Fig. 8. Relative instability temperature difference between the dielectric and ambient temperature. - - - - - at D.C. voltage; ——— at A.C. voltage

7. Determination of the thermal breakdown voltage at A.C. voltages

If an A.C. voltage is applied, the previous derivation is somewhat modified, because the losses are higher at A.C. voltages, for whose integrated characterization the so-called volume loss number has been introduced [16], [22]:

$$p'(\vartheta) = p'(\vartheta_0) \cdot e^{b(\vartheta - \vartheta_0)} = p'_0 \cdot e^{b(\vartheta - \vartheta_0)} = p'_a \cdot e^{b(\vartheta - \vartheta_a)}. \tag{38}$$

It must be noted that the validity of this expression applies to a not very wide temperature range and in the case of $\tan \delta$ curves with local minima it is only valid beyond the local extreme value. Let us again introduce relative units:

$$\Theta = b(\vartheta - \vartheta_a) \qquad \text{and} \qquad z = \frac{x}{h}. \tag{39}$$

Our differential equation for the model shown in Fig. 2 has now the following form:

$$\frac{d^2\Theta}{dz^2} + B \cdot e^{\Theta} = 0 \tag{40}$$

where

$$B = \frac{p'_a \cdot b \cdot h^2 \cdot E^2}{\lambda_1}. \tag{41}$$

By integrating the equation, with the determination of the integration constant from the boundary condition (6) and reintegrating, an inverse function $z = g(\Theta)$ of the function $\Theta = f(z)$ is obtained. Let us introduce the auxiliary parameter:

$$\beta = \sqrt{\frac{B}{2} \cdot e^{\frac{\Theta_m}{2}}}. \tag{42}$$

With the aid of this auxiliary parameter and the local temperature of the point $z = 0$ (which is the maximum temperature too) as a parameter, the temperature distribution may be expressed as:

$$\Theta(z, \Theta_m) = \Theta_m - 2 \cdot \ln\left[\cosh(\beta z)\right]. \tag{43}$$

The relative temperature of the boundary surface between the electrode and the dielectric can be determined by substituting $z = 1$ into this expression. Taking the linear temperature distribution developing in the electrode into account and also by satisfying the boundary conditions (7) and (8) we obtain the following implicit function relation between the electrical field strength (E) and the maximum temperature rise (Θ_m), (which is now the instability temperature rise):

$$F(E, \Theta_m) = 0{,}5 \cdot \ln\left(\frac{2 \cdot \beta^2}{B}\right) - \ln\left[\cosh(\beta)\right] - \frac{\beta \cdot \tanh \beta}{c} = 0. \tag{44}$$

If the function $F(E,\Theta_m)$ exists and is differentiable, then the instability condition may be reformulated. In the equilibrium state of the system $d\Theta_m/dE > 0$, whereas in the stable–instable limit state $d\Theta_m/dE \to \infty$, meaning that by increasing the field strength (deviating only by a constant from the voltage in the case of homogeneous fields) a critical field strength is reached, where the temperature of the dielectric increases monotonously and in prin-

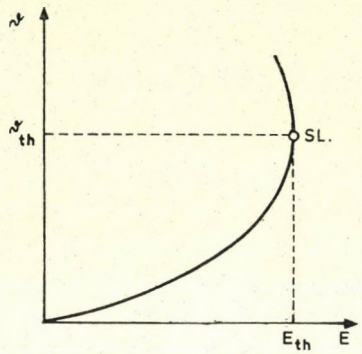

Fig. 9. Temperature of the dielectric versus the field strength. SL. — instability point

ciple it may become infinitive, i.e., more losses occur in the dielectric in the unit time than can be transferred to the environment. This condition is shown in Fig. 9. The instability criterion may also be formulated in the following way: $dE/d\Theta_m = 0$. As E and Θ_m are interrelated by $F(E, \Theta_m)$ and E is contained in it by way of the auxiliary parameter β, it is easily admissible that the condition $dF/d\beta = 0$ is equivalent with the condition $dE/d\Theta_m = 0$. By performing the differentiation the following function relationship between c and β is obtained:

$$c = \frac{\beta(\beta + \sinh\beta \cdot \cosh\beta)}{\cosh^2\beta\,(1 - \beta \cdot \tanh\beta)}\,. \tag{45}$$

The instability field strength or in the case of homogeneous fields the thermal breakdown voltage, respectively, may be expressed from (44) as:

$$U_{\tilde{th}} = \sqrt{\frac{2 \cdot \lambda_1}{b \cdot p'_a}} \cdot \varphi(c), \tag{46}$$

where

$$\varphi(c) = \frac{\beta}{\cosh\beta} \cdot e^{-\frac{\beta \tanh\beta}{c}} \tag{47}$$

The function $\varphi(c)$, as in the D.C. voltage case, is called Fok-function. For determining the interpretation range of the auxiliary parameter β the equation $1 - \beta\tanh\beta = 0$ must be solved. We have solved this equation by the Newton

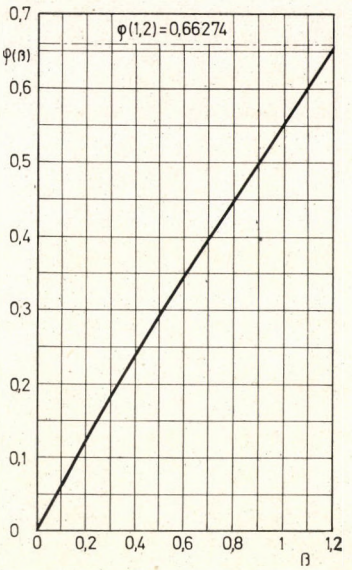

Fig. 10. The function $\varphi(\beta)$ for A.C. voltage

method with the aid of a digital computer [38] and obtained the result of $\beta_\infty = 1{,}19967864$. On this basis the interpretation ranges are as follows:

$$0 \leqq c \leqq \infty, \quad 0 \leqq \beta \leqq 1{,}19967864, \quad 0 \leqq \varphi(c) \leqq 0{,}6627434 .$$

With the knowledge of the interpretation ranges the functions were tabulated with the aid of the computer. The results are presented by the Appendix and in Figs 10 and 11. It is very interesting that similarly to the D.C. voltage

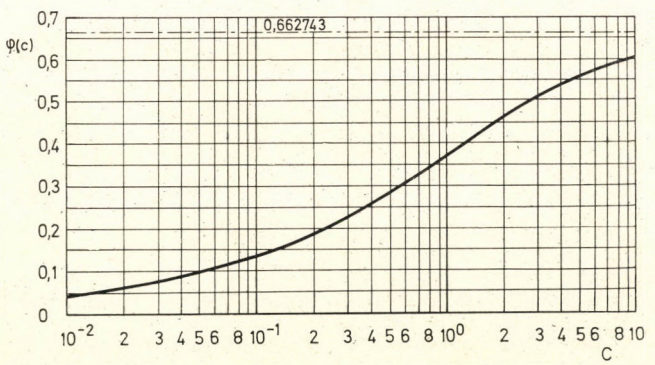

Fig. 11. The function $\varphi(c)$ for A.C. voltage

case, the thermal breakdown voltage tends to a maximum value with the increase of c also here:

$$U_{\widetilde{\text{thm}}} = U_{\text{th}}(c \to \infty) = 0{,}937226 \sqrt{\frac{\lambda_1}{b \cdot p'_a}} . \tag{48}$$

This result is rather remarkable, as it reflects the fact that the instability voltage cannot be increased unequivocally (and uniformly) by increasing the thickness of the insulating material or the intensity of the cooling. This is important for the practice, as it points out the possible and economical methods of increasing the stability voltage; such as e.g., the partition of the insulation and the insertion of a cooling canal, etc.

Naturally the individual temperature differences can be calculated for A.C. voltages as well, as given below, without the derivations [36]:

$$\Theta_m = b(\vartheta_m - \vartheta_a) = 2 \cdot \ln [\cosh \beta] + 2 \frac{\beta \cdot \tanh \beta}{c} \tag{49}$$

$$\Theta_m - \Theta_1 = b(\vartheta_m - \vartheta_1) = 2 \cdot \ln [\cosh \beta] \tag{50}$$

$$\Theta_1 = b(\vartheta_1 - \vartheta_a) = 2 \frac{\beta \cdot \tanh \beta}{c} \tag{51}$$

The relative temperature differences versus the parameter c are shown in Figs 6, 7 and 8. The results were obtained with the aid of the computer in this case, too. The fact that according to the expression (49) the relative instability temperature rise has a limit value:

$$\Theta_m(c \to \infty) = 1{,}186842$$

is very interesting and remarkable. The observed low values of the temperature rise do not mean to say that breakdown occurs at such low values, but only that the dielectric is in the stable–unstable boundary state under these temperature rise values. At D.C. voltages the situation is essentially different, as we have seen and also the reasons given.

8. Comparison between the cases of D.C. and A.C. voltage application

Two definitions: (31) and (46) were derived for calculating the thermal breakdown voltage. On comparing the obtained results a surprising — though not unexpected — agreement can be noted. This is naturally not accidental, as the fundamental physical contents of the processes have much in common and the deviations are caused only by the different origins of the lossess occurring in the dielectric. Both expressions are of a similar nature: the thermal coefficient $1/T$ characterizing the temperature dependence of the losses when D.C. voltage

is applied has its counterpart b in the case when A.C. voltage is used. A similar correspondence prevails between the conductivity in the case of the D.C. voltages and the volume loss number in the case of the A.C. voltages, both determining the developing losses. Also the ambient and the reference temperatures, respectively, influence both expressions of the thermal breakdown voltage in the same way. The obtained data are interesting also by the fact that these similar results, — based on deeper physical reasons, — were obtained by different mathematical apparatuses.

The expressions (31) and (46) show the greatest difference in their factorial functions $\Psi(c)$ and $\varphi(c)$, respectively. But on comparing Figs 5 and 11 it can be seen that practically both functions agree up to the value $c = 2$ (not meaning naturally the numerical agreement of the thermal breakdown voltages as well). But in the cases of $c > 2$ both functions deviate increasingly from each other and also their limit values are different.

The heat transfer relation and the data of the geometrical layout are represented by the factor c. It is worthwile investigating how the variations of these individual factors affect the value of the parameter c. The most interesting is naturally the effect of the variations of the heat transfer coefficient, illustrated by the following table:

Table I

The c parameter versus the heat coefficient (α)

α[W/m²°C]	5	10	20	30	50	100	500	∞
c	0,31249	0,62493	1,2497	1,8774	3,1232	6,243	31,077	5625

The main data of the dielectric are: $\lambda_1 = 0{,}16$ [W/m² °C], $\lambda_2 = 180$ [W/m² °C], $m = 0{,}002$ [m], $h = 0{,}01$ [m].

Very remarkable is the fact that in the case of $\alpha = \infty$, i.e., of ideal cooling (when the temperature of the dielectric equals the ambient temperature) the value of c is a finite number and is identical with the quotient of the thermal resistances of the dielectric and the electrode, respectively:

$$c(\alpha = \infty) = \frac{h \cdot \lambda_2}{m \cdot \lambda_1} .$$

This means that thermal breakdown may occur even under ideal heat transfer conditions, as $\Psi(c)$ and $\varphi(c)$ are limited functions.

The value of the parameter c is inversely proportional with the thermal conductivity of the dielectric. The effect of the electrode thickness is observable only when the thermal conductivity is very high.

Table II.

Fok-function for D.C. voltage and relative instability temperature rise

ξ[°]	c	$\Psi(c)$	$\Theta_m - \Theta_1 = \frac{1}{T}(\vartheta_m - \vartheta_a)$	β	c	$\varphi(c)$	$\Theta_m = b(\vartheta_m - \vartheta_a)$
0,0	0,000000	0,000000	1,000000	0,0000	0,000000	0,000000	1,000000
0,5	0,000152	0,005293	1,000025	0,0050	0,000050	0,003033	1,000008
1,0	0,000609	0,010586	1,000102	0,0100	0,000200	0,006065	1,000033
1,5	0,001372	0,015881	1,000229	0,0150	0,000450	0,009098	1,000075
2,0	0,002440	0,021176	1,000406	0,0200	0,000800	0,012130	1,000133
2,5	0,003815	0,026473	1,000635	0,0250	0,001250	0,015162	1,000208
3,0	0,005498	0,031772	1,000915	0,0300	0,001801	0,018193	1,000300
3,5	0,007491	0,027074	1,001247	0,0350	0,002451	0,021224	1,000408
4,0	0,009795	0,042378	1,001630	0,0400	0,003202	0,024255	1,000533
4,5	0,012413	0,047686	1,002064	0,0450	0,004053	0,027285	1,000674
5,0	0,015348	0,052997	1,002551	0,0500	0,005004	0,030314	1,000832
5,5	0,018600	0,058312	1,003090	0,0550	0,006056	0,033342	1,001006
6,0	0,022175	0,063632	1,003681	0,0600	0,007209	0,036370	1,001197
6,5	0,026075	0,068956	1,004325	0,0650	0,008462	0,039397	1,001405
7,0	0,030303	0,074286	1,005023	0,0700	0,009816	0,042423	1,001628
7,5	0,034864	0,079621	1,005774	0,0750	0,012271	0,045447	1,001868
8,0	0,039763	0,084962	1,006579	0,0800	0,012828	0,048471	1,002125
8,5	0,045002	0,090310	1,007439	0,0850	0,014485	0,051493	1,002397
9,0	0,050589	0,095665	1,008354	0,0900	0,016244	0,054514	1,002686
9,5	0,056527	0,101026	1,009325	0,0950	0,018105	0,057534	1,002991
10,0	0,062823	0,106396	1,010352	0,1000	0,020067	0,060553	1,003312
10,5	0,069482	0,111773	1,011435	0,1050	0,022132	0,063570	1,003649
11,0	0,076512	0,117159	1,012676	0,1100	0,024299	0,066585	1,004003
11,5	0,083919	0,122553	1,013776	0,1150	0,026568	0,069599	1,004372
12,0	0,091709	0,127957	1,015033	0,1200	0,028941	0,072611	1,004756
12,5	0,099892	0,133370	1,016351	0,1300	0,033994	0,078630	1,005573
13,0	0,108474	0,138793	1,017729	0,1400	0,039462	0,084641	1,006453
13,5	0,117465	0,144226	1,019168	0,1500	0,045347	0,090644	1,007394
14,0	0,126874	0,149670	1,020668	0,1600	0,051651	0,096638	1,008396
14,5	0,136710	0,155125	1,022232	0,1700	0,058376	0,102624	1,009459
15,0	0,146982	0,160592	1,023860	0,1800	0,065528	0,108599	1,010581
15,5	0,157702	0,166071	1,025552	0,1900	0,073107	0,114565	1,011761
16,0	0,168881	0,171561	1,027310	0,2000	0,081119	0,120520	1,013000
16,5	0,180531	0,177064	1,029134	0,2100	0,089567	0,126464	1,014295
17,0	0,192662	0,182581	1,031027	0,2200	0,098455	0,132397	1,015646
17,5	0,205290	0,188110	1,032988	0,2300	0,107787	0,138318	1,017052
18,0	0,218426	0,193653	1,035020	0,2400	0,117569	0,144226	1,018512
18,5	0,232085	0,199210	1,037123	0,2500	0,127806	0,150122	1,020024
19,0	0,246283	0,204782	1,039298	0,2600	0,138503	0,156005	1,021589
19,5	0,261034	0,210368	1,041548	0,2700	0,149665	0,161874	1,023023
20,0	0,276355	0,215969	1,043872	0,2800	0,161300	0,167730	1,024867
20,5	0,292263	0,221586	1,046274	0,2900	0,173413	0,173572	1,026578
21,0	0,308777	0,227218	1,048753	0,3000	0,186012	0,179399	1,028337
21,5	0,325914	0,232867	1,051312	0,3100	0,199105	0,185212	1,030141
22,0	0,343696	0,238532	1,053952	0,3200	0,212699	0,191010	1,031988
22,5	0,362142	0,244214	1,056675	0,3300	0,226803	0,196793	1,033879
23,0	0,381276	0,249913	1,059482	0,3400	0,241426	0,202561	1,035811
23,5	0,401118	0,255629	1,062375	0,3500	0,256578	0,208313	1,037782
24,0	0,421695	0,261363	1,065356	0,3600	0,272269	0,214050	1,039793
24,5	0,443030	0,267115	1,068427	0,3700	0,288510	0,219770	1,041840
25,0	0,465150	0,272885	1,071589	0,3800	0,305313	0,225475	1,043922
25,5	0,488083	0,278674	1,074845	0,3900	0,322690	0,231164	1,046039
26,0	0,511859	0,284482	1,078196	0,4000	0,340654	0,236837	1,048187
26,5	0,536507	0,290309	1,081645	0,4100	0,359220	0,242493	1,050367

Table II. continued

ξ[°]	c	$\Psi(c)$	$\Theta_m - \Theta_1 = \frac{1}{T}(\vartheta_m - \vartheta_a)$	β	c	$\varphi(c)$	$\Theta_m = b(\vartheta_m - \vartheta_a)$
27,0	0,562060	0,296155	1,085193	0,4200	0,378402	0,248133	1,052576
27,5	0,588552	0,302021	1,088843	0,4300	0,398216	0,253757	1,054813
28,0	0,616018	0,307907	1,092597	0,4400	0,418679	0,259365	1,057075
28,5	0,644496	0,313813	1,096458	0,4500	0,439810	0,264957	1,059362
29,0	0,674024	0,319740	1,100427	0,4600	0,461626	0,270532	1,061672
29,5	0,704644	0,325688	1,104508	0,4700	0,484149	0,276091	1,064003
30,0	0,736400	0,331656	1,108703	0,4800	0,507400	0,281634	1,066353
30,5	0,769336	0,337645	1,113014	0,4900	0,531403	0,287162	1,068721
31,0	0,803501	0,343656	1,117445	0,5000	0,556181	0,292673	1,071105
31,5	0,838946	0,349688	1,121998	0,5100	0,581761	0,298169	1,073503
32,0	0,875723	0,355742	1,126675	0,5200	0,608172	0,303649	1,075914
32,5	0,913889	0,361817	1,131481	0,5300	0,635442	0,309114	1,078336
33,0	0,953503	0,367915	1,136418	0,5400	0,663604	0,314563	1,080767
33,5	0,994627	0,374035	1,141488	0,5500	0,692692	0,319998	1,083206
34,0	1,037327	0,380177	1,146697	0,5600	0,722742	0,325418	1,085650
34,5	1,081672	0,386341	1,152046	0,5700	0,753793	0,330824	1,088099
35,0	1,127736	0,392528	1,157539	0,5800	0,785887	0,336216	1,090550
35,5	1,175596	0,398737	1,163131	0,5900	0,819068	0,341594	1,093002
36,0	1,225334	0,404969	1,168974	0,6000	0,853383	0,346958	1,095452
36,5	1,277036	0,411223	1,174922	0,6100	0,888885	0,352309	1,097900
37,0	1,330794	0,417501	1,181030	0,6200	0,925627	0,357647	1,100344
37,5	1,386704	0,423800	1,187301	0,6300	0,963669	0,362973	1,102782
38,0	1,444869	0,430123	1,193740	0,6400	1,003075	0,368287	1,105211
38,5	1,505397	0,436468	1,200351	0,6500	1,043912	0,373589	1,107632
39,0	1,568404	0,442836	1,207138	0,6600	1,086255	0,378880	1,110041
39,5	1,634010	0,449226	1,214106	0,6700	1,130182	0,384160	1,112438
40,0	1,702347	0,455639	1,221259	0,6800	1,175779	0,389429	1,114820
40,5	1,773549	0,462074	1,228603	0,6900	1,223139	0,394689	1,117187
41,0	1,847765	0,468531	1,236143	0,7000	1,272362	0,399939	1,119536
41,5	1,925148	0,475010	1,243883	0,7100	1,323557	0,405180	1,121866
42,0	2,005863	0,481511	1,251830	0,7200	1,376842	0,410413	1,124175
42,5	2,090086	0,488033	1,259988	0,7300	1,432345	0,415637	1,126462
43,0	2,178003	0,494577	1,268364	0,7400	1,490206	0,420855	1,128726
43,5	2,269814	0,501142	1,276963	0,7500	1,550577	0,426065	1,130964
44,0	2,365729	0,507728	1,285792	0,7600	1,613624	0,431268	1,133176
44,5	2,465976	0,514334	1,294856	0,7700	1,679531	0,436466	1,135359
45,0	2,570796	0,520960	1,304163	0,7800	1,748496	0,441659	1,137513
45,5	2,680447	0,527606	1,313718	0,7900	1,820739	0,446846	1,139636
46,0	2,795205	0,534271	1,323530	0,8000	1,896503	0,452030	1,141727
46,5	2,915364	0,540955	1,333604	0,8100	1,976053	0,457210	1,143784
47,0	3,041241	0,547658	1,343950	0,8200	2,059686	0,462386	1,145807
47,5	3,173174	0,554378	1,354573	0,8300	2,147728	0,467561	1,147792
48,0	3,311526	0,561115	1,365483	0,8400	2,240543	0,472733	1,149741
48,5	3,456687	0,567868	1,376687	0,8500	2,338538	0,477905	1,151651
49,0	3,609076	0,574638	1,388195	0,8600	2,442167	0,483075	1,153520
49,5	3,769141	0,581423	1,400014	0,8700	2,551938	0,488246	1,155349
50,0	3,937367	0,588222	1,412154	0,8800	2,668426	0,493417	1,157135
50,5	4,114276	0,595034	1,424625	0,8900	2,792277	0,498589	1,158878
51,0	4,300429	0,601860	1,437436	0,9000	2,924227	0,503763	1,160576
51,5	4,496433	0,608697	1,450598	0,9050	2,993495	0,506351	1,161408
52,0	4,702943	0,615546	1,464121	0,9100	3,065111	0,508940	1,162229
52,5	4,920666	0,622404	1,478016	0,9150	3,139197	0,511529	1,163038
53,0	5,150370	0,629271	1,492294	0,9200	3,215885	0,514120	1,163835
53,5	5,392882	0,636147	1,506968	0,9250	3,295318	0,516711	1,164620
54,0	5,649105	0,643028	1,522049	0,9300	3,377647	0,519303	1,165394

Table II. continued

$\xi[°]$	c	$\Psi(c)$	$\Theta_m - \Theta_1 = \frac{1}{T}(\vartheta_m - \vartheta_a)$	β	c	$\varphi(c)$	$\Theta_m = b(\vartheta_m - \vartheta_a)$
54,5	5,920016	0,649916	1,537551	0,9350	3,463037	0,521896	1,166155
55,0	6,206676	0,656807	1,553486	0,9400	3,551664	0,524491	1,166904
55,5	6,510241	0,663702	1,569869	0,9450	3,643719	0,527087	1,167640
56,0	6,831972	0,670598	1,586713	0,9500	3,739407	0,529684	1,168364
56,5	7,173243	0,677494	1,604034	0,9550	3,838951	0,532282	1,169076
57,0	7,535554	0,684389	1,621847	0,9600	3,942592	0,534882	1,169775
57,5	7,920547	0,691281	1,640169	0,9650	4,050592	0,537483	1,170461
58,0	8,330020	0,698168	1,659017	0,9700	4,163235	0,540086	1,171134
58,5	8,765945	0,705049	1,678407	0,9750	4,280831	0,542691	1,171794
59,0	9,230487	0,711922	1,698360	0,9800	4,403718	0,545298	1,172441
59,5	9,726030	0,718784	1,718893	0,9850	4,532265	0,547906	1,173075
60,0	10,255197	0,725636	1,740027	0,9900	4,666878	0,550517	1,173695
60,5	10,820885	0,732473	1,761783	0,9950	4,808001	0,553129	1,174303
61,0	11,426295	0,739294	1,784184	1,0000	4,956122	0,555744	1,174896
61,5	12,074970	0,746098	1,807252	1,0050	5,111782	0,558360	1,175477
62,0	12,770839	0,752881	1,831012	1,0100	5,275575	0,560979	1,176043
62,5	13,518271	0,759642	1,855489	1,0150	5,448163	0,563601	1,176596
63,0	14,322125	0,766378	1,880710	1,0200	5,630280	0,566224	1,177135
63,5	15,187823	0,773087	1,906704	1,0250	5,822744	0,568851	1,177660
64,0	16,121424	0,779766	1,933499	1,0300	6,026469	0,571479	1,178171
64,5	17,129713	0,786413	1,961127	1,0350	6,242482	0,574111	1,178668
65,0	18,220307	0,793024	1,989622	1,0400	6,471937	0,576745	1,179151
65,5	19,401774	0,799598	2,019017	1,0450	6,716138	0,579382	1,179620
66,0	20,683774	0,806132	2,049351	1,0500	6,976561	0,582022	1,180075
66,5	22,077229	0,812622	2,080661	1,0550	7,254890	0,584665	1,180515
67,0	23,594514	0,819065	2,112989	1,0600	7,553048	0,587311	1,180941
67,5	25,249691	0,825459	2,146379	1,0650	7,873242	0,589960	1,181352
68,0	27,058785	0,831800	2,180877	1,0700	8,218022	0,592612	1,181749
68,5	29,040107	0,838085	2,216534	1,0750	8,590347	0,595267	1,182132
69,0	31,214646	0,844311	2,253401	1,0800	8,993669	0,597926	1,182499
69,5	33,606538	0,850475	2,291537	1,0850	9,432041	0,600588	1,182852
70,0	36,243628	0,856572	2,331000	1,0900	9,910260	0,603254	1,183191
70,5	39,158156	0,862600	2,371856	1,0950	10,434034	0,605923	1,183515
71,0	42,387587	0,868554	2,414174	1,1000	11,010219	0,608595	1,183823
71,5	45,975621	0,874432	2,458029	1,1050	11,647120	0,611272	1,184118
72,0	49,973448	0,880229	2,503501	1,1100	12,354891	0,613952	1,184397
72,5	54,441278	0,885941	2,550679	1,1150	13,146089	0,616636	1,184661
73,0	59,450261	0,891565	2,599655	1,1200	14,036419	0,619324	1,184910
73,5	65,084873	0,897097	2,650533	1,1250	15,045793	0,622016	1,185144
74,0	71,445922	0,902532	2,703424	1,1300	16,199839	0,624712	1,185364
74,5	78,654353	0,907867	2,758449	1,1350	17,532110	0,627412	1,185568
75,0	86,856103	0,913097	2,815743	1,1400	19,087403	0,630117	1,185757
75,5	96,228341	0.918218	2,875450	1,1450	20,926900	0,632825	1,185931
76,0	106,987547	0,923226	2,937733	1,1500	23,136416	0,635538	1,186090
76,5	119,400084	0,928118	3,002770	1,1550	25,840179	0,638256	1,186234
77,0	133,796132	0,932887	3,070759	1,1600	29,225033	0,640977	1,186362
77,5	150,588271	0,937530	3,141921	1,1650	33,585583	0,643704	1,186475
78,0	170,296496	0,942044	3,216502	1,1700	39,414960	0,646435	1,186573
78,5	193,582324	0,946422	3,294781	1,1750	47,605939	0,649170	1,186656
79,0	221,295834	0,950661	3,377072	1,1800	59,958651	0,651911	1,186724
79,5	254,541484	0,954757	3,463734	1,1850	80,725944	0,654656	1,186776
80,0	294,771533	0,958705	3,555175	1,1900	122,948784	0,657406	1,186814
80,5	343,920835	0,962500	3,651867	1,1905	129,701059	0,657681	1,186816
81,0	404,604786	0,966138	3,754358	1,1910	137,231354	0,657957	1,186819
81,5	480,415793	0,969615	3,863286	1,1915	145,682361	0,658232	1,186822

Table II. continued

ξ [°]	c	$\Psi(c)$	$\Theta_m - \Theta_1 = \frac{1}{T}(\vartheta_m - \vartheta_a)$	β	c	$\varphi(c)$	$\Theta_m = b(\vartheta_m - \vartheta_a)$
82,0	576,377016	0.972926	3,979409	1,1920	155,233938	0,658507	1,186824
82,5	699,653840	0.976067	4,103627	1,1925	166,116053	0,658783	1,186826
83,0	860,700200	0.979034	4,237027	1,1930	178,627540	0,659058	1,186829
83,5	1075,163120	0.981822	4,380935	1,1935	193,163966	0,659334	1,186831
84,0	1367,149708	0.984427	4,536997	1,1940	210,260213	0,659610	1,186832
84,5	1775,147509	0.986845	4,707287	1,1945	230,657736	0,659885	1,186834
85,0	2362,945624	0.989071	4,894469	1,1950	255,414945	0,660161	1,186835
85,5	3241,603582	0.991103	5,102054	1,1955	286,096829	0,660437	1,186837
86,0	4615,772752	0.992936	5.334791	1,1960	325,119230	0,660713	1:186838
86,5	6890,348918	0.994566	5,599337	1,1965	376,418037	0,660988	1,186839
87,0	10942,014960	0.995989	5,905439	1,1970	446,867860	0,661264	1,186840
87,5	18908,291320	0.997202	6,268207	1,1975	549,654228	0,661540	1,186841
88,0	36930,895700	0.998201	6,712948	1,1980	713,672445	0,661816	1,186841
88,5	87540,815650	0.998984	7,287100	1,1985	1016,849398	0,662092	1,186842
89,0	295451,812800	0.999547	8,097158	1,1990	1766,767918	0,662369	1,186842
89,5	2363618,345200	0.999880	9,482925	1,1995	6714,610780	0,662645	1,186843
90,0	∞	1.000000	∞	1,2000	∞	0,662743	1,186853

The common effect of the ambient temperature and b, the temperature coefficient may be determined by the instability expression. With the above values and $\varphi(c) = 0{,}63$, for simplicity's sake, we have:

$$U_{\text{th}}^{\sim}(b, \vartheta_a) = \frac{52{,}3}{\sqrt{b}} \cdot \mathbf{e}^{-\frac{b}{2}(\vartheta_a - \vartheta_0)}$$

Our calculation results are seen in Fig. 12 showing clearly the value of the thermal breakdown voltage greatly decreasing with the variation of both ϑ_a

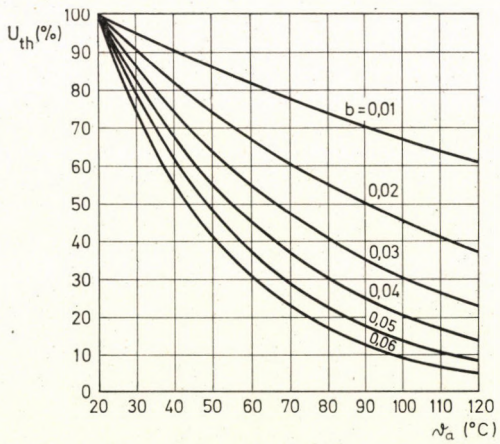

Fig. 12. Thermal breakdown voltage versus the ambient temperature with the parameter b

and the parameter b. We note that at D.C. voltages the effect of the variations of ϑ_a and T, respectively, is perfectly similar, only numerically different.

9. Summary

Two expressions were derived on the basis of the instability condition for calculating the thermal breakdown voltage at D.C. and A.C. voltage applications, respectively. Both expressions show a qualitative agreement, giving only numerically different values. As the losses are always higher at A.C. voltages, the numerical value of $U_{\text{th}}^{\sim}$ is always lower than that of $U_{\text{th}}^{=}$. The characteristic temperature distributions calculated for both cases show a fundamental difference. We have studied some factors influencing the value of the thermal breakdown voltage. The effect of the individual parameters can be taken into consideration, if they increase the value of the thermal breakdown voltage, e.g., by choosing insulation materials of lower temperature coefficients, etc.

Finally we note that the differential equation of the thermal conduction, which is of essential importance in the breakdown theories, may be solved for various boundary conditions with the aid of the digital computer. In addition to the above-mentioned boundary conditions also the possible external heat inflow may be easily allowed for. A possible solution of the differential equation for layouts of plane geometry with the aid of the computer is found in [39]. A more general process for the calculation of the thermal breakdown voltage with the aid of the computer, than those mentioned above, can also be given [40]. The above derivations are nevertheless useful, as they permit in many practical cases the fast estimation of the value of the thermal breakdown voltage.

Acknowledgements

The authors express herewith their thanks to professor Dr. EISLER János, academician Dr. GESZTI P. Otto and Dr. VAJDA György, honorary professor, for the careful recension of the manuscript and for their valuable comments.

Appendix

The derived relationships and functions were tabulated with the aid of a computer. The calculation program was prepared in the ALGOL—60 language and run on the computer type RAZDAN—3 of the Computation Centre of the Technical University of Budapest. The results are contained in the previous tables.

REFERENCES

1. ANDERSON, J. C.: Dielectrics, Chapman and Hall, London 1964
2. FRÖHLICH, H.: Theory of Dielectrics. Clarendon Press, Oxford 1950
3. *Handbuch der Physic*, editor in chief: FLÜGGE, S. Springer Verlag, Berlin 1956, vol. XVII.

4. HIPPEL, A.: Der Mechanismus des 'elektronischen' Durchschlages in festen Isolatoren I. *Zeitschrift der Physik*, **67** (1931), 707—724
5. HIPPEL, A.: Der Mechanismus des „elektrischen" Durchschlages in festen Isolatoren II. *Zeitschrift der Physik* **68** (1931), 309—324
6. JACKSON, W.: The Insulation of Electrical Equipment. Chapman and Hall, London 1954
7. GOODLET, B. L.—EDWARDS, F. S.—PERRY, F. R.: Dielectric Phenomena at High Voltages, *J.I.E.E.* **69** (1931)
8. GÜLLNER, G.: Zum Durchschlag fester Isolatoren, *Archiv für Elektrotechnik* **21** (1928), 267—288
9. HALBACH, K.: Untersuchungen über den Durchschlag und die Verluste einiger fester Isolierstoffe, *Archiv für Elektrotechnik* **21** (1929), 535—563
10. INGE, L.—WALTER, A.: Durchschlag von festen Isolatoren bei Hochfrequenz, *Archiv für Elektrotechnik* **21** (1928), 209—227
11. INGE, L.—WALTER, A.: Durchschlag von Isolatoren bei hohen Temperaturen, *Zeitschrift für Physik* **34** (1925), 15
12. INGE, L.—WALTER, A.: Über den Durchschlag fester Isolatoren, *Zeitschrift für Physik* **32** (1925), 273
13. INGE, L.—WALTER, A.: Durchschlag von Glas, *Zeitschrift für Physik* **37** (1926), 292
14. INGE, L.—WALTER, A.—SEMENOFF, N.: Über den Durchschlag fester Isolatoren, *Archiv für Elektrotechnik* **17** (1927), 543
15. RAYNER, E. H.: High-voltage Tests and Energy Losses in Insulating Materials, *J.I.E.E.* **49** (1912)
16. EISLER, J.: Bevezetés a nagyfeszültségű technikába (Introduction into the High Voltage Technics). Akadémiai Kiadó, Budapest 1966
17. VAJDA, GY.: Szigetelések romlása és romlásuk vizsgálata (The Deterioration of Insulations and the Investigation of Same). Akadémiai Kiadó, Budapest 1964
18. WHITEHEAD, S.: Dielectric Breakdown of Solids. Clarendon Press, Oxford 1951
19. ROGOWSKY, W.: Molekulare und technische Durchschlags-feldstärke fester elektrischer Isolatoren, *Archiv für Elektrotechnik* **18** (1927), 123—166
20. MOON, P. H.—NORCROSS, A. S.: Three Regions of Dielectric Breakdown, *Trans. A.I.E.E.* **49** (1930), 755—762
21. CSERNÁTONY, H. A.—HORVÁTH, T.: Nagyfeszültségű technika (High Voltage Technics). Tankönyvkiadó, Budapest 1969
22. SZKANAVI, G. I. Fizika dielektrikov (oblaszti szilnüh polej). Moszkva 1958
23. MIHEJEV, M. A.: A hőátadás gyakorlati számításának alapjai (The Basis of Practical Heat Transfer Calculations). Tankönyvkiadó, Budapest 1965
24. SIMONYI, K.: Elméleti villamosságtan (Theoretical Electrical Engineering). Tankönyvkiadó, Budapest 1967
25. CARSLAW, H. S.—JAEGER, J. C.: Conduction of Heat in Solids. Clarendon Press, Oxford 1959
26. BELLMAN, R.: On the Existence and Boundness of Solutions of Nonlinear Partial Differential Evaluations of Parabolic Type, *Trans. American Mathematical Society* (1948), No. 2.
27. WALKER, M.: Theory of Machine Design, *J.I.E.E.* **52** (1913), 51
28. WAGNER, K. W.: The Physical Nature of the Electrical Breakdown of Solid Dielectrics, *J.I.E.E.* **41** (1922), 1034—1044
29. ROGOWSKY, W.: Der Durchschlag fester Isolatoren, *Archiv für Elektrotechnik* **13** (1924), 153—174
30. KÁRMÁN, T.: Über das thermisch-elektrische Gleichgewicht in festen Isolatoren, *Archiv für Elektrotechnik* **13** (1924), 174—180
31. GEMANT, A.: Thermal Instability of Dielectrics under Continuous Voltages when the Conductivity is Dependent upon the Field Strength, *Journal of the Franklin Institute* **228** (1939), 79—90
32. GEMANT, A.—WHITEHEAD, S.: Thermal Instability of Dielectrics for Alternating Voltages, *Philosophical Magazin* **27** (1939), 582—595
33. WHITEHEAD, J. B.: The dielectric strength and life impregnated paper insulation I. III. Trans. A. I. E. E. **59,** (1040) 715—720.
Trans. A. I. E. E. **61,** (1942), 618—622.
34. WHITEHEAD, S.: Thermal Breakdown with Internal Defects, *ERA Rep. Ref.* L/T 193 (1948)
35. FOCK, V.: Zur Wärmetheorie des elektrischen Durchschlages, *Archiv für Elektrotechnik* **18** (1927), 71—81
36. VAJTA, M. jr.: Diplomaterv (Diplome work). B.M.E. Nagyfeszültségű Technika és Villamos Készülékek Tanszék, 1971 (Chair for High Voltage and Electric Apparatuses, Technical University of Budapest)

37. WHITEHEAD, S.—NETHERCOT, W.: The Breakdown of Dielectrics under High Voltage with Particular Reference to Thermal Instability. *Proceedings of the Royal Society of London* **47** (1935), 974
38. RALSTON, A.: Bevezetés a numerikus analízisbe (Introduction into the Numerical Analysis) Műszaki Könyvkiadó, Budapest 1969
39. VAJTA, M. jr.: Sík dielektrikumok stacioner hőfok-, potenciál- és térerősségeloszlásának számítása digitális számítógéppel (The Calculation of the Stationary Temperature, Potential- and Field Strength Distributions in Plane Dielectrics with the Help of a Digital Computer), *Számológép* **2** (1972), 48—60 No. 2.
40. VAJTA, M. jr.: Digital Computer Analysis of the Thermal Breakdown Voltages in Solid Dielectrics, *Periodica Polytechnica* **16** (1972), No. 3, 281—300.

Bestimmung der Wärmekippspannung für Gleich- und Wechselspannung. Nach Definition der Begriffe: Wärmedurchschlag und Wärmeinstabilität bringt die Arbeit einen kurzen Überblick über die Literatur, die sich mit der Theorie des Wärmedurchschlags beschäftigt. Für Gleichspannung wird der Ausdruck für die Wärmekippspannung nach Anschreiben der allgemeinen Labilitätsgleichungen auf die Temperaturabhängigkeit eines gegebenen spezifischen Widerstands angewendet, und dann wird in ähnlicher Weise der Ausdruck für die Wärmekippspannung auch für den Fall der Wechselspannung abgeleitet. In beiden Fällen wurden auch die einzelnen Temperaturverteilungen berechnet, die Ergebnisse tabelliert und die Wirkung von einigen Parametern wurde untersucht, die die Wärmekippspannung beeinflussen.

Определение напряжения лабильности при постоянном и переменном токах. В статье после изложения понятий теплоэлектрического пробоя и тепловой нестабильности дается краткое обобщение о формировании теорий теплоэлектрического пробоя. После вывода общих уравнений лабильности для постоянного тока выражение напряжения лабильности выводится для тепловой зависимости данного удельного сопротивления, после чего, аналогично приведенному выше, и для случая переменного тока выводится выражение напряжения лабильности. В обоих случаях вычисляются также отдельные распределения температур, а полученные результаты использовны для изготовления таблиц на ЭВМ и, далее, исследовано влияние некоторых параметров, воздействующих на величину напряжения лабильности.

Acta Technica Academiae Scientiarum Hungaricae, Tomus 76 (1—2), pp. 207—215 (1974)

AN INFINITE ELASTIC PLATE UNDER TENSION WITH A CRACK AND A CIRCULAR INCLUSION

R. D. BHARGAVA*

and

Miss R. R. BHARGAVA*

[Manuscript received 10 August, 1972]

In this paper, a procedure is presented for computing the stresses and displacements which arise in the body named in heading. Functions of complex variable are used. As starting-point, differential equations occurring in the two-dimensional theory of elasticity are applied. The results of a numerical example refer to the cases where the ratio of the elasticity constants of inclusion and matrix is 1/3, 1 and 3.

1. Introduction

The works on fracture and cracks were first started by INGLIS in 1913 [1]. But the interest in such problems was stemmed from GRIFFITH's paper [2] in 1921. The cases of straight crack, circular crack, star crack and penny-shaped crack have been investigated by many investigators. For further references see [3].

The inclusion problems were introduced in 1940 by MOTT [4] but a systematic investigation of ellipsoidal inclusion was undertaken in 1957 by ESHELBY [5]. Later the case of two-dimensional inclusion problem was discussed by JASWON and BHARGAVA [6]. Since then a number of papers have appeared [7], [8] where more references can be found.

An effort of combining the above two types of problems forms the subject matter of the present paper.

This paper deals with problem of an infinite isotropic elastic material, called the matrix, containing a straight crack and a circular inclusion. The matrix is subjected to load at infinity. The solution is obtained by an approach based upon complex variable formalism. The problem reduces to finding out two sets of complex potentials $\{\Phi(z), \Psi(z)\}$; one for the matrix and another for the circular inclusion.

* Indian Institute of Technology, Bombay—76, India.

2. Complex variable formalism

For the case of two dimensional theory of elasticity, the stress components $P_{ij}(i, j = x, y)$ are most conveniently calculated from the relations

$$\begin{aligned} P_{yy} + P_{xx} &= 2\,[\Phi(z)+\overline{\Phi(z)}], \\ P_{yy} - i\,P_{xy} &= \Phi(z) + \overline{\Phi(z)} + \overline{z\Phi'(z)} + \overline{\Psi(z)} \end{aligned} \tag{1}$$

where $\Phi(z)$, $\Psi(z)$ are analytic functions of complex variable $z = x + iy$. A bar indicates the complex conjugate operation and dash signifies differentiation [9]. Similarly, displacement components may be found from

$$2\mu\,(u_{x,x} + i\,u_{y,x}) = \varkappa\,\Phi(z) - z\,\overline{\Phi'(z)} + \overline{\Phi(z)} - \overline{\Psi(z)} \tag{2}$$

where $\varkappa = 3-4\nu$ under conditions of plane strain, and $\varkappa = (3-\nu)/(1+\nu)$ under conditions of generalized plane stress, ν being the Poisson's ratio and μ the shear modulus. The comma after the function stands for partial differentiation with respect to subscript following it.

As the geometry under consideration is circle, it is most convenient to introduce polar co-ordinates r, θ by $z = re^{i\theta}$. The stress and displacement components in polar co-ordinates can thus be written as

$$P_{rr} + P_{\theta\theta} = 2[\Phi(z) + \overline{\Phi(z)}]\,,$$

$$P_{rr} + i\,P_{r\theta} = \Phi(z) + \overline{\Phi(z)} = \overline{z\Phi'(z)} - (\bar{z}/z)\,\overline{\Psi(z)} \tag{3}$$

and

$$2\mu(u_{x,\theta} + i\,u_{u,\theta}) = iz\,[\varkappa\Phi(z) - \overline{\Phi(z)} + \overline{z\Phi'(z)} + (\bar{z}/z)\,\overline{\Psi(z)}]\,. \tag{4}$$

It is more useful to introduce the potential $\Omega(z)$ as follows:

$$\Omega(z) = \bar{\Phi}(z) + z\bar{\Phi}'(z) + \bar{\Psi}(z). \tag{5}$$

The relations $(1)_2$ and (2) may thus be written in terms of $\Phi(z)$ and $\Omega(z)$ as

$$P_{yy} - i\,P_{xy} = \Phi(z) + \Omega(\bar{z}) + (z - \bar{z})\,\overline{\Phi'(z)}\,. \tag{6}$$

$$2\mu(u_{x,x} + i\,u_{y,x}) = \varkappa\Phi(z) - \Omega(\bar{z}) - (z - \bar{z})\,\overline{\Phi'(z)}\,. \tag{7}$$

3. Formulation of the problem

We choose the reference frame in accordance with Fig. 1. The matrix of an elastic isotropic and homogeneous material contains a straight crack L from (a, o) to (b, o) and a hole of radius R and with centre at D (D may be complex). The crack and the hole do not overlap. The elastic circular inclusion of a different elastic material and of same radius R as that of the hole is welded

along the circumference of the hole. The boundary conditions of the problem can thus be stated as follows:

(i) The rims of the crack are free from stresses i.e., $P_{yy}^{\pm} - i\,P_{xy}^{\pm} = 0$. The superscripts $+$, $-$ indicate the limiting values from positive y-plane and negative y-plane respectively.

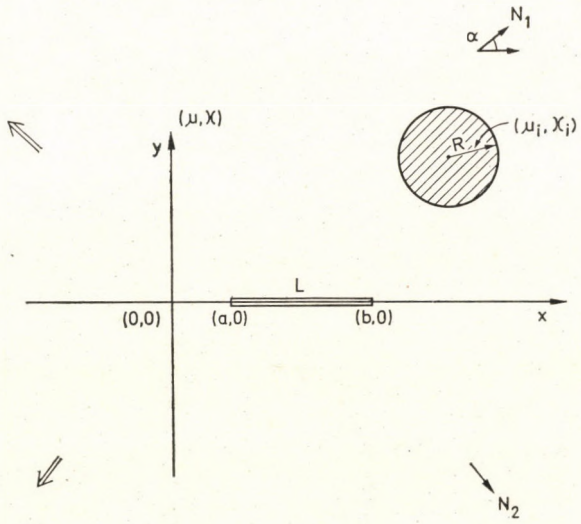

Fig. 1

(ii) At infinity the form of the potentials is

$$\Phi(z) = \Gamma_0 + 0\left(\frac{1}{z^2}\right),$$

$$\Psi(z) = \Gamma_1 + 0\left(\frac{1}{z^2}\right),$$

where

$$\Gamma_0 = \frac{1}{4}(N_1 + N_2); \quad \Gamma_1 = -\frac{1}{2}(N_1 - N_2)\,e^{-2i\alpha}.$$

The principal stresses at infinity are N_1 and N_2 and α is the angle between the x-axis and N_1. Rotation at infinity is neglected.

(iii) Along the inclusion boundary $r = R$, when origin is considered at D,

$$(P_{rr} + i\,P_{r\theta})_{\text{matrix}} = (P_{rr} + i\,P_{r\theta})_{\text{inclusion}},$$

$$(u_x + i\,u_y)_{\text{matrix}} = (u_x + i\,u_y)_{\text{inclusion}}.$$

4. Solution of the problem

The condition (i) when written in terms of the potentials $\Phi(z)$, $\Omega(z)$ using (6) yields dual homogeneous Hilbert problem.

$$\Phi^+(t) + \Omega^-(t) = 0; \qquad \Phi^-(t) + \Omega^+(t) = 0\,. \tag{8}$$

Superscripts $+$, $-$ have the same meaning as defined above and t is any point on the crack L other than end points. The solution of these equations may be written directly (taking into account that the potentials have poles of various orders at $z = D$ and considering condition (ii) as

$$\Phi(z) = -\frac{1}{2}\bar{\Gamma}_1 + \frac{1}{2}\sum_{2}^{\infty} A_n \left(\frac{1}{z-D}\right)^n + \frac{1}{2}X(z)\Bigg[(2\Gamma_0+\bar{\Gamma}_1)\cdot \left(z - \frac{a+b}{2}\right) + \sum_{1}^{\infty} B_n \left(\frac{1}{z-D}\right)^n\Bigg], \tag{9}$$

$$\Omega(z) = \frac{1}{2}\bar{\Gamma}_1 - \frac{1}{2}\sum_{2}^{\infty} A_n \left(\frac{1}{z-D}\right)^n + \frac{1}{2}X(z)\Bigg[(2\Gamma_0+\bar{\Gamma}_1)\cdot \left(z - \frac{a+b}{2}\right) + \sum_{1}^{\infty} B_n \left(\frac{1}{z-D}\right)^n\Bigg] \tag{10}$$

where

$$X(z) = (z-a)^{-1/2}(z-b)^{-1/2}.$$

The constants A_n's and B_n's are unknown.

The origin of co-ordinate system is now shifted to D. The functions $\{\Phi(z), \Psi(z)\}$ transform to new functions $\{\Phi_1(z_1), \Psi_1(z_1)\}$. We drop the suffix 1 for convenience but remember these are the potentials obtained after shifting the origin to D. The potentials $\Phi(z)$, $\Psi(z)$ may be expanded by Laurent series in the region $0 < |z| < |D|$

$$\Phi(z) = \sum_{-\infty}^{\infty} D_n z^n; \quad \Psi(z) = \sum_{-\infty}^{\infty} E_n z^n, \tag{12}$$

where

$$D_n = \frac{1}{2}\Bigg[-\bar{\Gamma}_1\delta_{0,n} + (2\Gamma_0+\bar{\Gamma}_1)P_{n-1}(1-\delta_{0,n}) + (2\Gamma_0+\bar{\Gamma}_1)\left(D - \frac{(a+b)}{2}\right)P_n + \sum_{k=1}^{\infty} P_{n+k}B_k\Bigg], \quad n \geq 0, \tag{13a}$$

$$D_{-n} = \frac{1}{2}\Bigg[A_n(1-\delta_{1,n}) + \sum_{k=0}^{\infty} P_k B_{n+k}\Bigg], \quad n \geq 1, \tag{13b}$$

$$E_n = \frac{1}{2}\Bigg[(\Gamma_1+\bar{\Gamma}_1)\,\delta_{0,n}+\big(\Gamma_1-\bar{\Gamma}_1-n\,(2\Gamma_0+\bar{\Gamma}_1)\big)\,P_{n-1}\,(1-\delta_{0,n})+$$

$$+\left\{\left(D-\frac{a+b}{2}\right)\big(\Gamma_1-\bar{\Gamma}_1-n\,(2\Gamma_0+\bar{\Gamma}_1)\big)-(n+1)\,(2\Gamma_0+\bar{\Gamma}_1)(D-\bar{D})\right\}\times$$

$$\times P_n+(2\Gamma_0+\bar{\Gamma}_1)(D-\bar{D})\left(D-\frac{a+b}{2}\right)(n+1)\,P_{n+1}+$$

$$+\sum_{k=1}^{\infty}\left\{\big(\bar{B}_k-(n+1)\,B_k\big)\,P_{n+k}-(D-\bar{D})\,(n+1)\,B_k\,P_{n+k+1}\right\}\Bigg],$$

$$n\geq 0\,, \qquad (14a)$$

$$E_{-n}=\frac{1}{2}\Bigg[\big\{(n-1)\,A_n-\bar{A}_n+(D-\bar{D})\,(n-1)\,A_{n-1}\,(1-\delta_{2,n})\big\}\times$$

$$\times(1-\delta_{1,n})+\sum_{k=0}^{\infty}\big\{\big((n-1)\,B_{n+k}+\bar{B}_{n+k}\big)\,P_k+ \qquad (14b)$$

$$+(D-\bar{D})\,(n-1)\,B_{n+k}\,P_{k+1}\big\}\Bigg], \qquad n\geq 1\,.$$

$\delta_{m,n}$ is usual Kronecker delta. The constants P_n's are known quantities determined from the relation

$$\sum_{0}^{\infty}P_n\,z^n=(z+D-a)^{-1/2}\,(z+D-b)^{-1/2}. \qquad (15)$$

The potentials $\Phi_i(z)$ and Ψi(z) for inclusion are analytic functions for the region $|z|\leq R$, hence can be written as

$$\Phi_i(z)=\sum_{0}^{\infty}G_n\,z^n;\ \Psi_i(z)=\sum_{0}^{\infty}H_n\,z^n. \qquad (16)$$

The subscript i indicates that these functions relate to the inclusion. Boundary conditions

(i) when written in terms of potentials

$$\{\Phi(z),\Psi(z)\}\ \text{ and }\ \{\Phi_i(z),\Psi_i(z)\}\ \text{ give}$$

$$\Phi(Re^{i\theta})+\overline{\Phi(Re^{i\theta})}-Re^{-i\theta}\,\overline{\Phi'(Re^{i\theta})}-e^{-2i\theta}\,\overline{\Psi(Re^{i\theta})}=$$

$$=\Phi_i(Re^{i\theta})+\overline{\Phi_i(Re^{i\theta})}-Re^{-i\theta}\,\overline{\Phi_i'(Re^{i\theta})}-e^{-2i\theta}\,\overline{\Psi_i(Re^{i\theta})}\,,$$

and

$$\frac{\mu_i}{\mu}\left[\varkappa\Phi(Re^{i\theta})-\overline{\Phi(Re^{i\theta})}+Re^{i\theta}\,\overline{\Phi'(Re^{i\theta})}+e^{-2i\theta}\,\overline{\Psi(Re^{i\theta})}\right]= \qquad (17)$$

$$=\varkappa_i\,\Phi_i\,(Re^{i\theta})-\overline{\Phi_i\,(Re^{i\theta})}+Re^{i\theta}\,\overline{\Phi_i'\,(Re^{i\theta})}+e^{-2i\theta}\,\overline{\Psi_i(Re^{i\theta})}.$$

Substituting the values from (12) and (16) into (17) and comparing various powers of $e^{i\theta}$ we get

$$R^n D_n+(n+1) R^{-n} \bar{D}_{-n} - R^{-n-2} \bar{E}_{-n-2} = R^n G_n+\bar{G}_0 \delta_{0,n}, \tag{18a}$$

$$\frac{\mu_i}{\mu} \varkappa R^n D_n - \frac{\mu_i}{\mu}(n+1) R^{-n} \bar{D}_{-n}+ \frac{\mu_i}{\mu} R^{-n-2} \bar{E}_{-n-2} = \varkappa_i R^n G_n - \bar{G}_0 \delta_{0,n} \quad n \geq 0, \tag{18b}$$

$$R^{-n} D_{-n} -(n-1) R^n \bar{D}_n - R^{n-2} \bar{E}_{n-2} = -(n-1) R^n \bar{G}_n - R^{n-2} \bar{H}_{n-2} \times (1-\delta_{1,n}), \tag{19a}$$

$$\frac{\mu_i}{\mu} \varkappa R^{-n} D_{-n} + \frac{\mu_i}{\mu}(n-1) R^n \bar{D}_n + \frac{\mu_i}{\mu} R^{n-2} \bar{E}_{n-2} = (n-1) R^n \bar{G}_n + R^{n-2} \bar{H}_{n-2}(1-\delta_{1,n}), \quad n \geq 1. \tag{19b}$$

When (18) and (19) are solved, the following expressions are obtained

$$G_n = \frac{\frac{\mu_i}{\mu}+1}{\varkappa_i+1} D_n - \frac{\frac{\mu_i}{\mu}-1}{\varkappa_i+1}(n+1) R^{-2n} \bar{D}_{-n}+ \frac{\frac{\mu_i}{\mu}-1}{\varkappa_i+1} R^{-2n-2} \bar{E}_{-n-2}, \tag{20a}$$

$$H_n = E_n - (n+2)^2 R^{-2n-2} \bar{D}_{-n-2}+(n+1) R^{-2n-4} \bar{E}_{-n-4}, \quad n \geq 0 \tag{20b}$$

and

$$D_{-1} = 0, \tag{21a}$$

$$D_{-n} = -\frac{\frac{\mu_i}{\mu}-1}{\frac{\mu_i}{\mu}\varkappa+1}\left[(n-1) R^{2n} \bar{D}_n + R^{2n-2} \bar{E}_{n-2}\right], \quad n \geq 2, \tag{21b}$$

$$E_{-1} = 0 \tag{22a}$$

$$E_{-n-2} = -\frac{\frac{\mu_i}{\mu}(\varkappa-1)-(\varkappa_i-1)}{2\frac{\mu_i}{\mu}+\varkappa_i-1} R^2 (D_0+\bar{D}_0) \delta_{0,n} + \left[-\frac{\frac{\mu_i}{\mu}\varkappa-\varkappa_i}{\frac{\mu_i}{\mu}+\varkappa_i} R^{2n+2} \bar{D}_n + (n+1) R^2 D_{-n}\right](1-\delta_{0,n}), \quad n \geq 0. \tag{22b}$$

By $(13)_2$ and $(21)_2$

$$A_n = -\sum_{k=0}^{\infty} P_k B_{n+k} - 2\frac{\frac{\mu_i}{\mu}-1}{\frac{\mu_i}{\mu}\varkappa+1}\left[(n-1)R^{2n}\bar{D}_n + R^{2n-2}\bar{E}_{n-2}\right], \quad (23)$$

$$n \geq 2$$

The equations (21a) and (22b) are transformed as

$$\sum_{k=0}^{\infty} P_k B_{k+1} = 0, \quad (24)$$

and

$$\sum_{k=0}^{\infty} P_k \bar{B}_{k+1} = 0. \quad (25)$$

Comparing (14b) and (22b)

$$\sum_{k=0}^{\infty}\left[(P_k+\bar{P}_k)\bar{B}_{n+k+2} - (D-\bar{D})(n+1)\left\{P_k B_{n+k+1}(1-\delta_{0,n}) - \right.\right.$$

$$\left.\left. - P_{k+1} B_{n+k+2}\right\}\right] =$$

$$= -2\frac{\frac{\mu_i}{\mu}(\varkappa-1)-(\varkappa_i-1)}{2\frac{\mu_i}{\mu}+\varkappa_i-1} R^2(D_0+\bar{D}_0)\delta_{0,n} - 2\frac{\frac{\mu_i}{\mu}\varkappa-\varkappa_i}{\frac{\mu_i}{\mu}+\varkappa_i} R^{2n+2}\bar{D}_n \times$$

$$\times(1-\delta_{0,n}) - 2\frac{\frac{\mu_i}{\mu}-1}{\frac{\mu_i}{\mu}\varkappa+1}\left[(n^2-1)R^{2n+2}\bar{D}_n + (n+1)R^{2n}\bar{E}_{n-2}\right]\times$$

$$\times(1-\delta_{0,n}-\delta_{1,n}) - 2\frac{\frac{\mu_i}{\mu}-1}{\frac{\mu_i}{\mu}\varkappa+1}\left[(n+1)R^{2n+4}D_{n+2} + R^{2n+2}E_n\right] +$$

$$+ 2\frac{\frac{\mu_i}{\mu}-1}{\frac{\mu_i}{\mu}\varkappa+1}\left[(n+1)^2 R^{2n+4}\bar{D}_{n+2} + (n+1)R^{2n+2}\bar{E}_n\right] +$$

$$+ 2(D-\bar{D})\frac{\frac{\mu_i}{\mu}-1}{\frac{\mu_i}{\mu}\varkappa+1}\left[n(n+1)R^{2n+2}\bar{D}_{n+1} + R^{2n}\bar{E}_{n-1}\right](1-\delta_{0,n}), \quad (26)$$

$$n \geq 0$$

The constants B_n's are determined from the equations (24), (25) and (26) by assigning values to Γ_0, Γ_1, μ_i/μ, $\varkappa$, $\varkappa_i$, D, a, b, R. The values of A_n's are determined from (23) using the values of B_n's determined earlier. Thus the potential $\{\Phi(z), \Psi(z)\}$ are completely known.

The coefficients G_n's and H_n's are determined by (20) with the help of the values of A_n's and B_n's determined previously. Hence $\{\Phi_i(z), \Psi_i(z)\}$ for inclusion is also known. The stress field for matrix and inclusion can now be determined with the help of (1).

5. Some numerical work

The length of the crack is taken as unity from $(-0{,}5, 0)$ to $(0{,}5, 0)$, along x-axis. The centre of the circular inclusion is taken at $(0, -2)$. The radius of circular inclusion is gradually increased from 0,5 to 1,75. As already stated μ_i and μ are the shear moduli of the inclusion and matrix; three cases have

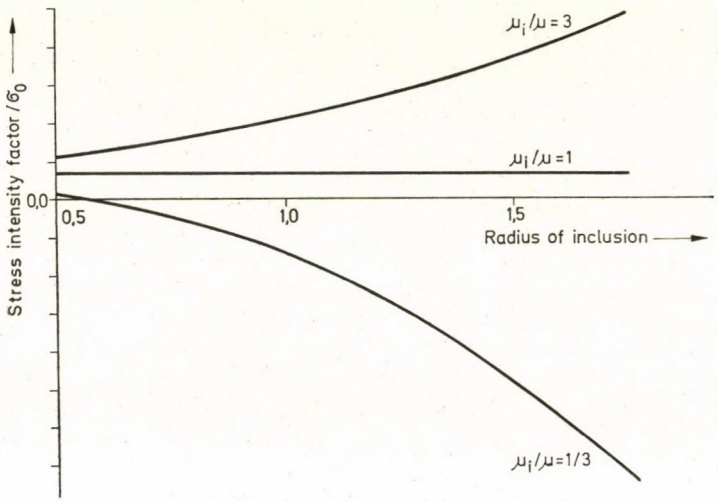

Fig. 2

been considered i.e., when $\mu_i/\mu = 1/3, 1, 3$. The matrix is subjected to a uniform tension σ_0 in the y-direction. The stress intensity factor at the crack tip is calculated. The curves in the graph are drawn for the three ratios of shear moduli (Fig. 2). Along the y-axis, is shown the (stress intensity factor)/σ_0; and along x-axis the radius of inclusion. For a constant length of the crack, it may be seen that as the radius of inclusion increases, the stress intensity factor also increases, as expected. Also when the radius of the inclusion is

small, the stress intensity factor is also small. This is expected, because the circular inclusion is far away from the crack tip. It may be verified from theoretical results given in this paper that when $\mu_i/\mu = 1$, we revert to the case of matrix with a single crack, under tension at infinity. Also when the length of the crack is zero, we get the results of circular inclusion in an infinite plate under tension.

REFERENCES

1. INGLIS, C. E.: *Trans. Instn. Naval Archit.* **55** (1913), 129
2. GRIFFITH, A. A.: *Phil. Trans.* A **221** (1921), 163
3. SNEDDON, I. N.—LOWENGRUB, M. L.: Crack Problems in Classical Theory of Elasticity, John Wiley and Sons, New—York
4. MOTT, N. F.—NABARRO: *Proc. Phys. Soc.* **52** (1940), 90
5. ESHELBY, J. D.: *Proc. Roy. Soc.* Ser. A. **241** (1957), 376
6. JASWON, M. A.—BHARGAVA, R. D.: *Proc. Cambridge-Philos. Soc.* **57** (1961), 669
7. DUNDURS, J.—MURA, T.: *J. Mech. Phys. Solids* **12** (1964), 177
8. WILLIAMS, M. L.: *J. Appl. Mech.* **28** (1961), 78
9. MUSKHELISHVILLI, N. I.: Some Basic Problems of the Mathematical Theory of Elasticity. Noordhoff: Groningen, Holland 1953

Zug einer unendlichen Schreibe, die einen geraden Einschnitt und eine kreisförmige Einbettung besitzt. Ein Verfahren wird entwickelt zur Berechnung der Spannungen und Verschiebungen, die in dem im Titel angegebenen Körper entstehen. Die aus der zweidimensionalen Elastizitätstheorie bekannten Differentialgleichungen bilden den Ausgangspunkt zu den Erörterungen. Funktionen von komplexer Veränderlichen werden benützt. Ein Zahlenbeispiel wird für die Fälle angeführt, wo das Verhältnis der Elastizitätskonstanten der Scheibe und Einbettung 1/3, 1 und 3 ausmacht.

Вытяжка бесконечной по размерам плоской пластины. Авторы описывают метод пригодный для вычисления напряжений и сдвигов в случае формы, указанной в заглавии. Они при своем способе используют тот метод плоскостной теории упругости, который основывается на использовании функций с комплексными переменными. Результаты числового примера на графике показаны для того случая, когда отношение числа упругости включений и плоской пластины равно 1/3, или 1 или 3.

Acta Technica Academiae Scientiarum Hungaricae, Tomus 76 (1—2), pp. 217—241 (1974)

ИТЕРАЦИОННЫЙ МЕТОД ДЛЯ РЕШЕНИЯ КОНТАКТНОЙ ЗАДАЧИ УПРУГИХ СИСТЕМ С ОДНОСТОРОННИМИ СВЯЗАМИ

ИШТВАН ПАЦЕЛЬТ*
КАНД. ТЕХН. НАУК

(Поступило 20 декабря 1971 г.)

В работе предлагается развитие метода В. М. Фридмана и В. С. Черниной для решения контактной задачи упругих систем с односторонними связями, причем предполагается, что между телами отсутствуют трение и сцепление. Этот метод, подобно основному методу, также основан на проверке выполнения условий контакта — отрыва в конечном числе точек. В такой постановке задача сводится к системе алгебраических уравнений — неравенств и к дополнительным уравнениям. Дополнительными уравнениями могут являться статические и кинематические уравнения (например: нулевое значение относительных смещений и углов поворота в точках сопряжения конструкций). Для решения этой системы предлагается циклический итерационный метод, основанный на градиентном методе. Минимизируется квадратичный функционал с ограничением на знак контактного усилия (т. е. они не могут быть отрицательными). Доказано, что существуют единственные решения контактных задач, которые могут быть найдены как предел последовательности, построенной по правилу итерации.

Введение

В настоящее время в практике машиностроения и строительства часто встречаются нонструкции, представляющие собой пластины, балки и оболочки. Эти элементы контактируются друг с другом или лежат на упругом основании.

Решение задачи о контакте упругих тел с произвольной поверхностью при произвольной нагрузке осложняется тем, что область контакта рассматриваемых тел заранее неизвестна. Это существенно затрудняет построение аналитического решения, однако разные приближенные методы — благодаря использованию ЭВМ — позволяют решить некоторые задачи.

Приближенный метод типа В. М. Фридмана—В. С. Черниной [5], [6] позволяет решить контактные задачи, возникающие в обширном классе упругих систем с предположением, что между контактирующими телами отсутствуют трение и сцепление.

При методе [6] относительное жесткое смещение** имеет только жесткое поступательное перемещение c_1, являющееся одной дополнительной величиной.

* Dr. Páczelt I., Győri kapu 37, 3531 Miskolc, Венгрия.

** Под относительным жестким смещением понимается такое перемещение, при котором проникнование одного из контактирующих тел в другое, а именно твердого, сопровождается сопротивлением.

Работа [3] позволяет учитывать между контактирующими телами не только относительное поступательное смещение, но и поворот (например, контакт балки, пластины на упругом основании для любого случая нагрузки). Предполагается, что в ненагруженном состоянии те части контактирующих поверхностей, вдоль которых могут возникать относительные жесткие смещения, являются плоскостями или слабо искривленными поверхностями.

Данная работа занимается дальнейшим развитием вышеуказанных методов [5], [6], [3]. Предполагают, что рассматриваемые системы являются упругими, имеют небольшие перемещения и деформации, а трение и сцепление между контактирующими телами отсутствуют. Таким образом, имеется возможность решить контактную задачу не только (на основе обычной механической схемы) одномерных, двумерных (балка, пластина, оболочка), а таких трехмерных упругих тел, при которых относительное жесткое смещение может быть любым, далее, рассчитать неизолированные системы, построенные из тел, имеющих относительно жесткие смещения (например: балки, пластины, лежащие на одной и той же упругой среде)* или решить такие задачи, в случае которых дополнительными уравнениями являются не обязательно только статические, но и кинематические уравнения, происходящие из построения конструкции (например, в данном месте перемещение, угол поворота равны нулю, или в месте соединения частей конструкции относительное смещение и угол поворота отсутствуют).

Как основной метод, так и этот метод основаны на проверке выполнения условий контакта — отрыва в конечном числе точек. В такой постановке задача сводится к системе алгебраических уравнений — неравенств и дополнительных уравнений. Для решения этой чистемы предлагается циклический итерационный процесс, основанный на градиентном методе. Минимизируется квадратичный функционал с ограничением на знак контактных усилий, т. е. они не могут быть отрицательными. Доказано, что существуют единственные решения всех сводящихся к системам алгебраических уравнений — неравенств (17)—(19) контактных задач, которые могут быть найдены как предел последовательности (37)—(41).

1. Вывод системы основных разрешающих уравнений — неравенств для упругих контактных задач

Возникающие в практике упругие системы очень разнообразны, часто резко отличаются друг от друга. Составить таким образом общую схему трудно и нецелесообразно. В данной работе будет показан принцип составления основной системы алгебраических уравнений — неравенств для нескольких конкретных упругих систем.

* Влияние одной из балок на другую перенесено общим основанием.

1.1. *Задача о контакте балки с упругим слоем, лежащим на жестком основании*

Предполагается, что пространственный стержень соответственно технической теории можно заменить его осью, т. е. задачу можно редуцировать к одномерной; нагрузка располагается в плоскости оси балки и одной из

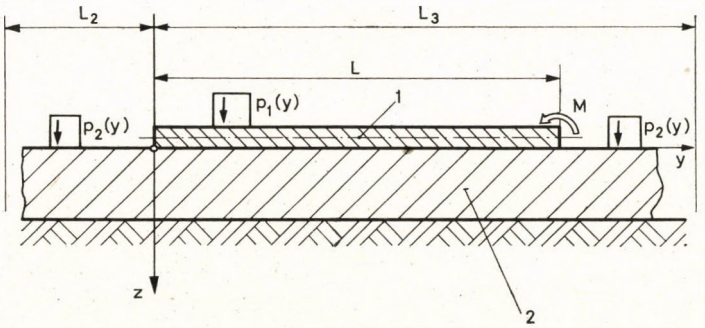

Рис. 1

главных осей поперечного сечения, далее, контактирующие в ненагруженном состоянии поверхности являются плоскостями (по использованной модели соответствующие плоские кривые являются прямыми) (рис. 1). Построим систему координат x, y, z по рис. 1.

Пусть y (или s) обозначает одномерную координату точек, поверхности $z = 0$ тела 2, а также оси балки. Балка перемещается в координатной плоскости yz. Степень свободы балки, как жесткого тела, $\lambda_{\max} = 2$.

Пусть $0 \leq y \leq L$ будет область Ω, а $-L_2 \leq y \leq 0$, $L \leq y \leq L_3 - \Omega_2$.

Приложим теперь к балке нагрузку

$$p_1(y) \qquad y \in \Omega,$$

а к упругому слою нагрузку

$$p_2(y) \qquad y \in \Omega_2.$$

Вследствие этого между балкой и верхней границей упругого основания возникнут перпендикулярные к границе контактные усилия (трением пренебрегаем).

Прогиб по направлению оси z будем считать положительным.

Введя следующие обозначения:
$w^2(y)$ — вертикальное перемещение края $z = 0$ упругого основания,
$w^1(y)$ — вертикальное перемещение (прогиб) оси балки с жестким на левом краю защемлением,

$q(y)$ — контактное давление (кг/см),
c_1 — вертикальное перемещение балки в точке $y = 0$,
c_2 — угол поворота балки, как твердого тела вокруг оси x,
$d(y)$ — перемещение, возникающее из-за движеня балки, как твердого тела,
Ω_0 — область отрыва, зазора,
Ω_Q — область контакта,

условия отрыва — контакта можно записать в следующем виде (рис. 2)*:
если

$$w^2(y) - w^1(y) - d(y) > 0, \quad \text{то} \quad q(y) = 0, \quad y \in \Omega_0 \tag{1}$$

и если

$$w^2(y) - w^1(y) - d(y) = 0, \quad \text{то} \quad q(y) \geq 0, \quad y \in \Omega_Q \tag{2}$$

где

$$d(y) = c_1 + c_2 y; \quad \Omega = \Omega_0 + \Omega_Q \tag{3)-(4}$$

и области Ω_0, Ω_Q заранее неизвестны.

Введем функцию влияния $K^1(y, s)$ для прогиба точки координатой y оси балки от единичной нагрузки, действующей в точке координатой s (балка на левом краю жестко защемлена), а также подобно определенную функцию влияния $K^2(y, s)$ для края $z = 0$ тела 2. Далее, обозначим через

$f^1(y)$ — вертикальное перемещение от известной нагрузки, действующей на защемленную левом конце балку,
$f^2(y)$ — перемещение вдоль оси z края тела 2 от нагрузки $p_2(y)$

В этом случае вертикальные перемещения будут (рис. 2а, б)

$$w^1(y) = -\int_{(\Omega)} K^1(y, s)\, q(s)\, ds + f^1(y), \tag{5}$$

$$w^2(y) = \int_{(\Omega)} K^2(y, s)\, q(s)\, ds + f^2(y). \tag{6}$$

Введя обозначения

$$K(y, s) = K^1(y, s) + K^2(y, s), \qquad f(y) = f^1(y) - f^2(y) \tag{7}$$

по (1) и (2) получим**

$$\int_{(\Omega)} K(y, s)\, q(s)\, ds - d(y) - f(y) > 0, \qquad q(y) = 0, \quad y \in \Omega_0, \tag{8}$$

$$\int_{(\Omega)} K(y, s)\, q(s)\, ds - d(y) - f(y) = 0, \qquad q(y) \geqslant 0, \quad y \in \Omega_Q \tag{9}$$

* Здесь и в дальнейшем цифрой, стоящей около букв вверху и внизу, подразумевается индекс. Наличие скобки указывает на возведение в степень, например: $(c_1)^2$.

** Здесь используем предположение о малости перемещения, т. е. $w^1(y) \cdot \cos c_2 \cong w^1(y)$

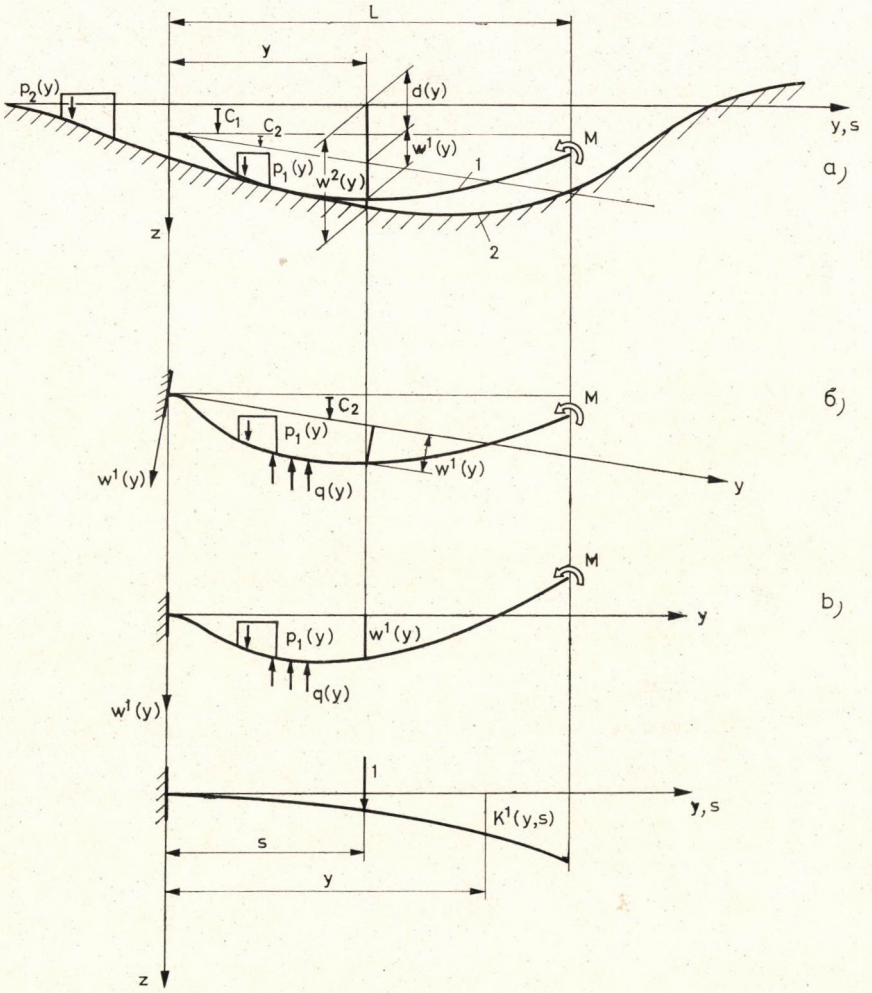

Рис. 2

В данной задаче дополнительными уравнениями являются записанные для тела 1 уравнения статики, т. е.

$$F^1 - \int_{(\Omega)} q(s)\, ds = 0 \tag{10}$$

$$M_x^1 - \int_{(\Omega)} q(s) \cdot s \cdot ds = 0\ , \tag{11}$$

где

$$\vec{\mathbf{F}}^1 = F^1\, \vec{\mathbf{k}}\,, \qquad \vec{q}(s) = -\, q(s)\vec{\mathbf{k}}$$

$$\vec{\mathbf{M}}_0^1 = M^1\, \vec{\mathbf{i}}\,, \qquad q(s) \geq 0$$

$[\vec{F}^1, \vec{M}_x^1]$ — дуальный вектор, вычисленный относительно начала системы координат. Его составляющими являются главный вектор и момент от известной нагрузки, действующей на тело 1.

Таким образом, контактная задача сводится к интегральному уравнению — неравенству первого рода (8)—(9) и дополнительным уравнениям (10)—(11) для определения неизвестных контактных усилий с интенсивностью $q(s)$ и компонентов относительного жесткого смещения c_1, c_2, причем области Ω_0 и Ω_Q заранее неизвестны.

Полученное интегральное уравнение — неравенство приближенно заменим системой алгебрических уравнений — неравенств. Для этого разобьем область Ω на k участков длинной Δs. В пределах каждого малого участка выберем точку с координатой s_j $j = 1, \ldots, k$ или на другом участке независимо от нее, точку с координатой y_i $i = 1, \ldots, k$, причем $y_i = s_i$. Распределенное усилие $q(s)$ заменим усилием $Q_j = q(s_j) \cdot \Delta s(s_j)$, далее $K(y,s)$, $f(y)$, $d(y)$ определим* во внутренней точке рассматриваемого малого участка, т. е.

$$\begin{aligned} \alpha_{ij} &= K(y_i, s_j), \quad f_i = f(y_i), \\ d(y_i) &= d_i = c_1 + c_2 \cdot y_i. \end{aligned} \tag{12}$$

Тогда получим следующую систему алгебраических уравнений — неравенств для некоторых значений индекса i

$$\sum_{j=1}^{k} \alpha_{ij} \cdot Q_j - d_i - f_i > 0; \quad Q_i = 0 \quad i \in \Omega_0 \tag{13}$$

и для остальных значений индекса i

$$\sum_{j=1}^{k} \alpha_{ij} \cdot Q_j - d_i - f_i = 0; \quad Q_i \geq 0, \quad i \in \Omega_Q \tag{14}$$

и сверх этого, уравнения статики 1-ого тела (дополнительные условия)

$$F^1 - \sum_{j=1}^{k} Q_j = 0; \quad M_x^1 - \sum_{j=1}^{k} y_j \cdot Q_j = 0. \tag{15}$$

Здесь заранее неизвестны номера i, при которых удовлетворяется условие зазора (отрыва) (13), или условия контакта (14).

Если ввести вектор неизвестных

$$\mathbf{x}^T = [Q_1, \ldots, Q_k, c_1, c_2]$$

* В тех случаях, когда при построении функций влияния под силой перемещение имеет бесконечное значение, сосредоточенную силу необходимо заменить распределяющейся по малой поверхности нагрузкой, являющейся статически эквивалентной единичному усилию.

Если имеется упругое основание типа Винклера ($w_i^2 = \alpha_{ii}^2 \cdot Q_i$, $\alpha_{ij}^2 = 0$ если $i \neq j$) и $d(y) = 0$, то вместо интегрального уравнения первого рода получается уравнение второго рода. Тогда оценку для приближения можно дать по методу Л. В. Канторовича [2].

(T — знак транспонирования)
и вектор известных величин

$$\mathbf{e}^T = [f_1, \ldots, f_k, -F^1 - M_x^1],$$

то систему (13)—(15) можно переписать в следующую матричную форму

		k	$k+1$	$k+2$					
	$[\alpha_{ij}]$	-1 $\vdots$ -1 $\vdots$ -1	$-y_1$ $\vdots$ $-y_i$ $\vdots$ $-y_k$	Q_1 $\vdots$ Q_i $\vdots$ Q_k	$-$	f_1 $\vdots$ f_i $\vdots$ f_k	$\geq$	0
k	$-1 \ . \ . \ -1 \ . \ . \ -1$	0	0	c_1		$-F^1$		
$k+1$							$=$	0
$k+2$	$-y_1 \ . \ . \ -y_j \ . \ . \ -y_k$	0	0	c_2		$-M_x^1$		

Итак, контактная задача сведена к решению матричного уравнения — неравенства

$$\mathbf{Ax} - \mathbf{e} \begin{cases} > 0 & Q_i = 0 & i \in \Omega_0 \\ = 0 & Q_i \geqq 0 & i \in \Omega_Q \\ = 0 & & i = k+\lambda, \ \lambda = 1,2 \\ & & c_\lambda \gtreqless 0 \end{cases} \tag{16}$$

причём области Ω_0 и Ω_Q заранее неизвестны.

1,2 Модифицированная задача о контакте балки с упругим слоем

Изображенная на рис. 3 задача отличается от изображенной на рис. 1 только тем, что в точке y_r есть заделка, обеспечивающая нулевое перемещение , т. е. $w(y_r) = 0$. Для того, чтобы использовать заранее введенные

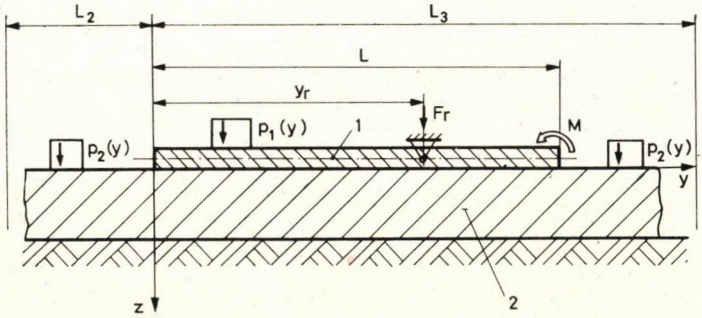

Рис. 3

величины, функции влияния α_{ij}^1 и перемещение f_i^1 будут определены для защемленной на левом конце балки. Итак, новым неизвестным является опорное усилие $F_r \gtrless 0$, и кроме уравнений статики, кинематическое уравнение

$$w^2(y_r) - w^1(y_r) - d(y_r) = 0$$

также является дополнительным уравнением. Здесь

$$d(y_i) = c_1 + c_2 \cdot y_i + F_r \cdot \alpha_{ir}^1,$$

В уравнении — неравенстве (16) матрица **A** имеет размер $(k+3) \cdot (k+3)$.

1.3 Задача о контакте цилиндрического резервуара с упругим основанием

Тонкостенные конструкции обычно построены из разных элементов. Трактовка контактной зачади этих систем возможна и так, что функции влияния α_{ij}^p и перемещения f_j^p будут определены для несопряженной системы, а только для отдельных частей конструкции. Таким образом, предварительное определение неизвестных внутренних усилий в точках сопряжения (например, в случае оболочек усилия и моменты) упускается столько раз, сколько имеется предполагаемых контактных точек. Вычисление внутренних усилий производится одновременно с определением контактных усилий. В этом случае дополнительными уравнениями, относящимися к вышесказанному, являются кинематические уравнения (например, в точке сопряжения частей конструкции относительное смещение и угол поворота имеют нулевые значения). Ниже для демонстрации сказанного будет показан простой пример.

Пусть цифры 1,2,3, обозначают соответственно цилиндрическую оболочку, плоское донышко и упругую среду (рис. 4). Нагрузка и деформация считаются осесимметричными.

Итак, неизвестными будут усилие Q_0 и момент M_0 в точке сопряжения цилиндрической оболочки с плоским донышком, контактные усилия Q_j $j = 1, \ldots, k$, возникающие между телами 1 и 3, а также 2 и 3, и далее, смещение c_1 тел 1 и 2, как твердых тел, вдоль оси z.

Для определения неизвестных кроме контактных усилий Q_0, M_0, c_1 в качестве дополнительного уравнения используем равенство перемещения цилиндрической оболочки $w^1 = w^1(z = L)$ перемещению плоского донышка $u^2 = u^2(r = R)$ в направления вектора $\vec{\mathbf{e}}_R$ и равенство углов поворота ϑ^1 и ϑ^2 в точке сопряжения 1-ого тела с 2-ым, далее уравнение статики, выражающее равновесие тела 2 вдоль оси z.

Положительное направление нормальных для отдельных тел перемещений w_i^p $p = 1,2,3$ показано на рис. 4 в. Если предположить, что удовлетворение условий отрыва — контакта будет проверено между телами 1 и 3 в

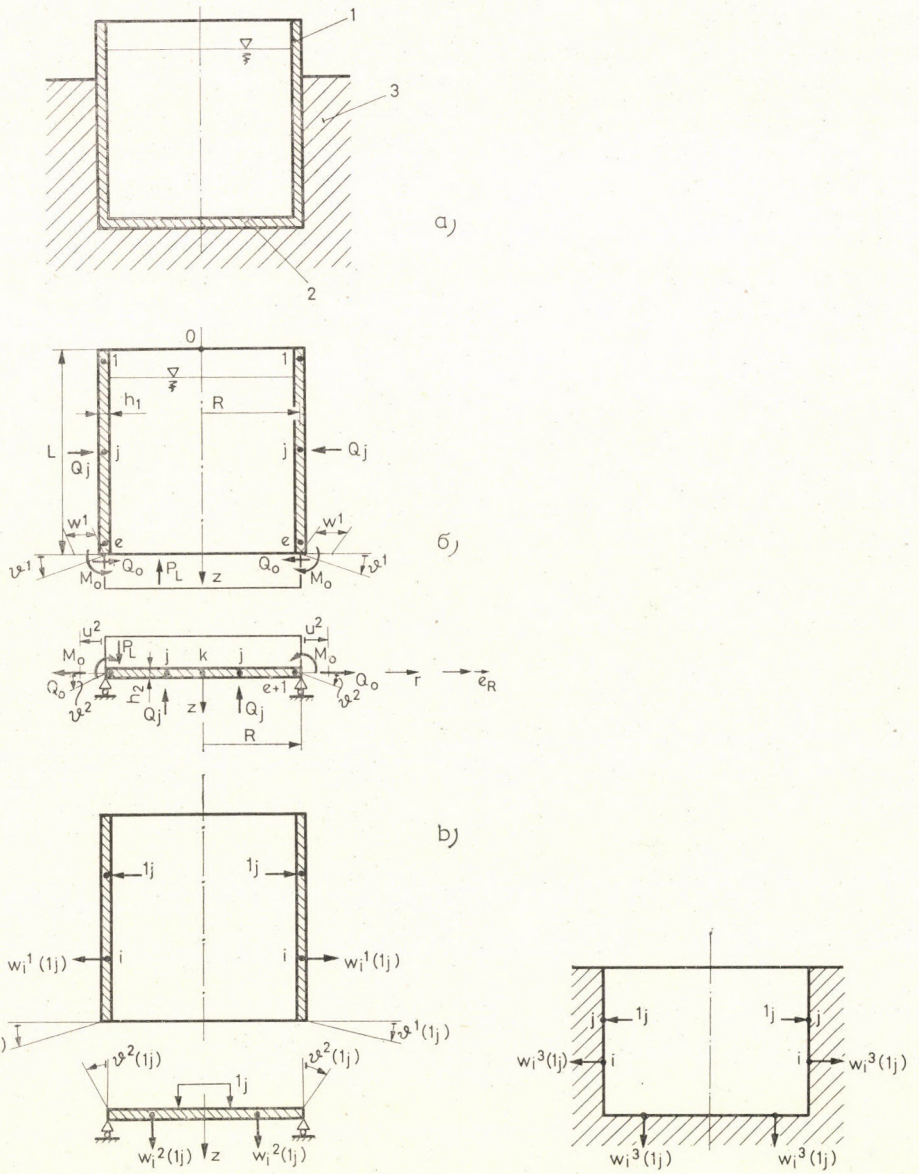

Рис.

точках $i \in \Omega^1 (i = 1, \ldots, e)$, а между телами 2 и 3 в точках $i \in \Omega^2 (i = e + 1, \ldots, k)$, то решение контактной задачи можно получить по матричному уравнению — неравенству $\mathbf{Ax} - \mathbf{e} \geq \mathbf{0}$, полученному из следующих уравнений — неравенств:

если

$$w_i^3 - w_i^1 > 0\,, \qquad \text{то} \qquad Q_i = 0 \qquad i \in \Omega_0^1\,,$$

$$
\begin{aligned}
&w_i^3 - w_i^1 = 0\,, && \text{то} && Q_i \geqq 0 && i \in \Omega_Q^1,\\
&w_i^3 - w_i^2 - d_i > 0, && \text{то} && Q_i = 0 && i \in \Omega_0^2,\\
&w_i^3 - w_i^2 - d_i = 0, && \text{то} && Q_i \geqq 0 && i \in \Omega_Q^2,\\
&\vartheta^1 - \vartheta^2 = 0\,, && && M_0 \gtreqless 0\,,\\
&w^1 - u^2 = 0\,, && && Q_0 \gtreqless 0\,,\\
&-\sum_{j=e+1}^{k} Q_j + F = 0\,, && && c_1 \gtreqless 0\,,
\end{aligned}
$$

где $d_i = c_1$, $\vec{\mathbf{F}} = F\vec{\mathbf{k}}$ собственные вес + вес содержания резервуара,

$$\Omega^1 = \Omega_0^1 + \Omega_Q^1\,, \qquad \Omega^2 = \Omega_0^2 + \Omega_Q^2\,.$$

1.4. *Матричное уравнение — неравенство* $\mathbf{Ax} - \mathbf{e} \geqq \mathbf{0}$, *являющееся основной системой для контактной задачи*

Подобно как и изложенные в пунктах 1.2 и 1.3 примеры, множество задач сводится к такой системе уравнений — неравенств как (13)—(15).

Основная система задач такого типа может быть записана в следующем виде: если

$$\sum_{j=1}^{k} \alpha_{ij} \cdot Q_j - d_i - f_i > 0\,, \qquad \text{то} \qquad Q_i = 0 \quad i \in \Omega_0 \tag{17}$$

и если

$$\sum_{j=1}^{k} \alpha_{ij} \cdot Q_j - d_i - f_i = 0\,, \qquad \text{то} \qquad Q_i \geqq 0 \quad i \in \Omega_Q \tag{18}$$

$$\Omega = \Omega_0 + \Omega_Q\,, \qquad i = 1, \ldots, k$$

и дополнительные уравнения

$$H_p = H_p(\Omega, [\vec{\mathbf{F}}^t, \vec{\mathbf{M}}_0^t],\ Q_1, \ldots, Q_k, c_1, \ldots, c_l) = 0 \tag{19}$$

$$p = 1, \ldots, l, \quad t \leq l.$$

Здесь $[\vec{\mathbf{F}}^t, \vec{\mathbf{M}}_0^t]$ — дуальный вектор, определяющийся известной нагрузкой, действующей на тело-t. Его составляющими являются главный вектор и момент, вычисленный относительно начала системы координат.

$c_1, \ldots, c_l$ — неизвестные кроме контактных усилий (компоненты вектора относительного жесткого смещения, внутренние усилия в точке сопряжения частей конструкции и. т. д. (связь является двухсторонней),

d_i — дополнительное смещение, значение которого зависит от $c_1, \ldots, c_l$.

(Остальные обозначения совпадают с введенными ранее обозначениями.) Если ввести вектор неизвестных*

* 1. $F_\lambda, \lambda = 1, \ldots, l$ — известные члены в дополнительных уравнениях

2. $d_i = -\sum_{\lambda=1}^{k} \alpha_{i,k+\lambda} \cdot c_\lambda$

$$\mathbf{x}^T = [Q_1, \ldots, Q_k, c_1, \ldots, c_l] \tag{20}$$

и вектор известных величин

$$\mathbf{e}^T = [f_1, \ldots, f_k, F_1, \ldots, F_l], \tag{21}$$

то контактная задача в широком классе упругих систем с односторонними связями сводится к решению следующего матричного уравнения — неравенства с ограничением на знак усилия

$$\begin{array}{c|c|c|c|c|c|c} & 1 & & k & k+l & & \\ 1 & & & \alpha_{1,k+\lambda}\cdots & \begin{matrix} Q_1 \\ \vdots \\ Q_i \\ \vdots \\ Q_k \end{matrix} & - & \begin{matrix} f_1 \\ \vdots \\ f_i \\ \vdots \\ f_k \end{matrix} \quad \geq \quad 0 \\ & & [\alpha_{ij}] & \alpha_{i,k+\lambda}\cdots & & & \\ & & & \alpha_{k,k+\lambda}\cdots & & & \\ k & & & \vdots & \begin{matrix} c_1 \\ c_\lambda \\ c_l \end{matrix} & & \begin{matrix} F_1 \\ F_\lambda \\ F_l \end{matrix} \quad = \quad 0 \\ k+l & \alpha_{k+p,1}\ldots\alpha_{k+p,j}\ldots\alpha_{k+p,k} & & \ldots\alpha_{k+p,k+\lambda} & & & \end{array} \tag{22}$$

т. е.

$$\mathbf{Ax} - \mathbf{e} \begin{cases} > 0 & Q_i = 0 & i \in \Omega_0 \qquad i = 1, \ldots, k \\ = 0 & Q_i \geq 0 & i \in \Omega_Q \\ = 0 & & i = k+\lambda, \lambda = 1, \ldots, l \\ & & c_\lambda \gtreqless 0 \end{cases} \tag{23}$$

где матрица $\mathbf{A}$ имеет размер $(k + l)$ $(k + l)$, при строках $i = 1, \ldots, k$ заранее неизвестны условия отрыва (неравенства) и условия контакта (равенства); при строках $i = k + 1, \ldots, k + l$ в силу уравнения (19) имеется только равенство.

2. Решение матричного уравнения — неравенства $\mathbf{Ax} - \mathbf{e} \geq 0$ с помощью циклического итерационного процесса, основонного на градиентном методе

2.1. *Введение квадратичного функционала*

Решение системы алгебраических уравнений — неравенств (17)—(19), или в более сжатом виде (22) — (23) можно найти следующим образом:

$$Q_i = \bar{Q}_i + \sum_{\lambda=1}^{l} c_\lambda \cdot Q^*_{\lambda,i} \qquad i = 1, \ldots, k \tag{24}$$

где $Q^*_{\lambda,i}$ есть решение приведенной ниже системы алгебраических уравнений:

$$\sum_{j=1}^{k} \alpha_{ij} \cdot Q^*_{\lambda,j} + \alpha_{i,k+\lambda} = 0 \qquad i = 1, \ldots, k, \lambda = 1, \ldots, l. \tag{25}$$

Подставляя (24) в (17)—(19) или в (22)—(23) и, далее, учитывая, что

$$-d_i = \sum_{\lambda=1}^{l} \alpha_{i,k+\lambda} \cdot c_\lambda$$

получим, с одной стороны,

$$\begin{aligned} &\sum_{j=1}^{k} \bar{\alpha}_{ij} \cdot \bar{Q}_j - \bar{f}_i > 0, \quad Q_i = 0, i \ni \Omega_0 \\ &\sum_{j=1}^{k} \bar{\alpha}_{ij} \cdot \bar{Q}_j - \bar{f}_i = 0, \quad Q_i \geq 0, i \ni \Omega_Q \end{aligned} \tag{26}$$

где

$$\bar{\alpha}_{ij} = \alpha_{ij}, / \alpha_{ii}\,, \quad \bar{f}_i = f_i / \alpha_{ii}\,,$$

а с другой

$$H_p = \sum_{j=1}^{k} \alpha_{k+p,j} \cdot \left(\bar{Q}_j + \sum_{\lambda=1}^{l} c_\lambda \cdot Q^*_{\lambda,j} \right) + \sum_{\lambda=1}^{l} \alpha_{k+p,k+\lambda} \cdot c_\lambda - F_p = 0\,, \qquad p = 1\,, \text{-...}, l. \tag{27}$$

Введем по [5]* квадратичный функционал от переменных

$$\bar{Q}_j, j = 1, \ldots, k \quad \text{и} \quad c_\lambda \quad \lambda = 1, \ldots, l:$$

$$G(\bar{Q}, C) = \frac{1}{2} \sum_{i=1}^{k} (\bar{Q}_i - \tilde{Q}_i) \cdot \left(\sum_{j=1}^{k} \bar{\alpha}_{ij} \bar{Q}_j - \bar{f}_i \right) + \sum_{p=1}^{l} \gamma_p (H_p)^2 \geq 0, \tag{28}$$

где $\bar{Q}_i$ есть решение системы алгебраических уравнений

$$\sum_{j=1}^{k} \bar{\alpha}_{ij} \bar{Q}_i - \bar{f}_i = 0\,, \quad i = 1, \ldots, k,$$

Значение выражения $H_p = H_p(\bar{Q}, C)$; $p = 1, \ldots, l$ можно вычислить по формуле (27) (оно в начале расчета имеет не нулевое значение), γ_p положитель-

* В этой пункте используем обозначения функционального анализа (см. например [1]). Q и C есть векторы $Q = (Q_1, \ldots, Q_i, \ldots, Q_k)$; $C = (c_1, \ldots, c_\lambda, \ldots, c_l)$.
В работе [5] в выражении $G(Q)$ член

$$\frac{1}{2} \sum_{p=1}^{l} \gamma_p (H_p)^2$$

отсутствует, так как там рассматриваются такие контактные задачи, где дополнительных уравнений нет. Из упругих систем следует, что матрица $[\alpha_{ij}]$ положительно определена.

ное число ($p = 1, \ldots, l$). Размерность γ_p изменяется с размерностью H_p. Чтобы вычислительная программа стала более универсальной, стоит в дальнейшем придерживаться констант γ_p.

2.2. *Использование градиентного метода для минимализации функционала* $G(\bar{Q}, C)$

Для определения неизвестных c_λ и $Q_i = Q_i(\tilde{Q}_i, c_\lambda, Q^*_{\lambda,i})$ строится циклический итерационный процесс, основанный на градиентном методе. Минимизируется квадратичный функционал (28) с ограничением на знак $Q_i \geq 0$

Итерационный процесс сгруппирован в циклы и состоит из последовательных приближений (шагов).

В некотором этапе обозначим через

s — номер цикла,
n — номер приближения.

Под n -ым приближением определенного по (20) искомого решения x системы уравнения — неравенства (23) подразумевается

$$x^n = (Q_1^n, \ldots, Q_k^n, c_1^n, \ldots, c_l^n) = (Q^n, C^n),$$

где

$$\begin{aligned} Q_i^n &= \bar{Q}_i^n + \sum_{\lambda=1}^{l} c_\lambda^n \cdot Q^*_{\lambda,i}, \quad i = 1, \ldots, k, \\ \bar{Q}^n &= (\bar{Q}_1^n, \ldots, \bar{Q}_k^n). \end{aligned} \tag{29}$$

Один цикл состоит из

k числа приближений типа a,
l числа приближений типа $б$,

т. е. всего $k + l$ шагов.

Под n подразумевается порядковый номер приближения. Если $n_* = (s-1) \cdot (k + l)$, то в s-ом цикле при приближениях типа a имеем $n_* < n \leq n_* + k$, а при приближениях типа $б$ имеем $n_* + k < n \leq n_* + k + l$.

Пусть при $(n + 1)$-ом приближении типа a $(n_* \leq n \leq n_* + k - 1)$:

$$\begin{aligned} &c_\lambda^{n+1} = c_\lambda^n, \lambda = 1, \ldots, l, \\ &Q_i^{n+1} = Q_i^n \quad \text{и} \quad \bar{Q}_i^{n+1} = \bar{Q}_i^n \quad \text{при} \quad i \neq n - n_* + 1, \end{aligned}$$

и

$$\bar{Q}_i^{n+1} = \bar{Q}_i^n + \varepsilon_i^n \left.\frac{\partial G}{\partial \bar{Q}_i}\right|_{\bar{Q}=\bar{Q}^n} \quad \text{при} \quad i = n - n_* + 1 \tag{30}$$

т. е. учитывая также (29)

$$Q_i^{n+1} = \bar{Q}_i^{n+1} + \sum_{\lambda=1}^{l} c_\lambda^{n+1} \cdot Q^*_{\lambda,i} = Q_i^n + \varepsilon_i^n \left.\frac{\partial G}{\partial \bar{Q}_i}\right|_{\bar{Q}=\bar{Q}^n} \quad \text{при} \quad i = n - n_* + 1, \tag{31}$$

далее при $(n+1)$-ом приближении типа *б*

$$
\begin{aligned}
&(n_*+k \leq n \leq n_*+k+l-1):\\
&c_\lambda^{n+1} = c_\lambda^n \quad \text{при} \quad \lambda \neq n-(n_*+k)+1\\
&c_\lambda^{n+1} = c_\lambda^n + \vartheta_\lambda^n \left.\frac{\partial G}{\partial c_\lambda}\right|_{C=C^n} \Bigg\} \text{ при } \lambda = n-(n_*+k)+1,\\
&\bar{Q}_i^{n+1} = \bar{Q}_i^n \;\; i=1,\ldots,k \Bigg\}
\end{aligned}
\tag{32}
$$

т. е. учитывая также (29) и (32)

$$
Q_i^{n+1} = \bar{Q}_i^{n+1} + \sum_{\lambda=1}^{l} c_\lambda^{n+1} \cdot Q_{\lambda,i}^* = Q_i^n + \vartheta_\lambda^n \left.\frac{\partial G}{\partial c_\lambda}\right|_{C=C^n} \cdot Q_{\lambda,i}^*,
\tag{33}
$$

$$
i=1,\ldots,\; k,\; \lambda = n-(n_*+k)+1.
$$

Производные функционала $G = G(Q, C)$, которые имеются в выражениях (30), (31) и (32), можно вычислить с помощью выражений (24), (25) и (27):

$$
\left.\frac{\partial G}{\partial \bar{Q}_i}\right|_{\bar{Q}=\bar{Q}^n} = \Delta_i^n + \bar{\Delta}_i^n
\tag{34}
$$

и

$$
\left.\frac{\partial G}{\partial c_\lambda}\right|_{C=C^n} = \Delta_\lambda^n,
$$

где величины Δ_i^n, $\bar{\Delta}_i^n$ и $\Delta_\lambda^n \equiv \Delta_{\lambda,s}^n$ находятся в выражениях (69).

Введя обозначения

$$
\bar{X} = (\bar{X}_1, \ldots, \bar{X}_k, \bar{X}_{k+1}, \ldots, \bar{X}_{k+l}) = (\bar{Q}, C) = (\bar{Q}_1, \ldots, \bar{Q}_k, c_1, \ldots, c_l),
$$

значения коэффициентов ε_i^n, ϑ_λ^n, имеющиеся в формулах (31)—(32), определяются по тому условию, что квадратичный функционал

$$
\begin{aligned}
G(\bar{X}^{n+1}) = G(\bar{X}^n) + \sum_{u=1}^{k+l} \left.\frac{\partial G}{\partial \bar{X}_u}\right|_{\bar{X}^n} \cdot (\bar{X}_u^{n+1} - \bar{X}_u^n) +\\
+ \frac{1}{2} \sum_{u=1}^{k+l} \sum_{v=1}^{k+l} \left.\frac{\partial^2 G}{\partial \bar{X}_u \partial \bar{X}_v}\right|_{\bar{X}^n} \cdot (\bar{X}_u^{n+1} - \bar{X}_u^n) \cdot (\bar{X}_v^{n+1} - \bar{X}_v^n)
\end{aligned}
\tag{35a}
$$

должен иметь минимальное значение, т. е.

$$
\frac{\partial G(\bar{X}^{n+1})}{\partial \varepsilon_i^n} = 0 \quad i=1,\ldots,k,
$$

$$
\frac{\partial G(\bar{X}^{n+1})}{\partial \vartheta_\lambda^n} = 0 \quad \lambda = 1,\ldots,l.
$$

На основе вычислений, детально приведенных ниже, независимо от порядкового номера приближения имеем:

при приближениях типа a $\varepsilon_i^n = \varepsilon_i \quad i = 1, \ldots, k,$
при приближениях типа $б$ $\vartheta_\lambda^n = \vartheta_\lambda \quad \lambda = 1, \ldots, l,$

(Величины ε_i, ϑ_λ находятся в выражениях (67).)
Действительно, принимая во внимание выражения (34), (69), (27) и третье уравнение (67), можно записать следующие зависимости

$$\left.\frac{\partial^2 G}{\partial \bar{Q}_i \partial \bar{Q}_i}\right|_{\bar{x}^n} = \frac{\partial}{\partial \bar{Q}_i}(\Delta_i + \bar{\Delta}_i)|_{\bar{x}^n} = 1 + \sum_{p=1}^{l} \gamma_p \cdot (\alpha_{k+p,i})^2,$$

$$\left.\frac{\partial^2 G}{\partial c_\lambda \partial c_\lambda}\right|_{\bar{x}^n} = \frac{\partial}{\partial c_\lambda}(\Delta_\lambda)|_{\bar{x}^n} = \sum_{p=1}^{l} \gamma_p \cdot (\Theta_{p,\lambda})^2,$$

и далее из соотношения (35-а) с учетом также (30), при приближениях типа a следует

$$G(\bar{X}^{n+1}) = G(\bar{X}^n) + \varepsilon_i^n \cdot (\Delta_i^n + \bar{\Delta}_i^n)^2 + \\ + \frac{1}{2}\left[1 + \sum_{p=1}^{l} \gamma_p \cdot (\alpha_{k+p,i})^2\right] \cdot (\varepsilon_i^n)^2 \cdot (\Delta_i^n + \bar{\Delta}_i^n)^2;$$

а при приближениях типа $б$, учитывая и выражение (32)

$$G(\bar{X}^{n+1}) = G(\bar{X}^n) + \vartheta_\lambda^n \cdot (\Delta_{\lambda,s}^n)^2 + \\ + \frac{1}{2}\left[\sum_{p=1}^{l} \gamma_p (\Theta_{p,\lambda})^2\right] \cdot (\vartheta_\lambda^n)^2 \cdot (\Delta_{\lambda,s}^n)^2,$$

откуда правильность нашего утверждения сразу же оказывается доказанной.

Подытоживая все сказанное выше, можно определить: в каждом цикле, при выполнении k приближений типа a при зафиксированном значении c_λ^n изменяются одно за другим усилия Q_i^n, определенные в конце предыдущего цикла, т. е. согласно выражениям (31) и (34) имеет место следующее правило

$$Q_i^{n+1} = Q_i^n + \varepsilon_i \cdot (\Delta_i^n + \bar{\Delta}_i^n) = Q_i^n - \bar{\delta}_i^n, \qquad (36)$$
$$i = 1, \ldots, k, \quad n = n_* + i - 1,$$

и далее при l приближениях типа $б$ изменяются одно за другим определенные в конце предыдущего цикла значения c_λ^n по правилу, полученному на основе выражений (32), (33) и (34):

$$c_\lambda^{n+1} = c_\lambda^n + \vartheta_\lambda \cdot \Delta_\lambda^n = c_\lambda^n + \beta_\lambda^n \qquad (37a)$$
$$\lambda = 1, \ldots, l, \quad n = n_* + k - 1 + \lambda$$

и вместе с тем, исходя из полученных в конце приближений типа *а* усилий Q_i^{n*+k}, все контактные усилия Q_i^n:

$$Q_i^{n+1} = Q_i^n + \vartheta_\lambda \cdot \Delta_{\lambda,}^n \cdot Q_{\lambda,i}^* = Q_i^n + \beta_\lambda^n \cdot Q_{\lambda,i}^* \qquad (37б)$$
$$i = 1, \ldots, k, \lambda = n - (n_* + k) + 1$$

(При приближениях типа *б* усилия $\bar{Q}_i$ не изменяются!)

Принимая во внимание, что величины c_λ^n изменяются только при приближениях типа *б*, а именно в рамках одного цикла только один раз, вместо уравнений (37а—б) можно записать

$$c_{\lambda,s+1} = c_{\lambda,s} + \beta_{\lambda,s}^n \qquad (37в)$$

$$Q_i^{n+1} = Q_i^n + \beta_{\lambda,s}^n \cdot Q_{\lambda,i}^* \qquad \lambda = 1, \ldots, l, \qquad (37г)$$

$$\beta_{\lambda,s}^n = \vartheta_\lambda \cdot \Delta_{\lambda,s}^n = \beta_\lambda^n, \qquad n = n_* + k + \lambda - 1,$$
$$i = 1, \ldots, k$$

где $c_{\lambda,s+1}$, $c_{\lambda,s}$ соответственно получены в s-ом и $(s-1)$-ом циклах ($\Delta_{\lambda,s}^n$, $\beta_{\lambda,s}^n$ см. (69)). Если еще учесть, что величины $\bar{Q}_i^n$ не изменяются при приближениях типа *б*, то условие (35а) можно записать в виде*

— при приближениях типа *а*

$$G(\bar{Q}^{n+1}, C_s) = \min, \qquad n = n_* + i - 1, \qquad i = 1, \ldots, k, \qquad (35б)$$

— при шагах типа *б*

$$G(\bar{Q}^{n'}, c_\lambda^{n+1}) = \min, \quad n' = n_* + k, \quad n = n_* + k + \lambda - 1, \quad \lambda = 1, \ldots, l. \qquad (35в)$$

Минимизирующая последовательность (36), (37) для функционала (28) все же не дает правильного решения контактной задачи, так как найденные в ходе вычислений усилия могут быть отрицательными. Поэтому при каждом шаге итерационного процесса надо учитывать ограничения, налагаемые на решение задачи о контакте с отрывом $Q_i \geq 0$.

Для этого выберем

$$Q_i^0 \geq 0, \qquad i = 1, \ldots, k \qquad (38)$$

и поскольку $Q_i^n - \bar{\delta}_i^n \geq 0$, то вычисляем Q_i^{n+1} по формуле (36) или же предполагаем $Q_i^{n+1} = 0$, если окажется, что $Q_i^n - \bar{\delta}_i^n \leq 0$. Таким образом, уже на каждом шагу итерации (приближении типа *а*) не реализуется условие $G(Q^{n+1}, C_s) = \min$, а обеспечивается лишь $G(Q^{n+1}, C_s) \leq G(Q^n, C_s)$. (Это утвер-

* $C_s = (c_{1,s}, c_{2,s}, \ldots, c_{\lambda,s}, \ldots, c_{l,s})$ — значение использованного при приближениях типа *а* s-ого цикла вектора C.

ждение будет доказано в следующем пункте.) Такое же рассуждение имеет место при приближениях типа *б*.

Если ищем $(n+1)$-ое приближение усилия при итерации типа *а* в следующем виде

$$Q_j^{n+1} = Q_j^n + \delta_{j,i}^n \qquad i,j = 1, \ldots, k, \tag{39}$$

то согласно вышесказанному

$$\begin{aligned} &\delta_{i,j}^n = 0 \quad \text{при} \quad i \neq j \quad \text{и при} \quad i = j \\ &\delta_{i,j}^n = \delta_i^n = -\bar{\delta}_i^n, \quad \text{если} \quad Q_i^n \geq \bar{\delta}_i^n, \\ &\delta_{i,j}^n = \delta_i^n = -Q_i^n, \quad \text{если} \quad Q_i^n \leq \bar{\delta}_i^n. \end{aligned} \tag{40}$$

При приближениях типа *б* вычисления по формулам (37) будут сделаны с удовлетворением условия

$$Q_i^{n+1} \geq 0 \tag{41}$$

2.3. *Теорема о циклической итерации* (37)—(41)

Теорема: Существуют единственные решения контактных задач рассматриваемых типов (22), которые могут быть найдены с удовлетворением условия (47), как пределы последовательностей, построенных по правилу (37)—(41).

Доказательство: Учитывая (33), (39) и (40), изменение функционала (28) при итерации типа *а* между $(n+1)$ и n-ми приближениями будет (Δ_i^n, $\bar{\Delta}_i^n$, χ_i см. (69), (67))

$$G(Q^{n+1}, C_s) - G(Q^n, C_s) = \delta_i^n \cdot (\Delta_i^n + \bar{\Delta}_i^n) + \frac{1}{2}\chi_i (\delta_i^n)^2$$

или

$$G(Q^{n+1}, C_s) - G(Q^n, C_s) = \frac{1}{2}\chi_i \cdot [2\delta_i^n \cdot \bar{\delta}_i^n + (\delta_i^n)^2].$$

Согласно полученной итерации (40)

$$G(Q^{n+1}, C_s) - G(Q^n, C_s) = \begin{cases} -1/2\ \chi_i \cdot (\delta_i^n)^2 \quad \text{при} \quad Q_i^n \geq 0 & (42) \\ -1/2\ \chi_i \cdot (Q_i^n)^2 \cdot [2\beta_i^n - 1] \quad \text{при} \quad \bar{\delta}_i^n \geq 0 & (43) \end{cases}$$

где $\beta_i^n \geq 1$.

Так как* $\chi_i \geq 1$,

* $Q^n = (Q_1^n, \ldots, Q_i^n, \ldots, Q_k^n)$,
$\delta^n = (0, \ldots, 0, \delta_i^n, 0, \ldots, 0)$,
$Q^{n+1} = Q^n + \delta^n$,
$Q^{n+1} = (Q_i^n, \ldots, Q_i^n + \delta_i^n, \ldots, Q_k^n) =$
$= (Q_1^{n+1}, \ldots, Q_i^{n+1}, \ldots, Q_k^{n+1})$, $n = n_* + i - 1$,
$i = 1, \ldots, k$.

$$G(Q^{n+1}, C_s) \leq G(Q^n, C_s) - \frac{1}{2}(\delta^n)^2 = G(Q^n, C_s) - \frac{1}{2}\|Q^{n+1} - Q^n\|^2, \qquad (44)$$
$$n = n_* + i - 1, \quad i = 1, \ldots, k.$$

Если имеется приближение типа *б*, то после подстановки выражения (33), (37) в функционал (28) получается, что в некоторых точки $i = i'$ из-за члена $\beta^n_{\lambda,s} \cdot Q^*_{\lambda,i}$ усилия Q_i^{n+1} могут быть отрицательными. Они должны быть скорректированы на нуль вследствие односторонних связей, т. е. $Q_i^{n+1} = 0$.

Таким образом, при номерах приближений $n = n_* + k + \lambda - 1$ приращение функционала (28) с учетом (41) равно:

$$G(Q^{n+1}, C^{n+1}) - G(Q^n, C^n) = -\frac{1}{2}\chi_i \cdot (\beta^n_{\lambda,s})^2 + \frac{1}{2}M_\lambda \qquad (45)$$

где*

$$M_\lambda = M_\lambda(Q^n, C^n, H^n_p, \beta^n_{\lambda,s}) \,. \qquad (46)$$

Если имеет место**

$$\frac{1}{2}\chi_\lambda \cdot (\beta^n_{\lambda,s})^2 \geq M_\lambda \,, \qquad (47)$$

то

$$G(^{n+1}, C^{n+1}) - G(Q^n, C^n) \leq -\frac{1}{2}\dot{\chi}_\lambda \cdot (\beta^n_{\lambda,s})^2$$

где

$$\dot{\chi}_\lambda = \chi_\lambda \cdot \pi_\lambda, \qquad 0 < \pi_\lambda \leq 1 \,, \qquad (48)$$
$$n = n_* + k + \lambda - 1, \quad \lambda = 1, \ldots, l.$$

Из (44) и (48) видно, что значение функционала на каждом шагу итерации уменьшается.

Введя новую величину ψ_λ, удовлетворяющую условиям

$$\psi_\lambda = \begin{cases} \dot{\chi}_\lambda & \text{если} \quad 1 \geq \dot{\chi}_\lambda > 0 \,, \\ 1 & \text{если} \quad \dot{\chi}_\lambda > 1 \,, \end{cases} \qquad (49)$$

получим неравенство

$$G(G^{n+1}, C^{n+1}) - G(Q^n, C^n) \leq -\frac{1}{2}\psi_\lambda \cdot (\beta^n_{\lambda,s})^2 .$$

Последовательность этих итерационных приближений дает следующее приращение функционала

$$G(Q^{n'+l}, C^{n'+l}) - G(Q^n, C^n) \leq -\frac{1}{2}\psi_\lambda \sum_{\lambda=1}^{l} (\beta^{n'+\lambda-1}_{\lambda,s})^2 \qquad (50)$$
$$n' = n_* + k, \qquad \lambda = 1, \ldots, l,$$

где $\psi = \min \psi_\lambda$

* H^n_p — есть значение p-ого дополнительного уравнения при n-ом приближении

** Если введение новой константы $0 \leq |\bar{\beta}^n_{\lambda,s}| \leq |\beta^n_{\lambda,s}|$ обеспечивает в выражениях (37) неравенства $Q_i^{n+1} \geq 0$, то $M_\lambda = 0$.

При приближениях типа a имеет место

$$G(Q^{n+m}, C_s) - G(Q^n, C_s) \leq$$
$$\leq -\frac{1}{2}\{\|\delta^n\|^2 + \|\delta^{n+1}\|^2 + \ldots + \|\delta^{n+m-1}\|^2\} = -\frac{1}{2}\|Q^{n+m} - Q^n\|^2, \tag{51}$$

при $m \geq 1$, так как $\delta^n \cdot \delta^{n+m-1} = 0$, если

$$n_* \leq n + m - 1 \leq n_* + k - 1 .$$

Из (50) и (51) следует, что в одном цикле

$$0 \leq G(Q^{n_*+k+l}, C^{n_*+k+l}) \leq G(Q^{n_*}, C^{n_*}) -$$
$$- \frac{1}{2}\psi\left\{\|Q^{n_*+k} - Q^{n_*}\|^2 + \sum_{\lambda=1}^{l}(\beta_{\lambda,s}^{n_*+k+l-1})^2\right\}. \tag{52}$$

Так как значение функционала при каждом шаге итерации уменьшается, то при номере — приближения $n = n_* \to \infty$ следует

$$\lim_{n=n_*}\left\{\|Q^{n+m} - Q^n\|^2 + \sum_{\lambda=1}^{l}(\beta_{\lambda,s}^{n+m+\lambda-1})^2\right\} = 0 \tag{53}$$

и существует

$$\lim_{n} Q^n = Q = (Q_1, \ldots, Q_k), \tag{54}$$

а также

$$\lim \beta_{\lambda,s}^n = \vartheta_\lambda \cdot \Delta_{\lambda,s}^n = \vartheta_\lambda \cdot \sum_{p=1}^{l} \gamma_p \cdot \Theta_{p,\lambda} \cdot H_p^n = 0 \tag{55}$$

$\lambda = 1, \ldots, l$ т.е.

$$H_p^n = 0 \qquad p = 1, \ldots, l \tag{56}$$

$$\lim_{n} C^n = C \tag{57}$$

и, кроме того, согласно (42) и (43) в пределе

либо $\delta_i = 0$ при $Q_i \geq 0$ $i \in \Omega_Q$
либо $Q_i = 0$ при $\delta_i \geq 0$ $i \in \Omega_0$

далее, согласно (56) дополнительные уравнения удовлетворены.

Таким образом доказано, что алгоритм (37)—(41) дает решение контактной задачи (22) (или (17)—(19)) с учетом односторонних связей.

Можно доказать, что *это решение является единственным*. Действительно, предположим, что существует два решения контактной задачи

$$Q_i^1, c_\lambda^1 \qquad \text{и} \qquad Q_i^2, c_\lambda^2,$$
$$i = 1, \ldots, k, \qquad \lambda = 1, \ldots, l,$$

или, используя обозначение (20)

$$X_i^1 \quad \text{и} \quad X_i^2 \qquad i = 1, \ldots, k+l$$

Тогда системы алгебраических уравнений-неравенств (17), (18), (23) имеют следующий вид:

$$\begin{aligned} &\sum_{j=1}^{k} \alpha_{ij} Q_j^1 - d_i^1 - f_i > 0 \qquad \text{при} \qquad Q_i^1 = 0 \\ &\sum_{j=1}^{k} \alpha_{ij} Q_j^1 - d_i^1 - f_i = 0 \qquad \text{при} \qquad \underset{i=1,\ldots,k}{Q_i^1 \geq 0} \end{aligned} \tag{58}$$

$$\sum_{j=1}^{k} \alpha_{k+p,j} Q_j^1 + \sum_{\lambda=1}^{l} \alpha_{k+p,\,k+\lambda} c_\lambda^1 = F_p \qquad p = 1, \ldots, l \tag{59}$$

и далее

$$\begin{aligned} &\sum_{j=1}^{k} \alpha_{ij} Q_j^2 - d_i^2 - f_i = 0 \quad \text{при} \quad Q_i^2 = 0 \\ &\sum_{j=1}^{k} \alpha_{ij} Q_j^2 - d_i^2 - f_i = 0 \qquad \text{при} \qquad \underset{i=1,\ldots,k}{Q_i^2 \geq 0} \end{aligned} \tag{60}$$

$$\sum_{j=1}^{k} \alpha_{k+p,j} Q_j^2 + \sum_{\lambda=1}^{l} \alpha_{k+p,\,k+\lambda} c_\lambda^2 = F_p, \qquad p = 1, \ldots, l. \tag{61}$$

Если введем величины

$$\begin{aligned} Y_i &= Q_i^1 - Q_i^2, & i &= 1, \ldots, k, \\ Z_\lambda &= c_\lambda^1 - c_\lambda^2, & \lambda &= 1, \ldots, l, \\ a_i &= d_i^1 - d_i^2 = \sum_{\lambda=1}^{l} \alpha_{i,k+\lambda} Z_\lambda & i &= 1, \ldots, k, \end{aligned} \tag{62}$$

то в силу уравнения-неравенства (58) и (60) при различных значениях индекса i возможны только следующие соотношения:

$$\begin{aligned} &\sum_{j=1}^{k} \alpha_{ij} Y_j - a_i \neq 0 \qquad \text{при} \qquad Y_i = 0 \\ &\sum_{j=1}^{k} \alpha_{ij} Y_j - a_i > 0 \qquad \text{при} \qquad Y_i \leq 0 \\ &\sum_{j=1}^{k} \alpha_{ij} Y_j - a_i < 0 \qquad \text{при} \qquad Y_i \geq 0 \end{aligned} \tag{63}$$

$$\sum_{j=1}^{k} \alpha_{ij} Y_j - a_i = 0 \qquad \text{при} \qquad Y_i \neq 0$$

Далее, из уравнений (59), (61) получим равенство

$$\sum_{j=1}^{k} \alpha_{k+p,j} Y_j + \sum_{\lambda=1}^{l} \alpha_{k+p,\,k+\lambda} Z_\lambda = 0\,. \tag{64}$$

С одной .стороны, из теоремы взаимности для упругих систем, а с другой стороны, из подобия между уравнениями статики и уравнениями перемещений жестких тел следует, что

$$\alpha_{k+p,j} = \alpha_{j,k+p} \quad \begin{matrix} p = 1, \ldots, l, \\ j = 1, \ldots, k\,. \end{matrix} \tag{65}$$

В силу (62), (65), (64)

$$\sum_{i=1}^{k} a_i Y_i = -\sum_{x=1}^{l} \sum_{\lambda=1}^{l} \alpha_{k+\lambda,\,k+x} Z_x Z_\lambda \leq 0$$

так как матрица $[\alpha_{k+\lambda,\,k+x}]$ неотрицательно-определена. (Если дополнительные уравнения (59), (61) не содержат уравнений статики, то матрица $[\alpha_{k+\lambda,\,k+x}]$ положительно-определена, так как в этом случае полученная квадратичная форма выражает, получаемую при разборке конструкции, работу внутренних усилий в местах сопряжений частей конструкции.)

Теперь из (63) получаем

$$\sum_{i=1}^{k} \sum_{j=1}^{k} \alpha_{ij} Y_j Y_j + \sum_{x=1}^{l} \sum_{\lambda=1}^{l} \alpha_{k+\lambda,\,k+x} Z_x Z_\lambda \leq 0$$

что возможно только при $Y_i = 0$, $i = 1, \ldots, k$ поскольку матрица $[\alpha_{ij}]$ положительно-определена. Тогда из соотношений (63) следует, что $a_i = 0 \quad i = 1, \ldots, k$, т. е. $Z_\lambda = 0$, $\lambda = 1, \ldots, l$. Таким, образом теорема доказана полностью.

Отметим, что приведенное в работе [5] докозательство для контактной задачи первого типа (относительное жесткое смещение между контактирующими телами отсуствует) является частным случаем данного выше доказательства.

При веденном выше доказательстве было предложено удовлетворение условия (47). Проверка этого в ходе итерации принципиально возможна, однако как расчеты показывают практически ее не стоит делать, поскольку при итерации всегда обеспечиваются условия $Q_i \geq 0, \quad i = 1 \ldots, k$ и итерация будет прекращена только тогда, когда дополнительные уравнения также будет удовлетворены. Так как было доказано, что решение единственно, мы получим это рещение для контактной задачи.

3. Основные шаги решения контактных задач, сводящихся к матричному уравнению — неравенству $\mathbf{Ax} - \mathbf{e} \geq \mathbf{0}$

Для того, чтобы легче осуществить практические расчеты, кратко подытожим проделанные шаги.

3.1 *Первая последовательность шагов*

После выбора расчетной схемы в первую очередь надо определить элементы матрицы **A** и вектора **e**, т. е. построить матрицу функций влияния $[\alpha_{ij}]$ с размером $(k \times k)$, затем вычислить коэффициенты $\alpha_{i,k+\lambda}$ $i = 1, \ldots, k$, $\lambda = 1, \ldots, l$, находящиеся в перемещении d_i, а, далее определить коэффициенты дополнительных уравнений $\alpha_{k+p,j}$ $p = 1, \ldots, l$, $j = 1, \ldots, k + l$, и окончательно можно вычислить перемещения f_i $i = 1, \ldots, k$ и величины $F_1, \ldots, F_l$.

Тот факт, что в наших расчетах имеются дополнительные уравнения, выражается через коэффициент $\gamma_p > 0$.

3.2 *Вторая последовательность шагов*

Если имеется хотя бы один коэффициент $\gamma_p \neq 0$, то в рамках второй последовательности шагов решаем следующую систему алгебраических уравнений относительно $Q^*_{\lambda,j}$:

$$\sum_{j=1}^{k} \alpha_{ij} Q^*_{\lambda,j} + \alpha_{i,k+\lambda} = 0\,, \qquad \begin{matrix} i = 1, \ldots, k, \\ p = \lambda = 1, \ldots, l. \end{matrix} \tag{66}$$

3.3 *Третья последовательность шагов*

Здесь будут вычислены неизменяющиеся в ходе итерационного процесса величины:

$$\varepsilon_i = -\frac{1}{1 + \sum_{p=1}^{l} \gamma_p \cdot (\alpha_{k+p,i})^2}\,, \qquad i = 1 \ldots, k$$

$$\vartheta_\lambda = -\frac{1}{\sum_{p=1}^{l} \gamma_p \cdot (\Theta_{p,\lambda})^2}\,, \qquad \lambda = 1, \ldots, l \tag{67}$$

$$\Theta_{p,\lambda} = \sum_{j=1}^{k} \alpha_{k+p,j} \cdot Q^*_{\lambda,j} + \alpha_{k+p,k+\lambda}\,,$$

$$p = 1, \ldots, l;\ \lambda = 1, \ldots, l.$$

3.4 *Осуществление циклического итерационного процесса* (n—номер приближения, s-номер цикла)

На каждом этапе итерации осуществленные шаги повторяются и при каждом шаге изменяется хотя бы одна величина. Необходимое условие сходимости итерации, чтобы в нулевом приближении все первые k проекции вектора $\mathbf{x}$ были не отрицательными, т. е.

$$Q_i^0 \geq 0 \qquad i = 1, \ldots, k, \tag{68}$$

причем члены $c_1, \ldots, c_l$ могут иметь любое значение.*

Пусть номер приближения в начале s-ого цикла $n_* = (s-1) \cdot (k+l)$ (при этом $(s-1)$ полное число пройденных циклов; каждый цикл содержит $k+l$ приближений; под n-ым приближением понимается $\mathbf{x}^n$-ое приближение вектора $\mathbf{x}$).

При итерации всегда вычисляются следующие величины**

$$\bar{\delta}_i^n = -\varepsilon_i \cdot (\Delta_i^n + \bar{\Delta}_i^n), \qquad \varepsilon_i = -\frac{1}{\chi_i}$$

$$\Delta_i^n = \frac{1}{\alpha_{ii}} \left(\sum_{j=1}^{k+l} \alpha_{ij} \cdot x_j^n - f_i \right),$$

или

$$\Delta_i^n = \frac{1}{\alpha_{ii}} \left(\sum_{j=1}^{k} \alpha_{ij} \cdot Q_j^n + \sum_{\lambda=1}^{l} \alpha_{i,k+\lambda} \cdot c_{\lambda,s} - f_i \right),$$

$$\bar{\Delta}_i^n = \sum_{p=1}^{l} \gamma_p \cdot H_p^n \cdot \alpha_{k+p,i}; \qquad \beta_{\lambda,s}^n = \vartheta_\lambda \cdot \Delta_{\lambda,s}^n,$$

$$\Delta_{\lambda,s}^n = \sum_{p=1}^{l} \gamma_p \cdot H_p^n \cdot \Theta_{p,\lambda} \qquad \vartheta_\lambda = -\frac{1}{\chi_\lambda}, \tag{69}$$

* Нулевое приближение $\mathbf{x}^0$ целесообразно получить по решению $\mathbf{x}$ системы (23), как уравнения, таким образом, что в тех местах, где $Q_i < 0$, изменяем его значение на нуль, т. е. $Q_i = 0$.

** При вычислениях можно поступать так, что величину $\bar{\Delta}_i^n$, которая находится в $\bar{\delta}_i^n$, определяется при приближении с номером n_* в начале s-ого цикла, и в дальнейшем ее неизменяем при итерации типа a.

$$H_p^n = H_p(\Omega, [\vec{\mathbf{F}}^t, \vec{\mathbf{M}}_0^t], \mathbf{x}^n).$$

s-ый цикл осуществляется с помощью последовательности приближения следующего типа: a, $б$.

Приближение типа а

При выполнении приближения типа a (k приближений) при фиксированном значении «дополнительных» неизвестных $c_{\lambda,s}$, определенных на $(s-1)$-

ом цикле (индекс указывает на то, что c_λ будет использовано на s-ом цикле), проверяются в области Ω (в точках $i = 1, \ldots, k$) условия контакта или отрыва (зазора). Далее, в зависимости от того, как удовлетворялись эти условия, изменяются усилия только в i-ой точке (номер приближения зависит от значения i).

По вышесказанному найдем $(n + 1)$-ое приближение в виде (39), (40).

С учетом (40) соотношение (39) можно представить в следующем векторном виде:

$$\mathbf{q}^{n+1} = \mathbf{q}^n + \boldsymbol{\delta}^n,$$

где

$$(\mathbf{q}^n)^T = [Q_1^n, \ldots, Q_i^n, \ldots, Q_k^n],$$

$$(\boldsymbol{\delta}^n)^T = [0, \ldots, 0, \delta_i^n, 0, \ldots, 0],$$

$$(\mathbf{q}^{n+1})^T = [Q_1^n, \ldots, Q_{i-1}^n, Q_i^n + \delta_i^n, Q_{i+1}^n, \ldots, Q_k^n] =$$

$$= [Q_1^{n+1} \ldots, , Q_i^{n+1}, \ \ldots, \ Q_k^{n+1}].$$

Приближение типа б

При выполнении приближения типа *б* проверяется степень удовлетворения дополнительных уравнений H_p $(p = 1, \ldots, l)$. При этом согласно (37) изменяются неизвестные величины c_λ^n, а также контактные усилия с условием* $Q_i^{n+1} \geq 0$.

После выполнения $k + l$ шагов начинается новый $(s + 1)$-ый цикл.

Итерационный процесс можно считать завершенным, если максимальное значение невязки

$$\max |Q_i(s) - Q_i(s-1)| \leq \vartheta \qquad i = 1, \ldots, k,$$

где ϑ есть впредь заданный предел. Здесь $Q_i(s)$ есть усилие, определенное в конце s-ого цикла в i-ой точке.

* Если при конкретных вычислениях из-за члена $\beta_{\lambda,s}^n \cdot Q_{\lambda,i}^*$ в некоторых точках i получаются $Q_i^{n+1} < 0$, то в этих точках условие $Q_i^{n+1} \geq 0$ обеспечим подстановкой $Q_i^{n+1} = 0$.

3.5 *Определение напряженного состояния*

Определение напряженного состояния можно осуществить двояким образом.

[1] Используется деформированная форма тела, полученная после итерации (т. е. после учета влияния одного тела на другое). При определенных видах тонкостенных элементов напряженное состояние можно получить путем дифференцирования деформированной формы.

[2] При построении функций влияния одновременно вычисляются напряжения, а затем на основе принципа суперпозиции определяется напряженное состояние частей упругой системы при помощи известных после итерации контактных усилий, внешней системы усилий и т. д.

ЛИТЕРАТУРА

1. Вулих, Б. З.: Введение в функциональный анализ изд. «Наука», М., 1967.
2. Канторович, Л. В., Крылов, В. И.: Приближенные методы высшего анализа. ГИТТЛ. М., 1949.
3. Пацельт, И.: Деформация торообразной оболочки на упругом винклеровском основании. Автореферат диссертации на соискание ученой степени к. т. н. ЛПИ, Ленинград, 1969.
4. Фаддеев, Д. К.—Фаддеева, В. Н.: Вычислительные методы линейной алгебры «Государственное изд. физико—математической литературы» М., Л., 1963.
5. Фридман, В. М.—Чернина, В. С.: Итерационный процесс для решения конечномерной контактной задачи. *Ж. ВМ и МФ. М.*, 7, (1967), 160—163.
6. Фридман, В. М.—Чернина, В. С.: Решение задачи о контакте упругих тел итерационным методом. Инженерный журнал МТТ. М., 1967, № 1, 116—120.

Iteration Method Applied to the Solution of Contact Problems of Elastic Systems Having Elements in Unilateral Relation. By the modification of the calculation process elaborated by V. M. FRIEDMANN and V. S. TCHERNJINA, an expanded method is discussed which can be applied to contact problems of constructional systems having unilateral relation in elements. Adhesion and friction between the contacting elements are disregarded. In the same way, as is done in the original process, the new method is reduced to the principle of an analysis, to find whether conditions of a contact or of a separation at a set of finite points are fulfilled. This process of reasoning leads to a system of equalities and inequalities including supplementary equations of equilibirium and kinematical conditions (e. g. zero-value of relative displacements between contacting elements, and/or of angular rotations.) A solution is found by a cyclic iteration applied on the basis of a gradient method. Essentially, a quadratic functional is minimized for which the sign of contact forces must be positive. It is clearly demonstrated that this solution is unique. Besides, it represents the limit value of a series formed in compliance with the iteration rule.

Iterationsverfahren zur Lösung der Kontakt-Fragen von elastischen Systemen mit einseitigem Anschluß. In diesem Aufsatz handelt es sich um eine Weiterentwicklung der durch W. M. FRIEDMANN und W. S. TSCHERNJINA ausgearbeiteten Lösungsmethode der Kontakt-Probleme von Konstruktionen mit einseitigem Anschluß. Reibung und Adhäsion bleiben hiebei außer acht. Im Einklang mit dem originalen Verfahren bildet auch hier die Analyse der Bedingungen der Entstehung des Kontaktes oder der Separation an einer endlichen Zahl von Punkten die prinzipielle Grundlage der Lösung. Die Ausarbeitung des Verfahrens führt zur Aufstellung eines Systems aus Gleichheiten und Ungleichheiten und ergänzenden Gleichungen. Die letzteren Gleichungen erscheinen als Gleichgewichtsbedingungen bzw. als kinematische Zusammenhänge. (Nullwert der relativen Verschiebungen, Winkelverschiebungen). Als Lösung des Systems ergibt sich eine zyklische Iteration aufgrund der Gradienten-Methode. Das Wesentliche darin ist das Minimalisieren eines quadratischen Funktionals, mit der Beschränkung, daß Kontaktkräfte nur mit positivem Vorzeichen figurieren können. Erwiesenermaßen ist dies die einzig mögliche Lösung uzw. als Grenzwert der nach Iterationsregeln gebildeten Wertreihe.

INDEX

Wedig, W.: Stabilitätsbedingungen für ein Schwingungssystem mit zufälliger Parametererregung — Conditions of Stability for a System under Random Parametric Excitation — *Ведиг, В.:* Условия стабильности колебательной системы, возбуждаемой случайным параметром 1

Kozarov, M.—Ivanov, Ts. P.: Wave Propagation in an Infinite Transversely Isotropic Cylinder of Elliptical Cross-Section — Wellenfortpflanzung in einem in der Querrichtung isotropen Zylinder elliptischen Querschnitts — *Козаров, М., Иванов, Ч. П.:* Распространение волн в поперечном направлении изотропном бесконечном цилиндре эллиптического сечения 21

Schatt, W.: Grundlegende Vorgänge bei der Gefügeentwicklung — Basic Phenomena in Structure Development — *Шатт, В.:* Основные процессы формирования материальной структуры 39

Kollár, L.: Continuum Method of Analysis for Double-Layer Space Trusses with Upper and Lower Chord Planes of Different Rigidities — Berechnung zweischichtiger Raumfachwerke mit unteren und oberen Gurtebenen von verschiedenen Steifigkeiten mit dem Kontinuumverfahren — *Коллар, Л.:* Расчет двухслойных пространственных ферм различной жесткости, имеющих верхнюю и нижнюю плоскости пояса 53

Bitó, J. F.—Antal, K. G.: A Capacitive Discharge Method for Determining Gas Impurities Quantitatively — Eine kapazitive Entladungsmethode für die quantitative Bestimmung von Gasverunreinigungen — *Бито, Я., Антал, К.:* Метод емкостных газовых разрядов для количественного определения газовых примесей 65

Buócz, Z.—Janositz, J.: Ein neues Verfahren zur Lösung der Doppelpunkteinschaltung durch Streckenmessung — A New Method of the Double-Point Insertion on the Basis of Distance Measurement — *Буоц, З., Яношитц, Я.:* Новый метод решения проблемы двойной привязки точки, основывающейся на данных измерения расстояния 87

Ecsedi, I.: An Approximate Method for the Analysis of Elastic Torsion of Round Bars of Variable Diameters — Eine Näherungsmethode zur Analyse der elastischen Verdrehung von Rundstäben mit veränderlichen Durchmessern — *Эчеди, И.:* Приближенный метод исследования упругого кручения круглых стержней переменного сечения 93

Misféth, E.: Dimensioning of Structures for Flood Discharge According to the Theory of Probability — Bemessung von Bauwerken für Hochwasser-Ableitung aufgrund der Wahrscheinlichkeitstheorie — *Миштет, Э.:* Расчет технических сооружений на основе теории вероятности на отвод паводковых вод 107

Kereszty, P.: Role of the Centre Plate and Side Bearing in the Safe Riding of Rail Vehicles — Rolle des Drehtellers und der Gleitstütze in der Fahrsicherheit der Schienenfahrzeuge — *Керести, П.:* Роль вагонного подпятника и боковой опоры в надежности движения железнодорожного подвижного средства 129

Hajdu, L.—Zahorán, J.: Hermetically Sealed Silver–Zinc Batteries Operating in the Silver (I) Oxide (Ag_2O) Phase — In der (Ag_2O)-Phase von Silber (I)-Oxyd funktionierender gasdicht verschlossener Silber-Zink-Akkumulator — *Хайду, Л., Захоран, Я.:* Герметизированный серебряно-цинковый аккумулятор, работающий в фазе одновалентного серебра (Ag_2O) 153

Somogyi, K.—Pődör, B.: A Simple Sample Holder and Cryostat for Measuring Thermoelectric Power of Semiconductors in the Temperature Range of 80—400 K — Ein einfacher Probenhalter und Kryostat für die Messung der thermoelektrischen Spannung von Halbleitern im Temperaturbereich 80—400 K — *Шомоди, К., Педер, Б.:* Простой держатель образца и криостат для измерения термо эдс полупроводников в интервале температур от 80 до 400 К 177

Patkó, J. —*Jr. Vajta, M.:* Determination of the Thermal Breakdown Voltage for D.C. and A.C. Voltages — Bestimmung der Labilitätsspannung für Gleich- und Wechselspannung — *Патко, Я., мл. Вайта, М.:* Определение напряжения лабильности при постоянном и переменном токах 138

Bhargava, R. D.—Miss Bhargava R. R.: An Infinite Elastic Plate under Tension with a Crack and a Circular Inclusion — Zug einer unendlichen Scheibe, die einen geraden Einschnitt und eine kreisförmige Einbettung besitzt — *Баргава, Р. Д., Баргава, Р. Р.:* Вытяжка бесконечной по размерам плоской пластины 207

Пацельт, И.: Итерационный метод для решеоия контактной заДачи систем с односторонними стязями — *Páczelt, I.e* Iteration Method Applied to the Solution of Contact Problems of Elastic Systems Having Elements in Unilateral Relation — Iterationsverfahren zur Lösung der Kontakt-Fragen von elastichen Systemen mit einseitigem Anschluß 217

Printed in Hungary

A kiadásért felel az Akadémiai Kiadó igazgatója. Műszaki szerkesztő: Zacsik Annamária

A kézirat nyomdába érkezett: 1973. V. 7 — Terjedelem: 21,7 (A/5) ív 92 ábra

73.75012 Akadémiai Nyomda, Budapest — Felelős vezető: Bernát György

REPRESENTATIVE ARCHITECTURAL ISSUE OF ACTA TECHNICA

The next issue No. 77 of Acta Technica will be especially rich and variegated in contents. Outstanding theoretical and historical problems of architecture will be considered with the same conceptions, to be assimilated to those of historical epochs. A copious report on a symposium held in Budapest by UNESCO's special fortress committee (IBI) to which is connected by László Gerő's survey of the development of fortresses in Europe. Ernő Marosi will give a report upon peculiar "tendencious" changes in plans of the gothic architecture pointing to social roots. Mrs. Rózsa Feuer, née Rózsa Tóth considers excavations for localizing king Mathias'- hanging garden proving the existence of engineer architecture in Hungary already in the early renaissance period. Jolán Balogh discusses another hitherto neglected major problem of the renaissance, the analyses of regular planned fortresses as evidenced by extensive unknown design material both from Hungary and abroad. Hungarian particularities in romantic architecture are shown by Dénes Komárik in connection with the competition conducted for the construction of the Parliament, whereas architectural principles of the secession style and its Hungarian traits are presented by Mihály Kubinszky summarizing the results on this subject at an international symposium held in Prague. Mutual implications of technical and historical problems are analyzed by Zoltán Szentkirályi with an original approach, and, finally, a new theory of mass shaping and space in architecture is established by Gyula Hajnóczy. In this way this volume can be looked at as a representative epitome of historical and theoretical research in architecture in our own days.

Redaction of the Acta Technica

RAUMGEOMETRIE IN DER TECHNISCHEN PRAXIS

von *I. PÁL*

Der fünfhundert Anaglyphen erhaltende Band bietet, nach Bereinigung der allgemeinen Grundbegriffe, einen Überblick über die raumgeometrischen Probleme der einzelnen Industriezweige. Namentlich die Raumprobleme der Maschinenindustrie (technische Zeichnung, charakteristische Kurven, Technologie der Spanabhebung), der Bauindustrie (Schalen- und Fachwerkkonstruktionen, Statik), der chemischen Industrie (Raumgitter, Kristallsymmetrien) sowie die auf diesem Gebiet erzielten Ergebnisse sind im Werk eingehend behandelt. Abschließend befaßt sich das Buch mit einigen im Grenzgebiet der Geometrie und der Mathematik gelegenen Problemen (Koordinatensysteme, Kurven, Flächen) sowie mit der Praxis entnommenen Fragen (Flächen zweiter Ordnung in der spanabhebenden Bearbeitung, Gewichtskurvenblatt, die empirische Funktion usw.). Die Auswahl der behandelten Probleme gestalten das Buch zu einem wichtigen Hilfsmittel der technischen Praxis.

In deutscher Sprache · Etwa 180 Seiten · Ganzleinen

DIMENSIONIERUNGSFRAGEN DER ZAHNRAD-PLANETENGETRIEBE

von *Z. TERPLÁN*

Das Zahnrad-Planetengetriebe ist eine spezielle Art der Zahnradgetriebe, das in den letzten anderthalb Jahrzehnten eine große Entwicklung durchgemacht hat. In diesem Buch werden in erster Linie die vom Verfasser oder von seinen Mitarbeitern beantworteten Fragen zusammengefaßt. Das Werk ist kurz gefaßt und komprimiert, dem leichteren Verständnis dienen zahlreiche Abbildungen und ein umfangreiches Tabellenmaterial. Ein reichhaltiges Literaturverzeichnis ergänzt das Buch.

In deutscher Sprache · Etwa 270 Seiten · Ganzleinen

AKADÉMIAI KIADÓ
Verlag der Ungarischen Akademie der Wissenschaften
B u d a p e s t

THE NITROGEN INDUSTRY I—II

edited by *Gy. Honti*

This work is both a monograph and an indispensable handbook for those working in the field of nitrogen industry and the various branch industries. It includes all the subjects of the ndustry; e.g. thermodynamics, technology, energetics, engineering design, construction and industrial practice, power and water supply. It treats also the question of most recent results, uch as, e.g. the ammonia synthesis based on high-capacity, single stream, hydrocarbon steam-reforming. The historical background and prospects for the future are outlined so that a ful] picture of an impetous young branch of industry is provided.

In English · Approx. 1360 pages · Cloth

2nd INTERNATIONAL SYMPOSIUM ON INFORMATION THEORY

Tsahkadsor, Armenia, USSR
September 2—8, 1971

edited by *B. N. Petrov* and *F. Csáki*

The 2nd International Symposium on Information Theory held in 1971 was organized by Soviet scientific organs in cooperation with the International Union of Radio Science (URSI). The lectures delivered by eminent scientists and researchers coming from 15 countries comprise the recent results of the modern information theory. The main topics were: general methods of information theory; coding theory and complexity estimates of encoders and decoders; feedback systems; algebraic methods of encoding; source encoding; statistical methods and learning systems.

In English · Approx. 350 pages · Cloth

AKADÉMIAI KIADÓ
Budapest

UNGARISCHE LOKOMOTIVEN UND TRIEBWAGEN

von K. Kopasz, M. Kubinszky, B. Manndorff und B. Varju

In diesem Werk wird jeder Dampf-, Diesel- und Elektro-Lokomotivtyp der 125 Jahre umfassenden Geschichte der ungarischen Eisenbahn ausführlich behandelt. Bei jeder Gattung werden die technischen Angaben mit charakteristischen Einzelheiten des Betriebes ergänzt. Es werden die in Ungarn hergestellten Lokomotive ausführlich behandelt und die Besprechung mit Typenskizzen und Photographien ergänzt, wobei die meisten Photographien Seltenheitswert besitzen. Besonders die Behandlung der Triebwagen von Ganz—Jendrassik und der elektrischen Lokomotiven des Systems Kandó ist sehr ausführlich, da es sich hier um spezielle ungarische Errungenschaften handelt. Das Buch beschäftigt sich auch mit vom Ausland beschafften Lokomotiven der Ungarischen Eisenbahnen. Das Werk ist mit biographischen Angaben berühmter ungarischer Lokomotivkonstrukteure, dem Nummernplan der MÁV und Typentabellen ergänzt.

In deutscher Sprache · Etwa 380 Seiten · Zahlreiche Abbildungen und Tabellen . Ganzleinen

AKADÉMIAI KIADÓ
Verlag der Ungarischen Akademie der Wissenschaften
Budapest

Acta Techn. Hung. **76** (1974), 1—19

WEDIG, W.: *Conditions of Stability for a System Random Parametric Excitation.*

The stability of a parametric excited system, the motions of which can be described by a differential equation with stochastic coefficients, is investigated by using the FOKKER—PLANCK equation. The conditions of the mean stability for the equilibrium position are approximately derived by applying a perturbation method. In case of stochastic coefficients, the spectral densities of which are distributed upon a broad frequency band, the critical spectral densities are giving instability regions, the lowest point of which is situated near twice the natural frequency of the system. In case of narrow band excitations one has to specify as first approximation the root of the critical exxcitation variance as a function of the mean excitation frequency.

Acta Techn. Hung. **76** (1974), 21—38

KOZAROV, M.—IVANOV, Ts. P.: *Wave Propagation in an Infinite Transversely Isotropic Cylinder of Elliptical Cross-Section*

The propagation of harmonic waves in a transversely isotropic clyinder of elliptical cross-section on the basis of the linear theory of elasticity was inevstigated. The result was obtained by Mathieu's function. The condition that the cylindrical surface is stressfree is given in the form of an infinite determinant which is equal to zero. From the general result it is possible to obtain two special cases: wave propagation in an isotropic cylinder of elliptical cross-section and wave propagation in a transversely isotropic cylinder of circular section.

Acta Techn. Hung. **76** (1974), 39—52

SCHATT, W.: *Basic Phenomena in Structure Development*

The author describes the most important phenomena of the structure development of metallic materials in solutions: edging with hydrogen development by reduction of an oxydizing agent and with formation of a complex. Subsequently the causes for the physical and chemical inhomogeneity of the real surface are discussed, which causes the structural components to be attacked selectively by the edging agent, so that they can be observed under the microscope.

Acta Techn. Hung. **76** (1974), 53—63

KOLLÁR, L.: ***Continuum Method of Analysis for Double-Layer Space Strusses with Upper and Lower Chord Planes of Different Rigidities***

A general method has been presented for determining equivalent continua of double-layer space trusses with two different, arbitrary chord plane meshes. Differential equation system and boundary conditions of the equivalent continuum are derived. In addition to the deflection functions describing the plate deformation, a stress function is still needed to describe the internal force system of the substituting continuum, similarly as for ribbed plates.

Acta Techn. Hung. **76** (1974), 65—85

BITÓ, J. F.—ANTAL, K. G.: ***A Capacitive Discharge Method for Determining Gas Impurities Quantitatively***

An original statistical model allowing theoretical determination of the critical breakdown field strength is presented. The applicability of the method is shown for argon. A good agreement has been found between the values of the critical breakdown field strength calculated by means of the proposed model and obtained experimentally. The revealed microphysical relationships lead to a quick quantitative method of gas analysis. By showing the possibilities of improving the model underlying theoretical considerations the importance of further information available is emphasized in this way.

Acta Techn. Hung. **76** (1974), 87—91

BUÓCZ, Z.—JANOSITZ, J.: ***A New Method of the Double-point Insertion on the Basis of Distance measurement.***

In this paper a new estimation method is described in order to find, in a certain way that deviates from the accustomed, the solution of the problem of how to carry out a double-point insertion on the basis of distance is defined by two independent informations, the latter being obtained from measured and calculated values. The numeric example, already published in the literary sources serves to demonstrate the advantages of the new nethod.

Acta Techn. Hung. **76** (1974), 93—105

ECSEDI, I.: *An Approximate Method for the Analysis of Flexible Torsion of Round Bars of Variable Diameters*

An approximate method for the analysis of round bars with variable diameter is being reported. The differential equation

$$\frac{\partial^2 \Phi}{\partial r^2} - \frac{3}{r}\frac{\partial \Phi}{\partial r} + \frac{\partial^2 \Phi}{\partial z^2} = 0 \qquad \text{(a)}$$

defining the stress function of torsion by taking into account the appropriate boundary conditions, is solved according to the method for the partial discretization with respect to z.

Acta Techn. Hung. **76** (1974), 107—128

MISTÉTH, E.: *Dimensioning of Structures for Flood Discharge According to the Theory of Probability*

The flood discharge capacity of structures is treated depending on the geometric proportions, discharge factor and random variables. Also an arbitrary probable value of the flood discharge in connection with the service life of the structure might be determined with the aid of one of the extremal distributions. The purpose of the new method of dimensioning is to ensure that the flood discharge capacity should, by a given probability, be higher than the design discharge. The risk incurred may, depending on the amount of damages caused by accidental failure, be established by only economical considerations.

Acta Techn. Hung. **76** (1974), 129—152

KERESZTY, P.: *Role of the Centre Plate and Side Bearing in the Safe Riding of Rail Vehicle*

In the construction technique of rail vehicles, the design of the support of the vehicle underframe on the bogie by a centre plate has been applied for nearly a century. This solution has the advantage of allowing the rocking of the vehicle body on its two bogies. However, if this motion becomes too intense, and causes oscillation of the body, this will already be unfavourable. Astonishingly the RIV and RIC-statutes regulating the change of railway cars on international level do not contain any prescriptions in this connection; in turn, in the PPV-regulation there are to be found some indications in respect to this question which, however, can only be considered as a first step in proposing a regulation.

Acta Techn. Hung. **76** (1974), 153—175

HAJDU, L.—ZAHORÁN, J.: *Hermetically Sealed Silver—Zinc Batteries Operating in the Silver (I) Oxide (Ag_2O) Phase*

The paper briefly reviews the characteristics of the hermetically sealed miniature silver—zinc storage cells enhancing the problems resulting primarily form their hermetic sealing. It deals in detail with the problem of gas fromation in sealed silver—zinc cells, and particularly with the factors which permit to influence the amount of gas formation. The influence of the silver structure on the size of the Ag_2O (silver monoxide) phase developing during the charging is analysed, then the design and experimental work is reviewed which enabled the development of hermetically sealed miniature silver—zinc cells working exclusively in the Ag_2O phase. Information is given on the electrical and storing characteristics and the life of such cells, finally they are compared to other cells, pointing out in what direction further research and development should proceed on the base of the very positive results obtained so far.

Acta Techn Hung. **76** (1974), 177—181

SOMOGYI, K.—PŐDÖR, B.: *A Simple Sample Holder and Cryostat for Measuring Thermoelectric Power of Semiconductors in the Temperature Range of 80—400 K*

A simple sample holder and cryostat system is described, suitable for measuring the temperature dependence of the thermoelectric power of semiconductors in the temperature range of 80—400 K.

Acta Techn. Hung. **76** (1974), 183—206

PATKÓ, J. —ifj. VAJTA, M.: *Determination of the Thermal Breakdown Voltage for D. C. and A. C. Voltages*

After the definition of the conceptions "thermal breakdown" and "thermal instability" a short survey of the history of the thermal breakdown theories is given. After writing up the general instability equations for D.C. voltages the expression of the thermal breakdown voltage for a specified temperature dependence of the resistivity is derived, then the same derivation for A.C. voltages is performed in a similar way. The individual temperature distributions are calculated for both cases, the obtained results tabulated by a computer are presented and the effects of some parameters on the value of the thermal breakdown voltage are investigated.

Acta Techn. Hung. **76** (1974), 207—215

BHARGAVA, H. D.—MISS BHARGAVA, R. R.: *An Infinite Elastic Plate Under Tension with a Crack and a Circular Inclusion*

In this paper, a procedure is presented for computing the stresses and displacements which arise in the body named in heading. Functions of complex variable are used. As starting-point, differential equations occurring in the two-dimensional theory of elasticity are applied. The results of a numerical example refer to the cases where the ratio of the elasticity constants of inclusion and matrix is 1/3, 1 and 3.

Acta Techn. Hung. **76** (1974), 217—241

PÁCZELT, I.: *Iteration Method Applied to the Solution of Contact Problems of Elastic Systems Having Elements in Unilateral Relation*

By the modification of the calculation process elaborated by V. M. FRIEDMANN and V. S. TSCHERNJINA, an expanded method is discussed which can be applied to contact problems of constructional systems having unilateral relation in elements. Adhesion and friction between the contacting elements are disregarded. In the same way, as is done in the original process, the new method is reduced to the principle of an analysis, to find whether conditions of a contact or of a separation at a set of finite points are fulfilled. This process of reasoning leads to a system of equalities and inequalities including supplementary equations of equilibrium and kinematical conditions (e.g. zero-value) of relative displacements between contacting elements, and/or of angular rotations). A solution is found by a cyclic iteration applied on the basis of a gradient method. Essentially a quadratic functional is minimized for which the sign of contact forces must be positive. It is clearly demonstrated that this solution is unique. Besides, it represents the limit value of a series formed in compliance with the iteration rule.

The *Acta Technica* publish papers on technical subjects in English, French, German and Russian.

The *Acta Technica* appear in parts of varying size, making up one volume.

Manuscripts should be addressed to

Acta Technica
1051 Budapest,
Münnich Ferenc u. 7.
Hungary

Correspondence with the editors and publishers should be sent to the same address.

The rate of subscription is $ 24.00 a volume. Orders may be placed with "Kultúra" Foreign Trade Company for Books and Newspapers (1389 Budapest 62, P.O.B. 149 Account No. 218 10990) or with representatives abroad.

Les *Acta Technica* paraissent en français, allemand, anglais et russe et publient des travaux du domaine des sciences techniques.

Les *Acta Technica* sont publiés sous forme de fascicules qui seront réunis en volumes.

On est prié d'envoyer les manuscrits destinés à la rédaction à l'adresse suivante:

Acta Technica
1051 Budapest,
Münnich Ferenc u. 7.
Hongrie

Toute correspondance doit être envoyée à cette même adresse.

Le prix de l'abonnement est de $ 24.00 par volume.

On peut s'abonner à l'Entreprise pour le Commerce Extérieur de Livres et Journaux «Kultúra» (1389 Budapest 62, P.O.B. 149 Compte courant No. 218 10990) ou à l'étranger chez tous les représentants ou dépositaires.

«*Acta Technica*» публикуют трактаты из области технических наук на русском, немецком, английском и французском языках.

«*Acta Technica*» выходят отдельными выпусками разного объема. Несколько выпусков составляют один том.

Предназначенные для публикации рукописи следует направлять по адресу:

Acta Technica
1051 Budapest,
Münnich Ferenc u. 7.
Венгрия

По этому же адресу направлять всякую корреспонденцию для редакции и администрации.

Подписная цена — $ 24.00 за том. Заказы принимает предприятие по внейшней торговле книг и газет «Kultúra» (1389 Budapest 62, P.O.B. 149 Текущий счет № 218 10990) или его заграничные представительства и уполномоченные.

Reviews of the Hungarian Academy of Sciences are obtainable at the following addresses:

ALBANIA

Drejtorija Qëndrone e Përhapjes dhe Propagandimit të Librit
Kruga Konferenca e Pazes
Tirana

AUSTRALIA

A. Keesing
Box 4886, GPO
Sydney

AUSTRIA

GLOBUS
Höchstädtplatz 3
A-1200 Wien XX

BELGIUM

Office International de Librairie
30, Avenue Marnix
1050 Bruxelles
Du Monde Entier
162, Rue du Midi
1000 Bruxelles

BULGARIA

HEMUS
11 pl Slaveikov
Sofia

CANADA

Pannonia Books
2, Spadina Road
Toronto 4, Ont.

CHINA

Waiwen Shudian
Peking
P. O. B. 88

CZECHOSLOVAKIA

Artia
Ve Směčkách 30
Praha 2
Poštovní Novinová Služba
Dovoz tisku
Vinohradská 46
Praha 2
Mad'arska Kultura
Václavské nám. 2
Praha 1
SLOVART A. G.
Gorkého
Bratislava

DENMARK

Ejnar Munksgaard
Nörregade 6
Copenhagen

FINLAND

Akateeminen Kirjakauppa
Keskuskatu 2
Helsinki

FRANCE

Office International de Documentation et Librairie
48, rue Gay-Lussac
Paris 5

GERMAN DEMOCRATIC REPUBLIC

Deutscher Buch-Export und Import
Leninstraße 16
Leipzig 701
Zeitungsvertriebsamt
Fruchtstraße 3—4
1004 Berlin

GERMAN FEDERAL REPUBLIC

Kunst und Wissen
Erich Bieber
Postfach 46
7 Stuttgart S.

GREAT BRITAIN

Blackwell's Periodicals
Oxenford House
Magdalen Street
Oxford
Collet's Subscription Import Department
Dennington Estate
Wellingsborough. Northants.
Robert Maxwell and Co. Ltd.
4—5 Fitzroy Square
London W. 1

HOLLAND

Swetz and Zeitlinger
Keizersgracht 471—487
Amsterdam C.
Martinus Nijhof
Lange Voorhout 9
The Hague

INDIA

Hind Book House
66 Babar Road
New Delhi 1

ITALY

Santo Vanasia
Via M. Macchi 71
Milano
Libreria Commissionaria Sansoni
Via La Marmora 45
Firenze
Techna
Via Cesi 16.
40135 Bologna

JAPAN

Kinokuniya Book-Store Co. Ltd.
826 Tsunohazu 1-chome
Shinjuku-ku
Tokyo
Maruzen and Co. Ltd.
P. O. Box 605
Tokyo-Central

KOREA

Chulpanmul
Phenjan

NORWAY

Tanum-Cammermeyer
Karl Johansgt 41—43
Oslo 1

POLAND

Ruch
ul. Wronia 23
Warszawa

ROUMANIA

Cartimex
Str. Aristide Briand 14—18
Bucureşti

SOVIET UNION

Mezhdunarodnaya Kniga
Moscow G—200

SWEDEN

Almquist and Wiksell
Gamla Brogatan 26
S—101 20 Stockholm

USA

F. W. Faxon Co. Inc.
15 Southwest Park
Westwood Mass. 02090
Stechert Hafner Inc.
31. East 10th Street
New York, N. Y. 10003

VIETNAM

Xunhasaba
19, Tran Quoc Toan
Hanoi

YUGOSLAVIA

Forum
Vojvode Mišića broj 1
Novi Sad
Jugoslovenska Knjiga
Terazije 27
Beograd

8. II. 1974. Index: 26.025

ACTA TECHNICA

ACADEMIAE SCIENTIARUM HUNGARICAE

REDIGIT: M. MAJOR

TOMUS 76
FASCICULI 3—4

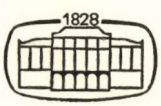

AKADÉMIAI KIADÓ, BUDAPEST 1974

ACTA TECHNICA

SZERKESZTŐ BIZOTTSÁG

BARTA ISTVÁN, BÖLCSKEI ELEMÉR, GESZTI P. OTTÓ,
HELLER LÁSZLÓ

Az *Acta Technica* angol, francia, német és orosz nyelven közöl értekezéseket a műszaki tudományok köréből.

Az *Acta Technica* változó terjedelmű füzetekben jelenik meg, több füzet alkot egy kötetet.

A közlésre szánt kéziratok a következő címre küldendők:

Acta Technica
1051 Budapest, Münnich Ferenc u. 7.

Ugyanerre a címre küldendő minden szerkesztőségi és kiadóhivatali levelezés.

Megrendelhető a belföld számára az „Akadémiai Kiadó"-nál (1363 Budapest Pf. 24. Bankszámla 215 11448) a külföld számára pedig a „Kultúra" Könyv- és Hírlap Külkereskedelmi Vállalatnál (1389 Budapest 62, P.O.B. 149 Bankszámla: 218 10990) vagy annak külföldi képviseleteinél és bizományosainál.

Die *Acta Technica* veröffentlichen Abhandlungen aus dem Bereiche der technischen Wissenschaften in deutscher, englischer, französischer und russischer Sprache.

Die *Acta Technica* erscheinen in Heften wechselnden Umfanges. Vier Hefte bilden einen Band.

Die zur Veröffentlichung bestimmten Manuskripte sind an folgende Adresse zu senden:

Acta Technica
1051 Budapest,
Münnich Ferenc u. 7.
Ungarn

An die gleiche Anschrift ist auch jede für die Schriftleitung und den Verlag bestimmte Korrespondenz zu richten. Abonnementspreis pro Band: $ 32.00

Bestellbar bei dem Buch- und Zeitungs-Außenhandels-Unternehmen »Kultúra« (1389 Budapest 62, P.O.B. 149 Bankkonto Nr. 218 10990) oder bei seinen Auslandsvertretungen und Kommissionären.

Acta Technica Academiae Scientiarum Hungaricae, Tomus 76 (3–4), pp 243–247 (1974)

J. A. VERŐ 70 JAHRE



Ein besonderes Erlebnis wurde allen jenen Teil, die am 26. Januar d. J. das Budapester Eisenforschungsinstitut betraten. Schon beim Eingang umwähte den Eintretenden eine unfaßbare Atmosphäre, die man nur bei sich zu Feierlichkeiten vorbereitenden, großen Familien, beim unerwarteten Eintreffen spürt. Jeder begrüßte im Institut aufs herzlichste József VERŐ, den Menschen, das Beispiel, den Freund, den Wissenschaftler und den amtlichen Chef.

József VERŐ wurde begrüßt, das mit dem Kossuth-Preis zweifach ausgezeichnete o. Mitglied der Ungarischen Akademie der Wissenschaften, das Beispiel seiner zahllosen Schüler, denn seine alltägliche Tätigkeit und sein ganzer Lebenslauf beweist, daß von Begabung begleiteter Fleiß und leidenschaftliche Liebe zum Fachgebiet nicht nur offizielle Anerkennung, sondern auch ausgeglichene Zufriedenheit mit sich bringen können. Dies zeigen alle Ereignisse der vergangenen 70 Jahre. Jetzt, da anläßlich des freudenvollen Feiertages alle Bekannten zu weiteren Erfolgen das Beste wünschen, wollen wir einige wesentliche Stationen jenes Lebenslaufes überblicken, durch die der Gefeierte zu einem der hervorragendsten Personalitäten des ungarischen wissenschaftlichen Lebens wurde.

Prof. VERŐ kam in Sopron, im Jahre 1904 auf die Welt. Sein Vater war Facharbeiter in einem kleingewerblichen Betrieb. Er absolvierte die Elementar- und die Mittelschule ebenfalls in Sopron, wo er auch sein Abitur mit Auszeichnung bestand. Danach wurde er an der damals in seiner Heimatstadt seßhaf-

ten Hochschule für Berg-, Hütten- und Forstwesen immatrikuliert. Im Eisenhütten-Fach studierte er so erfolgreich, daß er 1926 als Beweis der Anerkennung seiner Professoren nicht nur sein »vorzüglich« qualifiziertes Diplom erhielt, sondern zur Zeit des Überreichens des Diplomes schon Assistent am Lehrstuhl für Eisenhüttenkunde war. Nach kurzer, einjähriger Arbeit studierte er als Stipendiat an der Technischen Hochschule Berlin Metallographie und Materialprüfung. Nach seiner Heimkehr erhielt er von der Soproner Hochschule den Lehrauftrag, »Metallographie« und »Technologie der Metalle« zu lesen. Während seiner Hochschul- bzw. Universitäts-Tätigkeit wurde er 1934 zum Oberassistenten, 1940 zum Dozenten, 1943 zum a. o. Professor und endlich 1947 zum o. Professor ernannt.

Die Lehrtätigkeit und die pädagogische Arbeit hat Prof. VERŐ nie unterbrochen, bis er im Jahre 1968 seine bis dahin schon längst nach Miskolc übersiedelte, zur Technischen Universität umgestaltete, erste Arbeitsstelle verließ. Seit 1928 unterrichtete er Generationen der zukünftigen Hütteningenieure. Obwohl ihn die Regierung als Pädagogen mehrmals auszeichnete, bedeutet seine größte Anerkennung eher die Tatsache, daß seine Schüler nicht nur den Wissenschaftler in ihm ehren, sondern ihn liebevoll umgeben, als einen älteren Fachmann, den sie auch Jahre nach dem Erwerben ihre Diplome, mit allen ihren Problemen getrost aufsuchen können. Immer findet er Zeit für seine Schüler und Mitarbeiter, um mit ihnen, immitten seiner äußerst großen Inanspruchnahme, bestehende Schwierigkeiten zu besprechen, und ihnen zu helfen, die Schwierigkeiten zu überwinden. Vielleicht einzigartig ist seine Eigenschaft, daß seine immer objektive Kritik den ihn Aufsuchenden nicht verstimmt, sondern ermutigt. Jeder fühlt in seiner zum Ausdruck gebrachten Meinung die Hilfsbereitschaft und die uneigennützige Unterstützung.

Eine weitere Anerkennung seiner Lehrtätigkeit ist die Ehre, mit der ihn nicht nur die Lehrkräfte der Hüttenmännischen Fakultät, sondern alle Lehrkräfte der ganzen Miskolcer Technischen Universität für Schwerindustrie, auch heute noch, nach Jahren seines Abschiedes umgeben.

Während seiner ganzen Lehrtätigkeit befaßte sich Prof. VERŐ am liebsten mit Metallographie und mit Materialprüfung, obwohl er mitunter auch über andere Fachgebiete vorlas. Zur Zeit seiner ersten Assistentenjahre war die Metallographie nur ein Haufwerk phenomenologisch beobachteter Kenntnisse. Diese Kenntnisse erweiterte er nicht durch eigene Meß- und Forschungsergebnisse, sondern er suchte von Anfang an auch die erfahrungsmäßigen Tatsachen miteinander zu verbinden und die naturwissenschaftlichen Ursachen zu finden. In unserem Lande war er der Begründer jener Metallkunde, die mit ihren gut fundierten Gesetzen und Zusammenhängen ein natürliches Zubehör unseres sich auf Metalle und auf Legierungen bezüglichen Weltbildes ist.

In seiner pädagogischen Tätigkeit betonte er nicht nur, sondern verwirklichte auch seinen Standpunkt, nach dem ein hochstehender Universitäts-

unterricht nicht ohne zeitgemäße, wissenschaftliche Forschung bestehen kann. Deshalb arbeitete er immer auch an Forschungsaufgaben. Es ist sehr schwer, aus dieser Arbeit etwas herauszuheben, denn alle Ergebnisse sind eng in den naturwissenschaftlichen Begründungsvorgang der Metallographie eingelagert. Prof. VERŐ arbeitete zahlreiche Züge der Zustandsschaubilder der ternären Cu—Ni—Sn-, der Cu—Pb—Sn-, der Cu—P—Sn- und der Cu—Mn—Sn-Legierungsreihen aus, forschte aber auch bei Legierungen mit kompliziertesten Phasenverhältnissen des Cu—Sn-Systemes nach Einzelheiten der Gleichgewichtsbedingungen.

Im Interesse des besseren Verständnisses der Phasenverhältnisse der mehrkomponentigen Legierungssysteme untersuchte er die Kristallisationsbedingungen der Schmelzen, und deutete sie theoretisch. Er wies die auf die Kristallisation zurückzuführenden Ursachen der Warmrisse und der Seigerungen nach. Er erkannte nicht nur, sondern bewies auch die kornverfeinernde Wirkung der in die Schmelze eingeführten künstlichen Keime, und stellte die Stabilität dieser Keime fest.

Er erkannte, welche große Rolle jene Umwandlungen bei der Bestimmung der Eigenschaften der Metalle und der Legierungen spielen, die in den Metallen während des Verarbeitens, infolge der Temperaturänderungen vor sich gehen. Er führte quantitative Untersuchungen über die Temperatur- und zeitliche Abhängigkeit dieser Vorgänge durch, um sie als Ingenieur, den technologischen Umständen entsprechend in der Hand halten, und nach Möglichkeit auch beeinflußen zu können. Eng zum Wesen dieser Arbeit gehört der Umstand, daß im Stahl — in diesem in größter Menge hergestellten Konstruktionsmaterial — die während des Abkühlens vor sich gehenden Umwandlungen die mechanischen Eigenschaften festlegen. Zum Kennenlernen dieser Verhältnisse wurden von ihm jene Forschungen in die Wege geleitet, als deren Ergebnisse er feststellte, in welche Verteilung und Menge die verschiedenen Phasen im Stahl entstehen. Er forschte die Ausbildung der primären und sekundären Gefügebestandteile in Abhängigkeit von der Wanddicke und von der Wärmebehandlung, im Interesse der Qualitätsverbesserung der gegossenen Materialien. Die Meßergebnisse wurden von ihm naturwissenschaftlich gedeutet.

Prof. VERŐ stellte fest, wie der Kohlenstoffgehalt des unlegierten Stahles während der Wärmebehandlung in Abhängigkeit von der Temperatur und von der Glühdauer abnimmt. Um die Qualität der Schnellarbeitsstähle verbessern zu können, erforschte er die Verfeinerung der eutektischen Karbide während des Schmiedens.

Obige Forschungen waren seinerzeit bei Weitem nicht mit solchen modernen Mitteln versehen, wie dies heutzutage ziemlich selbstverständlich ist. Meistens entwickelte er deshalb die Methoden, mit denen er dann die gewünschten Versuche durchführen konnte. So entwickelte er eine ganze Reihe metallographischer Verfahren, unter Anderen zur quantitativen Gefügeanalyse

und eine Technik der Messung der Korngröße. Er brachte ein Verfahren zum Nachweis der Resultate der in gegossenen Gefügen mit Diffusion vor sich gehenden Homogenisierungsvorgänge zustande. Als Erster im Lande verwendete er das elektrolytische Polieren bei metallographischen Untersuchungen, und brachte dieses Verfahren der industriellen Anwendung näher. Erfolgreiche Forschungen führte er auch im Zusammenhang mit der Qualifizierung der Einschlüsse bei Stählen durch. Ein dilatometrisches Verfahren wurde von ihm zum Feststellen der Solidustemperatur der Zustandsschaubilder entwickelt; usw.

Es konnte nur ein Auszug jener wissenschaftlichen und technischen Forschungs- bzw. Entwicklungsarbeit angedeutet werden, der sich Prof. VERŐ immer mit so großer Liebe widmete, und mit der er auch Anderen Lust zur wissenschaftlichen Arbeit machte. Letzteres erreichte er nicht nur durch diese Erfolge, die seinen wissenschaftlichen Veröffentlichungen einheimische und internationale Anerkennung sicherten, sondern auch durch seine Anschauung, mit der seine Nachfolger die naturwissenschaftlichen Ergebnisse, im Dienste unserer Industrie, über die Laboratorien hinausgehend, auch bei großindustriellen Vorgängen in immer breiterem Kreise verwerten.

Unvergänglicher Dienst Prof. VERŐS ist das Zustandebringen einer einheimischen metallographischen bzw. metallkundlichen Schule, nicht nur durch seine Universitätsvorlesungen, sondern auch dadurch, daß bis jetzt acht Bücher von ihm erschienen sind. In diesen Bändern ist die jeweilige Entwicklung der Metallkunde klar zu verfolgen, denn er gab in ihnen immer die Zusammenfassung der modernsten Ergebnisse.

Über seine wissenschaftliche Tätigkeit berichtete er bis jetzt — außer in seinen acht Büchern —, in mehr als 140, in einheimischen und internationalen Zeitschriften erschienenen Mitteilungen. Er hielt anläßlich verschiedener Konferenzen Europas zahlreiche Vorträge. Obwohl seine Bücher größtenteils als Lehrmaterial herausgegeben worden sind, können sie nicht nur in der Bibliothek der Studenten der Hüttenmännischen Fakultät aufgefunden werden, sondern auch bei jedem praktizierenden Hütteningenieur und bei jedem anderen Fachmann, der irgendwie etwas mit der Technologie der metallischen Werkstoffe zu tun hat. Dies machte seinen Namen allgemein bekannt, und brachte ihm die aufrichtige Anerkennung bei. In seinen Büchern deutet und betont er klar das Wesen der inneren Zusammenhänge, und das ist für uns der beste Leitfaden im Labyrinth der Kenntnisse und der Technologien der Metalle.

Prof József VERŐ wurde von der Ungarischen Akademie der Wissenschaften im Jahre 1948 zum korrespondierenden, im Jahre 1949 zum ordentlichen Mitglied gewählt. Bei der Akademie nahm und nimmt er bis heute die verschiedensten Posten ein, und ist der angesehenste und gebildeteste Sachverständige der sich mit den Metallen und den Technologien befassenden Ausschüsse.

J. Prohászka

Auszeichnuugen von J. A. Verő

Kossuth Staatspreis II. (1949), Ehrenmedaille der Ungarischen Volksrepublik (1952), Ehrenmedaille der Ungarischen Volksrepublik (1954), Goldene Verdienst-Medaille (1956), Kossuth Staatspreis II. (1958), Heinrich Fassole-Ehrenmedaille (1958), Goldene Verdienstmedaille (1964), Goldene Verdienstmedaille (1969), GoldeneVerdienstmedaille (1974).

Fach-und Lehrbücher von J. A. Verő

1. *Metallográfia* (Metallographie). Herausgegeben von der Berg- und Hüttenmännischen Fakultät, Sopron 1942. und 1944.
2. *A mikroszkópos fémvizsgálat módszerei* (Methoden der mikroskopischen Metalluntersuchung) Mérnöki Továbbképző Intézet (Ingenieur-Fortbildungs-Institut), Budapest 1944. Nr. G 46.
3. *Az ipari vasötvözetek metallográfiája* (Metallkunde der industriellen Eisenlegierungen). Mérnöki Továbbképző Intézet (Ingenieur-Fortbildungs-Institut), Budapest, 1948. Nr. G 79.
4. *Vas- és fémipari anyagvizsgálat* (Materialprüfung in der Eisen- und Metallindustrie). Tankönyvkiadó, Budapest 1951, 1954, 1959 und 1966 (vier Auflagen).
5. *Általános metallográfia* (Allgemeine Metallkunde) Bd. I. und II. Akadémiai Kiadó, Budapest 1955, 1956.
6. *Az ipari vasötvözetek metallográfiája* (Metallkunde der industriellen Eisenlegierungen) Bd. I. und II. Akadémiai Kiadó, Budapest 1960, 1964.
7. *A vasötvözetek fémtana* (Metallkunde der Eisenlegierungen) Műszaki Kiadó, Budapest 1966 und 1971 (zwei Auflagen). (Gemeinsam mit M. KÁLDOR).
8. *Fémtan* (Metallkunde). Tankönyvkiadó, Budapest 1969, 1970 und 1973 (drei Auflagen).

Acta Technica Academiae Scientiarum Hungaricae, Tomus 76 (3—4), pp. 249—257 (1974)

A. MÁNDI

1891—1972

The death of Andor MÁNDI is a great loss for the science of heavy-current electric engineering and, particularly, for the field of electric machines. He was one of the most outstanding representatives of the "second generation" following the BLÁTHY, DÉRI, and ZIPERNOWSKY trio, dealing successfully with both the theory and practice of the electric machinery area. His engineering constructions, theoretical explanations, ingenious problem solvings, all characterize this excellent engineering scientist. And he exhibited similarly valuable human features. His associates, friends, and admirers loved him as a just man.

Andor MÁNDI was born in Budapest, on the 23rd of September, 1891. He has graduated from the Technical University of Berlin-Charlottenburg, and won his diploma of mechanical engineering in 1914.

In the First World War he joined the army, and as a wounded Serbian POW was released only in 1916. He was honorably discharged in 1918 as a first lieutenant of the signal corps.

In 1919, during the Councils' Republic, he was telegraph official of the District Headquarters, then manager of a coiler shop.

He was working as a designer in the Manfred Weiss Co., Csepel, in 1920, but in 1921 he joined the Ganz Electric Engineering enterprise where he stayed until 1959.

First, he was assigned to the transmission department, then to the machine design and calculation section which he was leading from 1933 on, at the beginning as senior engineer and subsequently as director. Simultaneously, from 1950 on, he was a professor of the Budapest Technical University, and was lecturing on "Large-size electric machines".

As a designer, he has dealt with the calculation and construction of all the electric machinery types; he was an innovator in every field. While with the Ganz Works, he has directed the production and development of new machine families, such as the medium output induction motors, or the distributed-polar-rotor-type synchronous generators and the synchronized asynchronous motors developed from the above induction motors. He was the first

one to derive from the commutation conditions of DC machines the proportionality of output to rotor diameter. He has elaborated the dimensioning specifications of single-armature converters, on which basis the 1000—1500-kW street-cars have been then produced. Some of them are still in operation.

He has solved independently a number of theoretical problems without any starting point available either home or abroad. Thus, for example, he has composed and published a study under the title "Asymmetries and overtones in electric machinery" where he suggested entirely new specifications for the coiling technique to be used with certain machine types. In 1930 he has studied the Scherbius pump motors and, by introducing a special connection, he could eliminate the oscillation of these machines.

In 1940 he has modified the old Dahlander connection of insufficient utilization possibility, and suggested a new 1 : 2 pole change-over. This solution was described in the Hungarian and foreign periodicals in detail, just like in the volumes by NÜRNBERG and SEQUENZ, well-known all over the world, who emphasized the advantage of the new solution in its making possible a much better utilization. In the Preface of his volume, NÜRNBERG made a special mention on Andor MÁNDI.

In 1929 MÁNDI joined the efforts to develop railway electrification. The Ganz Works entrusted to Otto BLÁTHY the supervision of the phase converter calculations, and to Andor MÁNDI that of the main driving motor. Kálmán KANDÓ accepted the suggestions submitted by MÁNDI, and the motors have been produced with these modifications. Subsequent engines employed the single-drive technique. The two experimental engines had squirrel cage rotors, where starting the motor with a low frequency represented a difficult problem. This, however, was recognized and successfully overcome by MÁNDI, as early as in the design stage.

After the Second World War the engines of the Hungarian Railways have been produced with a frequency converter of no separate driving motor but directly connected to slip-ring motors and phase converter, according to Mándi's patent.

Ever since 1930 Andor MÁNDI was the pupil and closest associate of Otto BLÁTHY in the calculation and construction of synchronous machines, particularly turbogenerators. In 1938, after BLÁTHY's death, the need of increasing the limit output achieved by high operational safety turborotors of the parallel slot type, and the necessity of their better utilization, have emerged. The solution suggested by MÁNDI, that is, the cross-coil rotor, increased the output limit to 50 MW maintaining, at the same time, all the advantages of the parallel slot rotor of BLÁTHY, and enhanced machine utilization by 25 to 40 per cent. Ganz Works still produce turbogenerators up to 50 MW. The cross-coil system was described in the periodical *Elektrotechnika*, and the Hungarian Electrotechnical Association awarded this publication

with the "Zipernowsky Anniversary Prize". The *Engineers Digest* published an article on Mándi's turbosystem in 1947.

MÁNDI has left the Ganz Works in 1959, and started working for the United Electric Machinery, dealing mainly with the overheat of large-size closed motors, in which context he has elaborated a completely new measurement method. The new method was highly appreciated as it has extended the indirect (idling and short) technique usually adopted for synchronous machines also to induction motors, by using reduced voltage measurement instead of shorting. Thereby, the measurement of warming up could be performed with motors of a capacity multiple of that of the test room and, at the same time, the additional losses could be determined with a high accuracy.

MÁNDI has, furthermore, composed studies for the Research Institute of Automation, Hungarian Academy of Sciences, on the autodyne dimensioning problems.

His textbook "Large-size Electric Machines", prepared to supplement his technical university lectures, had two editions, and its chapter on overheat was adopted by József LISKA for his volume "Electric Machinery".

In 1969, upon the commission of the State Office for Technical Development, MÁNDI wrote a comprehensive study under the title "Possibilities provided for by heat-resistant insulators in the production of electric machines".

He was member for life of the Heavy Current Electric Committee of the Hungarian Academy of Sciences, and was active in the Budapest Technical University even after he was pensioned, participating mainly in investigations on overheat problems.

The outstanding activity and the results of his long life have been awarded by the Emblem of Excellent Worker, Stachanovist, 5th Class of the Order of the Hungarian People's Republic, 2nd Class of the Kossuth Prize, and the Order of the Red Banner of Work.

On the occasion of his 80th birthday the Department of Electric Machines of the Budapest Technical University, the Ganz Works and the United Electric Machinery, his friends, associates, pupils, etc. organized a hearty celebration. The Hungarian Electrotechnical Association elected him honorary president.

During the anniversary celebration he still attempted to conceal with good spirit, strong will, and his old sense of humour the symptoms of tormenting pains caused by the fatal disease, although he must have felt the approaching end.

We all have escorted him on his last trip to the Farkasrét Cemetery on the 28th August. At his grave the representatives of the Hungarian Electrotechnical Association, the United Electric Machinery, the Ganz Works, and

the Technical University Department of Electric Machines bid a farewell to Andor MÁNDI, with the firm intention of never forgetting his exemplary career, creative activity, and exceptional human character.

K. P. Kovács

Scientific publications by Andor Mándi

1. Pole Conversion, 1 : 2 (modified Dahlander connection) — *Elektrotechnika*, 1940, No 4
2. New Development in the Structure of Turbogenerators — *Elektrotechnika*, 1946, No 1—5
3. Urgent Problems of Electric Railway Traction — *Elektrotechnika*, 1947, No 1
4. Aluminium Application in Electric Machinery, Transformers and Appliances (co-author: M. GOHÉR) — *MTI Aluminium Yearbook*, 1948
5. Asymmetries and Overtones in Electric Machines — *MTI* 1952—53 *Lecture Series*, No 2080
6. Overheat and Cooling of Synchronous Machines (in J. LISKA: Electric Machines, Vol III, Chapter XXV, 1955)
7. Asymmetries and Overtones in Electric Machines — *Hung. Acad. Sci., Dept. Eng. Sci.*, **23,** 1959, No 3—4
8. In Commemoration of Ottó Bláthy — *Hung. Acad. Sci., Dept. Eng. Sci.*, **28,** 1961, No 1—4
9. In Memory of Ottó Titus Bláthy — *Acta Techn. Hung.*, **34,** (in English), 1961 No 1—2
10. A New Method for Testing Induction Motors — *Elektrotechnika*, 1961, No 1—2
11. Measuring the Overheat of Induction Motors with an Indirect Method — *VK Bulletins*, Dec. 1962, No 2
12. Special Measurements in Electric Machines — *VK Anniversary Yearbook:* The 50 Years of the Electrice Machinery and Cable Works in the Development of the Hungarian Electric Industry, 1913—1963
13. Measurement of the Additional Losses of Induction Motors — *EVIG Bulletins*, 1964, No 1
14. Lamination Build-up for up-to-date Motors — *Elektrotechnika*, 1965, No 2—3, and *EVIG Bulletins*, 1965, No 2
15. Crane Motor Speed Control by Braking Mechanism — *Elektrotechnika*, 1963, No 11—12
16. Theoretical Problems of Autodyne Dimensioning — *Hung. Acad. Sci., Res. Inst. Aut.*, 1965, No 7
17. Development of the Four-pole Autodyne Family — *Hung. Acad. Sci., Res. Inst. Aut.*, 1965, No 9
18. Overheat and Cooling of Synchronous Machines, 1966 (2nd ed. of Chapter XXV under (6); J. LISKA: Electric Machines, Vol III)
19. Large-size Electric Machines (Manuscript, Tankönyvkiadó, Budapest 1968; 2nd revised ed. of author's textbook for the Budapest Technical University, 148 pp.; 1st ed. in 1951)
20. Possibilities Provided for by Heat Resistant Insulators in the Production of Electric Machines — *Elektrotechnika* 1969, No 2—3 (part of a study by the State Office of Technical Development on a similar subject)
21. Pole Conversion, 1 : 2 — *EuM* 1941 (in English)
22. New Development in the Design of High-speed Turbogenerators — *Engineers Digest* 1947, 1 (in English)
23. Wicklung für Polumschaltung 1 : 2, nach MÁNDI—NÜRNBERG: Die Asynchronmaschine, Springer Verlag, 1952, 316—318 (in German)
24. Schaltung von Ganz und Co, nach Andor MÁNDI -SEQUENZ: Die Wicklungen elektrischer Maschinen, III, 48—49, Springer Verlag 1954 (in German)
25. Liquid-cooled Rotor for Electric Machines — CIGRÉ 1956 (page 3, para. 5)
26. Ein Vorschlag zur Bestimmung des Wirkungsgrades und der Erwärmung von Induktionsmotoren — *EuM* 1962 August (in German)
27. Contribution to the Paper by Dr. M. SEIDNER: "Water-cooled Turbogenerator Rotors" — *Elektrotechnika* 1955, No 4
28. "Dr. Mihály SEIDNER" — *Elektrotechnika* 1968, No 12

Patents by A. Mándi

1. Pole Conversion, 1 : 2 (modified Dahlander connection) — Hungarian Standard No 123828, 3 Febr. 1939
2. Cross-coiled Turbogenerator — H.S. 131868, 27 Dec 1941
3. Electric Engine with Mechanically Switched Phase and Frequency Converter — H.S. 142132, March 1946 (descriptions in the 1947 issues of the periodicals *Elektrotechnika*, *Magyar Technika*, and *Nehézipar*)
4. Electric Machine with a Coil of p : 2p : 3p Convertible Pole Number (improvement of the patent under (1), 27 Sept 1954)
5. Liquid-cooled Rotor for Electric Machines, 20 Nov. 1954 (a new arrangement for the improvement of the heat transfer, as applied in the phase converter; introduced at the 1956 CIGRÉ session: Essais d'amélioration du refroidissement des turbo-alternateurs)

M. Gohér—K. P. Kovács

Acta Technica Academiae Scientiarum Hungaricae, Tomus 76 (3—4), p. 255 (1974)

CRITICAL SUMMARY OF THE DESIGN METHODS OF FORM-INDEPENDENT THIN TRIPLET SYSTEMS*

P. KALLÓ**

[Manuscript received January 18, 1974]

The creation of the very first objectives, as a result of deliberate calculations, should be attributed to József PETZVÁL and Harold Denis TAYLOR, in the late 19th century. PETZVÁL designed his objective somewhat earlier, whereas the construction by TAYLOR had a better concept, and was much more suitable for generalization. TAYLOR patented his triplet about 80 years ago, and this construction has been repeatedly subject to analysis ever since, because of its simplicity and diverse adaptabilities. However, the triplet theory cannot be considered as settled as yet, particularly if stricter requirements are set to the initial phase of design than was so far, just like the definition and solution of the problems related to the form-independent thin system of the triplet.

As a starting point, the specification or assumption of only the data concerning the whole of the triplet's thin system (focal length, overall length, relative aperture, image distance) is considered as permissible. Our aim is to determine the values of minimum objective length and the maximum focal length of the components for which a new method, entirely different from the starting methods and procedures found in the literature that we were in a position to review, will be described. The simplicity and high speed of the new method, as well as its capability to reveal all the relations of the whole problem will be illustratred by a numerical example.

The new method to be described is of conceptional importance, its validity goes far beyond the triplets, as it is suitable for the exploration of the possibilities hidden in triplet modifications as well (Tessar, Heliar etc.), and it has a construction whereby, on the basis of the promising results of the preliminary research, it appears to be adaptable for generalization in testing optical systems entirely different from the triplets, too. Finally, in our opinion an indispensable precondition of the fully automatic design of certain optical system types is the application of a new algorithm like the one described above, or similar thereto.

*) Preliminary Report.

**) P. KALLÓ, Kapy. u. 266, 1025 Budapest, Hungary.

Acta Technica Academiae Scientiarum Hungaricae, Tomus 76 (3—4), pp. 257—272 (1974)

EXAMINATION OF THE STRUCTURE OF FUNCTIONAL RELATIONS AMONG PHYSICAL QUANTITIES AND SOME APPLICATION THEREOF IN DISCHARGE PHYSICS

J. F. BITÓ*
DOCTOR OF TECHN. SC.

and

K. G. ANTAL**

(Manuscript received April 5, 1972)

Theorem π, the basis of the dimension theory, and starting from the same, the structure of functional relations among physical quantities, are being analyzed. The practical application of the theorem π is demonstrated on a classical mechanical example and its field of application is later extended to discharge physics. The dimension theory which is methodically simple but at the same time suitable for the deduction of useful conclusions may be advantegeously applied in discharge physics. The analysis of the function systems, requiring great mathematical apparatus and solvable only by the application of approximative methods, further the analysis of the working hypotheses is facilitated and accelerated by the application of theorem π.

1. Introduction

The physical rules determined in a theoretical or experimental way, may be characterized by the interactions and connections, characteristic of the single processes. The value of the investigated physical quantities depends on the chosen and applied unit system, but the examined rule is, of course, not influenced thereby. Consequently, the physical rules being independent of the chosen co-ordinate system have a special structure. That fact permits the exploration of the general interactions among the parameters, or group of parameters reflecting that rule [1].

2. The structure of functional connections among physical quantities

A quantity a, the dimension of which is given, may be produced as the function of parameters a_1, a_2, a_3, . . . , a_n, this also having a dimension, but being independent of each other:

$$a = f(a_1, a_2, a_3, \ldots, a_n) \tag{1}$$

* Dr. J. F. Bitó, Korompai u. 22/a, 1124 Budapest, Hungary
** K. G. Antal, Vécsey ltp. 4. ép. fsz. 3, 1204 Budapest, Hungary

The independence of parameters $a_1, a_2, a_3, \ldots, a_n$ means, in a given case, physical independence and not that of the measuring units; some of them may stand in the given process as a constant (e. g. in circumstances on the Earth, the value of the gravitation in certain physical models).

Establishing the structure of the function (1), we presuppose that the same is characteristic of a physical rule, i.e., it is independent of the applied unit system.

Let us regard the case when among the parameters

$$a_1, a_2, a_3, \ldots, a_k, a_{k+1}, \ldots, a_n \tag{2}$$

having dimension, the first k parameters ($k < n$) are independent in dimension of each other.

In the analysis of the structure of functional connections the subsidiary theorem may be applied that the dimension of whatever physical quantity may be unambigously given by the monomial power function of the basic dimensions of the chosen ground system of units. In the system CGS, e.g., any dimension D can be given by the following power function:

$$D = L^l M^m T^t \tag{3}$$

where L dimension of length,
M dimension of mass,
T dimension of time,
l, m, t exponents.

By the application of this subsidiary theorem it becomes evident that dimensions of length, velocity and energy, L, L/T and ML^2/T^2 are independent of each other, in contradiction to this, the dimensions of length, velocity and energy, L, L/T, resp. L/T^2, do not form an independent system. Among the mechanical quantities, in general, there are to be found not more than three dimensions independent of each other.

The dimensions of the above mentioned k parameters, being members of the parameter series (2) may be represented in the usual way:

$$[a_1] = A_1, \; [a_2] = A_2, \; [a_3] = A_3, \ldots, \; [a_k] = A_k \tag{4}$$

In this case, in accordance with the previous statements, the dimension of each parameter a_i, for the index i of which the one equality

$$k \leq i \leq n \tag{5}$$

is valid, may be produced as a power function of the dimension of parameters pertaining to number k, with an independent dimension. Accordingly, the

dimension of quantity a may be produced with the aid of the power function, containing the basic dimensions:

$$\begin{aligned} [a_{k+1}] &= A_1^{p_1} A_2^{p_2} A_3^{p_3} \dots A_k^{p_k} \\ &\vdots \\ [a_n] &= A_1^{q_1} A_2^{q_2} A_3^{q_3} \dots A_k^{q_k} \\ [a] &= A_1^{m_1} A_2^{m_2} A_3^{m_3} \dots A_k^{m_k} \end{aligned} \tag{6}$$

where

$$p_i,\ q_i,\ m_i \qquad [l \leq i \leq k]$$

are the exponents.

Let us change the measuring unit of the first, dimensionally independent k parameters in the (2) parameter series with the factors $\alpha_1, \alpha_2, \dots, \alpha_k$, respectively. In that case the numerical value of a, $a_{k+1} \dots a_n$ may be expressed in the new measuring system as follows:

$$\begin{aligned} a_1' &= \alpha_1 a_1, & a' &= \alpha_1^{m_1} \alpha_2^{m_2} \dots \alpha_k^{m_k} a\,, \\ a_2' &= \alpha_2 \alpha_2, & a_{k+1}' &= \alpha_1^{p_1} \alpha_2^{p_2} \dots \alpha_k^{p_k} a_{k+1}\,, \\ &\vdots & & \\ a_k' &= \alpha_k a_k, & a_n' &= \alpha_1^{q_1} \alpha_2^{q_2} \dots \alpha_k^{q_k} a_n\,. \end{aligned} \tag{7}$$

The justification of the product may be proved by the following subsidiary theorem:

$y = g(x_1, \dots, x_n)$ is a quantity, having a certain dimension. Let us change the measuring unit of parameters $x_1, \dots, x_n$ with the factors $\alpha_1, \alpha_2, \dots, \alpha_n$, respectively. It may be stated that for the quotient of the so attained y' and of the quantity y experessed in the original system of units, the following relation is valid:

$$\frac{y}{y'} = \varphi(\alpha_1, \alpha_2, \dots, \alpha_n) = \alpha_1^{m_1} \alpha_2^{m_2} \dots \alpha_n^{m_n}\,. \tag{8}$$

The subsidiary theorem is proved in a more simple case, when y means such a geometric quantity, which is only the function of distances x_1, $\dots$, x_n. The value of the same function y, expressed in another argument system, may be given by y'. Both the y and the y' depend on the measuring unit of parameters, but according to the previous comments, the physical contents of quantity are not influenced by the two different parameter systems. By changing the value of the distances for α_1, the following relation is valid:

$$\frac{y'}{y} = \frac{g(x_1', x_2', \dots, x_n')}{g(x_1, x_2, \dots, x_n)} = \frac{g(x_1' \alpha_1, x_2' \alpha_1, \dots, x_n' \alpha_1)}{g(x_1 \alpha_1, x_2 \alpha_1, \dots, x_n \alpha_1)} \tag{9}$$

i.e., the y'/y is constant independent of the chosen α_1. On the basis of relation (9)

$$\frac{g(x_1\alpha_1, x_2\alpha_2, \ldots, x_n\alpha_1)}{g(x_1, x_2, \ldots, x_n)} = \frac{g(x_1'\alpha_1, x_2'\alpha_1, \ldots, x_n'\alpha_1)}{g(x_1', x_2', \ldots, x_n')} \tag{10}$$

that is to say

$$\frac{y(\alpha_1)}{y(1)} = \frac{y'(\alpha_1)}{y(1)} = \varphi(\alpha_1) \tag{11}$$

the quotient of the examined quantities depends on the quotient of the applied measuring units of length.

Furthermore, the setting up of function y may be taken into account, in which case the extent of the distance is changed by the factor α_2. In this case, according to relation (11)

$$\frac{y(\alpha_1)}{y(1)} = \varphi(\alpha_1) \quad \frac{y(\alpha_2)}{y(1)} = \varphi(\alpha_2) \tag{12}$$

is valid, from which follows that

$$\frac{\varphi(\alpha_1)}{\varphi(\alpha_2)} = \varphi\left(\frac{\alpha_1}{\alpha_2}\right) \tag{13}$$

if

$$x_1' = x_1\alpha_2, \; x_2' = x_2\alpha_2, \ldots, \; x_n' = x_n\alpha_2 \tag{14}$$

transformation is carried out, on the basis of formula (11) it is clear that

$$\frac{y(\alpha_1)}{y(\alpha_2)} = \frac{y(\alpha_1/\alpha_2)}{y(1)} = \varphi\left(\frac{\alpha_1}{\alpha_2}\right). \tag{15}$$

Deriving equation (13) according to α_1, and using

$$\alpha_1 = \alpha_2 = \alpha \tag{16}$$

we obtain the following:

$$\frac{1}{\varphi(\alpha)}\frac{d\varphi}{d\alpha} = \frac{1}{\alpha}\left(\frac{d\varphi(\alpha)}{d\alpha}\right)_{\alpha=1} = \frac{m}{\alpha}. \tag{17}$$

By the integration of equation (17) we obtain the relation

$$\varphi = C\,\alpha^m \tag{18}$$

As in the case of $\alpha = 1$ $\varphi = 1$ and accordingly $C = 1$, so

$$\varphi = \alpha^m \tag{19}$$

It can easily be understood that in such a manner we get the relation we looked for also in a more general case by the the transformation with $\alpha_1, \alpha_2, \ldots, \alpha_n$, in the following form:

$$\varphi = \alpha_1^{m_1} \alpha_2^{m_2} \ldots \alpha_n^{m_n} \tag{20}$$

Our subsidiary theorem is proved thereby, production (7) is correct.

Accordingly, the original function given in equation (1) takes, in the new system of units (7), the following form:

$$\begin{aligned} a' = \alpha_1^{m_1} \alpha_2^{m_2} \ldots \alpha_k^{m_k} a = \alpha_1^{m_1} \alpha_2^{m_2} \ldots \alpha_k^{m_k} f(a_1, a_2, \ldots, a_n) = \\ = f(\alpha_1 a_1, \ldots, \alpha_k a_k, \alpha_1^{p_1} \alpha_2^{p_2} \ldots \alpha_k^{p_k} a_{k+1}, \ldots, \alpha_1^{q_1} \alpha_2^{q_2} \ldots \alpha_k^{q_k} a_n) \end{aligned} \tag{21}$$

which is evidently homogenous referring to transformation factors $\alpha_1, \alpha_2, \ldots, \alpha_n$ which are otherwise optional. Their arbitrary selection allows the application of the following transformation factors:

$$\alpha_1 = \frac{1}{a_1}, \quad \alpha_2 = \frac{1}{a_2}, \ldots, \quad \alpha_k = \frac{1}{a_k}, \tag{22}$$

so each of the first k, argumentum of function (1) might be replaced by a fixed constant, e.g., by 1.

In this new system the numerical values of parameters $a, a_{k+1}, \ldots, a_n$ are determined by the following formulas:

$$\begin{aligned} \Pi &= \frac{a}{a_1^{m_1} a_2^{m_2} \ldots a_k^{m_k}}, \\ \Pi_1 &= \frac{a_{k+1}}{a_1^{p_1} a_2^{p_2} \ldots a_k^{p_k}}, \\ &\ldots\ldots\ldots\ldots \\ \Pi_{n-k} &= \frac{a_n}{a_1^{q_1} a_2^{q_2} \ldots a_k^{q_k}} \end{aligned} \tag{23}$$

where $a, a_1, a_2, \ldots, a_n$ are the numerical values of the examined parameters, taken in the original measuring system. It is easily understandable that the numerical values $\Pi, \Pi_1, \ldots, \Pi_{n-k}$ are independent of the system of unit applied at the starting point, i.e., they are members of zero order — compared to dimensions $A_1, A_2, \ldots, A_k$. Accordingly, the quantities $\Pi, \Pi_1, \ldots, \Pi_{n-k}$ are considered as being without dimension. By the application of the transformed system of units, function (1) may be transcribed to the following form:

$$\Pi = f(1, 1, \ldots, 1, \Pi_1, \ldots, \Pi_{n-k}). \tag{24}$$

Thereby we have arrived at the so-called theorem Π, according to which the relation existing between quantities a, a_1, a_2, . . . , a_n and possessing dimension $n + 1$, may be replaced independently of the chosen system of measuring units by the relation among $n + 1 - k$ quantity without dimension, where $\Pi, \Pi_1, \ldots, \Pi_{n-k}$ result from the combination of the quantity, disposing of dimension $n + 1$.

In that case, if out of the first k arguments of function (1) one is 0 or infinitive and the function is at those values non-continuous, the transformation for 1 cannot be carried out. In such cases the number of arguments may even exceed $n-k$.

The less the number of parameters, determining the quantity under examination, the more restricted the functional relation, and accordingly, more simple is the analysis too. If the number of the basic dimensions of the basic unit system is the same as that of the parameters with independent dimension determining the physical process, i.e.,

$$n = k \tag{25}$$

then the functional relation may be determined up to a constant factor, on the basis of the theory of measure. Consequently, in the case of $n = k$, it is impossible to set up a combination without a dimension between parameters a_1, a_2, . . . , a_n, i.e., on the basis of equation (23)

$$a = \Pi a_1^{m_1} a_2^{m_2} \ldots a_n^{m_n} \tag{26}$$

relation is valid, where Π is, in that case, a constant without a dimension and the exponents m_1, m_2, . . . , m_n may be obtained on the basis of the exponents of the basic dimensions, characteristic of quantity a, by the solution of an algebraic equation system.

Summarizing what has been registered so far: each connection among physical quantities, having a dimension, may be expressed by a connection among parameters without dimension, formed of the combination of those quantities.

3. Indications of application

With the analysis of the physical process it is suitable to examine first the basic parameters determining that which is essentially important for the examination quantities, i.e., the models formed on the basis of primary consideration. The proper choice of the model, being the first condition for the right solution of the whole task, is often difficult. In many cases the necessity of an alteration of the basis or eventually of the starting hypotheses becomes evident only after the solution of the first task [1].

The system to be examined may be described by the characterization of each physical process only restricted to the phenomena, interests us; by parameters having a finite number of dimensions and by parameters without dimension. In accordance with the previous statements all parameters with dimension must be taken into account, independently of their being constants or variables in a given process. By such an adaptation of the theory of measure less data are needed than by the representation of the functional relation describling the examined process, but the above presented method is more restricted and does not give any information regarding the concrete form of the functions.

For the selection of the parameters determing the physical process, two possibilities are at hand:

a) In that case if the task is mathematically determined, all changing and constant parameters, with and without dimension in the equations and in the starting and boundary conditions as well, must be taken as determining parameters.

b) In the other case, in lack of mathematical relations, the assembly of the determining parameters must be chosen on the basis of the hypothesis regarding the phenomena.

The application of theorem *Π* helps, on the one hand, in the characterization of a quantity occurring in an equation, without the solution of the same, on the other, it helps in controlling our supposition regarding a certain physical process. In the following, some mechanical and discharge-physical examples are presented for the demonstration of the advantages resulting from the application of this method.

4. A mechanical example

Theorem *Π* has so far been applied only for a deeper analysis of the phenomena, occurring in mechanical systems and flowing media [1].

In the following, the applicability is demonstrated on a classical mechanical example, on the mathematical equilibrium (case "a").

Let us consider a mathematical equilibrium of pendiculum length l, and of mass m, for which the following equations of motion may be given, in the case of plane movement:

$$\frac{d^2\varphi}{dt^2} = -\frac{g}{l}\sin\varphi\,, \qquad m\left(\frac{d\varphi}{dt}\right)^2 l = N - mg\cos\varphi \tag{27}$$

with the following starting considerations:

$$t = 0;\ \varphi = \varphi_0; \frac{d\varphi}{dt} = 0 \tag{28}$$

where φ angle of deflection,
t time,
N force effecting the direction of the pendulum,
φ_0 angle of deflection at the moment $t = 0$,
g acceleration of gravitation.

In the following, the equations are not applied, in the knowledge of the same, however, the parameters determining the movement of the pendulum may be given as follows:

$$t,\ l,\ g,\ m,\ \varphi_0 \tag{29}$$

The parameters may be determined, however, also without equation (27) or premises (28), by the application of primary conceptions. Theorem M may be applied now for the determination of the duration of oscillations.

Parameters (29) unambiguously determine the movement of the pendulum and also the angle of deflection which is characterized by the following function:

$$\varphi = f(t,\ \varphi_0,\ l,\ g,\ m) \tag{30}$$

where f is a function without dimension.

By the application of system CGS we take the deflection of the angle as being without dimension. As in an implicite presentation (30) there are four parameters with dimensions, owing to the three basic dimensions of system CGS, one combination, without dimension may be produced. We present, e.g., a combination of time parameters without dimension in accordance with the previous comments, in the following form:

$$\Pi = \frac{t}{l^{m_1} m^{m_2} g^{m_3}} \tag{31}$$

where the dimensions of the determining parameters are:

$$[t] = T;\ [l] = L;\ [m] = M;\ [g] = LT^{-2} \tag{32}$$

Applying expression (31) for the dimensions we obtain relation

$$T = L^{m_1}\ M^{m_2} (LT^{-2})^{m_3} \tag{33}$$

The exponents may be interpreted by equations

$$\begin{aligned} m_1 + m_3 &= 0, \\ m_2 &= 0, \\ -2m_3 &= 1, \end{aligned} \tag{34}$$

with the solution of which, by substitution in equation (31), we get relation

$$\Pi = t \sqrt{\frac{g}{l}} . \tag{35}$$

The required function may be expressed in accordance with the previous comments by parameters without dimension in the form:

$$\varphi = f\left(\varphi_0, t \sqrt{\frac{g}{l}}\right) . \tag{36}$$

Defining the period of that time during which the pendulum returns from deviation φ_0 to its position characterized by deviation φ_0 on the same side, we get by substitution function $\varphi = \varphi_0$

$$\varphi = f\left(\varphi_0, T \sqrt{\frac{g}{l}}\right) . \tag{37}$$

Therefrom it follows that relation

$$T = \sqrt{\frac{l}{g}} \varphi\,(\varphi_0) \tag{38}$$

characterizes, in general cases, the period looked for. Restricting ourselves to small deviations and taking into account the fact that function $\varphi(\varphi_0)$ is even, making an extension with it in the ambiency of $\varphi_0 = 0$, we obtain:

$$\varphi = a_0 + a_1 \varphi_0^2 + a_2 \varphi_0^4 + \ldots \tag{39}$$

and taking into account only the member of zero order of the extension, we get the well-known relation:

$$T = a_0 \sqrt{\frac{l}{g}} . \tag{40}$$

The constant a_0 may be determined experimentally or on the basis of other assumptions, its value is equal to 2π.

Thus we get the period up to the exactness of one constant by the application of theorem Π without the solution of the differential equations, with the aid of elementary calculations.

5. Applications in discharge physics

a) *Plasma frequency*

The plasma frequency plays a very important role in the investigation of the different oscillation phenomena and in the diagnostic techniques in

discharge physics [2]. For the determination of the same up to one constant — also without the solution of the Poisson equation — theorem *II* is suitable (case "b"). On the basis of primary considerations it may be assumed that the plasma frequency may be produced as a function of charge e, of mass m and concentration n:

$$\omega_0 = f(e, m, n) . \tag{41}$$

Making our calculations in the CGS system, the dimensions of parameters are:

$$[\omega_0] = T^{-1};\ [e] = L^{3/2} M^{1/2} T^{-1};\ [m] = M;\ [n] = L^{-3} \tag{42}$$

In our case the number of parameters is the same as that of the basic dimensions. Corresponding to the previous facts, relation

$$\omega_0 = a e^{m_1} m^{m_2} n^{m_3} \tag{43}$$

is to be determined, from which follows

$$T^{-1} = (L^{3/2} M^{1/2} T^{-1})^{m_1} M^{m_2} (L^{-3})^{m_3} \tag{44}$$

From the above formula the following equations are given for the exponents:

$$\begin{aligned} 3/2\ m_1 - 3m_3 &= 0 \\ 1/2\ m_1 + m_2 &= 0 \\ -m_1 &= -1 \end{aligned} \tag{45}$$

by solution of which we obtain relation

$$\omega_0 = a \sqrt{\frac{e^2 n}{m}} \tag{46}$$

which gives the well-known plasma-frequency formula up to the exactness of one constant factor.

b) *Electron mobility*

Theorem *II* may, however, be applied also in more complicated cases correspondingly, it makes a very thorough analysis possible.

Let us consider the case when the charge carriers of the plasma of the discharge space cannot be characterized by the Maxwell–Boltzmann distribution of velocity [3, 4]. Such is the situation, e.g., in the cathode spaces of the discharges, where the distribution of the velocity is perturbated by the local

electric field strength to such an extent that the determination and characterization of the same would be possible only by the solution of a complicated integro-differential equation system. One of the most important microscopic parameters of those special plasmas is the mobility, which at the same time forms a transition between the micro- and macroparameters. That parameter contains, namely, on the one hand, the microparameters, on the other hand it is in connection with the construction, caused by the drift movements of the plasma, otherwise neutral in the state without perturbation. The latter may be measured indirectly and it is a well-determinated function of the perturbation field strength. The analysis of the structure of that function may furnish useful informations for experimental purposes.

Our purpose is the presentation of the possibility of such an adaptation of theorem Π, since the necessity of similar analysis often emerges in discharge physics. The advantages of the application of theorem Π appear explicitly by the extension and simplification of these analysis. By its application, a possibility is given for the comparison by experiments and correction of the theoretically designed models.

The mobility is determined by relation:

$$b = u/e \tag{47}$$

where b mobility
u drift velocity
E electric field strength.

On the basis of primary considerations (case "b") it may be assumed that the mobility depends on charge e, mass m, and collision frequency ν of electrons, and accordingly the relation

$$b = f(e,\ m,\ \nu) \tag{48}$$

may be given. Similarly, taking the system CGS as basis, by the application of theorem Π we obtain for the mobility relation:

$$b = a \frac{e}{m} \frac{1}{\nu}. \tag{49}$$

For a more thorough analysis of the same the collision frequency should be examined, which may be characterized by quotient

$$\nu = \frac{\lambda}{\bar{v}} \tag{50}$$

where λ mean free path of the electrons
$\bar{v}$ average velocity of electrons.

In the case of carrying on the analysis the dependence of the average velocity in certain cases upon certain parameters must be examined. However, for that purpose the simple considerations are not enough any longer. In the following, the previously set objective may be reached in a mathematically expressed case by the application of statistical methods and theorem Π (case "a").

The case being examined is, when the electrons, to be characterized by an arbitrary distribution function of velocity, are moving in a weak electric field. In describing the phenomenon we start from the Boltzmann–Vlasov equation:

$$\frac{\partial f_e}{\partial t} + v\frac{\partial f_e}{\partial r} + \frac{F}{m_e}\frac{\partial f_e}{\partial v} = S \tag{51}$$

where f_e distribution function of electrons,
v velocity of electrons, random velocity,
r coordinates,
m_e mass of the electron,
F external forces,
S collision integral.

In general cases, the external force may be given in the following form:

$$F = e\left(E + \frac{1}{C}v \times H\right). \tag{52}$$

In our case, however, the influence of an external magnetic field is not experienced.

The distribution function is sought for on the basis of the Lorentz extension, making use of its first member only in the following form:

$$f_e(v) = f_0(v) + \frac{u}{v} f_1(v) \tag{53}$$

where f_0 symmetric part of the distribution function f_e
f_1 asymmetric part of distribution function f_e perturbated by a field,
u drift velocity.

Substituting the division, given by equation (53) into equation (51) and applying the Davidov extension of the collision integral [5], we obtain the function system:

$$\frac{eE}{3v^2 m_e}\frac{d}{dv}(v^2 f_1) - \frac{1}{v^2}\frac{d}{dv}\left[\frac{v^3 kTg}{\lambda_e m_g}\frac{\partial f_0}{\partial v} + \frac{v^4 m_e}{\lambda_e m_g} f_0\right] = 0 \tag{54}$$

$$\frac{eE}{m_e}\frac{df_0}{dv} = -\frac{v}{\lambda_e} f_1$$

in the case, if

$$\frac{\partial f_0}{\partial t} = 0\,; \quad \frac{\partial f}{\partial r} = 0; \quad E = \text{const}\,; \quad H = 0 \tag{55}$$

are valid. The signs of the coupled equation system (54) are as follows:

k Boltzmann constant
T_g gas temperature
λ_e mean free path of the electrons
m_g mass of the gas atoms.

The drift velocity and, through it, the current carried by the electrons may be given by the solution of function system (54). In that case relation

$$u = \frac{4\pi}{3} \int f_1 \, v^3 \, \mathrm{d}v \tag{56}$$

may be obtained on the basis of equations (54) by the application of the relatively complicated approximation methods, known so far. For the sake of more exact expression, also the form of f_1 must be determined by the application of equations (54).

In the following, the analysis under different conditions of equations (54) was carried out with the aid of primary methods by the application of theorem *II* and after having solved the task given in a mathematically closed form, through the determination of $\bar{v}$ mean velocity up to the exactness of one constant factor, the drift velocity and the mobility were given.

By the analysis of equations (54), the discussion is treated in the following cases:

a) If the perturbation, caused by field strength E is very small, i.e., in the given equation it may formally be equal to zero.

In such a case in the calculation of the mean velocity in equation (54) the following parameters with independent dimension are to be found:

$$k \cdot T_g \text{ and } m_e$$

where $k \cdot T_g$ has in the CGS system — chosen also here as basis — an energy-dimensioned quantity. With these parameters the following form may be given:

$$\bar{v} = f(kT_g, \; m_e) \tag{57}$$

wherefrom the mean velocity $\bar{v}$ is with the application of theorem *II*:

$$\bar{v} = a \sqrt{\frac{kT_g}{m_e}} \tag{58}$$

determined up to the exactness of a constant factor a.

b) If the gas temperature may be neglected compared to the electron temperature, i.e., the formal substitution $T_g = 0$ may be carried out in the equation, the mean free path of the electrons is taken as being independent of the velocity, which is admissible with a good approximation in the case of some gases, e.g., neon gas.

The determining parameters will be as follows:

$$m_e,\ m_g,\ e,\ E,\ \lambda$$

Let us form thereof the parameter series

$$\frac{m_e}{m_g},\ m_e,\ e,\ E,\ \lambda$$

one member of the same has no dimension. The existence of the series justifies the extension by the introduction of a current dimension of the CGS system, applied so far, namely, in this way the occurring four dimensions become independent basic dimensions. By the application the theorem Π for the mean velocity we get an expression

$$\bar{v} = \Pi\left(\frac{m_e}{m_g}\right)\sqrt{\frac{e\,E\lambda}{m_e}} \tag{59}$$

where the inaccuracy may be eliminated by the correction of the constant deriving from the combination of m_e/m_g by another method. The obtained relation (59) is the average velocity, calculable from the Druyvesteyn distribution function, well-known in discharge physics.

c) Keeping the condition made in case *b)*, for gas temperature T_g, the following case is more general in that sense, that the mean free path of the electrons is taken as dependent on the random velocity. For the majority of gases this case is valid. In the following, we shall deal with gases by which the dependence may be given in the form:

$$\lambda = \Lambda\, v$$

This is valid also for mercury and helium.

The determining parameters in that case are as follows:

$$m_e,\ m_g,\ e,\ E,\ \Lambda$$

Taking again the CGS system of units extended by the current unit as basis, and in view of the fact that Λ is a constant and has a time dimension, we get, by the application of theorem Π, the following relation for the average velocity:

$$\bar{v} = \Pi \left(\frac{m_e}{m_g}\right) \frac{eE\Lambda}{m_e} . \tag{60}$$

The inaccuracy resulting from the application of the method itself appears also in that case in the form of a constant, produced as the combination of m_e/m_g. The examined three cases form a line of analysis becoming successively more and more refined. If the average velocities obtained in this way are substituted into relation (50) and successively into relation (49), we obtain the expressions of the sought for mobility, valid for the analyzed cases:

$$b = \Pi \frac{e}{m_e} \sqrt{\frac{kT_g}{m_e}} \frac{1}{\lambda} , \tag{61}$$

$$b = \Pi \left(\frac{m_e}{m_g}\right) \left(\frac{e}{m_e}\right)^{3/2} \frac{E^{1/2}}{\lambda^{1/2}} , \tag{62}$$

$$b = \Pi \left(\frac{m_e}{m_g}\right) \frac{e}{m_e} \frac{1}{\Lambda} . \tag{63}$$

The relations obtained by the application of theorem Π and by primary methods, offer a possibility for deeper analysis and may be directly controlled by experimental methods and the constants occurring in them may be determined in the course of examinations.

Accordingly, the applied system made the analysis easier in the given case and brought the same result which may be obtained in a more complicated way, by the mathematical solution of equation system (54).

REFERENCES

1. Sedov, A. I.: Methods of the Theory of Measure in Mechanics. Edition Science. Moscow 1967
2. Bitó, J. F.: Theoretical Basis of Plasma Diagnostics. University guide book. Budapest 1969
3. Bitó, J. F.—Antal, K. G.: Lecture on the Conference of "Closed systems" in Dubna (USSR) 1969
4. Bitó, J. F.—Antal, K. G.: *Acta Phys. Hung.* in print
5. Davidov, B. I., JEPT 7 (1937), 1064

Die Struktur von funktionellen Zusammenhängen zwischen physikalischen Größen und die Anwendung derselben in der Entladungsphysik. Das π-Theorem, das die Grundlage der Dimensionstheorie ist, wird analysiert und aufgrund dieser Theorie wird die Struktur der funktionellen Zusammenhänge zwischen den physikalischen Größen erläutert. Die praktische Anwendung des Theorems wird an einem klassisch-mechanischen Modell dargestellt und darauffolgend wird sein Anwendungsbereich auf die Entladungsphysik ausgedehnt. Die methodisch einfache, zugleich aber für wertvolle Folgerungen geeignete Dimensionstheorie kann vorteilhaft in der Entladungsphysik angewendet werden. Bei Analyse von Gleichungssystemen, die oft einen großen mathematischen Aufwand erfordern und nur durch die Anwendung von approximativen Methoden lösbar sind, wie auch bei der Analyse von Arbeitshypothesen bedeutet die Anwendung des π-Theorems eine Erleichterung und Beschleunigung.

Исследование структуры функциональных зависимостей между физическими величинами и ее применение для газовых разрядов. Анализируется теорема П, являющаяся основой для теории размерности, и, исходя из этой теоремы, рассчитывается структура функциональных зависимостей между физическими величинами. На одном классическом примере демонстрируется практическое применение и дается пример использования метода в области газовых разрядов. Простую в отношении методики и в то же время ценную для практики теорию размерности можно хорошо использовать в физике газовых разрядов. Для систем уравнений, которые решаются только приближенно, и для анализа рабочей гипотезы — использование теоремы П облегчает решение.

Acta Technica Academiae Scientiarum Hungaricae, Tomus 76 (3—4), pp. 273—292 (1974)

ANALYSIS OF DOUBLE-LAYER SPACE TRUSSES WITH DIAGONALLY SQUARE MESH BY THE CONTINUUM METHOD

L. KOLLÁR*
DOCTOR OF TECHN. SC.

[Manuscript received June 11, 1972]

A double-layer space truss is examined with both chord planes being of square mesh but at 45° to each other. The mode of supporting to provide rigidity, and number of redundacies are determined. A differential equation system of the substituting continuum as well as relationships for the calculation of the truss bar forces from continuum internal forces are established.

1. Generals on double-layer space trusses

Trusses consisting of two grids in parallel planes (chord planes) connected by diagonal bars are called double-layer space trusses.

For this structure with two chord planes consisting of bars in *three* directions an equivalent plate can be found, with bending and twisting rigidities equal to those of the truss, hence developing equal internal forces (stresses). Thus, from the aspect of stress determination, this structure is a hyperstatic one. In case of chord planes consisting of equilateral triangles and rods of uniform cross-section, this substituting plate will be isotropic [8], in any other case it will be orthotropic or aeolotropic [4]. Another feature of this truss with chord planes consisting of bars in three directions is that chord-bar forces can be determined from systems of three pure statical (equilibrium) equations and only from the stresses, without analysing strains. Thus, determination of the bar forces is a *statically determinate problem.*

If bars in the chord planes are parallel to *more than three* directions, then a substituting plate with equivalent rigidities can be found, just as for the tri-directional grid, though bar forces can only be determined from stresses by analysing also strains [2]. Hence, determination of bar forces is a *hyperstatic problem.*

Finally, if bars in the chord planes are parallel to less than three directions, then hyperstaticity of the grid, of importance for the determination of stresses in the equivalent plate, is reduced, since certain rigidities are lost. If, for instance, each chord plane consists of rods parallel to only two directions

* Dr. L. KOLLÁR, Karap u. 9, 1122 Budapest, Hungary

$x \perp y$ (Fig. 1) then none of the chord planes will be able to resist shear n_{xy}, hence, the structure as a whole will be soft to torque m_{xy}. Thus, the substituting plate will be of zero torsional rigidity and stresses (for an isotropic structure) and can be determined according to [7]:

$$w^{\mathrm{IV}} + w^{::} = \frac{p}{B}, \tag{1a}$$

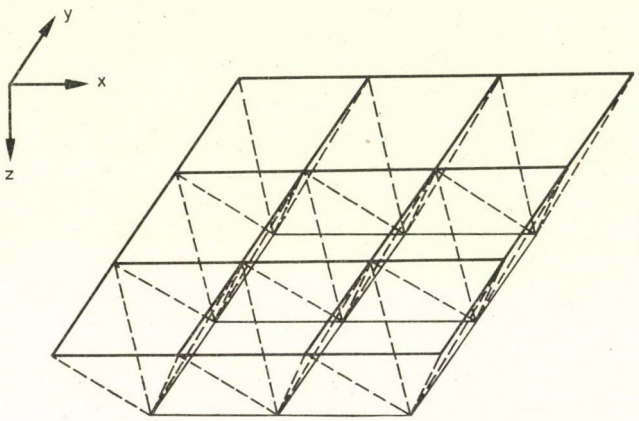

Fig. 1

instead of the equation for the ordinary solid plate

$$w^{\mathrm{IV}} + 2\,w''^{\cdot\cdot} + w^{::} = \frac{p}{B}. \tag{1b}$$

The truss will, however, not be rigid to any stress, just because of the missing torsional rigidity. If the two chord planes are relatively shifted in plan, as seen in Fig. 1, and connected by space diagonals, then they will be soft only to torque affecting the entire truss, thus, the truss will undergo deformation without resistance as seen in Fig. 2a. Thus, it has to be supported in at least four points (e.g. corners) that would displace vertically during twisting shown in Fig. 2a. If, however, bars of the two chord planes are above each other and connected by two grids of diagonals in vertical planes, then the truss may deform in its plan according to Fig. 2b, too. This also has to be prevented by the supports.

If the truss is designed so that the two directions of the rods in the upper chord plane include 45° with those in the lower plane ("diagonal-square mesh", Fig. 3), the resulting structure will have neither flexural nor torsional rigidity in itself (without supports), thus, it has no equivalent plate-like continuum in the usual sense of the word. Namely, the upper chord alone can absorb

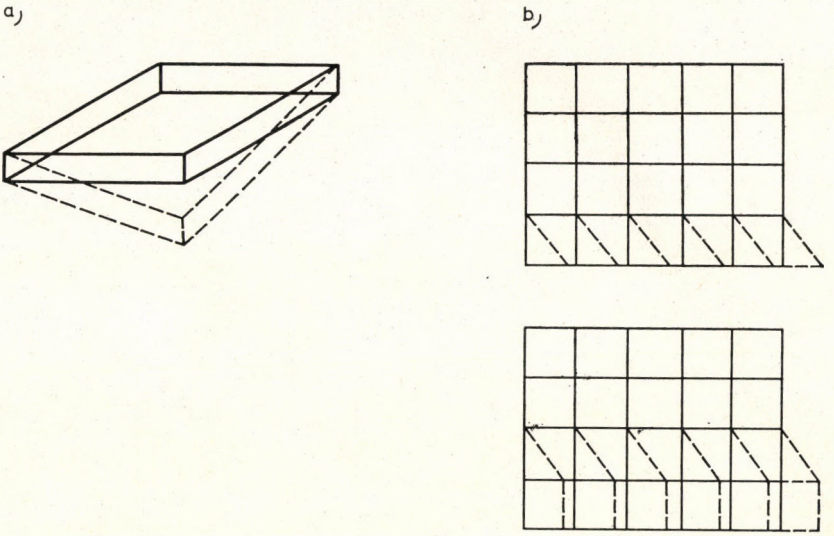

Fig. 2

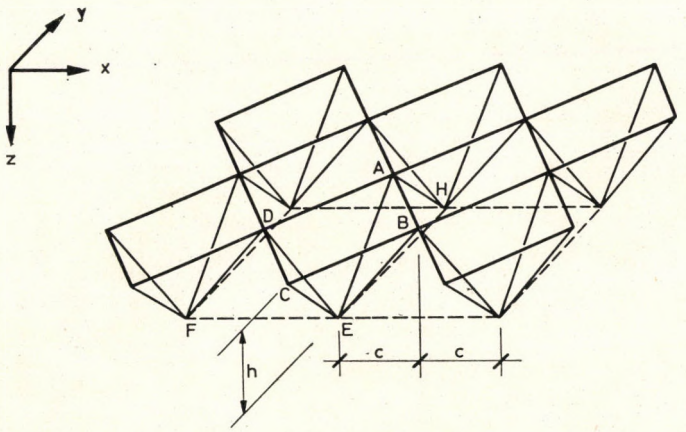

Fig. 3

only shear n_{xy}, while the lower one only normal forces n_x and n_y, these latter do not, however, correspond to n_{xy} in the upper chord, and so their combination develops no moments. Thus, the truss can resist bending moments only if aided by the supports.

In the following it is stipulated that the two systems of diagonals connecting the lower and upper chord plane are in the vertical plane, and parallel to the bars in the lower chord plane (Fig. 3). Hence, the structure may be considered as composed of pyramids standing on their peaks. Length of upper rods will be $1/\sqrt{2}$ times that of the lower ones.

This structure is advantageous by the buckling length of upper, compressed bars being $\sqrt{2}$ times less than that of the lower, tensile ones, and by the possibility of assembly from prefabricated pyramids.

KATO, TAKANASHI, TSUSHIMA and HIRATA [3] have been the first to analyze approximately the internal forces in a diagonal-square space truss as approximated by a continuum. An exact solution has been published by SOARE [5], [6] but not as a continuum but as a hyperstatic space truss, applying the method of finite differences for a special case.

In what follows, the diagonal-square truss will be examined in detail, determining first the kind of support needed for rigidity, then the condition of making the structure statically determinate, and the determination of the degree of hyperstaticity will be settled, followed by presenting the method of determination of stresses of the substituting continuum from its peculiarities, interpreting the notion "substituting continuum". At last, the determination of bar forces from stresses of the continuum will be described.

The continuum method is advantageous as compared to other methods, partly, by offering an illustrative picture of the internal forces, facilitating design, partly, by often reducing the problem to already solved plate problems, and partly, if the problem has no plate solution available because of variable rigidity or else, then either the stresses may be expressed in a closed form, or the mesh of the difference method can be assumed independently of the grid nodes, thus much reducing the computing work.

2. Degree of hyperstaticity of the diagonal-square space truss

Let the diagonal-square space truss, Fig. 3, be supported against vertical displacements at all the boundary points of the upper chord plane (indicated by circles in Fig. 4). To prevent horizontal displacements three, horizontal bracings (with no common intersection point) are needed, in conformity with the known law of statics (bars 1, 2, 3 in Fig. 4). Obviously, however, the structure will even so be liable to a distortion in horizontal plane where the pyramids are horizontally displaced and/or rotated around a vertical axis without deformation, and the squares between them become diamonds (Fig. 4). This is to be opposed by a fourth bracing.

Let us see now if the structure supported at its boundary points by vertical rods and four horizontal bracings is statically determinate or indeterminate.

The number X of statical redundancies is obtained from the known expression:

$$X = S + R - 3C \tag{2}$$

where S number of bars
R number of reaction components (bracings)
C number of hinges.

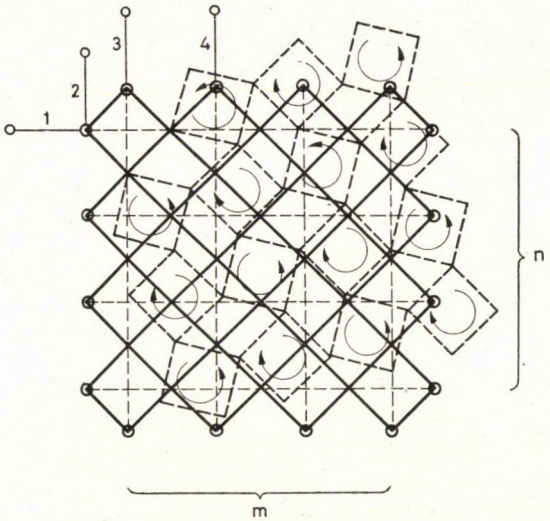

Fig. 4

Denoting the number of pyramids in x and y directions by m and n, respectively (Fig. 4), the number of bars is:

in the upper chord plane	$4\,mn$
in the lower chord plane	$(m-1)n + m(n-1)$
connecting diagonals	$4\,mn$
totalling	$S = 10\,mn - m - n$

Number of bracings:

vertical	$2\,m + 2\,n$
horizontal	4
totalling:	$R = 2\,m + 2\,n + 4$

Number of nodes:

in the upper chord plane	$(m+1)n + m(n+1)$
in the lower chord plane	mn
totalling	$C = 3\,mn + m + n$

Accordingly, the degree of hyperstaticity is:

$$X = mn + 4 - 2(m + n)\,. \tag{3}$$

Numerical values are compiled in Table I:

Cases of $m = 1$ and $n = 1$ have been omitted from the table since then the number of horizontal bracings to provide rigidity are to be determined upon special considerations, cases to be ignored now.

Table I

n \ m	2	3	4	5	6	7
2	0	0	0	0	0	0
3	0	1	2	3	4	5
4	0	2	4	6	8	10
5	0	3	6	9	12	15
6	0	4	8	12	16	20
7	0	5	10	15	20	25

From the table it appears that for $m = 2$ and/or $n = 2$, the structure is a statically determinate one, otherwise it has as many redundancies as it has "internal" pyramids.

3. Internal forces in a diagonal-square space truss

3.1. General features of the force system

For the time being, the effect of supports will be omitted and the space truss examined in itself.

For the sake of simplicity, only grids where upper and lower bars are of identical cross-sectional area each will be considered. Namely, then the substituting continuum is uniform rigidity.

The structure is immediately seen to be of zero torsional rigidity (in the assumed x, y co-ordinate system). Namely, the lower chord plane — lacking skew bars — cannot resist shear n_{xy}, besides, the plane of connecting diagonals being vertical, the torsional shear flow cannot close below. Accordingly, the plate equation will be of the simple form (1a).

Besides, force components in the upper chord plane should be in a relationship such as not to distort into diamonds the upper square planes of the pyramids, because the upper chord plane could not resist these forces.

Stability (rigidity) of one square is assured if forces acting at the corner points do not perform any work during a virtual distortion of the square into diamond. In this investigation any point of the square, among them midpoint O of the square shown in Fig. 5, can be considered as fixed. Namely, any other point taken as fixed, the corresponding displacement is obtained by adding to that in Fig. 5 a rigid body displacement and during this latter, equilibrium equations provide for performing zero work.

Thus, zero work (i.e. condition of rigidity of the square) is expressed by

$$(N_y^A - N_x^B + N_y^C - N_x^D)\,\Delta = 0\,,$$

i.e., by

$$N_x^B + N_x^D = N_y^A + N_y^C$$

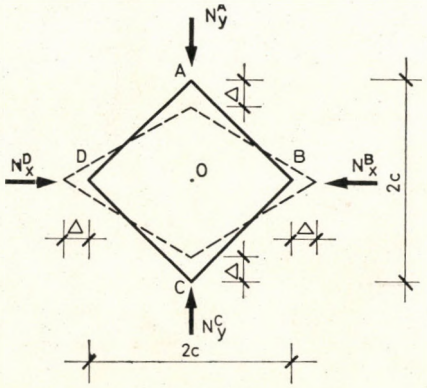

Fig. 5

and since (using the approximation usual in substituting the truss by a continuum)

$$\frac{N_x^B + N_x^D}{2} = N_x^0 = 2\,cn_x^0 = \frac{N_y^A + N_y^C}{2} = N_y^0 = 2cn_y^0\,, \tag{4a}$$

Eq. (4a) can be written as:

$$n_x = n_y. \tag{4b}$$

It follows also that the upper chord plane undergoes deformation according to the relationship $\varepsilon_x = -\varepsilon_y$ without resistance. Thus, normal forces n_x, n_y will be in no unambiguous relationship but to the mean value of the two strains $(\varepsilon_x + \varepsilon_y)/2$.

3.2. Rigidities of the space truss

The lower chord plane has tensile rigidity A_l in the directions of the two bar directions (Fig. 6). Tensile rigidity referred to unit width will be valid in both directions, due to the identity of bar cross-sections:

$$A_l = \frac{EF_l}{2c}\,. \tag{5}$$

The upper plane has no compressive rigidity A but to compressions equal in directions x and y, to be written, with notations in Fig. 7a as:

$$A = \frac{n}{\varepsilon} = \frac{N/(2c)}{2e/(2c)} \,. \tag{6a}$$

The e value is most simply obtained by means of the energy theorem (bar forces being $S = N/\sqrt{2}$):

$$4Ne = 4\,\frac{(N^2/2)\cdot\sqrt{2}\,c}{EF} \,,$$

i.e.

$$e = \frac{Nc}{\sqrt{2}\,EF} \,,$$

hence

$$A = \frac{EF}{\sqrt{2}\,c} \,. \tag{6b}$$

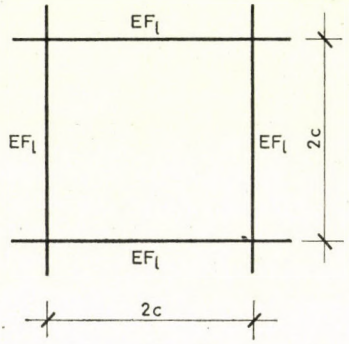

Fig. 6

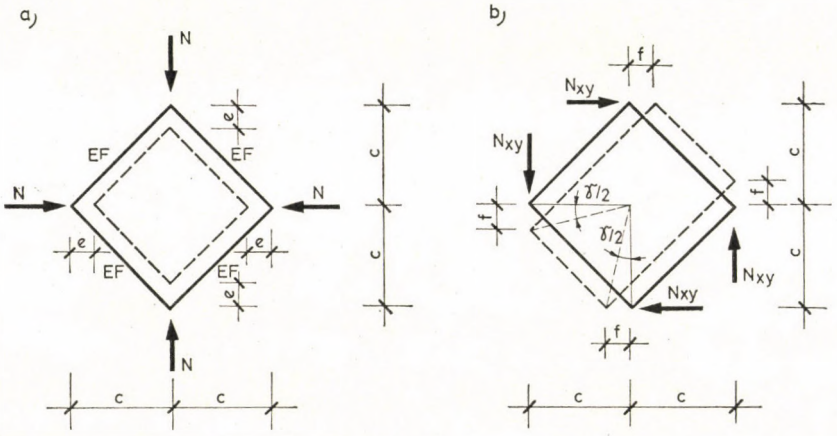

Fig. 7

The shear rigidity of the upper chord, A_{xy}, according to Fig. 7b, is:

$$A_{xy} = \frac{n_{xy}}{\gamma} = \frac{N_{xy}/(2c)}{2f/c} . \tag{7a}$$

Again, the f value can be obtained from the energy theorem: ($S = \pm N_{xy}/\sqrt{2}$):

$$\begin{aligned} 4N_{xy} f &= 4 \frac{(N_{xy}^2/2) \cdot \sqrt{2}\, c}{EF}, \\ f &= \frac{N_{xy} \cdot c}{\sqrt{2} EF}, \\ A_{xy} &= \frac{EF}{2\sqrt{2} c} . \end{aligned} \tag{7b}$$

Thus, the lower and upper chord planes have both quantitatively and qualitatively different rigidity characteristics. This is why — although there are less redundancies than for other space trusses — it is more intricate to analyse. The force system is somehow similar to the plate two-way ribbed on one side [1].

3.3. Strain state and equations of the space truss of constant rigidity, considered as a continuum

Strain state of a space truss is expedient to describe by composing it from two parts:

Let us ignore first the ability of the upper chord plane to deform without force effect of the kind $\varepsilon_x = -\varepsilon_y$ (that is, assume the chord plane to be rigid to deformations like $\varepsilon_x = -\varepsilon_y$), besides, assume it to have only rigidities like those of the lower chord plane (hence, only tensile rigidities in directions x and y), and be the rigidities of the upper chord plane k times those of the lower one, thus, in this case, tensile rigidity kA_l in both directions x and y. This coefficient of proportionality k is chosen arbitrarily, as it will fall out in the deductions and leaves the final result unaffected. Rigidities kA_l of the upper chord plane, taking part in bending, are only introduced to help illustratively expressing the force system in two parts.

Now, we can define the bending rigidity B of the entire space truss, also depending on the arbitrary parameter k:

$$B = h^2 A_l \frac{k}{1+k} \tag{8a}$$

and the distance of the upper and lower chord planes of the bending neutral axis (Fig. 8), to be found in the gravity centre of both chord plane rigidities:

$$h_u = h \frac{1}{1+k}, \tag{9a}$$

$$h_l = h \frac{k}{1+k}. \tag{9b}$$

For $k = 1$,

$$h_u = h_l = \frac{h}{2} \tag{9c}$$

and

$$B = \frac{h^2}{2} A_l. \tag{8b}$$

This modification of the upper chord plane rigidities causes the deformation to consist of only bending — namely, in general, no outer forces parallel to the middle plane act on double-layer trusses — described by the bending deflection function w_1. In the two chord planes, this bending deformation produces strains ε_1^u and ε_1^l as well as angular distortion γ_1^u and γ_1^l, respectively, (see the continuous skew line in Fig. 8), in conformity with the following known relationships [4]:

$$\varepsilon_{1x}^u = h_u w_1'', \tag{10a}$$

$$\varepsilon_{1y}^u = h_u \cdot w_1'', \tag{10b}$$

$$\gamma_1^u = h_u \cdot 2 w_1''. \tag{10c}$$

(Subscripts u are to be replaced by l for the lower chord plane).

It should be stressed that w_1 is only a part, due to pure bending of the final deformation, rather than a deformation to be calculated from the equilibrium of the truss of modified rigidity and to be corrected later in view of the real rigidity conditions.

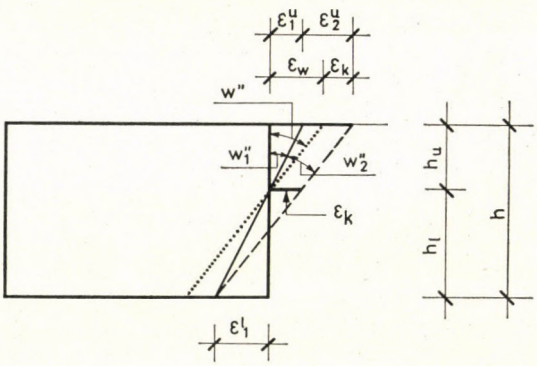

Fig. 8

The resulting states of deformation in the upper (and lower) chord planes are compatible (being derived from a single deformation function w_1), nevertheless, in the upper chord plane still a complementary plane deformation state has to develop, due to the following reasons:

a) Up to now, the rigidity to shear of the upper chord plane has been ignored (it being inexistent in the lower one). The angular distortion developing according to Eq. (10c) causes no shear n_{1xy} in the lower chord plane but does so in the upper one. In conformity with the plane equilibrium equations, this could only be balanced by the increments of forces n_{1x} and n_{1y} in their proper directions. Increments of bending forces n_{1x} and n_{1y} are, however, balanced by flexural shear developing in connecting diagonal bars along x and y, resp., thus, there is nothing to balance n_{1xy}. (This problem does not arise for the lower chord plane, the rigidities being there assumed realistically.)

b) The upper chord plane can only resist compressions equal in directions x and y, that is, equality $n_x = n_y$ has to be met, a condition frustrated by flexural deformation w_1 established according to properties of the lower chord plane.

c) Finally, the upper chord plane has no flexural rigidity kA_l along x and y, but only the mean of strains in both directions is known to be proportional to $n_x = n_y$, with the intermediary of compressive rigidity (6). In addition, however, the upper chord plane can undergo deformations of type $\varepsilon_x = -\varepsilon_y$ without developing forces.

These three contradictions are to be eliminated by the complementary plane deformation, the components of which will be marked by subscript 2. The diagonals connecting the two chord planes do not transmit this deformation to the lower chord plane. Thus, this plane deformation results in rotation (twist) of the cross-section shown with a dashed line in Fig. 8:

$$w_2'' = \frac{\varepsilon_{2x}^u}{h}, \tag{11a}$$

$$w_2'' = \frac{\varepsilon_{2y}^u}{h}, \tag{11b}$$

$$2w_2'' = \frac{\gamma_2^u}{h}. \tag{11c}$$

Hence, in spite of the attribute "plane", the complementary deformation 2 causes also bending deformation. The overall bending deflection will be the sum of both partial deflections (w_1 and w_2):

$$w = w_1 + w_2. \tag{12}$$

These two parts of deformation can only be determined at once. Let us express first the internal forces of the upper chord plane from w_1 and plane deformation 2.

Remembering that the tensile and shearing rigidities of the upper chord plane are kA_l and A_{xy}, resp., flexural deformation w_1 brings about membrane forces

$$n_{1x} = kA_l \varepsilon_{1x}, \tag{13a}$$

$$n_{1y} = kA_l \varepsilon_{1y}, \tag{13b}$$

$$n_{1xy} = A_{xy} \gamma_1, \tag{13c}$$

and bending moments

$$m_x = - Bw_1'', \tag{14a}$$

$$m_y = - Bw_1''. \tag{14b}$$

The subscript u has been omitted from the formulae. The negative sign serves to distinguish moments, considered positive if causing tension in the lower chord plane.

In conformity with formulae (8a), (9a), (10a –b), (13a –b) and (14a – b), it can be written that

$$n_{1x} = - \frac{m_x}{h}, \tag{14c}$$

$$n_{1y} = - \frac{m_y}{h}, \tag{14d}$$

following also from the definition of n_{1x} and n_{1y}.

From the complementary plane deformation nothing but the membrane shear force can be simply written down:

$$n_{2xy} = A_{xy} \gamma_2. \tag{15a}$$

This time, forces n_{2x} and n_{2y} are not directly related to strains ε_{2x} and ε_{2y} but only their sums with forces n_{1x} and n_{1y} are known to be equal in both directions:

$$n_{1x} + n_{2x} = n_{1y} + n_{2y}, \tag{15b}$$

and to be proportional to the average of the total strain in both directions:

$$n_{1x} + n_{2x} = A \frac{(\varepsilon_{1x} + \varepsilon_{2x}) + (\varepsilon_{1y} + \varepsilon_{2y})}{2}. \tag{15c}$$

Thereby all has been done to establish equations governing the system of internal forces.

First, equilibrium between vertical load p and two-way bending moments can be written as:

$$m_x'' + m_y'' = -p. \tag{16}$$

These moments m_x and m_y are due to deformation w_1 alone (8a—b), since internal forces of complementary deformation 2 are not matched in the lower chord plane, and besides — though they are eccentric with respect to the neutral axis of the truss — rather than by vertical (bending) shears, the moments due to their eccentricity are varied by horizontal (membrane) shears unfit to balance vertical loads.

Equilibrium equations of the complementary plane deformation have to include also membrane shears n_{1xy} due to deformation w_1, since forces with subscript 2 were necessary to balance the former ones:

$$n_{2x}' + (n_{1xy} + n_{2xy})^{\cdot} = 0, \tag{17a}$$

$$(n_{1xy} + n_{2xy})' + n_{2y}^{\cdot} = 0. \tag{17b}$$

Now, all variables in Eqs (16) and (17a—b) might be expressed by w_1 and w_2 making use of Eqs (14a—b) and (11a—c), (13a—c) (15a—c). Nevertheless, it is inexpedient to handle partial deflections w_1 and w_2 separately, since boundary conditions can only be set up for the entire deflection $w = w_1 + w_2$. Thus, Eqs (16) and (17a—b) will be rewritten so as to include nothing but the entire deflection w and a stress function Φ. This latter will be defined as usual:

$$\Phi^{\cdot\cdot} = n_{2x}, \tag{18a}$$

$$\Phi'' = n_{2y}, \tag{18b}$$

$$\Phi^{\cdot\prime} = -(n_{1xy} + n_{2xy}). \tag{18c}$$

Thus, Φ automatically meets equilibrium equations (17a—b), the but compatibility of the corresponding deformations remains still to be assured.

Remember that deformations in the upper chord plane due to w_1 are compatible, so it would be sufficient to include components of deformation 2 in the compatibility equation. This is, however, impossible, since Eq. (18c) already includes n_{1xy}. Hence, also the two strain components ε have to include strains due to w_1. Thus, the compatibility equation should be written for the entire deformation:

$$(\varepsilon_{1x} + \varepsilon_{2x})^{\cdot\cdot} + (\varepsilon_{1y} + \varepsilon_{2y})'' - (\gamma_1 + \gamma_2)^{\cdot\prime} = 0. \tag{19}$$

For changing to the new variables, let us consider Fig. 8 again. Rotation due to the entire deflection w is shown by a dotted line (parallel to the dashed one). As a matter of fact, this deformation ought to be increased by the defor-

mation (ε_{xk}, ε_{yk}, $\gamma_{ki}/2$) of the neutral plane, yet its h/h_u-fold, i.e. deformation 2 of the upper chord plane, that can be expressed by Φ, will be applied instead.

Let us express deformation components 1 by means of w and deformations 2. From (10a to c), according to (12) and (11a to c):

$$\varepsilon_{1x} = h_u(w'' - w_2'') = h_u\left(w'' - \frac{\varepsilon_{2x}}{h}\right), \tag{20a}$$

$$\varepsilon_{1y} = h_u\left(w'' - \frac{\varepsilon_{2y}}{h}\right), \tag{20b}$$

$$\gamma_1 = h_u\left(2w' - \frac{\gamma_2}{h}\right), \tag{20c}$$

and similarly rewriting (14a,b):

$$m_x = -B\left(w'' - \frac{\varepsilon_{2x}}{h}\right), \tag{21a}$$

$$m_y = -B\left(w'' - \frac{\varepsilon_{2y}}{h}\right). \tag{21b}$$

Express now deformations 2 by Φ making use of Eqs (15b,c), substituting the n_{1x} and n_{1y} values expressed from (13a,b), then eliminating ε_{1x} and ε_{1y} by means of (20a,b):

$$n_{2x} = -kA_l h_u\left(w'' - \frac{\varepsilon_{2x}}{h}\right) + A\,\frac{h_u\left(w''+w'' - \dfrac{\varepsilon_{2x}+\varepsilon_{2y}}{h}\right)+\varepsilon_{2x}+\varepsilon_{2y}}{2}, \tag{22a}$$

$$n_{2y} = -kA_l h_u\left(w'' - \frac{\varepsilon_{2y}}{h}\right) + A\,\frac{h_u\left(w''+w'' - \dfrac{\varepsilon_{2x}+\varepsilon_{2y}}{h}\right)+\varepsilon_{2x}+\varepsilon_{2y}}{2}. \tag{22b}$$

Therefrom ε_{2x} and ε_{2y} will be expressed, making use of (18a,b):

$$\varepsilon_{2x} = \frac{\left(\dfrac{A}{2}+A_l\right)\cdot\left[\Phi'' - \dfrac{A}{2}h_u w'' - \left(\dfrac{A}{2}-kA_l\right)h_u w''\right]}{\dfrac{kA_l(A+A_l)}{1+k}} - \frac{\dfrac{A}{2}\left[\Phi'' - \left(\dfrac{A}{2}-kA_l\right)h_u w'' - \dfrac{A}{2}h_u w''\right]}{\dfrac{kA_l(A+A_l)}{1+k}}, \tag{23a}$$

$$\varepsilon_{2y} = \frac{-\frac{A}{2}\left[\Phi'' - \frac{A}{2} h_u w'' - \left(\frac{A}{2} - kA_l\right) h_u w''\right]}{\frac{kA_l(A+A_l)}{1+k}} + \\ + \frac{\left(\frac{A}{2} + A_l\right)\left[\Phi'' - \left(\frac{A}{2} - kA_l\right) h_u w'' - \frac{A}{2} h_u w''\right]}{\frac{kA_l(A+A_l)}{1+k}} . \tag{23b}$$

By means of Eqs (13c), (15a) and (18c) the entire angular distortion can be expressed by Φ:

$$\gamma_1 + \gamma_2 = \frac{-\Phi''}{A_{xy}} . \tag{24}$$

Now, all variables in the basic equations (16) and (19) can be expressed by Φ and w such as:

Substituting (21a,b) and (23a,b) into (16):

$$\frac{h^2}{2} \frac{AA_l}{A+A_l} (w^{IV} + 2w''' + w'') + \\ + \frac{h}{2} \frac{A}{A+A_l} \left(\Phi^{IV} - 2\frac{A+2A_l}{A} \Phi''' + \Phi''\right) = p , \tag{25}$$

and substituting (20a, b), (23a, b) and (24) into (19):

$$-\frac{h}{2} \frac{A}{A+A_l} \left(w^{IV} - 2\frac{A+2A_l}{A} w''' + w''\right) + \\ + \frac{1}{2} \frac{A+2A_l}{A_l(A+A_l)} \left(\Phi^{IV} - 2\frac{A}{A+2A_l} \Phi''' + \Phi''\right) + \frac{\Phi''}{A_{xy}} = 0 . \tag{26}$$

Proportionality coefficient k is seen to fall out from the equations. Thus, it is unimportant how the fictitious rigidity of the upper chord had been assumed for the system of bending forces, since anyhow, in the subsequent steps this part has been corrected so as to achieve the real system of forces in the structure. In other words, how to divide the force system is of no matter, provided their sum yields the real system of forces.

Thus, w and Φ are to be determined from Eqs (25) and (26).

If the cross-sectional area of the lower chord bars is $\sqrt{2}$ times the upper one ($F_l = \sqrt{2}F$) then $A_l = A$ and Eqs (25) and (26) simplify into:

$$\frac{h^2}{4} A (w^{IV} + 2 w''^{\cdot\cdot} + w^{\cdot\cdot\cdot\cdot}) + \frac{h}{4} (\Phi^{IV} - 6 \Phi''^{\cdot\cdot} + \Phi^{\cdot\cdot\cdot\cdot}) = p , \tag{27}$$

$$- \frac{h}{4} (w^{IV} - 6 w''^{\cdot\cdot} + w^{\cdot\cdot\cdot\cdot}) + \frac{1}{4A} (3\Phi^{IV} - 2\Phi''^{\cdot\cdot} + 3\Phi^{\cdot\cdot\cdot\cdot}) + \frac{\Phi''^{\cdot\cdot}}{A_{xy}} = 0 . \tag{28}$$

3.4. Boundary conditions

For supporting conditions in item 2 (freely supported edges), boundary conditions of differential equations (25) and (26) are:

Along boundaries parallel to the x axis:

zero deflection: $w = 0;$ (29a)

zero bending moment normal to the boundary: $m_y = 0;$ (29b)

zero horizontal (membrane) force normal to the boundary in the upper chord plane: $n_y = n_{1y} + n_{2y} = 0;$ (29c)

zero (membrane) shear force in the upper chord plane, i.e., in conformity with (18c): $\Phi'' = 0 .$ (29d)

Conditions (29b) and (29c) are to be expressed by w and Φ. Making use of (14d), (29b) yields $n_{1y} = 0$, hence from (29c) taking (18b) into consideration:

$$\Phi'' = 0 . \tag{29c}^*$$

By means of (21b) and (23b), and taking into consideration that $w'' = 0$ along the boundary in direction x and that $\Phi'' = 0$ because of (29c)*, (29b) yields:

$$w^{\cdot\cdot} + \frac{1}{A_l h} \Phi^{\cdot\cdot} = 0 . \tag{29b}^*$$

For boundaries parallel to y, differentiations with respect to x and y have to be exchanged.

Because of conditions (29d) and (29b)*, the solution cannot be given as a sine series even for a quadratic ground plan, but in actual cases, some numerical method has to be involved.

3.5. Relationship between truss bar forces and internal forces of the equivalent continuum

w and Φ determined from differential equations (25) and (26) directly yield *internal forces of the continuum.* Eqs (21) and (23) deliver specific bending

moments. Derivation of Eqs (21) leads to the specific (flexural) shear forces:

$$t_x = m'_x = -B\left(w''' - \frac{\varepsilon'_{2x}}{h}\right), \tag{30a}$$

$$t_y = m'_y = -B\left(w''' - \frac{\varepsilon'_{2y}}{h}\right). \tag{30b}$$

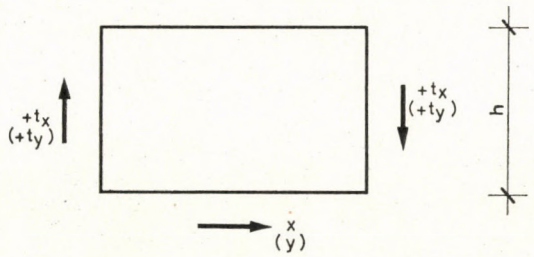

Fig. 9

Shear force in its positive sense is shown in Fig. 9. Finally, applying Eqs (18) to the stress function Φ, yields the complementary (membrane) internal forces of the upper chord plane.

For the determination of the *bar forces of the space truss*, their correlation to the internal forces of the continuum has to be established. This is most simply found for the lower chord plane since its bar forces multiplied by the truss depth h yield the bending moment acting on the width $2c$. (In conformity with the considerations introducing item 3.3, in the lower chord plane only internal forces n_{1x} and n_{1y} develop.) With notations in Fig. 3:

$$S_{EF} = \frac{2cm_x^D}{h} \tag{31a}$$

and

$$S_{EH} = \frac{2cm_y^A}{h}. \tag{31b}$$

Forces in connecting diagonals are due to flexural shear forces. Vertical equilibrium yields in direction x:

$$S_{DE} = 2c \cdot t_x^{DE} \cdot \frac{\sqrt{c^2+h^2}}{h} \tag{32a}$$

and

$$S_{EB} = -2c \cdot t_x^{EB} \cdot \frac{\sqrt{c^2+h^2}}{h}, \tag{32b}$$

and in direction y:

$$S_{CE} = 2c \cdot t_y^{CE} \cdot \frac{\sqrt{c^2+h^2}}{h} \tag{32c}$$

and

$$S_{EA} = -2c \cdot t_y^{EA} \cdot \frac{\sqrt{c^2+h^2}}{h}. \tag{32d}$$

Connecting diagonal forces have to be calculated from the shear force t valid in the vertical section going through the mid-bar.

Upper chord-bar forces are somewhat more complex to calculate. For the sake of illustration, Fig. 10 shows the four possible force systems meeting rigidity condition (4a) and thereby acting as equilibrium force system at the

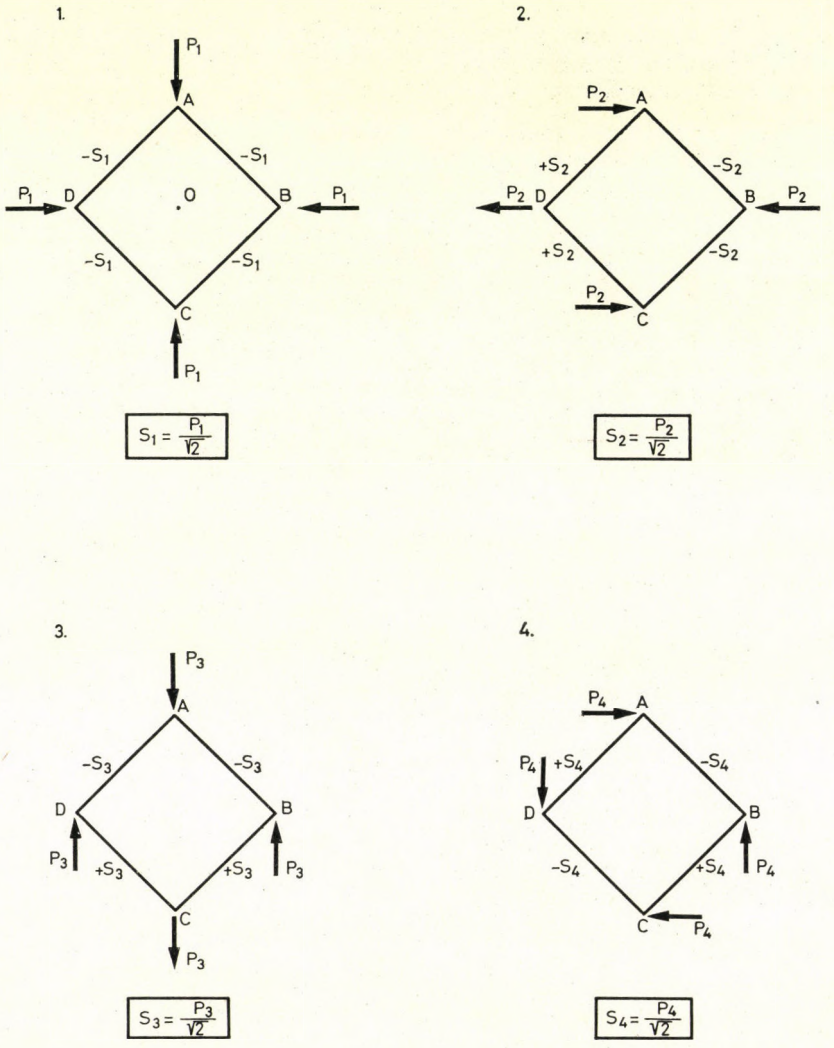

Fig. 10

corners of the upper square planes of the pyramids. To determine the upper chord-bar forces, forces acting at the corners of each square are advisably decomposed into these four force systems:

Force system 1 essentially corresponds to the forces $n_x = n_y$ referred to the square centre O. According to Eqs (21), (23) and (18):

$$P_1 = 2c\left(\frac{m_x^0}{h} - \Phi''\right) = 2c\left(\frac{m_y^0}{h} - \Phi''\right). \tag{33a}$$

Force system 2 is most simply obtained from the increment n_{xy} in direction y. Making use of Eq. (18c):

$$P_2 = 2c\,\frac{n_{xy}^A - n_{xy}^C}{2} = c\,(\Phi'_C - \Phi'_A)\,, \tag{32b}$$

and similarly, from increment n_{xy} in direction x:

$$P_3 = c\,(\Phi'_D - \Phi'_B)\,. \tag{33c}$$

Force system 4 is obtained by averaging the n_{xy} acting at the four corners:

$$P_4 = -\,c\,(\Phi'_A + \Phi'_C) = -\,c\,(\Phi'_B + \Phi'_D)\,. \tag{33d}$$

Upper chord-bar forces resulting from these four force systems are shown in Fig. 10.

REFERENCES

1. GIENCKE, E.: Die Grundgleichungen für die orthotrope Platte mit exzentrischen Steifen. *Der Stahlbau* **24** (1955), 128—129
2. HEGEDÜS, I.: Analysis of Meshes with Bars in Four or More Directions by means of the Continuous Computational Model. *Acta Techn. Hung.* (In press)
3. KATO, B.—TAKANASHI, K.—TSUSHIMA, Y.—HIRATA, Y.: The Analysis of a Space Truss Composed of Square Pyramid Units. Space Structures (R. N. Davies Editor), Oxford and Edinburgh, Blackwell Scientific Publications 1967, 201- 212
4. KOLLÁR, L.—HEGEDÜS, I.: Solution of Double-layer Space Trusses of General Triangular Grid by the Equivalent Continuum Method. *Acta Techn. Hung.* **74** (1972), 363—381.
5. SOARE, M.: Cylindrical Bending of Double-layer Diagonal Square Mesh Grids. *Acta Techn. Hung.* **69** (1971)
6. SOARE, M.: Contribuţii la studiul reţelelor spaţiale planar pătrate diagonale. *Construcţii şi materiale de construcţie* (1970) 8, 423—440
7. TIMOSHENKO, S.—WOINOWSKI-KRIEGER, S.: Theory of Plates and Shells. McGraw-Hill, New York—Toronto—London 1959
8. WRIGHT, D. T.: A Continuum Analysis for Double-layer Space Frame Shells. *Publ. Int. Ass. Bridge Struct. Eng.* Zürich, **26** (1966)

Berechnung zweischichtiger, im Grundriß diagonal-viereckiger Raumfachwerke mit dem Kontinuumverfahren. Ein zweischichtiges Raumfachwerk mit beiden Gurtebenen aus Vierecknetz aber zu 45° zueinander wird untersucht. Es werden die die Steifigkeit gewährleistende Stützungsart bzw. der Grad der statischen Unbestimmtheit festgestellt. Das Differential-

gleichungssystem des mit dem Raumfachwerk gleichwertigen Kontinuums und die Zusammenhänge für die Berechnung der Fachwerk-Stabkräfte aus den Schnittkräften des Kontinuums werden ermittelt.

Расчет двухслойных пространственных решеток с диагонально-квадратным планом методом континуума. В работе рассматривается двухслойная пространственная конструкция решеток, оба поясных листа которой имеют квадратно-сетевой вид, но повернуты по отношению друг к другу на 45°. Определяется способ опоры, необходимый для жесткости, а также степень статической неопределенности. Устанавливаются система дифференциальных уравнений континуума, равнозначного решетчатой конструкции, и зависимости для вычисления стержневых усилий из разрезных усилий континуума.

Acta Technica Academiae Scientiarum Hungaricae, Tomus 76 (3—4), pp. 293—306 (1974)

A COMPARATIVE STUDY OF SOME CREEP-RUPTURE EXTRAPOLATING FORMULAE

J. S. MURTY*

[Manuscript received July 20, 1972]

A comparative study of some creep-rupture extrapolating formulae is made. The basic differences between the different parametric formulae are discussed. It is shown that the basic differences between the parametric formulae lie in the rate-controlling mechanisms which are different in the different parametric formulae and this is implied in the assumptions made by different authors while deriving their parametric formulae. Using the creep-rupture data of a Cr-Mo-V steel, the various formulae are compared for their extrapolating ability by the standard deviation. It is found, in general, that the iso-thermal relations have a better correlation with the rupture data. All the parametric formulae, which are considered, have given the standard deviation of the same order of magnitude. Rupture stresses were predicted for rupture times of 10^4 and 10^5 hours by the different methods.

1. Introduction

The long-time high-temperature stress-rupture strength of engineering materials is generally predicted by various extrapolation formulae. In these formulae, the stress, temperature and rupture time are related by an equation. Currently, two types of these formulae are in wide use. In the first type, the time and temperature are incorporated in a parameter which is equated to a function of stress, while in the other type, the rupture time and applied stress are related by an iso-thermal relationship. The chief parametric formulae, in present day use, include the Larson—Miller [1], the Orr, Sherby and Dorn [2], the Conrad [3], the Manson—Haferd [4] and the Murry [5]. Two iso-thermal relationships, which are in wide practice presently, the Russian method [6] and the Krish method [7], are compared with the parametric formulae and their extrapolating ability is determined. This comparative study is made by using the creep-rupture data of a Cr—Mo—V steel, which is mostly used in the construction of power-plant equipment.

2. Creep-rupture formulae

Larson and Miller [1] were the first persons to propose a parametric formula, which they have suggested on the lines of Holloman and Jaffe's relation

* J. S. MURTY, Aspirant, Department of Electrical Engineering Material Technology, the Institute of Mechanical Technology and Metal Research, Technical University, 1111 Budapest, Hungary

[8] between tempering time and temperature. They suggested the relation:

$$f_1(\sigma) = T(C + \log t_r) \tag{1}$$

where $f_1(\sigma)$ is a function of stress, T is temperature in absolute degrees, t_r is rupture time and C is a constant. Although LARSON and MILLER proposed a constant value of 20 for C, others [9, 10] obtained a better fit with the Larson — Miller method by using an optimized value for C. The Larson —Miller parameter is derived basically from the Arrhenius rate equation:

$$\frac{1}{t_r} = Ae^{-Q/RT} \tag{2}$$

by assuming that the activation energy, Q, is a function of stress and temperature. The equation (2) can be reduced to equation (1) by writing in logarithmic form and substituting C and $f_1(\sigma)$ for $\log A$ and $Q/2, 3R$, respectively. In this parameter it is implied that the iso-stress plots of $\log t$ versus $1/T$ are linear and intersect the axis, $1/T = 0$, at $\log t = -C$. The slope of these plots is a function of stress. Stress dependency of the activation energy is followed when cross-slip is the rate-controlling mechanism for creep, according to SCHOECK and SEEGER [11]. It suggests, therefore, that the Larson —Miller parameter should best fit the data obtained in the temperature and stress range where cross-slip is rate-controlling.

MANSON and HAFERD [4], on a pure emperical basis, have proposed the parameter:

$$f_2(\sigma) = \frac{T - T_a}{\log t - \log t_a} \tag{3}$$

where $f_2(\sigma)$ is a function of stress, T_a and $\log t_a$ are material constants without any physical significance. The iso-stress plots of $\log t_r$ versus T are implied to be linear and meet at the point $(\log t_a, T_a)$ and the slopes of the plots are a function of stress. A comparative study by GOLDHOFF [9] showed that the Manson — Haferd parameter, in general, is superior to others and the most accurate and conservative one among the various extrapolating methods. This equation is (2) recently [12] derived from the basic equation (2) by assuming that the activation energy be a function of stress and temperature:

$$Q = F_1(\sigma).\ T - F_2(\sigma) \cdot T^2 \tag{4}$$

But so far, such a behaviour has not been reported experimentally.

ORR, SHERBY and DORN have obtained the relation:

$$f_3(\sigma) = \log t_r - \frac{Q}{2{,}3\,RT} \tag{5}$$

from the basic equation (2) by assuming that the activation energy, Q, is constant and equal to the activation energy for self-diffusion and the pre-exponential term, A, is a function of stress. This implies that this parameter is applicable when the diffusion-controlled mechanisms, such as, dislocation climb [13], movement of jogged screw dislocations [14], diffusion creep [15] etc. are rate-controlling. The iso-stress plots, in this parameter, are linear and parallel to one another and their intercepts with the axis, $1/T = 0$, are a function of stress.

CONRAD [4] proposed the formula:

$$B\sigma = C_1 + \frac{C_2}{T} + \log t_r \tag{6}$$

where B is a temperature-dependent constant and C_1 and C_2 are constants independent of stress and temperature. This equation is derived from the basic equation:

$$\frac{1}{t_r} = C_3 \, e^{B'\sigma} \cdot e^{-Q/RT} \tag{7}$$

where C_3 is a constant. As in the Orr, Sherby and Dorn parameter, in this parameter also, the activation energy, Q, is constant and equal to the activation energy for self-diffusion, thereby implying that the diffusion-based mechanisms are rate-controlling. The exponential dependence on stress of creep rate is believed to be followed in the high-stress range [16] and therefore the parameter is expected to fit well the data obtained in the high-stress range where the rate-controlling mechanism is diffusion-enhanced by the intersection vacancies.

MURRY [5] derived the following formula:

$$f_4(\sigma) = T(f_3(\sigma) + \log t_r) \tag{8}$$

from the basic equation (2), assuming that both the pre-exponential term, A, and the activation energy, Q, are functions of stress. In this parameter, the iso-stress plots of $\log t_r$ versus $1/T$ are linear and their slopes, as well as their intercepts with the axis, $1/T = 0$, are dependent on stress. Such a behaviour is expected when the rate-controlling mechanism is a dislocation glide [17].

KRISH [7] proposed the following iso-thermal relation between rupture time and stress:

$$\log \sigma = a + b(\log t_r)^2 \tag{9}$$

where a and b are temperature-dependent.

The Russian method [8] is another iso-thermal relation between stress and rupture time:

$$\log \sigma = a_1 + a_2 \log t \tag{10}$$

where a_1 and a_2 are temperature-dependent and are obtained by:

$$a_1 = \frac{1}{n}\left(\sum_{i=1}^{n} y_i - a_2 \sum_{i=1}^{n} x_i\right)$$

$$a_2 = \sqrt{\frac{n\sum_{i=1}^{n}(y_i)^2 - \left(\sum_{i=1}^{n} y_i\right)^2}{n\sum_{i=1}^{n}(x_i)^2 - \left(\sum_{i=1}^{n} x_i\right)^2}}$$

where y_i and x_i are the logarithms of stress and rupture time, respectively, of the ith specimen and n is the number of specimens tested at each temperature.

3. Materials and methods

The chemical composition of the steels investigated in the present study, is given in Table I. These steels are used in making steam-conveying pipes. Though the basic composition of the four steels are of the same standard, they are in different heat-treated conditions due to the difference in the thickness of the tubes. Constant load creep-rupture tests were conducted by EROKAR on the above steels; most of the tests were conducted at 540 °C, and 580 °C, while a few were conducted at 550 °C, 565 °C and 570 °C also.

Table I

Chemical composition of the steels

Steel	Per cent									
	C	Si	Mn	P	S	Cr	Mo	V	Ni	Cu
I	0,13	0,27	0,61	0,008	0,019	1,07	0,33	0,20	—	0,13
II	0,13	0,27	0,69	0,012	0,017	1,15	0,33	0,20	—	0,16
III	0,12	0,25	0,61	0,008	0,019	1,09	0,32	0,19	0,23	0,12
IV	0,13	0,26	0,69	0,009	0,017	1,09	0,33	0,19	0,17	0,15

4. Results and discussion

The experimental data are fitted into the various formulae considered above, by the least squares method and the coefficients derived are presented in Table II. Using these coefficients, the stresses are recalculated by each method at the given rupture time and temperature. The calculated stresses and their deviation from the applied stresses are given in Table III, along with the

Table II

Values of the coefficients of various formulae

a) Larson–Miller parameter

Equation: $a + b \log \sigma = \frac{T}{1000} [C + \log t_n]$

Steel	a	b	c
I	23,92	—4,892	19,05
II	25,77	—5,527	20,55
III	31,49	—4,423	26,50
IV	31,93	—4,796	27,80

b) Manson–Haferd parameter

Equation: $a + b\,\sigma = \frac{(\log t - \log t_a)}{T - Ta} \times 10^3$

Steel	a	b	T_a	log t_a
I	1,33364	9,42014	386,5	7,76
II	1,80471	3,27958	425,0	6,65
III	—3,77454	100,90108	618,0	1,34
IV	—0,87874	65,84383	776,0	—7,40

c) Orr, Sherby and Dorn parameter

Equation: $a + b \log \sigma = \log t_r - \frac{C}{T}$

Steel	a	b	c
I	9,9626	7,60438	$17{,}81672 \times 10^3$
II	14,6528	6,79941	$21{,}00163 \times 10^3$
III	24,4741	9,50545	$32{,}77425 \times 10^3$
IV	18,45625	6,47750	$24{,}87240 \times 10^3$

d) Conrad parameter

Equation: $B\,\sigma = C_1 + \frac{C_2}{T} + \log tr$

Steel	B		C_1	C_2
	540 °C	580 °C		
I	0,219225	0,28197	1,32584	$4{,}22786 \times 10^3$
II	0,212060	0,28468	3,43347	$2{,}39150 \times 10^3$
III	0,357580	0,17364	—89,37195	$81{,}16080 \times 10^3$
IV	0,268800	0,23871	—30,88360	$32{,}47600 \times 10^3$

e) Murry parameter

Equation: $a + b \log \sigma = \frac{T}{1000} [c + d \log \sigma + \log t_r]$

Steel	a	b	c	d
I	24,998	— 5,8793	20,173	— 1,0288
II	61,737	+ 76,0950	—83,400	+ 97,0000
III	226,107	—160,6700	258,000	—185,0000
IV	143,170	— 94,3780	160,000	—106,5000

f) Krish isothermal relation

Equation: $\log \sigma = a + b (\log t_r)^2$

Steel	a			b		
	540°	560°	580°	540°	560°	580°
I	7,53512	7,11958	6,70405	3,0779	3,17713	3,2764
II	7,27318	7,02690	6,78062	2,9445	3,19905	3,4536
III	13,62525	9,90991	6,19468	6,1020	4,14225	2,1825
IV	11,57759	10,09293	8,60828	4,6793	4,15620	3,6331

g) Russian isothermal relation

Equation: $\log \sigma = a_1 + a_2 \log t_r$

Steel	a_1			a_2		
	540°	560°	580°	540°	560°	580°
I	1,63601	1,57133	1,50660	0,14205	0,14542	0,14880
II	1,66672	1,56161	1,45651	0,15280	0,14590	0,13900
III	1,50921	1,62762	1,74603	0,06333	0,12271	0,18210
IV	1,57673	1,58019	1,58365	0,07557	0,09488	0,11420

creep-rupture data. The Figs 1 to 5 show the parametric relations and the Figs 6 and 7 show the iso-thermal relations. In Table IV, the various methods are compared by their standard deviation, which is calculated by the following formula:

$$S = \left(\frac{1}{n} \sum_{i=1}^{n} d^2 \right)^{1/2} \tag{11}$$

where S is the standard deviation, n is number of test points and d is the deviation at each test point. In Table V, the predicted rupture-stress values for rupture-times of 10^4 and 10^5 hours at 560 °C are presented.

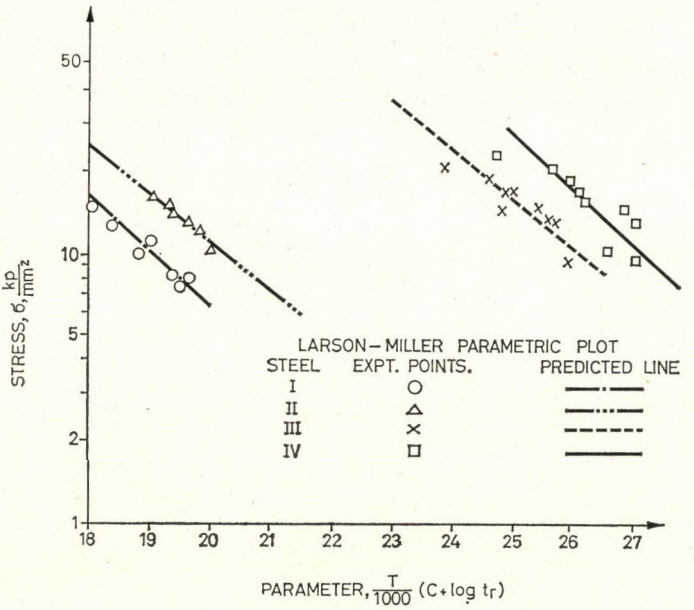
LARSON–MILLER PARAMETRIC PLOT
STEEL EXPT. POINTS. PREDICTED LINE
I
II
III
IV
STRESS, σ, kp/mm²
PARAMETER, T/1000 (C+log tr)

Fig. 1

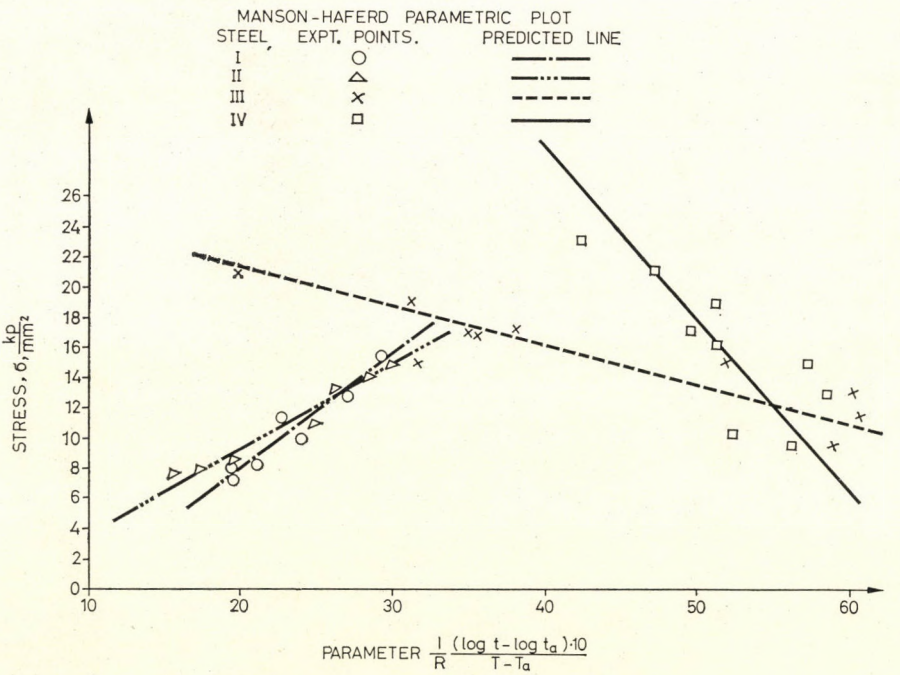
MANSON-HAFERD PARAMETRIC PLOT
STEEL EXPT. POINTS. PREDICTED LINE
I
II
III
IV
STRESS, σ, kp/mm²
PARAMETER 1/R (log t - log ta)·10 / T - Ta

Fig. 2

Table III

A comparison of experimental and predicted

Steel	σ_e	Temp. °C	Rupture time hrs	Larson—Miller		Manson—Haferd	
				σp	deviation %	σp	deviation %
I	13,0	540	4745	13,01	+ 0,1	12,89	— 0,88
	15,0	540	1729	15,39	+ 2,6	15,03	+ 0,179
	7,6	565	18292	7,91	+ 4,02	7,61	+ 0,182
	10,0	565	2922	10,82	+ 8,22	10,98	+ 9,76
	8,0	580	9345	7,50	— 5,80	7,62	— 4,74
	11,0	580	2092	9,79	—11,02	10,14	— 9,82
	13,0	580	341	13,43	+ 3,33	13,19	+ 1,48
II	13,0	540	4152	12,82	— 1,37	12,94	— 0,440
	14,0	540	2548	13,78	— 1,58	13,92	— 0,572
	11,0	550	3626	11,83	+ 7,54	11,82	+ 7,454
	7,6	565	28420	7,45	+ 2,0	7,51	— 1,185
	8,5	575	4874	8,80	+ 3,4	8,81	+ 3,64
	8,0	580	9204	7,58	— 5,3	7,64	— 4,513
	13,0	580	332	12,66	— 2,62	12,45	— 4,231
	15,0	580	95	15,36	+ 2,40	14,97	— 0,20
III	17,1	540	19273	15,52	— 9,30	16,73	— 2,1202
	19,0	540	5950	18,51	— 2,58	18,47	— 2,815
	21,0	540	782	25,09	+19,40	21,46	+ 2,17
	9,5	565	29190	10,47	+10,2	11,11	+17,031
	15,1	565	1020	17,63	+16,70	18,39	+21,80
	17,0	575	711	16,46	— 3,21	17,42	+ 2,452
	11,5	580	4391	11,49	— 0,06	10,68	— 7,114
	13,0	580	4273	11,66	—10,31	10,76	—17,20
	15,0	580	2088	13,05	—13,00	12,93	—13,75
	17,0	580	499	16,35	— 3,85	17,26	+ 1,16
IV	17,1	549	21794	16,39	— 4,20	18,33	+ 7,18
	21,0	540	6199	20,28	— 3,5	20,96	+ 3,62
	23,0	540	428	31,64	+37,5	29,34	+27,56
	10,4	550	28212	13,44	+29,2	15,2586	+46,72
	9,5	565	29190	10,59	+11,0	10,94	+23,54
	16,0	565	2851	15,90	— 0,70	16,48	+ 2,98
	13,0	580	12148	9,81	—24,52	8,25	—36,55
	15,0	580	4601	11,66	—22,7	10,7	—28,68
	18,0	580	456	17,6	— 6,91	16,53	—12,58

σe = experimental stress; σp = predicted stress

rupture-stress values (stress in kp/mm²)

Orr, Sherby—Dorn		Conrád		Murry		Krish		Russian	
σp	deviation %	σp	deviation %	σp	deviation %	σp	deviation %	σp	deviation %
12,26	— 5,74	13,0	0	12,95	— 0,4	13,17	+1,31	13,0	0
14,00	— 6,7	15,0	0	15,24	+ 1,6	15,20	1,33	15,0	0
8,42	+10,7	8,16	+10,736	7,97	+ 4,8	7,6	0	7,6	0
10,72	+ 7,15	11,24	+12,42	10,82	+ 8,22	10,0	0	10,0	0
8,21	+ 2,60	8,20	+ 2,25	7,60	— 5,1	8,19	+ 2,38	8,24	+ 2,96
10,00	— 9,10	10,50	— 4,50	9,86	—10,4	10,4	— 5,45	10,39	— 5,53
12,69	— 2,37	13,30	+ 2,30	13,36	+ 2,74	13,44	+ 3,38	13,48	+ 3,69
12,94	— 0,44	13,00	0	13,49	+ 3,77	13,0	0	13,02	+ 0,15
13,92	— 0,55	14,0	0	15,58	+11,30	13,95	— 0,36	14,04	+ 0,36
11,82	+ 7,47	12,08	+ 9,78	11,56	+ 5,13	12,05	+ 9,55	12,09	+ 9,94
7,51	— 1,20	7,12	— 6,30	7,10	— 6,53	7,47	— 1,71	7,87	+ 2,89
8,81	+ 3,60	9,31	+ 9,52	8,93	+ 5,0	9,22	+ 8,47	9,20	+ 8,20
7,60	— 4,60	7,98	— 0,20	8,06	+ 0,7	8,0	0	8,05	+ 0,56
12,45	— 4,23	13,05	+ 0,41	12,39	— 4,70	12,9	— 0,77	12,77	— 1,77
14,97	— 0,20	14,96	— 0,27	14,51	— 3,24	15,11	+ 0,73	15,2	+ 0,33
16,42	— 3,96	17,26	+ 0,94	17,14	+ 0,23	17,27	+ 0,99	17,29	+ 1,01
18,58	— 2,24	18,69	— 1,65	18,8	— 1,0	18,65	— 1,84	18,63	— 1,95
23,01	+ 9,50	21,15	+ 0,72	22,5	+ 7,14	21,2	+ 0,95	21,18	+0,86
11,75	+23,6	12,42	+30,74	11,36	+19,5	9,5	0	9,5	0
16,72	+10,72	18,42	+22,80—	18,7	+23,84	15,1	0	15,1	0
15,53	— 8,65	17,72	+ 4,245	18,17	+ 6,9	17,12	+ 0,71	16,52	— 2,82
12,14	+ 5,56	12,28	+ 6,8	8,85	—23,0	12,06	+ 4,87	12,1	+ 5,22
12,17	— 6,36	12,35	— 4,98	8,92	—31,38	12,13	— 6,69	12,16	— 6,48
13,13	—12,49	14,14	— 5,7	11,04	—26,4	14,05	— 6,3	13,85	— 7,65
18,35	+ 7,91	17,72	+ 4,25	16,9	— 0,59	18,44	+ 8,47	17,98	+ 5,76
16,00	— 6,47	17,57	+ 2,77	16,9	— 1,17	17,53	+ 2,51	17,74	+ 3,72
19,42	— 7,6	19,61	— 6,64	19,23	— 8,43	19,46	— 7,3	19,5	— 7,14
26,56	+15,47	23,92	+ 4,10	25,40	+10,43	24,14	+ 4,96	23,87	+ 3,78
13,48	+29,49	15,80	+51,87	14,56	+40,0	15,20	+46,2	13,70	+31,73
11,05	+16,30	13,63	+43,4	11,02	+16,0	9,54	+ 0,4	9,51	+ 0,10
15,83	— 1,07	17,66	+10,39	16,12	+ 0,75	16,00	0	16,0	0
10,51	—19,20	13,0	0	8,8	—32,30	13,06	+ 0,46	13,08	+ 0,58
12,2	—18,7	14,77	— 1,53	10,21	—31,90	14,7	— 2,0	14,63	— 2,44
17,45	— 7,70	18,98	+ 0,4	17,84	— 5,60	10,95	+ 0,79	19,05	+ 0,79

Table IV

Standard deviation

Method	Steel			
	I	II	III	IV
Larson & Miller	0,0566	0,0383	0,1074	0,1993
Orr, Sherby & Dorn	0,0675	0,0371	0,1071	0,1755
Manson & Haferd	0,0480	0,0524	0,1152	0,2366
Conrad	0,0662	0,0533	0,1268	0,2298
Murry	0,0542	0,0580	0,1806	0,2144
Krish	0,0279	0,0456	0,0431	0,1579
Russian	0,0305	0,0484	0,0513	0,1102

Table V

Extrapolated rupture-stress values at 560 C°

Method	Time hrs.	Steel			
		I	II	III	IV
		(Stress in kp/mm²)			
Larson & Miller	10^4	9,22	9,20	13,22	13,66
	10^5	6,23	6,49	9,28	9,15
Orr, Sherby & Dorn	10^4	9,47	9,22	13,92	13,90
	10^5	7,00	6,57	10,93	9,73
Manson & Haferd	10^4	9,40	9,06	14,58	14,87
	10^5	5,46	4,96	10,01	9,60
Conrad	10^4	9,58	10,87	15,29	16,17
	10^5	5,59	6,15	11,52	12,23
Murry	10^4	9,29	8,62	15,75	14,40
	10^5	6,34	5,73	11,76	10,25
Krish	10^4	9,79	9,55	15,65	16,25
	10^5	6,56	6,25	12,27	12,80
Russian	10^4	9,77	9,51	13,00	15,87
	10^5	6,99	6,80	10,33	12,76

A comparison of the standard deviation for the different steels with various formulae show that no single method gives the minimum value of standard deviation for all the four steels. The iso-thermal relations have a better correlation with the experimental data when compared with the parametric methods. However, these methods have the disadvantage, that for better reliability the tests are to be conducted at the temperatures at which the material is put to use. The larger deviations of some of the test points in steels III

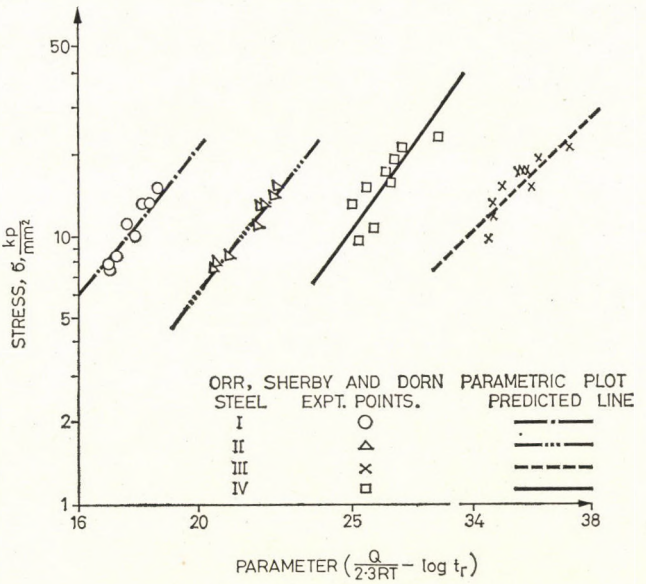
50
10
5
2
1
STRESS, σ, kp/mm²
ORR, SHERBY AND DORN PARAMETRIC PLOT
STEEL EXPT. POINTS. PREDICTED LINE
I
II
III
IV
16
20
25
34
38
PARAMETER (Q/2·3RT − log t_r)

Fig. 3

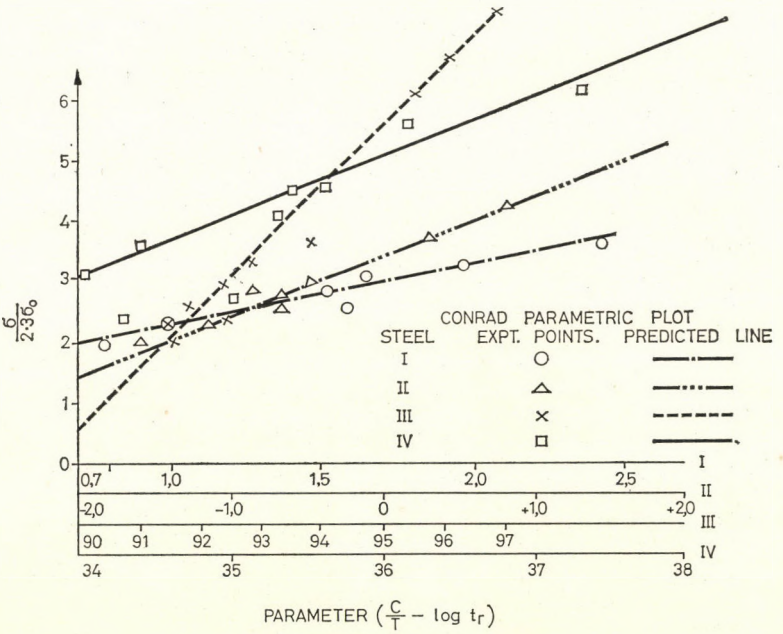
σ/2·36₀
6
5
4
3
2
1
0
CONRAD PARAMETRIC PLOT
STEEL EXPT. POINTS. PREDICTED LINE
I
II
III
IV
0,7
1,0
1,5
2,0
2,5
-2,0
-1,0
0
+1,0
+2,0
90
91
92
93
94
95
96
97
34
35
36
37
38
PARAMETER (C/T − log t_r)

Fig. 4

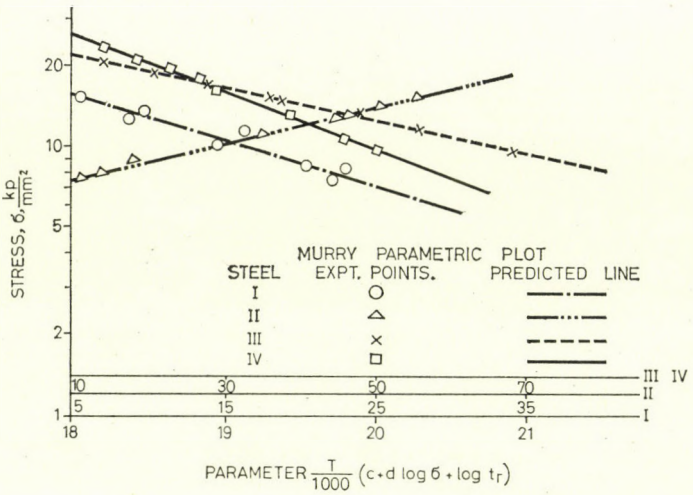

Fig. 5

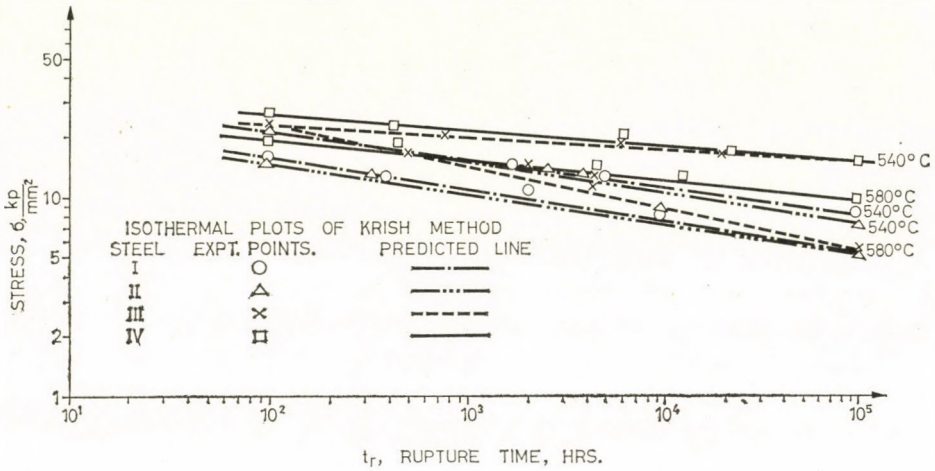

Fig. 6

and IV may be partly because of the termination of the tests before rupture. The lowest standard deviation is given by the Krish method for steels I and III, while the Orr, Sherby and Dorn method and the Russian method have given the minimum standard deviation for steels II and IV, respectively. This shows that for better correlation no single method is to be relied upon. Among the parametric methods, though there is a slight difference in the standard deviation given by different methods, their order of magnitude is the same.

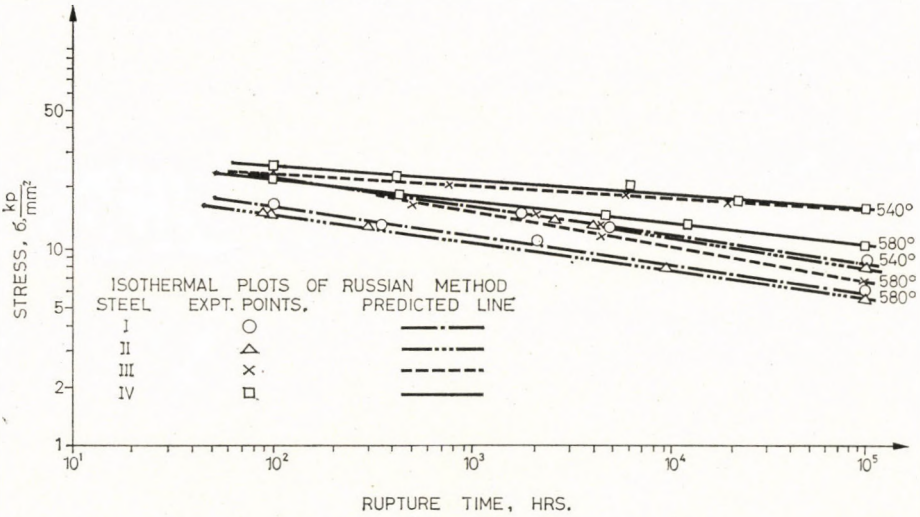

Fig. 7

5. Conclusions

Some methods which are currently in practice for extrapolating the creep-rupture data, are outlined and their ability to correlate and extrapolate the creep-rupture data is compared by standard deviation. No single method is found to give the minimum value of standard deviation for all four steels. In general, the iso-thermal relations have the better correlation with the creep-rupture data than the parametric methods. Among the parametric methods, all the methods have given the standard deviation of the same order of magnitude, even though there are slight differences in the standard deviation values.

Acknowledgements

The author expresses his deep sense of gratitude to Prof. Prohászka János for his valuable guidance and constant encouragement in this work. He is highly thankful to Mr. Süle János who was kind enough to provide the creep-rupture data. He is thankful to the Hungarian Academy of Sciences for providing a scholarship.

REFERENCES

1. Larson, F. R.—Miller, J.: *Trans. ASME*, **74** (1952), 765
2. Orr, R. L.—Sherby, O. D.—Dorn, J. E.: *Trans. ASM*, **46** (1954), 113
3. Conrad, H.: *J. Basic Engg., Trans. ASME*, 81 (1959), 617
4. Manson, S. S.—Haferd, A. M.: NACA TN 2890, March, 1952.
5. Murry, G.: "Joint International Conference on Creep", 1963, p. 6—87.
6. Cited by J. Prohászka S.: "Symposium on Metallurgy and Material Testing", Balatonszéplak, 1971, p. 241.
7. Krish, A.: *Archiv f. d. Eisenhüttenw.*, **33** (1962), 107

8. HOLLOMAN, J. H.—JAFFE, L. C.: *Trans. ASME*, Iron and Steel Division, **162** (1945), 223
9. GOLDHOFF, R. M.: *J. Basic Engg., Trans. ASME* **81** (1959), 629
10. KRISH, A.—WERNER: *Archiv f. d. Eisenhüttenw.*, **28** (1957), 339
11. SCHOECK, G.—SEEGER, A.: "Defects in Crystalline Solids", Physical Society of London, 1955
12. MURTY, M. N.—PATEL, T. S.: *Indian J. Tech.*, **6** (1968), 99
13. WEERTMAN, J.: *J. Appl. Physics*, **26** (1955), 1213
14. BARRET, C. R.—NIX, W. D.: *Acta Met.*, **13** (1965), 1247
15. NABARRO, F. R. N.: "Report on a conference on strength of Solids", Physical Society, London, 1948, p. 75.
16. SHERBY, O. D.—BURKE, P. M.: *Progress in Material Science Journal*, **13** (1968), 360
17. ARDEL, A. J.—SHERBY, O. D.: *Trans. AIME*, **239** (1967), 1547

Vergleichende Untersuchung einiger Extrapolationsformeln für die Auswertung von Zeitdauern. Im Beitrag wird über die vergleichende Untersuchung einiger Extrapolationsformeln der Zeitmessungen berichtet. Die grundlegenden Unterschiede zwischen den verschiedenen Parameterformeln werden behandelt. Es wird nachgewiesen, daß der Grund für diese in den die Geschwindigkeit bestimmenden Mechanismen liegt, die in den verschiedenen Parameterformeln unterschiedlich sind und durch die die von verschiedenen Verfassern bei der Ableitung ihrer Parameterformeln gemachten Annahmen zum Ausdruck kommen. Anhand der bei Dauerprüfungen von Cr-Mo-V-Stahl erhaltenen Meßwerte werden mit Hilfe der Standardabweichung die Extrapolationsmöglichkeiten verschiedener Formeln verglichen. Es ergab sich, daß in der Regel die isothermischen Beziehungen mit den Dauerprüfungsergebnissen besser korrelieren. Alle hier behandelten Parameterformeln ergaben Standardabweichungen gleicher Größenordnung. Es werden nach verschiedenen Verfahren die zu Zeitdauern von 10^4 und 10^5 gehörenden Bruchspannungen angegeben.

Сравнительное исследование некоторых экстраполяционных формул для оценки продолжительностей. В работе дается обзор сравнительной проверки некоторых экспраполяционных формул измерения времени. Излагаются основные различия между разными параметрическими формулами. Доказано, что причина этих основных различий заключается в определяющих скорость механизмах, которые различаются друг от друга в отдельных параметрических формулах, и это выражает предположения, сделанные различными авторами при выводе своих собственных параметрических формул. Используя данные, полученные при измерении времени для хромомолибденованадиевой стали, сравнивается экстраполяционная способность формул стандартного отклонения. Получено, что в общем данные измерения времени имеют лучшую корреляцию с изотермическими зависимостями. Каждая из приведенных параметрических формул дала стандартное отклонение аналогичного порядка. Для продолжительностей в 10^4 и 10^5 *час* задается разрушающее напряжение путем различных методов.

Acta Technica Academiae Scientiarum Hungaricae, Tomus 76 (3—4), pp. 307—336 (1974)

SPHERICAL GRIDS OF TRIANGULAR NETWORK

T. TARNAI*

(Manuscript received March 28, 1971)

The network of single-layered spherical grids consisting of triangles is geometrically analysed. The answer sought for is how a sphere surface might be divided into the greatest possible number of spherical triangles with a small number of different side-lengths in such a way that the division be as uniform as possible. With the aid of regular or semi-regular solids approximately uniform triangular division is produced on the surface of the sphere from which the densest network should be selected. A new method of division is suggested and the resulting configurations are compared to those obtained by Fuller's methods of subdivision.

1. Symbols

The following symbols are used in this paper:

c number of all vertices of a polyhedron,
c_k number of different solid angles of a polyhedron,
e number of all edges of a polyhedron,
e_k number of different edges of a polyhedron,
E_i $(i = 1, 2, \ldots, e_k)$ ith differing edge of a polyhedron or corresponding side of a spherical triangle,
l number of all faces of a polyhedron,
l_k number of different faces of a polyhedron,
L_i $(i = 1, 2, \ldots, l_k)$ ith different face of a polyhedron or a corresponding spherical triangle,
L_i' mirror image related to the plane of a great circle of face L_i or a spherical triangle,
n fineness grade of network meaning in most cases into how many parts the side of a spherical triangle of the basic configuration has been subdivided,
s_k number of different dihedral angles of a polyhedron.

2. Introduction

In the past two decades a number of spherical cupolas have been constructed of metallic frame mounted in situ from prefabricated units. In planning the structures, the designers strove to assemble them from as many uniform elements as possible.

The object of constructing a spherical network from a number of elements as small as possible was originated by FULLER [9]. On the basis of his conceptions a number of spherical tents [5] and domes [9, 8, 2] have been built.

* T. TARNAI, Klauzál tér 2, 6720 Szeged, Hungary

However, the geometry of the network of these spherical grids is only partly known. FULLER divided the surface of the sphere into spherical triangles with the aid of geodesic lines, i.e. the great circles. A geometric system (the so-called energetic—synergetic geometry) developed by FULLER served as basis for the network construction. Two basic types of Fuller's geodesic systems are known [5, 6, 3] for which as basic configuration of division the regular icosahedron and the convex polyhedron consisting of regular pyramids placed upon the faces of the regular pentagondodecahedron, i.e., the spherical projection of the network of their edges have been chosen.

A special type of the spherical grids was also analysed by TUPOLEV [10].

In this paper the geometric analysis of the network of single-layered spherical grids will be dealt with. The purpose is to establish whether an inscribed convex polyhedron confined by triangular faces or a spherical network configuration consisting of spherical triangles exists or not to a given sphere which might be selected for a finer network by subdividing the spherical triangles of the network configuration, like that obtainable by refining the network of the spherical icosahedron or completed dodecahedron with the reservation that the number of the different types of faces or edges of the originating polyhedrons should be the same. Another purpose is that, if Fuller's principle is not rigorously followed (according to which, within a spherical triangle of a spherical network configuration serving as basis for the division, a dividing line is always an arc of a great circle whose end points fall on the two sides of the spherical triangle), in some cases a definite method should be given for carrying out the division.

Lastly, the data of the constructed polyhedrons (spherical networks) will be confronted with the data of Fuller's familiar polyhedrons (spherical networks).

3. Basic concepts[1]

In the paper certain geometrical basic concepts are used. Among these the most elementary ones are: the *polygon*; *side*, *vertex*, *angle of the polygon*; *the polyhedron*; *face*, *edge*, *vertex*, *edge angle*, *dihedral angle of the polyhedron*; *the great circle of the sphere*; these will not be defined here, they only will be referred to in [7], where the meanings of these concepts are explained.

Some important, partly commonly familiar concepts will be interpreted as follows:

3.1. A configuration is *convex* if all points of a straight segment connecting any two points of the configuration belong to the configuration.

3.2. A convex polygon is *regular* if all of its sides and angles are equal. In the plane there is only one single point whose distances to the vertices, respectively sides of the regular polygon are equal. This is the *centre* of the regular polygon.

[1] Those discussed below are detailed, for example, in [7, 1, 4].

3.3. If to the points of a region of polygons from a point outside the plane of the polygon half-lines are drawn, an *infinite pyramid* is obtained. The polyhedron which is produced by intersecting the infinite pyramid by the plane of the polygon, is called *pyramid*. The polygon is the *base-face* of the pyramid. The other faces are triangles and they are the *side-faces* of the pyramid. The side-faces together constitute the *mantle* of the pyramid. The edges confining the base-face are the *base-edges* of the pyramid, the rest are the *side-edges* of this latter. The origin of the half-lines partaking in originating the pyramid is the *vertex* of the pyramid. The half-lines in the side-faces from the origin to the base-edges are the *generatrices* of the pyramid.

The pyramid is *regular* if its base-face is a regular polygon and its vertex lies in the vertical line standing in the centre of the base-face normal to it.

3.4. An infinite pyramid which is confined by regions of angles adjoining through their legs, are called *solid angles (solid angle ranges)*. The confining solid angle ranges are the *sides* of the solid angle, the adjoining half-lines are the *edges* of the solid angle and the dihedral angles formed by the adjoining solid angle ranges are the *angles* of the solid angle. The common origin of the edges is the *vertex* of the solid angle. The convex solid angle region is called *trihedron*. A solid angle is *regular* if its faces and angles are equal. If a polyhedron is singly connected, and in all of its edges only two faces meet, than to each vertex of the polyhedron only one solid angle may be adapted whose vertex is the same as that of the polyhedron, its edges comprise the edges of the polyhedron which converge in the vertex, its faces are the edge angles of the polyhedron, and the angles are the dihedral angles of the polyhedron. This solid angle is the *solid angle* of the polyhedron.

3.5. A convex polyhedron is a *regular solid* if all of its edges, angles formed by the edges (edge angles), and dihedral angles are equal. In the space there is only one single point which lies at equal distances from the vertices, respectively faces of the regular solid. This point is the *centre* of the regular solid.

The faces and solid angles of the regular solid are regular and congruent.

3.6. If in the case of a convex polyhedron regularity is required for the faces and congruence for the solid angles or conversely, then a *semi-regular solid* is obtained. In order not to classifyby this definition the regular solids among the semi-regular solids, it should be stated that regularity and congruence cannot be simultaneously fulfilled in respect to the faces and solid angles. Accordingly, the semi-regular solids may be grouped into two classes:

In class 1 the convex polyhedrons are included whose faces are all regular polygons and all of their solid angles are congruent but not regular.

In class 2 the convex polyhedrons are comprised whose faces are all congruent but not regular, and all of their solid angles are regular.

To each of the polyhedrons belonging to class 1, another one may be found in class 2 which has as many vertices as that in class 1 has faces and vice versa. This polyhedron of the 2nd class is the *dual* of that of class 1. The semi-regular solids included in class 1 are called the *Archimedean polyhedrons*. All edges of the Archimedean polyhedron are equal. For the designation of the Archimedean polyhedrons a set of numbers will be used on the basis of [4]: $(i, j, \ldots, m)$. The meaning of the numbers in this set is: a set of numbers consists of as many numbers, as many polygon-faces meet in one vertex, and the numbers $i, j, \ldots, m$ mean that each polygon has $i, j, \ldots, m$ angles. For example, (4, 6, 8) means that in every vertex three polygons meet, among these there is a tetragon, a hexagon and an octagon. The Archimedean polyhedrons are shown in Figs 5 to 19 with heavy lines.

3.7. A configuration cut out from a spherical surface by a trihedron, is called the *spherical triangle*, if the vertex of the trihedron is identical with the centre of the sphere.

3.8. If a surface of a polyhedron having an inscribed sphere (all of the faces of the polyhedron touches a sphere) or a circumscribed sphere (all of the vertices of the polyhedron lie on the surface of a sphere) will be projected from the centre to the surface of the sphere, then the projection of the edges of the polyhedron on the sphere will be a system of lines consisting of arcs of great circles which is called the *spherical network of the edges (network)* of the polyhedron.

The surface of the sphere subdivided by the spherical network which is the spherical projection of the polyhedron, is called the *entire spherical network configuration (spherical network configuration)*.

3.9. By the term *density* of the spherical network of edges the ratio of the length of the network and the diameter of the sphere is meant. If a network configuration such as is merely consisting of spherical triangles and the triangles are approximately equilateral, and approximately equiform, the density of the network is fairly well characterized by the numbers of the sides of the spherical triangles (that is, those of the polyhedron edges corresponding to the spherical configuration) or by the numbers of the spherical triangles (that is, the corresponding

polyhedron faces). In fact, the polyhedron corresponding to the spherical network configuration is confined by triangle faces, and in this case

$$e = \frac{3}{2} l .$$

3.10. The shortest line on a surface connecting two points of this surface is the *geodesic line*. The geodesic lines of a spherical surface are the great circles. The spherical cupolas constructed on the basis of the spherical network consisting of arcs of great circles, are called *geodesic domes*.

4. Approximate polyhedrons of the sphere

If a spherical structure — for example, a dome — is to be constructed from prefabricated units, then, from the viewpoint of manufacturing and assembling, it seems to be convenient that the units whose longitudinal, or longitudinal and lateral dimensions are large in comparison to the other dimensions do not possess longitudinal and lateral curvature, that is, these units should be either straight bars or plane plates. With the help of such structural units, as a matter of course, a spherical surface cannot be produced but only an approximating polyhedron of the sphere.

It is stated that a polyhedron approaches a sphere of radius r up to a degree ε if all points of the surface of the polyhedron lies within the region confined by the concentric spherical surfaces of $r + \varepsilon$, $r - \varepsilon$ radii.

Among the different kinds of polyhedrons it is convenient to select two types easy to treat:

a) a polyhedron which is an inscribed convex polyhedron of the sphere,

b) a polyhedron which is a circumscribed polyhedron of the sphere.

In the case of a given sphere an inscribed or circumscribed polyhedron approaches the sphere closer than another one if its edges and faces are of smaller dimensions.

For certain values of ε also the regular and semi-regular solids may be considered as the approximating polyhedron of the sphere. The regular solids belong to both types, the Archimedean polyhedrons belong to type *a)*; the duals of the Archimedean polyhedrons belong to type *b)*.

If a structure consists of bars and nodal elements connecting the bars, it is called a *bar structure*. If a structure consists of plane slabs and elements connecting them along their edges, it is called a *plate structure*.

In a *bar structure* built up on an edge network of a polyhedron, the nodal elements assure the dihedral angles of the polyhedron and when assembling, the faces of the polyhedron will be automatically developed by the two kinds of the elements (bars and nodal elements).

In a *plate structure* built up on an edge network of a polyhedron, the edge elements assure the dihedral angles of the polyhedron, and

when assembling, the solid angles of the polyhedron will be automatically developed by the two types of elements (f a c e s a n d e d g e e l e m e n t s).

The edge angles of the polyhedron are automatically assured by the nodal elements and faces, respectively, at both types of structures.

The bar structures are well-known. For the plate structures Fig. 1 shows an example, here the faces are constituted of triangular frames. In Fig. 2, the connection of the faces, the elements assuring the dihedral angles and the node (solid angle) developed are to be seen. The vertices of the polyhedron serving



Fig. 1. Spherical grid assembled of triangular frames

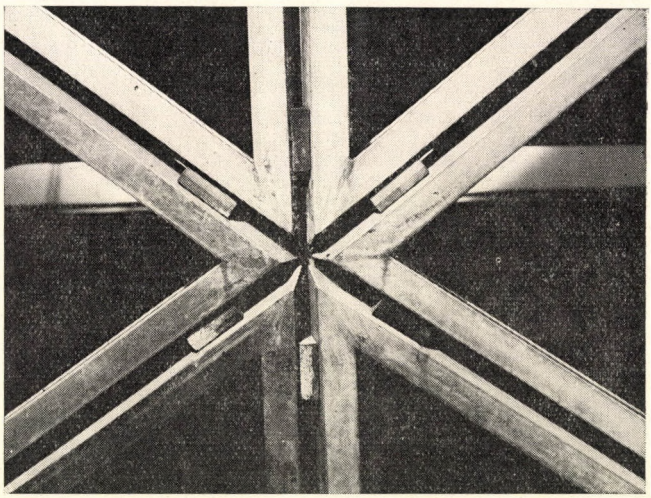

Fig. 2. A joint of the grid

as basis of the construction of the structure are located on a sphere surface of a diameter of 15 m; the number of the confining faces is 240. The structure was designed by I. KÁDÁR.

5. The problem of subdivision

If a spherical configuration of a given radius should be constructed from straight bars and nodal elements as a single-layered grid, than the following requirements should be fulfilled:

a) The form of the grid should approach the sphere as closely as possible. The network of the grid should correspond to the edge network of one of the approximating polyhedrons of the sphere.

b) The network of the grid should merely consist of triangles because among the grids enclosing the part of space singly connected, only a grid built up of triangles is rigid.

c) The greatest dimension of the elements should not surpass the limit of transportability and mountability. The buckling wave- length of the bars should be as short as possible.

d) The structural members should be of the same dimensions so that they should be suitable for mass production and to be uniform and attractive in appearance.

Condition *a)* can be satisfied in several ways. In section 4, among the feasible ways, the two most significant ones have been mentioned. *In the following, the case will be dealt with where the approaching polyhedron is the inscribed convex polyhedron of the sphere.*

Let us now see which polyhedrons meet the above requirements.

The regular solids comply with requirements *a)* and *d)*, in fact, the inscribed convex polyhedrons of the sphere and all their edges and solid angles are equal. Among the five kinds of regular solids only three fulfil the requirement *b)*: these are the tetrahedron, ($c = 4$, $e = 6$, $l = 4$, in a vertex three edges meet); the octahedron ($c = 6$, $e = 12$, $l = 8$, in a vertex four edges meet); and the icosahedron ($c = 12$, $e = 30$, $l = 20$, in a vertex five edges adjoin).

Let us fix the dimension prescribed in point *c)* which gives the upper limit of the edge length and let us increase the radius of the sphere. Consider now the above three polyhedrons. In the case of the tetrahedron, the edge length rapidly reaches the given limit.

Let us consider now the octahedron. The radius of the sphere may be augmented in order to keep the edge length below the given limit. However, by further augmenting the radius of the sphere, also the edge length of the octahedron surpasses the limit and, in this case only the icosahedron (Fig. 3) could be taken into account. Thus, it can be stated that, as long as the radius of the sphere does not surpass the 1/1,0515fold value of the given limit, but is $1/\sqrt{2}$

times greater than this limit, among the regular solids only the icosahedron satisfies condition *c)*.

However, if the radius of the sphere is large, then also the edges of the inscribed icosahedron will be large and might exceed the limit defined by condition *c)*; therefore, such polyhedrons should be found, the edge network of which is more refined and accordingly, its edges are shorter.

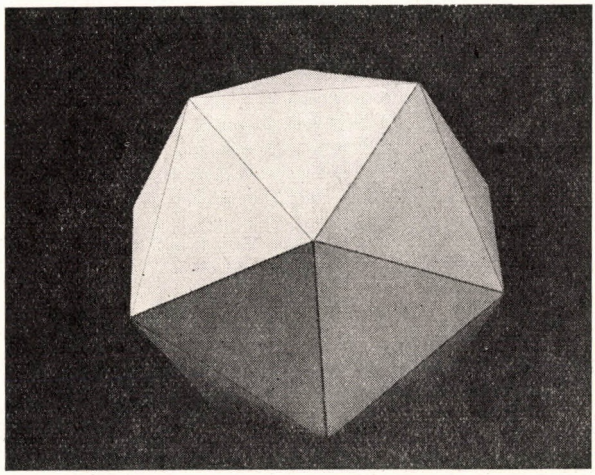

Fig. 3. Regular icosahedron

Polyhedrons of this kind may be found among the semi-regular solids. For example, the Archimedean solid (3, 4, 5, 4) has 60 vertices, 120 edges, and 62 faces. The Archimedean polyhedrons satisfy the requirements *a)* and *d)*, being the inscribed convex polyhedrons of the sphere, and their edges and angles are equal. They also fulfil the condition *c)* for spheres of not very large radii to which the icosahedron does not fit any longer. However, the Archimedean polyhedrons are confined by polygons of 3, 4, 5, 6, 8 and 10 angles and no polyhedrons are confined merely by triangles. Therefore, these polyhedrons do not satisfy condition *b)*. But on the faces of the Archimedean polyhedrons which are not triangles, regular pyramids may be located so that the base-face of the pyramid is the face of the polyhedron and the vertex of the pyramid is on the surface of the sphere circumscribed about the polyhedron.

Thereby it is attained that all of the faces of the new polyhedron thus developed are triangles and the side-edges of the pyramids give one or more new edge lengths which differ from the edge length of the Archimedean polyhedron defining the base-edges of the pyramids. Since among the inscribed convex polyhedrons of the sphere there are no other polyhedrons except those discussed above, the edge lengths of which would be equal, and since the edge network of the Archimedean polyhedrons does not consist merely of triangles,

the requirement that all of the edges of the polyhedron should be equal, could not be fulfilled.

In lieu of the condition *d)* one could take into account the following two conditions valid simultaneously:

*d.*1*)* The structure should consist of many equal, but only of a few different types of units, for assuring the economy of the prefabrication.

*d.*2*)* The dimensions of the units should differ from each other only little for assuring the appearance of uniformity of the units and to give a pleasing aspect of the structure, further, with the purpose that the structure could be constructed from bars of identical length in a way that the differences in length could be assured with the aid of the nodal connections.

Those mentioned above concerned the bar structures. Comparable conditions could be established in respect to plate structures by taking plates in lieu of bars and connecting members along the edges in lieu of nodal units. In the case of plate structures in condition *b)* other polygons than triangles could be selected. The plate structure consisting of solid plates is, as a matter of fact, a surface structure, however, if only the edges of the plates participate in load bearing, then the plate structure becomes a spatial framework. If the frame network consists of triangles, then a grid is obtained. In the following, when dealing with plate structures, only those constructed from triangles will be considered for which, essentially, the very same conditions will be valid as for those of the bar structures.

It is easy to understand that the inscribed convex polyhedron of a sphere confined by triangular faces might reciprocally unequivocally be correlated with its spherical network configuration if for each spherical triangle of the network configuration the following condition *(the condition of reciprocally unequivocal correlation)* is fulfilled: the calotte covering the spherical triangle, the base circle of which passes through all the three vertices of the spherical triangle, does not cover any more vertices. Having made this statement, in the case of accomplishing condition *a)*, the requirements *b* to *d.*2 could be summarized as follows *(problem of the subdivision)*:

Let us divide a sphere of given radius with the aid of great circles into spherical triangles in a way that

α*)* also the longest side of the spherical triangle should be shorter than a given length,

β*)* as few different types of sides of the spherical triangles and spherical triangles themselves should occur as possible; the sides of equal length of the spherical triangles and the congruent spherical triangles be as many as possible,

γ*)* the sides of the spherical triangles and the spherical triangles should differ as little as possible, that is, the subdivision should be as uniform as possible. It is required that the condition of reciprocally unequivocal correlation should be fulfilled.

To the spherical network configuration satisfying the conditions of the problem of subdivision a polyhedron is associated which satisfies the conditions of the primary problem.

The investigations should be carried out on the sphere of unit radius.

Among the regular and semi-regular solids there are such as those satisfying in invariable form or by *pyramid completion* the conditions except those to be found under point *c)* and *α)*. In order to fulfil also the conditions *c)* and *α)*, these polyhedrons or their spherical projections should further be subdivided as long as the lengths of the edges and sides do not come under the given limit.

It should be investigated in the case of $e_k = 1, 2, 3$ (for plate structures $l_k = 1, 2$) which are the polyhedrons in the case of which the ratio of the longest and shortest edges is the lowest. The spherical network of the polyhedrons developed in this way will be refined by subdivision and from the network configurations so obtained the densest networks should be selected.

In principle, it should still further be investigated whether a certain densest triangular subdivision of a sphere surface has been produced from an earlier spherical configuration (for example, from spherical icosahedron) by a certain further subdivision (all vertices of the earlier configuration will also become vertices of the subdivided configuration), however, this investigation will not be dealt with here.

6. The regular solids and their pyramid completions

Let us now ignore the conditions *c)* and *α)* of Section 5.

In the case of bar structures, the polyhedrons in respect to which the condition $e_k = 1$ and also the other conditions are fulfilled, are some kinds of regular solids. Among them — as has been seen — it is the icosahedron which satisfies the conditions best.

In the case of plate structures for $l_k = 1$, the polyhedron satisfying the other conditions best may be derived in the following way:

Consider the regular dodecahedron inscribed in the sphere. The faces of the dodecahedron are regular pentagons (at a vertex three edges meet). Let us project the centres of the faces from the centre of the dodecahedron on the sphere surface. Connect these projected points by straight line segments with the points of edges confining each of the faces. Thus, on each face of the dodecahedron a regular pyramid has been positioned whose vertex lies in the sphere surface. The mantles of the pyramids give an inscribed convex polyhedron of the sphere (Fig. 4), which is designated by $(5, 5, 5)_g$.[(5, 5, 5) designates the dodecahedron. This notation is in agreement with that given for the Archimedean polyhedrons in Section 3.8. The subscript g refers to the fact that the

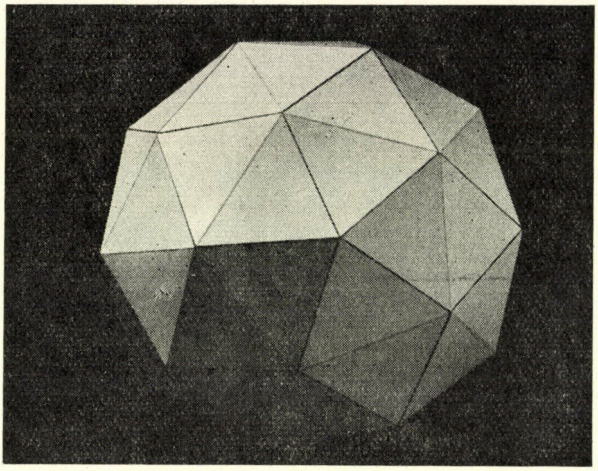

Fig. 4. $(5, 5, 5)_g$

polyhedron was obtained from (5, 5, 5) by pyramid completion]. The polyhedron $(5, 5, 5)_g$ is confined by 60 congruent isosceles triangles. The ratio of length of the two kinds of edges is 1,11. The dimensionless characteristic data are to be found in Table V at $n = 1$. At the vertices of the $(5, 5, 5)_g$, five and six edges meet.

7. The Archimedean polyhedrons and their pyramid completions

If from the solids $(4, 4, n)$ and $(3, 3, 3, n)$ only those defined by a given n (for example, $n = 5$) are considered, then 15 kinds of semi-regular solids of congruent solid angles are obtained.

They are as follows:

(3, 6, 6)	(3, 3, 3, n)	(3, 3, 3, 3, 4)
(3, 8, 8)	(3, 4, 3, 4)	(3, 3, 3, 3, 5)
(3, 10, 10)	(3, 4, 4, 4)	
(4, 4, n)	(3, 4, 5, 4)	
(4, 6, 6)	(3, 5, 3, 5)	
(4, 6, 8)		
(4, 6, 10)		
(5, 6, 6)		

Consider now each of the 15 kinds of Archimedean polyhedrons inscribed in the sphere of unit radius and put on each polygonal face with more than three vertices, regular pyramids in the way shown in Section 6. In this way polyhedrons are obtained which will be denoted as $(i, j, \ldots, m)_g$.

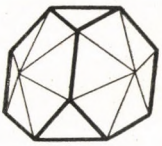

Fig. 5. $(3, 6, 6)_g$

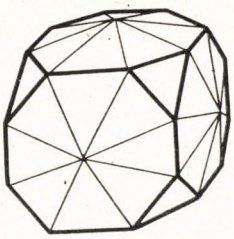

Fig. 6. $(3, 8, 8)_g$

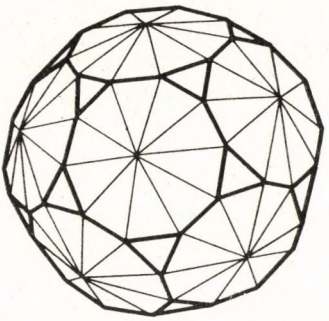

Fig. 7. $(3, 10, 10)_g$

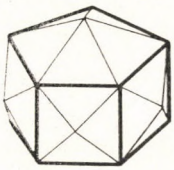

Fig. 8. $(4, 4, 5)_g$

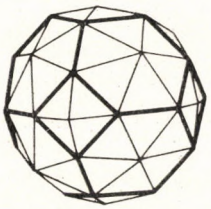

Fig. 9. $(4, 6, 6)_g$

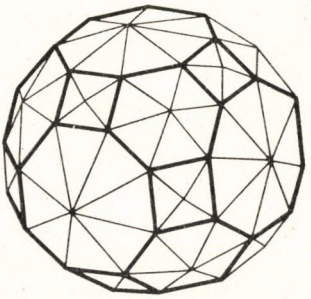

Fig. 10. $(4, 6, 8)_g$

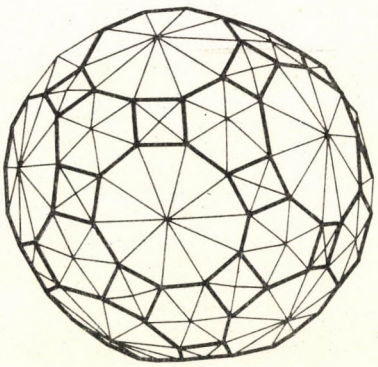

Fig. 11. $(4, 6, 10)_g$

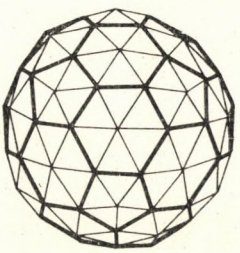

Fig. 12. $(5, 6, 6)_g$

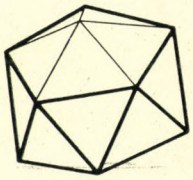

Fig. 13. $(3, 3, 3, 5)_g$

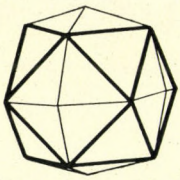

Fig. 14. $(3, 4, 3, 4)_g$

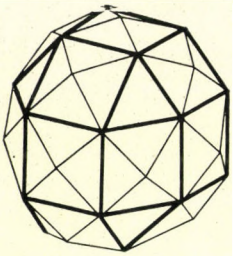

Fig. 15. $(3, 4, 4, 4)_g$

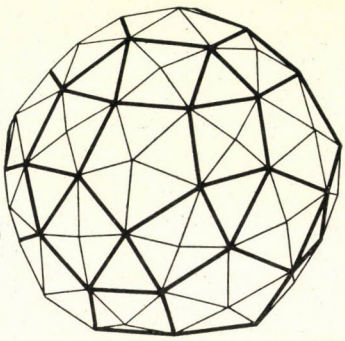

Fig. 16. $(3, 4, 5, 4)_g$

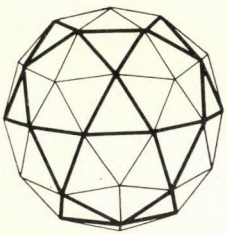

Fig. 17. $(3, 5, 3, 5)_g$

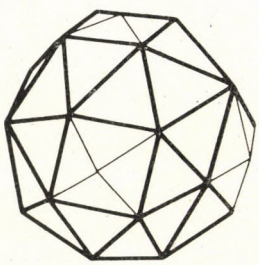

Fig. 18. $(3, 3, 3, 3, 4)_g$

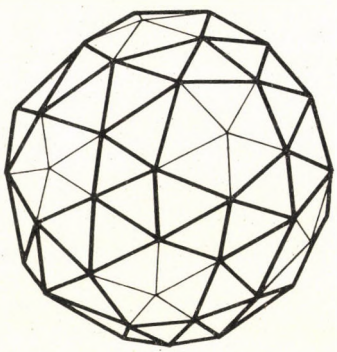

Fig. 19. $(3, 3, 3, 3, 5)_g$

The subscript g again refers to the new polyhedron being obtained from the Archimedean polyhedron $(i, j, \ldots, m)$ by pyramidal completion.

The polyhedrons now completed and confined only by triangles, are shown in Figs 5 to 19. The dimensionless characteristics of the polyhedrons are listed in Table I. From among these polyhedrons those should be selected for different e_k-s, whose networks are the densest and which satisfy the conditions of Section 5, except those given under *c)* and *α)*, respectively.

Among the completed polyhedrons there is only one in the case of which $e_k = 1$. This is the polyhedron $(3, 3, 3, 5)_g$ which is identical with the icosahedron.

However, on the basis of the data to be found in Table I, for the higher values of e_k it cannot be decided which polyhedron satisfies the conditions of Section 5 best and the network of which polyhedron is more refined, because it may happen that at two polyhedrons c_k, c, e_k, e, l_k, l, s_k are identical as, for example, in the case of $(3, 10, 10)_g$ and $(3, 3, 3, 3, 5)_g$. Therefore, the edge-

Table I

Dimensionless characteristic data of the Archimedean polyhedrons completed by regular pyramids

Polyhedron	c_k	c	e_k	e	l_k	l	s_k
$*(3,6,6)_g$	2	16	2	42	2	28	3
$(3, 8, 8)_g$	2	30	2	84	2	56	3
$(3, 10, 10)_g$	2	72	2	210	2	140	3
$(4, 4,n)_g$, n = 5	3	17	3	45	2	30	4
$(4, 6, 6)_g$	3	32	3	108	2	72	4
$(4, 6, 8)_g$	4	74	4	216	3	144	6
	(5)						
$(4, 6, 10)_g$	4	182	4	540	3	360	6
	(5)						
$*(5, 6, 6)_g$	3	92	3	270	2	180	4
$*(3, 3, 3, n)_g$, n = 5	1	12	1	30	1	20	1
$(3, 4, 3, 4)_g$	2	18	2	48	2	32	2
$(3, 4, 4, 4)_g$	2	42	2	120	2	80	3
$(3, 4, 5, 4)_g$	3	102	3	300	3	200	4
$*(3, 5, 3, 5)_g$	2	42	2	120	2	80	2
$(3, 3, 3, 3, 4)_g$	2	30	2	84	2	56	3
$*(3, 3, 3, 3, 5)_g$	2	72	2	210	2	140	3

Starred polyhedrons satisfy the requirements in Section 5, point *d.* 2.
Cyphers in brackets are valid in that case if two elements of the same size, which can only be brought into congruence by mirroring, are considered to be different.

lengths of each polyhedron should be determined and the ratio of the longest and shortest edges for each polyhedron produced. In the case of the polyhedrons at which this ratio is not much higher than 1, the condition *d*.2 of Section 5 will be considered to be satisfied. The polyhedrons will be selected out and established for which of them the requirement *d*.1 of Section 5 is fulfilled. The results of the calculation are listed in Table II. In Table II the edge-length of the Archimedean polyhedron is denoted by k and the edge-lengths of the different regular pyramids applied on the faces, by a_1, a_2, a_3.

Table II

Edge-lengths of Archimedean polyhedrons completed by regular pyramids inscribed in the sphere of unit radius

No.	$(i, j, \ldots, m)_g$	k	a_1	a_2	a_3	$\frac{\max(k, a_1, a_2, a_3)}{\min(k, a_1, a_2, a_3)}$
1	$*(3, 6, 6)_g$	0,8528	0,9775	—	—	1,15
2	$(3, 8, 8)_g$	0,5622	0,8017	—	—	1,43
3	$(3, 10, 10)_g$	0,3363	0,5675	—	—	1,69
4	$(4, 4, 5)_g$	1,0135	0,7778	0,9932	—	1,30
5	$(4, 6, 6)_g$	0,6325	0,4595	0,6714	—	1,46
6	$(4, 6, 8)_g$	0,4315	0,3088	0,4424	0,5900	1,91
7	$(4, 6, 10)_g$	0,2630	0,1868	0,2653	0,4360	2,33
8	$*(5, 6, 6)_g$	0,4035	0,3486	0,4124	—	1,18
9	$*(3, 3, 3, 5)_g$ icosahedron	1,0515	1,0515	—	—	1
10	$(3, 4, 3, 4)_g$	1,0000	0,7654	—	—	1,31
11	$(3, 4, 4, 4)_g$	0,7148	0,5237	—	—	1,36
12	$(3, 4, 5, 4)_g$	0,4478	0,3208	0,3883	—	1,40
13	$*(3, 5, 3, 5)_g$	0,6178	0,5465	—	—	1,13
14	$(3, 3, 3, 3, 4)_g$	0,7724	0,5698	—	—	1,36
15	$*(3, 3, 3, 3.5)_g$	0,4638	0,4028	—	—	1,15

Starred polyhedrons satisfy the requirements in Section 5, point *d*.2.

It may be stated that from among the 15 kinds of polyhedrons only in the case of five is the condition fulfilled that the ratio of the longest and shortest edge is lower than 1,2. In the case of the other polyhedrons this ratio is 1,3 or higher. Thus, the five polyhedrons in the case of which the requirement *d*.2) is fulfilled, are as follows: $(3, 6, 6)_g$ (Fig. 5), $(5, 6, 6)_g$ (Figs 12 and 20), $(3, 3, 3, 5)_g$ (Figs 3 and 13), $(3, 5, 3, 5)_g$ (Figs 17 and 21) and $(3, 3, 3, 3, 5)_g$ (Figs 19 and 22).

At the vertices of these polyhedrons five or six edges meet. From among these five polyhedrons — since there cannot be found among them two poly-

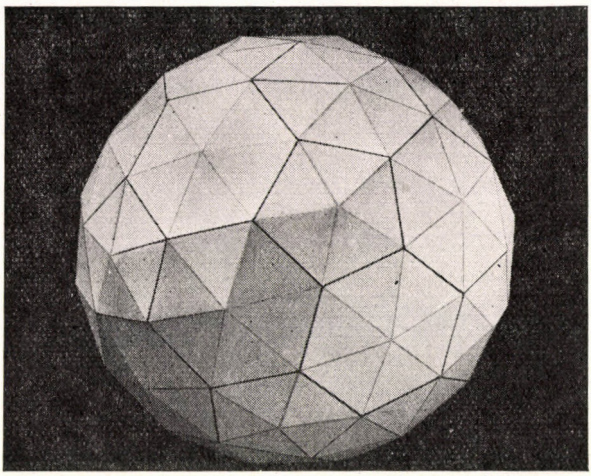

Fig. 20. $(5, 6, 6)_g$

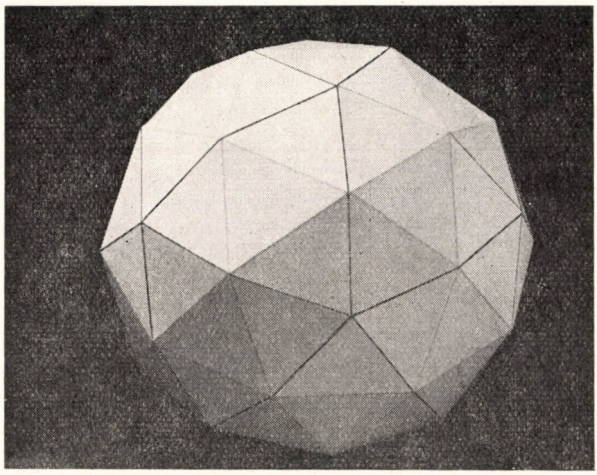

Fig. 21. $(3, 5, 3, 5)_g$

hedrons in the case of which c, e, l, would be the same — the polyhedron defined by the values $e_k = 2$ and $e_k = 3$, consisting of the greatest number of faces might be selected.

These are:

in the case of $e_k = 2$: $(3, 3, 3, 3, 5)_g$, and

in the case of $e_k = 3$: $(5, 6, 6)_g$.

The polyhedron $(3, 3, 3, 3, 5)_g$ consists of two kinds of triangular faces. One of them is regular, the other one is an isosceles triangle. The polyhedron $(5, 6, 6)_g$ consists of two kinds of isosceles triangle faces.

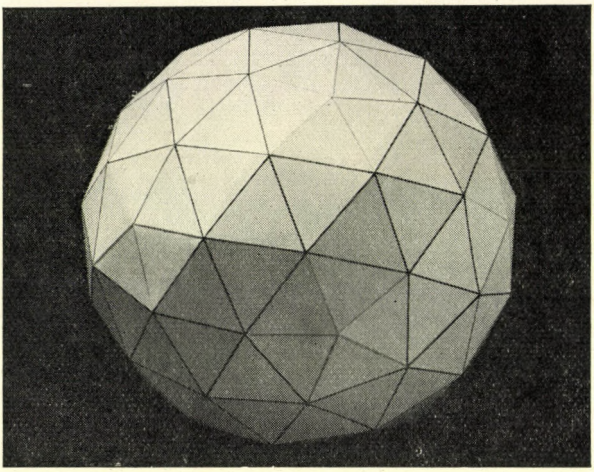

Fig. 22. $(3, 3, 3, 3, 5)_g$

8. Methods of refinement of the network and subdivision of the spherical triangles

It was seen in Sections 6 and 7 that in the case of polyhedrons for which the requirement *d.2)* of Section 5 is fulfilled and which have more faces than the octahedron, at each vertex five or six edges meet. The icosahedron, the $(5, 5, 5)_g$, the $(3, 3, 3, 3, 5)_g$ and the $(5, 6, 6)_g$ will be considered as the basic configurations of the subdivision and their spherical network will be refined according to certain principles, by taking care that also at each vertex of the polyhedron produced by further subdivision, five or six edges meet.

The refinement of the spherical network of the basic configuration is carried out by the subdivision of the confining spherical triangles into smaller spherical ones. Some of the methods of subdivision are described below.

8.1. *Methods of subdivision also applicable to general spherical triangles (Refinement of a network consisting of different triangles)*

8.1.1. *Procedure of side bisection.* Connect the median points of the sides of the spherical triangles by arcs of great circles. Thus, the given spherical triangle has been divided into four spherical triangles. The median points of the sides of the spherical triangles obtained should again be connected by arcs of great circles, and so on. The subdivision may be continued up to optional density. With the aid of this procedure the subdivision of the sides of the original spherical triangles into equal parts (of 2^k) is achieved.

8.1.2. *Refinement by the centre of the circle circumscribed about the spherical triangle.* Consider a spherical triangle of a spherical configuration of any

kind of spherical triangles. Let us connect the centre of the circle circumscribed about the spherical triangle by arcs of great circles with the three vertices of the spherical triangle and with the centre of the circle circumscribed about the three spherical triangles each having a common side with the spherical triangle in question. By carrying out this procedure for every spherical triangle, a new network is obtained three times finer than the original one.

8.2. *Fuller's method of division of isosceles spherical triangles*

Division of the isosceles spherical triangles resulting in the lowest number of different side-lengths, originates from FULLER. His method is described on the basis of [3].

Consider an isosceles acute-angled spherical triangle. Its spherical symmetry line perpendicularly halves the base and also bisects the edge angle ω of the spherical triangle. Then divide the segment of the symmetry line within the triangle into n parts of equal lengths (Fig. 23a). At the points of divi-

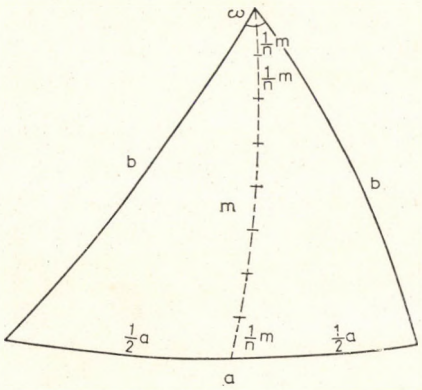

Fig. 23a. Fuller's method of division of isosceles spherical triangle

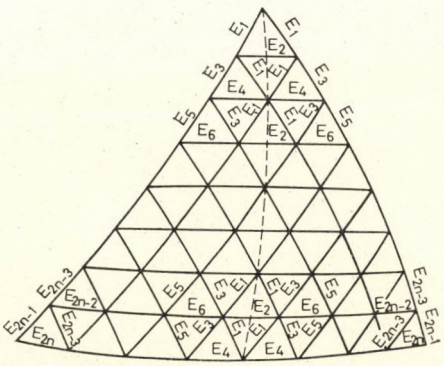

Fig. 23b

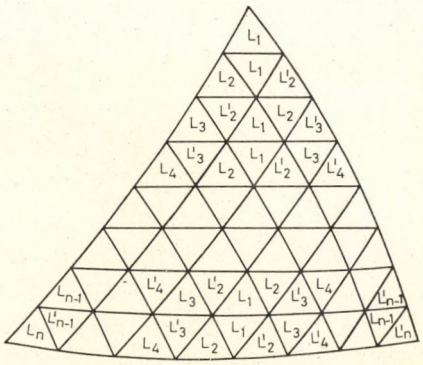

Fig. 23c

sion draw the great circles which are perpendicular to the symmetry line. These intersect the legs of the spherical triangle. Starting from the vertex of the spherical triangle, at the angle of the legs, connect the points of intersection obtained on both legs, with the help of arcs of great circles with every second point of division on the symmetry line. Thus, one can proceed only up to the half of the leg. Therefore, rotate the segment of the symmetry line divided into equal parts on the sphere, about the midpoint of the base by 180 degrees and by making use of the points of division so obtained, continue the procedure. Thereby the isosceles spherical triangle has been divided into n^2 spherical triangles. In the direction of the symmetry line under each other spherical triangles are to be found which can be brought into congruence by mirroring. By this procedure the leg of the spherical triangle will be divided into n segments of arcs of different lengths of great circle, and the base into $n/2$ or $(n + 1)/2$ segments of arcs of great circle, depending, whether n is an even or odd number. On the first dividing great circle above the base $n/2$ or $(n - 1)/2$ arc segments of different lengths of great circle are produced, depending, whether n is an even or odd number.

Thus, this division of an isosceles spherical triangle results in

$2n$ different side-lengths,

n or $2n - 1$ different spherical triangles (depending, whether two spherical triangles of identical dimensions which can only be brought into congruence by mirroring, might be considered as identical or not), and

n^2 spherical triangles.

The result of the division is illustrated in Figs 23b and 23c for the case where n is an even number.

8.3. *Subdivisions of equilateral triangles*

8.3.1. *Fuller's method of division of equilateral spherical triangles.* Fuller's method will be described on the basis of [5] and [6]. In subdividing the equilateral spherical triangles, Fuller sets out essentially from two basic cases:

a) Connect the midpoints of the sides of the equilateral spherical triangle by arcs of great circles. Thereby the spherical triangle has been divided in such a way that within it a new equilateral spherical triangle has been produced whose vertices are the midpoints of the sides of the given equilateral spherical triangle.

b) Draw through the centre of the equilateral spherical triangle arcs of great circle perpendicularly to the symmetry lines.

These define six points of intersection with the sides. Two points of intersection being nearest to the vertices of the spherical triangle connecting in pairs by arcs of great circles, a subdivision is obtained which, within the original spherical triangle, results in a regular spherical hexagon.

If a finer subdivision is required than the equilateral spherical triangle obtained by the subdivision *a)* should be subdivided by one of the *a)* or *b)* basic methods. The points of subdivision obtained outside the inner regular spherical triangle are definitely determined by the great circles perpendicular to the symmetry line.

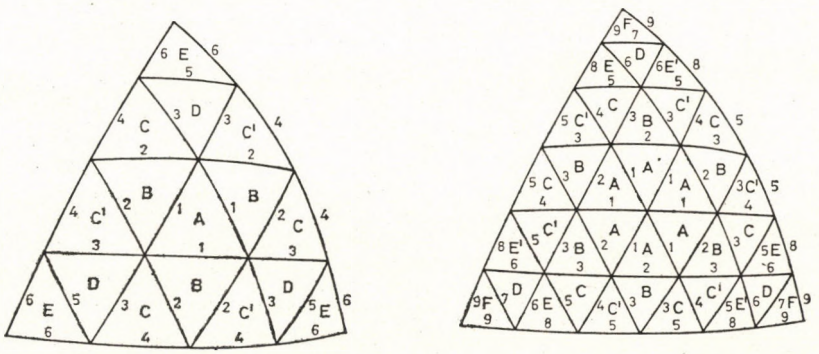

Fig. 24. Fuller's method of division of a triangle of the spherical icosahedron

The subdivision to $n = 2$ is given by the basic version *a)* whereas to $n = 3$, it is obtained by version *b)*; the subdivision to $n = 4$ and $n = 6$ is shown in Fig. 24. In the figure, the cyphers denote the different sides and the capitals denote the different spherical triangles.

8.3.2. *The method of subdivision suggested by the author.* Let us subdivide the three sides of the equilateral spherical triangle into n arcs of equal lengths. At each vertex of the spherical triangle connect the points of division nearest to the vertices with the aid of arcs of great circles. Consider the spherical altitude line (symmetry line) intersecting the vertex of the spherical triangle and the second segment counted from the vertex on the subdivided side of the triangle as well as the perpendicular midline of this segment. This one intersects the altitude line of the triangle. By connecting the point of intersection with the first and second point of subdivision counted from the vertices, isosceles spherical triangles are produced. Let us put on the sides of the original spherical triangle on each of the other segments the same kinds of isosceles spherical triangles. Hitherto three different side-lengths were obtained. The vertices of the isosceles triangles at their leg angles will lie at equal spherical distances from each other along a side of the original spherical triangle because these vertices lie on the sphere also on a plane parallel to that of the side of the spherical triangle. Connect these vertices with the help of arcs of great circles. Thus, the fourth kind of side-length has been obtained. Thereby a configuration has been formed within the original spherical triangle, resembling this latter, whose "sides" (which are now spherical broken lines) are divided through the break points into n—2 equal segments.

The procedure should be repeated as long as a point or spherical triangle has been obtained, depending, whether n could be divided by three or not.

In applying this method, the spherical triangles obtained are all or all but one, isosceles (this one being a regular triangle of central position), depending, whether n could be divided by three or not.

9. Polyhedrons produced by network refinement

In Section 8, with the exception of 8.1.2, some important procedures have been presented, showing how one single spherical triangle of a network configuration consisting of spherical triangles, could be so subdivided that by the subdivision as few new side-lengths as possible should be obtained. Now, by making use of the methods of subdivision, all of the spherical triangles of the sphere network configuration should be divided. Thereby, a finer spherical network configuration consisting of spherical triangles will be produced. In this section the characteristics of the polyhedrons associated with the spherical network configurations (Sections 3.8 and 5) will be analysed.

9.1. *Refinement of the network of the spherical icosahedron*

The subdivision of the icosahedron according to Section 8.1.1. in a second step — if the icosahedron itself is assumed to be the first one — yields the configuration $(3, 5, 3, 5)_g$. Some first steps of the refinement of the network are shown in Table III, point *a)*. By the second step of the refinement of the network according to Section 8.1.2 the configuration $(5, 5, 5)_g$ is obtained. The data of the configurations obtained for the further values of n are to be found in Table III, point *b)*.

The subdivision described in Section 8.3.1 was developed by FULLER, especially for the spherical icosahedron. The regularity involved in this method of subdivision also asserts itself in that for $n = 2$ and $n = 3$, the configurations $(3, 5, 3, 5)_g$ and $(5, 6, 6)_g$, respectively, will be obtained (earlier, these configurations were derived from the Archimedean polyhedrons). Thus, Fuller's subdivision of the icosahedron for certain values of n also yields at the same time the division of the spherical configuration $(5, 6, 6)_g$.

For the higher values of n a more advantageous subdivision than the former ones is assured by the procedure suggested in Section 8.3.2. By making use of this method, in the case of subdivision of a side into n parts, then:

$$
\begin{aligned}
c_k &= n, \\
c &= 10\ n^2 + 2, \\
e_k &= n, \\
e &= 30\ n^2, \\
l &= 20\ n^2.
\end{aligned}
$$

Table III

Refinement of the network of the spherical icosahedron

a) Method of side bisection

No. n	c_k	c	e_k	e	l_k	l	s_k
2	2	42	2	120	2	80	2
3	4	162	5	480	5 (6)	320	5
4	10 (12)	642	15	1920	15 (22)	1280	20

b) Method by centres of circles circumscribed about triangles

No. n	c_k	c	e_k	e	l_k	l	s_k
2	2	32	2	90	1	60	2
3	3	92	3	270	2	180	4
4	6	272	6	810	4 (5)	540	10

c) Method of division suggested by the author

No. n	c_k	c	e_k	e	l_k	l	s_k
1	1	12	1	30	1	20	1
2	2	42	2	120	2	80	2
3	3	92	3	270	3	180	4
4	4	162	4	480	5	320	6
5	5	252	5	750	6	500	7
6	6 (7)	362	6	1080	7	720	9
7	7 (8)	492	7	1470	9	980	11
8	8 (9)	642	8	1920	10	1280	12
9	9 (11)	812	9	2430	11	1620	14
10	10 (12)	1002	10	3000	13	2000	16

Cyphers in brackets are valid if two elements of the same size which can only be brought into congruence by mirroring, are considered to be different.

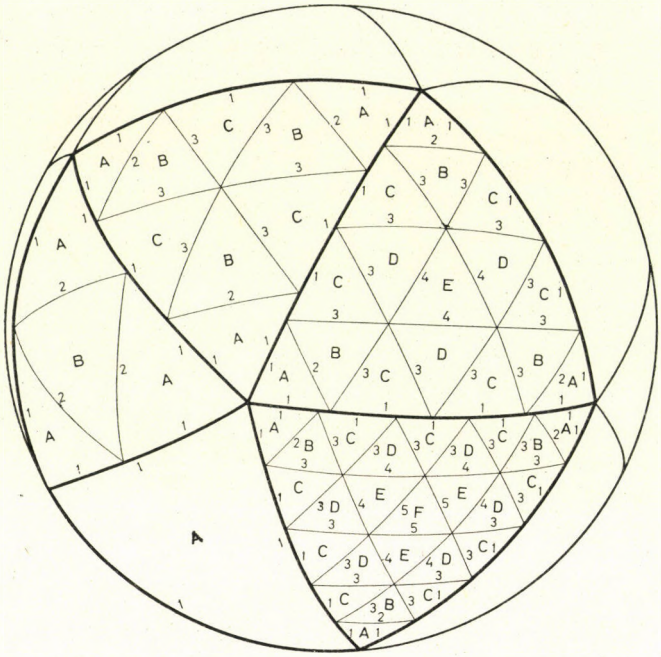

Fig. 25. Refinement of the network of the spherical icosahedron in the cases of $n = 1, 2, 3, 4, 5$

The first five steps of the refinement of the network with this method are shown in Fig. 25. The different cyphers denote the different sides and the different letters designate the different spherical triangles. The data of the obtained configurations are listed in Table III, point *c)*.

9.2. *Refinement of the network of the spherical configuration* $(5, 5, 5)_g$

The spherical configuration $(5, 5, 5)_g$ could be subdivided in the most successful way by making use of the method described in Section 8.2. This method was used by FULLER, in particular for the refinement of the spherical network of the configuration $(5, 5, 5)_g$. If a side has been subdivided into n parts, then the characteristic dimensionless data of the polyhedron will be as follows:

$c_k = 2n,$
$c = 30\ n^2 + 2,$
$e_k = 2\ n,$
$e = 90\ n^2,$
$l_k = n$ ($2n-1$, if two faces of the same size which could only be brought into congruence through mirroring, are considered to be different),
$l = 60\ n^2,$
$s_k = 3n-1.$

The subdivisions for the cases $n = 1, 2, 3, 4, 5$ are shown in Fig. 26. The polyhedrons obtained for $n = 2$, may be seen in Figs 1 and 27. The characteristic data are also listed in Table IV.

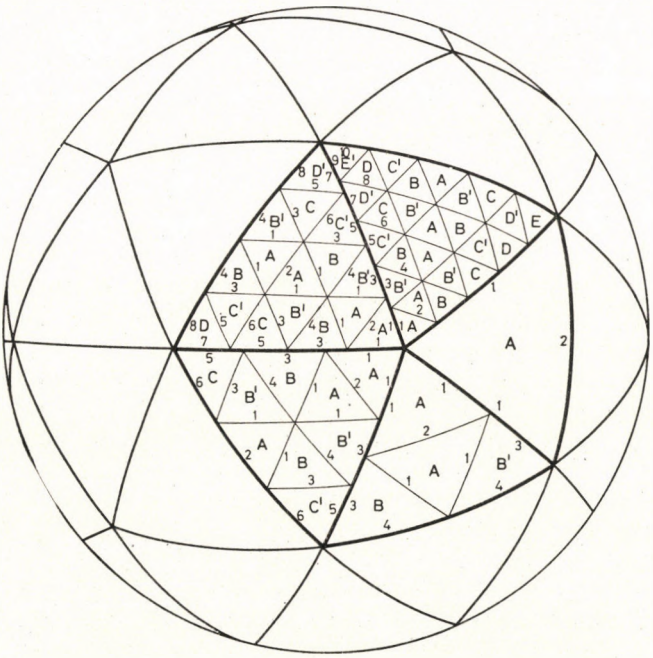

Fig. 26. Division of the network of the spherical configuration $(5, 5, 5)_g$ with the aid of Fuller's method

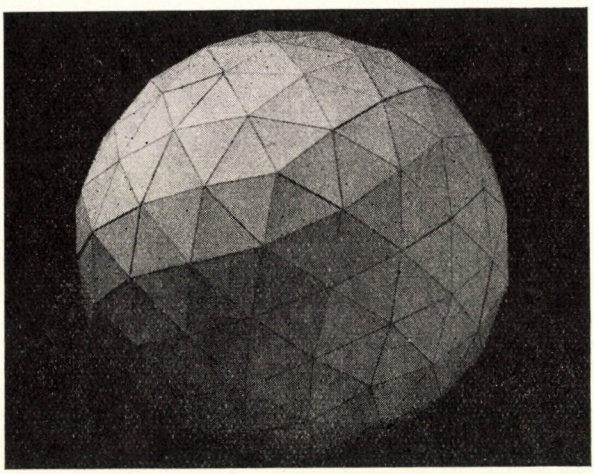

Fig. 27. Division of $(5, 5, 5)_g$ by making use of Fuller's method, in the case of $n = 2$

Table IV

Fuller's method for network refinement of a spherical configuration $(5, 5, 5)_g$

No. n	c_k	c	e_k	e	l_k	l	s_k
1	2	32	2	90	1	60	2
2	4	122	4	360	2 (3)	240	5
3	6	272	6	810	3 (5)	540	8
4	8	482	8	1440	4 (7)	960	11
5	10	752	10	2250	5 (9)	1500	14

Cyphers in brackets are valid if two elements of the same size which can only be brought into congruence by mirroring, are considered to be different.

9.3. *Refinement of the network of the spherical configuration* $(3, 3, 3, 3, 5)_g$

The spherical network of the polyhedron $(3, 3, 3, 3, 5)_g$, as was seen, consists of isosceles and equilateral spherical triangles. Both the isosceles and

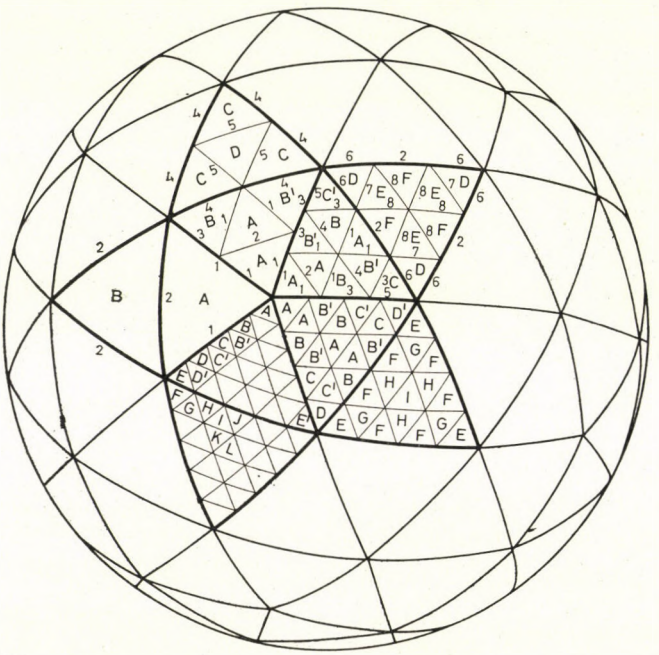

Fig. 28. Refinement of the network of the spherical configuration $(3, 3, 3, 3, 5)_g$ in the cases of $n = 1, 2, 3, 4, 5$

the equilateral spherical triangles are congruent. To the isosceles spherical triangles at the legs again isosceles spherical triangles are adjoining, to the base an equilateral spherical triangle is attached. The refinement of the network has been carried out as follows:

Let us divide the isosceles spherical triangle according to those mentioned in Section 8.2. This division of triangles induces a symmetrical division on the basis of the isosceles spherical triangle. The same division should be transferred to the other two sides of the equilateral spherical triangle. Then let us apply the method described in Section 8.3.2. Since the side has not been divided into equal segments, and thus, on the segments congruent spherical

Table V

Network refinement of the spherical configuration $(3, 3, 3, 3, 5)_g$

a) Method of side bisection

No. n	c_k	c	e_k	e	l_k	l	s_k
1	2	72	2	210	2	140	3
2	5	282	5	840	5 (6)	560	7

b) Method by centres of circles circumscribed about triangles

No. n	c_k	c	e_k	e	l_k	l	s_k
1	2	72	2	210	2	140	3
2	5	212	5	630	3 (4)	420	7

c) Method of division suggested by the author

No. n	c_k	c	e_k	e	l_k	l	s_k
1	2	72	2	210	2	140	3
2	5	282	5	840	4 (5)	560	7
3	8	632	8	1890	6 (8)	1260	13
4	12	1122	11	3360	9 (12)	2240	18

Cyphers in brackets are valid in that case if two elements of the same size which can be brought into congruence only by mirroring, are considered to be different.

triangles cannot be positioned, 8.3.2 should be modified in a way that the leg-length of the isosceles triangles placed on the segments should be identical. The first steps of the subdivision are shown in Fig. 28. The data of the polyhedrons associated with the configurations are indicated in Table V under point *c)*. For the sake of comparison, also the divisions according to Sections 8.1.1 and 8.1.2 have been carried out for $n = 2$ (Table V, points *a)* and *b)*).

9.4. *Refinement of the network of the spherical configuration* $(5, 6, 6)_g$

As was seen in 9.1, the subdivision of the spherical network of the polyhedron $(5, 6, 6)_g$ with the aid of geodesic lines is, in fact, the consequence of the division of the spherical icosahedron according to 8.3.1.

The spherical network of the polyhedron $(5, 6, 6)_g$ consists of two kinds of isosceles spherical triangles. Two different spherical triangles are connected by their bases. Having dealt with isosceles spherical triangles, the method of subdivision presented in Section 8.2 may be employed. This may be done without any change for $n = 2$. However, in the case of $n > 2$, the procedure should be modified.

Let us divide the first kind of the isosceles spherical triangles according to that mentioned in Section 8.2. This division of the spherical triangle results

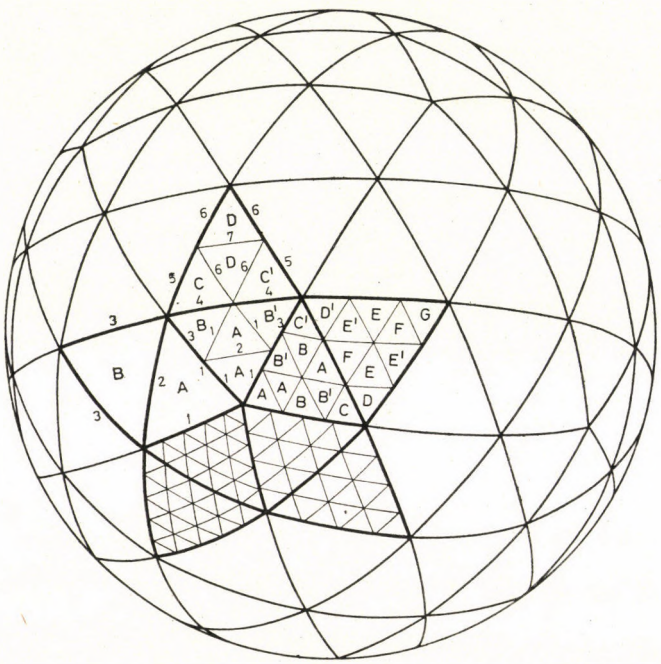

Fig. 29. Refinement of the network of the spherical configuration $(5, 6, 6)_g$ in the cases of $n = 1, 2, 3, 4, 5$

on the base in a symmetrical division. The second kind of the isosceles triangle should be so divided that the points of division obtained on the base, are the same as those obtained earlier. Accordance of the points of division of the base yields that for higher values of n this procedure is no longer suitable, the values of e_k and l_k will — at the same density — be higher than those of the polyhedrons obtained with the aid of the previous methods. The procedure and data of the configurations are indicated in Fig. 29 and Table VI, respectively.

Table VI

Network refinement of the spherical configuration $(5, 6, 6)_g$

No. n	c_k	c	e_k	e	l_k	l	s_k
1	3	92	3	270	2	180	4
2	6	362	7	1080	4 (6)	720	9
3	10	812	11	2430	7 (11)	1620	16

Cyphers in brackets are only valid if two elements of the same size which can be brought into congruence only by mirroring, are considered to be different.

10. Comparison and evaluation

Besides the configurations known from the special literature [icosahedron, $(5, 5, 5)_g$, their Fuller divisions, as well as $(5, 6, 6)_g$] a number of configurations could be constructed — partly by making use of Fuller's method — according to that mentioned above. This permits to set the configurations of the densest network obtained by the new divisions together with those known so far, in a range according to the increasing values of e_k and l_k by taking into account the requirements raised in Section 5. From the polyhedrons treated, those of the densest network are listed for the bar structures in Table VII, for the plate structures in Table VIII, points *a)* and *b)*.

From the results obtained it is clear that in the case of *plate structures*, if the faces of the triangles of the same size but of opposed encompassment are considered to be identical, then the densest edge-network is produced merely by the configuration $(5, 5, 5)_g$ and its polyhedrons derived by Fuller's method of division 8.2. If the triangle faces of the same size, but of opposed encompassment, are not considered to be identical, then the configuration $(5, 5, 5)_g$ and its Fullerian polyhedrons, as well as the configuration $(5, 6, 6)_g$, the configuration $(3, 3, 3, 3, 5)_g$ and the polyhedrons obtained by the subdivision of this latter will alternately be the polyhedrons of the densest network.

Table VII

Polyhedrons of densest network for bar structures

Configuration	c_k	c	e_k	e	l_k	l
Icosahedron	1	12	1	30	1	20
$(3,3,3,3,5)_g$	2	72	2	210	2	140
$(5,6,6)_g$	3	92	3	270	2	180
icosahedron division n = 4	4	162	4	480	5	320
$(3, 3, 3, 3, 5)_g$ division n = 2	5	282	5	840	4 (5)	560
icosahedron division n = 6	6 (7)	362	6	1080	7	720
icosahedron division n = 7	7 (8)	492	7	1470	9	980
icosahedron division n = 8	8 (9)	642	8	1920	10	1280
icosahedron division n = 9	9 (11)	812	9	2430	11	1620

Cyphers in brackets are valid if two elements of the same size which can be brought into congruence only by mirroring, are considered to be different.

Table VIII

Polyhedrons of densest network for plate structures

a) If two triangular faces of the same size — which can be brought into congruence only by mirroring — are considered to be the same

Configuration	c_k	c	e_k	e	l_k	l	s_k
$(5, 5, 5)_g$	2	32	2	90	1	60	2
$(5, 5, 5)_g$ Fullerian division, n = 2	4	122	4	360	2	240	5
$(5, 5, 5)_g$ Fullerian division, n = 3	6	272	6	810	3	540	8
$(5, 5, 5)_g$ Fullerian division, n = 4	8	482	8	1440	4	960	11
$(5, 5, 5)_g$ Fullerian division, n = 5	10	752	10	2250	5	1500	14

In the case of the *bar structures*, being from the viewpoint of the practice of great importance, considering the increasing values of n, after the polyhedrons derived from the icosahedron and from the two semi-regular solids [$(3, 3, 3, 3, 5)_g$ and $(5, 6, 6)_g$], the polyhedrons giving the densest edge network are those produced from the icosahedron by the subdivision suggested in this

b) If two triangular faces of the same size — which can be brought into congruence only by mirroring — are considered to be different

Configuration	c_k	c	e_k	e	l_k	l	s_k
$(5, 5, 5)_g$	2	32	2	90	1	60	2
$(5, 5, 6)_g$	3	92	3	270	2	180	4
$(5, 5, 5)_g$ Fullerian division, n=2	4	122	4	360	3	240	5
$(3, 3, 3, 3, 5)_g$ refined by centres of circles circumscribed about triangles, n=2	5	212	5	630	4	420	7
$(3, 3, 3, 3, 5)_g$ division, n = 2	5	282	5	840	5	560	7
$(5, 5, 6)_g$ division, n = 2	6	362	7	1080	6	720	9
$(5, 5, 5)_g$ Fullerian division, n = 4	8	482	8	1440	7	960	11
$(3, 3, 3, 3, 5)_g$ division, n = 3	8	632	8	1890	8	1260	13
$(5, 5, 5)_g$ Fullerian division, n = 5	10	752	10	2250	9	1500	14

paper, in Section 8.3.2. Thus, it can be established that the polyhedron $(3, 3, 3, 3, 5)_g$ and that, obtained by its subdivision as well as the polyhedrons produced with the aid of the subdivision of the spherical icosahedron suggested in Section 8.3.2, fulfil for $n \geq 2$, $n \neq 3$ the conditions prescribed in Section 5 in a more satisfying way than any other polyhedrons did so far.

REFERENCES

1. Brückner, M.: Vielecke und Vielflache. Verlag von B. G. Teubner, Leipzig 1900
2. Buray, Z.—Kádár, I.: Load-bearing Aluminium Engineering Structures. (In Hungarian) ÉM Építésügyi Dokumentációs Iroda, Budapest 1965
3. Doernach, R.: Sphärische Raumfachwerke. *Der Stahlbau* **29** (1960), 97—104
4. Fejes Tóth, L.: Lagerungen in der Ebene, auf der Kugel und im Raum. Springer-Verlag, Berlin—Göttingen—Heidelberg 1953
5. Fuller, R. B.: Geodesic tent. United States Patent Office, patent 2,914,074, Nov. 24, 1959
6. Fuller, R. B.: Item "M". Boston Blue Print Data Archive, (without date year)
7. Hajós, Gy.: Introduction to Geometry. (In Hungarian) Tankönyvkiadó, Budapest 1964
8. Makowski, Z. S.: Räumliche Tragwerke aus Stahl. Stahleisen-Verlag, Düsseldorf 1963
9. McHale, J.: R. Buckminster Fuller. Otto Maier Verlag, Ravensburg 1964
10. Tupolev, M. S.: Géométrie sphérique et coupoles préfabriquées. *L'architecture d'aujourd'hui*, N° 141 (1968)—(1969), 62—64

Sphärische Dreiecksfachwerke. Die Geometrie des Dreiecksnetzes von einschichtigen sphärischen Fachwerken wird untersucht. Auf die Frage: auf welche Weise eine Kugelfläche in soviel sphärische Dreiecke wie möglich mit wenigen unterschiedlichen Seiten aufgeteilt werden kann, daß die Aufteilung möglichst gleichförmig sei, wird eine Antwort gesucht. Mit Hilfe von regelmäßigen und halbregelmäßigen Körpern wurden auf der Kugelfläche annähernd gleichförmige Dreiecksaufteilungen hergestellt, von denen dieselben von dichtesten Netzen ausgewählt werden können. Es wird eine neue Aufteilungsmethode vorgeschlagen und die durch Anwendung dieser Methode als Ergebnis erhaltenen Konfigurationen werden denselben, die durch die Fullerschen Aufteilungen erhalten wurden, entgegengestellt.

Сферические решетчатые конструкции с треугольной сеткой. Работа занимается геометрическим анализом сетки однослойных сферических решетчатых конструкций с треугольной сеткой. В работе поставлена цель, найти ответ на вопрос, каким образом можно сферическую поверхность с небольшим числом различных по длине сторон разбить на максимально наибольшее количество сферических треугольников так, чтобы разбивка по возможности была бы равномерной. С помощью тел правильной и полуправильной формы на сферической поверхности создается приближенно равномерная разбивка на треугольники, из которых выбирают те, которые имеют наиболее густую сеть. Предлагается метод разбивки, и формы, получающиеся в результате разбивки на треугольники, сравнивают с формами, полученными при разбивке по Фулеру.

Acta Technica Academiae Scientiarum Hungaricae, Tomus 76 (3—4), pp. 337—353 (1974)

L'APPROVISIONNEMENT EN EAU DES VILLES ET CHÂTEAUX-FORTS

L. ZOLNAY*

[Manuscrit reçu le 5 mai 1969]

1. Introduction

L'approvisionnement en eau potable pure et salubre avait été l'une des préoccupations majeures des habitants des villes médiévales, décimées par les épidémies. Bien que les anciens habitants de la région sud-ouest de la Hongrie, les Romains de Pannonie nous aient laissé leurs aqueducs, brillants souvenirs de leur civilisation matérielle, rien ne prouve que leurs conduites d'eau avaient survécu pendant les siècles de la migration des peuples et que l'homme du moyen-âge a pu les utiliser. Tout un millénaire devait s'écouler avant que le moyen-âge eût atteint le degré de développement de la civilisation romaine, mais dès qu'il l'a atteint, il l'a aussitôt dépassé.

Tout en se servant de l'eau des sources et des puits, utilisés de tout temps à la campagne, les habitants de nos villes et châteaux-forts ont mis au point de bonne heure une nouvelle technique d'adduction d'eau qui devait, dès le XVe siècle, dépasser par son niveau les aqueducs de l'antiquité. Si l'on pense à la magnifique citerne du palais royal d'Esztergom construite au XIIe siècle et à celle de la citadelle de Visegrád des XIIIe—XIVe siècles, ou si l'on regarde le puits d'Esztergom creusé dans la roche, il apparaît aussitôt évident que l'eau de pluie recueillie dans des citernes et le rendement des puits n'avaient point dû suffire aux agglomérations de montagne médiévales.

Lors de la fondation de la ville de montagne de Buda, l'approvisionnement en eau était un facteur déterminant de l'implantation. Dans le choix de l'emplacement, les avens aux eaux abondantes de la partie septentrionale du mont du château entraient en ligne de compte tout comme l'eau du Danube, proche de l'extrémité sud de la montagne où devait se construire le château royal.

Le problème de l'eau se posait dans toute son acuité aux habitants du mont du château au XIIIe siècle. Outre la proximité du Danube, la présence de sources thermales situées sur le versant nord du mont Gellért et au côté sud-est de la colline Rózsadomb avaient sependant allégé leurs soucis. La satisfaction des besoins en eau des premiers habitants se trouvait facilitée,

* Zolnay, L., Nagymező u. 3, 1065 Budapest, Hungary

de plus, par les eaux abondantes provenant d'une couche d'argile sous-jacente au tuf calcaire du mont du Château. Mais ces eaux n'étaient pas superficielles. Le mont du Château n'a que deux sources, dont l'une surgit dans la cour du n° 8 de la rue Hunfalvy et l'autre en contre-bas du Bastion des Pêcheurs, l'une et l'autre étant déjà d'un très faible débit. Dans la partie nord du mont, un vaste système de cavités souterraines accumulait les eaux de précipitation et il semble plausible de supposer que l'exploitation de ces avens avait dû commencer dès le XIIIe siècle. Dans les diplômes du moyen-âge on trouve même mention des puits et salles d'eau du mont du Château.

Evlia Tchelebi (1660—1664) énumère, pour le quartier de la forteresse, soixante-quinze puits communs et quarante puits privés creusés dans la roche, ajoutant que cent soixante-dix citernes souterraines recueillent les égouts des toits de maisons. Dans les quatre-vingt cavernes aujourd'hui connues du mont du Château, Henrik Horusitzky a découvert aux années 1920 treize avens toujours utilisables, dont le niveau d'eau va de 150,65 à 158,47 m au-dessus du niveau de la mer.

Dans un autre travail j'ai montré que la cour royale n'avait quitté la ville fortifiée fondée par Adalbert IV (1235—1270) que sous le règne de Louis le Grand (1342—1382), dans la seconde moitié du XIVe siècle, pour venir s'établir sur l'emplacement de l'actuel château royal. Depuis l'époque d'Adalbert IV jusqu'aux années 1350, la résidence royale se trouvait au nord du mont du Château, sur l'emplacement du n° 9 de la rue Mihály Táncsics. C'est confirmé d'ailleurs par l'absence de couches géologiques aquifères au sud de la place Dísz, sur le versant méridional du mont. Sur la partie nord, la couche supérieure est un recouvrement en calcaire d'eau douce, de quelques mètres d'épaisseur, disloqué par en-dessous par les sources thermales d'autrefois. C'est leur reste qu'il faut voir dans l'énorme système de cavernes, riche en puits, qui s'étend dans les parties centrale et septentrionale du mont du Château. Au niveau de la place Dísz, ce recouvrement en calcaire d'eau douce disparaît, tandis que dans la partie sud du mont, au-dessous du château royal, la couche marneuse primitive qui forme, dans la partie nord, le sol des cavernes, réapparaît en surface. Or cette couche marneuse de Buda est entièrement dépourvue d'eau. Alors que le système des cavernes du versant nord constitue une vraie citerne naturelle, le versant sud ne possède comme ressources, pour son approvisionnement en eau, que le Danube ou les sources groupées au pied du mont Gellért. Plus au sud de la place Dísz, le système naturel de cavernes et ses citernes naturelles disparaissent avec la nappe calcaire.

Lors de la construction, au XIVe siècle, du château royal du sud, on était parti sans doute de la conception que la partie sud de la forteresse, terrain dépourvu d'eau, devait couvrir ses besoins par les eaux du Danube. Sans ses bastions flanquants donnant sur le fleuve, le château royal ne pouvait, en cas de siège, assurer son approvisionnement en eau que par ses citernes.

En comparaison du bourg situé sur le versant nord, le château avait donc le double désavantage d'être situé près de quinze mètres plus bas et de ne point disposer de ressources en eau naturelle sur son propre territoire. C'est à cet inconvénient que devait remédier la relative proximité du Danube. L'histoire nous montre que les deux bastions flanquants donnant sur le fleuve devaient jouer un rôle décisif dans le sort du château. (En 1541, Rosetti, ambassadeur de Ferrara à Buda rapporte que les forces impériales assiégeant Buda ont privé d'eau les habitants du château, en détruisant les chemines et escaliers par lesquels les gens de la forteresse allaient prendre de l'eau au Danube.)

Jusqu'au tournant du XIVe et du XVe siècle, le château royal et le bourg de Buda ne montrent aucune trace de conduites artificielles. L'approvisionnement en eau potable du bourg et du château royal était assuré par des citernes, des puits et des porteurs d'eau (Wasserträger) puisant l'eau dans le fleuve.

Les importants travaux d'agrandissement que le roi Sigismond avait fait faire au château et aux fortifications du mont — parmi lesquels figuraient la construction d'un bastion au bord du Danube et la fabrication d'une chaîne attachée à ce même bastion pour bâcler le fleuve — étaient déjà les résultats de nouvelles considérations tactiques. A quoi étaient destinés le bastion de Buda construit sur l'emplacement de l'actuelle place Miklós Ybl et celui de Pest, avec la chaîne tendue entre les deux, servant à bâcler le fleuve? Ils étaient évidemment destinés à protéger *Buda regia* ou *Buda imperialis*, ainsi que le bastion abritant la conduite d'eau, ce point névralgique du château royal. Après Nicapolis et Galambóc, l'art militaire hongrois devait déjà tenir compte de la nouvelle arme, jusque-là ignorée, des forces ottomanes, à savoir de la flotte turque du Danube.

Ce n'est point par hasard que les premiers documents relatifs aux conduites d'eau artificielles du mont du château de Buda proviennent du XVe siècle, de l'époque même des vastes travaux de reconstruction de la forteresse. La crainte des attaques turques, le développement du Buda en une grande ville européenne et les exigences plus élevées émanant de la cour royale et impériale faisaient naître ensemble le besoin de construire des conduites d'eau.

Mon travail entrepris il y a une quinzaine d'années pour éclaircir le système technique de distribution d'eau de nos villes et châteaux-forts du moyen-âge ne pouvait s'appuyer que sur un nombre bien réduit de recherches préliminaires hongroises. En ce qui concerne même les auteurs étrangers classiques, VIOLLET-LE-DUC par ex., n'examinéaient que les conduites d'eau des maisons d'habitation et les travaux d'histoire technique de FELDHAUS franchissent tout le moyen-âge avec des pas de géant. (Pour l'Europe occidentale, FELDHAUS mentionne comme première conduite d'eau après les aqueducs de

l'Antiquité, le réseau de tuyaux de fonte de Versailles, de l'époque de Louis XIV. Or ces constatations ont pu être dépassées même par la recherche archéologique hongroise, retardée pourtant, dans ce sens, par sa forte orientation esthétique.)

Sándor GARÁDY avait mis à jour et relevé, aux années trente, de nombreux restes de conduites d'eau médiévales sur le territoire de Budapest. Il est à regretter que sa mort survenue pendant la guerre l'ait empêché de faire la monographie qu'il avait projeté d'écrire sur l'histoire des conduites d'eau médiévales et contemporaines de Budapest. Des résultats importants ont été également obtenus par les ingénieurs du Service des Eaux de la Ville de Budapest. Au cours de poses de tuyaux, ils ont découvert de nombreuses conduites plus anciennes, trouvailles qui ont été réunies au musée du Service des Eaux qui fut détruit en 1944—45. De nos jours, quand la distribution d'eau dans la capitale remonte à cinq siècles et demi en arrière, il paraît actuel d'affirmer, une fois de plus, la nécessité d'écrire l'histoire de notre approvisionnement en eau.

2. Les types de distribution d'eau au moyen-âge

Abstraction faite des puits, avens, citernes et sources, les modes de distribution d'eau au moyen-âge peuvent se classer en trois catégories techniques. Les trouvailles archéologiques prouvent — en accord avec les documents écrits — que nous avions:

a) des conduites de distribution d'eau apparentes, fonctionnant par gravitation, semblables aux aqueducs de l'Antiquité;

b) des conduites de distribution d'eau par pression, fonctionnant sur le principe des vases communicants;

c) des pompes actionnées par moulin à manège ou cabestan.

Buda, capitale du pays et centre de rayonnement de notre culture médiévale, joue aussi un rôle de premier plan dans l'histoire de notre technique. On peut démontrer la présence, à Buda, de nos trois systèmes de distribution d'eau utilisés au moyen-âge.

a) Conduites de distribution par gravitation

Ce type, le plus fréquent et le plus simple, du point de vue technique, de nos systèmes de distribution d'autrefois, conduit l'eau des sources situées à un niveau supérieur à l'agglomération, à des fontaines placées plus bas. Des conduites fonctionnant sur ce principe avaient assuré l'approvisionnement en eau de Bártfa (la première mention écrite date de 1426), Körmöcbánya (1442) et d'après les livres de compte municipaux du XVe siècle, des villes d'Eperjes, Kassa, Besztercebánya, Újbánya, Lőcse, Brassó et Pécs.

La plus grande partie de nos monuments écrits du moyen-âge, — et surtout les documents d'archives de la Hongrie centrale — avaient été détruits pendant la domination turque et cette lacune n'a pas pu être comblée intégralement par les archéologues. Aussi bien, dans la première moitié de notre siècle, on a attribué encore à l'époque romaine des tuyaux de poterie provenant du moyen-âge (leur «marque énigmatique» s'avérait être celle des potiers médiévaux de Vienne et de Tulln). Et avant que ne soient faites des analyses plus approfondies des matériaux, le chercheur ne pourra point se prononcer s'il faut attribuer certains éléments de conduite à l'antiquité, au moyen-âge, à l'époque de la domination turque ou à l'âge moderne.

Parmi les maîtres ayant exécuté le canal de Bártfa, deux nous sont connus par leurs noms. Il s'agit de Michel (1434) et de Nicolas de Cracovie (1436), venus de Pologne. Du fontainier (Roerenmaister) Michel, on sait qu'il avait, à une époque antérieure, construit le canal de Cracovie et le bain des Juifs de cette ville.

Parmi nos agglomérations du bord du Danube, c'est l'ancien bourg d'Esztergom qui paraît avoir été approvisionné en eau au moyen de cette conduite en tuyaux de poterie qui partait du puits Saint-Jean et dont les restes ont été enlevés il y a quelques années par des écoliers trop zélés. Une autre conduite, la pierrée partant du versant sud du mont du Château de Visegrád, aboutissait au palais de cette ville. Elle devait sans doute assurer le début des fontaines gothiques et renaissance, ainsi que celui des bains genre sauna du roi Mathias. A Buda, on trouve également un bon nombre de restes de conduites — surtout en tuyaux de poterie — ayant utilisé le principe de la gravitation. De tels éléments ont été mis à jour rue Váralja, au Ier arrondissement parmi les ruines du couvent de la rue Bugát, et dans les rues Kiscelli et Gyűrű, au IIIe arrondissement de la capitale. Sur l'emplacement de l'ancien monastère pauliste, au voisinage de l'actuel Ságvári-liget (n° 91—93 rue Budakeszi, au XIIe arrondissement) on a déterré une pierrée destinée à conduire l'eau par gravitation, dont le constructeur devrait être cherché — d'après des données de la fin du XVe siècle — en la personne du prieur pauliste János Kámánczi, maître d'œuvre de sa profession (aux environs de 1490—1492).

Les tuyaux de poterie retrouvés sur les terrains situés entre le mont Szabadság et le mont du Château, à Buda ne sont pas, comme nous allons le voir, les fragments d'une simple conduite par gravitation, mais les restes d'un système de distribution fonctionnant sur le principe des vases communicants, construit sous le règne du roi Mathias.

b) Le système de distribution fonctionnant sur le principe des vases communicants

Le système était peut-être le plus important des biens assurés par le roi Mathias (1458—1490) aux habitants de la capitale.

Des quatre sources de jadis des monts de Buda, qui prenaient naissance sur le versant est de l'actuel mont Szabadság, les hydrotechniciens du roi avaient choisi trois (figure 1), dont les eaux réunies étaient refoulées jusqu'au mont du château de Buda.

Parmi les édicules qui protégeaient les sources, celui de la Fontaine de ville, magnifique construction gothique du XVe siècle, existe toujours; sa restauration projetée est appelée à enrichir la faible série de monuments techniques dont on dispose.

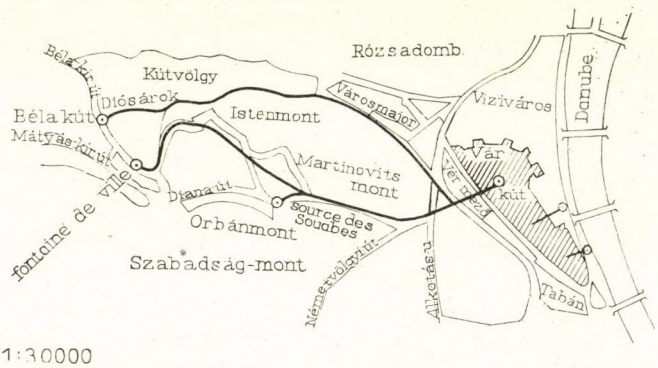

Fig. 1. Levé de plan des trois conduites d'eau médiévales de Buda

Les eaux de la Fontaine de ville de l'avenue du roi Béla, au XIIe arrondissement (354 m au-dessus du niveau de la mer), réunies à celles de la Fontaine du roi Béla (348 m) et de la Source dite des Souabes de la rue Diana (XIIe arrondissement) que des travaux de canalisation ont fait disparaître depuis, étaient conduites par des tuyaux de plomb et de poterie et accumulées aux alentours de l'actuel Vérmező, d'où leur propre pesanteur les avait fait monter, selon le principe des vases communicants, jusqu'au parvis de l'église Notre-Dame appelé aujourd'hui Szentháromság tér (place de la Trinité). La différence de niveau entre les sources et la fontaine centrale de la forteresse de Buda est de 160 à 190 mètres. Les bassins de rétention et de refoulement se trouvaient au voisinage de l'actuelle place Orbán et ont été détruits au cours de la construction du bassin moderne du Service des Eaux.

De la citerne centrale de la Grande Place de Buda, l'eau des sources de montagne avait été amenée par des tuyaux aux fontaines du château royal et du bourg de Buda et à l'ancien puits de trop-plein de l'actuel Víziváros. La citerne centrale située devant l'église Notre-Dame de Mathias était surmontée d'une fontaine décorative. Le fragment en marbre blanc d'un

écusson au corbeau, qui fut retrouvé au siècle dernier, non loin de là, dans la cour du n° 14 rue Országház, appartenait probablement à cette fontaine centrale. Aujourd'hui, il est exposé au Lapidaire du Musée des Beaux-Arts.

L'usage fréquent de conduites de distribution par gravitation est démontrée par le grand nombre de trouvailles archéologiques dont on dispose. Des éléments de conduites, des tuyaux de poterie et de bois, accompagnés d'autres trouvailles provenant du moyen-âge ont été mis à jour à Esztergom, à Pécs, au château-fort de Fülek, à la limite de Gödöllő, au village de Páty dans les environs de Buda, à Pilisszentkereszt, au château-fort de Nógrád, au château-fort de Munkács, à Kőszeg et à Gyulafehérvár.

Une portion plus longue d'une conduite faite en mélèze se trouve *in situ* dans la partie est de la galerie d'observation souterraine du château-fort d'Eger. Vido Pataki a démontré que cette partie du château-fort avait été bâtie par l'ingénieur militaire Ottavio Baldigara, aux alentours de 1568—70. Baldigara avait construit d'ailleurs une conduite d'eau semblable dans les casemates du château-fort de Pozsony

Les conduites du temps du roi Mathias, détruites à l'époque de la domination ottomane, avaient été rénovées en 1718 par Konrád Kerschensteiner, un architecte jésuite de Buda, après quoi elles restaient en service jusqu'à la seconde moitié du XIXe siècle, époque de la construction du service de distribution moderne de Budapest.

Ces conduites de distribution par gravitation de la Hongrie médiévale présentent cependant, du point de vue de l'histoire de la technique, un intérêt moindre que

c) Les stations de pompage actionnées par moulin à manège ou cabestan

En 1416 Sigismond, roi de Hongrie et de Bohême et empereur du Saint-Empire, qui siégait à Buda, avait fait payer au «Rohrschmidt» (en traduction littérale: batteur de tuyaux) Hartmann de Nuremberg, mille ducats rhénans prélevés sur les impôts de la ville de Nuremberg. Maître Hartmann «vor Zeiten das Wasser in Ofen den Berg geleitet hat» (avait antérieurement conduit l'eau sur le mont de Buda). D'après cette donnée, Buda était notre premier château-fort et ville de montagne fortifiée possédant des conduites d'eau. Ce système de distribution d'eau de Buda, construit au temps du roi Sigismond, s'intègre bien d'ailleurs dans le tableau européen général, les premières mentions relatives aux canalisations d'eau de Leipzig et d'Augsbourg datant respectivement de 1412 et 1450.

Les conduites d'eau de Buda, construites dans la première décennie des années 1400 paraissent avoir été utilisées sans interruption. En 1424, un diplôme émis à Diósgyőr par le roi Sigismond enjoint à la ville de Kassa de payer, sur les impôts de la ville, quarante florins à maître Pierre, fontainier

du roi (aqueductori nostro). En 1417, Ambrosio Traversari mentionne les étangs créés à Buda, sur le côté ouest du jardin du château, étangs qui devaient être alimentés, évidemment, par des conduites. C'est de même aux conduites d'eau de l'époque de Sigismond qu'il convient de rattacher le fragment d'une fontaine gothique qui, selon la reconstitution de Mme Istvàn FEUER, avait décoré la petite cour sud du château royal.

Certaines sources écrites d'une date ultérieure, complétées en partie par des trouvailles archéologiques, nous autorisent à penser que la station de pompage construite par le maître Hartmann avait fonctionné dans le

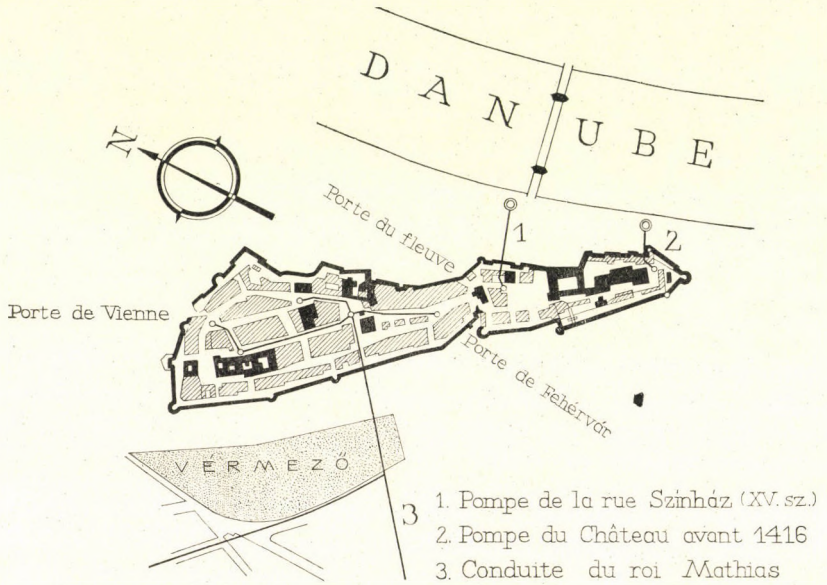

Fig. 2. Levé de plan des conduites d'eau médiévales de Buda

bastion circulaire du bord du Danube, qui se rattachait à la courtine sud flanquant le château royal en direction du fleuve (figure 2), et que cette pompe actionnée par cabestan approvisionnait, avec l'eau du Danube, le château de Sigismond. (Le bastion circulaire a été démoli dans la première décade du XIXe siècle; la galerie du canal existe toujours dans la courtine sud du château.)

Une autre pompe analogue, actionnée par cabestan, a été construite aux années 1440 sur l'ordre du roi Uladislas Ier, pour satisfaire aux besoins non plus du château, mais de la ville. L'enveloppe de la pompe, située sur le bord du Danube, se trouvait sur l'emplacement du n° 3—5 rue Fő. La fontaine (figure 3) était à l'ouest de l'actuel théâtre du quartier du château, sur l'emplacement du bâtiment en ruines de l'ancien Ministère de la Défense Nationale. J'ai pu retrouver, en 1950, la galerie souterraine qui les reliait

ensemble et qui avait été rénovée au XVIIIe siècle (figure 4). Cette galerie souterraine, pratiquée dans le flanc de la montagne et s'étendant de la rue Színház à l'avenue János Hunyadi, a été remblayée depuis.

Les deux pompes du XVe siècle du château de Buda fonctionnaient jusqu'au début de l'occupation turque (1541—1686). Le débit de la station de pompage était emmagasiné dans des réservoirs d'eau en plusieurs points

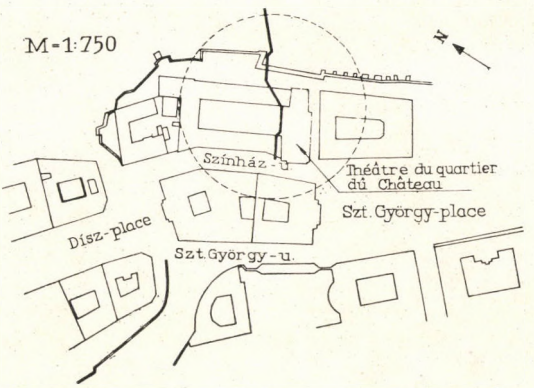

Fig. 3. Trace du puits de la pompe médiévale conduisant à l'ancien couvent franciscain de Buda

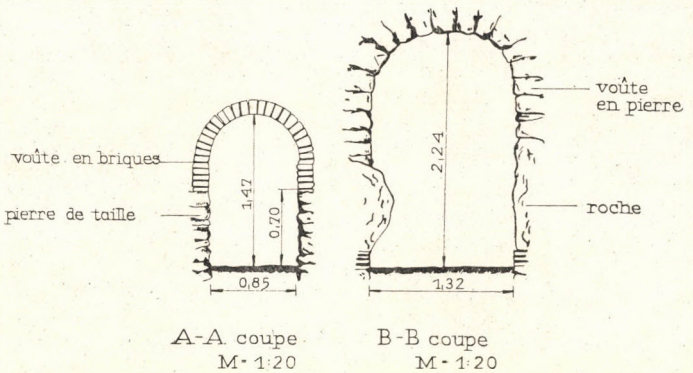

Fig. 4. Puits du temps moderne et du moyen-âge sous l'ancien couvent franciscain de Buda

de la forteresse de Buda (dans la citerne située près de la maison de l'argentier — domus tavernicalis — appartenant au château royal, ainsi que dans les réservoirs de la place Dísz, de la place Szentháromság et de la place András Hess). Le débit continu, enrichi depuis le temps du roi Mathias par les eaux de source du mont Szabadság, avait été amené en partie dans les jardins du château royal. Le trop-plein des eaux alimentant la ville se trouvait dans le quartier Víziváros, aux alentours de l'actuelle rue Iskola.

Une station de pompage analogue à celle de Buda fonctionnait à Esztergom. Dselalzade, l'historiographe du grand Soliman en parle dans ces termes, vers les années 1540: «en certain endroit de la ville basse, ils ont fait un réservoir d'eau; un certain volume d'eau s'y déverse depuis le Danube. Ils ont monté une roue au-dessou du réservoir et fabriqué d'étroits tuyaux de cuivre pratiqués dans les murailles, qu'ils conduisaient jusqu'en haut du château. La roue — tournée artificiellement — refoule l'eau par ces tuyaux jusqu'au château-fort.»

Les restes architecturaux de la station de pompage d'Esztergom, qui attendent toujours d'être mis au jour et exposés au public, existent actuellement sous forme d'un ancien «château d'eau» au n° 20 rue Zsigmond Berényi, d'une galérie voûtée souterraine pratiquée dans le flanc de la montagne et du puits, resp. de la citerne du bastion circulaire nord de la forteresse.

Énumérer tous nos châteaux-forts et villes fortifiées bâtis en montagne où fonctionnaient jadis des stations de pompage analogues à celle de Buda nous mènerait peut-être trop loin. Parmi nos châteaux-forts construits au bord du Danube, celui de Pozsony avait reçu du roi Sigismond, en 1434, six cents florins en chiffres ronds pour son installation de pompage. Plus en aval, Esztergom, Visegrád et, aux confins sud du pays, Nándorfehérvár — aujourd'hui Belgrade — avaient recours à une solution semblable. En 1521, après la chute de Nándorfehérvár, le chroniqueur écrit: «La cause de la perte de Nándorfehérvár était que l'eau du canal venait à être complètement épuisée». De même en 1543, Esztergom passa aux mains des Turcs à cause de l'occupation, par ces derniers, du «château d'eau» du bord du Danube.

Du point de vue de l'histoire de la technique, l'utilisation du moulin à manège et du cabestan comme sources d'énergie de ce système à pompe est une conquête médiévale importante. De 1416, année d'émission du document relatif au maître Hartmann, une autre donnée nous apprend que le roi Sigismond a rendu obligatoire, pour les futainiers hongrois, de marcher dans les moulins à manège qui actionnaient les métiers. La pompe à eau et le métier à tisser étaient donc actionnés d'après le même principe mécanique. Les pompes reçoivent une importance encore plus grande dans l'épuisement des eaux des mines de la Haute-Hongrie.

Ce qui précède fait donc tomber cette hypothèse, admise autrefois dans la littérature, que les installations de nos châteaux-forts de montagne auraient été analogues aux chaînes à godets utilisées actuellement pour le dragage des lits de fleuve. Si l'on considère, en effet, que le cabestan utilisé pour élever l'eau du Danube au mont de la forteresse de Buda, à soixante mètres de hauteur, était actionné par des chevaux, si l'on observe les couloirs des conduites, creusés dans le flanc de la montagne (leur hauteur intérieure va de 1,5 à 1,7 m en moyenne) et que l'on tienne compte du tracé oblique et brisé des conduites, cette hypothèse tombe d'elle-même. Des godets puiseurs

n'étaient utilisés que pour l'exhaure dans les mines, où la machine hydraulique fonctionnant à la surface enlevait les eaux d'infiltration suivant un parcours vertical.

A Körmöcbánya, ville ayant jadis appartenu à la Haute Hongrie, le capitaine des mines Conrad Rollner avait construit, dans les années 1440—41, la première pompe d'exhausse. En 1462, les mines d'or et d'argent de Körmöc possèdent déjà six installations de pompage. En 1475 János Thurzó, sénateur de Cracovie et technicien réputé des mines de cette époque, passe un contrat avec la Chambre hongroise, aux termes duquel il s'engage à épuiser les eaux des mines de Selmec avec ses installations d'élévation d'eau. En contrepartie, il reçoit un sixième du métal précieux extrait, plus un florin or par semaine et par machine. Cette entreprise, qui devait devenir l'une des bases du consortium Thurzó—Fugger réalisé en 1495, était couronnée d'un tel succès que le roi Mathias ne tardait pas à étendre l'activité de Thurzó à toutes les mines de la Haute Hongrie, faisant payer à Thurzó quatre florins or par marc d'argent extrait.

En 1518, un nommé Hans, «Kunstmeister» de Besztercebánya, fait fonctionner dans cette ville sa machine à élever l'eaux. Notre littérature spéciale a bien nettement établi le fait que les mines de Körmöc et de Selmec devaient à ces pompes à eau leur floraison de la fin du XVe siècle. Dès que ces installations furent détruites par un incendie, au début du XVIe siècle, la production des mines de la Haute Hongrie s'en trouve aussitôt paralysée.

Les deux pompes à eau du bord du Danube, à Buda, construites par des maîtres du XVe siècle, furent détruites en 1686 lors du siège qui se termina par l'expulsion des Turcs. La ville aussi bien que la pompe du château royal ont été rénovées au XVIIIe siècle. Farkas Kempelen, l'éminent constructeur du système de distribution d'eau de Schönbrunn avait lui-même pris part à la reconstruction de cette dernière (1777).

3. Fontainiers du moyen-âge

A l'époque médiévale, la construction des canalisations d'eau occupait les spécialistes de nombreuses branches de la technique et de l'industrie, depuis les architectes — comme Léonard de Vinci, ou Chimenti Camicia qui travaillait aussi en Hongrie — jusqu'aux artisans des métiers les plus divers.

Maîtres d'œuvres, potiers, tuiliers, armuriers, meuniers, serruriers et charpentiers travaillaient ensemble à la construction des ouvrages. Le fait qu'on n'a point méconnu l'importance de leurs travaux nous est bien prouvé par la rémunération de leurs activités.

Dans la première moitié du XVe siècle, les porteurs d'eau (Wasserträger) de Buda, gens de bas étage dans la société locale, qui transportaient

l'eau dans des hottes, devaient monter 2240 litres d'eau à la forteresse de Buda pour gagner une pièce d'or. Le maître Hartmann, lui, recevait en 1416 du roi Sigismond mille florins or pour son ouvrage assurant l'approvisionnement en eau du château de Buda, somme qui équivaut, en chiffres ronds, au transport de deux millions et quart de litres d'eau !

Le maître Hartmann est appelé «batteur de tuyaux» et «cylindreur» par le roi Sigismond. Le maître Pierre, son contemporain d'origine française, également au service du roi, est architecte et fontainier — architector, sive aqueductor. Les deux fontainiers cracoviens de Bártfa étaient nommés, comme nous l'avons vu, «Roerenmaister». Un autre fontainier vivant à Bártfa, était invité par János Drugeth à venir dans son château-fort de Jessena, pour y construire une installation d'élévation d'eau. La même année, le fontainier Hans de Besztercebánya en construit une, à son tour, pour la ville de Selmec. En 1525, le fontainier de Buda au service du roi Louis II, le maître Orbán porte le signe de son métier dans son surnom: on l'appelle, en effet, Orbán-des-canaux. C'est lui qui repare le canal du château-fort de Buda, détérioré par le gel d'hiver.

Le fontainier d'Esztergom du temps de la domination ottomane s'appelait Imanuel Uveiss et son métier était «kouïodchi», ce qui signifie chaudronnier.

En dehors des maîtres médiévaux mentionnés, il est à supposer que l'architecte et ingénieur militaire italien Paolo Santini di Duccio, qui travaillait à Buda aux années 1430—1440, avait lui aussi participé à la construction de l'installation hydraulique de Buda. Il est certain, d'autre part, que la construction de la pompe du château-fort d'Esztergom, au XVe siècle, et celle de la grande installation de pompage que faisait réaliser le roi Mathias, s'associent au nom du maître florentin Chimenti Camicia qui travaillait entre 1470 et 1490 à Buda aussi bien qu'à Esztergom. Vasari, ce grand chroniqueur de la Renaissance, note l'épitaphe de Camicia, dont il ressort que le maître avait surtout construit, au cours de sa vie, des installations hydrauliques, et que la mort elle-même le surprit en Hongrie lors d'un voyage en bâteau, au moment où il travaillait au projet de construction d'un moulin.

Les données dont on dispose nous apprennent qu'en plus des maîtres hongrois, des maîtres allemands, polonais, italiens et français avaient concouru à la construction des installations hydrauliques de la Hongrie médiévale. L'«aqueductor» ou le «Wasserkünstler» du moyen-âge était un maître aussi recherché et apprécié dans la construction des châteaux-forts et des villes que les tailleurs de pierre, les maîtres d'œuvres ou les charpentiers.

4. Trouvailles archéologiques

Bien peu de chose nous reste des installations hydrauliques mentionnées. Nous avons déjà parlé de l'emplacement de nos réseaux de distribution par gravitation et de nos pompes. La construction des réseaux de distribution modernes devait causer la destruction non seulement d'une grande partie de nos installations du moyen-âge, mais aussi de la totalité de celles construites au XVIIIe siècle.

Le dernier moulin à manège servant à l'élévation des eaux a été vu par Kornél DIVALD en 1910, au château-fort de Zólyom-Lipcse.

Comme matériau de leurs conduites d'eau, nos maîtres du moyen-âge avaient utilisé le plomb, la poterie et le bois de sapin. C'est le plomb que mentionne Bonfini, comme matériau des tuyaux dont était construit le canal de montagne du roi Mathias. Ces tuyaux étaient combinés avec des tuyaux de poterie ou de bois de sapin. Le plomb était tellement précieux qu'au début du XIXe siècle encore, la ville de Buda avait dû faire garder les tuyaux de plomb posés à un mètre de profondeur environ, de peur qu'on ne les vole, ce qui aurait privé la ville de son eau potable. Les données de Bonfini se trouvent confirmées par un tronçon de tuyau de plomb du XVe siècle, muni d'un robinet de bronze, que nos archéologues ont découvert au-dessous de l'aile sud-ouest du château royal de Buda (Musée Historique de Budapest).

A partir de 1823, les tuyaux de plomb, de poterie et de bois, d'un caractère médiéval, ont été remplacés à Buda par des tuyaux de fonte que l'on faisait venir de Mariazell. En 1828, le conseil municipal de la ville de Buda a fait vendre aux enchères les tuyaux de plomb enlevés.

Une partie des tuyaux de poterie de Buda provenant du XVe siècle portent les signes de potiers de Vienne et de Tulln, mais il est certain que la majeure partie de nos tuyaux de poterie du XVe siècle avaient été fabriqués par des potiers hongrois. Nos maîtres du moyen-âge avaient raccordé leurs tuyaux de poterie de 40 à 70 cm de long et d'un diamètre d'entrée de 8 à 12 cm, en emboîtant le bout rétréci d'un élément dans le bout plus large de l'autre et en les couvrant, au point de raccordement, de mortier à chaux et à sable additionné d'huile.

Les tuyaux de poterie étaient supportés par endroits, dans le sol meuble, par des lits de pierres jointes avec du mortier. En 1951, un tel tronçon de conduite a été mis à jour avenue Istenhegyi, à Buda, par les collaborateurs du Musée Historique de Budapest.

D'après une description de l'époque, à Buda on utilisait la poterie vernissée, le bois et le plomb, tandis qu'à Visegrád on recourait même à l'usage du bronze pour la fabrication des tuyaux.

Les tuyaux de bois, faits en mélèze, étaient frottés de poix à l'extérieur. Le raccordement se faisait au moyen d'anneaux de fer (fig. 5). On cerclait

à leurs extrémités les troncs de bois percés, pour les protéger contre l'éclatement, puis en intercalant l'anneau de jointure et de raccordement formant arête dans les deux sens, on battait le nouveau tuyau sur celui déjà posé. Cette opération s'appelait battage des tuyaux, expression qui a survécu jusqu'à nos jours. Les branchements des tuyaux de bois étaient faits en fer. Il est intéressant de noter que Léonard de Vinci avait construit une machine pour percer les tuyaux de bois, dont le dessin existe encore. Quant aux tuyaux de plomb, ils étaient faits de feuilles pliées et fermées par soudure avec du plomb fondu.

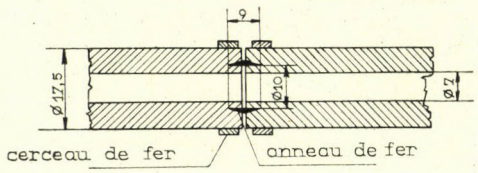

Fig. 5. Tuyaux de bois raccordés au moyen de cerceaux de fer (reconstitution de Á. JAKAB)

5. Conditions techniques de l'approvisionnement en eau au moyen-âge

Les descriptions contemporaines donnent une idée des possibilités et de l'état de l'approvisionnement en eau au moyen-âge.

L'apparition des tuyaux de fonte se situe selon toute vraisemblance à la première moitié du XVe siècle, puisqu'on savait déjà couler le fer au tournant des XIVe et XVe siècles. Et selon le livre de compte château-fort de Dillenbourg on y utilisait, en effet, dès l'an 1455, des tuyaux de fonte.

L'application de tuyaux de fonte en Hongrie n'est établie par des données qu'à partir du XVIIIe siècle. En 1777, le conseil municipal de Buda envoie le fontainier de la ville en Styrie, pour y étudier la fabrication des tuyaux de fonte. Cependant, les premiers tuyaux de fonte n'avaient été posés à Buda qu'en 1823. Ils n'étaient pas de fabrication hongroise; on les importait de Mariazell, d'Autriche.

Pour l'élévation des eaux, on avait déjà la pompe. D'après F. W. ROBINS, les installation hydrauliques des villes anglaises du moyen-âge comportaient souvent des pompes. Celles-ci étaient généralement faites en bois (fig. 6) avec cerclage en fer; le cylindre était souvent en métal; la garniture étanche du

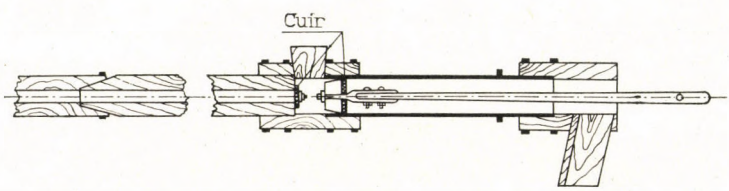

Fig. 6. Pompe à tuyau de bois et cylindre métallique

piston devait être un manchon de cuir graissé. Au début, les pompes n'étaient que des pompes élévatoires qui déversaient l'eau à l'extrémité des cylindres prolongés jusqu'à la hauteur voulue.

Dans le manuscrit technico-militaire illustré de Konrad KYESER von Eichstadt, intitulé: «Bellifortis», qui date de 1405, on trouve cependant des solutions indiquant sans doute possible, qu'il devait exister déjà des mécanismes qui permettaient l'élévation des eaux jusqu'aux châteaux-forts construits en haut des montagnes. Si l'une des figures ne laisse que présumer leur existence pratique, la seconde (fig. 7) montre avec évidence qu'il s'agit d'une

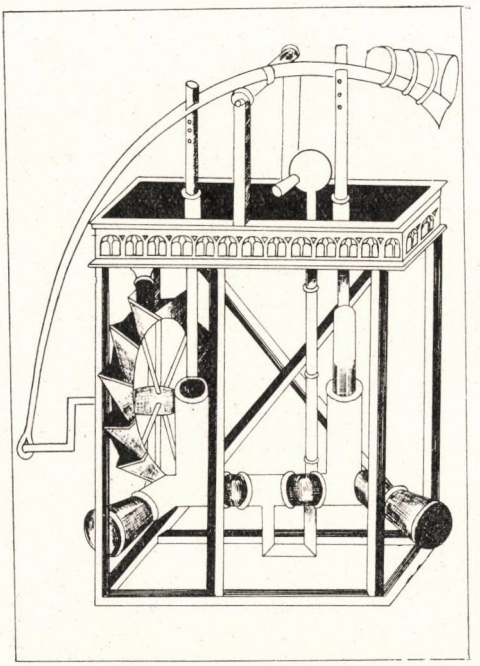

Fig. 7. Pompe actionnée par roue hydraulique de Konrad KYESER von Eickstadt, 1405 (peut être considérée comme le modèle de la pompe construite à Buda vers 1410)

pompe foulante. L'entraînement se fait par roue hydraulique et le mouvement rectiligne des pistons est assuré au moyen de balanciers.

Deux manuscrits antérieurs aux années 1430, conservés dans une bibliothèque de Munich, contiennent des schémas qui présupposent la connaissance de l'arbre à manivelle. Le principe de fonctionnement des pompes est identique à celui de la pompe de Nuremberg construite à une époque postérieure (fig. 8). Les possibilités techniques existaient donc, au début du XVe siècle, pour élever les eaux à des hauteurs plus importantes. Tout ceci rend évident que des installations analogues devaient aussi fonctionner à Buda. Il est, en effet, peu probable que la cour du roi et empereur Sigismond se fût

contentée d'un confort inférieur à celui dont elle aurait pu jouir dans les villes et châteaux-forts d'Allemagne. En raison des fluctuations du niveau d'eau du Danube, on actionnait les pompes du château-fort de Buda non pas par des roues hydrauliques, mais au moyen de cabestans à traction animale, ce qui assurait un rendement constant, indépendant des circonstances extérieures. Dans les tuyaux de bois, la hauteur d'élévation ne provoquait pas une tension pouvant causer des difficultés techniques, grâce à la grande épaisseur de paroi et au calibre relativement faible des tuyaux. Et l'élévation de la quantité d'eau nécessaire à l'alimentation d'une ou de deux fontaines pouvait être assurée par le travail de deux chevaux, malgré la faible efficience du cabestan en bois.

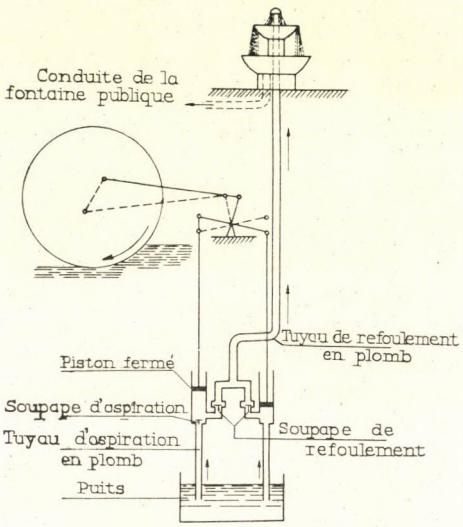

Fig. 8. Pompe (Manuscrit, Munich, 1430.)

Ce qui précède peut paraître plutôt un curieux détail de l'histoire de la civilisation qu'un enseignement positif intéressant l'ingénieur de nos jours.

Nous n'avons certes pas donné réponse à des questions fondamentales. On ne sait point quel était le débit des pompes de Buda ou celui des conduites de montagne, construites au moyen-âge, et l'on ignore de même la consommation d'eau journalière dans le Buda médiéval.

Ces questions restent forcément irrésolues, puisqu'on ignore jusqu'au nombre d'habitants de nos villes médiévales, comme Buda, Esztergom ou Pozsony (Bratislava).

Néanmoins, l'analyse de notre civilisation technique d'autrefois fait progresser nos connaissances. Des hypothèses et datations anciennes perdent leur validité, tandis que certains faits du passé, plus proches de la réalité,

s'expliquent. Aussi est-il à souhaiter que les recherches d'histoire de la technique qui prennent seulement leur essor, étudient plus à fond, par des méthodes plus modernes, les vestiges de la culture matérielle des temps passés.

LITTERATURE

Documentation plus détaillée et littérature hongroise du sujet traité:

ZOLNAY, L.: Vízművek a magyar középkorban (Ouvrages hydrauliques dans la Hongrie médiévale) *Comptes Rendus* de la Section des Sciences Techniques de l'Académie des Sciences de Hongrie, Tome XII (Budapest, 1956), pp. 1—15

ZOLNAY, L.: Buda középkori vízművei (Les ouvrages hydrauliques de Buda au moyen-âge). *Történelmi Szemle* (Revue Historique), 1961, n° 1, pp. 16—55

JAKAB, Á.—ZOLNAY, L.: Városaink és váraink vízellátása a középkorban (L'approvisionnement en eau de nos villes et châteaux-forts au moyen-âge). *Épületgépészet* (L'Installation), XIV (1965), n° 5, pp. 178—184

Note

Les dessins ont été exécutés par Mme S. KISS, en partie d'après les reconstructions de M. Á. JAKAB et les levés de M. A. VIRÁGH.

Water Supply of Mediaeval Hungarian Towns and Fortresses. As was proved by the evidence of Hungarian diplomatics and archeology, the towns of Hungary — Transylvania and Northern Hungary (Slovakia) included — were equipped in the 14th and 15th centuries with gravity watermains. The pumps for the water supply of mountain fortresses represented a considerable progress in comparison with these aqueducts, well-known already in antique Pannonia. According to written records, the first pump was installed in Buda in 1416. In the 15th century the fortresses of Pozsony (Bratislava), Visegrád and Belgrade were equipped with similar pump works by the Kings of Hungary. Still more important was the water-conduit of King Mathias Corvinus. Based on the law of communication vessels, this conduit carried the water of the Buda mountain sources down into the valley and from there on up to the castle hill. The architect was probably Chimenti Camicia of Firenze. Most of Hungary's important monuments of technical history were destroyed during the Turkish occupation (16—17th century).

Wasserversorgung mittelalterlicher ungarischer Städte und Burgen. Funde aus dem Bereich ungarischer Diplomatik und Archäologie lassen erkennen, daß die ungarischen Städte — sowohl in Siebenbürgen als auch im Oberland (Slowakei) — im Laufe des 14—15. Jh. mit Gravitations-Wasserleitungen versehen wurden. Im Vergleich zu diesen Wasserwerken, die bereits im antiken Pannonien wohlbekannt waren, bedeuteten die Pumpenanlagen zur Wasserversorgung der Bergfestungen einen bedeutenden technischen Fortschritt. Die erste Pumpe wird aus dem Jahre 1416 in Buda (Ofen) schriftlich erwähnt. Ähnliche Einrichtungen ließen die Ungarnkönige im 15. Jh. auch in den Festungen von Preßburg (Bratislava), Visegrád und Belgrad anlegen. Noch bedeutender war die Wasserleitung des Matthias Corvinus in den Budaer Bergen. Nach dem Gesetz der kommunizierenden Gefäße wurde das Wasser der Budaer Gebirgsquellen in das Tal geleitet und von dort auf den Burghügel. Der Architekt war vermutlich Chimenti Camicia aus Florenz. Die bedeutenden technischen Denkmäler Ungarns wurden größtenteils während der Türkenzeit (16—17. Jh.) zerstört.

Acta Technica Academiae Scientiarum Hungaricae, Tomus 76 (3—4), pp. 355—370 (1974)

TESTING THE PLASTIC PROPERTIES OF COHESIVE- AND INTERMEDIATE-TYPE SOILS BY EXTRUSION

A. TIMÁR*

[Manuscript received January 27, 1972]

The author describes a simple apparatus designed on the extrusion principle, a technique widely used in cold-plastic working of metals, and suggests its use for testing the plastic properties of soils. A comparative study of the extrusion technique has verified a new concept of the liquid limit and plastic limit of soils, on an energy theory basis, as one truly reflecting physical behaviour. The suggested method permits liquid limit and plastic limit to be determined within a single bar-extrusion test. As the procedure is fully mechanized, test results are relatively free from subjective errors. A statistical evaluation of a large number of tests has revealed a fair correlation between results furnished by conventional and extrusion methods. In order to clarify certain details, further investigations are suggested.

1. Interpretation of the liquid limit

In soil mechanics, the term liquid limit is used as defined by the fundamental research work of ATTERBERG, A. [1] and later elaborated by CASAGRANDE, A. [2], and it means the water content w_F at which a groove of standard dimensions in a specimen contained by the Casagrande dish will just close over a length of 10 mm upon 25 blows, under standardized conditions. Arbitrary as they are, test results thus obtained can be excellently used for a practical classification of soils and for the evaluation of their behaviour with respect, for example, to frost hazard, and have been generally adopted all over the world for such purposes without, however, any exact definition of the physical fundamentals of the liquid state.

Similarly, an arbitrary test is used for the determination of the plastic limit w_P, which means the water content at which the soil when rolled into threads of 3 mm diameter begins to crumble. The physical basis and explanation of this test and its correlation with the liquid limit have not been clarified yet.

Among the authors studying the plastic properties of soils, VASILIEV [3] and OHDE [4] should be mentioned first who attempted to elaborate new methods. Others tried to reduce the subjective errors of the Casagrande test to

* Dr. A. TIMÁR, Budapest Ráth Gy. u. 25, 1122 Hungary

an acceptable degree by statistical or mathematical methods (CASAGRANDE [6], NORMAN [5], PESTI [7]).

Recently the mechanization of methods, formerly used for the determination of the liquid limit, was also attempted, for example, by KAISER and GAY [8]. At the same time, in the rapidly developing colloid chemical-rheological research new devices designed on the extrusion (plastometric) principle have been increasingly adopted for the determination of viscosity (shear stress).

Experimental results obtained by the method described below are, owing to the instrumented character of the test, comparatively free from errors that depends on the individual running the test. The method also makes it feasible for the consistency limits and the plasticity index to be determined from the data of a single test.

KÉZDI [9] has shown that a certain activation energy is needed to initiate viscous yield in soils which may be considered as macromeritic liquids. He found that the energy "stored" in the soil (i.e., the energy required during sedimentation to produce a given density of the soil) would depend not only on density itself, but also on the shape and size of the grains, and on the frequency distribution of the different grain sizes; that is, it would be different for cohesive and intermediate soils even if their densities were the same. This means that the same "stored" energy level may correspond to different densities depending on the soil type. Results obtained by the Casagrande apparatus reveal that the "stored" energy of a soil with high liquid limit must be reduced to a relatively greater extent by remoulding the soil or otherwise increasing its water content in order to start viscous yield by the transfer of some arbitrarily chosen constant activation energy (influenced by the mass of the dish plus the soil cake in it, by the drop height, and by other factors).

At the same time, the work spent on remoulding and increasing the water content, i.e., on loosening the soil, cannot be measured, only its eventual difference.

It follows that although the densities of sand and of highly cohesive clay under natural conditions can be identical in theory, a reduction of the "stored" energy level to that of the Casagrande apparatus will require different work according to the soil type.

In order to provide for a basis of comparability, the Casagrande test is always performed, theoretically, with two-phase (saturated) soil samples. In such a state the water content can be regarded as an index of density. With the symbols (s, v, l) introduced by KÉZDI [10] to numerically express the phase composition, the water content may be written as

$$w = \frac{v\gamma_v}{s\gamma_s}, \tag{1}$$

or, in the saturated state ($v = 1 - s$)

$$w = \frac{(1 - s)\gamma_v}{s\gamma_s} \tag{2}$$

whence

$$s = \frac{1}{1 + \frac{w\gamma_s}{\gamma_v}} \tag{3}$$

where s is the volume per cent of the solid part,
γ_s is the specific gravity of the soil, and
γ_v is that of the water.

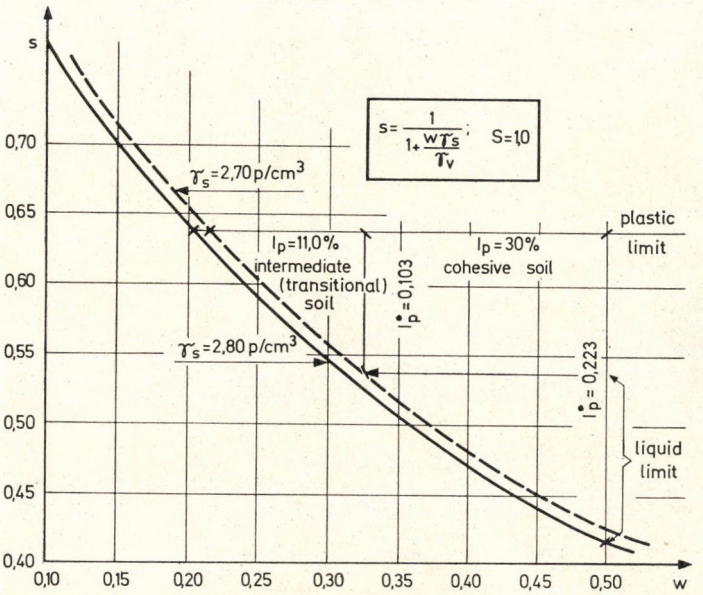

Fig. 1

On the basis of Eq. (3), the liquid limit could be expressed by the volume per cent (s) of the solid part instead of the water content, as the former is directly related to the density of the soil and is, therefore, in closer correlation with the idea of the "stored" energy, expressing it implicitly in a numerical form.

This concept is reflected by Fig. 1, the graphic illustration of Eq. (3). The "stored" energy level of highly cohesive soils is higher than that of the intermediate soil types, so a reduction of their energy to some arbitrarily predetermined level triggering viscous yield (neglecting here, for the sake of illustration, the otherwise significant surface effects) would require far more work, remoulding, or loosening (the w_F and w_P values have been selected on the basis of empirical data).

It should be noted here that the plasticity index which is generally used today ($I_p = w_F - w_P$) to describe the plastic behaviour of soils, and to serve as a basis for soil classification, might be expressed in the form

$$I_p = \frac{s_P - s_F}{s_P \cdot s_F} \cdot \frac{\gamma_v}{\gamma_s} \tag{4}$$

is proportional to the loss of energy characteristic of the plastic domain.

In the process of remoulding and of viscous flow it is the most likely that not the lubricating effect of the water, but its action as an energy level stabilizer by maintaining the phase composition will manifest itself, so it can readily be understood why consistency-limit tests must be performed with two-phase saturated soil samples.

Accordingly, saturated soils will start out as behaving like viscous liquids, when the molecular forces of attraction among the particles have decreased to a certain critical threshold value because of the structural rearrangement, that is, permanent displacement of the grains. The particles of granular soils have reached this state, and can be distinguished from cohesive and intermediate soil types precisely by their fusible character.

The molecular forces of attraction among the particles of intermediate and cohesive soils can be reduced to the critical value by a forcible rearrangement of the grains (water content increase, loosening). This again may be expressed numerically in the most convenient way (although somewhat inaccurately) by certain density characteristics (s, e, n). In other words, the liquid limit and the plastic limit might be expressed, instead of using the saturation water contents, by liquid and plastic porosity (or liquid and plastic void ratio) indicating a conveniently selected energy level measured in the saturated state. Such an energy level is easy to determine.

Experiments conducted in the Geotechnical Department of the Budapest Technical University revealed (KÉZDI—VARGA—TIMÁR [11]) that the shear strength of intermediate soil types was dependent on the phase composition to a degree readily expressed numerically. The following correlation was found:

$$\log \sigma_u = As + Bv + C \tag{5}$$

which, under saturation conditions, may be rewritten as

$$\log \sigma_u = A's + B'; \quad A' = A - B \qquad B' = B + C \tag{6}$$

With the liquid limit of the experimental soils determined by the Casagrande apparatus, the shear stress at the liquid limit defined by CASAGRANDE can be calculated by making use of Eqs (3) and (6):

$$\tau = \frac{\sigma_u}{2} = 0{,}10 - 0{,}15 \text{ kp/cm}^2$$

(provided that no volume change occurs, and thus $\Phi = 0$ during the whole loading period). This experimental result, however, does not agree with statement of SZILVÁGYI [12] who claimed that the value of the Casagrande liquid limit would be equal to the water content at which the shear stress is 10^4 din per $cm^2 = 0{,}01$ kp/cm^2. These latter results have been determined for soils in the liquid limit state, by using a torsional viscosimeter. The discrepancy may obviously be due to the different experimental methods.

If the ideas accepted in practice about 40 years ago are to be maintained, then the porosity (void ratio) of the saturated granular mass exhibiting viscous yield under the action of a shear stress of $\tau = 0{,}1-0{,}15$ kp/cm^2 might be termed as yield porosity (void ratio), and the water content which can still be calculated (measured) in this state as the liquid limit.

2. Extrusion

Extrusion is a technique known for quite some time for metal forming, and accepted increasingly in recent years. During extrusion, a punch exerts on a cylindrical block located in a similarly cylindrical chamber, the so-called

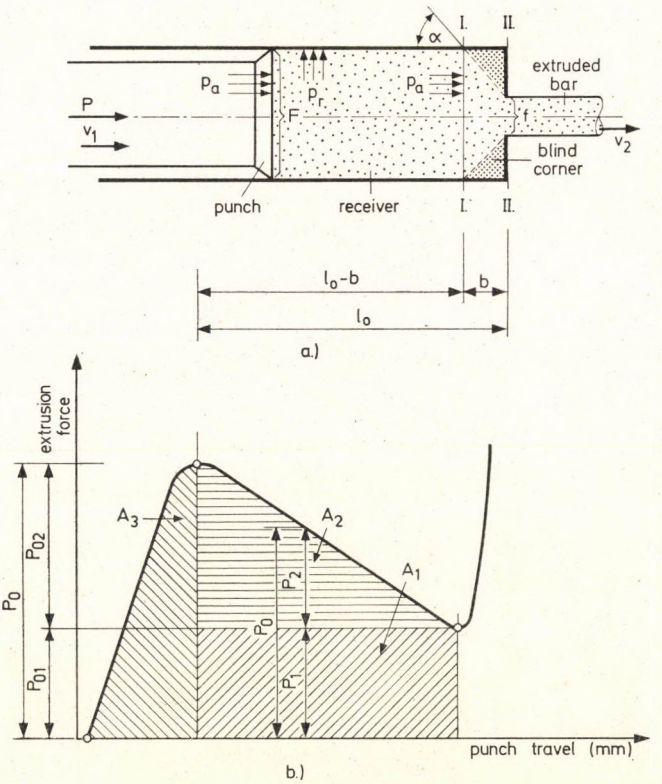

Fig. 2

receiver, such a pressure that the material in the latter will flow through the contoured orifice of the receiver's bottom cover (the die), see Fig. 2a. The material flowing through the orifice has a bar shape, with a cross-section identical to that of the orifice.

As GELEJI [13] pointed out, although many attempts have been made to determine the forces produced by extrusion, no experimental investigation conducted so far has led to acceptable results. Yet the only way to obtain satisfactory correlations in the field of extrusion seems to be experimentation.

Fig. 2b illustrates the variation of the extrusion force with the punch travel, so this may be regarded as the work diagram of extrusion, which may be divided into 3 parts. Field A_3 signifies the expansion work required for making the block fill up the receiver. Field A_1 is the deformation work needed to transform the block of cross-section F into a bar of a cross-section f. Finally, field A_2 is equal to the work necessary to overcome internal material displacements and the receiver wall friction.

Literature on metal working offers calculation techniques for the determination of forces P_0, P_1, and P_2, so these will not be dealt with here. From metal working (machine design) aspects, by the way, the determination of the P_0 and P_2 forces is the most important, whereas our experiments are primarily aimed at the determination of force P_1 and the deformation work.

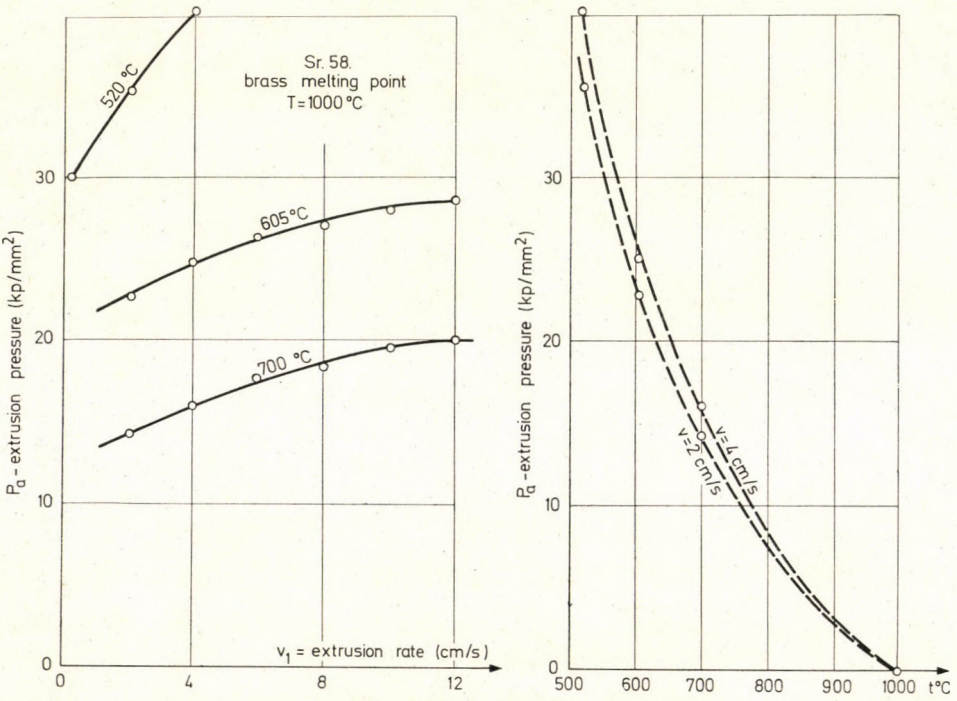

Fig. 3

The amount of energy stored in solids depends on pressure and temperature. By using the example of the melting point of mixtures, KÉZDI [9] proved that the temperature of solid bodies and the porosity of granular assemblies were analogous notions. In metal extrusion the deformation work, or force P_0, depends critically on the pressing temperature (Fig. 3) and, theoretically, it can be realized that if the melting point T^0 of the material and the extrusion temperature t^0 are identical, then the deformation work, or the value of force P_1, will be zero, that is, the value of function

$$P_a = f(t^0)$$

will be 0 when $t^0 = T^0$. However, literature discussing metal working does not contain any information on the shape of this function.

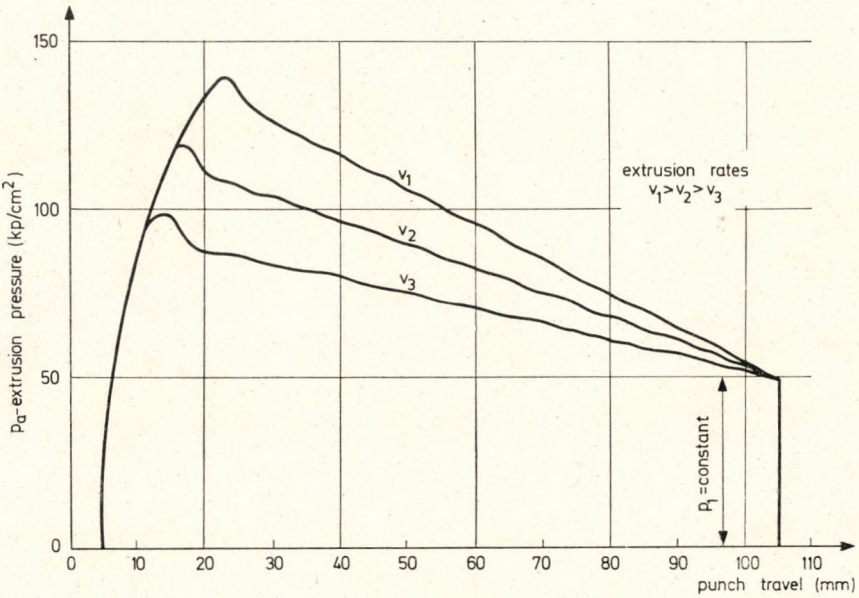

Fig. 4

In metal extrusion, when pressing is at the same temperature but at different rates, the speed does not affect the deformation force P_1 (GELEJI [13]), see Fig. 4.

According to GELEJI, the effect of the reduction in cross-section from F to f may be taken into account as follows:

The mean moulding resistance in the tapered drawing zone formed behind the punch will be

$$k_k = \frac{k_f}{1 - \dfrac{(F-f) + Q\mu_i}{2F}} = \frac{k_f}{1 - \dfrac{(F-f)}{2F}\left(1 + \dfrac{\mu_i}{\sin\alpha}\right)} \tag{7}$$

where
k_f — the moulding strength of the extruded material, kp/cm²
F — cross-section of the receiver, cm²
f — cross-section of the extruded bar, cm²
$Q = (F - f)/\sin \alpha$ — internal surface of the tapered drawing zone formed in the material, cm²
α — angle of the blind corner
μ_i — coefficient of internal friction.

In the opening of the stamp die (cross section *II* in Fig. 2), the moulding resistance is zero in theory. Accordingly, the same in cross-section *I* will equal $k_I = 2\,k_k$.

The axial stress in cross-section *I* reads

$$\sigma = p_a = 2k_k - k_f\,. \tag{8}$$

On the basis of experimental results, metal technology assumes that the axial and radial stresses in cross-section *I* are approximately equal ($p_a = p_r$).

Eq. (8) helps in calculating

— the force or stress passing the material through the orifice, if the material characteristics are known,

— the material characteristics, after the force of deformation, has been experimentally determined.

In the extrusion of soils the latter procedure is followed. If it is assumed that in the saturated soil at a sudden stress increase $\Phi = 0$ and $k_f = \text{const}$ (characteristic of the soil), — these assumptions are justified by the shear strength parameters: $\Phi \approx 0$, and $c = \text{const}$, obtained from the undrained, quick triaxial compression tests, — then the deformation stress ratios can be calculated by substituting the data of the three stamping dies we have used in our work in Eqs (7) and (8):

$F_1 \cong 2{,}5$ cm²
$F_2 \cong 4{,}2$ cm² $\quad f = 1{,}0$ cm²
$F_3 \cong 7{,}1$ cm²

$p_{11} = 1{,}82\ k_f$
$p_{12} = 2{,}22\ k_f$
$p_{13} = 2{,}56\ k_f$
$p_{a2}/p_{a1} = 1{,}2$
$p_{a3}/p_{a1} = 1{,}4$

(if $f \to F$, then $p_1 \to k_f$).

Thus a receiver or die of any convenient dimensions could be used for extrusion since the results can be evaluated in a uniform way.

In soil extrusion, the work values characteristic of metal extrusion may be interpreted in a similar manner. Force P_1, or the deformation work, depends on the density of the soil, and will equal zero when the porosity of the soil is equal to the yield porosity. It follows that the yield point or liquid limit could be defined as

> the water content of a saturated soil sample having such a density that the moulding stress in the extrusion test is zero, i.e., $p_1 = 0$.

In practice, however, since the soils never behave exactly in the same way as viscous liquids, the theoretical moulding stress p_1 pertaining to the liquid limit should be considered as higher than 0, such as 0,1 kp/cm² in order to ensure a better agreement with the results hitherto used in practical work.

In this case, after having established the empirical relationships

$$p_a = f(s) \quad \text{or} \quad p_a = f(w)$$

the liquid limit of individual soils could be directly determined.

The course of the function could be expected to characterize the behaviour of the respective soil in the plastic domain.

Just as the liquid limit is associated with a certain moulding stress value, the plastic limit and some other moulding stress value, say, the hundredfold of that pertaining to the liquid limit, that is, $p_1 = 10{,}0$ kp/cm², might also be related to each other. The following paragraphs describe the experimental results supporting the above theoretical statements.

3. Testing equipment

The soil extrusion tests were carried out by using the apparatus shown in detail in Figs 5, 6, and 7, mounted onto a motor-driven shear-box apparatus. Extrusion rate was 7,5 mm/min, the cross-sectional area of the circular receiver $F = 4{,}2$ cm², and that of the circular opening type die $f = 1{,}0$ cm². The natural soil sample was thoroughly mixed with distilled water, saturated, then filled into the receiver. After the die was placed into the shear-test machine, the motor was started and, from the very beginning of the extrusion of the soil bar, dial readings were taken at certain extrusion-path intervals (or, assuming a uniform rate, after certain time intervals). The test was continued until the extrusion force was decreasing, then its minimum, that is, the deformation force P_1 was determined. When the punch approached the cross-section I (Fig. 2), a sample of about 10 to 20 g was collected from the extruded soil bar into a watch-glass, and its water content was determined.

After the completion of the experiment the receiver and the die were washed and dried, then the test was several times repeated with gradually increased water contents, but otherwise as described above, until the minimum of the extrusion stress assumed a value approximating zero.

The test data ($P_a/F = p_a$; w) enabled us to determine the function

$$p_a = f(w)$$

sought for.

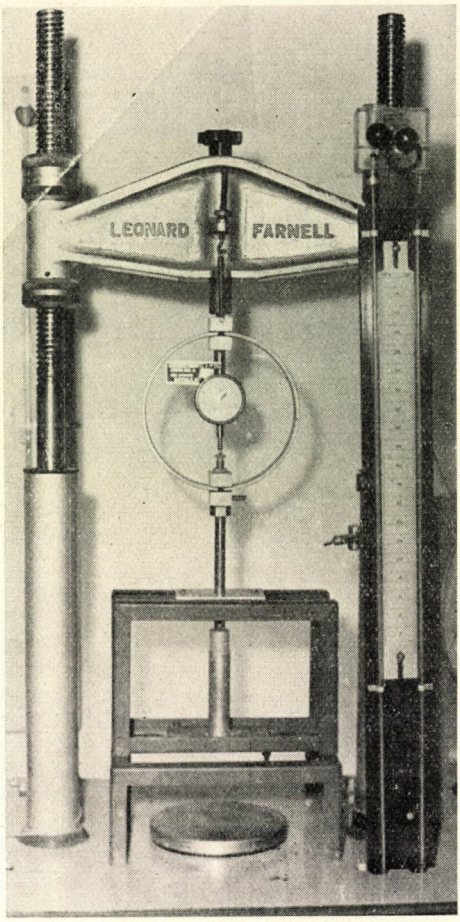

Fig. 5

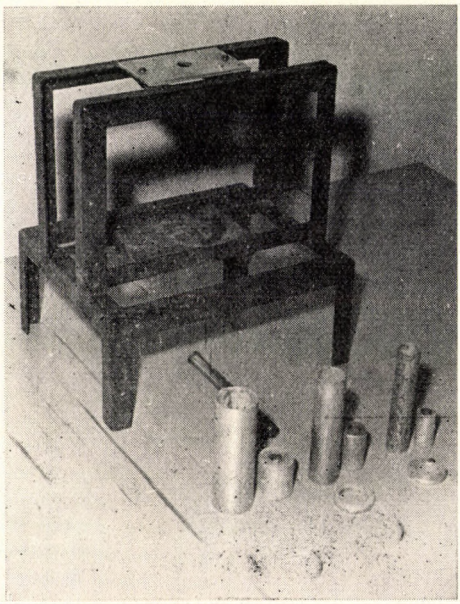

Fig. 6

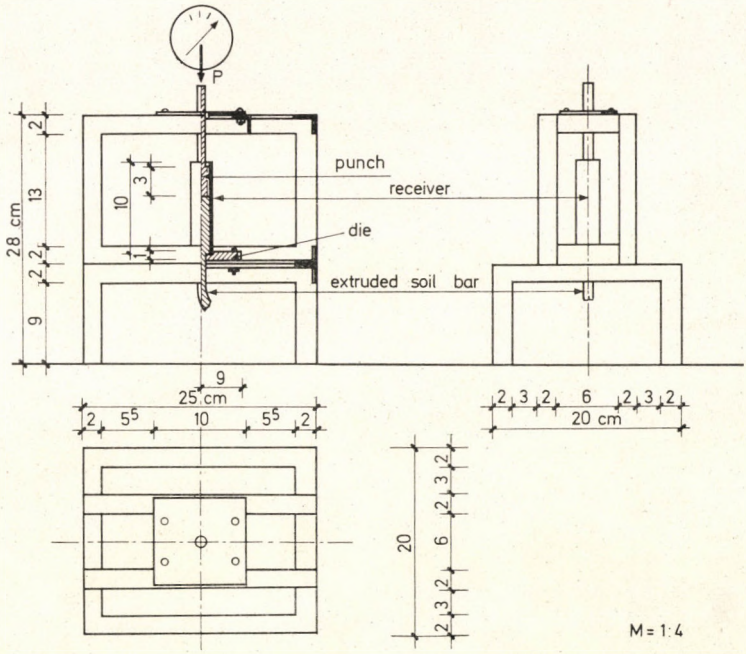

Fig. 7

4. Evaluation of the experimental results

In the laboratory of the Geotechnical Department of the Budapest Technical University about 50 soil samples, mainly cohesive, a few intermediate ones, were used for more than 250 extrusion tests.

These investigations included the measurement of the minimum extrusion force, and of the water content of the extruded samples, as well as the calculation of the volume per cent of the solid phase (s) from the water content (with complete saturation assumed).

Fig. 8 presents a typical experimental result. The character of the experimental curves was similar to that illustrated in this figure with each tested sample.

Assuming that the Casagrande relation

$$N^{(\text{impact no})} = ae^{-\text{bw}} \quad (10 \leq N \leq 40) \tag{9}$$

has the form

$$p_1^{(\text{minimum forming stress})} = ae^{-\text{bw}} \tag{10}$$

in the case of extrusion, the validity of this assumption had to be and was checked. Using the method of least squares revealed that the assumed expo-

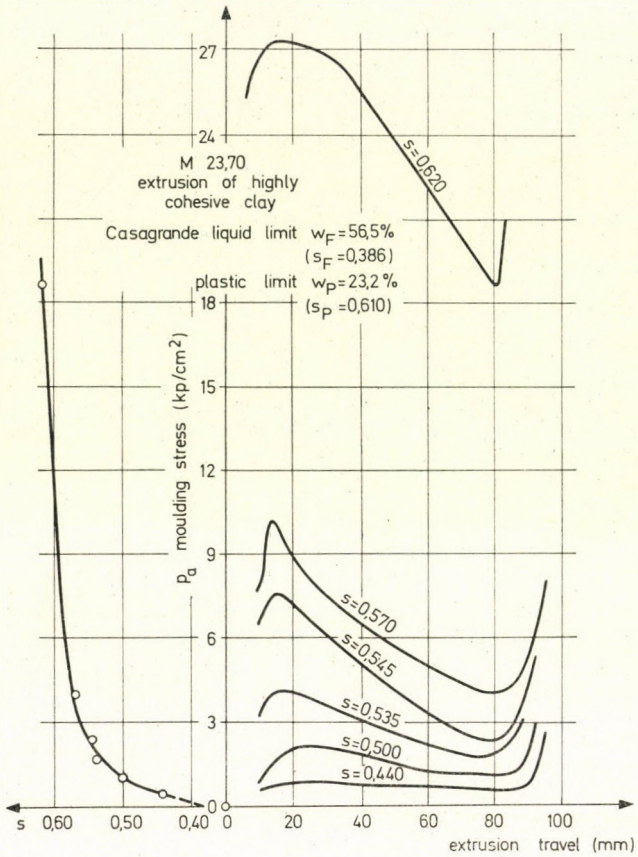

Fig. 8

nential curve fitted very well the test data, with an average correlation coefficient of $r_a = 0{,}980$, for 42 tested samples. Thus, according to our check-up tests, the correlation of the data pairs obtained with the Casagrande liquid limit apparatus is the same as for the exponential function. In addition, the b coefficients are of the same order of magnitude.

All these prove the adaptability of the extrusion experiment for testing the plastic properties of soils. With the experimental results plotted in a semi-logarithmic co-ordinate system, the best fitting line can be readily obtained (Fig. 9).

Assuming the w_F^x value of the liquid limit at $p_1 = 0{,}1$ kp/cm², and the w_P^x value of the plastic limit at $p_1 = 10$ kp/cm² on the basis of the theoretical considerations explained above, these characteristics can be determined for each soil, if the function $p_a = f(w)$ is known.

Based on the data of $n = 40$ samples, the linear correlation coefficient between the Casagrande liquid limit w_F and that obtained by extrusion w_F^x

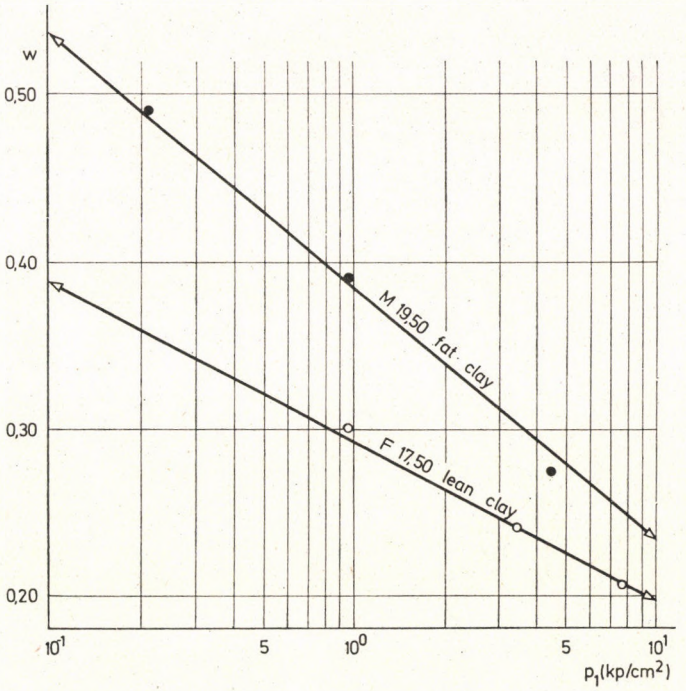
w
0,50
0,40
0,30
0,20
M 19,50 fat clay
F 17,50 lean clay
10^-1
5
10^0
5
10^1
p_1(kp/cm^2)

Fig. 9

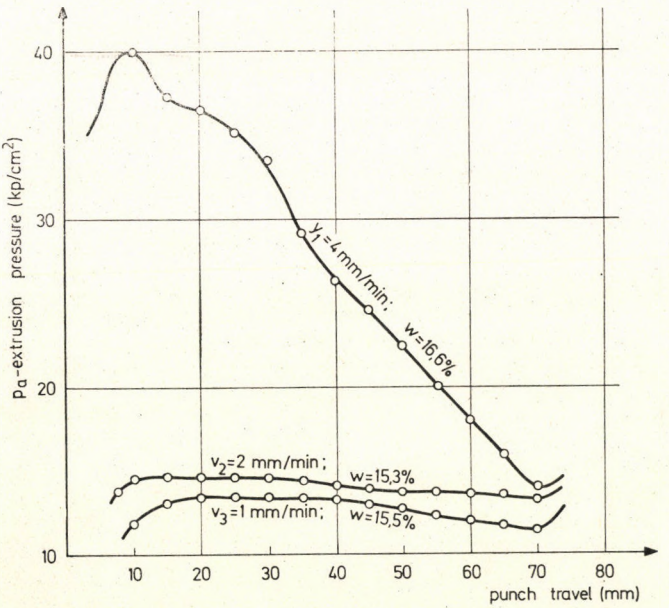
40
30
20
10
p_a-extrusion pressure (kp/cm^2)
v_1=4 mm/min; w=16,6%
v_2=2 mm/min; w=15,3%
v_3=1 mm/min; w=15,5%
10
20
30
40
50
60
70
80
punch travel (mm)

Fig. 10

is $r = 0{,}586$ ($a = 26{,}2$ and $b = 0{,}49$), while that between w_P determined by rolling-out test and w_P^x obtained by extrusion will be $r = 0{,}591$ ($a = 8{,}8$ and $b = 0{,}49$). Both cases exhibit a significant difference from zero which verifies the existence of the relation.

Consequently, extrusion as an experimental method may be introduced without changing the liquid limit concept used at present in soil mechanics.

Calculations were also made to prove whether the values quickly obtained from a semilogarithmic plot might be accepted to replace the exact values, to obtain which would require lengthy calculations in the absence of a computer.

Based on the data of $n = 45$ samples, the linear correlation between the accurate values calculated by a Hewlett-Packard computer, and those obtained graphically: w_F^x and w_P^x, proved to be very close ($r = 0{,}891$ and $r = 0{,}936$, resp.) which confirms the acceptable accuracy of the rapid graphic evaluation.

In order to study the effect of the rate of extrusion soil samples of identical water content were extruded at different rates (7,5; 4; 2, and 1 mm per min). The results of such a comparative test series are shown in Fig. 10.

As seen in this figure, the experience in metal working, namely, that the extrusion rate does not significantly affect the force of deformation, as it will only change the amount of work required to overcome internal resistances and wall friction, will hold true also for saturated soils.

To study the effect of varying receiver/die cross- section ratios, saturated soil samples of an identical water content were extruded with the same die in the three different receivers described under 2 ($F_1 = 2{,}5$, $F_2 = 4{,}2$, $F_3 = 7{,}1$ cm^2, and $f = 1{,}0$ cm^2). Experiments completed so far, although small in number, revealed that the ratios in metal working (see under 2) cannot be applied to soils without modification. Clarification of this problem requires further investigation.

6. Summary and recommendations

The extrusion technique described above offers a new soil testing method, in addition to those already adopted internationally, with the extra merit of permitting:

— direct measurement of the work spent on the plastic deformation of soils;

— determination of the liquid and plastic limits within a single test;

— elimination of the subjective errors from the measurement results.

The testing equipment is inexpensive to produce, and can be operated by any existing shear-test machine. Assuming an extrusion rate of a 4,0 to

8,0 mm/min, the duration of the test does not exceed that of the Casagrande liquid limit test and the plastic limit test together.

The interpretation of the "yield point" or liquid limit of soils as macromeritic grain assemblies, on an energy theory basis, which better reflects physical reality, has been illustratively and convincingly verified by extrusion tests.

Thus it is fully justified to continue these experiments, mainly to compare the results obtained with conventional and extrusion techniques, and to completely clarify their interrelation. If the initial promising results are verified on a large scale, the method may, in future, gain general acceptance as a routine test.

REFERENCES

1. ATTERBERG, A.: Die Plastizität der Tone — *Int. Mitt. Bodenkd. Översatt fr. Svenska ur Kungl. Landbruksakademiens Handlingar och Tidskr*, **50** (1911)
2. CASAGRANDE, A.: Research on the Atterberg Limits of Soils — *Public Roads*, **13** (1932—1933)
3. VASILIEV, A. M.: Uproshtchenny sposob opredelenya granicy tekutchesty glinisty gruntov — *Stroitelstvo dorog*, 1942, No 11
4. OHDE, J.: Neue Erdstoffkennwerte — *Bautechnik*, **27** (1950), 11
5. NORMAN, L. E.: A Comparison of Values of Liquid Limit Determined with an Apparatus Having Bases of Different Hardness — *Geotechnique* **2** (1958)
6. CASAGRANDE, A.: Notes on the Design of the Liquid Limit Device — *Geotechnique* **8** (1958)
7. PESTI, A.: Contribution to the Philosophy of the Liquid Limit Test — *Proceedings, 3rd Budapest Conference on Soil Mechanics*, Budapest 1968
8. KAISER, W.—GAY, G. C. W.: Die Mechanisierung der Bodenprobenaufbereitung und der Bestimmung der Ausrollgrenze nach Atterberg — *Straße und Autobahn* **23** (1972)
9. KÉZDI, Á.: Fundamentals of a New Soil Physics — Paper presented at the Hungarian Academy of Sciences, Budapest 1964 (in Hungarian)
10. KÉZDI, Á.: Soil Mechanics I — University textbook, Tankönyvkiadó, Budapest 1969
11. KÉZDI, Á.—VARGA, L.—TIMÁR, A.: Strength of Transition Soils — *Proceedings of the 4th Budapest Conference on Soil Mechanics*, 1971
12. SZILVÁGYI, I.: Laboratory Investigations — Engineering Planning, FTI Budapest 1965 (in Hungarian)
13. GELEJI, S.: Theory of Plastic Metal Forming — Akadémiai Kiadó, Budapest 1967 (in Hungarian)

Untersuchung der plastischen Eigenschaften von bindigen und Übergangsböden mit Hilfe von Stangenpressung. Der Autor schlägt eine einfache, beim Kaltformen der Metalle angewandte und nach dem Prinzip der Stangenpressung wirkende Vorrichtung zur Untersuchung von bindigen und Übergangsböden vor. Mit Hilfe der Stangenpressungsverfahren wird bewiesen, daß die aufgrund der Energietheorie erfolgende Beurteilung der Fließ- und Plastizitätsgrenzen der Bodenarten als makrometrischen Körnerhaufwerken, die physische Realität gut widerspiegelt. Die Fließ- und Plastizitätsgrenzen des Bodens kann mit einem einzigen Versuch ermittelt werden, der von den subjektiven Meßfehlern nur geringfügig belastet ist. Durch zahlreiche Versuche wird die Übereinstimmung zwischen den durch die herkömmliche Versuchsmethode und durch die Stangenpressung erhaltenen Werten mit Hilfe der Korrelationsrechnung nachgewiesen. Zur Untersuchung der noch ungeklärten Teilprobleme werden weitere Versuche vorgeschlagen.

Исследование пластических свойств связанных и переходных грунтов прессованием прутков. Автор предлагает для исследования пластических свойств связаных и переходных грунтов простой прибор, работающий по принципу прессования прутков, используемому при холодной обработке металлов. При помощи метода прессования прутков автор подтверждает хорошо отражающую физическую действительность трактовку пределов текучести и пластичности грунтов, как макрометрических множеств зерен, на энерготеоретической основе. Пределы текучести и пластичности грунтов могут быть определены при помощи одного единственного опыта прессования прутков, на который только в небольшой степени воздействуют субъективные ошибки измерения. На основе большого числа проведенных опытов с помощью корреляционного вычисления доказывается зависимость между результатами, которые получаются с помощью обычно применяемого экспериментального метода и метода прессования прутков. Для изучения еще невыясненных деталей автор предлагает выполнение дальнейших серий опытов.

Acta Technica Academiae Scientiarum Hungaricae, Tomus 76 (3—4), pp. 371—389 (1974)

DISPLACEMENT FUNCTIONS OF ORTHOGONALLY ANISOTROPIC CYLINDRICAL SHELLS

L. VARGA*

[Manuscript received December 20, 1971]

Displacement functions describing the stress state of orthotropic, anisotropic cylindrical shells are analysed and determined on the assumption of homogeneous anisotropy. By introducing the displacement functions, the exact and approximate solutions of the set of differential equations derived from the equilibrium conditions are presented. The relation between the displacements and displacement functions rendering general solutions to the homogeneous part and performing particular solutions to the non-homogeneous system are detailed. The differential equations furnishing the establishment of the displacement functions are reported. Last, the relations existing between the displacements caused by the membrane forces and the displacement functions, as well as the differential equation including the displacement functions and its solution are shown.

Introduction

Investigations on determining the stress state of shell structures was initiated by LOVE [1]. In connection with cylindrical shells also the works of TIMOSHENKO [2], FLÜGGE [3], WLASSOW [4], DONNEL [5], NOVOZHILOV [6], and GOLDENVEIZER [7], may be considered as of fundamental importance among which [4] and [7] deserve special attention due to their methods of the discussion of the problem. Namely, the stress functions giving the approximate solutions of the isotropic cylindrical shells are dealt with in these works, the terms analogous to which and relating to the orthotropic shells, are called displacement functions by the author of this paper.

In the investigations of pressurized reservoirs, the determination of the stress state of cylindrical shells by introducing the displacement function representing the displacements of the middle surface of the shell shows itself to be especially advantageous. In fact, to the cylindrical mantle of the shell, fittings of different forms and of different rigidity (closing surfaces limiting the extremities, supporting devices transmitting the forces etc.), are connected. The stress pattern developed at the connections and in their neighborhood will be determined by satisfying the constraints of fitting. The fitting constraints describing the identity of the deformations, may directly be expressed by the displacement functions. The displacement functions being familiar, as a matter of course, also the internal forces may readily be calculated.

* Dr. L. VARGA, Gábor Áron u. 42, 1026 Budapest, Hungary

The adoption of the displacement functions provides further advantages in handling and easily understanding the problem of such shells which might be considered as homogeneous, anisotropic structures. Structures of this type are, for example, shells of plastic material reinforced with fibreglass (fibreglass-skeleton shells) which, due to the great number of fibres embedded into the plastic material, may be considered as uniformly distributed and treated as a homogeneous anisotropic matter. Due to its elastic properties — in the range of deformation permissible from the viewpoint of safety — follow Hooke's law with a close approximation.

Also the cylindrical shells are constructed from such structural material, and it is characteristic that their wall-thickness — in comparison to the other dimensions and to the radius of curvature — is relatively small.

Hence, for the thin shells, the following assumptions and neglections may be made:

1. Straight lines being normal to the middle surface remain straight lines also after deformation and normal to the middle surface of the shell.

2. The stresses acting perpendicularly to the middle surface of the shell, may be disregarded in comparison to the stresses acting within the plane of the middle surface or in layers parallel to it.

3. The specific deformations developing perpendicularly to the middle surface may be disregarded.

Accordingly, the stresses and deformations induced at a point $P(x_1,x_2x_3)$ of the shell, may be represented by the following symmetric tensors:

$$\begin{matrix} \mathfrak{S} = (\sigma_{ik}) \\ \mathfrak{D} = (\varepsilon_{ik}) \end{matrix} \quad (i, k = 1, 2) \qquad \text{(a)}$$

As thin-walled structures satisfying the above conditions are to be considered according to references [2] and [3], the cylindrical shells having a thickness to the radius of curvature ratio $s/R - 1/10$, and according to reference [6], those, having a thickness to radius ratio $s/R - 1/20$. By virtue of the above assumptions the cylindrical shell may be analysed as an anisotropic, homogeneous structure. For the principal directions of the orthotropy, the direction of the generatrix and that of the circumference may be adopted. The characteristics of elasticity in respect to the principal directions may be measured or calculated.

The displacement functions of cylindrical shells to be considered orthogonally anisotropic homogeneous, may, in the simplest way, be derived by solving the set of differential equations describing the equilibrium conditions, by making use of the operator calculus. The paper treats the actual functional relations between the displacements and displacement functions representing the exact and approximate solutions of the set of equations in case of different loads. The differential equations furnishing the determination of the dis-

placement functions and the solutions of the set of equations are described. However, their solution will not be discussed here. The solution was treated in an earlier paper of the author [10] in which the introduction and definition of the displacement function including the approximate solutions of the set of homogeneous equations may be found.

1. *Relations between the internal forces and deformations*

The relations between the stresses developing in the principal directions of rigidity of the orthotropic shell and the deformations — according to Hooke's law — may be written down as follows:

$$\sigma_{11} = \frac{E_1}{1 - \nu_{12}\nu_{21}} (\varepsilon_{11} + \nu_{12}\varepsilon_{22})$$

$$\sigma_{22} = \frac{E_2}{1 - \nu_{12}\nu_{21}} (\varepsilon_{22} + \nu_{21}\varepsilon_{11}) \qquad (1a—c)$$

$$\sigma_{12} = \sigma_{21} = G\varepsilon_{12} = G\varepsilon_{21}$$

Expressing the specific deformations by the deformations of the middle surface yields

$$\varepsilon_{11} = \frac{u^{\prime}}{R} - x_3 \frac{w^{\prime\prime}}{R^2}$$

$$\varepsilon_{22} = \frac{\dot{v}}{R} - \frac{x_3}{R} \frac{\ddot{w}}{R+x_3} + \frac{w}{R+x_3} \qquad (2a—c)$$

$$\varepsilon_{12} = \frac{\dot{u}}{R+x_3} + \frac{R+x_3}{R^2} v^{\prime} - \frac{w^{\prime\cdot}}{R}\left(\frac{x_3}{R} + \frac{x_3}{R+x_3}\right).$$

The meanings of notations denoting the differentiation are as follows:

$$\frac{\partial(\ )}{\partial \frac{x_1}{R}} = \frac{\partial(\ )}{\partial \bar{x}_1} = (\ )^{\prime}$$

$$\frac{\partial(\ )}{\partial \frac{x_2}{R}} = \frac{\partial(\ )}{\partial \bar{x}_2} = (\ )^{\cdot}. \qquad (b)$$

By making use of relations (1a—c) and (2a—c) the section forces and moments may be produced depending on the displacements. Using the notations

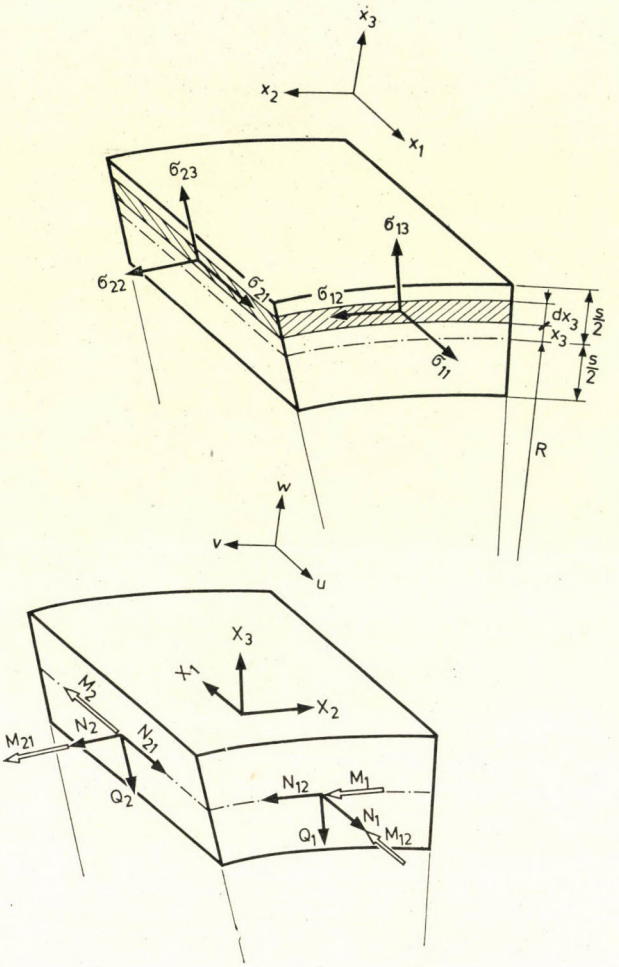

Fig. 1. Interpretation of the stresses, sectional forces and moments as well as external loads

of Fig. 1, the following may be written:

$$N_1 = \int_{-s/2}^{s/2} \sigma_{11} \left(1 + \frac{x_3}{R}\right) dx_3 = \frac{D_1}{R}(u' + \nu_{12} v' + \nu_{12} w) - \frac{B_1}{R^3} w''$$

$$N_2 = \int_{-s/2}^{s/2} \sigma_{22}\, dx_3 = \frac{D_2}{R}(\nu_{21} u' + v' + w) + \frac{B_2}{R^3}(\ddot{w} + w)$$

$$N_{12} = \int_{-s/2}^{s/2} \sigma_{12} \left(1 + \frac{x_3}{R}\right) dx_3 = \frac{D_3}{R}(u' + v') + \frac{B_3}{R^3}(v' - w'') \qquad (3a—d)$$

$$N_{21} = \int_{-s/2}^{s/2} \sigma_{21}\, dx_3 = \frac{D_3}{R}(u' + v') + \frac{B_3}{R^3}(u' + w'')$$

$$M_1 = -\int_{-s/2}^{s/2} \sigma_{11}\left(1+\frac{x_3}{R}\right) x_3\, dx_3 = \frac{B_1}{R^2}\left(w^{\mathrm{II}}+\nu_{12}\, w^{\cdot\cdot}-u^{\mathrm{I}}-\nu_{12}\, v^{\cdot}\right)$$

$$M_2 = -\int_{-s/2}^{s/2} \sigma_{22}\, x_3\, dx_3 = \frac{B_2}{R^2}\left(w^{\cdot\cdot}+\nu_{21}\, w^{\mathrm{II}}+w\right)$$

$$M_{12} = -\int_{-s/2}^{s/2} \sigma_{12}\left(1+\frac{x_3}{R}\right) x_3\, dx_3 = 2\,\frac{B_3}{R^2}\left(w^{\mathrm{I}\cdot}-v^{\mathrm{I}}\right) \qquad \text{(3e—f)}$$

$$M_{21} = -\int_{-s/2}^{s/2} \sigma_{21}\, x_3\, dx_3 = 2\,\frac{B_3}{R^3}\left(w^{\mathrm{I}\cdot}+\frac{u^{\cdot}}{2}-\frac{v^{\mathrm{I}}}{2}\right)$$

where

$$D_1 = \frac{E_1\, s}{1-\nu_{12}\,\nu_{21}}, \qquad B_1 = \frac{E_1\, s^3}{12(1-\nu_{12}\,\nu_{21})}$$

$$D_2 = \frac{E_2\, s}{1-\nu_{12}\,\nu_{21}}, \qquad B_2 = \frac{E_2\, s^3}{12(1-\nu_{12}\,\nu_{21})} \qquad \text{(4a—f)}$$

$$D_3 = Gs \qquad B_3 = \frac{Gs^3}{12}$$

are the elongation and flexural rigidities with respect to the principal directions of rigidity.

2. *The differential equations of the stress state*

The differential equations — as is known — may be established by writing down the equilibrium equations. The equilibrium of the forces and moments acting on an element of the shell, as is to be seen in Fig. 1, are represented by the following relations:

$$\begin{aligned} N_1^{\mathrm{I}} + N_{21}^{\cdot} &= X_1 R \\ N_2^{\cdot} + N_{12}^{\mathrm{I}} - Q_2 &= X_2 R \\ N_2 + Q_1^{\mathrm{I}} + Q_2^{\cdot} &= X_3 R \\ M_1^{\mathrm{I}} + M_{21}^{\cdot} - RQ_1 &= 0 \\ M_2^{\cdot} + M_{12}^{\mathrm{I}} - RQ_2 &= 0 \\ M_{21} + RN_{12} - RN_{21} &= 0 \end{aligned} \qquad \text{(5a—f)}$$

Expressing the transversal forces from formulas (5d—e) and substituting into Eqs (5b—c) yields:

$$\begin{aligned} N_1^{\mathrm{I}} + N_{21}^{\cdot} &= X_1 R \\ RN_2^{\cdot} + RN_{12}^{\mathrm{I}} - M_2^{\cdot} - M_{12}^{\mathrm{I}} &= X_2 R^2 \\ M_2^{\cdot\cdot} + M_{12}^{\mathrm{I}\cdot} + M_{21}^{\mathrm{I}\cdot} + M_1^{\mathrm{II}} + RN_2 &= X_3 R^2 \end{aligned} \qquad \text{(6a—c)}$$

Let us now replace the expressions (3a—h) of the sectional forces and moments into Eqs (6a—c) then, after reduction, we arrive at the required differential equations:

$$\frac{E_1}{E_2}u^{II}+\frac{G}{E_2^*}(1+k)u^{\cdot\cdot}+\left(\frac{G}{E_2^*}+\nu_{21}\right)v^{I\cdot}+\nu_{21}w^{I}+k\left(\frac{G}{E_2^*}w^{I\cdot\cdot}-\frac{E_1}{E_2}w^{III}\right)=X_1^*$$

$$\left(\frac{G}{E_2^*}+\nu_{21}\right)u^{I\cdot}+v^{\cdot\cdot}+\frac{G}{E_2^*}(1+3k)\,v^{II}+w^{\cdot}-k\left(3\frac{G}{E_2^*}+\nu_{21}\right)w^{II\cdot}=X_2^*$$

$$\nu_{21}u^{I}+v^{\cdot}+w+k\left[\frac{G}{E_2^*}u^{I\cdot\cdot}-\frac{E_1}{E_2}u^{III}-\left(3\frac{G}{E_2^*}+\nu_{21}\right)v^{II\cdot}+\right. \tag{7a—c}$$

$$\left.+\frac{E_1}{E_2}w^{IV}+2\left(2\frac{G}{E_2^*}+\nu_{21}\right)w^{II\cdot\cdot}+w^{\cdot\cdot\cdot\cdot}+2w^{\cdot\cdot}+w\right]=X_3^*$$

where

$$E_i^*=\frac{E_i}{1-\nu_{12}\nu_{21}};\quad k=\frac{B_i}{R^2D_i}=\frac{1}{12}\frac{s^2}{R^2};\quad X_i^*=\frac{R^2}{D_2}X_i. \tag{c}$$

The solution of the set of differential equations (7a—c) representing the stress state may be carried out as described in the following chapter.

3. *Solution to the differential equations by introducing the displacement function*

Eqs (7a—c) describing the stress state of the orthotropic cylindrical shell may be handled as a non-homogeneous set of linear equations whose solutions — as is known — are composed of the general solutions of the homogeneous part and of the particular solutions of the non-homogeneous system. Thus, the displacements giving the solution might be written in the following form:

$$\begin{aligned} u &= u_0+u_p \\ v &= v_0+v_p \\ w &= w_0+w_p \end{aligned} \tag{8a—c}$$

The solutions may be relatively simply obtained by introducing the displacement function

$$\mathfrak{F}=\mathfrak{F}(\bar{x}_1,\bar{x}_2) \tag{9}$$

in such a way that the displacements should be sought in the form

$$\begin{aligned} u &= U(\mathfrak{F}) \\ v &= V(\mathfrak{F}) \\ w &= W(\mathfrak{F}) \end{aligned} \tag{10a—c}$$

It is practicable and reasonable to divide the displacement function into two parts, i.e., to write it down as the following sum:

$$\mathfrak{F}(\bar{x}_1, \bar{x}_2) = \mathfrak{F}_0(\bar{x}_1, \bar{x}_2) + \mathfrak{F}_p(\bar{x}_1, {}_2\bar{x}) \tag{11}$$

in such a way that the solutions to the homogeneous part are included in the function $\mathfrak{F}_0$, and those of the non-homogeneous system in the function $\mathfrak{F}_p$. For the sake of lucidity and easy handling also the displacement function $\mathfrak{F}_p$ should conveniently be considered as a sum

$$\mathfrak{F}_p(\bar{x}_1, \bar{x}_2) = \mathfrak{F}_1(\bar{x}_1, \bar{x}_2) + \mathfrak{F}_2(\bar{x}_1, \bar{x}_2) + \mathfrak{F}_3(\bar{x}_1, \bar{x}_2) \tag{12}$$

where $\mathfrak{F}_1$ first displacement function including displacements u_1, v_1 and w_1 caused by loading X_1,

$\mathfrak{F}_2$ second displacement function comprising displacements u_2, v_2 and w_2 caused by load X_2,

$\mathfrak{F}_3$ third displacement function including displacements u_3, v_3 and w_3 caused by load X_3.

On the whole, the displacements may be written in the form

$$\begin{aligned} u &= u_0 + u_1 + u_2 + u_3 = U_0(\mathfrak{F}_0) + U_1(\mathfrak{F}_1) + U_2(\mathfrak{F}_2) + U_3(\mathfrak{F}_3) \\ v &= v_0 + v_1 + v_2 + v_3 = V_0(\mathfrak{F}_0) + V_1(\mathfrak{F}_1) + V_2(\mathfrak{F}_2) + V_3(\mathfrak{F}_3) \\ w &= w_0 + w_1 + w_2 + w_3 = W_0(\mathfrak{F}_0) + W_1(\mathfrak{F}_1) + W_2(\mathfrak{F}_2) + W_3(\mathfrak{F}_3) \end{aligned} \tag{13a–c}$$

The effective relation between the displacements and displacement functions will be determined in the following chapter.

4. *The relation between the displacement of the middle surface and displacement functions*

The relation between the displacement of the middle surface and displacement functions may be determined by the application of the operator calculus. Treating the relations (7a–c) as an algebraic set of equations, the determinant produced from the coefficients of the desired u, v and w can be written as follows

$$\mathfrak{D} = \begin{vmatrix} d_{11} & d_{12} & d_{13} \\ d_{21} & d_{22} & d_{23} \\ d_{31} & d_{32} & d_{33} \end{vmatrix} \tag{14}$$

The meanings of the coefficients d_{ij} are given by the differential operators indicated in Table I.

Table I

Operators denoting the coefficients of displacements

d_{11}	$\frac{E_1}{E_2}\frac{\partial^2}{\partial \bar{x}_1^2} + \frac{G(1+k)}{E_2^*}\frac{\partial^2}{\partial \bar{x}_2^2}$
$d_{12} = d_{21}$	$\left(\frac{G}{E_2^*} + \nu_{21}\right)\frac{\partial^2}{\partial \bar{x}_1 \partial \bar{x}_2}$
$d_{13} = d_{31}$	$\nu_{21}\frac{\partial}{\partial \bar{x}_1} + k\left(\frac{G}{E_2^*}\frac{\partial^3}{\partial \bar{x}_1 \partial \bar{x}_2^2} - \frac{E_1}{E_2}\frac{\partial^3}{\partial \bar{x}_1^3}\right)$
d_{22}	$\frac{G(1+3k)}{E_2^*}\frac{\partial^2}{\partial \bar{x}_1^2} + \frac{\partial^2}{\partial \bar{x}_2^2}$
$d_{23} = d_{32}$	$\frac{\partial}{\partial \bar{x}_2} - k\left(3\frac{G}{E_2^*} + \nu_{21}\right)\frac{\partial^3}{\partial \bar{x}_1^2 \partial \bar{x}_2}$
d_{33}	$1 + k\left[1 + \frac{E_1}{E_2}\frac{\partial^4}{\partial \bar{x}_1^4} + 2\left(2\frac{G}{E_2^*} + \nu_{21}\right)\frac{\partial^4}{\partial \bar{x}_1^2 \partial \bar{x}_2^2} + \frac{\partial^4}{\partial \bar{x}_2^4} + 2\frac{\partial^2}{\partial \bar{x}_2^2}\right]$

The solutions of the set of equations (7a—c) are sought in the following form:

$$\begin{aligned} u &= u_0 + u_p = \mathfrak{D}_{11}(\gamma_1^0 + \gamma_1^p) + \mathfrak{D}_{12}(\gamma_2^0 + \gamma_2^p) + \mathfrak{D}_{13}(\gamma_3^0 + \gamma_3^p) \\ v &= v_0 + v_p = \mathfrak{D}_{21}(\gamma_1^0 + \gamma_1^p) + \mathfrak{D}_{22}(\gamma_2^0 + \gamma_2^p) + \mathfrak{D}_{23}(\gamma_3^0 + \gamma_3^p) \\ w &= w_0 + w_p + \mathfrak{D}_{31}(\gamma_1^0 + \gamma_1^p) + \mathfrak{D}_{32}(\gamma_2^0 + \gamma_2^p) + \mathfrak{D}_{33}(\gamma_3^0 + \gamma_3^p) \end{aligned} \qquad (15a-c)$$

Substitution of these solutions into the set of differential equations — on the basis of the theory of the linear algebraic equations — yields the set of homogeneous and non-homogeneous equations:

$$\begin{aligned} \mathfrak{D}\gamma_1^0 &= 0 \\ \mathfrak{D}\gamma_2^0 &= 0 \\ \mathfrak{D}\gamma_3^0 &= 0 \end{aligned} \qquad (16a-c)$$

and

$$\begin{aligned} \mathfrak{D}\gamma_1^p &= X_1^* \\ \mathfrak{D}\gamma_2^p &= X_2^* \\ \mathfrak{D}\gamma_3^p &= X_2^* \end{aligned} \qquad (17a-c)$$

To derive the solving equation comprising the general solution of the set of homogeneous equations, it is convenient to select the roots in the form

$$\gamma_1^0 = \gamma_2^0 = 0, \qquad \gamma_3^0 = \frac{E_2^*}{G}\mathfrak{F}_0 \qquad (18a-c)$$

Thus, the solutions are included in the equivalent differential equation

$$\mathfrak{D}^* \mathfrak{F}_0 = 0 \tag{19}$$

wherein

$$\mathfrak{D}^* = \frac{E_2^*}{G} \mathfrak{D} \tag{20}$$

The particular solutions of the non-homogeneous system can be written in the form

$$\gamma_1^p = \frac{E_2^*}{G} \mathfrak{F}_1$$

$$\gamma_2^p = \frac{E_2^*}{G} \mathfrak{F}_2 \tag{21a—c}$$

$$\gamma_3^p = \frac{E_2^*}{G} \mathfrak{F}_2$$

The displacement functions including the solutions will be given as the particular solutions of the differential equations

$$\begin{aligned} \mathfrak{D}^* \mathfrak{F}_1 &= X_1^* \\ \mathfrak{D}^* \mathfrak{F}_2 &= X_2^* \\ \mathfrak{D}^* \mathfrak{F}_3 &= X_3^* \end{aligned} \tag{22a—c}$$

In accordance with what has been said above, the relation between the displacements and displacement functions is represented by the equations

$$\begin{aligned} u &= \mathfrak{D}_{11}^* \mathfrak{F}_1 + \mathfrak{D}_{12}^* \mathfrak{F}_2 + \mathfrak{D}_{13}^* (\mathfrak{F}_3 + \mathfrak{F}_0) \\ v &= \mathfrak{D}_{21}^* \mathfrak{F}_1 + \mathfrak{D}_{22}^* \mathfrak{F}_2 + \mathfrak{D}_{23}^* (\mathfrak{F}_3 + \mathfrak{F}_0) \\ w &= \mathfrak{D}_{31}^* \mathfrak{F}_1 + \mathfrak{D}_{32}^* \mathfrak{F}_2 + \mathfrak{D}_{33}^* (\mathfrak{F}_3 + \mathfrak{F}_0) \end{aligned} \tag{23a—c}$$

In consequence of the above mentioned facts, the displacement functions can be considered as potential functions, whose detailed analysis is to be found in the chapters following hereafter.

5. *The displacement function comprising the solution of the homogeneous system*

On the basis of relations (23a—c) deduced in the preceding chapter — taking into account the terms of the operators indicated in Table I, and the interpretation by (20) — the effective functional relation between the displacements solving the homogeneous system and the displacement function takes the form:

$$u_0 = U_{01}\mathfrak{F}_0^{III} + U_{02}\mathfrak{F}_0^{I:} + k(U_{03}\mathfrak{F}_0^{III} + U_{04}\mathfrak{F}_0^{V} + U_{05}\mathfrak{F}_0^{III:} + U_{06}\mathfrak{F}_0^{I::}) + \\ + k^2(U_{07}\mathfrak{F}_0^{V} + U_{08}\mathfrak{F}_0^{III:})$$

$$v_0 = V_{01}\mathfrak{F}_0^{II\cdot} + V_{02}\mathfrak{F}_0^{\cdot\cdot} + k(V_{03}\mathfrak{F}_0^{\cdot\cdot} + V_{04}\mathfrak{F}_0^{IV\cdot} + V_{05}\mathfrak{F}_0^{II:\cdot}) + k^2 V_{06}\mathfrak{F}_0^{II:\cdot}$$

$$w_0 = W_{01}\mathfrak{F}_0^{IV} + W_{02}\mathfrak{F}_0^{II:} + W_{03}\mathfrak{F}_0^{::} + k(W_{04}\mathfrak{F}_0^{IV} + W_{05}\mathfrak{F}_0^{II:} + \\ + W_{06}\mathfrak{F}_0^{:::}) + k^2 W_{07}\mathfrak{F}_0^{II:} \qquad (24a-c)$$

The terms of the coefficients are indicated in Table II.

Table II

Coefficients of the homogeneous solutions

j	U_{0j}	V_{0j}	W_{0j}
1	$-\nu_{21}$	$\nu_{21} - \frac{E_1}{G}$	$\frac{E_1}{E_2}$
2	1	-1	$\frac{E_1}{G} - 2\nu_{21}$
3	$-3\nu_{21}$	-1	1
4	$\frac{E_1}{E_2}$	$2\frac{E_1}{E_2}$	$3\frac{E_1}{E_2}$
5	$\frac{E_1}{G} - 4\left(\frac{G}{E_2^*} + \nu_{21}\right)$	$2\left(2\frac{G}{E_2^*} + \nu_{21}\right)$	$4\frac{G}{E_2^*}$
6	-1	$3\frac{G}{E_2^*} + \nu_{21}$	1
7	$3\frac{E_1}{E_2}$		$3\frac{G}{E_2^*}$
8	$-3\frac{G}{E_2^*}$		

The differential equation [19] furnishing the determination of the displacement function takes the form

$$\mathfrak{F}_0^{VIII} + a_{01}\mathfrak{F}_0^{VI:} + a_{02}\mathfrak{F}_0^{IV::} + a_{03}\mathfrak{F}_0^{II:::} + a_{04}\mathfrak{F}_0^{::::} + a_{05}\mathfrak{F}^{VI} + \\ + a_{06}\mathfrak{F}_0^{IV:} + a_{07}\mathfrak{F}_0^{II::} + a_{08}\mathfrak{F}_0^{:::} + a_{09}\mathfrak{F}_0^{IV} + a_{010}\mathfrak{F}_0^{II:} + a_{011}\mathfrak{F}_0^{::} = 0 \qquad (25)$$

The coefficients are as shown in the relations listed in Table III.

The displacement function — in case of given boundary condition — can be calculated from the general solutions of Eq. (25).

Table III

Expressions furnishing the exact determination of the coefficients

a_0	$k\left(\frac{E_1}{E_2}\right)^2(1+2k-3k^2)$
a_{01}	$\frac{k}{a_0}\frac{E_1}{E_2}\left[\frac{E_1}{G}+4\frac{G}{E_2^*}-k\left(\frac{E_1}{G}-15\frac{G}{E_2^*}-8\nu_{21}\right)+9k^2\frac{G}{E_2^*}\right]$
a_{02}	$\frac{k}{a_0}\left[6\frac{E_1}{E_2}+2\nu_{21}\frac{E_1}{G}-8\nu_{21}\frac{G}{E_2^*}-8\nu_{21}^2+k\left(6\frac{E_1}{E_2}-6\nu_{21}\frac{G}{E_2^*}-3\nu_{21}^2\right)-k^2\nu_{21}^2\right]$
a_{03}	$\frac{k}{a_0}\left[\frac{E_1}{G}+4\frac{G}{E_2^*}+k\left(7\frac{G}{E_2^*}+2\nu_{21}\right)+3k^2\frac{G}{E_2^*}\right]$
a_{04}	$\frac{k}{a_0}(1+k)$
a_{05}	$2\frac{k}{a_0}\frac{E_1}{E_2}\nu_{21}(1+3k)$
a_{06}	$\frac{k}{a_0}\left[6\frac{E_1}{E_2}+2\nu_{21}\frac{E_1}{G}-8\nu_{21}\frac{G}{E_2^*}-8\nu_{21}^2+6k\left(\frac{E_1}{E_2}-\nu_{21}\frac{G}{E_2^*}\right)\right]$
a_{07}	$\frac{k}{a_0}\left[8\frac{G}{E_2^*}+2\frac{E_1}{G}-2\nu_{21}+k\left(14\frac{G}{E_2^*}+2\nu_{21}\right)+6k^2\frac{G}{E_2^*}\right]$
a_{08}	$2\frac{k}{a_0}(1+k)$
a_{09}	$\frac{k}{a_0}\left(4\frac{E_1}{E_2}-3\nu_{21}^2+3k\frac{E_1}{E_2}\right)+\frac{1}{a_0}\left(\frac{E_1}{E_2}-\nu_{21}^2\right)$
a_{010}	$\frac{k}{a_0}\left(\frac{E_1}{G}+4\frac{G}{E_2^*}-2\nu_{21}+7k\frac{G}{E_2^*}+3k^2\frac{G}{E_2^*}\right)$
a_{011}	$\frac{k}{a_0}(1+k)$

In connection with the thin shells investigated herein, $R/s > 10$, therefore $k < 0{,}001$ and thus, neglection of k in comparison to the unit is justified. This neglection permits an accuracy in the calculation being satisfactory for the practice, by using the coefficients indicated on Table IV.

A further significant simplification can be made by introducing, on the basis of the above consideration, the approximations

$$(1+k)\,u'' \approx u'' \qquad (1+3k)v^{II} \approx v^{II} \qquad \text{(26a—b)}$$

Table IV

Expressions furnishing the approximate determination of the coefficients

a_0	$k\left(\frac{E_1}{E_2}\right)^2$
a_{01}	$4\left(\frac{G}{E_1^*}+\frac{1}{4}\frac{E_2}{G}\right)$
a_{02}	$6\frac{E_2}{E_1}\left(1+\frac{1}{3}\frac{E_2}{G}\nu_{21}-\frac{4}{3}\frac{G}{E_2^*}\nu_{12}-\frac{4}{3}\nu_{12}\nu_{21}\right)$
a_{03}	$4\frac{E_2}{E_1}\left(\frac{G}{E_1^*}+\frac{1}{4}\frac{E_2}{G}\right)$
a_{04}	$\left(\frac{E_2}{E_1}\right)^2$
a_{05}	$2\nu_{12}$
a_{06}	$6\frac{E_2}{E_1}\left(1+\frac{1}{3}\frac{E_2}{G}\nu_{21}-\frac{4}{3}\frac{G}{E_2^*}\nu_{12}-\frac{4}{3}\nu_{12}\nu_{21}\right)$
a_{07}	$2\frac{E_2}{E_1}\left(4\frac{G}{E_1^*}+\frac{E_2}{G}-\nu_{12}\right)$
a_{08}	$2\left(\frac{E_2}{E_1}\right)^2$
a_{09}	$\frac{1}{k}\frac{E_2}{E_1^*}+\frac{E_2}{E_1}(4-3\nu_{12}\nu_{21})$
a_{010}	$\frac{E_2}{E_1}\left(4\frac{G}{E_1^*}+\frac{E_2}{G}-2\nu_{12}\right)$
a_{011}	$\left(\frac{E_2}{E_1}\right)^2$

Namely, in this case, the coefficients will be

$$U_{03}=U_{07}=U_{08}=0$$
$$V_{03}=V_{06}=0$$
$$W_{04}=W_{05}=W_{06}=W_{07}=0$$

and Eqs (24a—c) take the form

$$u_0=U_{01}\mathfrak{F}_0^{\mathrm{III}}+U_{02}\mathfrak{F}_0^{\mathrm{I}:}+k(U_{04}\mathfrak{F}_0^{\mathrm{V}}+U_{05}\mathfrak{F}_0^{\mathrm{III}:}+U_{06}\mathfrak{F}_0^{\mathrm{I}::})$$
$$v_0=V_{01}\mathfrak{F}_0^{\mathrm{II}\cdot}+V_{02}\mathfrak{F}_0^{::}+k(V_{04}\mathfrak{F}_0^{\mathrm{IV}\cdot}+V_{05}\mathfrak{F}_0^{\mathrm{II}:\cdot}) \qquad (27\mathrm{a—c})$$
$$w_0=W_{01}\mathfrak{F}_0^{\mathrm{IV}}+W_{02}\mathfrak{F}^{\mathrm{II}:}+W_{03}\mathfrak{F}_0^{::}$$

The differential equation (19) serving for the determination of the displacement function can be written as

$$\mathfrak{F}_0^{\mathrm{VIII}} + a_{01}\mathfrak{F}_0^{\mathrm{VI}:} + a_{02}\mathfrak{F}_0^{\mathrm{IV}::} + a_{03}\mathfrak{F}_0^{\mathrm{II}:::} + a_{04}\mathfrak{F}_0^{::::} + a_{05}\mathfrak{F}_0^{\mathrm{VI}} + \\ + a_{06}\mathfrak{F}_0^{\mathrm{IV}:} + a_{07}\mathfrak{F}^{\mathrm{II}::} + a_{08}\mathfrak{F}^{:::} + a_{09}^{*}\mathfrak{F}_0^{\mathrm{IV}} + a_{010}^{*}\mathfrak{F}_0^{\mathrm{II}:} + a_{011}\mathfrak{F}_0^{::} = 0 \tag{28}$$

The coefficients can be calculated according to Table IV from the relations

$$a_{09}^{*} = \frac{1}{k}\,\frac{E_2}{E_1^{*}} + \frac{E_2}{E_1}$$

$$a_{010}^{*} = \frac{E_2}{E_1}\left(\frac{E_2}{G} - 2\nu_{12}\right)$$

6. *The displacement function comprising the particular solutions of the non-homogeneous equations*

The particular solutions of the set of non-homogeneous differential equations — as is known — represent the effect of the uniformly distributed forces acting on the shell surface. In their determination simplifying assumptions may be made [5] by applying the following neglections:

The terms multiplied by B_i, in the expression of the sectional forces (N_1, N_2, N_{12}, N_{21}) can be neglected in comparison to those multiplied by D_i.

In the expression of the moments (M_1, M_2, M_{12}, M_{21}) the first derivatives of u and v (v', $\dot{v}$, u', $\dot{u}$) can be disregarded beside the second derivatives of w (w'', $\dot{w}$, $\dot{w}'$).

In the equation describing the peripheral equilibrium of the forces, the component of the transverse force Q_2 smaller than this latter itself being relatively insignificant.

The magnitude of the error due to the neglections depends on the coefficient k. In case of shells commonly used (where $k < 0{,}001$), the error may be disregarded [8], [9].

As a consequence of the neglections, the set of differential equations (7a—c) takes the form

$$\frac{E_1}{E_2}u'' + \frac{G}{E_2^{*}}\ddot{u} + \left(\frac{G}{E_2^{*}} + \nu_{21}\right)v'' + \nu_{21}w' = X_1^{*}$$

$$\left(\frac{G}{E_2^{*}} + \nu_{21}\right)u'' + \ddot{v} + \frac{G}{E_2^{*}}v'' + \dot{w} = X_2^{*} \tag{29a—c}$$

$$\nu_{21}u' + \dot{v} + w + k\left[\frac{E_1}{E_2}w'''' + 2\left(2\frac{G}{E_2'} + \nu_{21}\right)w'':: + \ddot{w}\right] = X_3^{*}\,.$$

The expressions comprising the particular solutions of the non-homogeneous set of equations (29a—c) can be introduced according to the method described in Chapter 4, by taking into account the determinant

$$\mathfrak{D}^p = \begin{vmatrix} d_{11}^p & d_{12}^p & d_{13}^p \\ d_{21}^p & d_{22}^p & d_{23}^p \\ d_{31}^p & d_{32}^p & d_{33}^p \end{vmatrix} \tag{30}$$

Table V

Approximating operators representing the coefficients of displacements

d_{11}^p	$\frac{E_1}{E_2}\frac{\partial^2}{\partial \bar{x}_1^2} + \frac{G}{E_2^*}\frac{\partial^2}{\partial \bar{x}_2^2}$
$d_{12}^p = d_{21}^p$	$\left(\frac{G}{E_2^*} + \nu_{21}\right)\frac{\partial^2}{\partial \bar{x}_1 \partial \bar{x}_2}$
$d_{13}^p = d_{31}^p$	$\nu_{21}\frac{\partial}{\partial \bar{x}_1}$
d_{22}^p	$\frac{G}{E_2^*}\frac{\partial^2}{\partial \bar{x}_1^2} + \frac{\partial^2}{\partial \bar{x}_2^2}$
$d_{23}^p = d_{32}^p$	$\frac{\partial}{\partial \bar{x}_2}$
d_{33}^p	$1 + k\left[\frac{E_1}{E_2}\frac{\partial^4}{\partial \bar{x}_1^4} + 2\left(2\frac{G}{E_2^*} + \nu_{21}\right)\frac{\partial^4}{\partial \bar{x}_1^2 \partial \bar{x}_2^2} + \frac{\partial^4}{\partial \bar{x}_2^4}\right]$

formed from the coefficients of the displacement. Meanings of the coefficients d_{ij}^p are now given by the differential operators indicated in Table V.

Based on the relations (20), (22a—c) and (23a—c), the following relations serve for the determination of the displacement functions as well as for expressing the connection between the displacements and displacement functions:

$$\begin{aligned} \mathfrak{D}^{p*}\mathfrak{F}_1 &= X_1^* \\ \mathfrak{D}^{p*}\mathfrak{F}_2 &= X_2^* \\ \mathfrak{D}^{p*}\mathfrak{F}_3 &= X_3^* \end{aligned} \tag{31a—c}$$

and

$$\begin{aligned} u &= u_1 + u_2 + u_3 = \mathfrak{D}_{11}^{p*}\mathfrak{F}_1 + \mathfrak{D}_{12}^{p*}\mathfrak{F}_2 + \mathfrak{D}_{13}^{p*}\mathfrak{F}_3 \\ v &= v_1 + v_2 + v_3 = \mathfrak{D}_{21}^{p*}\mathfrak{F}_1 + \mathfrak{D}_{22}^{p*}\mathfrak{F}_2 + \mathfrak{D}_{23}^{p*}\mathfrak{F}_3 \\ w &= w_1 + w_2 + w_3 = \mathfrak{D}_{31}^{p*}\mathfrak{F}_1 + \mathfrak{D}_{32}^{p*}\mathfrak{F}_2 + \mathfrak{D}_{33}^{p*}\mathfrak{F}_3 \end{aligned} \tag{32a—c}$$

On the basis of the relations (32a—c) — by taking into account the expression of the operators comprised in Table V — the displacements can be written as

Table VI

Coefficients of the non-homogeneous solutions

j	U_{1j}	$V_{1j}=U_{2j}$	$W_{1j}=U_{3j}=U_{0j}$	V_{2j}	$W_{2j}=V_{3j}=V_{0j}$	$W_{3j}=W_{0j}$
1	1	-1	$-\nu_{21}$	$\frac{E_1}{G}$	$\nu_{21}-\frac{E_1}{G}$	$\frac{E_1}{E_2}$
2	$\frac{E_1}{E_2}$	$-\left(\frac{E_1}{E_2}+\nu_{21}\frac{E_1^*}{G}\right)$	1	1	-1	$\frac{E_1}{G}-2\nu_{21}$
3	$\frac{E_1^*}{G}+4\frac{G}{E_2^*}+2\nu_{21}$	$-\left(4\frac{G}{E_2^*}+2\nu_{21}^2\frac{E_2^*}{G}+6\nu_{21}\right)$		$\frac{E_1^*}{G}\frac{E_1}{E_2}$		1
4	$2\nu_{21}\frac{E_2^*}{G}+5$	$-\left(1+\nu_{21}\frac{E_2^*}{G}\right)$		$5\frac{E_1}{E_2}+2\nu_{21}\frac{E_1^*}{G}$		
5	$\frac{E_2^*}{G}$			$\frac{E_1^*}{G}+4\frac{G}{E_2^*}+2\nu_{21}$		
6				1		

follows:

$$\begin{aligned} u_1 &= U_{11}\mathfrak{F}_1^{\mathrm{II}} + k(U_{12}\mathfrak{F}_1^{\mathrm{VI}} + U_{13}\mathfrak{F}_1^{\mathrm{IV}\cdot} + U_{14}\mathfrak{F}_1^{\mathrm{II}\cdot\cdot} + U_{15}\mathfrak{F}_1^{\cdot\cdot\cdot}) \\ v_1 &= V_{11}\mathfrak{F}_1^{\mathrm{I}\cdot} + k(V_{12}\mathfrak{F}_1^{\mathrm{V}\cdot} + V_{13}\mathfrak{F}_1^{\mathrm{III}\cdot\cdot} + V_{14}\mathfrak{F}_1^{\mathrm{I}\cdot\cdot\cdot}) \\ w_1 &= W_{11}\mathfrak{F}_1^{\mathrm{III}} + W_{12}\mathfrak{F}_1^{\mathrm{I}\cdot} \end{aligned} \tag{33a–c}$$

further

$$\begin{aligned} u_2 &= U_{21}\mathfrak{F}_2^{\mathrm{I}\cdot} + k(U_{22}\mathfrak{F}_2^{\mathrm{V}\cdot} + U_{23}\mathfrak{F}_2^{\mathrm{III}\cdot\cdot} + U_{24}\mathfrak{F}_2^{\mathrm{I}\cdot\cdot\cdot}) \\ v_2 &= V_{21}\mathfrak{F}_2^{\mathrm{II}} + V_{22}\mathfrak{F}_2^{\cdot\cdot} + k(V_{23}\mathfrak{F}_2^{\mathrm{VI}} + V_{24}\mathfrak{F}_2^{\mathrm{IV}\cdot} + V_2\mathfrak{F}_2^{\mathrm{II}\cdot\cdot} + V_{26}\mathfrak{F}_2^{\cdot\cdot\cdot}) \\ w_2 &= W_{21}\mathfrak{F}_2^{\mathrm{II}\cdot} + W_{22}\mathfrak{F}_2^{\cdot\cdot} \end{aligned} \tag{34a–c}$$

and

$$\begin{aligned} u_3 &= U_{31}\mathfrak{F}_3^{\mathrm{III}} + U_{32}\mathfrak{F}_3^{\mathrm{I}\cdot} \\ v_3 &= V_{31}\mathfrak{F}_3^{\mathrm{II}\cdot} + V_{32}\mathfrak{F}_3^{\cdot\cdot} \\ w_3 &= W_{31}\mathfrak{F}_3^{\mathrm{IV}} + W_{32}\mathfrak{F}_3^{\mathrm{II}\cdot} + W_{33}\mathfrak{F}_3^{\cdot\cdot} \end{aligned} \tag{35a–c}$$

The coefficients U_{ij}, V_{ij} and W_{ij} can be calculated from the relations given in Table VI.

The displacement functions expressing the displacements are furnished by the particular solutions of the differetial equations established on the basis of relations (31a–c):

$$\mathfrak{F}_i^{\mathrm{VIII}} + a_{01}\mathfrak{F}_i^{\mathrm{VI}\cdot} + a_{02}\mathfrak{F}_i^{\mathrm{IV}\cdot\cdot} + a_{03}\mathfrak{F}_i^{\mathrm{II}\cdot\cdot\cdot} + a_{04}\mathfrak{F}_i^{\cdot\cdot\cdot\cdot} + a_{09}^{**}\mathfrak{F}_i^{\mathrm{IV}} = a_{09}^{**}\frac{E_2^*}{E_1}X_i^*. \tag{36}$$

$$(i = 1, 2, 3)$$

The coefficients can be calculated according to Table IV, and from the relation

$$a_{09}^{**} = \frac{1}{k}\,\frac{E_2}{E_1^*}\,. \tag{f}$$

It is interesting to note [8], [9], [10] that the stress state, formed under the effect of the edge loads might be analysed with suitable accuracy by solving the homogeneous part of the set of equations (29a–c). Investigations of similar character — in connection with orthotropic cylindrical shell — may be found in a previous paper [10] of the author.

7. *Displacement functions relating to the membrane-stress state*

In practical calculations the determination of membrane stresses and consequent deformations developed in cylindrical shells has a special importance. Therefore, it will be interesting to present the displacement function associated with the membrane-stress state.

The analysis can entirely be carried out by making use of the relations already presented by assuming that $B_i = 0$ and $k = 0$, being characteristic for the membrane-stress state. Thus, by making use of the relations (33a—c), (34a—c) and (35a—c), the displacements caused by the membrane forces can be written in the form

$$\begin{aligned} u_{1M} &= U_{11}\mathfrak{F}^{\mathrm{II}}_{1M} \\ v_{1M} &= V_{11}\mathfrak{F}^{\mathrm{I}\cdot}_{1M} \\ w_{1M} &= W_{11}\mathfrak{F}^{\mathrm{III}}_{1M} + W_{12}\mathfrak{F}^{\mathrm{I}:}_{1M} \end{aligned} \qquad (37a-c)$$

further

$$\begin{aligned} u_{2M} &= U_{21}\mathfrak{F}^{\mathrm{I}\cdot}_{2M} \\ v_{2M} &= V_{21}\mathfrak{F}^{\mathrm{II}}_{2M} + V_{22}\mathfrak{F}^{\cdot\cdot}_{2M} \\ w_{2M} &= W_{21}\mathfrak{F}^{\mathrm{II}\cdot}_{2M} + W_{22}\mathfrak{F}^{\cdot\cdot}_{2M} \end{aligned} \qquad (38a-c)$$

and

$$\begin{aligned} u_{3M} &= U_{31}\mathfrak{F}^{\mathrm{III}}_{3M} + U_{32}\mathfrak{F}^{\mathrm{I}:}_{3M} \\ v_{3M} &= V_{31}\mathfrak{F}^{\mathrm{II}\cdot}_{3M} + V_{32}\mathfrak{F}^{\cdot:}_{3M} \\ w_{3M} &= W_{31}\mathfrak{F}^{\mathrm{IV}}_{3M} + W_{32}\mathfrak{F}^{\mathrm{II}:}_{3M} + W_{33}\mathfrak{F}^{::}_{3M} \end{aligned} \qquad (39a-c)$$

and the differential equation (36) furnishing the determination of the displacement functions will be reduced to the following simple form:

$$\mathfrak{F}^{\mathrm{IV}}_{iM} = \frac{E_2^*}{E_1} X_i^* \qquad (i = 1, 2, 3)\,. \qquad (40)$$

By introducing the interpretation of the load function

$$\mathfrak{I}_{4i} = \frac{E_2^*}{E_1} X_i^* \qquad (41)$$

the solution of the differential function (40) will be obtained in the form

$$\mathfrak{F}_{iM} = \mathfrak{I}_{0i} + \sum_{n=1}^{4} C_n(\bar{x}_2)\,\bar{x}_1^{n-1} \qquad (42)$$

where $\mathfrak{F}_{0i}$ can be calculated from the relation

$$\mathfrak{I}_{(k-1)i} = \int \mathfrak{I}_{ki}\, d\bar{x}_1 \qquad (k = 1, 2, 3, 4)\,. \qquad (43)$$

In the knowledge of the displacement functions, besides the displacements, as a matter of course, also the membrane forces can be determined.

REFERENCES

1. Love, H.: The Mathematical Theory of Elasticity. Univ. Press, Oxford 1952
2. Timoshenko, S.: Theory of Plates and Shells. McGraw-Hill, New York 1959
3. Flügge, W.: Stresses in Shells. Springer-Verlag, Berlin 1960
4. Wlassow, S.: Allgemeine Schalentheorie und ihre Anwendung in der Technik. Akademie-Verlag, Berlin 1958
5. Donnel, H.: Stability of Thin-walled Tubes under Torsion. NACA, Tech. Rep. 1933
6. Novozhilov, V.: The Theory of Thin Shells. Noordhoff, 1959
7. Goldenveizer, L.: Theory of Elastic Thin Shells. Pergamon Press, Oxford 1961
8. Hoff, J.: The Accuracy of Donnel's Equations. *J. Appl. Mech.* **22** (1955) 117–118
9. Kempner, J.: Remarks on Donnel's Equations. *J. Appl. Mech.* **22** (1955) 117–118
10. Varga, L.: Discussion of the Bending Theory of Cylindrical Shells of Orthogonally Anisotropic Structural Material, by Introducing the Displacement Function. *Acta. Techn. Hung.* **73** (1972), 175

Notation

The following symbols are used in this paper:

s = shell thickness (cm)
$u, u_0, u_p, u_1, u_2, u_3$ = displacements in the direction of the generatrix (cm)
$v, v_0, v_p, v_1, v_2, v_3$ = displacement in the peripheral direction (cm)
$w, w_0, w_p, w_1, w_2, w_3$ = radial displacements (cm)
x_1 = co-ordinate of the direction of the generatrix (cm)
x_2 = co-ordinate in the peripheral direction (cm)
x_3 = co-ordinate in the radial direction (cm)
$\bar{x}_1 = x_1/R$, $\bar{x}_2 = x_2/R$ = dimensionless co-ordinates
B_1 = flexural rigidity in respect to the direction of the generatrix (kp/cm)
B_2 = flexural rigidity in respect to the direction of the periphery (kp/cm)
B_3 = torsional rigidity (kp/cm)
D_1 = elongation rigidity in respect to the direction of the generatrix (kp/cm)
D_2 = elongation rigidity in respect to the direction of the periphery (kp/cm)
D_3 = shear rigidity (kp/cm)
E_1 = Young's modulus in respect to the direction of the generatrix (kp/cm^2)
E_2 = Young's modulus in respect to the direction of the periphery (kp/cm^2)
$\mathfrak{F}, \mathfrak{F}_0, \mathfrak{F}_p, \mathfrak{F}_1, \mathfrak{F}_2, \mathfrak{F}_3$ = displacement functions (cm)
G = Young's modulus of shear (kp/cm^2)
M_1, M_2 = specific bending moments (cm kp/cm)
M_{12}, M_{21} = specific torsional moments (cm kp/cm)
N_1, N_2 = normal forces (kp/cm)
N_{12}, N_{21} = shear forces (kp/cm)
R = radius of curvature of middle surface (cm)
Q_1, Q_2 = radial shear forces (kp/cm)

X_1, X_2, X_3 = uniformly distributed external forces applied to the shell surface (kp/cm^2)
ε_{11} = specific elongation in the direction of the generatrix
ε_{22} = specific elongation in the direction of the periphery
$\varepsilon_{12}, \varepsilon_{21}$ = specific rotations
ν_{12}, ν_{21} = Poisson's ratio (first subscript denotes direction of deformation, the second one that of force)
σ_{11}, p_{22} = normal stresses (kp/cm^2)
σ_{12}, σ_{21} = shear stresses (kp/cm^2)

Meanings of other symbols are to be found in the text.

Verschiebungsfunktionen von ortogonal-anisotropischen zylindrischen Schalen. Behandelt werden die Untersuchung und Ermittlung von zylindrische Schalen kennzeichnenden Verschiebungsfunktionen unter der Voraussetzung der Anisotropie. Durch Einführung der Verschiebungsfunktionen werden sowohl die exakten als auch die Näherungslösungen des Differentialgleichungssystems dargestellt, das sich aus den Gleichgewichtsbedingungen ergibt.

Der Zusammenhang zwischen den Verschiebungen, die die allgemeinen Lösungen des homogenen Teils und die partikularen Lösungen des inhomogenen Systems bedeuten, und den Verschiebungsfunktionen wird eingehend erörtert. Ferner werden die Differentialgleichungen zur Ermittlung der Verschiebungsfunktionen vorgelegt. Abschließend werden die Zusammenhänge zwischen den durch die Membrankräfte hervorgerufenen Verschiebungsfunktionen enthaltende Differentialgleichung und deren Lösung erörtert.

Функции смещение ортогональных анизотропных цилиндрических оболочек. Работа при предположении гомогенной анизотропии занимается анализом и определением функций смещения, характерных для напряженного состояния ортотропных цилиндрических оболочек. Введением функций смещения излагается строгое и приближенное решение системы дифференциальных уравнений, получающейся на основе условий равновесия. Детально рассматривается связь между функциями смещения и смещениями, отражающими общие решения гомогенной части и партикулярные решения и ингомогенной системы. Далее сообщаются дифференциальные уравнения, служащие для определения функций смещения. Наконец, описываются зависимости между смещениями от мембранных усилий и функциями смещения, далее дифференциальное уравнение, содержащее функции смещения, и его решение.

Acta Technica Academiae Scientiarum Hungaricae, Tomus 76 (3—4), pp. 391—411 (1974)

THE EFFECT OF THE CROSS-SECTION DIMENSIONS ON THE DUCTILITY OF CONCRETE

MEGAHID AHMED, A.*

and

P. LENKEI**

CAND. OF TECHN. SC.

[Manuscript received December 6, 1972]

A test program was carried out to investigate the effect of the cross-sectional dimensions on the ductility of concrete. 60 axially and eccentrically loaded concrete prisms of various cross-sectional dimensions as well as 14 r.c. beams with variable dimensions of compression zone (depth and breadth) under pure bending were tested. The investigations proved, that the stress-strain curve of concrete is depending on the type of loading (centric or eccentric compression, bending). The ultimate strain in the extreme compressed fibers of the axially compressed concrete prisms increased, but that of the eccentrically compressed concrete prisms and of the compressed zone of the r.c. beams decreased with the increase of the depth of the compressed concrete. These changes were due to the corresponding changes in the plastic parts of the ultimate concrete strains.

Symbols

a, c	— constants
b_0, x_0	— the exact measured breadth and depth of the prism cross-section, respectively
e	— the measured eccentricity of the applied load
E_c	— the secant modulus of elasticity of concrete
f_0	$= P/(b_0 x)$ — average stress according to load
f_1, f_2, f_3	— the measured deflections in the beam tests at the applied loads and at the mid span (mm) resp.
m_0	$= M/(b_0 x^2)$ — average stress according to moment
M	— bending moment, in general,
M_c	— the calculated internal moment
n	— number of the loading steps for each specimen
P	— applied load, in general,
P_1, P_2	— the applied concentrated loads in the beam tests
P_c	— calculated internal force
x	— depth of the neutral axis, in general,
ε	— strain, in general,
ε_{ce}, ε_{cp}, ε_{cu}	— the elastic, plastic and the ultimate concrete strain at the extreme fibers in the tested beams
$\varepsilon_{\text{el. ecc.}}$	— the elastic part of strain in the eccentric prisms
$\varepsilon_{\text{el. cent.}}$	— the elastic part of strain in the centric prisms
$\varepsilon_{\max}$	— the max. concrete compressive strain
$\varepsilon_{\text{max. el.}}$	— the elastic part of the max. concrete compressive strain
$\varepsilon_{\text{max. pl.}}$	— the plastic part of the max. concrete compressive strain
$\varepsilon_{\text{max. cen.}}$	— the max. concrete compressive strain in centric prisms
$\varepsilon_{\text{max. ecc.}}$	— the max. concrete compressive strain at the extreme fibers in the eccentric prisms
σ	— stress
$\sigma_{\max}$	— max. stress
σ_{cube}	— the cubic strength of concrete

* MEGAHID AHMED, A., Assuit University, Civil Engineering Department, Egypt
** Dr. P. LENKEI, Szakasits Árpád u. 4., 1119 Budapest, Hungary

α_1 — $\varepsilon_{\text{el. ecc.}}/\varepsilon_{\text{el. cent}}$
α_2 — $\varepsilon_{\text{pl. ecc.}}/\varepsilon_{\text{pl. cent.}}$
α_0 — $\varepsilon_{\text{max. ecc.}}/\varepsilon_{\text{max. cent.}}$
β_0 — $\sigma_{\text{max. ecc.}}/\sigma_{\text{max. cent.}}$
Φ — curvature, in general,
Φ_u — the ultimate curvature
Φ_{up} — the plastic part of the ultimate curvature

Note: i = index refers to the number of the loading step

1. Introduction

The idea to utilize the plastic behaviour of reinforced concrete structures for design purposes originated some 50 years ago. This problem was and is object of extensive research activity in a wide range of countries. Both theoretical and experimental investigations proved the plastic design hypotheses.

Progress in plastic design of statically indeterminate r.c. linear structures offered this method to be adopted as one of the design criteria by various codes of practice.

In the plastic design of r.c. linear structures the compatibility conditions should be fulfilled on equal terms along with the equilibrium conditions [4]. The compatibility conditions mean that for full redistributions of moments the required plastic rotations should not exceed the so-called plastic rotation capacities in the formed plastic hinges.

The plastic rotation capacity of a bar subjected to bending largely depends on the plastic part of the ultimate concrete compressive strain in the extreme fibers. In addition to this, usually the value of the max. concrete compressive strain is a basic data in any code prescriptions on the design of r.c. cross-sections.

The value of the ultimate concrete compressive strain and its plastic part at failure have been assumed as independent values on the cross-sectional dimensions. Recent investigations [1, 2, 5, 6] showed contradictory results concerning the effect of the cross-sectional dimensions on the ultimate concrete compressive strain developed in r.c. flexural members. Hence, the effect of the cross-sectional dimensions, or rather the dimensions of the compression zone in r.c. beams, on the deformation capacity is not quite clear and, therefore, this problem is still in need of further clarification [4].

To clarify this problem, a test program was carried out in two parts. In the first part of the program, axially and eccentrically loaded concrete prisms of various cross-sectional dimensions were investigated. In the second part of the test program r.c. beams with variable dimensions of the compression zone (depth and breadth) were investigated in the pure bending length.

2. Tests on Prisms

2.1. The test prgram

Centric and eccentric prisms were made from a concrete composition having the same proportionality. Both the technology of casting and curing were identical. 60 prisms were cast in the form of 10 variable cross-sectional dimensions groups of 6 replicate from each group. The breadth varied between 15 and 30 cm, the depth between 10 and 25 cm in increments of 5 cm. The length of the prisms were so chosen as to avoid both the buckling and influence of the loading plates. The cross-sectional dimensions were selected to correspond with the compression zone of real r.c. beams. From each group 3 specimens were tested axially and the other 3 were tested eccentrically.

The age of the prisms at the date of the test was between 62 and 327 days, the prism strength was between 400 and 575 kp/cm^2, but there was no significant difference in the mechanical characteristics connected with the age of the specimens.

The longitudinal and transversal deformations of the prisms were measured by electric resistance-strain gages of 6 cm length (production of Orion-EMG) 4 longitudinal and 4 transversal gages were mounted on the middle height of the each surface in the case of axially loaded prisms. However, in case of the eccentric prisms, 10 longitudinal and 12 transversal gages were mounted on the surfaces of the specimens. Figs 1, 2, 3 show the mounting of strain gages as well as the shape of the failures.

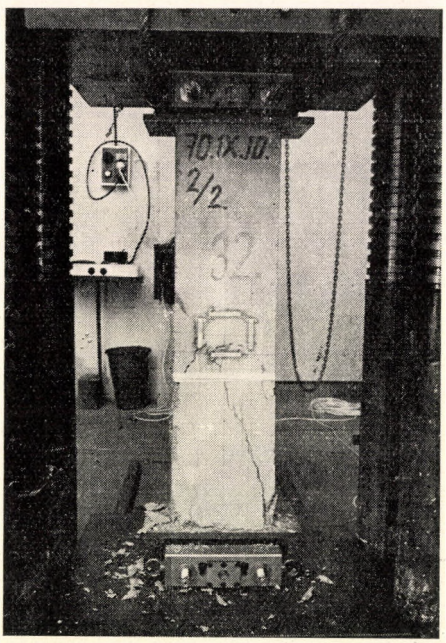

Fig. 1. Eccentric prism in the testing machine with the adjustable loading plates used

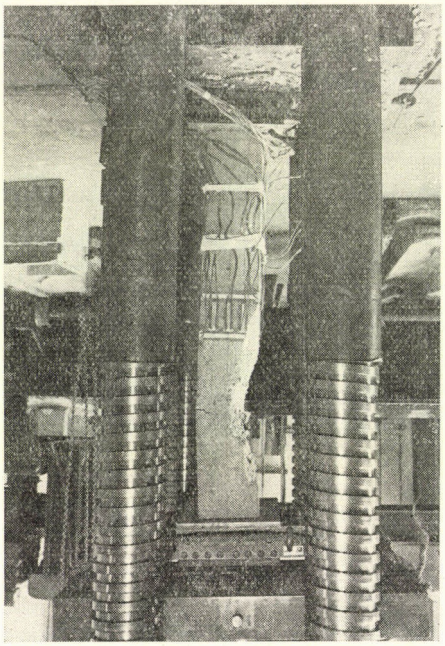

Fig. 2. Eccentric prism in the testing machine after failure showing the mounting of the strain gages on one side



Fig. 3. Centric prism after failure showing the mounted gages

2.2. The testing

The centric and eccentric specimens of the same dimensions were tested one after the other in succession. The axial load was established and adjusted on the basis of the strain-gage readings. In case of eccentrically loaded prisms from the beginning of the test up to failure, the eccentricity was maintained by means of specially developed adjustable upper and lower loading plates specially made for this purpose. The eccentricity at each step of loading was varied so as to have zero strain on one surface of the prism. In this way the neutral axis was modeled. The eccentricity was measured by two special scales, mounted on both sides of the loading plates. The load was applied to conform with the international recommendations on short-time static loading. At each loading step the longitudinal strains were determined as an average of the readings of the four longitudinal gages in case of axially loaded specimens, however, in case of eccentrically loaded specimens it was based on the average readings of the two longitudinal gages on the max. and min. stressed surfaces.

2.3. Evaluation of the test data

The Poisson's ratios for each loading step were determined by means of the longitudinal and transversal strains, to check the mechanical conditions of the specimens. The specimens found to be not reaching its plastic state at the failure were excluded from further evaluation.

The strain distribution along the depth of the eccentric specimens were drawn to be able to check the plane-section hypothesis and for the determination of the exact positions of the neutral axis. The plane-section hypothesis was valid for all the eccentric specimens with a max. deviation of $\pm 15\%$.

The stress-strain curves were plotted for both the axial and eccentric specimens. In case of eccentric specimens the stress-strain diagram for each specimen was indirectly determined from the measured test data, as well as a coefficient called "modified coefficient of variation", μ, which is analogous to the term "standard error of estimate" often used in connection with regression analysis, was also calculated. The value of μ ranged between 1,48% and 5,23% which seems to be quite small (see Appendix).

The corresponding deformations were separated into their elastic and plastic parts in case of centric and eccentric specimens on the basis of the calculated initial modulus of elasticity.

Due to the large dispersion of the measured strains at failure, the one before the last reading was taken into account ($94 \div 97\%$ of the max. loading step).

The evaluated test data of the specimens in groups are tabulated in Table I.

Table I

Data of prisms in groups

Group No.	Type of loading	Dimensions [cm] x_i* / x_b	Dimensions [cm] b_0	Max. strains 10^{-6} ε_{max}*	Max. strains 10^{-6} $\varepsilon_{max.\,el}$*	Max. strains 10^{-6} $\varepsilon_{max.\,pl.}$*	strength [kp/cm²] σ_{cube}	strength [kp/cm²] $\sigma_{max.}$	$\frac{\sigma_{max.}}{\sigma_{cube}}$	$\frac{\varepsilon_{el.ecc.}}{\varepsilon_{el.cen.}}$ (α_1)	$\frac{\varepsilon_{max.\,ecc.}}{\varepsilon_{max.cen.}}$ (α_0)	$\frac{\varepsilon_{pl.ecc.}}{\varepsilon_{pl.cen.}}$ (α_2)	$\frac{\sigma_{max.ecc.}}{\sigma_{max.cen.}}$ (β_0)
1	++	21,0	19,9	1836	1340	496	588	709,0	1,207	1,155	1,238	1,653	1,262
	+	19,90	20	1460	1160	300	588	562,0	0,956				
2	++	15,4	15	1694	1284	410	682	647,0	0,944	1,244	1,438	2,828	1,340
	+	15	14,9	1177	1032	145	682	483,0	0,708				
3	++	9,925	19,95	1770	1285	485	555	568,0	1,023	1,243	1,541	4,409	1,226
	+	10	20	1143	1033	110	450▲	463,0	1,029				
4	++	9,925	15	2303	1362	941	450▲	634,0	1,407	1,490	1,992	4,091	1,367
	+	9,83	14,95	1156	914	242	589	463,3	0,786				
5	++	14,43	20,1	1849	1182	667	508	545,0	1,973	1,135	4,358	4,084	1,073
	+	15	19,95	1362	1041	321	601	508,0	0,845				
6	++	19,5	25	1690	1257	433	672	568,0	0,877	1,296	1,331	1,300	1,209
	+	19,9	25,04	1291	970	320	632	470	0,743				
7	++	25	20,2	1496	1106	392	633	570,0	0,900	1,140	1,177	1,177	1,212
	+	25,04	19,9	1291	970	320	632	470	0,743				
8	++	14,43	25,3	1646	1082	564	621	520	0,837	1,201	1,463	2,518	1,212
	+	15,2	25	1125	901	224	640	427	0,667				
9	++	24,5	30	1513	1068	445	649	531	0,818	1,080	1,175	1,343	1,063
	+	25	30	1287	988	299	675	500	0,740				
10	++	15,05	29,8	1789	1196	593	697	574	0,823	1,211	1,346	1,744	1,095
	+	15,1	30,1	1327	987	340	704	524	0,744				

* This value at a level equal to 94—97% of the max. load

▲ Only one cube from this mix had been prepared.

++ Eccentric specimens

\+ Centric specimens

The ultimate overall and plastic strains were plotted with respect to the prism dimensions or rather the depth of the neutral axis (x_i), as well as a mathematical expression for these relations were also derived, as shown in Fig. 4.

2.4. Discussion on prisms

1. In case of the axially loaded specimens the ultimate strains slightly increase with the increase of the cross-sectional dimensions (depth and breadth), which values are indicated by x_0 in Fig. 4. This increase is mainly due to the increase of the plastic part of the strains.

This result can be motivated by the phenomena that the average plastic deformations are less sensitive to the local defects in case of larger cross-sectional dimensions, where the individual fibers have bigger possibility for the redistribution of stresses and strains. There is also another explanation based on the microcracking concept for this result [3].

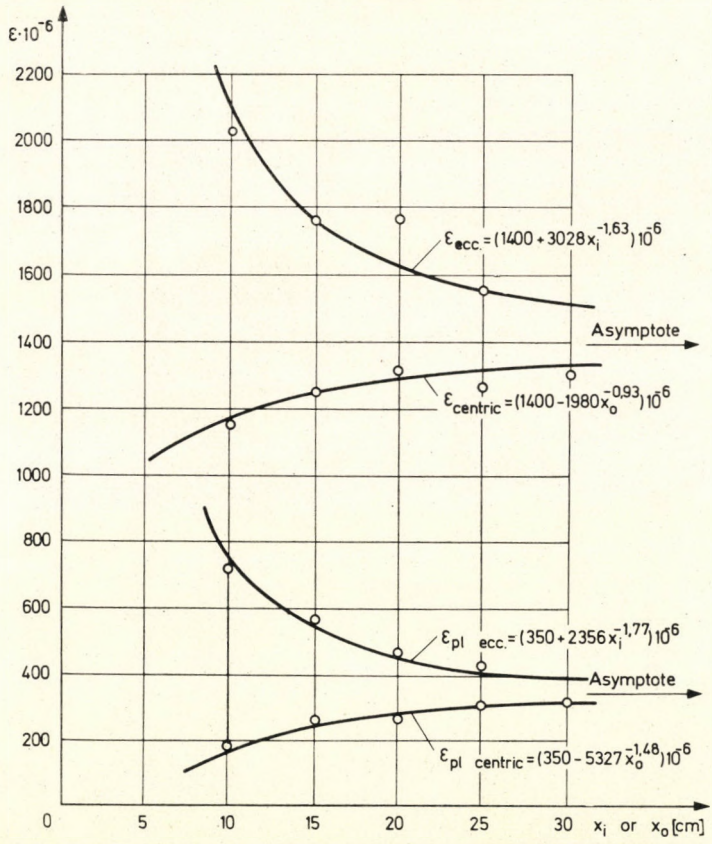

Fig. 4. The overall and the plastic strains versus the cross-sectional dimensions relationships

2. In case of the eccentrically loaded specimens the ultimate strain has a larger absolute value than in the case of axially loaded prisms of the same dimensions, but the value of these strains decrease with the increase of the depth of the neutral axis, the values of which are indicated by x_i in Fig. 4. This decrease is mainly due to the decrease of the plastic part of the strain.

This result can be interpreted by the phenomena that in case of smaller dimensions the less strained fibers are closer to the most strained ones, and, consequently, there will be a greater possibility for redistribution of stresses and strains between the fibers. Also for this result there is another explanation, based on the concept that the strain gradient retards the microcracking phenomena [8].

From the extrapolation of the above results it can be assumed that this increasing tendency in case of axially loaded prisms and the decreasing tendency in case of eccentrically loaded prisms have theoretically a common value (asymptote) when $x_i \to \infty$, i.e., the eccentric load becomes axial. This asymptote was determined on the assumption of the intersections of the linear relationship of these two phenomena (Fig. 4).

3. The breadth of the specimen has no significant effect on both the plastic and overall strains in case of eccentric prisms in comparison with the effect of the depth.

4. If the overall strains and the associated elastic and plastic deformations of the eccentric specimens are compared with the corresponding strains of the centric specimens of the same dimensions in the form of α_0, α_1, and α_2 ratios respectively, where

$$\alpha_1 = \frac{\varepsilon_{\text{el. ecc.}}}{\varepsilon_{\text{el. cent.}}}, \qquad \alpha_0 = \frac{\varepsilon_{\text{max. ecc.}}}{\varepsilon_{\text{max.cent.}}}$$

$$\alpha_2 = \frac{\varepsilon_{\text{pl. ecc.}}}{\varepsilon_{\text{pl. cent.}}}$$

then the following condition is fulfilled:

$$\alpha_2 > \alpha_0 > \alpha_1.$$

Generally, all the α ratios are bigger than one and decrease with the increase of the depth of the cross-section.

5. The ratio of the max. concrete stresses developed in the eccentric prisms to that developed in the axial prisms of the same dimensions, i. e., β_0 ratio, decreases with the increase of the size dimensions, namely, by the breadth of the cross-section.

3. Test on beams

3.1. The test program

The test of 14 under- and over-reinforced concrete beams were conducted as simple span beams loaded with two concentrated loads.

The concrete composition and technology were the same as those in prisms.

The beams were without stirrups or bent bars and without any compression reinforcements. To avoid shear failure, the beams were strengthened by two outside removable constrained steel casing fittings along the shear span lengths (Fig. 5).

The pure bending length and the overall depth of the beams were constant (2,45 m and 35 cm, respectively). The width and the depth of the neutral

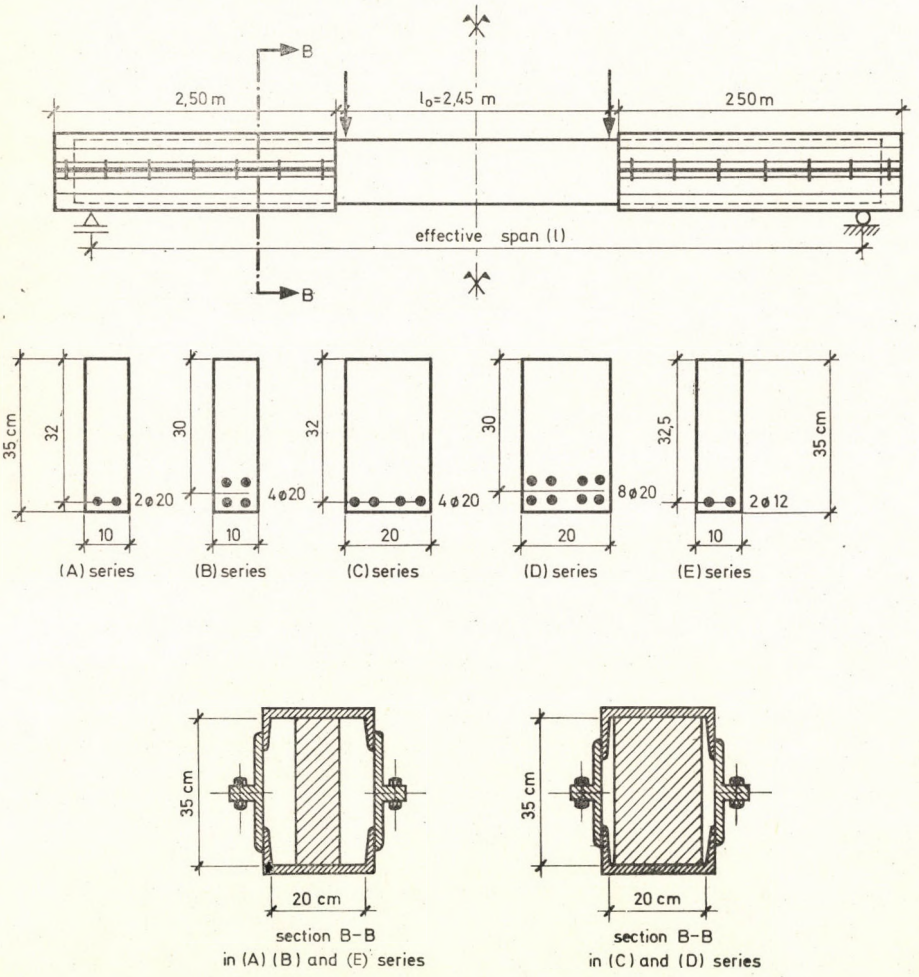

Fig. 5. The test-beams geometry and details

axis of the tested beams were variable. The latter was maintained by varying the amount of tension reinforcements. The data of the beams' description is listed in Table II, and shown in Fig. 5.

The beams were instrumented in three main gaged sections in the pure bending region, to measure the following:

— the strains of concrete at the extreme compression fibers and along the depth of the compression zone by means of 28 electrical resistance-strain gages, 10 of these gages were mounted on the top surface of the beam;

— the steel strains at a level as near as possible to the centroid of the used steel in the longitudinal direction by means of a mechanical deformeter over eleven base lengths distributed all along the pure bending length;

— the deflections near the applied loads and at the midspan by means of inductive displacement pick-ups;

— the loads applied to the tested beam monitored by means of two load cells;

— the inclinations close to the applied loads and at the midspan with the aid of 3 mechanical clinometers.

The instrumentation of the beams was installed and established to measure and record the loads at any step of loading, the strains in concrete and the deflections until failure.

3.2. The testing

The arrangement of a specimen under test, as well as the instrumentations can be shown by Figs 6, 7, 8. The load was applied first under the weight of the upper steel girder which transmits and distributes the load from the lever of the machine to the tested beam. The loads, after that, were applied in a rate equal to $10 \div 15\%$ of the probable max. load. The rate of load was maintained at constant all over the beam tests. At each step of loading the load was maintained for 20 minutes to register three times all the readings. Also the cracks directly visible to the naked eye were marked and measured by means of a hand microscope. The shape of failure of some beams is shown in Figs 9, 10.

3.3. Evaluation of the test data

The age of the tested beams was between 45 and 170 days. There is no great deviation between the average strengths of the 3 ($15 \times 15 \times 60$ cm) prisms made specially from the same mix and cured alongside the beams.

The value of the concrete compressive strain at the extreme fibers were taken to be the average of the readings of the 10 strain gages mounted on the top surface of the beam. The steel strains were based on the average of the eleven deformeter readings.

Table II

Beam descriptions

Series No	Beam No	Breadth [cm]	Effective depth [cm]	Overall depth [cm]	Effective span [m]	Tension reinforcement				Cube strength [kp/cm²]	Prism strength [kp/cm²]	Type of beam	Age of beam at date of test in days
						Bars in mm	Area [cm²]	% of reinforc.	Yield strength [kp/cm²]				
	1	10	32	35	7,35	2Ø20	6,28	1,96	4400	453,3	392,29	+	97
A	2	10	32	35	7,35	2Ø20	6,28	1,96	4400	523,3	446,66	+	—
	3	10	32	35	7,35	2Ø20	6,28	1,96	4400	475,6	419,33	+	125
	4	10	30	35	7,35	4Ø20	12,56	4,18	4400	506,6	438,51	++	132
B	5	10	30	35	7,35	4Ø20	12,56	4,18	4400	531,5	453,32	++	135
	6	10	30	35	7,35	4Ø20	12,56	4,18	4400	555,8	461,47	++	141
	7	20	32	35	7,35	4Ø20	12,56	1,96	4400	532,3	488,88	+	165
C	8	20	32	35	7,35	4Ø20	12,56	1,96	4400	440,6	364,44	+	167
	9	20	32	35	8,85	4Ø20	12,56	1,96	4400	458,0	404,44	+	163
	10	20	30	35	7,35	8Ø20	25,12	4,18	4400	530,8	459,25	++	165
D	11	20	30	35	7,35	8Ø20	25,12	4,18	4400	531,6	408,58	++	166
	12	20	30	35	7,35	8Ø20	25,12	4,18	4400	480,8	425,18	++	167
E	13	10	32,5	35	6,00	2Ø12	2,26	0,70	4400	433,2	337,77	+	45
	14	10	32,5	35	6,00	2Ø12	2,26	0,70	4400	391,2	248,88	+	45

\+ Under = reinforced beams.
++ Over = reinforced beams.

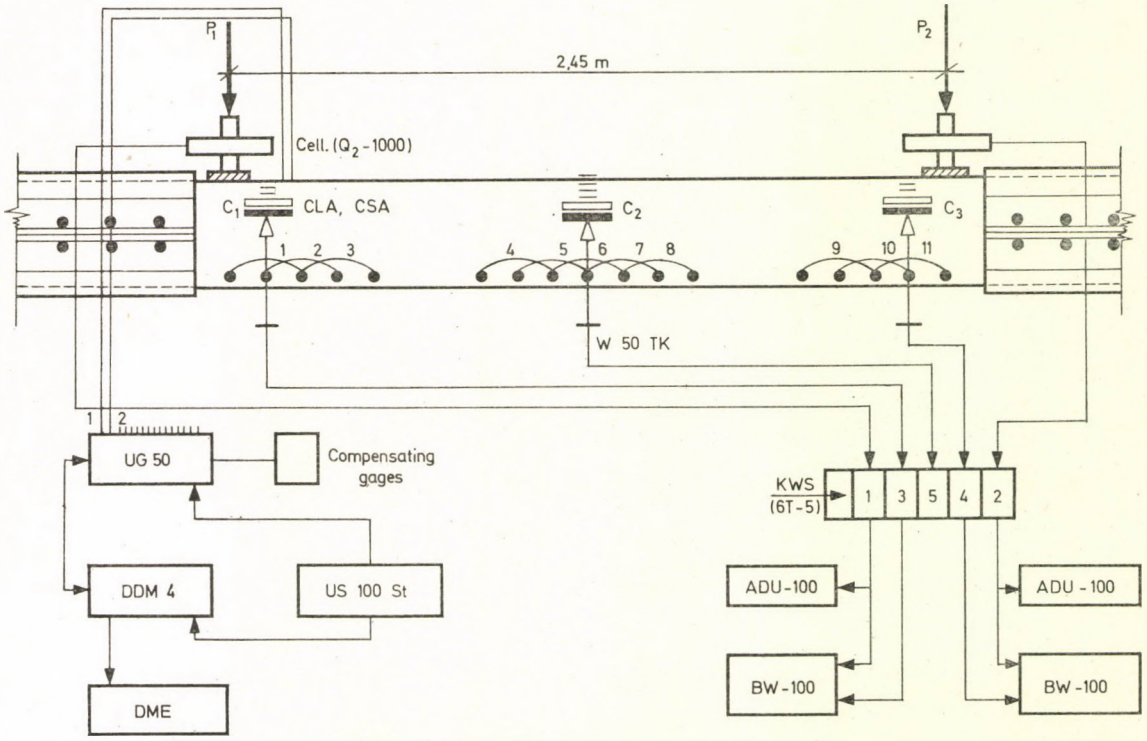

Fig. 6. The instrumentation of the beam

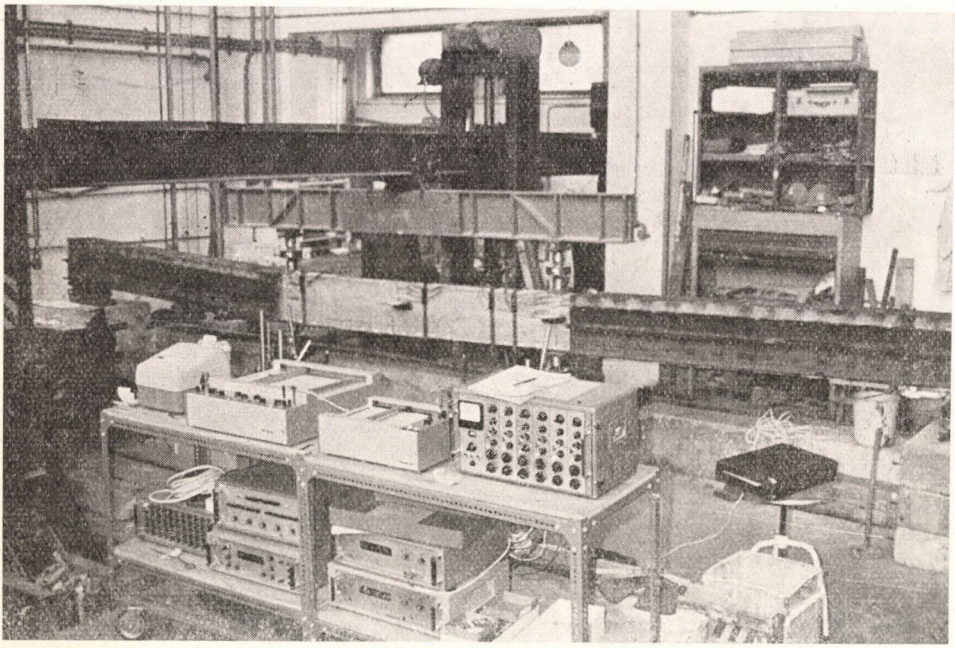

Fig. 7. The used instruments

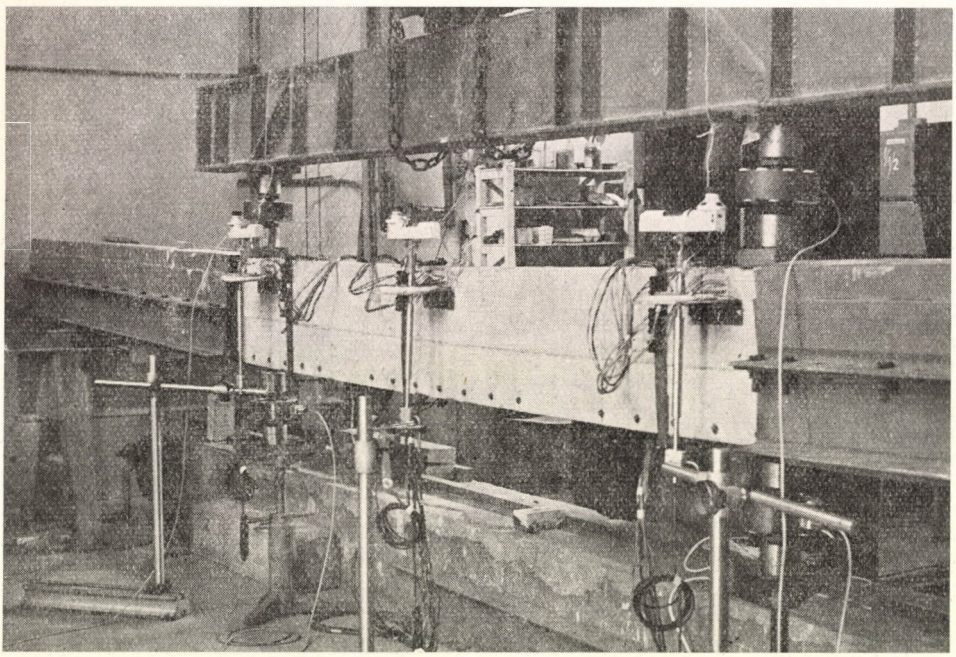

Fig. 8. The set-up of the beam before testing

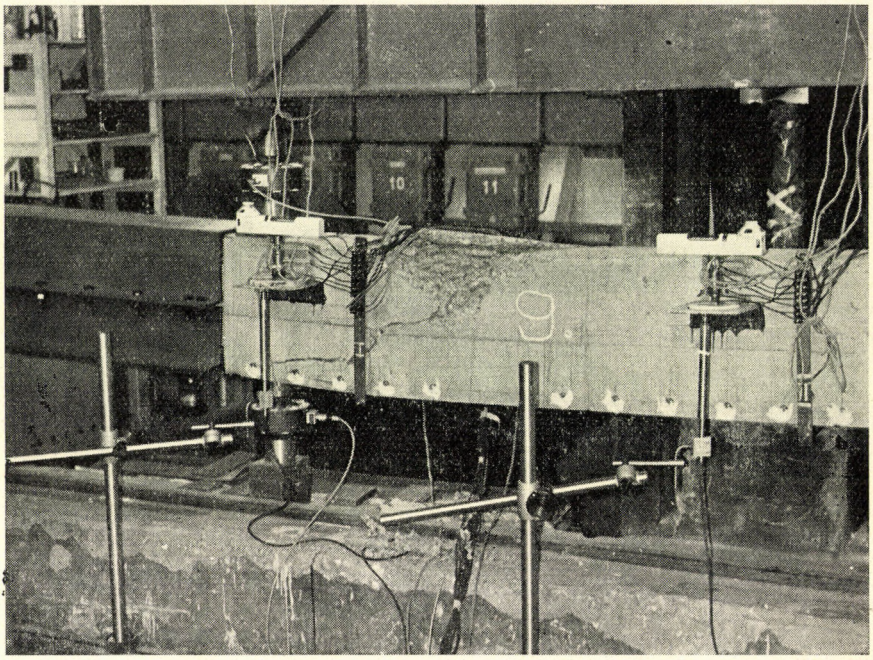

Fig. 9. The shape of failure of beam No 9

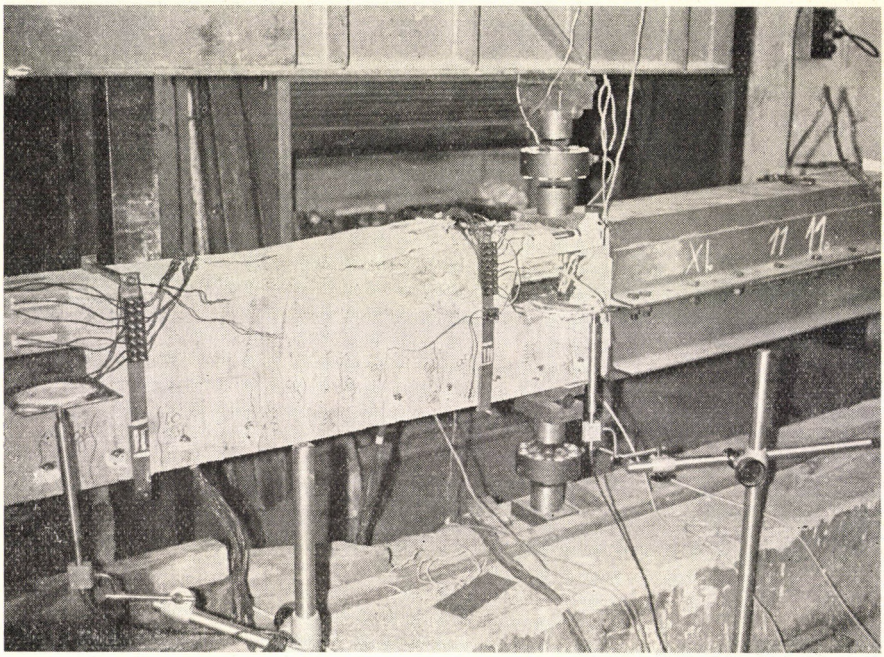

Fig. 10. The shape of failure of beam No 11

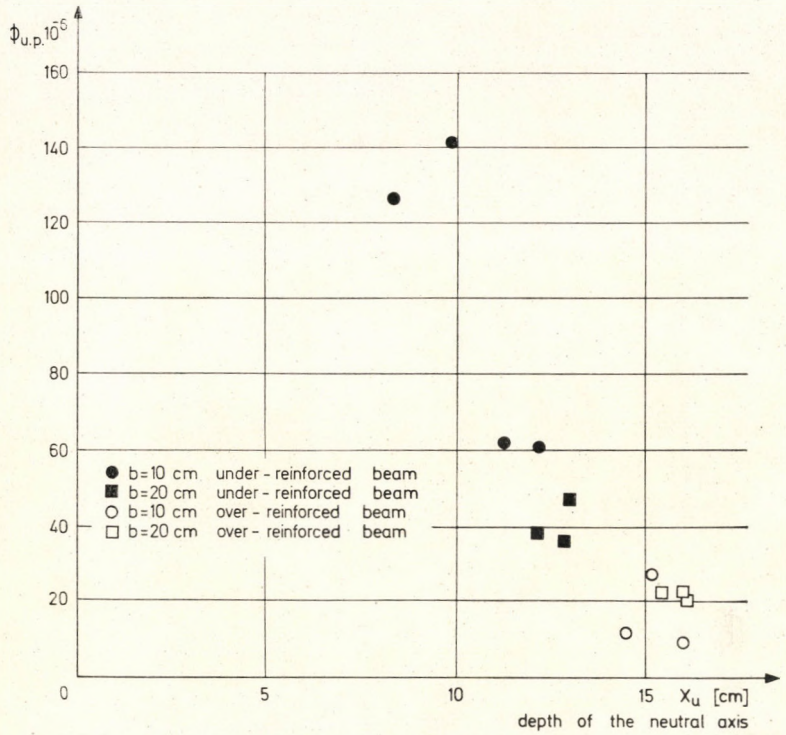

Fig. 11. The plastic part of the curvature versus the neutral axis-depth relation in the tested beams

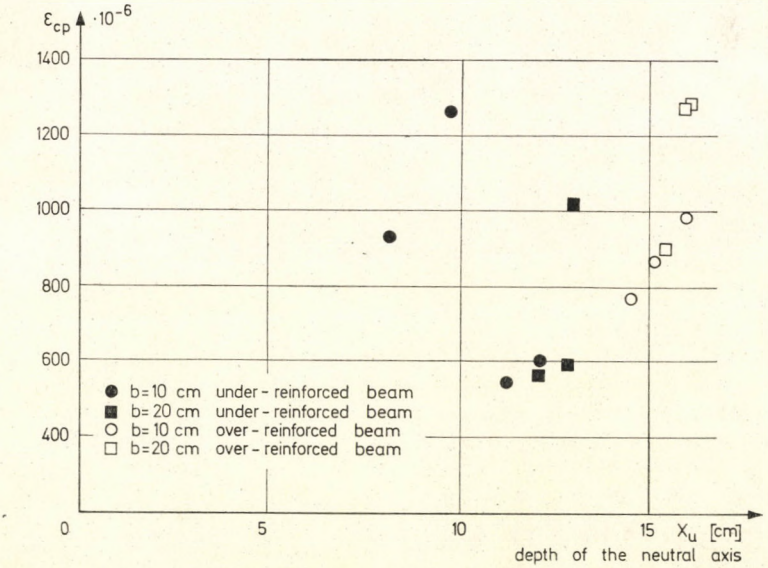

Fig. 12. The plastic part of the ultimate concrete compressive strain versus the neutral axis-depth relation in the tested beam

Table III

Data of the tested

Series	Beam No	Loads and deflections at ultimate					Moments and curvatures at ultimate			
		P_1 [kp]	P_2 [kp]	f_1 [mm]	f_2 [mm]	f_3 [mm]	Moment M_u [kp · cm]	Curvature Φ [cm^{-1}] · 10^{-6}		
								Φ_c	Φ_P	Φ_u
A	1	2900	2850	74,0	73,0	85,70	704 375,0	102	60,60	162,60
	3	2950	2965	86,0	86,0	99,00	724 587,5	111	62,20	173,20
B	4	3625	3650	55,0	54,0	61,20	8 911 875,0	113*	11,00*	124,00*
	5	4250	4100	64,0	62,0	71,20	1 022 875,0	123	12,50	135,50
	6	4000	3920	64,0	59,5	70,10	1 019 700,0	110	28,00	138,00
C	7	6050	5850	77,0	78,0	86,70	1 580 250,0	113	39,00	152,00
	8	5750	5760	70,5	67,0	77,70	1 409 975,0	110	35,90	145,90
	9	5775	5775	71,0	68,0	79,10	1 414 875,0	111	47,70	158,70
D	10	8650	8725	68,5	67,5	76,30	2 128 437,5	116	21,20	137,20
	11	8700	8675	67,5	67,5	76,20	2 128 437,5	120	23,80	143,80
	12	9500	9500	68,0	72,0	78,50	2 327 500,0	117	23,50	140,50
E	13	1570	1576	84,9	84,0	99,31	279 952,5	104	141,60	245,60
	14	1470	1462	82,6	83,4	98,02	259 235,0	122	126,20	248,20

* One before the last loading level.
[1] This value is the average of three prisms.
[2] This value corresponds to only one individual prism.

The moments were calculated as the average of the moments produced from the external forces along the pure bending length.

The curvature was calculated on the assumption of linear strain distribution along the overall depth of the beam.

The stress-strain curves of the concrete at the compression zone were evaluated following an approach similar to that used in case of eccentric prisms. However, the modified coefficient of variation was much larger than that in the case of eccentric prisms due to the neglection of the strain-hardening effect of the reinforcing steel in analysis. (μ was ranged between 4,6% and 16,88%.)

The moment-curvature as well as the load-deflection diagrams were plotted from zero loading level until ultimate load.

The elastic and the plastic parts of the obtained curves of both stress-strain and moment-curvature diagrams were separated.

The measured and evaluated data are given in Table III.

beams at failure

Stresses and strains at ultimate							Depth of the neutral axis x_u [cm]
Concrete in extreme compression fiber				prisms 15×15×60 [cm]		Max. steel strain $\varepsilon_{su} \cdot 10^{-6}$	
$\varepsilon_{re} \cdot 10^{-6}$	$\varepsilon_{cp} \cdot 10^{-6}$	$\varepsilon_{cu} \cdot 10^{-6}$	$\sigma_{max\ flex.}$ [kp/cm²]	Max.¹ strength [kp/cm²]	Max.² strain 10^{-6}		
1376	599	1975	400	392,29	1784	3227	12,149
1437	548	1985	432	419,33	1624	3658	11,250
1023*	988*	2011*	388*	438,51	1930	1760*	15,998*
1197	770	1967	531	453,32	1258	2100	14,509
1230	868	2098	510	461,47	1522	2042	15,200
1270	571	1841	499	488,88	1805	3024	12,110
1275	595	1870	436	364,44	1448	2797	12,822
1037	1023	2060	375	404,44	1598	3016	12,986
937	1282	2219	443	459,25	1869	1896	16,177
1005	1286	2291	426	408,58	1305	2022	15,935
1264	900	2164	509	425,18	1490	2050	15,405
1128	1264	2392	348	337,77	1820	5590	9,730
1111	924	2035	275	248,88	1852	6030	8,200

3.4. Discussion on beams

1. The ductility of r.c. sections defined by the ultimate curvature decreases by increasing the depth of the neutral axis. This decrease is mainly due to the plastic part of the moment-curvature relationship as shown in Fig. 11. This agrees with Ref. [5].

2. The ultimate compressive strain at the extreme fibers developed in r.c. beams subjected to pure bending depends mainly on the type of the beam (under- or over-reinforced beam).

3. In under-reinforced beams, the larger the neutral axis depth, the smaller will be the expected ultimate concrete compressive strain, the decrease of which is attributed to the plastic part of the strain, as is clear from Fig. 12. This agrees with the result found in case of eccentric prisms.

4. The breadth of the beam has no significant effect on the ultimate concrete compressive strain on any type of beams as was found in the case of eccentric prisms.

5. The mechanical behavior of the concrete in the compressed zone of r.c. beams subjected to bending is quite different from that in the centric prisms as supported in Ref. [8].

6. The stresses associated with max. concrete compressive strains at the extreme fibers are not significantly affected by the dimensions of the compressed zone as in the case of the eccentric prisms.

4. Concluding remarks

The following conclusions can be summarized:

1. For given cross-section dimensions the stress-strain diagram of the compressed concrete differs according to the type of loading, i.e., the stress-strain curve of an eccentric specimen is not the same as that in the compressed zone of r.c. beams subjected to flexure or as that of a centric specimen of the same dimensions, although these curves, in case of the eccentric loading and flexure, are quite similar.

2. In the centric prisms the increase of the cross-section dimensions tends to increase the ultimate compressive strain. However, in case of eccentric specimens and in under-reinforced beams the ultimate concrete compressive strain in the extreme fibers considerably increases with the decrease of the depth of the compression zone. The increase of strain is mainly due to the increase of the associated plastic part of the strain. However, the breadth has no significant effect upon the plastic and upon the max. concrete compressive strains in comparison with the effect of the depth.

3. The stresses associated with the max. concrete compressive strains are not significantly affected by the compressed zone dimensions.

It should be emphasized that the above findings refer only to the tested r.c. beams without any type of confinement and without compression reinforcements, subjected to pure bending and to the plain concrete prisms in the investigated range of cross-sectional dimensions under short-time loading, and they do not include the effect of creep or other long-time processes.

APPENDIX

Determination of the stress-strain relationship of the concrete in eccentric specimens

The determination of the $\sigma - \varepsilon$ diagram followed the approach given in ref. [7] with some modifications.

Assumptions

— Equilibrium of both internal and external forces and moments should be maintained.

— Sections plane before loading, remain plane under and after loading.

— The stress-strain function in tension of concrete is assumed to be the same as that in compression up to that strain at which the concrete cracks in tension.

At each step of loading the available data were the load P_i, the average extreme fiber compression strain, ε_{max_i}, the average extreme fiber minimum strain (tension or compres-

sion), $\varepsilon_{\min_i}$ and the eccentricity, e_i, using the notation in Fig. 13, the equilibrium condition can be expressed as follows*

$$\text{load} = P = \int_0^x f(y) b_0 \, dy - \int_0^s f(y) b_0 \, dy \tag{1}$$

$$\text{moment} = M = P\left(e + x - \frac{x_0}{2}\right) = \int_0^x f(y) y \, b_0 \, dy \mp \int_0^{|s|} f(y) y \, b_0 d_y \tag{2}$$

where the moment is taken about the neutral axis and
$\sigma = f(y)$ is the unknown function of the stress.

The compatibility of plane sections can be expressed as

$$\varepsilon = \frac{y}{x} \cdot \varepsilon_{\max} \tag{3}$$

then

$$y = \frac{x}{\varepsilon_{\max}} \cdot \varepsilon \tag{4}$$

and

$$dy = \frac{x}{\varepsilon_{\max}} \cdot d\varepsilon \,. \tag{5}$$

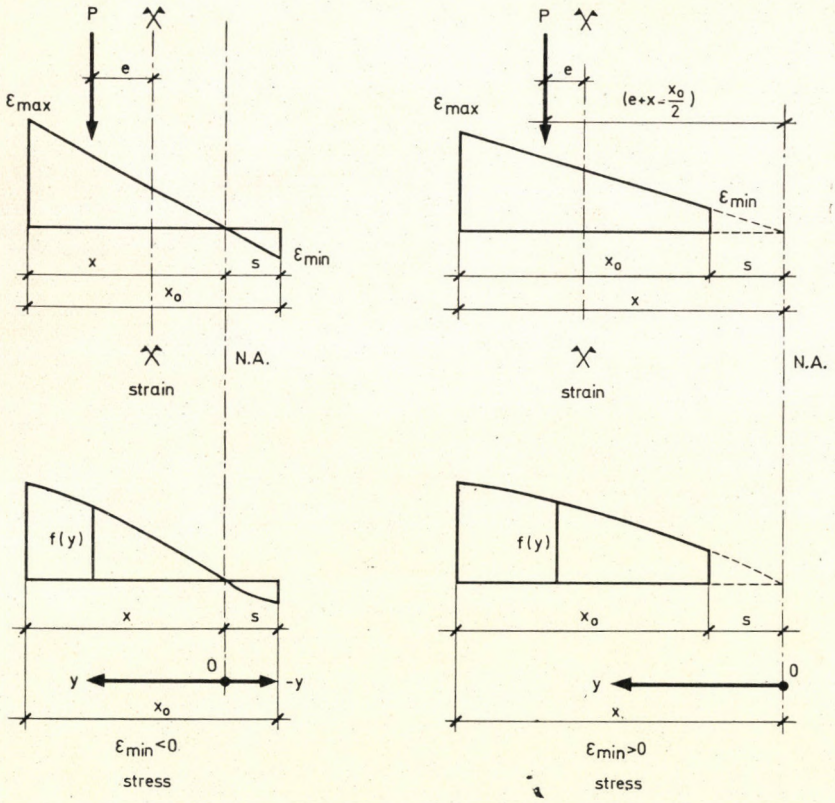

Fig. 13. Notations for the analysis of the eccentric prisms

* Use (+) if s is smaller than zero (see Fig. 13).

The depth of the neutral axis may be determined from the measured strains, i.e.,

$$x = x_0 \cdot \frac{\varepsilon_{max}}{\varepsilon_{max} - \varepsilon_{min}} . \tag{6}$$

Substituting the above values in equations (1) and (2) then**

$$P = \frac{b_0 x}{\varepsilon_{max}} \left[\int_0^{\varepsilon_{max}} f(\varepsilon)\, d\varepsilon - \int_0^{|\varepsilon_{min}|} f(\varepsilon) d\varepsilon \right], \tag{7}$$

$$M = \frac{b_0 x^2}{\varepsilon_{max}^2} \left[\int_0^{\varepsilon_{max}} f(\varepsilon) \cdot \varepsilon \cdot d\varepsilon \mp \int_0^{|\varepsilon_{min}|} f(\varepsilon) \cdot \varepsilon \cdot d\varepsilon \right] \tag{8}$$

where $\sigma = f(\varepsilon)$ is the desired stress-strain function.

To facilitate the calculations, the second two terms in equations (7) and (8) were neglected as a result of the small values of ε_{min}. (The max. measured value of ε_{min} in all the specimens at any step of loading did not exceed $150 \cdot 10^{-6}$ cm/cm.) So the equations (7) and (8) will be

$$P = \frac{b_0 x}{\varepsilon_{max}} \int_0^{\varepsilon_{max}} f(\varepsilon)\, d\varepsilon , \tag{9}$$

$$M = \frac{b_0 x^2}{\varepsilon_{max}^2} \int_0^{\varepsilon_{max}} f(\varepsilon)\, \varepsilon d\varepsilon . \tag{10}$$

Putting $P/b_0 x = f_0$ and $M/b_0 x^2 = m_0$ and assuming the depth of the neutral axis as constant between two successive steps of loading, and differentiating these equations with respect to the variable ε_{max}, we can obtain:

$$\sigma = f_0 + \varepsilon_{max} \cdot \frac{df_0}{d\varepsilon_{max}} , \tag{11}$$

$$\sigma = 2m_0 + \varepsilon_{max} \frac{dm_0}{d\varepsilon_{max}} . \tag{12}$$

The last terms in the above equations (11) and (12) can be approximately determined by evaluating the change in the values of f_0 and m_0 over small increments of strains. Accordingly, equations (11) and (12) can be set down in the following form:

$$\sigma = f_0 + \frac{\Delta f_0}{\Delta \varepsilon_{max}} \cdot \varepsilon_{max}, \tag{13}$$

$$\sigma = 2m_0 + \frac{\Delta m_0}{\Delta \varepsilon_{max}} \cdot \varepsilon_{max} . \tag{14}$$

It was found that if the results obtained from the tests were directly applied to these equations, a very large scatter in the calculated values of σ would be obtained. This is due to the sensitivity of the equations to any slight inaccuracy in determining the incremental terms beside the experimental error involved in calculating the m_0 value. The numerical error in the differential terms can be minimized by rearranging the equations (13) and (14) in the form of the secant modulus of elasticity E_c instead of σ:

$$E_c = \frac{\sigma}{\varepsilon_{max}} = \frac{f_0}{\varepsilon_{max}} + \frac{\Delta f_0}{\Delta \varepsilon_{max}} , \tag{15}$$

$$E_c = \frac{\sigma}{\varepsilon_{max}} = \frac{2m_0}{\varepsilon_{max}} + \frac{\Delta m_0}{\Delta \varepsilon_{max}} . \tag{16}$$

The average value of E_c according to the equations (15) and (16) was taken into consideration and, therefore, the E_c and ε_{max} relation was represented by a straight-line equation in the form of

$$E_c = a + c\varepsilon_{max} , \tag{17}$$

and hence the constant values a and c can be determined. Accordingly, the stress function can be easily determined, i.e.

$$\sigma = a\, \varepsilon_{max} + c\, \varepsilon_{max}^2 . \tag{18}$$

** Use (+) when $\varepsilon_{min} < 0$. (See Fig. 13.)

To check the equilibrium conditions, a coefficient called modified coefficient of variation, μ was computed, following that developed by ref. [8] using the following expression:

$$\mu = 100 \sqrt{\frac{\sum_{i=1}^{n}\left[\left(\frac{P_{ci}-P_i}{P_i}\right)^2+\left(\frac{M_{ci}-M_i}{M_i}\right)^2\right]}{2n}} \tag{19}$$

where

P_i and M_i are the measured values for the loads and moments respectively;

P_{ci} and M_{ci} are the calculated load and moment from the determined stress-function equation (18) after substituting it in equations (7) and (8) respectively;

n is the number of the data points for each specimen individually, i.e., n is equal to the number of the loading steps for each specimen individually.

REFERENCES

1. Baker, A. L. L.—Amarakone, A. M. N.: Analysis and Application of CEB International Correlated Tests. *Bulletin d'Information du Comité Européen du Béton*, Paris, No. 52, (1965), 1—94
2. Corley, W. G.: Rotation Capacity of R. C. Beams. *Journal of Structural Division*, ASCE, **92** (1966), 121—146
3. Hsu Thomas, T. C.—Slate, O.—Sturman, G. M.—Winter, G.: Microcracking of Plain Concrete and Shape of the Stress-strain Curve. *Journal of ACI*, **60** (1963), 209—224
4. Lenkei, P.: Compatibility Condition in Plastic Design of Statically Indeterminate Reinforced Concrete Linear Structures. *Acta Techn. Hung.* **72** (1972), 341—346
5. Mattock, A. H.: Rotation Capacity of Hinging Regions in R. C. Beams. *Proceedings of the International Symp. on Flexural Mechanics of R. C.*, Miami, Nov. 1964, ASCE-ACI (1965), 143—181
6. Rüsch, H.—Stöcki, S.: Versuche zur Festigkeit der Biegedruckzone. Einflüsse der Querschnittsform. *Deutscher Ausschuß für Stahlbeton*, Heft, 207 (1969),
7. Soliman, M. T. M.—Yu, C. W.: The Flexural Stress-strain Relationship of Concrete Confined by Rectangular Reinforcement. *Magazine of Concrete Research*, **19** (1967), 223—238
8. Sturman, G. M.—Shah, S. P.—Winter, G.: Effects of Flexural Strain Gradients on Microcracking and Stress-strain Behavior of Concrete. *Journal of ACI* **63** (1965), 805—821

Einfluß der Querschnittsdimensionen auf die Verformungsfähigkeit des Betons. Im Rahmen eines Versuchsprogrammes wurde die Wirkung der Querschnittabmessungen auf die Verformungsfähigkeit des Betons untersucht. Es wurden 60 mittig und außermittig gedruckte Prismen von verschiedenen Durchmessern und 14 auf reine Biegung beanspruchte Stahlbetonträger mit Druckzonen von verschiedenen Dimensionen (Längen, Höhen) geprüft. Die Versuche bewiesen, daß das Spannungs-Verformungs-Diagramm des Betons von der Art der Belastung (mittiger oder außermittiger Druck, Biegung) abhängig ist. Die Bruchverformung des mittig gedruckten Betonprismas nimmt zu, während die Bruchverformung des Randfasers der Druckzone des außermittig gedruckten Betonprismas und des auf Biegung beanspruchten Stahlbetonträgers mit der Zunahme der Querschnitthöhe des gedruckten Betons abnimmt. Diese Veränderungen werden durch die entsprechenden Änderungen des plastischen Teiles der Bruchverformung des Betons verursacht.

Влияние поперечных размеров на предельные деформации бетона. Разработана экспериментальная программа для исследования влияния поперечных размеров на предельные деформации бетона. Было исследовано 60 центрально и внецентренно нагруженных бетонных призм различного поперечного сечения и 14 изгибаемых ж. б. балок с различными размерами сжатой зоны (ширины и высоты) на участке чистого изгиба. Исследования показали, что кривая напряжения — деформации бетона зависит от рода прикладываемой нагрузки (центральное или внецентренное сжатие, изгиб). Предельные деформации в крайнем сжатом волокне в случае центрально сжатых бетонных призм возрастали, а в случае внецентренно сжатых призм и изгибаемых ж. б. балок уменьшались с ростом высоты сжатого бетонного сечения. Эти изменения являлись результатом соответствующих изменений пластической части предельных деформаций.

Acta Technica Academiae Scientiarum Hungaricae, Tomus 76 (3—4), pp. 413—423 (1974)

NUMERICAL ALGORITHM TO DETERMINE THE DIFFERENCE OPERATORS OF BOUNDARY-VALUE PROBLEMS

D. HOLNAPY*
CAND. OF TECHN. SC.

[Manuscript received October 26, 1972]

The present paper suggests an algorithm for the determination of the linear equation systems for solving of boundary-value problems by means of the finite difference technique. The method involves the production of the difference operator, and enables the interpolation polynome approximating the solution area to satisfy such conditions that can be specified by the linear combination of the derivatives. Thus, the process includes the most frequently employed methods based on the Lagrange interpolation. The plurilocal method (Mehrstellenverfahren) satisfying the differential equation at a number of points may be considered as a special version of this technique.

1. Introduction

In the mathematical models of engineering problems the boundary-value problems of partial and ordinary differential equations are often encountered. Among others, determination of the internal forces of plates and shells also demands the solution of a boundary-value problem.

Solution of a second-order boundary-value problem, with respect to the Dirichlet condition, is relatively easy and accurate, by making use of the finite difference technique based on the traditional Lagrange interpolation. In addition to several comprehensive papers, the solution of such problems has been dealt with in detail, by BEREZIN and ZHIDKOV [2], and later by SOARE [9], so the mechanization of the calculations involved can now be directly carried out. However, by taking into account the boundary values expressed by the linear combination of higher-order derivatives (as the moment-free curved plate edge in the engineering practice), still no generally adaptable numerical algorithm can be found.

Although the calculations of COLLATZ [3, 4] and ZURMÜHL [12] are of a general character, their final conclusions reckon only with the aspects of increased accuracy and the simplest boundary conditions, whereas for the determination of the difference-operator weights they supply individual derivations instead of an algorithm.

Nevertheless, by making use and adopting the numerical method of FEKETE [6], it is possible to develop a technique easy to program in a general

* D. HOLNAPY, Öv u. 150, 1147 Budapest, Hungary

manner [7], and the present paper deals with the extension of its application possibilities.

Without this method, each problem would require the build-up of a system like that elaborated by BALAŠ and HANUŠKA [1], and also by ZURMÜHL [13].

The present paper, in general, describes the integration of the expressions formed by the linear combination of the derivatives into the difference operator, with particular respect to the mechanization possibilities of the method.

The difference operator is formed by the determination of the derivatives of an interpolation surface. In addition to the function values and derivatives, their linear combinations are also made use of in order to obtain the interpolation surface to be employed. Consequently, any such linear combination may be added to the unknowns of the difference operator.

As an advantage of the mathematical method described below, the difference operators can be produced by means of the same algorithm system under different conditions, and the adaptability of the method is not restricted by the irregularity of the mesh, either. At the boundary and the intermediate points the method permits the consideration of such secondary conditions that consist of the linear combinations of function values and derivatives.

With this method the boundary condition systems consisting of first-, second- and third-order derivatives or their linear combinations, often encountered in the engineering practice, can be readily manipulated, even in the case of curved edges. In addition, the method has generalized the plurilocal method (Mehrstellenverfahren).

Discussion will cover ordinary and partial (single and two-variable) differential equations. Detailed discussion of the ordinary differential equations is only intended to facilitate understanding. The method applies to the formation of the difference operators used with n-variable functions as well, and represents a basis for generalization including also the partial differential equation systems.

2. Ordinary differential operators

Let us have the following differential equation to be solved:

$$\mathfrak{L}[f(x)] \equiv d_0(x)f^{(0)}(x) + d_1(x)f'(x) + \ldots + d_n(x)f^{(n)}(x) = p(x) \qquad (1)$$

which, if written in the form of a scalar product, much easier to treat, will read:

$$\mathfrak{L}[f(x)] \equiv [d_0(x)\ d_1(x)\ \ldots\ d_n(x)] \begin{bmatrix} f^{(0)}(x) \\ f'(x) \\ \vdots \\ f^{(n)}(x) \end{bmatrix} = p(x)\,. \qquad (2)$$

Here $d_i(x)$ is a known function, the coefficient of the differential equation term containing the i-th derived function. In engineering practice, many of the $d_i(x)$ functions of such differential equations equal zero. Taking now the $x = x_0$ substitution value of (2), and using a condense expression form, we obtain

$$\mathfrak{L}[f(x)]\Big|_{x=x_0} \equiv \underset{1\times(n+1)}{d^*}(x_0) \cdot \underset{(n+1)\times 1}{t}(x_0) = p(x_0). \tag{3}$$

Now let us approximate the solution surface with an n-th degree polynome. Let the conditions required for the determination of the interpolation surface of the form be

$$\hat{f}(x_\nu) = \sum_{k=0}^{n} c_{\nu k} f^{(k)}(x_\nu).$$

These conditions contain the Lagrange interpolation when $c_{\nu k}$ is selected as 1, if $k = 0$, and as zero in any other case. With the above conditions the following expression may be written, which is of a far more general character than those suggested by COLLATZ [3, 4] or SOARE [10]:

$$P \equiv \sum_{\nu=1}^{m} s_\nu \left\{ \sum_{k=0}^{n} c_{\nu k} f^{(k)}(x_\nu) \right\} - \mathfrak{L}[f(x)]\Big|_{x=x_0} = 0 \tag{4}$$

where ν is the index of the conditions to be satisfied by the interpolation surface,
s_ν means the weight of the ν-th linear condition ("generalized function value", the unknown in the differential equation of the difference method), and
$c_{\nu k}$ indicates the coefficient of the term containing the k-th derivative in the ν-th linear condition.

In (4), the term $f^{(k)}(x_\nu)$ may be substituted by the k-th derivative of the Taylor polynome from the n-th degree interpolation polynome pertaining to point x_0. Thereafter what (4) will express is that the weighed sum of the linear conditions associated with the ν-th point will determine the differential operator value in point x_0 by means of the error due to the neglection of the higher order Taylor terms. Our next task is to determine these weights.

Written in a matrix form, (4) will read:

$$P \equiv \underset{1\times m}{[\ \mathbf{s}_0^*\ ]} \cdot \underbrace{\overset{(n+1)}{\overbrace{\begin{bmatrix} \\ \mathbf{A}_0 \\ \\ \end{bmatrix}}}\ \underset{(n+1)\times 1}{\begin{bmatrix} \mathbf{t}_0 \end{bmatrix}}}_{\substack{m \\ \hat{f}_0 \\ m\times 1}} - \underset{1\times(n+1)}{[\ \mathbf{d}_0^*\ ]} \underset{(n+1)\times 1}{\begin{bmatrix} \mathbf{t}_0 \end{bmatrix}} = 0 + \text{error} \tag{5}$$

where

$$\underset{1\times(n+1)}{\left[\quad a_\nu^*\quad\right]}=\underset{1\times(n+1)}{\left[\quad c_\nu^*\quad\right]}\begin{bmatrix} 1 & \frac{x_\nu-x_0}{1!} & \frac{(x_\nu-x_0)^2}{2!} & \cdots & \frac{(x_\nu-x_0)^n}{n!} \\ 0 & 1 & \frac{x_\nu-x_0}{1} & \cdots & \frac{(x_\nu-x_0)^{n-1}}{(n-1)!} \\ 0 & 0 & 1 & \cdots & \frac{(x_\nu-x_0)^{n-2}}{(n-2)!} \\ \vdots & & & & \cdots\cdots \\ & & & & 1 \end{bmatrix} \tag{6}$$

and

$$\underset{1\times(n+1)}{a_\nu^*}\cdot\underset{(n+1)\times 1}{t_0}=\hat{f}(x_\nu). \tag{7}$$

Vector $\underset{1\times m}{s_0^*}$ containing the weights, can be obtained by solving the equation

$$\underset{1\times m}{s_0^*}=\underset{1\times(n+1)}{d_0^*}\ \underset{(n+1)\times m}{\mathbf{A}_0^+}\ . \tag{8}$$

In (8), the symbol $\mathbf{A}_0^+$ indicates the generalized inverse of matrix $\mathbf{A}_0$ [5]. However, the $\mathbf{A}_0^+$ inverse can only be accepted if the equation

$$\underset{1\times m}{s_0^*}\ \underset{m\times(n+1)}{\mathbf{A}_0}=\underset{1\times(n+1)}{d_0^*} \tag{9}$$

is satisfied. This is necessary to make the columns of matrix $\mathbf{A}_0^*$ contain all the linearly independent vectors whose linear combination d can be then obtained from.

Now, by means of the differential operator, the differential equation may be approximated as follows:

$$\mathfrak{L}\,[f(x)]\Big|_{x=x_0}\cong\underset{1\times m}{\mathbf{s}_0^*}\ \underset{m\times(n+1)}{\mathbf{A}_0}\ \underset{(n+1)\times 1}{\mathbf{t}_0}=\underset{1\times m}{s_0^*}\ \underset{m\times 1}{\hat{f}_0}=p(x_0)\ . \tag{10}$$

Each line of matrix $\mathbf{A}_0$ contains a restriction (condition) for the interpolation area. In order, for example, that Eq. (7) should express a function value, the line in question of matrix $\mathbf{A}_0$ must be composed by making use of vector

$$c^*=[1\ 0\ 0\ \ldots].$$

If

$$c^*=[0\ 0\ \ldots\ 1\ \ldots\ 0]$$

is used, then the i-th derivative can be considered as unknown. Naturally, in special cases $c^*=d^*$ may also be selected, which represents the basic idea of the plurilocal method. In this case the corresponding element in the right-hand side of Eq. (7) is not an unknown, but equals the right-hand side of the differential equation, whereby the number of unknowns will not be increased in (10).

As an example, let us examine the difference operator related to the x_3 boundary point (Fig. 1) of the differential equation

$$\frac{d^4}{dx^4}f(x)=p(x)$$

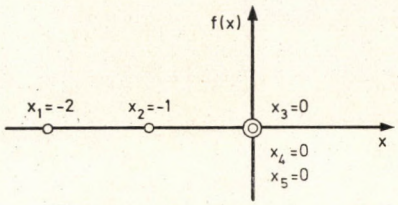

Fig. 1

satisfying the boundary conditions

$$\frac{d^2}{dx^2} f(x_3) = g_1(x_3)$$

and

$$\frac{d^3}{dx^3} f(x_3) = g_2(x_3).$$

The requirements $\nu = 1$, 2 and 3 are, that the interpolation area must rely on an unknown function value, the fourth condition is the satisfaction of $f''(x_3) = g_1(x_3)$, while the fifth that of $f'''(x_3) = g_2(x_3)$. In the case of $\nu = 1$, 2 and 3, vectors

$$\underset{1\times 5}{c_\nu^*} = [1\ 0\ 0\ 0\ 0],$$

$$\underset{1\times 5}{c_\nu^*} = [0\ 0\ 1\ 0\ 0],$$

$$\underset{1\times 5}{c_\nu^*} = [0\ 0\ 0\ 1\ 0].$$

The system built up by lines corresponding to (7) will in this case be

$$\begin{bmatrix} 1 & -2 & 2 & -\frac{4}{3} & \frac{2}{3} \\ 1 & -1 & \frac{1}{2} & -\frac{1}{6} & \frac{1}{24} \\ 1 & 0 & 0 & 0 & 0 \\ 0 & 0 & 1 & 0 & 0 \\ 0 & 0 & 0 & 1 & 0 \end{bmatrix} \cdot \begin{bmatrix} f^{(0)}(x_3) \\ f^{\mathrm{I}}(x_3) \\ f^{\mathrm{II}}(x_3) \\ f^{\mathrm{III}}(x_3) \\ f^{\mathrm{IV}}(x_3) \end{bmatrix} = \begin{bmatrix} f(x_1) \\ f(x_2) \\ f(x_3) \\ f^{\mathrm{II}}(x_3) \\ f^{\mathrm{III}}(x_3) \end{bmatrix}. \tag{11}$$

The differential equation written for point x_3, with the weights $\underset{1\times 5}{s_3^*}$ obtained by making use of the inverse of matrix $\mathbf{A}_0$ thus composed, and vector

$$\underset{1\times 5}{d^*(x_3)} = [0\ 0\ 0\ 0\ 1]$$

representing the differential operator that contains the fourth derivative, will

assume the following form:

$$\underset{1\times 5}{s^*(x_3)}\ \underset{5\times 1}{\hat{f}(x_3)} \equiv \underset{1\times 5}{d^*(x_3)}\ \underset{5\times 5}{\mathbf{A}^+}\ \underset{5\times 1}{\hat{f}(x_3)} = \tag{12}$$

$$= [+1{,}714 f(x_1) - 3{,}428 f(x_2) + 1{,}714 f(x_3) - 1{,}714 f''(x_3) + 1{,}714 f'''(x_3)].$$

Fig. 2 illustrates the weights with the usual difference asterisk indication. The next example applies to the "Mehrstellenverfahren" operator formation.

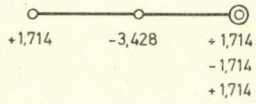

Fig. 2. Function-value weights. Second derivative weights. Third derivative weights

Let us express the difference operator of differential equation

$$y''(x) + (1 + x^2)y(x) = -1 \tag{13}$$

for the locus $x = 0$ (literature has repeatedly given this equation as a classical example, see [3], [11]). Conditions 1, 2 and 3 (Fig. 3) defining the interpolation surface should be function values, while the fourth and fifth conditions the differential equation Eq. (13), interpreted for the relevant point.

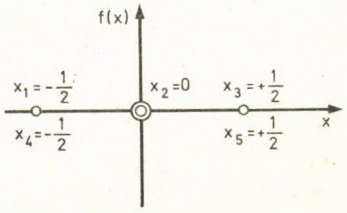

Fig. 3

Matrix $\mathbf{A}_0$ consisting of lines according to (7) by making use of vectors

$$\underset{1\times 6}{d^*(x_0)} = [(1+x_0^2)\ 0\ 1\ 0\ 0\ 0] = [1\ 0\ 1\ 0\ 0\ 0]$$

and

$$c^* = \left[\frac{5}{4}\ 0\ 1\ 0\ 0\ 0\right]$$

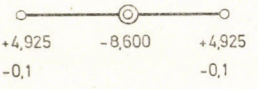

Fig. 4. Function-value weights. Differential-equation weights

which means the satisfaction of conditions (4) and (5), will take the following form:

$$\begin{bmatrix} 1 & -\frac{1}{2} & \frac{1}{8} & -\frac{1}{48} & \frac{1}{384} & -\frac{1}{3840} \\ 1 & 0 & 0 & 0 & 0 & 0 \\ 1 & \frac{1}{2} & \frac{1}{8} & \frac{1}{48} & \frac{1}{384} & \frac{1}{3840} \\ \frac{5}{4} & -\frac{5}{8} & \frac{37}{32} & -\frac{101}{192} & \frac{197}{1536} & -\frac{325}{15\,360} \\ \frac{5}{4} & \frac{5}{8} & \frac{37}{32} & \frac{101}{192} & \frac{197}{1536} & \frac{325}{15\,360} \end{bmatrix} \begin{bmatrix} f^{(0)}(x_2) \\ f'(x_2) \\ f''(x_2) \\ f'''(x_2) \\ f^{IV}(x_2) \\ f^{V}(x_2) \end{bmatrix} = \begin{bmatrix} f(x_1) \\ f(x_2) \\ f(x_3) \\ -1 \\ -1 \end{bmatrix} \tag{14}$$

The final result obtained by means of Eq. (8) is illustrated in Fig. 4.

3. Partial differential operators

In the case of partial differential operators a process similar to that described for the ordinary differential equations is followed. In the most frequent bivariate cases the scalar product form of the differential equation is

$$\underset{1\times r}{\mathfrak{L}\,[f(x,y)] \equiv [d_{01}(x,y)\ d_{11}(x,y)\ d_{12}(x,y)\ \ldots\ d_{n,n+1}(x,y)]} \underset{r\times 1}{\begin{bmatrix} f(x,y) \\ f_x(x,y) \\ f_y(x,y) \\ f_{xx}(x,y) \\ f_{xy}(x,y) \\ f_{yy}(x,y) \\ \vdots \\ f_{y\ldots\overset{n}{y}}(x,y) \end{bmatrix}} = p\,(x,y) \tag{15}$$

where

$$r = 1 + \frac{3}{2}n + \frac{1}{2}n^2.$$

To obtain $\underset{1\times r}{a_\nu^*}$ it is best to use the following equation:

$$\underset{1\times r}{a_\nu^*} = \begin{bmatrix} & \underset{1\times r}{c_\nu^*} & \end{bmatrix} \begin{bmatrix} 1 & \dfrac{x_\nu - x_0}{1!} & \dfrac{y_\nu - y_0}{1!} & \dfrac{(x_\nu - x_0)^2}{2!} \ldots \\ 0 & 1 & 0 & \dfrac{x_\nu - x_0}{1!} \ldots \\ 0 & 0 & 1 & 0 \ldots \\ \ldots\ldots\ldots\

(given moment at the boundary):

$$c^* = [0 \quad 0\ 0 \quad -\mu K\ 0\ -K \quad 0\ 0\ 0\ 0 \quad 0\ 0\ 0\ 0\ 0].$$

(c) Taking into consideration the boundary condition

$$-K(f_{yyy}(x, y) + (2 - \mu) f_{yxx}(x, y)) = Q_y^*$$

(given substituting stress resultant):

$$c^* = [0 \quad 0\ 0 \quad 0\ 0\ 0 \quad 0 \quad -K(2-\mu)\ 0\ -K \quad 0\ 0\ 0\ 0\ 0].$$

(d) Taking into consideration the boundary condition

$$\frac{\partial f(x, y)}{\partial n} = g(x, y)$$

at a point of the normal

$$\bar{n} = (\cos \alpha,\ \sin \alpha)$$

(oblique clamping):

$$c^* = [0 \quad \cos \alpha\ \sin \alpha \quad 0\ 0\ 0 \quad 0\ 0\ 0\ 0 \quad 0\ 0\ 0\ 0\ 0].$$

(e) Taking into consideration the boundary condition

$$-K(f_{nn}(x, y) + \mu f(x, y) = m_n$$

(given moment at an oblique plate edge):

$$c^* = [0 \quad 0\ 0 \quad -K(\cos^2 \alpha + \mu \sin^2 \alpha) \quad -2K(1 - \mu)\cos \alpha \sin \alpha \quad -K(\sin^2 \alpha + \mu \cos^2 \alpha)\ 0\ 0\ 0\ 0 \quad 0\ 0\ 0\ 0\ 0]$$

(f) When solving the biharmonic equation, vector c^* for an increased accuracy by the plurilocal method will be

$$c^* = [0 \quad 0\ 0 \quad 0\ 0\ 0 \quad 0\ 0\ 0\ 0 \quad 1\ 0\ 2\ 0\ 1].$$

New equations must be added, when the linear combination of the derivatives introduce new unknowns (Fig. 5). These new equations can be obtained by derivating the differential equation. In the case of bent plates, therefore, in addition to equation

$$\left(\frac{\partial^4}{\partial x^4} + 2\frac{\partial^4}{\partial x^2 \partial y^2} + \frac{\partial^4}{\partial y^4}\right) w(x, y) = \frac{p(x, y)}{K(x, y)} \tag{17}$$

equations

$$\frac{\partial}{\partial x}\left(\frac{\partial^4}{\partial x^4}+2\frac{\partial^4}{\partial x^2\,\partial y^2}+\frac{\partial^4}{\partial y^4}\right)w(x,y)=\frac{\partial}{\partial x}\left(\frac{p(x,y)}{K(x,y)}\right) \tag{18}$$

and

$$\frac{\partial}{\partial y}\left(\frac{\partial^4}{\partial x^4}+2\frac{\partial^4}{\partial x^2\,\partial y^2}+\frac{\partial^4}{\partial y^4}\right)w(x,y)=\frac{\partial}{\partial y}\left(\frac{p(x,y)}{K(x,y)}\right) \tag{19}$$

must also be reckoned with, if the two tangents of co-ordinate axis direction of the $w(x, y)$ solution function are also considered as unknown at the point in question, besides the function value. All these reveal that the possibility described above hides the Hermite approximation of the load function as well.

This method can be applied without any difficulties to partial differential equations of optional variables.

REFERENCES

1. Balaš, J.—Hanuška, A.: Der Einfluß der Querdehnungszahl auf den Spannungszustand einer 45° schiefen Platte — *Der Bauingenieur* **36** (1961), 100—107
2. Berezin, I. S.—Zhidkov, N. P.: Computing Methods. Pergamon Press, Oxford, London, etc., 1965
3. Collatz, L.: The Numerical Treatment of Differential Equations. Springer Verlag, Berlin 1960
4. Collatz, L.: Das Mehrstellenverfahren bei Plattenaufgaben. *ZAMM* **30** (1950), 385—388
5. Egerváry, J.: Generalization of the Inverse Matrix (in Hungarian). *Bulletins of the Research Institute of Mathematics*, Hungarian Academy of Sciences, **1** (1956), 315—324
6. Fekete, S.: Numerical Generation of Difference Operators (in Hungarian). IASS Shell Conference, Budapest 1968
7. Holnapy, D.: A New Numerical Method for the Mechanical Calculation of Plates and Shells. (Cand. Thesis in Hungarian), Budapest 1970
8. Kantorovich, L. V.—Krylov, V. I.: Approximation Methods of Higher-order Analysis. (Hungarian translation), Akadémiai Könyvkiadó, Budapest 1953
9. Soare, M.: Application des équations aux différences finies au calcul des coques. Ed. Acad. Roumanie, Ed. Eyrolles, Paris 1962
10. Soare, M.: Über das verbesserte Mehrstellenverfahren. *Bulletin Mathématique* (Bucarest), **4** (52) (1960), 91—98
11. Szabó, J.: Girder Statics, III. (University textbook in Hungarian). Tankönyvkiadó, Budapest 1968
12. Zurmühl, R.: Matrizen und ihre technischen Anwendungen. Springer Verlag, Berlin, Göttingen, Heidelberg 1964
13. Zurmühl, R.: Behandlung der Plattenaufgabe nach dem verbesserten Differenzenverfahren. *ZAMM* **37** (1957), 1—16

Numerischer Algorithmus zur Ermittlung der Differenzenoperatoren von Randwertaufgaben. Ein Algorithmus wird gegeben zur Ermittlung des linearen Gleichungssystems der mit Hilfe der Methode der endlichen Differenzen durchgeführten Randwertaufgabenlösung. Das Verfahren bezieht sich auf die Bildung des Differenzenoperators und ermöglicht, daß das der Lösungsfläche sich nähernde Interpolationspolynom Bedingungen befriedige, die durch die lineare Kombination der Derivierten angegeben werden können. Demgemäß enthält das Verfahren auch die am häufigsten angewandten und auf die Lagrangesche Interpolation aufgebauten Verfahren. Auch die mit der auf mehreren Punkten durchgeführten Befriedigung der Differentialgleichungen arbeitende Mehrstellenmethode kann als ein Spezialfall des oben beschriebenen Verfahrens betrachtet werden.

Численный алгоритм для определения разностных операторов задач краевых значений (Д· Хольнапи). В настоящей работе автор дает алгоритм для определения системы линейных дифференциальных уравнений решения задачи краевых значений с помощью метода конечных разностей. Метод действителен для образования разностного оператора и допускает, чтобы интерполяционный полином, приближающий поверхность решения, удовлетворял бы таким условиям, которые можно задавать линейной комбинацией производных. Таким образом, метод охватывает также наиболее часто применяемые и основанные на интерполяцию Лагранжа методы. Также в качестве специального случая описанного метода можно принять многоточечный метод, основанный на уравнении дифференциального уравнения во многих точках.

Acta Technica Academiae Sceintiarum Hungaricae, Tomus 76 (3—4), pp. 425—433 (1974)

RATIONAL ASSUMPTION OF INTERPOLATION REFERENCE POINTS IN THE CASE OF BIVARIATE LAGRANGE INTERPOLATION

KIS, S.*

[Manuscript received October 26, 1972]

The paper deals with the bivariate Lagrange interpolation with respect to the unicity of the interpolating polynome. Such an interpolation (regular) point pattern is defined where the interpolation can be unequivocally performed. The properties of regular point patterns are studied, and a practical method is introduced for their production. Finally, some regular interpolation-point patterns are presented as examples for the application of the method described.

1. Introduction

Interpolation is an important aid in numerical mathematics. If a function is substituted by its interpolating polynome, it will be much easier to deal with from calculation engineering or computer aspects (determination of the substitute value, derivation, integration, etc). This is how it can be reduced, for example, to the solution of a differential equation. Literature has discussed this method in detail for ordinary and partial differential equations, and for interpolation at regular, as well as irregular gratings [2—4, 6—9].

The success of this approach greatly depends on the advantageous assumption of the interpolation-reference points (hence point pattern). It is known from literature that in the case of an interpolation-point pattern, optionally selected for functions of a single variable, there will be only one minimum-degree Lagrange interpolating polynome existing, whereas for bivariate interpolation this unequivocality, from a number of aspects very advantageous, is not ensured at all.

It follows that the difference method applied to partial differential equations would raise stability problems in the case of optionally selected patterns [4, 6], and could not lead to success, except with the so-called regular point patterns.

In the first part of the present paper the definition of the regular point pattern will be given, and interpreted for interpolations of a single, as well as two variables. As a consequence, the close correlation between the stability

* Kis, S., Újvidék u. 66/b, 1145 Budapest, Hungary

of the difference method and the Lagrange interpolation will seem to be quite obvious.

In the second part certain properties of the regular pattern of bivariate interpolation will be determined whereby the sufficient condition of regularity can then be defined.

With this condition known, the third part of the paper offers a method for plotting regular patterns. The condition of regularity contains geometrical stipulations, thus, because of its illustrative character, it can be successfully employed for practical plotting.

Finally, some examples on pattern assumption will be shown which, in addition to those at regular rectangular and triangular gratings, include the so-called "most general" pattern as well.

2. Definition of the regular point pattern

Let the linear space R be the set $\{u\}$ of the u functions of a certain common property. To any of these u functions a real or complex number can be assigned by the symbol $L(u)$. The assignment will be linear, if the equality

$$L(\alpha u + \beta v) = \alpha L(u) + \beta L(v)$$

is true for any $u, v \in R$ and α, β real or complex pair of numbers.

The set $\{L\}$ of the L linear assignments is also a linear space, called the conjugate space of R, and indicated by R^*. If space R is n-dimensional, then R^* is similarly n-dimensional (see the proof in [5]).

If a base of R is represented by $r_1, r_2, \ldots, r_n$, and that of R^* by $L_1, L_2, \ldots, L_n$, then the following determinant will surely not equal zero:

$$\Delta = |L_i(r_j)| \neq 0, \tag{2.1}$$

and vice versa: if $\Delta \neq 0$, then $\{L_i\}$ and $\{r_i\}$ are bases (proved, for example, in [3] and [5]).

In this case R will have such an $l_1, l_2, \ldots, l_n$ base, whose vectors are orthogonal to the $L_1, L_2, \ldots, L_n$ vectors in the following sense:

$$L_i(l_j) = \delta_{ij} = \begin{cases} 1, & \text{if } i = j, \\ 0, & \text{if } i \neq j. \end{cases} \tag{2.2}$$

Here $\{L_i\}$ and $\{l_i\}$ are called reciprocal bases, which can be defined as follows:

Let $\alpha_{1,k}, \alpha_{2,k}, \ldots, \alpha_{n,k}$ be the co-ordinates of vector l_k as related to base $\{r_i\}$. Now, on the basis of (2.2), the following condition system may be

written for the determination of the above co-ordinates:

$$L_i(l_k) = L_i\left(\sum_{j=1}^{n} \alpha_{jk}\, r_i\right) = \sum_{j=1}^{n} \alpha_{jk}\, L_i(r_j) = \delta_{ik}\,, \qquad (2.3)$$
$$(i = 1, 2, \ldots, n)\,.$$

Since the determinant of the equation system (Δ) is not zero, the α_{jk} co-ordinates can be unequivocally determined.

The correlation of what has been said above to the Lagrange interpolation will seem to be quite obvious, if the vectors involved are interpreted as in the following two examples:

(a) *In the first example* R is the linear space of the maximum kp-th degree polynomes of a single variable. The dimensional number of this space is: $n = p + 1$. Now let us select bases $\{r_i\}$ and $\{L_i\}$ as follows:

$$\begin{aligned} r_1 = 1, \quad r_2 = x, \quad r_3 = x^2, \ldots, r_n = x^{n-1}, \\ L_1(u) = u(x_1), \quad L_2(u) = u(x_2), \ldots, L_n(u) = u(x_n) \end{aligned} \qquad (2.4)$$

where $x_1, x_2, \ldots, x_n$ are optional but having different values.

In this case the determinant according to (2.1) will be the so-called Vandermonde determinant:

$$\Delta = V(x_1, x_2, \ldots, x_n) = |r_j(x_i)| = \begin{vmatrix} 1 & 1 & \ldots & 1 \\ x_1 & x_2 & \ldots & x_n \\ \vdots & \vdots & & \vdots \\ x_1^{n-1} & x_2^{n-1} & \ldots & x_n^{n-1} \end{vmatrix} \neq 0 \qquad (2.5)$$

As is known, the Vandermonde determinant does not disappear at different x_i values, so $\{L_i\}$ and $\{r_i\}$ are actually bases. The vectors of the reciprocal base $\{l_i\}$ of base $\{L_i\}$ are, in this case, the Lagrange interpolating base polynomes:

$$L_i(l_j) = l_j(x_i) = \delta_{ij}. \qquad (2.6)$$

Any function (polynome) u can be written as the linear combination of the base vectors:

$$u = \alpha_1 l_1 + \ldots + \alpha_n l_n.$$

For the determination of the co-ordinates, let us make use of the L_i linear assignment with respect to u:

$$L_i(u) = u(x_i) = L_i(\alpha_1 l_1 + \ldots + \alpha_n l_n) = L_i(\alpha_i l_i) = \alpha_i,$$

that is

$$u = u(x_1) l_1 + \ldots + u(x_n) l_n. \qquad (2.7)$$

(b) *In the second example* R is the linear space of the maximum p-th degree bivariate polynomes. The dimensional number of the space is : $n = 1/2(p+1)(p+2)$. This is easy to realize, if we remember that a p-th degree polynome has maximum a number of $1/2(p+1)(p+2)$ coefficients assumed optionally. Now let us assume in the range of interpretation a pattern consisting of n points: $P_1, P_2, \ldots, P_n$, and select the $\{r_i\}$ and $\{L_i\}$ bases as follows:

$$r_1 = 1,\ r_2 = x,\ r_3 = y,\ r_4 = x^2,\ r_5 = xy,\ r_6 = y^2,\ \ldots,\ r_n = y^p,$$
$$L_1(u) = u(P_1),\ L_2(u) = u(P_2),\ \ldots,\ L_n(u) = u(P_n). \tag{2.8}$$

Since $\{r_i\}$ is obviously a base of R, vectors $L_1, L_2, \ldots, L_n$ can obviously be linearly independent, only if the Δ determinant produced according to (2.1) is not zero:

$$\Delta = |r_i(P_j)| = \begin{vmatrix} 1 & 1 & \ldots & 1 \\ x_1 & x_2 & \ldots & x_n \\ y_1 & y_2 & \ldots & y_n \\ x_1^2 & x_2^2 & \ldots & x_n^2 \\ \vdots & \vdots & & \vdots \\ y_1^p & y_2^p & \ldots & y_n^p \end{vmatrix} = W(x_1, y_1; x_2, y_2; \ldots; x_n, y_n)\,. \tag{2.9}$$

Hence this is called, after (2.5), bivariate *Vandermonde determinant*, and indicated by $W(x_1, y_1; x_2, y_2; \ldots x_n, y_n)$.

If $W \neq 0$, then the reciprocal base $\{l_i\}$ can be produced unequivocally, and any u element of the space R may be written in the form

$$u = u(P_1)l_1 + \ldots + u(P_n)l_n. \tag{2.10}$$

The value of the bivariate Vandermonde determinant cannot be expressed explicitely, and its being other than zero will not be ensured in the case of any point pattern.

Definition

A pattern consisting of points $P_1, P_2, \ldots, P_n$ *where the associated determinant* W *is other than zero, is called a p-th-degree regular point pattern.*

In the two above examples an optional element (polynome) of space R has been produced as the linear combination of the Lagrange base polynomes. In an interpolation problem the function to be approximated is generally not a polynome, so it is not an element of R, and thus the construction under (2.7) and (2.10) gives only the "projection" of the function as related to R. It follows that the approximation may be considered as correct or incorrect only

as far as it can be correctly or incorrectly substituted by its projection related to the R space (from this aspect, R should be regarded as the hyperplane of the linear space pertaining to the continuous functions).

The two above examples lead to the following conclusions: a function u can be unequivocally produced or approximated in the form (2.7) or (2.10), if the vector system L_i expressing the interpolation conditions is linearly independent, that is, if the interpolation pattern is regular in the sense of the definition given above.

Let us now examine how the regularity of the pattern could be provided for in the case of bivariate functions.

3. Properties of regular point patterns

In the following paragraphs three properties of the p-th-degree regular point patterns will be discussed on the basis of which the following pattern types can be constructed:

I^0. *Determinant W pertaining to a given pattern is invariant as against co-ordinate transformation*

Validity of the above statement can be realized if we consider that the transformation of the co-ordinate system can be characterized by variables v, z, and ψ, of which v means the x-direction displacement, z the same in direction y, and ψ the angle of rotation.

Let us study the various movements separately, and derivate W according to the subsequent variables. The derivative of an n-th-order determinant is equal to the sum of n determinants, where a line is derived in each. It is easy to realize that, owing to the special structure of W, any derived line will coincide with another non-derived one, or one of their linear combinations or, again, it will be zero, whereby

$$\frac{dW}{dv} = 0, \qquad \frac{dW}{dz} = 0, \qquad \frac{dW}{d\psi} = 0. \tag{3.1}$$

The three equalities presented above are equivalent to the statement I^0.

II^0. *In a p-th-degree regular pattern maximum $p + 1$ points can be fitted to a straight line.*

In order to prove the above statement, let us express the Lagrange base polynomes of variables x and y:

$$l_i(x_j, y_j) = \delta_{ij} \tag{3.2}$$

where x_j, y_j are the co-ordinates of point P_j $(i, j = 1, 2, \ldots, n)$. Let us have points $P_{\nu 1}, P_{\nu 2}, \ldots, P_{\nu k}$ on the straight line $y = \alpha x + \beta$, and then let us consider the p-th-degree polynome $z = l_{\nu i}(x, \alpha x + \beta)$ of a single variable whose zero loci are $x_{\nu 1}, \ldots, x_{\nu i-1}, x_{\nu i+1}, \ldots, x_{\nu k}$, and at $x = x_{\nu i}$ we have $z = 1$. Since the polynome is of a *p-th* degree in z, the number of the different real roots of $x_{\nu j}$ is maximum p. We must have, therefore,

$$k \leq p + 1 \tag{3.3}$$

whereby the above statement has been proved.

III^0. *If a number of* $p + 1$ *points on a straight line are omitted from a p-th-degree regular pattern, then the remaining points will form a* $(p - 1)$*-th-degree regular point pattern.*

We shall now demonstrate that the determinant $W^{(p)}$ can be obtained as the product of a determinant other than zero, and the determinant $W^{(p-1}$ of the leftover $(p - 1)$-th degree pattern.

Let the points $P_1, P_2, \ldots, P_{p+1}$ be on a straight line: axis X. This condition is all the more permissible as the numbering of the points is optional and, on the other hand, the reference system can also be assumed optionally according to I^0. Now let us rearrange the lines of determinant $W^{(p)}$ according to the increasing powers of co-ordinates y and x therein, while the number of line exchanges is t_p. In this case W^p will assume the following form:

$$W^{(p)} = (-1)^{t_p} \begin{vmatrix} 1 & \ldots & 1 & 1 & \ldots & 1 & 1 \\ x_1 & \ldots & x_{p+1} & x_{p+2} & \ldots & x_{n-1} & x_n \\ x_1^2 & \ldots & x_{p+1}^2 & x_{p+2}^2 & \ldots & x_{n-1}^2 & x_n^2 \\ \vdots & & \vdots & \vdots & & \vdots & \vdots \\ x_1^p & \ldots & x_{p+1}^p & x_{p+2}^p & \ldots & x_{n-1}^p & x_n^p \\ 0 & \ldots & 0 & y_{p+2} & \ldots & y_{n-1} & y_n \\ 0 & \ldots & 0 & x_{p+2}\, y_{p+2} & \ldots & x_{n-1}\, y_{n-1} & x_n\, y_n \\ 0 & \ldots & 0 & x_{p+2}^2\, y_{p+2} & \ldots & x_{n-1}^2\, y_{n-1} & x_n^2\, y_n \\ \vdots & & \vdots & \vdots & & \vdots & \vdots \\ 0 & \ldots & 0 & x_{p+2}^{p-1}\, y_{p+2} & \ldots & x_{n-1}^{p-1} y_{n-1} & x_n^{p-1} y_n \\ 0 & \ldots & 0 & y_{p+2}^2 & \ldots & y_{n-1}^2 & y_n^2 \\ 0 & \ldots & 0 & x_{p+2}\, y_{p+2}^2 & \ldots & x_{n-1}\, y_{n-1}^2 & x_n y_n^2 \\ \vdots & & \vdots & \vdots & & \vdots & \vdots \\ 0 & \ldots & 0 & y_{p+2}^p & \ldots & y_{n-1}^p & y_n^p \end{vmatrix} = \left| \begin{array}{c|c} V^{(r)} & Z \\ \hline & M^{(p-1)} \end{array} \right| \tag{3.4}$$

The lower left block will be zero because of the condition set. Using the Laplace

expansion rule we obtain

$$W^{(p)} = (-1)^{t_p} V^{(p)} M^{(p-1)} \tag{3.5}$$

where $V^{(p)} = V(x_1, x_2, \ldots, x_p)$, that is, the Vandermonde determinant. We can now factor out y_k from the determinant $M^{(p-1)}$ per column ($k = p + 2, \ldots, n$), whereafter $W^{(p)}$ may be written as

$$W^{(p)} = (-1)^{t_p} V^{(p)} y_{p+2} y_{p+3} \ldots y_n (-1)^{t_{p-1}} W^{(p-1)}. \tag{3.6}$$

If we introduce

$$G^{(p)} = (-1)^{t_p + t_{p-1}} V^{(p)} \prod_{k=p+2}^{n} y_k, \tag{3.7}$$

then

$$W^{(p)} = G^{(p)} W^{(p-1)}.$$

$G^{(p)}$ is not zero as the Vandermonde determinant does not disappear at the different values and since, according to our condition, the y_k co-ordinates are also other than zero if $p + 2 \leq k \leq n$. Thereby the statement III^0 has also been verified.

4. Construction of a regular point pattern

If a pattern includes, after the omission of a $p + 1$ number of points, p points on a straight line, then the process described under III^0 may be continued: let us assume a pattern structure where each "residual" r-th-degree pattern contains $r + 1$ points readily fitted on a straight line. In this case the $W^{(p)}$ determinant is

$$W^{(p)} = G^{(p)} G^{(p-1)} \ldots G^{(1)} W^{(0)} \tag{4.1}$$

and it is obvious that $W^{(0)} = 1$.

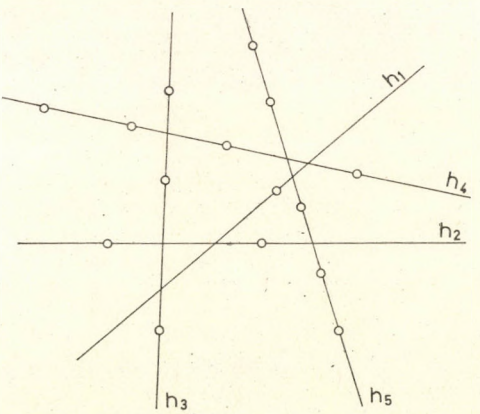

Fig. 1

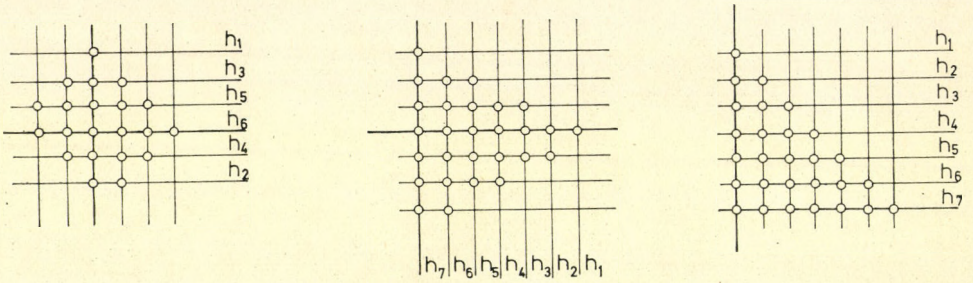

Fig. 2

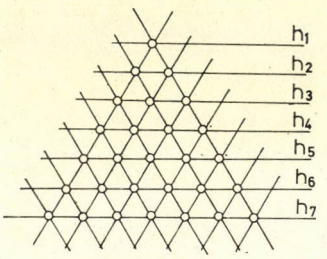

Fig. 3

Reverting the process, and starting from a 0-th-degree regular pattern consisting of a single point, a p-th-degree regular point pattern can be obtained in $p + 1$ steps. The general (k-th) step of this process will be to assume a straight line (h_k), and a number of k points thereon ($k = 1, 2, \ldots, p + 1$).

The straight lines assumed in the individual steps must obviously differ, and the points assumed in the previous steps certainly cannot be fitted to the lines assumed in the next steps.

Fig. 1 illustrates a fourth-degree pattern obtained with the method described above, in the case of an irregular grating. Figs 2 and 3 show fifth and sixth-degree patterns, respectively, obtained with regular gratings.

REFERENCES

1. Booth, A. D.: Numerical Methods — Butterworths Scientific Publications, London 1957
2. Collatz, L.: Numerical Treatment of Differential Equations — Springer Verlag, Berlin—Göttingen—Heidelberg 1960
3. Davis, Ph. J.: Interpolation and Approximation — Blaisdell Publishing Co, New York, Toronto, London 1965
4. Fekete, S.: Numerical Generation of Differential Operators — *NIM Számítástechnikai Közlemények* **12** (1968) (in Hungarian)
5. Gelfand, I. M.: Linear Algebra Lectures — Akadémiai Kiadó, Budapest 1955 (in Hungarian)
6. Holnapy, D.: New Numerical Method for the Mechanical Calculation of Surface Structures — Cand. Thesis, Budapest 1970

7. KANTOROVITCH, L. V.—KRYLOV, V. I.: Approximation Methods for Higher-order Analysis — Akadémiai Kiadó, Budapest 1953 (Hungarian translation)
8. KOROVKIN, P. P.: Linear Operators and Approximation Theory — Hindustan Publishing Corp., Delhi 1960
9. KUNZ, K. S.: Numerical Analysis — McGraw-Hill Book Co Inc, New York—Toronto—London 1957
10. RALSTON, A.: Introduction to Numerical Analysis — Műszaki Könyvkiadó, Budapest 1969 (Hungarian translation)
11. STEFFENSEN, J. F.: Interpolation — Chelsea Publishing Co, New York 1950
12. THIELE, T. N.: Interpolationsrechnung — Commission von B. G. Teubner, Leipzig 1909

Zweckmäßige Festlegung der Grundpunkte für die Lagrangesche Interpolation bei zwei Variablen. Die Arbeit untersucht die Lagrangesche Interpolation für zwei Veränderliche vom Standpunkt der Unizität des interpolierenden Polynoms. Der Begriff eines solchen Punktsystems wird definiert (reguläres Punktsystem), für welches die Interpolation eindeutig durchgeführt werden kann. Die Eigenschaften des regulären Punktsystems werden untersucht und ein praktisches Verfahren für die Darstellung eines solchen Punktsystems wird gezeigt. Als Beispiele für die Anwendung der Methode werden einige reguläre Interpolationspunktsysteme gezeigt.

Целесообразное принятие интерполяционных опорных точек в случае интерполяции Лагранжа с двумя переменными. В работе интерполяция Лагранжа с двумя переменными исследуется с точки зрения инцитивности интерполирующего полинома. Определяется понятие такого точечного отображения (регулярное точечное отображение), на котором можно однозначно произвести интерполирование. Анализируются свойства регулярных точечных отображений, и описывается практический метод получения таких точечных отображений. В качестве примера применения метода приводится несколько регулярных интерполяционных точечных отображений.

Acta Technica Academiae Scientiarum Hungaricae, Tomus 76 (3—4), pp. 435—451 (1974)

CIRCULAR PLATE FOUNDATIONS OF SPHERICAL GAS TANKS ON POINT SUPPORTS

GY. MÁRKUS*
CANDIDATE OF TECHN. SCIENCES

[Manuscript received Dec. 8, 1971]

The paper gives the solution for a fundament circular plate on the undersoil, which is loaded by an eccentric force. The results may be used for the calculation of circular ground plates of buildings, tanks, towers, resting on columns, or point supports, also in the case when the arbitrarily situated columns pass onto the plate forces of different magnitudes resulting from wind pressure.

Spherical steel gas tanks are very often supported by bars situated in planes tangential to the middle surface of the shell. It is practical to transmit the load onto the bars by insetting a fundamental circular plate of reinforced concrete on the undersoil (Fig. 1). The supports pass on to the ground plate forces of different magnitudes resulting from wind pressure.

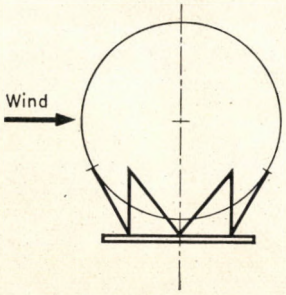

Fig. 1

We may consider as solved the play of forces on the plate if we know the internal forces of the circular plate under one concentrated load. We must apply superposition in case of some loads. We assume the distribution of the ground reaction as varying linearly (Fig. 2).

The problem of a circular plate under a concentrated load was solved by A. CLEBSCH [1]. The simply supported and clamped circular plates were treated by A. FÖPPL [2]. The problem when a circular ring plate is clamped along the inner edge and loaded by a concentrated force at the outer boundary was worked out by H. REISSNER [3]. We followed the above-named authors

* Dr. GY. MÁRKUS, Süveg u. 4/a, 1112 Budapest, Hungary

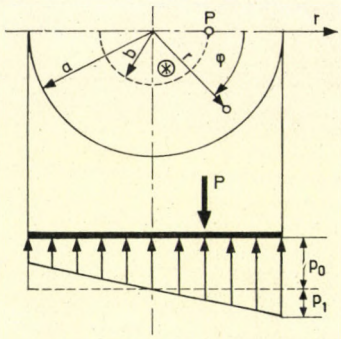

Fig. 2

in the solution of our task and will discuss the problem in the polar co-ordinate system r and φ. The final result obtained in such a system may be programmed more simply on an electronic computer — assuming the determination of stress conditions in several points — than in bipolar coordinates, in which the problem is also solved by E. MELAN [4], W. FLÜGGE [5] and H. SCHMIDT [6].

We composed the circular plate as having radius a of an inner circular plate having radius b and an outer circular ring plate of radii b, a. The concentrated force P is applied at distance b from the centre at the angle $\varphi = 0$. We will give its representation in form of an infinite Fourier's series written along the dividing circle:

$$p(\varphi) = \frac{P}{b\pi}\left(\frac{1}{2} + \sum_{m=1}^{\infty} \cos m\varphi\right), \quad (m = 1, 2, 3, \ldots). \tag{1}$$

The ground reaction p consists of a uniformly distributed member p_0 and a linearly varying antisymmetrical load p_1, depending on the place of the concentrated force P:

$$p = p_0 + p_1 \frac{r}{a} \cos \varphi\,, \tag{2}$$

where

$$p_0 = -\frac{P}{a^2\pi} \quad \text{and} \quad p_1 = -\frac{4bP}{a^3\pi}\,. \tag{3}$$

The differential equation of the circular plate of uniform thickness may be written in polar co-ordinates in the following well-known form:

$$\Delta\Delta w = \left(\frac{\partial^2}{\partial r^2} + \frac{1}{r}\frac{\partial}{\partial r} + \frac{1}{r^2}\frac{\partial r}{\partial \varphi^2}\right)\left(\frac{\partial w}{\partial r^2} + \frac{1}{r}\frac{\partial w}{\partial r} + \frac{1}{r^2}\frac{\partial^2 w}{\partial \varphi^2}\right) = \frac{p}{K}\,, \tag{4}$$

where K is the so-called flexural rigidity of the plate as follows:

$$K = \frac{Eh^3}{12(1-\mu^2)}\,. \tag{5}$$

The general solution of the above-mentioned inhomogeneous equation of the outer circular ring plate can be taken in the form of the following series:

$$w = w_0 + w_1 + \sum_{m=2}^{\infty} w_m, \quad (m = 2, 3, 4 \ldots), \tag{6}$$

in which, instead of r and b, with dimensionless quantities

$$\varrho = \frac{r}{a}; \quad \beta = \frac{b}{a}, \tag{7}$$

$$\begin{aligned} w_0 &= \frac{p_0 a^4 \varrho^4}{64K} + A_0 + B_0 \varrho^2 + C_0 \ln \varrho + D_0 \varrho^2 \ln \varrho , \\ w_1 &= \left(\frac{p_1 a^4 \varrho^5}{192K} + A_1 \varrho + B_1 \varrho^3 + C_1 \varrho^{-1} + D_1 \varrho \ln \varrho \right) \cos \varphi , \\ w_m &= (A_m \varrho^m + B_m \varrho^{m+2} + C_m \varrho^{-m} + D_m \varrho^{-m+2}) \cos m\varphi . \end{aligned} \tag{8}$$

The constants A, B, C, D in these expressions must be determined from the boundary conditions. It may be seen in the formulas that from the foot indexes

0 signify the symmetry,
1 the antisymmetry and
m the period above one

of the periodical function. Now, with the deflection w we can express the slopes ϑ_r and ϑ_φ; the bending and twisting moments M_r, M_φ, $M_{r\varphi}$; the shearing force Q_r; and the reactive force V_r with the aid of the customary relations:

$$\left.\begin{aligned} \vartheta_r &= -\frac{1}{a}\frac{\partial w}{\partial \varrho} = \vartheta_{r0} + \vartheta_{r1} + \sum_{m=2}^{\infty} \vartheta_{rm}, \\ \vartheta_{r0} &= -\frac{1}{a}\left[\frac{p_0 a^4 \varrho^3}{16K} + 2B_0 \varrho + C_0 \varrho^{-1} + D_0 \varrho(1 + 2 \ln \varrho) \right], \\ \vartheta_{r1} &= -\frac{1}{a}\left[\frac{5p_1 a^4 \varrho^4}{192\,K} + A_1 + 3B_1 \varrho^2 - C_1 \varrho^{-2} + D_1(1 + \ln \varrho) \right] \cos \varphi , \\ \vartheta_{rm} &= -\frac{1}{a}\Big[m A_m \varrho^{m-1} + (m+2) B_m \varrho^{m+1} - \\ &\qquad - m C_m \varrho^{-m-1} - (m-2) D_m \varrho^{-m+1} \Big] \cos m\varphi , \\ \vartheta_\varphi &= -\frac{1}{a\varrho}\frac{\partial w}{\partial \varphi} = \vartheta_{\varphi 0} + \vartheta_{\varphi 1} + \sum_{m=2}^{\infty} \vartheta_{\varphi m}, \\ \vartheta_{\varphi 0} &= 0 , \end{aligned}\right\} \tag{9a}$$

$$\left.\begin{aligned}
\vartheta_{\varphi 1} &= \frac{1}{a}\left(\frac{p_1 a^4 \varrho^4}{192\,K} + A_1 + B_1\varrho^2 + C_1\varrho^{-2} + D_1 \ln\varrho\right)\sin\varphi\,,\\
\vartheta_{\varphi m} &= \frac{m}{a}\left(A_m\varrho^{m-1} + B_m\varrho^{m+1} + C_m\varrho^{-m-1} + D_m\varrho^{-m+1}\right)\sin m\varphi\,,\\
M_r &= -\frac{K}{a^2}\left[\frac{\partial^2 w}{\partial\varrho^2} + \mu\left(\frac{1}{\varrho}\,\frac{\partial w}{\partial\varrho} + \frac{1}{\varrho^2}\,\frac{\partial^2 w}{\partial\varphi^2}\right)\right] =\\
&= M_{r0} + M_{r1} + \sum_{m=2}^{\infty} M_{rm}\,,\\
M_{r0} &= -\frac{K}{a^2}\left\{(3+\mu)\,\frac{p_0 a^4\varrho^2}{16\,K} + 2(1+\mu)B_0 - (1-\mu)\,C_0\varrho^{-2} +\right.\\
&\qquad \left. + [3+\mu+2(1+\mu)\ln\varrho]D_0\right\},\\
M_{r1} &= -\frac{K}{a^2}\left[(5+\mu)\,\frac{p_1 a^4\varrho^3}{48\,K} + 2(3+\mu)B_1\varrho + 2(1-\mu)C_1\varrho^{-3} +\right.\\
&\qquad \left. + (1+\mu)\,D_1\varrho^{-1}\right]\cos\varphi,\\
M_{rm} &= -\frac{K}{a^2}\left\{(1-\mu)m(m-1)A_m\varrho^{m-2} + (m+1)[m+\right.\\
&\qquad + 2 - \mu(m-2)]B_m\varrho^m + (1-\mu)m(m+1)\,C_m\varrho^{-m-2} +\\
&\qquad \left. + (m-1)[m-2-\mu(m+2)]D_m\varrho^{-m}\right\}\cos m\varphi\,,\\
M_\varphi &= -\frac{K}{a^2}\left(\frac{1}{\varrho}\,\frac{\partial w}{\partial\varrho} + \frac{1}{\varrho^2}\,\frac{\partial^2 w}{\partial\varphi^2} + \mu\,\frac{\partial^2 w}{\partial\varrho^2}\right) =\\
&= M_{\varphi 0} + M_{\varphi 1} + \sum_{m=2}^{\infty} M_{\varphi m}\,,\\
M_{\varphi 0} &= -\frac{K}{a^2}\left\{(1+3\mu)\,\frac{p_0 a^4\varrho^2}{16\,K} + 2(1+\mu)B_0 + (1-\mu)C_0\varrho^{-2} +\right.\\
&\qquad \left. + [1+3\mu+2(1+\mu)\ln\varrho]D_0\right\},\\
M_{\varphi 1} &= -\frac{K}{a^2}\left[(1+5\mu)\,\frac{p_1 a^4\varrho^3}{48\,K} + 2(1+3\mu)B_1 - 2(1-\mu)C_1\varrho^{-3} +\right.\\
&\qquad \left. + (1+\mu)\,D_1\varrho^{-1}\right]\cos\varphi\,,
\end{aligned}\right\} \quad (9b)$$

$$
\left.
\begin{aligned}
M_{\varphi m} &= -\frac{K}{a^2}\{-(1-\mu)m(m-1)A_m\varrho^{m-2} + (m+1)\times \\
&\times[\mu(m+2) - m + 2]B_m\varrho^m - (1-\mu)\,m\,(m+1)\times \\
&\times C_m\,\varrho^{-m-2} + (m-1)[\mu(m-2) - m - 2]D_m\varrho^{m-}\}\cos m\varphi,
\end{aligned}
\right.
$$

$$
M_{r\varphi} = -(1-\mu)\frac{K}{a^2}\left(\frac{1}{\varrho}\,\frac{\partial^2 w}{\partial\varrho\,\partial\varphi} - \frac{1}{\varrho^2}\,\frac{\partial w}{\partial\varphi}\right) =
$$

$$
= M_{r\varphi 0} + M_{r\varphi 1} + \sum_{m=2}^{\infty} M_{r\varphi m}\,,
$$

$$
M_{r\varphi 0} = 0,
$$

$$
M_{r\varphi 1} = (1-\mu)\frac{K}{a^2}\left(\frac{p_1 a^4 \varrho^3}{48\,K} + 2B_1\varrho - 2C_1\varrho^{-3} + D_1\varrho^{-1}\right)\sin\varphi\,,
$$

$$
M_{r\varphi m} = (1-\mu)\frac{K}{a^2}\,m\,[(m-1)A_m\varrho^{m-2} + (m+1)\,B_m\varrho^m -
$$

$$
-(m+1)\,C_m\varrho^{-m-2} - (m-1)D_m\varrho^{-m}]\sin m\varphi\,,
$$

$$
Q_r = -\frac{K}{a^3}\left(\frac{\partial^3 w}{\partial\varrho^3} + \frac{1}{\varrho}\,\frac{\partial^2 w}{\partial\varrho^2} - \frac{1}{\varrho^2}\,\frac{\partial w}{\partial\varrho} - \frac{2}{\varrho^3}\,\frac{\partial^2 w}{\partial\varphi^2} + \frac{1}{\varrho^2}\,\frac{\partial^3 w}{\partial r\,\partial\varphi^2}\right) =
$$

$$
= Q_{r0} + Q_{r1} + \sum_{m=2}^{\infty} Q_{rm}\,, \qquad \text{(9c)}
$$

$$
Q_{r0} = -\frac{K}{a^3}\left(\frac{p_0 a^4\,\varrho}{2K} + 4D_0\,\varrho^{-1}\right),
$$

$$
Q_{r1} = -\frac{K}{a^3}\left(\frac{3p_1 a^4\,\varrho^2}{8K} + 8B_1 + 2D_1\varrho^{-2}\right)\cos\varphi\,,
$$

$$
Q_{rm} = -\frac{4K}{a^3}\,m[(m+1)B_m\varrho^{m-1} + (m-1)D_m\varrho^{-m-1}]\cos m\varphi\,,
$$

$$
V_r = \mp\frac{K}{a^3}\left(\frac{\partial^3 w}{\partial\varrho^3} + \frac{1}{\varrho}\,\frac{\partial^2 w}{\partial\varrho^2} - \frac{1}{\varrho^2}\,\frac{\partial w}{\partial\varrho} + \frac{2-\mu}{\varrho^2}\,\frac{\partial^3 w}{\partial\varrho\,\partial\varphi^2} -
$$

$$
-\frac{3-\mu}{\varrho^3}\,\frac{\partial^2 w}{\partial\varphi^2}\right) = V_{r0} + V_{r1} + \sum_{m=2}^{\infty} V_{rm}\,,
$$

$$
V_{r0} = \pm\frac{K}{a^3}\left(\frac{p_0 a^4\,\varrho}{2K} + 4D_0\varrho^{-1}\right),
$$

$$
V_{r1} = \pm\frac{K}{a^3}\left[(17+\mu)\,\frac{p_1 a^4\,\varrho^2}{48K} + 2(3+\mu)B_1 + 2(1-\mu)C_1\varrho^{-4} -\right.
$$

$$
\left.-(3-\mu)\,D_1\varrho^{-2}\right]\cos\varphi\,,
$$

$$V_{rm}=\pm\frac{K}{a^3}m\{-(1-\mu)m(m-1)A_m\varrho^{m-3}+(m+1)\times \\ \times[4-(1-\mu)m]B_m\varrho^{m-1}+(1-\mu)m(m+1)C_m\varrho^{-m-3}+ \\ +(m-1)[4+(1-\mu)m]D_m\varrho^{-m-1}\}\cos m\varphi\,. \tag{9d}$$

We have found double signs in the expression of the reactive force. The upper sign refers to the boundary form farther off the centre, the lower one to the nearer, namely, we call the reaction force operating upwards form to be below positive. Similar expressions may be written for the inner portion of the circular plate of radius b, too. There we apply an asterisk foot index in all formulas for the sake of distinction. From the condition that the deflection, the slope and the moments must be finite at the centre of the plate, we obtain

$$\begin{aligned} C_{*0}&=D_{*0}=0,\\ C_{*1}&=D_{*1}=0,\\ C_{*m}&=D_{*m}=0. \end{aligned} \tag{10}$$

Our next task is to determine the missing six integration constants. The six equations needed for this determination can be obtained from the boundary conditions at the edge of the plate and from the continuity conditions along the circle of radius b. The outer edge of the plate is assumed to be free, therefore the corresponding boundary conditions are:

$$1\ldots\ (M_r)_{\varrho=1}=0; \qquad 2\ldots\ (V_r)_{\varrho=1}=0. \tag{11}$$

Accordingly, the conditions are in detail:

$$1\ldots(3+\mu)\frac{p_0a^4}{16K}+2(1+\mu)B_0-(1-\mu)C_0+(3+\mu)D_0+ \\ +\left[(5+\mu)\frac{p_1a^4}{48K}+2(3+\mu)B_1+2(1-\mu)C_1+(1+\mu)D_1\right]\cos\varphi+ \\ +\sum_{m=2}^{\infty}\{(1-\mu)m(m-1)A_m+(m+1)[m+2-\mu(m-2)]B_m+ \\ +(1-\mu)m(m+1)C_m+(m-1)[m-2-\mu(m+2)]D_m\}\cos m\varphi=0,$$

$$2\ldots\frac{p_0a^4}{2K}+4D_0+ \\ +\left[(17+\mu)\frac{p_1a^4}{38K}+2(3+\mu)B_1+2(1-\mu)C_1-(3-\mu)D_1\right]\cos\varphi+ \\ +\sum_{m=2}^{\infty}\{-(1-\mu)m^2(m-1)A_m+m(m+1)[4-(1-\mu)m]B_m+ \\ +(1-\mu)m^2(m+1)C_m+m(m-1)[4+(1-\mu)m]D_m\}\cos m\varphi=0\,. \tag{12}$$

The edges of the circular and annular plates connected along the circle of radius b undergo the same deformation, consequently, the boundary conditions are:

$$3 \ldots (w)_{\varrho=\beta} = (w_*)_{\varrho=\beta}\,; \qquad 4 \ldots \left(\frac{\partial w}{\partial \varrho}\right)_{\varrho=\beta} = \left(\frac{\partial w}{\partial \varrho}\right)_{\varrho=\beta}. \tag{13}$$

These conditions are also written as:

$$\begin{aligned}
3 \ldots & \frac{p_0 a^4 \beta^4}{64K} + A_0 + B_0 \beta^2 + C_0 \ln \beta + D_0 \beta^2 \ln \beta + \\
& + \left(\frac{p_1 a^4 \beta^5}{192K} + A_1 \beta + B_1 \beta^3 + C_1 \beta^{-1} + D_1 \beta \ln \beta\right) \cos \varphi + \\
& + \sum_{m=2}^{\infty} (A_m \beta^m + B_m \beta^{m+2} + C_m \beta^{-m} + D_m \beta^{-m+2}) \cos m\varphi = \\
& = \frac{p_0 a^4 \beta^4}{64K} + A_{*0} + B_{*0} \beta^2 + \\
& + \left(\frac{p_1 a^4 \beta^5}{192K} + A_{*1} \beta + B_{*1} \beta^3\right) \cos \varphi + \\
& + \sum_{m=2}^{\infty} (A_{*m} \beta^m + B_{*m} \beta^{m+2}) \cos m\varphi\,, \qquad (14) \\
4 \ldots & \frac{p_0 a^4 \beta^3}{16K} + 2B_0 \beta + C_0 \beta^{-1} + D_0 \beta(1 + 2 \ln \beta) + \\
& + \left[\frac{5p_1 a^4 \beta^4}{192K} + A_1 + 3B_1 \beta^2 - C_1 \beta^{-2} + D_1(1 + \ln \beta)\right] \cos \varphi + \\
& + \sum_{m=2}^{\infty} \left[mA_m \beta^{m-1} + (m+2) B_m \beta^{m+1} - mC_m \beta^{-m-1} - \right. \\
& \left. - (m-2) D_m \beta^{-m+1}\right] \cos m\varphi = \frac{p_0 a^4 \beta^3}{16K} + 2B_{*0} \beta + \\
& + \left[\frac{5p_1 a^4 \beta^4}{192K} + A_{*1} + 3B_{*1} \beta^2\right] \cos \varphi + \\
& + \sum_{m=2}^{\infty} \left[mA_{*m} \beta^{m-1} + (m+2) B_{*m} \beta^{m+1}\right] \cos m\varphi\,.
\end{aligned}$$

Since there are no external moments applied along the circle of radius b, the second-grade differential quotients must be identical along the neighbouring edges

$$5 \ldots \left(\frac{\partial^2 w}{\partial \varrho^2}\right)_{\varrho=\beta} = \left(\frac{\partial^2 w_*}{\partial \varrho^2}\right)_{\varrho=\beta}. \tag{15}$$

The last equation is obtained from the consideration that the difference of the shearing forces along the dividing circle represents the external concentrated load P:

$$6\ldots - (Q_r)_{\varrho=\beta} + (Q_{r*})_{\varrho=\beta} = \frac{P}{a\beta\pi}\left(\frac{1}{2} + \sum_{m=1}^{\infty}\cos m\varphi\right). \tag{16}$$

Let us write the fifth and sixth boundary conditions also in the form of equations:

$$\begin{aligned}
5\ldots\ & \frac{3p_0 a^4\beta^2}{16K} + 2B_0 - C_0\beta^{-2} + D_0(3 + 2\ln\beta) + \\
& + \left(\frac{5p_1 a^4\beta^3}{48K} + 6B_1\beta + 2C_1\beta^{-3} + D_1\beta^{-1}\right)\cos\varphi + \\
& + \sum_{m=2}^{\infty}\left[m(m-1)A_m\beta^{m-2} + (m+1)(m+2)B_m\beta^m + \right. \\
& \left. + m(m+1)C_m\beta^{-m-2} + (m-1)(m-2)D_m\beta^{-m}\right]\cos m\varphi = \\
& = \frac{3p_0 a^4\beta^2}{16K} + 2B_{*0} + \left(\frac{5p_1 a^4\beta^3}{48K} + 6B_{*1}\beta\right)\cos\varphi + \\
& + \sum_{m=2}^{\infty}\left[m(m-1)A_{*m}\beta^{m-2} + (m+1)(m+2)B_{*m}\beta^m\right]\cos m\varphi\,,
\end{aligned} \tag{17}$$

$$\begin{aligned}
6\ldots\ & \frac{p_0 a^4\beta}{2K} + 4D_0\beta^{-1} + \left(\frac{3p_1 a^4\beta^2}{8K} + 8B_1 + 2D_1\beta^{-2}\right)\cos\varphi + \\
& + 4\sum_{m=2}^{\infty}\left[m(m+1)B_m\beta^{m-1} + m(m-1)D_m\beta^{-m-1}\right]\cos m\varphi - \\
& - \frac{p_0 a^4\beta}{2K} - \left(\frac{3p_1 a^4\beta^2}{8K} + 8B_{*1}\right)\cos\varphi - \\
& - 4\sum_{m=2}^{\infty}\left[m(m+1)B_{*m}\beta^{m-1}\right]\cos m\varphi = \frac{P}{a\beta\pi}\left(\frac{1}{2} + \sum_{m=1}^{\infty}\cos m\varphi\right).
\end{aligned}$$

We have found after the substitution of p_0 and p_1, the execution of abbreviations and arrangement of the equations, that each two of the present equations identify the members with foot indices 0 and 1, and according to the given conditions, are not sufficient for determining the integration constants. We can obtain a further equation for the integration constants with foot indices 0 and 1 if we stipulate that the boundary of the plate of radius a

cannot deflect in case of symmetrically and antisymmetrically distributed loads (rigid body displacement):

$$7\ldots\ (w_0)_{\varrho=1} = 0; \qquad (w_1)_{\varrho=1} = 0. \tag{18}$$

This means after all that the plate has no initial deflection. We obtain the following equations after detailed inscription:

$$\begin{aligned} 7\ldots\ &\frac{p_0 a^4}{64K} + A_0 + B_0 = 0\ ; \\ &\frac{p_1 a^4}{192K} + A_1 + B_1 + C_1 = 0\ . \end{aligned} \tag{19}$$

Hereupon there is no difficulty in solving the equations of conditions. The obtained integration constants are:

$$0 \leqq \varrho \leqq \beta$$

$$A_{*0} = \frac{Pa^2}{8K\pi}\left[7 + 3\mu - 4(3+\mu)\beta^2 + 8(1+\mu)\beta^2 \ln \beta\right]\frac{1}{8(1+\mu)}\ ,$$

$$B_{*0} = \frac{Pa^2}{8K\pi}\left[1 + 3\mu + 2(1-\mu)\beta^2 + 4(1+\mu)\ln \beta\right]\frac{1}{4(1+\mu)}\ ,$$

$$C_{*0} = D_{*0} = 0\ ,$$

$$A_{*1} = \frac{Pa^2}{8K\pi}\left[4(1+\mu) + 12(3+\mu)\ln \beta + 3(1-\mu)\beta^2\right]\frac{-\beta}{6(3+\mu)}\ ,$$

$$B_{*1} = \frac{Pa^2}{8K\pi}\left[8(2+\mu) + 3(1-\mu)\beta^2 - 3(3+\mu)\beta^{-2}\right]\frac{\beta}{6(3+\mu)}\ , \tag{20}$$

$$C_{*1} = D_{*1} = 0\ ,$$

$$A_{*m} = \frac{Pa^2}{8K\pi}\left[\frac{4-(1-\mu)m}{(3+\mu)m}(m\beta^2 - m - 1) + \frac{4+(1-\mu)m}{m(1-\mu)} - \beta^2 + \beta^{-2m+2}\right]\frac{\beta^m}{m(m-1)}\ ,$$

$$B_{*m} = \frac{Pa^2}{8K\pi}\left[\frac{1-\mu}{3+\mu}(m\beta^2 - m - 1) - \beta^{-2m}\right]\frac{\beta^m}{m(m+1)}\ ,$$

$$C_{*m} = D_{*m} = 0\ .$$

$$\beta \leq \varrho \leq 1$$

$$A_0 = \frac{Pa^2}{8K\pi}\left[7 + 3\mu - 4(1-\mu)\beta^2\right]\frac{1}{8(1+\mu)},$$

$$B_0 = \frac{Pa^2}{8K\pi}\,\frac{2(1-\mu)\beta^2 - (3+\mu)}{4(1+\mu)},$$

$$C_0 = \frac{Pa^2}{8K\pi}\beta^2, \qquad D_0 = \frac{Pa^2}{8K\pi},$$

$$A_1 = \frac{Pa^2}{8K\pi}\left[4(1+\mu) + 3(1-\mu)\beta^2\right]\frac{-\beta}{6(3+\mu)},$$

$$B_1 = \frac{Pa^2}{8K\pi}\left[8(2+\mu) + 3(1-\mu)\beta^2\right]\frac{\beta}{6(3+\mu)},$$

$$C_1 = \frac{Pa^2}{8K\pi}\left(-\frac{\beta^3}{2}\right), \qquad D_1 = \frac{Pa^2}{8K\pi}(-2\beta), \tag{21}$$

$$A_m = \frac{Pa^2}{8K\pi}\left[\frac{4-(1-\mu)m}{(3+\mu)m}(m\beta^2 - m - 1) + \right.$$

$$\left. + \frac{4+(1-\mu)m}{(1-\mu)m} - \beta^2\right]\frac{\beta^m}{m(m-1)},$$

$$B_m = \frac{Pa^2}{8K\pi}\,\frac{(1-\mu)(m\beta^2 - m - 1)}{(3+\mu)m(m+1)}\beta^m,$$

$$C_m = \frac{Pa^2}{8K\pi}\,\frac{-\beta^{m+2}}{m(m+1)}, \qquad D_m = \frac{Pa^2}{8K\pi}\,\frac{\beta^m}{m(m-1)}.$$

We can calculate every statical quantity with the aid of the integration constants.

We had a computer programme made to obtain numerical results and to study the kind of convergence of the series. We prescribed to get a certain accuracy in the results. If this accuracy was not attainable at the points near the dividing circle, we took no more then fifty members of the series into consideration.

Table I and the Fig. 3 show the bending moments belonging to the ratio $\beta = 0{,}7$ in case of $\mu = 1/6$. Such a circular plate is especially suitable for founding a building which stands on six bars at an equal distance from each other (Fig. 4), namely, the negative and positive field bending moments have the same order of magnitude. Table II and the Fig. 5 give the moments in this case.

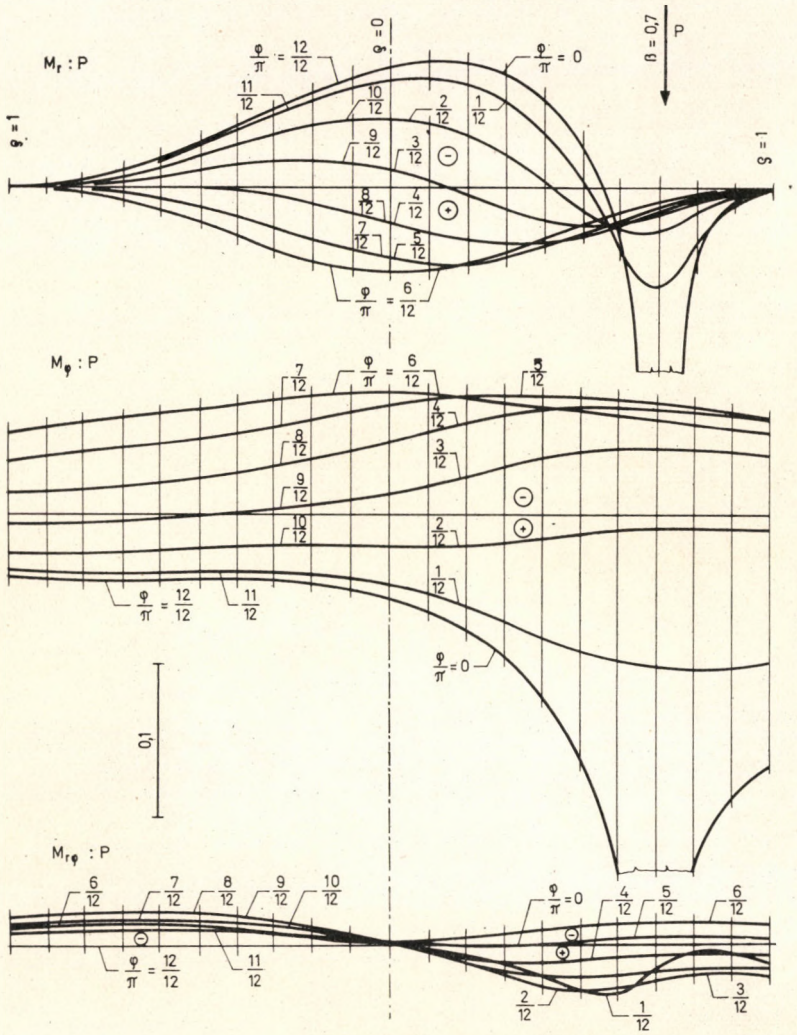

Fig. 3

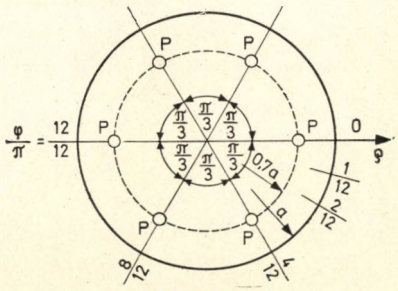

Fig. 4

Table I

$\beta = 0{,}7$	$w : \frac{Pa^2}{K}$ $M_r : P$ $M_\varphi : P$ $M_{r\varphi} : P$										
$\varphi : \pi$ \ ϱ	0	0,1	0,2	0,3	0,4	0,5	0,6	0,7	0,8	0,9	1,0
0	−0,0014	+0,0002	+0,0027	+0,0063	+0,0109	+0,0162	+0,0221	+0,0280	+0,0327	+0,0371	+0,0419
	−0,0813	−0,0854	−0,0847	−0,0777	−0,0612	−0,0298	+0,0333	+0,3411	+0,0492	+0,0052	0
	+0,0554	+0,0640	+0,0763	+0,0940	+0,1193	+0,1576	+0,2249	+0,4014	+0,2395	+0,1875	+0,1656
	0	0	0	0	0	0	0	0	0	0	0
$\frac{1}{12}$	−0,0014	+0,0001	+0,0024	+0,0056	+0,0095	+0,0140	+0,0186	+0,0231	+0,0271	+0,0310	+0,0349
	−0,0722	−0,0741	−0,0709	−0,0607	−0,0404	−0,0062	+0,0393	+0,0642	+0,0350	+0,0092	0
	+0,0462	+0,0523	+0,0606	+0,0711	+0,0828	+0,0926	+0,0944	+0,0986	+0,1021	+0,1021	+0,0973
	0	+0,0039	+0,0089	+0,0153	+0.0234	+0,0321	+0,0346	+0,0198	+0,0070	+0,0081	+0,0130
$\frac{2}{12}$	−0,0014	−0,0002	+0,0015	+0,0036	+0,0060	+0,0085	+0,0109	+0,0130	+0,0149	+0,0167	+0,0185
	−0,0471	−0,0444	−0,0367	−0,0234	−0,0052	+0,0136	+0,0250	+0,0267	+0,0134	+0,0040	0
	+0,0212	+0,0215	+0,0213	+0,0198	+0,0161	+0,0108	+0,0067	+0,0099	+0,0084	+0,0094	+0,0093
	0	+0,0065	+0,0141	+0,0224	+0,0298	+0,0337	+0,0318	+0,0262	+0,0219	+0,0209	+0,0221
$\frac{3}{12}$	−0,0014	−0,0006	+0,0003	+0,0011	+0,0017	+0,0020	+0,0021	+0,0018	+0,0013	+0,0007	−0,0001
	−0,0130	−0,0063	+0,0028	+0,0127	+0,0208	+0,0241	+0,0213	+0,0165	+0,0065	+0,0010	0
	−0,0130	−0,0180	−0,0241	−0,0311	−0,0378	−0,0427	−0,0450	−0,0430	−0,0445	−0,0434	−0,0420
	0	+0,0071	+0,0143	+0,0205	+0,0244	+0,0251	+0,0232	+0,0206	+0,0189	+0,0184	+0,0186
$\frac{4}{12}$	−0,0014	−0,0010	−0,0010	−0,0015	−0,0024	−0,0038	−0,0056	−0,0077	−0,0101	−0,0126	−0,0153
	+0,0212	+0,0281	+0,0338	+0,0364	+0,0347	+0,0290	+0,0208	+0,0129	+0,0047	+0,0004	0
	−0,0471	−0,0538	−0,0603	−0,0657	−0,0693	−0,0709	−0,0709	−0,0690	−0,0684	−0,0664	−0,0639
	0	+0,0056	+0,0102	+0,0130	+0,0138	+0,0128	+0,0110	+0,0094	+0,0087	+0,0088	+0,0090

	−0,0014	−0,0015	−0,0021	−0,0034	−0,0053	−0,0077	−0,0105	−0,0137	−0,0171	−0,0206	−0,0243
5/12	+0,0462	+0,0496	+0,0492	−0,0450	+0,0375	+0,0283	+0,0188	+0,0102	+0,0041	+0,0005	0
	−0,0722	−0,0762	−0,0789	−0,0799	−0,0794	−0,0779	−0,0760	−0,0739	−0,0714	−0,0688	−0,0660
	0	+0,0026	+0,0038	+0,0035	+0,0020	+0,0001	−0,0017	−0,0029	−0,0029	−0,0023	−0,0017
	−0,0014	−0,0018	−0,0028	−0,0045	−0,0067	−0,0093	−0,0123	−0,0156	−0,0190	−0,0226	−0,0263
6/12	+0,0554	+0,0534	+0,0479	+0,0401	+0,0311	+0,0222	+0,0143	+0,0070	+0,0033	+0,0006	0
	−0,0813	−0,0805	−0,0784	−0,0754	−0,0721	−0,0688	−0,0657	−0,0637	−0,0600	−0,0572	−0,0543
	0	−0,0009	−0,0029	−0,0056	−0,0084	−0,0108	−0,0125	−0,0133	−0,0128	−0,0117	−0,0107
	−0,0014	−0,0020	−0,0031	−0,0047	−0,0066	−0,0088	−0,0112	−0,0137	−0,0164	−0,0192	−0,0220
7/12	+0,0462	+0,0402	+0,0327	+0,0252	+0,0182	+0,0123	+0,0077	+0,0031	+0,0020	+0,0006	0
	−0,0722	−0,0672	−0,0620	−0,0571	−0,0527	−0,0489	−0,0455	−0,0437	−0,0400	−0,0375	−0,0352
	0	−0,0040	−0,0083	−0,0123	−0,0157	−0,0182	−0,0197	−0,0202	−0,0194	−0,0179	−0,0167
	−0,0014	−0,0021	−0,0031	−0,0041	−0,0053	−0,0063	−0,0078	−0,0091	−0,0105	−0,0119	−0,0133
8/12	+0,0212	+0,0144	+0,0088	+0,0046	+0,0019	+0,0004	−0,0000	−0,0009	+0,0004	+0,0005	0
	−0,0471	−0,0410	−0,0355	−0,0309	−0,0270	−0,0236	−0,0207	−0,0192	−0,0161	−0,0144	−0,0130
	0	−0,0060	−0,0114	−0,0158	−0,0192	−0,0215	−0,0227	−0,0229	−0,0219	−0,0204	−0,0190
	−0,0014	−0,0022	−0,0027	−0,0031	−0,0034	−0,0035	−0,0034	−0,0033	−0,0031	−0,0029	−0,0027
9/12	−0,0130	−0,0168	−0,0181	−0,0172	−0,0148	−0,0114	−0,0077	−0,0045	−0,0013	+0,0002	0
	−0,0130	−0,0090	−0,0057	−0,0028	−0,0003	+0,0019	+0,0040	+0,0053	+0,0071	+0,0080	+0,0084
	0	−0,0064	−0,0017	−0,0158	−0,0187	−0,0205	−0,0214	−0,0215	−0,0206	−0,0192	−0,0179
	−0,0014	−0,0022	−0,0024	−0,0021	−0,0014	−0,0004	+0,0008	+0,0023	+0,0039	+0,0055	+0,0072
10/12	−0,0471	−0,0460	−0,0420	−0,0361	−0,0289	−0,0213	−0,0140	−0,0074	−0,0028	−0,0000	0
	+0,0212	+0,0210	+0,0211	+0,0216	+0,0224	+0,0225	+0,0246	+0,0258	+0,0263	+0,0265	+0,0260
	0	−0,0054	−0,0095	−0,0126	−0,0147	−0,0160	−0,0165	−0,0165	−0,0158	−0,0147	−0,0138

$\beta = 0{,}7$	$w : \frac{Pa^2}{K}$ $M_r : P$ $M_\varphi : P$ $M_{r\varphi} : P$										
$\varphi : \pi$ \ ϱ	0	0,1	0,2	0,3	0,4	0,5	0,6	0,7	0,8	0,9	1,0
	−0,0014	−0,0021	−0,0021	−0,0013	−0,0000	+0,0018	+0,0039	+0,0062	+0,0088	+0,0114	+0,0141
11/12	−0,0722	−0,0666	−0,0584	−0,0487	−0,0383	−0,0279	−0,0182	−0,0092	−0,0037	−0,0002	0
	+0,0462	+0,0420	+0,0395	+0,0381	+0,0376	+0,0378	+0,0382	+0,0394	+0,0389	+0,0386	+0,0375
	0	−0,0030	−0,0053	−0,0069	−0,0080	−0,0087	−0,0090	−0,0089	−0,0085	−0,0080	−0,0075
	−0,0014	−0,0021	−0,0019	−0,0010	+0,0005	+0,0025	+0,0050	+0,0077	+0,0105	+0,0136	+0,0166
12/12	−0,0813	−0,0739	−0,0643	−0,0532	−0,0416	−0,0302	−0,0197	−0,0098	−0,0041	−0,0003	0
	+0,0554	+0,0496	+0,0460	+0,0439	+0,0430	+0,0428	+0,0430	+0,0441	+0,0433	+0,0428	+0,0415
	0	0	0	0	0	0	0	0	0	0	0

Table II

$\beta = 0{,}7$	$w : \frac{Pa^2}{K}$ $M_r : P$ $M_\varphi : P$ $M_{r\varphi} : P$										
$\varphi : \pi$ \ ϱ	0	0,1	0,2	0,3	0,4	0,5	0,6	0,7	0,8	0,9	1,0
0	−0,0086	−0,0083	−0,0074	−0,0059	−0,0040	−0,0018	−0,0004	+0,0020	+0,0021	+0,0017	+0,0013
	−0,0778	−0,0742	−0,0640	−0,0490	−0,0296	+0,0010	+0,0550	+0,3554	+0,0553	+0,0065	0
	−0,0778	−0,0760	−0,0694	−0,0554	−0,0303	+0,0114	+0,0847	+0,2693	+0,1136	+0,0686	+0,0533
	0	0	0	0	0	0	0	0	0	0	0
$\frac{1}{12}$	−0,0086	−0,0083	−0,0074	−0,0059	−0,0041	−00,0022	−0,0005	+0,0004	+0,0006	+0,0004	−0,0000
	−0,0778	−0,0741	−0,0627	−0,0438	−0,0169	+0,0192	+0,0612	+0,0804	+0,0425	+0,0113	0
	−0,0778	−0,0761	−0,0707	−0,0618	−0,0498	−0,0372	−0,0300	−0,0173	−0,0077	−0,0009	+0,0003
	0	+0,0000	+0,0003	+0,0017	+0,0060	+0,0134	+0,0168	+0,0044	−0,0075	−0,0059	−0,0011
$\frac{2}{12}$	−0,0086	−0,0083	−0,0073	−0,0059	−0,0042	−0,0033	−0,0012	−0,0006	−0,0005	−0,0008	−0,0013
	−0,0778	−0,0740	−0,0615	−0,0387	−0,0060	+0,0291	+0,0505	+0,0526	+0,0279	+0,0092	0
	−0,0778	−0,0761	−0,0720	−0,0680	−0,0670	−0,0691	−0,0688	−0,0559	−0,0506	−0,0426	−0,0378
	0	0	0	0	0	0	0	0	0	0	0

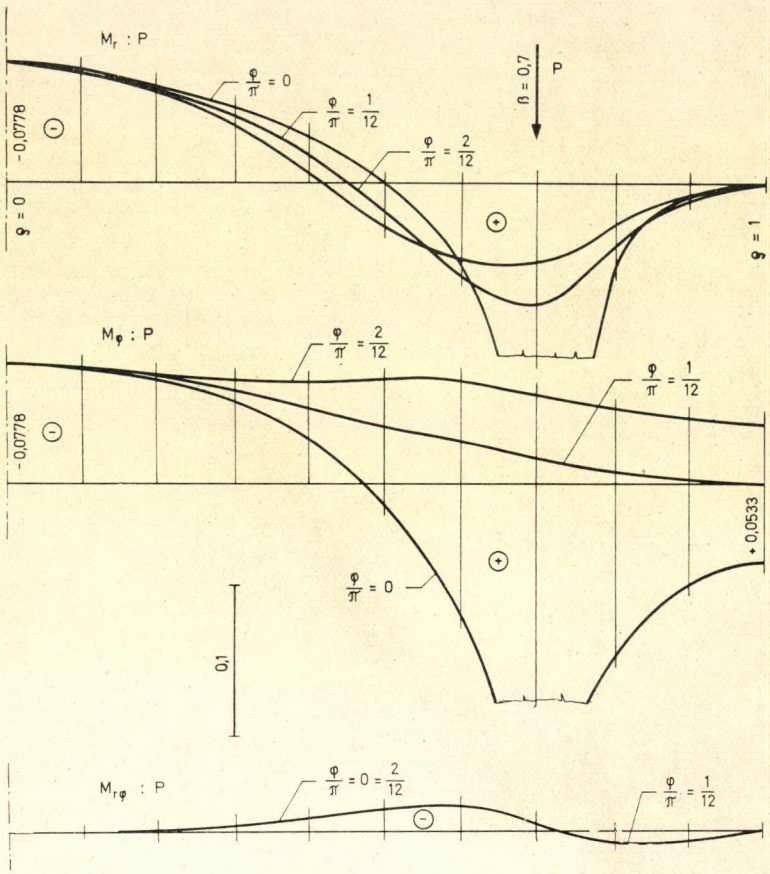

Fig. 5

REFERENCES

1. CLEBSCH, A.: Theorie der Elasticität fester Körper. Leipzig, Druck und Verlag von B. G. Teubner 1862
2. FÖPPL, A.: *Sitzber. Bayer. Akad. Wiss.* (1912), 155
3. REIßNER, H.: Über die unsymmetrische Biegung dünner Kreisringplatten. *Ingenieur-Archiv* **1** (1929), 72—83
4. MELAN, E.: *Eisenbau* (1920), 190
5. FLÜGGE, W.: Die strenge Berechnung von Kreisplatten unter Einzellasten mit Hilfe von krummlienigen Koordinaten und deren Anwendung auf die Pilzdecke. Verlag von Julius Springer, Berlin 1928
6. SCHMIDT, H.: *Ingenieur-Archiv.* **1** (1930), 147
7. TIMOSHENKO, S.—WOINOWSKY-KRIEGER, S.: Theory of Plates and Shells. Second Edition. McGraw-Hill Book Company, New York 1959

Kreisplatten-Fundamente von Kugelgasbehältern mit punktförmigen Abstützungen. Der Artikel gibt die Lösung einer auf den Untergrund gelegten Kreisplatte, welche einer exzentrischen Einzellast unterworfen wird. Die Ergebnisse können bei der Berechnung von

Kreisgrundplatten angewendet werden, welche auf Säulen oder punktförmigen Stützungen liegende Gebäude, Behälter oder Türme tragen, selbst im Falle wenn die nach Belieben gestellten Säulen zufolge der Windbelastung verschiedene Kräfte auf die Platte ausüben.

Круглая плита фундамента шарового газгольдера, покоящегося на точечных опорах. В статье дается решение круглых покоящихся на грунте, плит, на которые действует эксцентричная сосредоточенная сила. Результаты работы распространяются на решение задачи о расчете круглых плит в случае передачи на плиту нагрузки от колонн, а также сооружений, покоящихся на точенных опорах (резервуары, башни). Результаты работы также дают возможность рассчитывать круглые фундаментные плиты и при случае, когда вследствие ветровой нагрузки произвольно расположенные колонны передают на фундаментную плиту различные по величине силы.

INDEX

Verő J. A., 70 Jahre — For *Verő J. A.* 70th Anniversary 243

Mándi A. 1891—1972 249

Kalló, P.: Critical Summary of the Design Methods of Form-independent Thin Triplet Systems — Kritische Zusammenfassung der Entwurfsmethode der gestaltunabhängigen dünnen Schichten des Triplex — Критическое об-обшение метода проэктирования форманезависимой тоской системы триплета 255

Bitó, J. F.—Antal, K. G.: Examination of the Structure of Functional Relations among Physical Quantities and some Application thereof in Discharge Physics — Die Struktur von funktionellen Zusammenhängen zwischen physikalischen Größen und die Anwendung derselben in der Entladungsphysik — Исследования структуры функциональных зависимотей между физическими величинами и ее применение для газовых разрядов 257

Kollár, L.: Analysis of Double-Layer Space Trusses with Diagonally Square Mesh by the Continuum Method — Berechnung zweischichtiger, im Grundriß diagonalviereckiger Raumfachwerke mit dem Kontinuumverfahren — Расчет двухслойных пространственных решеток с диагонально-квадратным планом методом континуума 273

Murty, J. S.: A Comparative Study of some Creep-rupture Extrapolating Formulae — Vergleichende Untersuchung einiger Extrapolationsformeln für die Auswertung von Zeitdauern — Сравнительное исследование некоторых экстраполяционных формул для оценки продолжительностей 293

Tarnai, T.: Spherical Grids of Triangular Network — Sphärische Dreiecksfachwerke — Сферические решетчатые конструкциис треугольной сеткой..... 367

Zolnay, L.: L'approvisionnement en eau des villes et châteaux-forts hongrois au moyen-âge — Water Supply of Mediaeval Hungarian Towns and Fortresses — Wasserversorgung mittelalterlicher ungarischer Städte und Burgen 337

Timár, A.: Testing the Plastic Properties of Cohesive- and Intermediate-Type Soils by Extrusion — Untersuchung der plastischen Eigenschaften von bindigen und Übergangsböden mit Hilfe der Stangenpressung — Исследование пластических свойств связанных и переходных грунтов прессованием прутков 355

Varga, L.: Displacement Functions of Orthogonally Anisotropic Cylindrical Shells — Verschiebungsfunktionen von ortogonal-anisotropischen zylindrischen Schalen — Функиии смешение ортогонамьнцх анизотропных цилиндрическиу оболочек 371

Megahid Ahmed, A.—Lenkei, P.: The Effect of the Cross-Section Dimensions on the Ductility of Concrete — Einfluß der Querschnittsdimensionen auf die Verformungsfähigkeit des Betons — Влияние поперечных размеров на предельные деформации бетона 391

Holnapy, D.: Numerical Algorithm to Determine the Difference Operators of Boundary-Value Problems — Numerischer Algorithmus zur Ermittlung der Differenzoperatoren von Randwertaufgaben — Численный алгоритм для определения разностных операторов задач краевых значений 413

Kis, S.: Rational Assumption of Interpolation Reference Points in the Case of Bivariate Lagrange Interpolation — Zweckmäßige Festlegung der Grundpunkte für die Lagrangesche Interpolation bei zwei Variablen — Целесообразное принятие интерполяционных опорных точек в случае интерполяции Лагранжа с двумя переменными 425

Márkus, Gy.: Circular Plate Foundations of Spherical Gas Tanks on Point Supports — Kreisplatten-Fundamente von Kugelgasbehältern mit punktförmigen Abstützungen — Круглая плита фундамента шарового газгольдера, покоящегося на точечных опорах 435

Printed in Hungary

A kiadásért felel az Akadémiai Kiadó igazgatója. Műszaki szerkesztő: Zacsik Annamária
A kézirat nyomdába érkezett: 1973. X. 12. — Terjedelem: 18,9 (A/5) ív 46 ábra

74.75565 Akadémiai Nyomda, Budapest — Felelős vezető: Bernát György

RAUMGEOMETRIE IN DER TECHNISCHEN PRAXIS

von *I. PÁL*

Der fünfhundert Anaglyphen erhaltende Band bietet, nach Bereinigung der allgemeinen Grndbegriffe, einen Überblick über die raumgeometrischen Probleme der einzelnen Industriezweige Namentlich die Raumprobleme der Maschinenindustrie (technische Zeichnunng, charakteristische Kurven, Technologie der Spanabhebung), der Bauindustrie (Schalen- und Fachwerkkonstruktionen, Statik), der chemischen Industrie (Raumgitter, Kristallsymmetrien) sowie die auf diesem Gebiet erzielten Ergebnisse sind im Werk eingehend behandelt. Abschließend befaßt sich das Buch mit einigen im Grenzgebiet der Geometrie und der Mathematik gelegenen Problemen (Koordinatensysteme, Kurven, Flächen) sowie mit der Praxis entnommenen Fragen (Flächen zweiter Ordnung in der spanabhebenden Bearbeitung Gewichtskurvenblatt, die empirische Funktion usw.). Die Auswahl der behandelten Probleme gestalten das Buch zu einem wichtigen Hilfsmittel der technischen Praxis.

In deutscher Sprache · 1974 · 176 Seiten · 555 Abbildungen · Ganzleinen

DIMENSIONIERUNGSFRAGEN DER ZAHNRAD-PLANETENGETRIEBE

von *Z. TERPLÁN*

Das Zahnrad-Planetengetriebe ist eine spezielle Art der Zahnradgetriebe, das in den letzten anderthalb Jahrzehnten eine große Entwicklung durchgemacht hat. In diesem Buch werden in erster Linie die vom Verfasser oder von seinen Mitarbeitern beantworteten Fragen zusammengefaßt. Das Werk ist kurz gefaßt und komprimiert, dem leichteren Verständnis dienen zahlreiche Abbildungen und ein umfangreiches Tabellenmaterial. Ein reichhaltiges Literaturverzeichnis ergänzt das Buch.

In deutscher Sprache · 1974 · 304 Seiten · 114 Abbildungen · 9 Tabellen · Ganzleinen

1828

AKADÉMIAI KIADÓ

Verlag der Ungarischen Akademie der Wissenschaten

B u d a p e s t

THE NITROGEN INDUSTRY I—II

edited by *Gy. Honti*

This work is both a monograph and an indispensable handbook for those working in the field of nitrogen industry and the various branch industries. It includes all the subjects of the ndustry; e.g. thermodynamics, technology, energetics, engineering design, construction and ndustrial practice, power and water supply. It treats also the question of most recent results, uch as, e.g. the ammonia synthesis based on high-capacity, single stream, hydrocarbon steam-reforming. The historical background and prospects for the future are outlined so that a picture of an impetous young branch of industry is provided.

In English · Approx. 1360 pages · Cloth

2nd INTERNATIONAL SYMPOSIUM ON INFORMATION THEORY

Tsahkadsor, Armenia, USSR
September 2—8, 1971

edited by *B. N. Petrov* and *F. Csáki*

The 2nd International Symposium on Information Theory held in 1971 was organized by Soviet scientific organs in cooperation with the International Union of Radio Science (URSI). The lectures delivered by eminent scientists and researchers coming from 15 countries comprise the recent results of the modern information theory. The main topics were: general methods of information theory; coding theory and complexity estimates of encoders and decoders; feedback systems; algebraic methods of encoding; source encoding; statistical methods and learning systems.

In English · 451 pages · Cloth

AKADÉMIAI KIADÓ
Budapest

UNGARISCHE LOKOMOTIVEN UND TRIEBWAGEN

von K. Kopasz, M. Kubinszky, B. Manndorff und B. Varju

In diesem Werk wird jeder Dampf-, Diesel- und Elektro-Lokomotivtyp der 125 Jahre umfassenden Geschichte der ungarischen Eisenbahn ausführlich behandelt. Bei jeder Gattung werden die technischen Angaben mit charakterstischen Einzelheiten des Betriebes ergänzt. Es werden die in Ungarn hergestellten Lokomotive ausführlich behandelt und die Besprechung mit Typenskizzen und Photographien ergänzt, wobei die meisten Photographien Seltenheitswert besitzen. Besonders die Behandlung der Triebwagen von Ganz—Jendrassik und der elektrischen Lokomotiven des Systems Kandó ist sehr ausführlich, da es sich hier um spezielle ungarische Errungenschaften handelt. Das Buch beschäftigt sich auch mit vom Ausland beschafften Lokomotiven der Ungarischen Eisenbahnen. Das Werk ist mit biographischen Angaben berühmter ungarischer Lokomotivkonstrukteure, dem Nummernplan der MÁV und Typentabellen ergänzt.

In deutscher Sprache · Etwa 380 Seiten · Zahlreiche Abbildungen und Tabellen . Ganzleinen

AKADÉMIAI KIADÓ
Verlag der Ungarischen Akademie der Wissenschaften
Budapest

THE THEORY OF GRINDABILITY AND THE COMMINUTION OF BINARY MIXTURES

by K. Reményi

This book deals with the theory as well as the experimental aspects of the grinding behaviour of various materials. A critical evaluation of the most important theories and procedures of comminution is followed by examination of the behaviour of the components of mixtures during grinding. In this part, the author clarifies the fundamental physical law of the grindability of mixtures. Several conclusions can be drawn from the author's investigations: changes of the grinding time of mixtures involve changes in the proportional amount of the crushing energy in relation of the different components; in case of grinding mixtures, the size distribution curves of the components follow either a regular log-normal or an RRB distribution, hence, the resulting ground product of the compounds will have neither lognormal nor RRB distribution; the value of the relative grindability index is not of an additive character.

In English • Approx. 130 pages • Cloth

– ISBN 963 05 0231 3

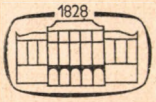

AKADÉMIAI KIADÓ
Budapest

Acta Techn. Hung. **76** (1974), *257—272*

BITÓ, J. F.—ANTAL, K. G. *Examination of the Structure of Functional Relations Among Physical Quantities and Some Application thereof in Discharge Physics*

Theorem π, the basis of the dimension theory, and starting from the same, the structure of functional relations among physical quantities, are being analyzed. The practiced application of the theorem π is demonstrated on a classical mechanical example and its field of application is later extended to discharge physics. The dimension theory which is methodically simple but at the same time suitable for the deduction of useful conclusion may be advantageously applied in discharge physics. The analysis of the function systems, requiring great mathematical apparatus and solvable only by the application of approximative methods, further the analysis of the working hypotheses is facilitated and accelerated by the application of theorem π.

Acta Techn. Hung. **76** (1974, *273—292*

KOLLÁR, L.: *Analysis of Double-Layer Space Trusses with Diagonally Square Mesh by the Continuum Method*

A double-layer space truss is examined wit both chord planes being of square mesh but at 45° to each other. The mode of supporting to provide rigidity, and number of redundacies are determined. A differential equation system of the substituting continuum as well as relationships for the calculation of the truss bar forces from continuum internal forces are established.

Acta Techn. Hung. **76** (1974), *293—306*

MURTY, J. S.: *A Comparative Study of some Creep-rupture Extrapolating Formulae*

A comparative study of some creep-rupture extrapolating formulae is made. The basic differences between the different parametric formulae are discussed. It is shown that the basic differences between the parametric formulae lie in the rate-controlling mechanisms which are different in the different parametric formulae and this is implied in the assumptions made by different authors while deriving their parametric formulae. Using the creep-rupture data of a Cr-Mo-V steel, the various formulae are compared for their extrapolating ability by the standard deviation. It is found, in general, that the iso-thermal relations have a better correlation with the rupture data. All the parametric formulae, which are considered, have given the standard deviation of the same order of magnitude. Rupture stresses were predicted for rupture times of 10^4 and 10^5 hours by the different methods.

Acta Techn. Hung. **76** (1974), *307—336*

TARNAI, T.: *Spherical Grids of Triangular Network*

The network of single-layered spherical grids consisting of triangles is geometrically analysed. The answer sought for is how a sphere surface might be divided into the greatest possible number of spherical triangles with a small number of different side-lengths in such a way that the division be as uniform as possible. With the aid of regular or semi-regular solids approximately uniform triangular division is produced on the surface of the sphere from which the densest network should be selected. A new method of division is suggested and the resulting configurations are compared to those obtained by Fuller's methods of subdivision.

Acta Techn. Hung. **76** (1974), *337—353*

ZOLNAY, L.:

Water Supply of Mediaeval Hungarian Towns and Fortresses. As was proved by the evidence of Hungarian diplomatics and archeology, the towns of Hungary — Transsylvania and Northern Hungary (Slovakia) included — were equipped in the 14th and 15th centuries with gravity watermains. The pumps for the water supply of mountain fortresses represented a considerable progress in comparison with these aqueducts, well-known already in antique Pannonia. According to written records, the first pump was installed in Buda in 1416. In the 15th century the fortresses of Pozsony (Bratislava), Visegrád and Belgrade were equipped with similar pump works by the Kings of Hungary. Still more important was the water-conduit of King Mathias Corvinus. Based on the law of communication vessels, this conduit carried the water of the Buda mountain sources down into the valley and from there on up to the castle hill. The architect was probably Chimenti Camicia of Firenze. Most of Hungary's important monuments of technical history were destroyed during the Turkish occupation (16—17th century).

Acta Techn. Hung. **76** (19744), *355—370*

TIMÁR, A.: *Testing the Plastic Properties of Cohesive-and Intermediate-Type Soils by Extrusion*

The author describes a simple apparatus designed on the extrusion principle, a technique widely used in cold-plastic working of metals, and suggests its use for testing the plastic properties of soils. A comparative study of the extrusion technique has verified a new concept of the liquid limit and plastic limit of soils, on an energy theory basis, as one truly reflecting physical behaviour. The suggested method permits liquid limit and plastic limit to be determined within a single bar extrusion test. As the procedure is fully mechanized, test results are relatively free from subjective errors. A statistical evaluation of a large number of tests has revealed a fair correlation between results furnished by conventional and extrusion methods. In order to clarify certain details further investigations are suggested.

Acta Techn. Hung. **76** (1974), *371—389*

VARGA, L.: *Displacement Functions of Orthogonelly Anisotropic Cylinotrical Shells*

Diplacement functions describing the stress state of orthotropic, anisotropic cylindrical shells are analysed and determined on the assumption of homogeneous anisotropy. By introducing the displacement functions, the exact and approximate solutions of the set of differential equations derived from the equilibrium conditions are presented. The relation between the displacement and isplacement functions rendering general solutions to the homogeneous part and performing particular solutions to the non-homogeneous system are detailed. The differential equations furnishing the establishment o) the displacement functions are reported. Last, the relations existing between the displacements caused by the membrane forces and the displacement functions, as well as the differential equation including the displacement functions and its solution are shown.

Acta Techn. Hung. **76** (1974), *391—411*

MEGAHID AHMED A.—LENKEI, P.: *The Effect of the Cross-Section Dimensions on the Ductility of Concrete*

A test program was carried out to investigate the effect of the cross-sectional dimensions on the ductility of concrete. 60 axially and eccentrically loaded concrete prisms of various cross-sectional dimensions as well as 14 r.c. beams with variable dimensions of compression zone (depth and breadth) under pure bending were tested. The investigations proved, that the stress-strain curve of concrete is depending on the type of loading (centric or eccentric compression, bending). The ultimate strain in the extreme compressed fibers of the axially compressed concrete prisms increased, but that of the eccentially compressed concrete prisms and of the compressed zone of the r.c. beams decreased with the increase of the depth of the compressed concrete. These changes were due to the corresponding changes in the plastic parts of the ultimate concrete strains.

Acta Techn. Hung. **76** (1974), *412—423*

HOLNAPY, D.: *Numerical Algorithm to Determine the Difference Operators of Boundary-Value Problems*

The present paper suggests an algorithm for the determination of the linear equation systems for solving of boundary-value problems by means of the finite difference technique. The method involves the production of the difference operator, and enables the interpolation polynome approximating the solution area to satisfy such conditions that can be specified by the linear combination of the derivatives. Thus, the process includes the most frequently employed methods based on the Lagrange interpolation. The plurilocal method (Mehrstellenverfahren) satisfying the differential equation at a number of points may be considered as a special version of this technique.

Acta Techn. Hung. **76** (1974), *425—433*

KIS, S.: *Rational Assumption of Interpolation Reference Points in the Case of Bivariate Lagrange Interpolation*

The paper deals with the bivariate Lagrange interpolation with respect to the unicity of the interpolating polynome. Such an interpolation (regular) point pattern is defined where the interpolation can be unequivocally performed. The properties of regular point patterns are studied, and a practical method is introduced for their production. Finally, some regular interpolation point patterns are presented as examples for the application of the method described.

Acta Techn. Hung. **76** (1974), *435—451*

MÁRKUS, GY.: *Circular Plate Foundations of Spherical Gas Tanks on Point Supports*

The paper gives the solution for a fundament circular plate on the undersoil, which is loaded by an eccentric force. The results may be used for the calculation of circular ground plates of buildings, tanks, towers resting on columns, or point supports, also in the case when the arbitrarily situated columns pass onto the plate forces of different magnitudes resulting from wind pressure.

The *Acta Technica* publish papers on technical subjects in English, French, German and Russian.

The *Acta Technica* appear in parts of varying size, making up one volume.

Manuscripts should be addressed to

Acta Technica
1051 Budapest,
Münnich Ferenc u. 7.
Hungary

Correspondence with the editors and publishers should be sent to the same address.

The rate of subscription is $ 32.00 a volume. Orders may be placed with "Kultúra" Foreign Trade Company for Books and Newspapers (1389 Budapest 62, P.O.B. 149 Account No. 218 10990) or with representatives abroad.

Les *Acta Technica* paraissent en français, allemand, anglais et russe et publient des travaux du domaine des sciences techniques.

Les *Acta Technica* sont publiés sous forme de fascicules qui seront réunis en volumes.

On est prié d'envoyer les manuscrits destinés à la rédaction à l'adresse suivante:

Acta Technica
1051 Budapest,
Münnich Ferenc u. 7.
Hongrie

Toute correspondance doit être envoyée à cette même adresse.

Le prix de l'abonnement est de $ 32.00 par volume.

On peut s'abonner à l'Entreprise pour le Commerce Extérieur de Livres et Journaux «Kultúra» (1389 Budapest 62, P.O.B. 149 Compte courant No. 218 10990) ou à l'étranger chez tous les représentants ou dépositaires.

«*Acta Technica*» публикуют трактаты из области технических наук на русском, немецком, английском и французском языках.

«*Acta Technica*» выходят отдельными выпусками разного объема. Несколько выпусков составляют один том.

Предназначенные для публикации рукописи следует направлять по адресу:

Acta Technica
1051 Budapest,
Münnich Ferenc u. 7.
Венгрия

По этому же адресу направлять всякую корреспонденцию для редакции и администрации.

Подписная цена — $ 32.00 за том. Заказы принимает предприятие по внешней торговле книг и газет «Kultúra» (1389 Budapest 62, P.O.B. 149 Текущий счет № 218 10990) или его заграничные представительства и уполномоченные.

Reviews of the Hungarian Academy of Sciences are obtainable at the following addresses:

ALBANIA

Drejtorija Qändrone e Pärhapjes dhe Propagandimit të Librit
Kruga Konferenca e Päzes
Tirana

AUSTRALIA

A. Keesing
Box 4886, GPO
Sydney

AUSTRIA

GLOBUS
Höchstädtplatz 3
A-1200 Wien XX

BELGIUM

Office International de Librairie
30, Avenue Marnix
1050 Bruxelles
Du Monde Entier
162, Rue du Midi
1000 Bruxelles

BULGARIA

HEMUS
11 pl Slaveikov
Sofia

CANADA

Pannonia Books
2, Spadina Road
Toronto 4, Ont.

CHINA

Waiwen Shudian
Peking
P. O. B. 88

CZECHOSLOVAKIA

Artia
Ve Směčkách 30
Praha 2
Poštovní Novinová Služba
Dovoz tisku
Vinohradská 46
Praha 2
Mad'arska Kultura
Václavské nám. 2
Praha I
SLOVART A. G.
Gorkého
Bratislava

DENMARK

Ejnar Munksgaard
Nörregade 6
Copenhagen

FINLAND

Akateeminen Kirjakauppa
Keskuskatu 2
Helsinki

FRANCE

Office International de Documentation et Librairie
48, rue Gay-Lussac
Paris 5

GERMAN DEMOCRATIC REPUBLIC

Deutscher Buch-Export und Import
Leninstraße 16
Leipzig 701
Zeitungsvertriebsamt
Fruchtstraße 3—4
1004 Berlin

GERMAN FEDERAL REPUBLIC

Kunst und Wissen
Erich Bieber
Postfach 46
7 Stuttgart S.

GREAT BRITAIN

Blackwell's Periodicals
Oxenford House
Magdalen Street
Oxford
Collet's Subscription Import Department
Dennington Estate
Wellingsborough. Northants.
Robert Maxwell and Co. Ltd.
4—5 Fitzroy Square
London W. I

HOLLAND

Swetz and Zeitlinger
Keizersgracht 471—487
Amsterdam C.
Martinus Nijhof
Lange Voorhout 9
The Hague

INDIA

Hind Book House
66 Babar Road
New Delhi I

ITALY

Santo Vanasia
Via M. Macchi 71
Milano
Libreria Commissionaria Sansoni
Via La Marmora 45
Firenze
Techna
Via Cesi 16.
40135 Bologna

JAPAN

Kinokuniya Book-Store Co. Ltd.
826 Tsunohazu 1-chome
Shinjuku-ku
Tokyo
Maruzen and Co. Ltd.
P. O. Box 605
Tokyo-Central

KOREA

Chulpanmul
Phenjan

NORWAY

Tanum-Cammermeyer
Karl Johansgt 41—43
Oslo I

POLAND

Ruch
ul. Wronia 23
Warszawa

ROUMANIA

Cartimex
Str. Aristide Briand 14—18
Bucureşti

SOVIET UNION

Mezhdunarodnaya Kniga
Moscow G—200

SWEDEN

Almquist and Wiksell
Gamla Brogatan 26
S—101 20 Stockholm

USA

F. W. Faxon Co. Inc.
15 Southwest Park
Westwood Mass. 02090
Stechert Hafner Inc.
31. East 10th Street
New York, N. Y. 10003

VIETNAM

Xunhasaba
19, Tran Quoc Toan
Hanoi

YUGOSLAVIA

Forum
Vojvode Mišića broj 1
Novi Sad
Jugoslovenska Knjiga
Terazije 27
Beograd

24. V. 1974. **Index: 26.025**